Analysis of a nonlinear dynamics model of the saccadic system

Akman, Ozgur

2003

MIMS EPrint: **2006.28**

ISSN 1749-9097

Contents

List of Figures

List of Tables

Acknowledgements

First and foremost, I would like to thank my supervisor Prof. David Broomhead, for his guidance and support throughout this study. I would also like to thank Prof. Richard Abadi and Dr Richard Clement for their encouragement and interest. A particular mention is due to Dr Jerry Huke for many enlightening discussions, mathematical and otherwise.

I would also like to acknowledge the friendship and collaboration of my fellow graduate students Paul B, Paul L, Demetris, Anupap, Eleni and Dan, and to thank Natasha for her love and patience.

Last, but by no means least, I am indebted to my mother, father and grandmother for their continuing love, support and understanding.

Declaration

No portion of the work referred to in this thesis has been submitted in support of an application for another degree or qualification of this or any other university, or other institute of learning.

Abstract

Models of the mechanisms of saccadic eye movements are typically described in terms of the block diagrams used in control theory. Recently, a nonlinear dynamics model of the saccadic system was developed. The model comprises a symmetric piecewise-smooth system of six first-order autonomous ordinary differential equations, which were obtained by combining parts of the existing control models with data from experimental observations of saccadic dynamics. A preliminary numerical investigation of the model revealed that in addition to generating normal saccades, it could also simulate inaccurate saccades, and an oscillatory instability known as congenital nystagmus (CN). By varying the parameters of the model, several types of CN oscillations could be produced, including jerk, bilateral jerk and pendular nystagmus.

The aim of this study was to investigate the bifurcations and attractors of the nonlinear dynamics model, in order to obtain a classification of the simulated oculomotor behaviours. The application of standard local and global stability analysis techniques, together with numerical work, revealed that the equations have a rich bifurcation structure. In addition to Hopf, homoclinic and saddlenode bifurcations organised by a Takens-Bogdanov point, the equations can undergo nonsmooth pitchfork bifurcations and nonsmooth gluing bifurcations. These nonsmooth bifurcations were observed to result from simultaneous transcritical and homoclinic bifurcations in a pair of related smooth systems. Evidence was also found for the existence of Hopf-initiated canards, and for a global bifurcation involving the catastrophic destruction of a symmetry-invariant limit cycle. Unlike the pitchfork and gluing bifurcations, this bifurcation could not be explained in terms of the related smooth systems.

The simulated jerk CN waveforms were found to correspond to a pair of post-canard symmetry-related limit cycles, which exist in regions of parameter space where the equations are a slow-fast system. The slow and fast phases of the simulated oscillations were

attributed to the geometry of an underlying slow manifold. This provides an alternative explanation for the shape of the jerk oscillation, which contrasts with the prevalent control model view that CN is caused by structural abnormalities. The simulated bilateral jerk and pendular waveforms were attributed to a symmetry invariant limit cycle produced by the gluing of the asymmetric cycles.

The bifurcation structure of the model suggests the possibility of moving between the different simulated behaviours by varying the parameters of the model. This was in agreement with experimental evidence showing that subjects can exhibit several different types of behaviour in a single recording period. In addition, the bifurcation analysis places restrictions on which kinds of behaviour are likely to be associated with each other in parameter space. On the basis of these restrictions, several experiments were suggested to assess the validity of the model as a predictor of saccadic behaviour. In particular, it was proposed that reducing the level of attention of a subject in a controlled way could induce a change from a jerk to a pendular oscillation.

Chapter 1

Introduction

The study of eye movements is a source of important information for both clinicians and physical scientists. To clinicians, the presence of abnormal eye movement behaviour in a patient is often the indicator of a specific pathology. For physical scientists, the study of eye movements presents a unique opportunity to understand the workings of the brain. This is in part due to the relative simplicity of the oculomotor control system, in comparison to other neurobiological control systems, and the wealth of quantitative data on eye movements that has been collected in the last four decades [2], [5], [6]. Traditionally, the investigation of oculomotor control has been dominated by control systems theory [2], [3], [5], [6], [7], [8], [9], [10], [11]. In the last few years, however, there has been some interest in using the techniques of nonlinear dynamics to model oculomotor control, and to anlayse eye movement time series [12], [13], [14], [15], [16], [17].

The oculomotor control subsystem that is responsible for the generation of fast eye movements, or saccades, has been the focus of much theoretical and experimental work [2], [3], [5]-[11]. A recent nonlinear dynamics model of the saccadic system proposed by Broomhead et al was found to be able to simulate both normal saccades and an oscillatory oculomotor instability known as congenital nystagmus (CN) [14]. The existence of a single model able to generate both normal saccades and CN oscillations conflicts with an influential control theory model proposed by Optican et al, which suggested that CN results from structural abnormalities in the oculomotor control system [7]. The work presented here is an analysis of the nonlinear dynamics model of Broomhead et al, with a view to interpreting the possible implications that the predictions of the model may have for understanding saccadic abnormalities and the aetiology of CN.

The remainder of this chapter is a brief discussion of some characteristics of the oculomotor control system relevant to this study, followed by a description of the context in which the mathematical analysis of the model was carried out. Thereafter, chapter 2 describes the construction of the model, with chapters 3 to 5 detailing the analysis of the bifurcations and attractors of the model. In chapter 6 a full classification of the simulated saccadic behaviours is proposed, based on the bifurcation analysis. This classification is then used as the framework for a discussion of the biological implications of the model. Finally, in chapter 7, a summary of the preceding analysis is presented. A number of suggestions for further development of the model are also suggested. The more technical proofs from Chapters 3 to 5, together with other results which were omitted for brevity, are given in an Appendix.

1.1 Oculomotor control, saccades and congenital nystagmus

1.1.1 Eye movement control

Figure (1-1) shows the major structures of the eye in transverse section. Light enters the eye through the pupil and is focused onto the retina by the lens. The retina contains photoreceptors which absorb the incoming light, generating electrical impulses that are relayed to the visual cortex via the optic nerve [1]. The density of photoreceptors is greatest in a small region of the retina known as the fovea. Optimal visual performance is only attained when images are held steady on the fovea; the ability of the eye to resolve distinct points in the visual field (visual acuity) decreases sharply away from the fovea. In addition, visual acuity is also degraded if images slip over the fovea at velocities greater than a few degrees per second [1]. In broad terms, the brain controls the movement of the eyes to ensure that the image of the object of interest falls on the fovea [1], [2]. This is a process referred to as **foveation** [2].

Ocular movements are carried out by six extraocular muscles that are attached to the outer wall of the eye (sclera). Figure (1-2) is a transverse section through the skull, showing the orientation of the extraocular muscles. The medial and lateral rectus muscles produce predominately horizontal movements, the superior and inferior rectus muscles produce predominately vertical movements, while the superior and inferior oblique muscles produce mainly rotary movements. The extraocular muscles receive commands from motoneurons

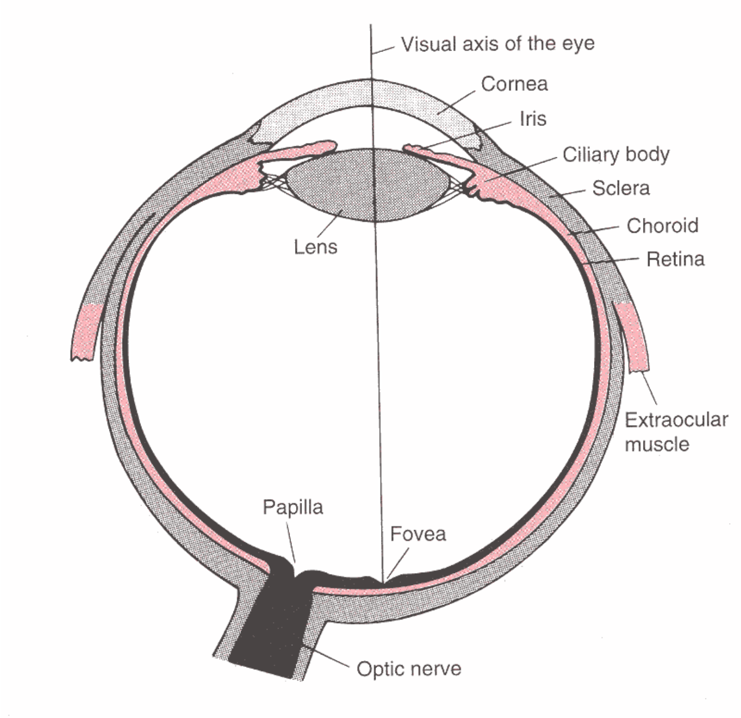

Figure 1-1: Transverse section through the right eye, seen from above (Reproduced from figure 8.2 of [1]).

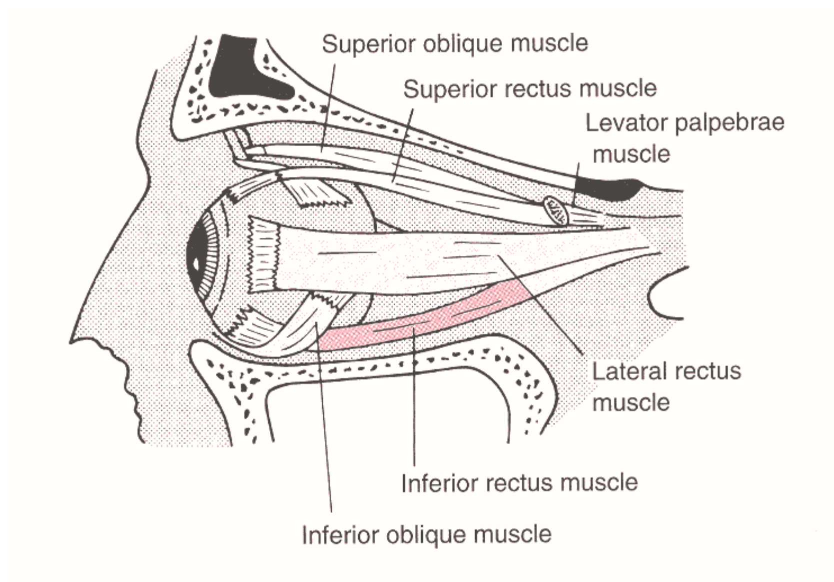

Figure 1-2: Transverse section through the skull, showing the extraocular muscles. The medial rectus is obscured from view by the eyeball. (Reproduced from figure 16.24 in [1]).

in the nuclei of the abducent, trochlear and oculomotor nerves, situated in the brain stem [1], [2]. The activity of these motoneurons is coordinated by a complex set of interconnected neuronal groups. Physiological studies of such 'preoculomotor' nuclei and networks through single neuron recording, electrical stimulation and lesion have identified many of the pathways associated with different types of eye movement. This has led to the isolation of six major preoculomotor networks: the saccadic system, the smooth pursuit system, the vestibular system, the optokinetic system, the vergence system and the gaze-holding system [1], [2], [5], [6], [18]. The saccadic system provides rapid shifts of gaze, or **saccades**, to bring about foveation of new targets. The smooth pursuit system matches eye velocity with target velocity to provide a stable foveal image when tracking objects in the visual field. The function of the vestibular system is to stabilise gaze during brief head rotations by generating an involuntary eye movement which has velocity equal and opposite to the velocity of the head. The optokinetic system is responsible for matching eye velocity to the velocity of the visual field to enable stable gaze during sustained head motion. The vergence system acts so as to keep the target image on the fovea during motion of the target away from or towards the eyes. Finally, the function of the gaze-holding system is to maintain a stable foveal image during sustained fixation at a given gaze angle.

1.1.2 Saccades

Saccades are fast, conjugate eye movements which redirect gaze to bring the image of the object of interest onto the fovea. In the following work, only horizontal saccades will be considered. A schematic of the major neural pathways involved in the generation of a horizontal saccade is given in figure (1-3). Physiological studies indicate that saccades are initiated in response to signals from the visual cortex specifying the spatial location to which the eyes are to be driven. These signals are conveyed via the superior colliculus in the midbrain to **burst neurons** (or **bursters**) situated in the brain stem. The burst neurons are normally prevented from discharging by inhibitory **omnipause neurons**. Just prior to the onset of a saccade, an inhibitory trigger to the omnipause neurons releases their inhibition of the bursters, which generate a signal referred to as the **pulse**. This signal creates the initial 'push' of the eye to overcome orbital viscous drag. The pulse is conveyed to a complex of neuronal feedback circuits, collectively referred to as the **neural integrator (NI)**, which integrate the pulse producing a signal called the **step**. This signal generates the forces necessary to hold the eye in its new position against orbital elastic

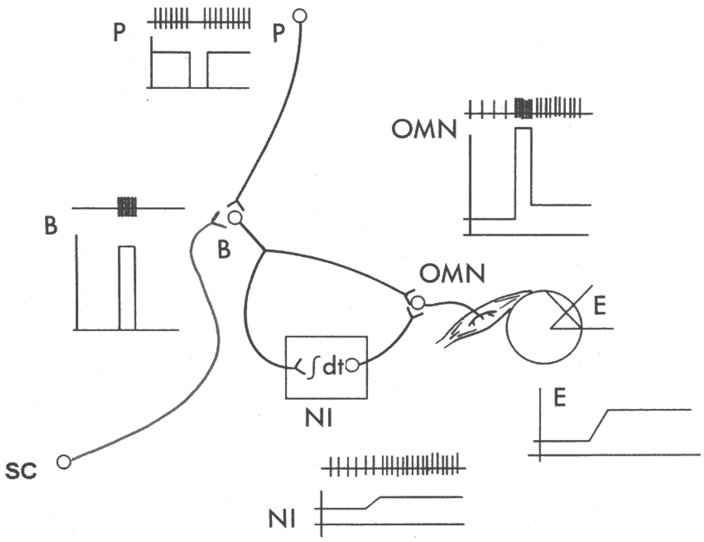

Figure 1-3: Schematic of the main neural pathways involved in the production of horizontal saccades. P=omnipause neurons, B=burst neurons, SC=superior colliculus, OMN=ocular motoneurons, E=saccadic eye movement, NI=neural integrator. Vertical lines represent individual discharges of neurons. Underneath the schematised neural discharge is a plot of discharge rate versus time. The schematic plot E shows horizontal eye position versus time. (Adapted from figure 3.6 of [2]).

restoring forces. The step and pulse signals are then transmitted together to the relevant motoneurons. These combine the signals to produce a final motor command which is sent to the extraocular muscles. The muscles then move the eye to the required gaze angle [2], [5], [6], [18]. In control models of the saccadic system, the ocular motoneurons and extraocular muscles are collectively referred to as the **muscle plant**.

The peak velocity of a 30 degree saccade frequently exceeds 500 deg/sec and the movement can be completed in just 80 msec. Experimental investigation of the dynamic characteristics of saccades has revealed that the peak velocities and durations of saccades are related to their amplitudes. This relationship is often referred to as the **main sequence** [2], [18]. Saccades can be **normometric** (accurate) or **dysmetric** (inaccurate), depending on factors such as the eccentricity of the target, the type of saccadic task and the state of the subject [2], [15]. Saccades which overshoot the target are referred to as **hypermetric** while those which undershoot are called **hypometric**. Figure (1-4) shows the time course of a normometric rightward saccade generated by a normal subject (i.e. one with no known ocular pathology). As with all eye movement plots presented here, positive eye position corresponds to rightward gaze, and negative eye position corresponds to leftward gaze.

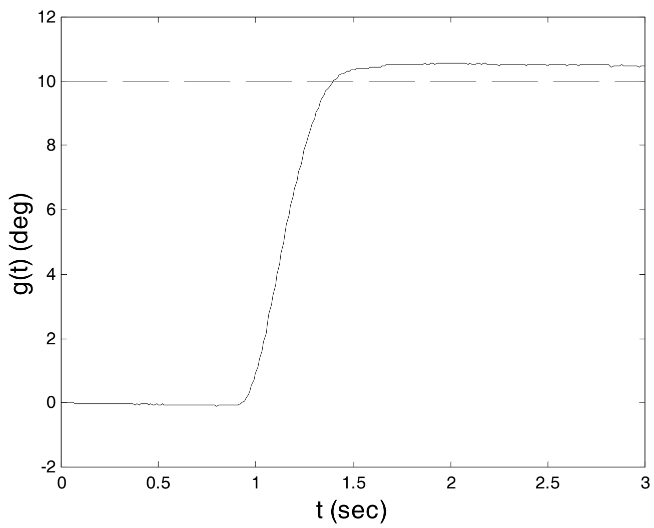

Figure 1-4: Recording of a normometric rightward saccade. t = time, $g(t)$ = horizontal eye position. The position of the target is indicated by the dotted line.

A particular class of hypermetric saccades which are of interest to this study are those involving a **dynamic overshoot**. These are small, damped oscillations that follow the primary saccade with no delay. Dynamic overshoots have been observed in both normal subjects and those with an ocular pathology [2], [15]. Figure (1-5) shows the time course of a hypermetric rightward saccade with dynamic overshoot.

1.1.3 Congenital nystagmus

The term **nystagmus** refers to an oscillatory movement of the eyes. The particular type of nystagmus which is of interest here is a condition known as **congenital nystagmus** (CN). CN is an involuntary, bilateral oscillation of the eyes that is present in approximately 0.025% of the population. The movements are conjugate and occur predominately in the horizontal plane. CN develops at birth, or shortly afterwards, and persists throughout life [2], [18], [19], [20], [21]. In the last three decades, infrared reflection and electro-oculography techniques have been used to accurately record CN time series, enabling CN waveforms to be objectively analysed. It has been found that considerable variation in the mean amplitude (1°-10°) and frequency (2 Hz-5 Hz) of the oscillation occurs between subjects [21]. The ability to record CN oscillations has also led to the classification of CN waveforms into subclasses. This classification is based on the decomposition of the oscillation into fast and slow phases, depending on the magnitude of the instantaneous eye velocity. In general,

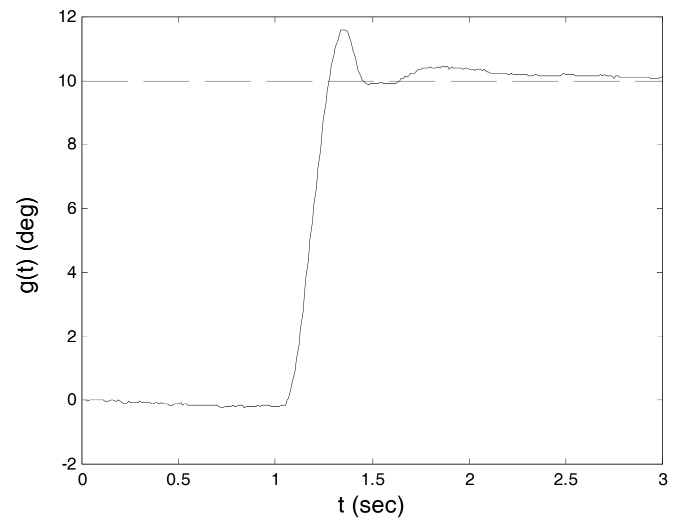

Figure 1-5: Recording of a hypermetric rightward saccade with dynamic overshoot. t = time, $g(t)$ = horizontal displacement of the eye. The position of the target is indicated by the dotted line.

the retinal image is held on the fovea for a short time before a slow phase takes the target off the fovea. The slow phase is then interrupted by a fast or slow phase which moves the target towards, or directly onto the fovea [2], [18]-[20]. As a consequence of the reduced foveation time, nystagmats tend to have poor visual acuity [2], [18], [19]. Schematics of some typical CN waveforms are shown in figure 1-6, together with the positions of the fast and slow phases. Some of these oscillation types will now be described in greater detail.

Jerk nystagmus is composed of an increasing exponential slow phase followed by a saccadic fast phase. The nystagmus is referred to as right-beating or left-beating in accordance with the direction of the fast phase [2], [19], [20]. Figure (1-7) is a time series of a left-beating jerk nystagmus. A variation on the jerk waveform is **jerk with extended foveation (JEF)** [20]. As the name suggests, JEF has a longer slow phase than the plain jerk waveform. Figure (1-8) is a time series of a left-beating JEF oscillation (compare with figure (1-7)). In some subjects, an extended period of jerk oscillations is followed by a shorter period of jerks that beat in alternate directions. After this bidirectional phase, the oscillation reverts to a unidirectional jerk. This phenomenon is known as **bias reversal** [2], [20]. The bidirectional waveform associated with bias reversal will be referred to in the following work as **bilateral jerk**. Figure (1-9) is a time series of a bilateral jerk oscillation.
Pendular nystagmus consists of sinusoidal slow phase movements. Pendular oscillations tend to be of larger amplitude than jerk oscillations, and are seen more often in infants

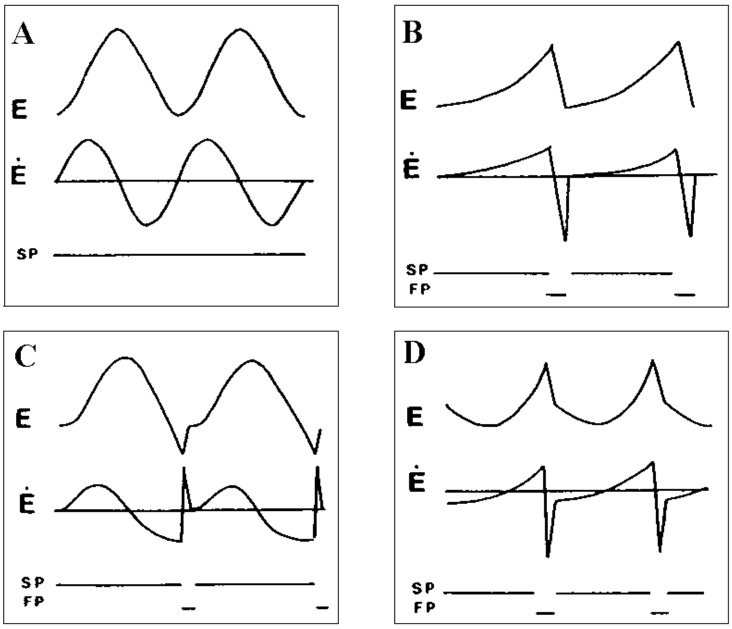

Figure 1-6: Schematic illustration of 4 waveform types found in congenital nystagmus. E=eye position, Ė=eye velocity. The durations of the slow phases (SP) and fast phases (FP) of the waveforms are indicated by the upper and lower solid lines respectively. The waveforms depicted are: A) pure pendular, B) pure jerk, C) pendular with foveating saccades and D) pseudocyloid.

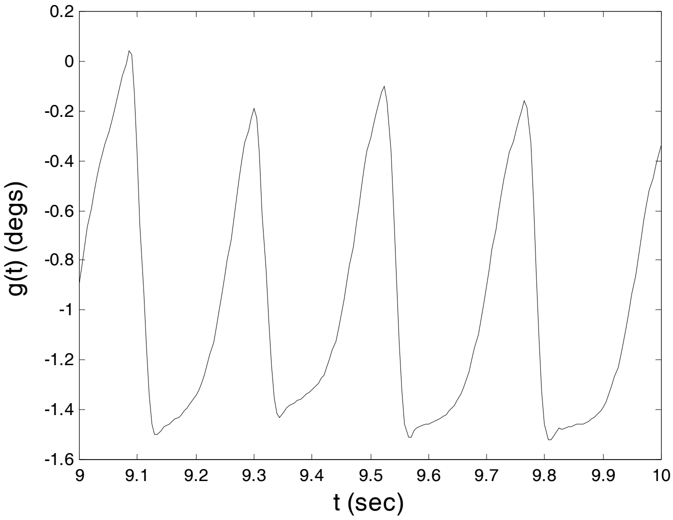

Figure 1-7: Recording of a jerk nystagmus waveform. t = time, $g(t)$ = horizontal displacement of the eye.

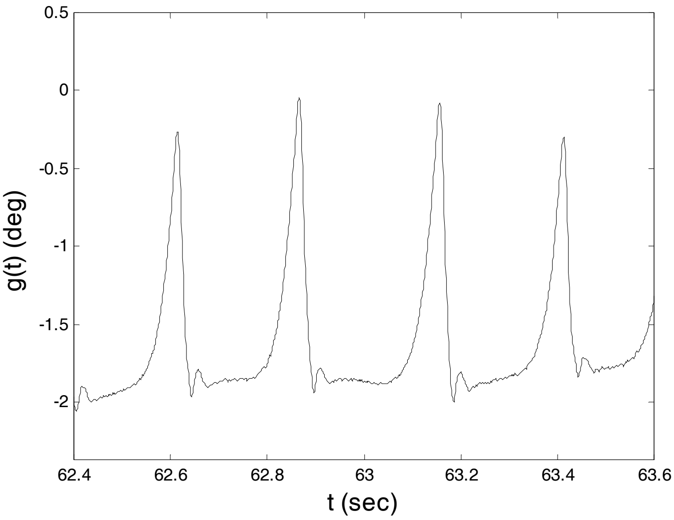

Figure 1-8: Recording of a jerk with extended foveation waveform. t = time, $g(t)$ = horizontal displacement of the eye.

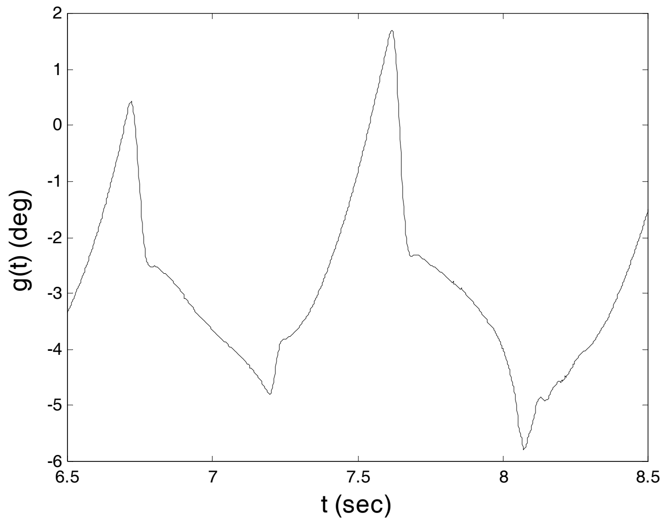

Figure 1-9: Recording of a bilateral jerk waveform. t = time, $g(t)$ = horizontal displacement of the eye.

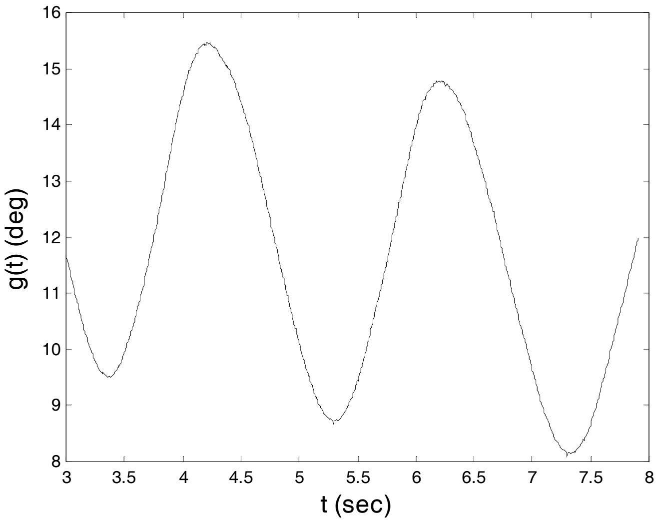

Figure 1-10: Recording of a pendular waveform. t = time, $g(t)$ = horizontal displacement of the eye.

than adults [2], [20]. Figure (1-10) is a time series of a pendular nystagmus.

Fourier analysis of CN waveforms has shown that there are marked differences in the frequency spectra of waveforms from different CN classes, although all CN waveforms have a strong periodic component [22]. Despite this variety, it has long been postulated by some researchers that there is a common CN mechanism responsible for generating the different types of oscillation that have been observed [7], [19], [20]. The most compelling evidence for this idea is that many CN subjects can exhibit a range of different oscillations over the same recording period. The type of waveform observed has been found to depend on environmental factors, and in particular, on the level of attention of the subject [20], [21]. An example of this, which is of interest here, is the finding that some subjects who exhibit a jerk nystagmus during a fixation task can switch to a pendular nystagmus upon entering a state of low attention, such as when closing their eyes or daydreaming [20], [21].

The explanation for CN provided by the control theory model of Optican et al is that the oscillations result from a malfunction of the gaze-holding system due to neural miswiring. In this scheme, the malfunction causes drift of the eye away from the target, which is followed by saccades to bring the eye back to the target [7]. Explicit in this idea is the assumption that the fast phases of nystagmus are corrective; saccades are in fact assumed to be generated when the retinal error exceeds a set threshold. By modifying parameters, such as the gain of position and velocity feedback loops in both the gaze-holding and saccadic units of their model, Optican et al were able to generate a broad range of CN waveforms [7]. The nonlinear dynamics model of the saccadic system proposed by Broomhead et al was obtained by converting parts of the existing control models of the oculomotor system into corresponding sets of ordinary differential equations. The model also incorporated some characteristics of burst neurons obtained from empirical data that had been ignored in the control models. By varying parameters governing the burst neuron characteristics, and the speed at which burst neurons react to their input signal, Broomhead et al were able to simulate saccadic dysmetrias-such as dynamic overshoot-and CN oscillations-such as jerk, bilateral jerk and pendular nystagmus. These simulated eye movements were found to be attributable to fixed point and limit cycle attractors of the model. The derivation of the model due to Broomhead et al will be described in greater detail in the next chapter. The following section presents the mathematical setting for the analysis of the model in chapters 3-6.

1.2 The general system of first order autonomous ODEs

The material presented here is based on [4], [23], [24], [25], [26], [27] and [28]. Throughout this section and the following chapters, $\|.\|$ will be taken to represent the vector and matrix p norm, unless otherwise specified. Also, $\mathbf{1}_n$ represents the $n \times n$ identity matrix and $\mathbf{0}_{n\times m}$ the $n \times m$ zeros matrix. The expression $(\mathbf{x}, \mathbf{y})^T$ where $\mathbf{x} \in \mathbb{R}^m$ and $\mathbf{y} \in \mathbb{R}^n$ will be implicitly taken to mean the vector:

$$\begin{pmatrix} \mathbf{x} \\ \mathbf{y} \end{pmatrix}$$

The object of interest in this section will be the general system of n first order autonomous ordinary differential equations (ODEs) below:

$$\begin{aligned} \dot{x}_1 &= F_1\left(x_1, x_2, \dots, x_n\right) \\ \dot{x}_2 &= F_2\left(x_1, x_2, \dots, x_n\right) \\ &\vdots \\ \dot{x}_n &= F_n\left(x_1, x_2, \dots, x_n\right) \end{aligned} \tag{1.1}$$

In (1.1), the dot represents differentiation with respect to time $\frac{d}{dt}$. Thus, $\dot{x}_i = \frac{dx_i}{dt}$ $\forall 1 \leq$

$i \leq n$. By setting $\mathbf{x} = (x_1, x_2, \dots, x_n)^T$ and $\mathbf{F}(\mathbf{x}) = (F_1(\mathbf{x}), F_2(\mathbf{x}), \dots, F_n(\mathbf{x}))^T$, (1.1) can be written in the vectorised form below:

$$\dot{\mathbf{x}} = \mathbf{F}(\mathbf{x}) \tag{1.2}$$

It is assumed that $\mathbf{x} \in W$, where W is an open subset of $\mathbb{R}^n$, and that $\mathbf{F} : W \to \mathbb{R}^n$ is a locally Lipschitz function. The set W is called the *state space* of the system. The map $\mathbf{F}$ is called the *vector field.* Given $1 \leq i \leq n$, the subset of the state space on which $F_i(x_1, x_2, \dots, x_n) = 0$ is referred to as the x_i *nullcline.*

The existence and uniqueness of solutions of $\dot{\mathbf{x}} = \mathbf{F}(\mathbf{x})$ will be covered first in this section. This will followed by a discussion of ω-limit sets, and two of the most simple types of ω-limit sets, fixed points and limit cycles will be defined. Next, the idea of linearising the system about a fixed point will be introduced. Following this, the asymptotic behaviour of systems in which solutions can be extended infinitely far forward in time, and are also eventually confined to a compact subset of W will be discussed. This will lead to a definition of an attractor which will be used throughout the rest of this work. The section will finish with a brief discussion of symmetries of vector fields.

1.2.1 Existence and uniqueness of solutions

It can be shown that given $\mathbf{x} \in W$, there is a maximal open interval $J(\mathbf{x}) = (a, b)$ containing 0, such that a solution $\mathbf{x}(t)$ of $\dot{\mathbf{x}} = \mathbf{F}(\mathbf{x})$ with $\mathbf{x}(0) = \mathbf{x}$ exists, and is unique on $J(\mathbf{x})$ (a may be $-\infty$ and b may be $+\infty$). For each $\mathbf{x} \in W$, write the solution $\mathbf{x}(t)$ as $\phi(\mathbf{x}, t)$. The set $\{\phi(\mathbf{x}, t) : t \in J(\mathbf{x})\}$ is referred to as the *trajectory* or *orbit* of $\dot{\mathbf{x}} = \mathbf{F}(\mathbf{x})$ passing through $\mathbf{x}$. Define the set $\Omega \subseteq W \times \mathbb{R}$ by $\Omega = \left\{(\mathbf{x}, t)^T : \mathbf{x} \in W, t \in J(\mathbf{x})\right\}$. Then Ω is open in $W \times \mathbb{R}$ and the map $\phi : \Omega \to W$ defined by $\phi : (\mathbf{x}, t) \mapsto \phi(\mathbf{x}, t)$ is continuous. The function ϕ is referred to as the *flow* of the system. Define the *time set* $T \subseteq \mathbb{R}$ by $T = \{t \in \mathbb{R} : \exists \mathbf{x} \in W \text{ for which } t \in J(\mathbf{x})\}$. Also, given $t \in T$, define the t *set* $U_t \subseteq W$ by $U_t = \{\mathbf{x} \in W : t \in J(\mathbf{x})\}$ and the *time* t *map* $\phi_t : U_t \to W$ by $\phi_t(\mathbf{x}) = \phi(\mathbf{x}, t)$ $\forall \mathbf{x} \in U_t$. Then $\forall t \in T$, U_t is open in W, $-t \in T$ with $U_{-t} = \phi_t(U_t)$ and $\phi_t : U_t \to U_{-t}$ is a homeomorphism with $\phi_t^{-1} = \phi_{-t}$. Moreover, 0 is always an element of T, and $U_0 = W$ with $\phi_0 = id|_W$, where $id : \mathbb{R}^n \to \mathbb{R}^n$ is the identity map. Also, for $\mathbf{x} \in W$ and $s, t \in \mathbb{R}$ such that $\phi_t(\mathbf{x}), \phi_s(\phi_t(\mathbf{x}))$ and $\phi_{s+t}(\mathbf{x})$ all exist, $\phi_s(\phi_t(\mathbf{x})) = \phi_{s+t}(\mathbf{x})$. If $\mathbf{F}$ is not just locally Lipschitz but is in fact C^k for some $k \geq 1$, the map ϕ is C^k and $\phi_t : U_t \to U_{-t}$ is a

C^k diffeomorphism $\forall t \in T$.

A subset S_W of W is defined to be *invariant* if given $\mathbf{x} \in S_W$, $J(\mathbf{x}) = \mathbb{R}$ and $\phi_t(\mathbf{x}) \in S_W$ $\forall t \in \mathbb{R}$. S_W is defined to be *positively invariant* if given $\mathbf{x} \in S_W$, $[0, \infty) \subset J(\mathbf{x})$, and $\phi_t(\mathbf{x}) \in S_W$ $\forall t \geq 0$. Similarly, S_W is defined to be *negatively invariant* if given $\mathbf{x} \in S_W$, $(-\infty, 0] \subset J(\mathbf{x})$, and $\phi_t(\mathbf{x}) \in S_W$ $\forall t \leq 0$. If S_W is invariant, then $\{\phi_t(\mathbf{x}_0) : t \in \mathbb{R}, \mathbf{x}_0 \in S_W\}$ is said to be a *dense orbit* of S_W if given $\mathbf{y} \in S_W$, $\forall \epsilon > 0$ there is some $t' \in \mathbb{R}$ for which $\|\phi_{t'}(\mathbf{x}_0) - \mathbf{y}\| < \epsilon$.

Remark: Note that solutions of C^k systems are C^{k+1} functions of time. To see this, let $\mathbf{x}(t)$ be a solution of $\dot{\mathbf{x}} = \mathbf{F}(\mathbf{x})$ where $\mathbf{F}$ is C^k for some $k \geq 0$. Then by the discussion above, $\mathbf{x}(t) = \phi(\mathbf{x}(0), t)$ $\forall t \in J(\mathbf{x}(0))$, where the flow $\phi : \Omega \to W$ is a C^k function of $(\mathbf{x}, t)^T$ on Ω. It follows that $\mathbf{x}(t)$ is a C^k function of t on $J(\mathbf{x}(0))$. Now $\forall t \in J(\mathbf{x}(0))$, $\dot{\mathbf{x}}(t) = \mathbf{F}(\mathbf{x}(t))$. Thus, since a composition of C^k functions is itself C^k, $\dot{\mathbf{x}}(t)$ is C^k on $J(\mathbf{x}(0))$. This implies that $\mathbf{x}(t)$ is C^{k+1} on $J(\mathbf{x}(0))$.

1.2.2 ω-limit sets of $\dot{\mathbf{x}} = \mathbf{F}(\mathbf{x})$

Given $\mathbf{x} \in W$ for which $[0, \infty) \subset J(\mathbf{x})$, the *$\omega$-limit set* $\omega(\mathbf{x}) \subseteq W$ of $\mathbf{x}$ is defined as below:

$$\omega(\mathbf{x}) = \left\{\mathbf{y} \in W : \exists (t_n) \subset [0, \infty) \text{ with } t_n \to \infty \text{ as } n \to \infty \text{ and } \phi_{t_n}(\mathbf{x}) \to \mathbf{y} \text{ as } n \to \infty\right\}$$

Each element of $\omega(\mathbf{x})$ is referred to as an *ω-limit point* of $\mathbf{x}$. It can be shown that $\omega(\mathbf{x})$ is closed.

Fixed points

A point $\bar{\mathbf{x}} \in W$ is called a *fixed point* of $\dot{\mathbf{x}} = \mathbf{F}(\mathbf{x})$ if $\mathbf{F}(\bar{\mathbf{x}}) = 0$. It follows that $\bar{\mathbf{x}}$ is invariant. Also $\omega(\mathbf{y}) = \bar{\mathbf{x}}$ for all $\mathbf{y} \in W$ such that $\phi_t(\mathbf{y}) \to \bar{\mathbf{x}}$ as $t \to \infty$. In particular, $\omega(\bar{\mathbf{x}}) = \bar{\mathbf{x}}$.

Given $\delta > 0$, and $\mathbf{x} \in \mathbb{R}^n$, define the ball $B_\delta(\mathbf{x}) \subseteq W$ by:

$$B_\delta(\mathbf{x}) = \{\mathbf{y} \in W : \|\mathbf{y} - \mathbf{x}\| < \delta\}$$

A fixed point $\bar{\mathbf{x}}$ is defined to be *Liapunov stable* if $\forall \epsilon > 0$, $\exists \delta > 0$ such that $\forall \mathbf{y} \in B_\delta(\bar{\mathbf{x}})$, $\phi_t(\mathbf{y}) \in B_\epsilon(\bar{\mathbf{x}})$ $\forall t \geq 0$. $\bar{\mathbf{x}}$ is defined to be *quasi-asymptotically stable* if $\exists \delta > 0$ such that

$\forall \mathbf{y} \in B_\delta(\bar{\mathbf{x}})$, $\phi_t(\mathbf{y}) \to \bar{\mathbf{x}}$ as $t \to \infty$. $\bar{\mathbf{x}}$ is defined to be *asymptotically stable* (or simply *stable*) if it is both Liapunov stable and quasi-asymptotically stable. $\bar{\mathbf{x}}$ is defined to be *unstable* if it is not Liapunov stable.

Limit cycles

A *periodic orbit* of $\dot{\mathbf{x}} = \mathbf{F}(\mathbf{x})$ of period T is a set $\mathcal{S} \subset W$ which can be written as

$$\mathcal{S} = \{\phi_t(\mathbf{y}) : 0 \le t < T\}$$

for some $\mathbf{y} \in W$ for which $[0, T] \subset J(\mathbf{y})$, $\phi_T(\mathbf{y}) = \mathbf{y}$ and $\phi_t(\mathbf{y}) \neq \mathbf{y}$ for all $0 < t < T$. It can be shown that $\mathcal{S}$ is invariant, with $\mathcal{S} = \{\phi_t(\mathbf{y}') : 0 \le t < T\}$ for all $\mathbf{y}' \in \mathcal{S}$. Also, $\omega(\mathbf{y}) = \mathcal{S}\ \forall \mathbf{y} \in \mathcal{S}$. $\mathcal{S}$ is called a *limit cycle* of period T if there is an open neighbourhood U of $\mathcal{S}$ which contains no periodic orbits other than $\mathcal{S}$ itself.

Given $\delta > 0$, and a set $V \subseteq W$, define the δ-neighbourhood $N(V, \delta) \subseteq W$ of V by:

$$N(V, \delta) = \{\mathbf{y} \in W : \exists \mathbf{x} \in V \text{ with } \|\mathbf{y} - \mathbf{x}\| < \delta\}$$

A limit cycle $\mathcal{S}$ is defined to be *Liapunov stable* if $\forall \epsilon > 0$, $\exists \delta > 0$ such that $\forall \mathbf{y} \in N(\mathcal{S}, \delta)$, $\phi_t(\mathbf{y}) \in N(\mathcal{S}, \epsilon)\ \forall t \ge 0$. $\mathcal{S}$ is defined to be *quasi-asymptotically stable* if $\exists \delta > 0$ such that $\forall \mathbf{y} \in N(\mathcal{S}, \delta)$, $\phi_t(\mathbf{y}) \to \mathcal{S}$ as $t \to \infty$. $\mathcal{S}$ is defined to be *asymptotically stable* (or simply *stable*) if it is both Liapunov stable and quasi-asymptotically stable. $\mathcal{S}$ is defined to be *unstable* if it is not Liapunov stable. A related concept is that of a phase-coherent limit cycle. A limit cycle $\mathcal{S}$ is defined to be *phase-coherent* if $\exists \delta > 0$ such that $\forall \mathbf{y} \in N(\mathcal{S}, \delta)$, $\exists \mathbf{x} \in \mathcal{S}$ with $\phi_t(\mathbf{y}) \to \phi_t(\mathbf{x})$ as $t \to \infty$. If $\mathbf{F}$ is C^1 it can be shown that, generically, a stable limit cycle is a phase-coherent limit cycle. It will be assumed in the following work that all stable limit cycles of the saccadic system model are phase-coherent.

There is another type of orbit of $\dot{\mathbf{x}} = \mathbf{F}(\mathbf{x})$ which will be of importance later. Let $\bar{\mathbf{x}} \in W$ be a fixed point of $\dot{\mathbf{x}} = \mathbf{F}(\mathbf{x})$ and assume $\mathbf{y} \in W \setminus \{\bar{\mathbf{x}}\}$ such that $J(\mathbf{y}) = \mathbb{R}$. The orbit $\Gamma = \{\phi_t(\mathbf{y}) : t \in \mathbb{R}\}$ is defined to be *homoclinic* to $\bar{\mathbf{x}}$ if $\phi_t(\mathbf{y}) \to \bar{\mathbf{x}}$ as $t \to \infty$ and as $t \to -\infty$. It can be shown that Γ is invariant, $\Gamma \cap \{\bar{\mathbf{x}}\}$ is empty, and for any $\mathbf{y}' \in \Gamma$, $\Gamma = \{\phi_t(\mathbf{y}') : t \in \mathbb{R}\}$ with $\phi_t(\mathbf{y}') \to \bar{\mathbf{x}}$ as $t \to \pm\infty$.

1.2.3 Linearising $\dot{\mathbf{x}} = \mathbf{F}(\mathbf{x})$ about a fixed point

Assume that the vector field $\mathbf{F} : W \to \mathbb{R}^n$ is C^1. Let $\bar{\mathbf{x}} \in W$ be a fixed point of $\dot{\mathbf{x}} = \mathbf{F}(\mathbf{x})$, and write $D\mathbf{F}(\bar{\mathbf{x}})$ for the Jacobian matrix of partial derivatives of $\mathbf{F}$ evaluated at $\bar{\mathbf{x}}$. By Taylor expanding $\mathbf{F}$ about $\mathbf{0}$, $\dot{\mathbf{x}} = \mathbf{F}(\mathbf{x})$ can be written as $\dot{\mathbf{w}} = D\mathbf{F}(\bar{\mathbf{x}})\mathbf{w} + O\left(\|\mathbf{w}\|^2\right)$, where $\mathbf{w} = \mathbf{x} - \bar{\mathbf{x}}$. The *linearisation* of $\dot{\mathbf{x}} = \mathbf{F}(\mathbf{x})$ about $\bar{\mathbf{x}}$ is the linear system defined on $\mathbb{R}^n$ which is obtained by ignoring the $O\left(\|\mathbf{w}\|^2\right)$ term:

$$\dot{\mathbf{z}} = D\mathbf{F}(\bar{\mathbf{x}})\mathbf{z} \tag{1.3}$$

The vector field of (1.3) is obviously Lipschitz (it is in fact C^∞), and so solutions exist and are unique. It can be shown that $\forall \mathbf{z} \in \mathbb{R}^n$, $J(\mathbf{z}) = \mathbb{R}$. Hence, the time set is $\mathbb{R}$, and $\forall t \in \mathbb{R}$ the t set is $\mathbb{R}^n$. Moreover, $\forall t \in \mathbb{R}$ the time t map $L_t : \mathbb{R}^n \to \mathbb{R}^n$ is C^∞, and is defined by:

$$L_t(\mathbf{x}) = e^{D\mathbf{F}(\bar{\mathbf{x}})t}\mathbf{x} \tag{1.4}$$

Write $\{\lambda_1, \ldots, \lambda_n\}$ for the eigenvalues of the Jacobian matrix $D\mathbf{F}(\bar{\mathbf{x}})$. $\bar{\mathbf{x}}$ is defined to be *hyperbolic* if none of $\{\lambda_1, \ldots, \lambda_n\}$ have zero real part. In this case, $D\mathbf{F}(\bar{\mathbf{x}})$ is invertible and so $\mathbf{0} = (0, 0, \ldots 0)^T$ is the unique fixed point of $\dot{\mathbf{z}} = D\mathbf{F}(\bar{\mathbf{x}})\mathbf{z}$. The importance of the linearisation is that the behaviour of $\dot{\mathbf{x}} = \mathbf{F}(\mathbf{x})$ about a hyperbolic fixed point $\bar{\mathbf{x}}$ is determined by the behaviour of $\dot{\mathbf{z}} = D\mathbf{F}(\bar{\mathbf{x}})\mathbf{z}$ about $\mathbf{0}$. More precisely, the Hartman-Grobman Theorem states that there is a homeomorphism H mapping some open neighbourhood $U_{\bar{\mathbf{x}}}$ of $\bar{\mathbf{x}}$ in W to an open neighbourhood $V_{\mathbf{0}}$ of $\mathbf{0}$ in $\mathbb{R}^n$ with the following properties:

1. $H(\bar{\mathbf{x}}) = \mathbf{0}$.

2. If $\mathbf{x} \in U_{\bar{\mathbf{x}}}$ then $\forall t$ such that $\phi_t(\mathbf{x}) \in U_{\bar{\mathbf{x}}}$:

$$H \circ \phi_t(\mathbf{x}) = L_t \circ H(\mathbf{x}) \tag{1.5}$$

The conjugacy (1.5) shows that H maps trajectories of $\dot{\mathbf{x}} = \mathbf{F}(\mathbf{x})$ in $U_{\bar{\mathbf{x}}}$ to trajectories of $\dot{\mathbf{z}} = D\mathbf{F}(\bar{\mathbf{x}})\mathbf{z}$ in $V_{\mathbf{0}}$ in such a way as to preserve the parameterisation of trajectories with time. An important consequence of this is that the stability of $\bar{\mathbf{x}}$ as a fixed point of $\dot{\mathbf{x}} = \mathbf{F}(\mathbf{x})$ is determined by the stability of $\mathbf{0}$ as a fixed point of $\dot{\mathbf{z}} = D\mathbf{F}(\bar{\mathbf{x}})\mathbf{z}$: $\bar{\mathbf{x}}$ is stable if all the λ_ks have negative real part and unstable if any of the λ_ks have positive real part.

If $\mathbf{F}: W \to \mathbb{R}^n$ is C^k for some $1 \leq k \leq \infty$ and $\{\lambda_1, \dots, \lambda_n\}$ satisfy nonresonance conditions, the map H is not just a homeomorphism, but is a C^k diffeomorphism. The fixed point $\bar{\mathbf{x}}$ is then said to be C^k *linearisable*. $\{\lambda_1, \dots, \lambda_n\}$ are said to have a *resonance* of order j if there is some i with $1 \leq i \leq n$ and a vector $(\alpha_1, \dots, \alpha_n)^T \in \mathbb{Z}^n$ with $\sum_{m=1}^n \alpha_m = j$ and $\lambda_i = \sum_{m=1}^n \alpha_m \lambda_m$. An extended version of the Hartman-Grobman Theorem states that H is a C^1 diffeomorphism, provided that there is no reordering of $\{\lambda_1, \dots, \lambda_n\}$ for which $\lambda_1 = \lambda_2 + \lambda_3$ with $\mathrm{Re}\{\lambda_2\} < 0$ and $\mathrm{Re}\{\lambda_3\} > 0$. Sternberg's Theorem states that when $k \geq 2$, H is a C^k diffeomorphism with $DH(\bar{\mathbf{x}}) = \mathbf{1}_n$ if and only if $\{\lambda_1, \dots, \lambda_n\}$ have no resonances of order r with $2 \leq r \leq k$.

In the case where $k \geq 2$ and the eigenvalues of linearisation have no resonances of order 2, H is C^2 and so can be expanded as a Taylor series about $\bar{\mathbf{x}}$, giving:

$$H(\mathbf{x}) = \mathbf{x} - \bar{\mathbf{x}} + O\left(\|\mathbf{x} - \bar{\mathbf{x}}\|^2\right)$$

Using the above, it can be shown that given λ with $\lambda > \max_{1 \leq i \leq n} \mathrm{Re}\{\lambda_i\}$, there is a $\delta > 0$ with $B_\delta(\bar{\mathbf{x}}) \subset U_{\bar{\mathbf{x}}}$ and a constant $K > 0$ such that if $\mathbf{x} \in B_\delta(\bar{\mathbf{x}})$, then $\forall t \geq 0$ for which $\phi_t(\mathbf{x}) \in B_\delta(\bar{\mathbf{x}})$

$$\phi_t(\mathbf{x}) - \bar{\mathbf{x}} = L_t(\mathbf{x} - \bar{\mathbf{x}}) + \mathbf{S}(t) \tag{1.6}$$

where:

$$\|\mathbf{S}(t)\| \leq K e^{\lambda t} \delta^2 \tag{1.7}$$

If $\mathrm{Re}\{\lambda_i\} < 0 \; \forall\, 1 \leq i \leq n$ (so $\bar{\mathbf{x}}$ is a stable fixed point of $\dot{\mathbf{x}} = \mathbf{F}(\mathbf{x})$), it can be shown that given λ with $\max_{1 \leq i \leq n} \mathrm{Re}\{\lambda_i\} < \lambda < 0$, there is a $\delta > 0$ with $B_\delta(\bar{\mathbf{x}}) \subset U_{\bar{\mathbf{x}}}$, and a constant $K > 0$ such that if $\mathbf{x} \in B_\delta(\bar{\mathbf{x}})$, then $\phi_t(\mathbf{x}) \in U_{\bar{\mathbf{x}}} \; \forall t \geq 0$ with

$$\phi_t(\mathbf{x}) - \bar{\mathbf{x}} = L_t(\mathbf{x} - \bar{\mathbf{x}}) + \mathbf{S}(t) \tag{1.8}$$

where:

$$\|\mathbf{S}(t)\| \leq K e^{\lambda t} \|\mathbf{x} - \bar{\mathbf{x}}\|^2 \tag{1.9}$$

Note that in this case, for a given $\mathbf{x}$ with $\|\mathbf{x} - \bar{\mathbf{x}}\| < \delta$, the difference $\mathbf{S}(t)$ between the solution $\{L_t(\mathbf{x} - \bar{\mathbf{x}}) : t \geq 0\}$ of the linearised dynamics and the shifted solution $\{\phi_t(\mathbf{x}) - \bar{\mathbf{x}} : t \geq 0\}$

of the nonlinear dynamics goes to $\mathbf{0}$ as $t \to \infty$.

1.2.4 Eventually compact systems

Assume that all solutions of $\dot{\mathbf{x}} = \mathbf{F}(\mathbf{x})$ can be extended infinitely far forward in time. i.e. $[0, \infty) \subset J(\mathbf{x})\ \forall \mathbf{x} \in W$. It follows that the time set is $\mathbb{R}$, and $\forall t \geq 0$ the t set is W. Also assume that there is some compact subset C of W such that solutions are eventually confined to C (i.e. $\forall \mathbf{x} \in W$, $\exists t'(\mathbf{x}) > 0$ such that $\phi_t(\mathbf{x}) \in C\ \forall t \geq t'(\mathbf{x})$). A system which satisfies these conditions will be referred to in the following as *eventually compact*. For such a system, given $\mathbf{x} \in W$, the ω-limit set $\omega(\mathbf{x})$ of $\mathbf{x}$ can be shown to have the following properties:

1. $\omega(\mathbf{x})$ is nonempty, compact and invariant.

2. $\omega(\mathbf{x}) \subseteq C$.

3. $\phi_t(\mathbf{x}) \to \omega(\mathbf{x})$ as $t \to \infty$.

The asymptotic behaviour of all solutions is therefore determined, in that as $t \to \infty$, every point in W converges to its ω-limit set, which is an invariant, compact subset of W lying in C. It is useful to partition W on the basis of the ω-limit sets. For each $\mathbf{x} \in W$, define the set $[\mathbf{x}] \subseteq W$ by:

$$[\mathbf{x}] = \{\mathbf{y} \in W : \omega(\mathbf{y}) = \omega(\mathbf{x})\} \tag{1.10}$$

It is possible to find an index set I and a set of points $\{\mathbf{x}_i : i \in I\}$ in W such that every point of W lies in one and only one $[\mathbf{x}_i]$. W can then be written as the disjoint union $\bigcup_{i \in I} [\mathbf{x}_i]$ and the ω-limit sets as the distinct collection $\{\omega(\mathbf{x}_i) : i \in I\}$. For each $i \in I$, all points in $[\mathbf{x}_i]$ converge to $\omega(\mathbf{x}_i)$ as $t \to \infty$. This scheme is illustrated schematically in figure (1-11).

Attractors of eventually compact systems

An ω-limit set $\mathcal{A} = \omega(\mathbf{x}_i)$ is defined to be an *attractor* of the eventually compact system $\dot{\mathbf{x}} = \mathbf{F}(\mathbf{x})$ if it has a dense orbit, and there is some open subset N of W with $\mathcal{A} \subset N$ such that N is positively invariant, and $\phi_t(N) \to \mathcal{A}$ as $t \to \infty$. With this definition,

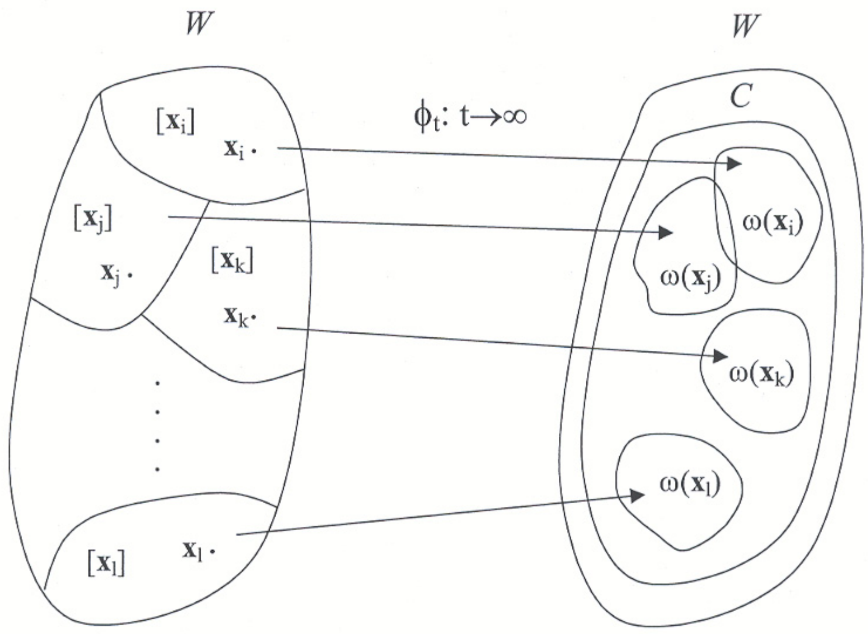

Figure 1-11: ω-limit sets of the eventually compact system $\dot{\mathbf{x}} = \mathbf{F}(\mathbf{x})$.

quasi-asymptotically stable fixed points and quasi-asymptotically stable limit cycles of $\dot{\mathbf{x}} = \mathbf{F}(\mathbf{x})$ are attractors. Also, assuming that no unstable fixed point of $\dot{\mathbf{x}} = \mathbf{F}(\mathbf{x})$ is quasi-asymptotically stable, unstable fixed points are not attractors. Similarly, assuming that no unstable limit cycle is quasi-asymptotically stable, unstable limit cycles are not attractors. If $\mathcal{A} = \omega(\mathbf{x}_i)$ is an attractor, its *basin of attraction* $\mathcal{B}(\mathcal{A})$, is defined by:

$$\mathcal{B}(\mathcal{A}) = \{\mathbf{y} \in W : \phi_t(\mathbf{y}) \to \mathcal{A} \text{ as } t \to \infty\} \tag{1.11}$$

Since every point of W converges to its ω-limit set, $[\mathbf{x}_i] \subseteq \mathcal{B}(\mathcal{A})$. It follows that $\mathcal{B}(\mathcal{A}) = [\mathbf{x}_i]$ if $\mathcal{A}$ is a quasi-asymptotically stable fixed point.

1.2.5 Symmetries of F

A diffeomorphism $\sigma : W \to W$ is called a *symmetry* of the vector field $\mathbf{F}$ if for all $\mathbf{x} \in W$, $J(\sigma(\mathbf{x})) = J(\mathbf{x})$ with $\phi_t(\sigma(\mathbf{x})) = \sigma(\phi_t(\mathbf{x}))\ \forall t \in J(\mathbf{x})$. σ therefore maps the trajectories of the system into each other, in that if $\mathbf{x}(t)$ is the unique solution of $\dot{\mathbf{x}} = \mathbf{F}(\mathbf{x})$ with $\mathbf{x}(0) = \mathbf{x}$, then $\mathbf{y}(t)$ defined by $\mathbf{y}(t) = \sigma\mathbf{x}(t)$ is the unique solution with $\mathbf{y}(0) = \sigma\mathbf{x}$. It can be shown that if σ is a symmetry of $\mathbf{F}$, then for each $k \in \mathbb{Z}$, σ^k is also a symmetry of

$\mathbf{F}$. i.e. for all $\mathbf{x} \in W$, $J\left(\sigma^k(\mathbf{x})\right) = J(\mathbf{x})$ with $\phi_t\left(\sigma^k(\mathbf{x})\right) = \sigma^k(\phi_t(\mathbf{x}))$ $\forall t \in J(\mathbf{x})$. Define the set G_σ by:

$$G_\sigma = \left\{\ldots, \sigma^{-2}, \sigma^{-1}, id, \sigma, \sigma^2 \ldots\right\}$$

(Here $id : W \to W$ is the identity map. Also given $r \geq 1$, σ^r is defined as the r-fold composition of σ, and similarly, σ^{-r} is defined as the r-fold composition of σ^{-1}). G_σ is a group under the group operation of composition, and will be referred to as the *symmetry group* generated by σ. For the case that $\sigma^p = id$ for some $p \geq 2$, G_σ is the finite group $G_\sigma = \left\{id, \sigma, \sigma^2 \ldots, \sigma^{p-1}\right\}$, which is isomorphic to $\mathbb{Z}_p$.

If solutions of $\dot{\mathbf{x}} = \mathbf{F}(\mathbf{x})$ can be extended infinitely far forward in time, it follows that $\forall \rho \in G_\sigma$:

$$\rho \circ \phi_t = \phi_t \circ \rho : t \geq 0$$

For each $\rho \in G_\sigma$, ρ therefore conjugates the time t map ϕ_t $\forall t \geq 0$. If solutions are also eventually confined to a compact set $C \subset W$ (so $\dot{\mathbf{x}} = \mathbf{F}(\mathbf{x})$ is eventually compact), then for each $\rho \in G_\sigma$ the ω-limit sets of the system can be shown to have the following properties:

1. $\forall i \in I$, $\rho(\omega(\mathbf{x}_i)) = \omega(\rho(\mathbf{x}_i))$ and $[\rho(\mathbf{x}_i)] = \rho([\mathbf{x}_i])$.

2. $\bar{\mathbf{x}}$ is a fixed point of $\dot{\mathbf{x}} = \mathbf{F}(\mathbf{x})$ iff $\rho(\bar{\mathbf{x}})$ is a fixed point. Additionally, $\bar{\mathbf{x}}$ is stable iff $\rho(\bar{\mathbf{x}})$ is stable and $\bar{\mathbf{x}}$ is unstable iff $\rho(\bar{\mathbf{x}})$ is unstable.

3. $\mathcal{S}$ is a limit cycle of $\dot{\mathbf{x}} = \mathbf{F}(\mathbf{x})$ of period T iff $\rho(\mathcal{S})$ is a limit cycle of period T. Additionally, $\mathcal{S}$ is stable iff $\rho(\mathcal{S})$ is stable, and $\mathcal{S}$ is unstable iff $\rho(\mathcal{S})$ is unstable.

4. $\mathcal{A} = \omega(\mathbf{x}_i)$ is an attractor of $\dot{\mathbf{x}} = \mathbf{F}(\mathbf{x})$ with basin of attraction $\mathcal{B}(\mathcal{A})$ iff $\rho(\mathcal{A}) = \omega(\rho(\mathbf{x}_i))$ is an attractor with basin of attraction $\rho(\mathcal{B}(\mathcal{A}))$.

5. The set $\digamma(\rho) \subseteq W$ defined by:

$$\digamma(\rho) = \{\mathbf{x} \in W : \rho(\mathbf{x}) = \mathbf{x}\}$$

is positively invariant.

Chapter 2

The saccadic system model

The construction of the nonlinear dynamics model proposed by Broomhead et al is described in this chapter. Following this, the analysis of the model presented in chapters 3-6 is outlined.

2.1 Local feedback hypotheses for saccade generation

Recall from section 1.1.2 that during a saccade, burst neurons discharge in response to a signal from the visual cortex which specifies the required eye location. Current knowledge of the firing characteristics of burst neurons is based on a comprehensive study conducted by Van Gisbergen et al [3]. Through single neuron recordings from alert monkeys, Van Gisbergen et al found that the rate of firing of burst neurons is a nonlinear, saturating function of the dynamic motor error, which is the difference between the required eye position and the current eye position. The existing control theory models of the saccadic system are based on one of two hypotheses regarding how the dynamic motor error signal is computed. In the **position feedback** hypotheses, the motor error ε, is assumed to be given by $\varepsilon = g^* - n$, where g^* is the desired gaze angle supplied by the visual cortex, and n is the output of the neural integrator (the step), which is taken to be an estimate of the current eye position [3], [7], [8]. In the **displacement feedback** hypotheses, the output of the burst neurons b (the pulse) is assumed to be integrated by a separate **resettable integrator** (**RI**) to obtain an estimate of current eye displacement s. The motor error is then obtained from $\varepsilon = \Delta g - s$, where Δg is the desired gaze displacement provided

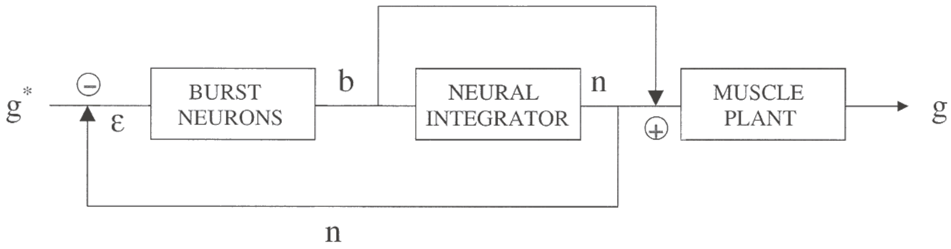

Figure 2-1: Position feedback hypotheses of saccadic generation. A copy of the step n, is fed back from the neural integrator to generate the motor error ε. The gaze angle is denoted by g.

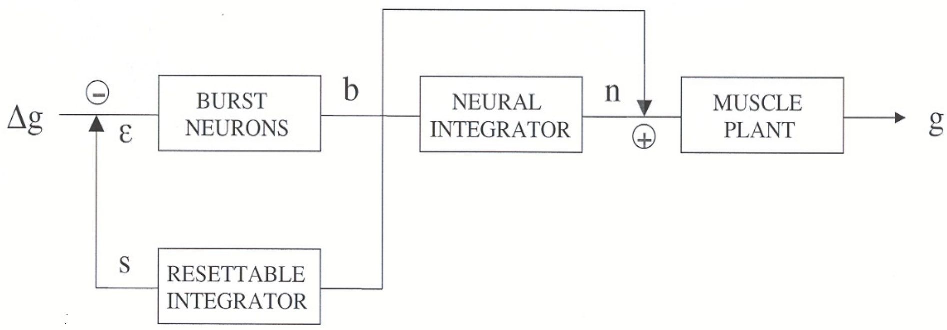

Figure 2-2: Displacement feedback hypotheses of saccadic generation. A copy of the pulse b, is integrated to obtain an estimate of current eye displacement s, which is fed back to generate the motor error ε. The gaze angle is denoted by g.

by the visual cortex. The epithet 'resettable' refers to the fact that in this scheme, s is required to be set to 0 at the beginning of each saccade [9], [10], [11]. In both schemes, ε is driven to 0, causing the gaze angle g to be bought to the required value. The position and displacement feedback hypotheses are illustrated in figures (2-1) and (2-2) respectively.

More recent models of the saccadic system have been based on the displacement feedback hypothesis, owing to neurophysiological studies of the superior colliculus, which have provided strong evidence for a neural correlate of Δg [9]. The model of Broomhead et al also assumes the displacement feedback hypothesis [14]. It does not, however, include the input from the omnipause neurons (cf. section 1.1.2). This is in contrast to the control models, which incorporate the contribution of the omnipause neurons. The derivation of the model equations will now be described.

2.2 Equations for the muscle plant and NI

In the control models of the saccadic system, the muscle plant is assumed to behave like a second order linear system with time constants T_1 and T_2 such that $T_2 \gg T_1$ [3], [7], [8]. This characterisation of the muscle plant is based on experimental measurements of eye dynamics during saccades, and leads to the following second order ODE for the gaze angle g

$$\ddot{g} + \left(\frac{1}{T_1} + \frac{1}{T_2}\right)\dot{g} + \frac{1}{T_1T_2}g = \frac{1}{T_1T_2}n + \left(\frac{1}{T_1} + \frac{1}{T_2}\right)b$$

where n and b are the driving signals from the neural integrator and bursters respectively. Writing v for the eye velocity $\dot{g}$, the above system can be expressed as the pair of coupled first order ODEs below:

$$\begin{aligned} \dot{g} &= v & (2.1)\\ \dot{v} &= -\left(\frac{1}{T_1} + \frac{1}{T_2}\right)v - \frac{1}{T_1T_2}g + \frac{1}{T_1T_2}n + \left(\frac{1}{T_1} + \frac{1}{T_2}\right)b & (2.2) \end{aligned}$$

Similarly, the neural integrator is modelled as a first-order linear system with time constant T_N such that $T_N \gg 0$ [3], [7], [8]. This characterisation leads to the equation:

$$\dot{n} = -\frac{1}{T_N}n + b \tag{2.3}$$

It should be noted that the neural integrator is not assumed to be a perfect integrator, but is 'leaky' (a perfect integrator would have a time constant of ∞). This reflects the experimental observation that following a saccade, there is a slow, exponential drift of the eye back towards its initial position [2], [5], [6]. Equations (2.1)-(2.3) will be collectively referred to as the **plant equations.**

2.3 Equations for the burst neurons and RI

In order to understand the reasoning behind the derivation of the equations corresponding to the burst neurons and resettable integrator, it is necessary to first describe the properties of the burst neurons in slightly more detail. The material presented here relating to burst neuron characteristics is based on the results of Van Gisbergen et al [3].

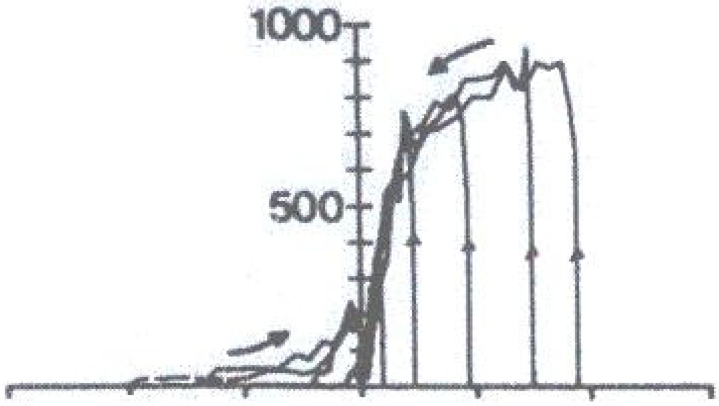

Figure 2-3: Trajectories in the firing rate against motor error phase plane obtained from recordings of a right burst neuron during saccades of different amplitudes. The vertical axis denotes firing rate in spikes/sec while the horizontal axis denotes motor error in steps of 10 degrees. (Reproduced from figure 7 of [3]).

Individual burst neurons are divided into those that fire maximally for rightward saccades and those that fire maximally for leftward saccades. The direction of eye movement for which a burster fires maximally is referred to as its 'on' direction and the opposite direction is referred to as its 'off' direction. The net burst signal b is then given by $r - l$, where r is the output of the right burst neurons and l is the output of the left burst neurons. Van Gisbergen et al investigated the responses of individual right and left burst neurons by recording their firing rates during saccades made over a range of amplitudes, and plotting the corresponding trajectories in the firing rate against motor error phase plane. It was found that the trajectories contracted quickly to a unique curve in the phase plane before converging slowly to the origin (cf. figure (2-3). By flipping the response curves from left burst neurons about the firing rate axis, and then averaging over all response curves, Van Gisbergen et al were able to obtain a single curve describing the mean response of all neurons (cf. figure (2-4)). In the on direction, this mean burster response curve was observed to have the form of an increasing exponential function that saturates at large motor errors. In the off direction, the curve was found to be approximately zero except for a small maximum close to zero error (cf. figure (2-4)). The off response is believed to correspond to a **braking saccade**; this is a small tug at the end of the saccade in the direction opposite to that of the eye movement. The braking saccade helps prevent the inertia of the eye causing overshoot of the target. Van Gisbergen et al also proposed that

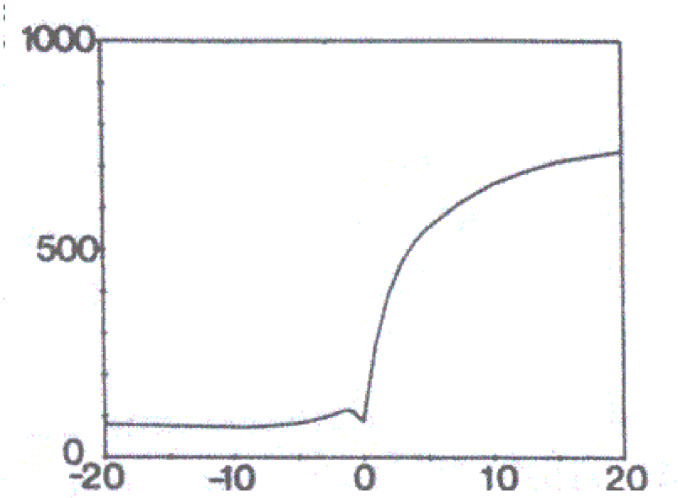

Figure 2-4: Mean burst neuron response curve obtained by Van Gisbergen et al. The vertical axis denotes firing rate in spikes/sec while the horizontal axis denotes motor error in degrees. (Reproduced from figure 7 of [3]).

the left and right bursters exhibit **mutual inhibition;** that is the firing of the left bursters inhibits that of the right bursters and vice versa.

The control models of the saccadic system that have been referred to here ignore both the off response and the effect of mutual inhibition [3], [7], [8]. In these models, the mean right and left burster responses are represented by the functions $F_C(\varepsilon)$ and $F_C(-\varepsilon)$ respectively where:

$$F_C(\varepsilon) = \begin{cases} \alpha'\left(1 - e^{-\varepsilon/\beta'}\right) & \text{if} \quad \varepsilon \geq 0 \\ 0 & \text{if} \quad \varepsilon < 0 \end{cases}$$

Here α' and β' are positive parameters [3], [7], [8]. As $\varepsilon \to \infty$, $F_C(\varepsilon) \to \alpha'$. α' therefore determines the magnitude of the saturated on response. Also, $F_C(\beta') = \alpha'(1 - e^{-1})$, and hence β' determines how quickly the saturation occurs as ε is increased. The following pair of ODEs are a model of the burst neurons and resettable integrator based on the assumptions of the control models:

$$\begin{aligned} \dot{b} &= \frac{1}{\epsilon}\left(-b + H_C(\varepsilon)\right) \\ \dot{s} &= b \end{aligned}$$

In the above, ϵ is a small positive parameter, and $H_C(\varepsilon)$ is given by:

$$H_C(\varepsilon) = F_C(\varepsilon) - F_C(-\varepsilon) = \alpha' \operatorname{sign}(\varepsilon)\left(1 - e^{-|\varepsilon|/\beta'}\right)$$

Note that the resettable integrator is assumed to be a perfect integrator. Using $\varepsilon = \Delta g - s$, the ODEs can be written in terms of ε and b only as:

$$\dot{b} = \frac{1}{\epsilon}\left(-b + H_C(\varepsilon)\right) \tag{2.4}$$

$$\dot{\varepsilon} = -b \tag{2.5}$$

Equations (2.4)-(2.5) are an example of a so-called **slow-fast** system [4], [27], [29], [30]. Slow-fast systems have the general form

$$\begin{aligned} \dot{\mathbf{x}} &= \frac{1}{\epsilon}\mathbf{f}(\mathbf{x}, \mathbf{y}) \\ \dot{\mathbf{y}} &= \mathbf{g}(\mathbf{x}, \mathbf{y}) \end{aligned}$$

or

$$\begin{aligned} \dot{\mathbf{x}} &= \mathbf{f}(\mathbf{x}, \mathbf{y}) \\ \dot{\mathbf{y}} &= \epsilon\mathbf{g}(\mathbf{x}, \mathbf{y}) \end{aligned}$$

where $\mathbf{x} \in \mathbb{R}^m$, $\mathbf{y} \in \mathbb{R}^n$, $\mathbf{f} : \mathbb{R}^{m+n} \to \mathbb{R}^m$, $\mathbf{g} : \mathbb{R}^{m+n} \to \mathbb{R}^n$ and $\epsilon > 0$ is small. Such systems are common when modelling physical behaviour with 2 time scales, such as heart and nerve cell dynamics [29]. There is a standard way to deduce the behaviour of slow-fast systems. Since ϵ is assumed to be small, $|\dot{\mathbf{x}}| \gg |\dot{\mathbf{y}}|$ except in the neighbourhood of the solution set of $\mathbf{f}(\mathbf{x}, \mathbf{y}) = \mathbf{0}$. This set is referred to as the **slow manifold** (SM)**.** Assuming that the slow manifold is attracting, trajectories contract rapidly onto it with $\mathbf{y}(t) \approx \mathbf{y}(0)$. On the SM, the motion is governed by the equation for $\mathbf{y}$. As ϵ is decreased, trajectories contract onto the SM more quickly and follow it more closely [4], [27], [29], [30]. In the case of equations (2.4)-(2.5), the slow manifold is the b nullcline, $b = H_C(\varepsilon)$. Trajectories outside the neighbourhood of $b = H_C(\varepsilon)$ will therefore contract rapidly onto it, parallel to the b axis. On $b = H_C(\varepsilon)$, the motion is governed by the equation for $\dot{\varepsilon}$. As $\operatorname{sign}(H_C(\varepsilon)) = \operatorname{sign}(\varepsilon)$, it follows that trajectories on the SM will move along it to the stable fixed point at the origin $(0, 0)^T$. The origin is thus the unique attractor of the system, with basin of attraction $\mathbb{R}^2$. Figure (2-5) is a plot of several trajectories generated by (2.4)-

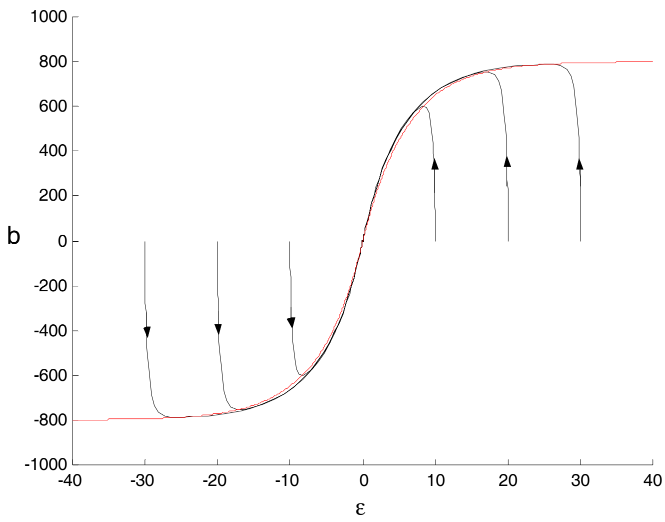

Figure 2-5: Plot of trajectories of (2.4)-(2.5) generated by the initial condition $(0, \Delta g)^T$ for $\Delta g = -30, -20, -10, 0, 10, 20$ and 30 when $\alpha' = 800$, $\beta' = 6$ and $\epsilon = 0.001$ (black lines). The slow manifold $b = H_C(\varepsilon)$ is indicated by the red line.

(2.5) for initial conditions of the form $(0, \Delta g)^T$ when $\alpha' = 800$, $\beta' = 6$ and $\epsilon = 0.001$. Such trajectories correspond to saccades of Δg degrees. The slow manifold $b = H_C(\varepsilon)$ is also shown. The behaviour of the trajectories is seen to be as predicted in the discussion above. Comparing figure (2-5) to figure (2-3) indicates that the model has captured the basic properties of trajectories in the firing rate against motor error phase plane observed by Van Gisbergen et al: namely that the trajectories undergo fast contraction onto a unique curve followed by a slower convergence to the origin. The parameter ϵ can be thought of as a measure of how quickly bursters respond to the motor error signal, with the response time decreasing as ϵ is decreased.

A more physiologically realistic model of the bursters needs to include the off response and mutual inhibition neglected by the control models. One approach to incorporating the off response is to represent the mean right and left burster responses by the functions $F(\varepsilon)$ and $F(-\varepsilon)$ respectively, where:

$$F(\varepsilon) = \begin{cases} \alpha'\left(1 - e^{-\varepsilon/\beta'}\right) & \text{if} \quad \varepsilon \geq 0 \\ -\frac{\alpha}{\beta}\varepsilon e^{\varepsilon/\beta} & \text{if} \quad \varepsilon < 0 \end{cases} \tag{2.6}$$

Here α', β', α and β are all positive parameters. $F(\varepsilon)$ preserves the form of the on response used by the control models and also accounts for the off response through the function

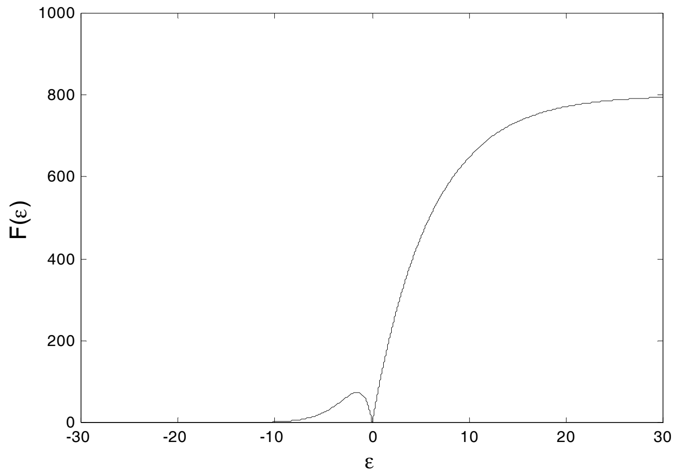

Figure 2-6: Plot of the burster response function $F(\varepsilon)$ defined in (2.6) for $\alpha' = 800$, $\beta' = 6$, $\alpha = 200$, $\beta = 1.5$.

$-\frac{\alpha}{\beta}\varepsilon e^{\varepsilon/\beta}$. For $\varepsilon \leq 0$, $F(\varepsilon)$ is a nonnegative function of ε with a global maximum at $(-\beta, \frac{\alpha}{e})$, such that $F(\varepsilon) \to 0$ as $\varepsilon \to -\infty$. α therefore determines the magnitude of the off response, while β determines the range over which this response is effective. Note that F is continuous on $\mathbb{R}$. Figure (2-6) is a plot of the burster response function $F(\varepsilon)$ for the parameter values $\alpha' = 800$, $\beta' = 6$, $\alpha = 200$, $\beta = 1.5$ (cf. figure (2-4)). The following set of ODEs for the burst neurons and resettable integrator has a similar structure to the model (2.4)-(2.5), but incorporates both the off response and mutual inhibition:

$$\dot{r} = \frac{1}{\epsilon}\left(-r - \gamma r l^2 + F(\varepsilon)\right) \tag{2.7}$$

$$\dot{l} = \frac{1}{\epsilon}\left(-l - \gamma l r^2 + F(-\varepsilon)\right) \tag{2.8}$$

$$\dot{\varepsilon} = -(r - l) \tag{2.9}$$

Again, ϵ is a small positive parameter determining the response time of the bursters. $\gamma \geq 0$ is a parameter which represents the strength of the mutual inhibition. The functional form of each mutual inhibition term has been taken to be quadratic in the activity of the inhibiting neuron. This turns out to be the simplest polynomial term that gives a system which cannot be reduced to one that depends only on b and ε [17]. Equations (2.7)-(2.9) will be collectively referred to as the **burster equations.** In contrast to (2.4)-(2.5), the burster equations consider the right and left bursters separately, and therefore comprise a bilateral model of burst neuron dynamics.

2.4 The bilateral saccadic model

Combining the plant equations (2.1)-(2.3) with the burster equations (2.7)-(2.9) and using $b = r - l$ leads to the bilateral model of the saccadic system proposed by Broomhead et al [14]:

$$\begin{aligned}
\dot{g} &= v && (2.10)\\
\dot{v} &= -\left(\frac{1}{T_1}+\frac{1}{T_2}\right)v - \frac{1}{T_1T_2}g + \frac{1}{T_1T_2}n + \left(\frac{1}{T_1}+\frac{1}{T_2}\right)(r-l) && (2.11)\\
\dot{n} &= -\frac{1}{T_N}n + r - l && (2.12)\\
\dot{r} &= \frac{1}{\epsilon}\left(-r - \gamma r l^2 + F(\varepsilon)\right) && (2.13)\\
\dot{l} &= \frac{1}{\epsilon}\left(-l - \gamma l r^2 + F(-\varepsilon)\right) && (2.14)\\
\dot{\varepsilon} &= -(r-l) && (2.15)
\end{aligned}$$

This set of 6 coupled ODEs will be referred to as the **saccadic equations.** The time constants of the plant and neural integrator are set to the values used in the control model proposed by Optican et al [7]. These are $T_1 = 0.15$, $T_2 = 0.012$ and $T_N = 25$. γ is fixed at 0.05. The parameters α' and β' are fixed at $\alpha' = 600$ and $\beta' = 9$, on the basis that saccades modelled using these values have durations and peak velocities which follow the main sequence for nystagmats (cf. section 1.1.2) [14]. The parameters of the model are therefore α, β and ϵ, representing the off response magnitude, off response range and burst neuron response time respectively. These can be combined to give the parameter vector $\boldsymbol{\alpha} = (\alpha, \beta, \epsilon)^T$. By assumption, $\boldsymbol{\alpha} \in \Pi$ where:

$$\Pi = \left\{(\alpha, \beta, \epsilon)^T : \alpha, \beta, \epsilon > 0\right\} \tag{2.16}$$

Solutions of the saccadic equations with initial condition $(0, 0, 0, 0, 0, \Delta g)^T$ simulate saccades to the gaze angle Δg from an initial angle of 0. Such solutions will be referred to from now on as **saccade-modelling solutions**. The ultimate objects of interest in the following work are the gaze time series $\{g(t) : t \geq 0\}$ of saccade modelling solutions obtained for $\boldsymbol{\alpha}$ in the subset Π_P of Π defined below:

$$\Pi_P = \left\{(\alpha, \beta, \epsilon)^T : 0 < \alpha < \alpha', 1.5 < \beta < 6, 0 < \epsilon < 0.05\right\} \tag{2.17}$$

Broomhead et al found that for many choices of $\boldsymbol{\alpha}$ in Π_P, the saccade modelling-solutions gave biologically realistic gaze time series [14] . Π_P will henceforth be referred to as the **physiological parameter range**.

2.5 Outline of the model analysis

By setting $\mathbf{x} = (g, v, n)^T$ and $\mathbf{y} = (r, l, \varepsilon)^T$, the saccadic equations can be written in the form

$$\begin{aligned} \dot{\mathbf{x}} &= A\mathbf{x} + B\mathbf{y} && (2.18) \\ \dot{\mathbf{y}} &= \mathbf{Y}(\mathbf{y}) && (2.19) \end{aligned}$$

where

$$A = \begin{pmatrix} 0 & 1 & 0 \\ -P_2 & -P_1 & P_2 \\ 0 & 0 & -\frac{1}{T_N} \end{pmatrix} \tag{2.20}$$

$$B = \begin{pmatrix} 0 & 0 & 0 \\ P_1 & -P_1 & 0 \\ 1 & -1 & 0 \end{pmatrix} \tag{2.21}$$

with

$$\begin{aligned} P_1 &= \frac{1}{T_1} + \frac{1}{T_2} && (2.22) \\ P_2 &= \frac{1}{T_1 T_2} && (2.23) \end{aligned}$$

and:

$$\mathbf{Y}(r, l, \varepsilon) = \begin{pmatrix} \frac{1}{\epsilon}\left(-r - \gamma r l^2 + F(\varepsilon)\right) \\ \frac{1}{\epsilon}\left(-l - \gamma l r^2 + F(-\varepsilon)\right) \\ -(r - l) \end{pmatrix} \tag{2.24}$$

By setting $\mathbf{z} = (\mathbf{x}, \mathbf{y})^T = (g, v, n, r, l, \varepsilon)^T$, the saccadic equations can also be written as

$$\dot{\mathbf{z}} = \mathbf{Z}(\mathbf{z}) \tag{2.25}$$

where:

$$\mathbf{Z}(\mathbf{z}) = \begin{pmatrix} A\mathbf{x}+B\mathbf{y} \\ \mathbf{Y}(\mathbf{y}) \end{pmatrix} \tag{2.26}$$

The plant equations (2.18) are seen to be a linear set of equations which are forced by the output $\mathbf{y}(t)$ of the autonomous burster equations (2.19). The saccadic equations are therefore a skew-product [31]. This fact simplifies their analysis, as it enables many important properties to be inferred from the burster equations. In particular, the skew-product structure implies that there is a one-to-one correspondence between the attractors of the burster and saccadic equations, when the attractors are stable fixed points or stable limit cycles.

Chapters 3 and 4 are an analysis of the burster equations. This analysis culminates in a proposed classification of the attractors of the burster equations in an $\boldsymbol{\alpha}$ range $\hat{\Pi}_P$ containing Π_P, in which the attractors are argued to be stable fixed points or stable limit cycles. The classification includes a description of the morphology of the error time series associated with limit cycle attractors. Chapter 5 is an analysis of the saccadic equations modelled on that of the burster equations. It finishes with a classification of the attractors of the saccadic equations for $\boldsymbol{\alpha}$ in $\hat{\Pi}_P$. This classification includes a description of the morphology of the gaze time series associated with limit cycle attractors. In chapter 6, the work of the preceding chapters is used to obtain a classification of the gaze angle times series associated with saccade-modelling solutions that simulate biologically realistic eye movements for $\boldsymbol{\alpha}$ in Π_P.

2.6 The rescaled burster equations

In analysing the burster equations, it is useful to rescale time by $\tau = \frac{t}{\epsilon}$. Doing so introduces the related system of equations

$$\frac{d\mathbf{y}}{d\tau} = \mathbf{X}(\mathbf{y}) \tag{2.27}$$

where the vector field $\mathbf{X} : \mathbb{R}^3 \to \mathbb{R}^3$ is defined by:

$$\mathbf{X}(\mathbf{y}) = \epsilon \mathbf{Y}(\mathbf{y}) \tag{2.28}$$

Given $\mathbf{v}_0 \in \mathbb{R}^3$, if $\mathbf{v}(\tau)$ solves $\frac{d\mathbf{y}}{d\tau} = \mathbf{X}(\mathbf{y})$ on the open interval (a,b) with $\mathbf{v}(0) = \mathbf{v}_0$, then $\mathbf{w}(t)$ defined by $\mathbf{w}(t) = \mathbf{v}\left(\frac{t}{\epsilon}\right)$ $\forall t \in (\epsilon a, \epsilon b)$ solves $\dot{\mathbf{y}} = \mathbf{Y}(\mathbf{y})$ on $(\epsilon a, \epsilon b)$ with $\mathbf{w}(0) = \mathbf{v}_0$. Conversely, if $\mathbf{w}(t)$ solves $\dot{\mathbf{y}} = \mathbf{Y}(\mathbf{y})$ on (a,b) with $\mathbf{w}(0) = \mathbf{v}_0$, then $\mathbf{v}(\tau)$ defined by $\mathbf{v}(\tau) = \mathbf{w}(\epsilon\tau)$ $\forall \tau \in \left(\frac{a}{\epsilon}, \frac{b}{\epsilon}\right)$ solves $\frac{d\mathbf{y}}{d\tau} = \mathbf{X}(\mathbf{y})$ on $\left(\frac{a}{\epsilon}, \frac{b}{\epsilon}\right)$ with $\mathbf{v}(0) = \mathbf{v}_0$. The dynamics of $\dot{\mathbf{y}} = \mathbf{Y}(\mathbf{y})$ and $\frac{d\mathbf{y}}{d\tau} = \mathbf{X}(\mathbf{y})$ are therefore equivalent, up to the rescaling of time $t \to \tau$. Both systems will be referred to in the following work as the burster equations. Also, $\frac{d\mathbf{y}}{d\tau}$ will be written as $\dot{\mathbf{y}}$, unless the two different time scales are being explicitly considered.

Chapter 3

Analysis of the burster equations I: Fixed points

This chapter and the following chapter comprise an analysis of the (rescaled) burster equations $\dot{\mathbf{y}} = \mathbf{X}(\mathbf{y})$. In this chapter, basic properties of the equations are discussed such as the existence/uniqueness of solutions and the existence of attractors. The chapter finishes with a full classification of the fixed points of the equations in the (β, α) plane. Included in this classification are curves on which bifurcations of the equations are believed to occur.

3.1 Vector field

Equations (2.24) and (2.28) imply that the vector field $\mathbf{X} : \mathbb{R}^3 \to \mathbb{R}^3$ is as below:

$$\mathbf{X}(r, l, \varepsilon) = \begin{pmatrix} -r - \gamma r l^2 + F(\varepsilon) \\ -l - \gamma l r^2 + F(-\varepsilon) \\ -\epsilon(r - l) \end{pmatrix} \tag{3.1}$$

The (rescaled) burster equations $\dot{\mathbf{y}} = \mathbf{X}(\mathbf{y})$ are therefore given explicitly by:

$$\dot{r} = -r - \gamma r l^2 + F(\varepsilon) \tag{3.2}$$

$$\dot{l} = -l - \gamma l r^2 + F(-\varepsilon) \tag{3.3}$$

$$\dot{\varepsilon} = -\epsilon(r - l) \tag{3.4}$$

As F is continuous on $\mathbb{R}$, $\mathbf{X}$ is continuous on $\mathbb{R}^3$. Also since $F(0) = 0$ for all parameter values, the origin $\mathbf{0} = (0,0,0)^T$ is always a fixed point of the burster system.

3.1.1 Smoothness of the vector field

The existence/uniqueness and smoothness properties of solutions of $\dot{\mathbf{y}} = \mathbf{X}(\mathbf{y})$ are determined by the smoothness properties of the vector field $\mathbf{X}$ (cf. section 1.2). The latter is addressed in this section.

In order to examine the smoothness of F, it is useful to introduce the functions $f, h : \mathbb{R} \to \mathbb{R}$ defined $\forall \varepsilon \in \mathbb{R}$ by

$$f(\varepsilon) = \alpha' \left(1 - e^{-\varepsilon/\beta'}\right) \tag{3.5}$$

and:

$$h(\varepsilon) = -\frac{\alpha}{\beta} \varepsilon e^{\varepsilon/\beta} \tag{3.6}$$

It follows from (2.6) that F can be written as:

$$F(\varepsilon) = \begin{cases} f(\varepsilon) & \text{if} \quad \varepsilon \geq 0 \\ h(\varepsilon) & \text{if} \quad \varepsilon < 0 \end{cases} \tag{3.7}$$

The vector field $\mathbf{X}$ can then be expressed as a piecewise function involving f and h in the following way:

$$\mathbf{X}(r, l, \varepsilon) = \begin{cases} \begin{pmatrix} -r - \gamma r l^2 + f(\varepsilon) \\ -l - \gamma l r^2 + h(-\varepsilon) \\ -\epsilon(r - l) \end{pmatrix} & \text{for} \quad \varepsilon \geq 0 \\ \begin{pmatrix} -r - \gamma r l^2 + h(\varepsilon) \\ -l - \gamma l r^2 + f(-\varepsilon) \\ -\epsilon(r - l) \end{pmatrix} & \text{for} \quad \varepsilon < 0 \end{cases} \tag{3.8}$$

f and h are both C^∞ on $\mathbb{R}$ with kth derivatives $D^k f$ and $D^k h$ given by

$$D^k f(\varepsilon) = \frac{(-1)^{k-1} \alpha'}{(\beta')^k} e^{-\varepsilon/\beta'} \tag{3.9}$$

and:

$$D^k h(\varepsilon) = -\frac{\alpha}{\beta^k}\left(k + \frac{1}{\beta}\varepsilon\right) e^{\varepsilon/\beta} \tag{3.10}$$

As f and h are C^∞ on $\mathbb{R}$, $\mathbf{X}$ is C^∞ on $\mathbb{R}\backslash P$, where P is defined to be the plane:

$$P = \left\{(r, l, \varepsilon)^T \in \mathbb{R}^3 : r, l \in \mathbb{R}, \varepsilon = 0\right\} \tag{3.11}$$

$\mathbf{X}$ is, however, not differentiable at P as F is not differentiable at 0. To see this, note that F is right differentiable at 0 with right derivative $\Lambda_+ = Df(0)$ and left differentiable at 0 with left derivative $\Lambda_- = Dh(0)$. Explicitly:

$$\Lambda_+ = \frac{\alpha'}{\beta'} \tag{3.12}$$

$$\Lambda_- = -\frac{\alpha}{\beta} \tag{3.13}$$

It follows that $\Lambda_+ > 0$ and $\Lambda_- < 0$. Hence, $\Lambda_+ \neq \Lambda_-$, and so F is not differentiable at 0. $\mathbf{X}$ is therefore not smooth at P, and so is a piecewise C^∞ function about P. Note that when Λ_+ and Λ_- are considered as functions of the system parameters, $\Lambda_- = \Lambda_-(\alpha, \beta)$ and Λ_+ is a constant (the exact value of Λ_+ is $\frac{200}{3}$).

Smoothness of the vector field as a function of $\mathbf{y}$ and $\boldsymbol{\alpha}$

It will be useful when examining the bifurcations of $\dot{\mathbf{y}} = \mathbf{X}(\mathbf{y})$ to consider $\mathbf{X}$ as a function of both the space variable $\mathbf{y}$ and the parameter variable $\boldsymbol{\alpha}$, $\mathbf{X} : \mathbb{R}^3 \times \Pi \to \mathbb{R}^3$. Noting that the α and β dependence of $\mathbf{X}$ comes from the α and β dependence of F, and hence from the α and β dependence of h, $\mathbf{X}(\mathbf{y}; \boldsymbol{\alpha})$ can be written as

$$\mathbf{X}(r, l, \varepsilon; \alpha, \beta, \epsilon) = \begin{cases} \begin{pmatrix} -r - \gamma r l^2 + f(\varepsilon) \\ -l - \gamma l r^2 + h(-\varepsilon; \alpha, \beta) \\ -\epsilon(r - l) \end{pmatrix} & \text{for} \quad \varepsilon \geq 0 \\ \begin{pmatrix} -r - \gamma r l^2 + h(\varepsilon; \alpha, \beta) \\ -l - \gamma l r^2 + f(-\varepsilon) \\ -\epsilon(r - l) \end{pmatrix} & \text{for} \quad \varepsilon < 0 \end{cases}$$

where $h : \mathbb{R} \times (0, \infty) \times (0, \infty) \to \mathbb{R}$ is defined in (3.6) above. It can be seen from equation (3.6) that $h(\varepsilon; \alpha, \beta)$ is C^∞ on $\mathbb{R} \times (0, \infty) \times (0, \infty)$. It follows that as a function of both $\mathbf{y}$

and $\boldsymbol{\alpha}$, $\mathbf{X}$ is C^{∞} on $\left(\mathbb{R}^3 \backslash P\right) \times \Pi$.

3.1.2 Existence and uniqueness of solutions of the burster system

It can be shown that the vector field $\mathbf{X}$ of the burster system is locally Lipschitz on $\mathbb{R}^3$. Solutions of $\dot{\mathbf{y}} = \mathbf{X}(\mathbf{y})$ therefore exist and are unique (cf. section 1.2.1). Additionally, it is possible to show that all solutions of $\dot{\mathbf{y}} = \mathbf{X}(\mathbf{y})$ can be extended infinitely far forward in time: i.e. for each $\mathbf{y} \in \mathbb{R}^3$, $[0, \infty) \subset J(\mathbf{y})$, where $J(\mathbf{y})$ is the maximal open interval on which the unique solution $\mathbf{y}(\tau)$ with $\mathbf{y}(0) = \mathbf{y}$ exists. Proofs of these claims are given in sections A.1.1 and A.1.2. It follows from these results that the time set of $\dot{\mathbf{y}} = \mathbf{X}(\mathbf{y})$ is $\mathbb{R}$, and that the τ set is $\mathbb{R}^3$ $\forall \tau \geq 0$. In addition, the flow ϕ is continuous, and $\forall \tau \geq 0$, the time τ map $\phi_\tau : \mathbb{R}^3 \to \phi_\tau\left(\mathbb{R}^3\right)$ is a homeomorphism with $\phi_\tau^{-1} = \phi_{-\tau}$.Moreover, for $\mathbf{y} \in \mathbb{R}^3$ and $\tau_1, \tau_2 \in \mathbb{R}$ such that $\phi_{\tau_2}(\mathbf{y}), \phi_{\tau_1}\left(\phi_{\tau_2}(\mathbf{y})\right)$ and $\phi_{\tau_1+\tau_2}(\mathbf{y})$ all exist $\phi_{\tau_1}\left(\phi_{\tau_2}(\mathbf{y})\right) = \phi_{\tau_1+\tau_2}(\mathbf{y})$. In particular, given $\mathbf{y} \in \mathbb{R}^3$, $\phi_{\tau_1}\left(\phi_{\tau_2}(\mathbf{y})\right) = \phi_{\tau_1+\tau_2}(\mathbf{y})$ $\forall \tau_1, \tau_2 \geq 0$. Finally, if $\mathbf{y}(\tau)$ is a solution of $\dot{\mathbf{y}} = \mathbf{X}(\mathbf{y})$, $\mathbf{y}(\tau)$ is C^1 on $J(\mathbf{y}(0))$.

3.1.3 C^{∞} extensions of the vector field

Define $N_+, N_- \subset \mathbb{R}^3$ by:

$$\begin{aligned} N_+ &= \left\{(r, l, \varepsilon)^T : r, l \in \mathbb{R}, \varepsilon \geq 0\right\} && (3.14) \\ N_- &= \left\{(r, l, \varepsilon)^T : r, l \in \mathbb{R}, \varepsilon \leq 0\right\} && (3.15) \end{aligned}$$

Then $\mathbb{R}^3 = N_+ \cup N_-$ and $N_+ \cap N_- = P$. It will be useful in the analysis of the burster system to extend $\mathbf{X}|_{N_+}$ out into N_- and $\mathbf{X}|_{N_-}$ out into N_+ so as to generate two C^{∞} vector fields $\mathbf{X}_+$ and $\mathbf{X}_-$ which agree with $\mathbf{X}$ in N_+ and N_- respectively. This can be done in a natural way by using the C^{∞} maps f and h. Define the maps $\mathbf{X}_+, \mathbf{X}_- : \mathbb{R}^3 \to \mathbb{R}^3$ as follows:

$$\mathbf{X}_+(r, l, \varepsilon) = \begin{pmatrix} -r - \gamma r l^2 + f(\varepsilon) \\ -l - \gamma l r^2 + h(-\varepsilon) \\ -\epsilon(r - l) \end{pmatrix} \tag{3.16}$$

$$\mathbf{X}_{-}(r,l,\varepsilon) = \begin{pmatrix} -r-\gamma r l^2 + h(\varepsilon) \\ -l-\gamma l r^2 + f(-\varepsilon) \\ -\epsilon(r-l) \end{pmatrix} \tag{3.17}$$

Then since f and h are both C^∞ on $\mathbb{R}$ it follows that $\mathbf{X}_+$ and $\mathbf{X}_-$ are C^∞ on $\mathbb{R}^3$. Moreover, equations (3.8), (3.16) and (3.17) imply that $\mathbf{X}_+|_{N_+} = \mathbf{X}|_{N_+}$ and $\mathbf{X}_-|_{N_-} = \mathbf{X}|_{N_-}$.

Smoothness of the extended vector fields as functions of y and $\boldsymbol{\alpha}$

When discussing bifurcations of $\dot{\mathbf{y}} = \mathbf{X}(\mathbf{y})$ in chapter 4, it will be necessary to discuss the bifurcations of the systems $\dot{\mathbf{y}} = \mathbf{X}_+(\mathbf{y})$ and $\dot{\mathbf{y}} = \mathbf{X}_-(\mathbf{y})$ associated with the extended vector fields $\mathbf{X}_+$ and $\mathbf{X}_-$. Consequently, $\mathbf{X}_\pm$ will be considered as a function of both the space variable $\mathbf{y}$ and the parameter variable $\boldsymbol{\alpha}$, $\mathbf{X}_\pm : \mathbb{R}^3 \times \Pi \to \mathbb{R}^3$. Recall from section 3.1.1 that when considered as functions of both ε and the parameters α and β, h is C^∞ on $\mathbb{R}\times(0,\infty)\times(0,\infty)$. If follows easily that $\mathbf{X}_\pm(\mathbf{y};\boldsymbol{\alpha})$ is a C^∞ function of $\mathbf{y}$ and $\boldsymbol{\alpha}$ on $\mathbb{R}^3\times\Pi$.

3.1.4 Existence and uniqueness of solutions of the extended systems

Since $\mathbf{X}_\pm$ is C^∞, it is Lipshitz, and so solutions of the extended systems $\dot{\mathbf{y}} = \mathbf{X}_+(\mathbf{y})$ and $\dot{\mathbf{y}} = \mathbf{X}_-(\mathbf{y})$ exist and are unique (cf. section 1.2.1). Given $\mathbf{y}\in\mathbb{R}^3$, denote the maximal open interval on which the unique solution $\mathbf{y}_\pm(\tau)$ of $\dot{\mathbf{y}} = \mathbf{X}_\pm(\mathbf{y})$ with $\mathbf{y}_\pm(0) = \mathbf{y}$ exists by $J_\pm(\mathbf{y})$. Additionally, denote the flow of $\dot{\mathbf{y}} = \mathbf{X}_\pm(\mathbf{y})$ by $\phi^\pm$, the time set by $T_\pm$ and the τ set by $U^\pm_\tau$ for $\tau\in T_\pm$. The following facts about the extended system $\dot{\mathbf{y}} = \mathbf{X}_\pm(\mathbf{y})$ can then be easily deduced.

1. $\phi^\pm$ is C^∞.

2. $\forall\tau\in T_\pm$, the map $\phi^\pm_\tau : U^\pm_\tau \to U^\pm_{-\tau}$ is a C^∞ diffeomorphism with $\left(\phi^\pm_\tau\right)^{-1} = \phi^\pm_{-\tau}$.

3. For $\mathbf{y}\in\mathbb{R}^3$ and $\tau_1,\tau_2\in\mathbb{R}$ such that $\phi^\pm_{\tau_2}(\mathbf{y}), \phi^\pm_{\tau_1}\left(\phi^\pm_{\tau_2}(\mathbf{y})\right)$ and $\phi^\pm_{\tau_1+\tau_2}(\mathbf{y})$ all exist, $\phi^\pm_{\tau_1}\left(\phi^\pm_{\tau_2}(\mathbf{y})\right) = \phi^\pm_{\tau_1+\tau_2}(\mathbf{y})$.

4. If $\mathbf{y}(\tau)$ is a solution of $\dot{\mathbf{y}} = \mathbf{X}_\pm(\mathbf{y})$, $\mathbf{y}(\tau)$ is C^∞ on $J_\pm(\mathbf{y}(0))$.

Also, note that $\mathbf{X}_\pm(\mathbf{0}) = \mathbf{0}$, and so the origin is a fixed point of $\dot{\mathbf{y}} = \mathbf{X}_\pm(\mathbf{y})$.

The relation between the vector fields $\mathbf{X}_{\pm}$ and $\mathbf{X}$ can be translated into a relation between the associated flows $\phi_\tau^{\pm}$ and ϕ_τ. Given $\mathbf{y} \in \mathbb{R}^3$, assume that $(\tau_1, \tau_2) \subseteq J(\mathbf{y})$ with $\phi_\tau(\mathbf{y}) \in N_+ \ \forall \tau \in (\tau_1, \tau_2)$. Define $\mathbf{y}(\tau)$ by $\mathbf{y}(\tau) = \phi_\tau(\mathbf{y}) \ \forall \tau \in (\tau_1, \tau_2)$. Then $\mathbf{y}(\tau)$ solves $\dot{\mathbf{y}} = \mathbf{X}(\mathbf{y})$ on (τ_1, τ_2). Hence since $\mathbf{X}_+|_{N_+} = \mathbf{X}|_{N_+}$, $\mathbf{y}(\tau)$ solves $\dot{\mathbf{y}} = \mathbf{X}_+(\mathbf{y})$ on (τ_1, τ_2), implying that $(\tau_1, \tau_2) \subseteq J_+(\mathbf{y})$ with $\phi_\tau^+(\mathbf{y}) = \phi_\tau(\mathbf{y}) \ \forall \tau \in (\tau_1, \tau_2)$. Similarly if $\mathbf{y} \in \mathbb{R}^3$ such that $(\tau_1, \tau_2) \subseteq J(\mathbf{y})$ with $\phi_\tau(\mathbf{y}) \in N_- \ \forall \tau \in (\tau_1, \tau_2)$, then $(\tau_1, \tau_2) \subseteq J_-(\mathbf{y})$ with $\phi_\tau^-(\mathbf{y}) = \phi_\tau(\mathbf{y}) \ \forall \tau \in (\tau_1, \tau_2)$.

3.2 Physiological state space and attractors

The state space of the burster system $\dot{\mathbf{y}} = \mathbf{X}(\mathbf{y})$ is $\mathbb{R}^3$. However, r and l represent the spiking rates of neurons, and so are nonnegative quantities. All biologically feasible trajectories of $\dot{\mathbf{y}} = \mathbf{X}(\mathbf{y})$ must therefore be confined to the set S defined below:

$$S = \mathbb{R}^{2+} \times \mathbb{R} = \left\{ (r, l, \varepsilon)^T \in \mathbb{R}^3 : r, l \geq 0, \varepsilon \in \mathbb{R} \right\} \tag{3.18}$$

S will be referred to as the physiological state space of the burster system. Conveniently, S is positively invariant. To see this, let $\mathbf{y}(\tau) = (r(\tau), l(\tau), \varepsilon(\tau))^T$ be a solution of $\dot{\mathbf{y}} = \mathbf{X}(\mathbf{y})$ with $\mathbf{y}(0) \in S$. Then $r(0), l(0) \geq 0$. The r equation (3.2) shows that $\dot{r}(\tau) > 0$ whenever $r(\tau) < 0$. It follows that $r(\tau) \geq 0 \ \forall \tau \geq 0$. Similarly, $l(\tau) \geq 0 \ \forall \tau \geq 0$. Thus, $\mathbf{y}(\tau) \in S \ \forall \tau \geq 0$. Note that since the trajectories of ultimate interest have initial condition $(0, 0, \Delta g)^T$, these are confined to S for all $\tau \geq 0$, limiting the possibility of biologically unrealistic behaviour.

It will further be assumed in the following work that for the choices of $\boldsymbol{\alpha}$ of interest, all trajectories are eventually confined to a compact set $C = C(\boldsymbol{\alpha}) \subset S$ of the form:

$$C = \left\{ (r, l, \varepsilon)^T \in \mathbb{R}^3 : 0 \leq r, l \leq \alpha_M, |\varepsilon| \leq \varepsilon_M \right\} \tag{3.19}$$

(By all trajectories being eventually confined to C is meant that given $\mathbf{y} \in \mathbb{R}^3$, there is $\tau_C(\mathbf{y}) > 0$ such that $\phi_\tau(\mathbf{y}) \in C \ \forall \tau \geq \tau_C(\mathbf{y})$). Consequently, $\dot{\mathbf{y}} = \mathbf{X}(\mathbf{y})$ is eventually compact, by assumption (cf. section 1.2.4). Given $\mathbf{y} \in \mathbb{R}^3$, write $\omega(\mathbf{y})$ for the ω-limit set of $\mathbf{y}$ in $\dot{\mathbf{y}} = \mathbf{X}(\mathbf{y})$. Then, as discussed in detail in section 1.2.4, there is an index set I_B and a set of points $\{\mathbf{y}_i : i \in I_B\}$ in $\mathbb{R}^3$ such that $\mathbb{R}^3$ can be written as the disjoint union $\bigcup_{i \in I_B} [\mathbf{y}_i]$, and the ω-limit sets can be written as the distinct collection $\{\omega(\mathbf{y}_i) : i \in I_B\}$

where for each $i \in I_B$:

$$[\mathbf{y}_i] = \left\{ \mathbf{y} \in \mathbb{R}^3 : \omega(\mathbf{y}) = \omega(\mathbf{y}_i) \right\}$$

Moreover, $\forall i \in I_B$, $\omega(\mathbf{y}_i)$ is a compact, invariant set lying in C, and all points in $[\mathbf{y}_i]$ converge to $\omega(\mathbf{y}_i)$ as $\tau \to \infty$. Also recall that $\mathcal{A} = \omega(\mathbf{y}_i)$ is defined to be an attractor of $\dot{\mathbf{y}} = \mathbf{X}(\mathbf{y})$ if it has a dense orbit, and there is some open subset N of $\mathbb{R}^3$ with $\mathcal{A} \subset N$ such that N is positively invariant and $\phi_\tau(N) \to \mathcal{A}$ as $\tau \to \infty$. Given an attractor $\mathcal{A}$, its basin of attraction $\mathcal{B}(\mathcal{A})$ is the set of all points which converge to it as $\tau \to \infty$.

It should be noted that since the ω-limit sets of $\dot{\mathbf{y}} = \mathbf{X}(\mathbf{y})$ all lie in C, they must all lie in S. Thus all fixed points, limit cycles and attractors of the burster system lie in the physiological state space.

3.3 Symmetry

Define the map $\sigma : \mathbb{R}^3 \to \mathbb{R}^3$ through the 3×3 matrix below:

$$\sigma = \begin{pmatrix} 0 & 1 & 0 \\ 1 & 0 & 0 \\ 0 & 0 & -1 \end{pmatrix} \tag{3.20}$$

Given $\mathbf{y} = (r, l, \varepsilon)^T \in \mathbb{R}^3$, $\sigma\mathbf{y} = (l, r, -\varepsilon)^T$. Hence by (3.1):

$$\mathbf{X}(\sigma\mathbf{y}) = \mathbf{X}(l, r, -\varepsilon) = \begin{pmatrix} -l - \gamma l r^2 + F(-\varepsilon) \\ -r - \gamma r l^2 + F(\varepsilon) \\ -\epsilon(l - r) \end{pmatrix} = \sigma \begin{pmatrix} -r - \gamma r l^2 + F(\varepsilon) \\ -l - \gamma l r^2 + F(-\varepsilon) \\ -\epsilon(r - l) \end{pmatrix} = \sigma\mathbf{X}(\mathbf{y})$$

This holds $\forall \mathbf{y} \in \mathbb{R}^3$ and so:

$$\mathbf{X} \circ \sigma = \sigma \circ \mathbf{X} \tag{3.21}$$

The conjugacy (3.21) implies that if $\mathbf{y}(\tau)$ solves $\dot{\mathbf{y}} = \mathbf{X}(\mathbf{y})$ on the interval (a, b), then $\sigma\mathbf{y}(\tau)$ also solves $\dot{\mathbf{y}} = \mathbf{X}(\mathbf{y})$ on (a, b). Moreover, $\sigma^2 = \mathbf{1}_3$, and so for all $\mathbf{y} \in \mathbb{R}^3$, $J(\sigma\mathbf{y}) = J(\mathbf{y})$ with $\phi_\tau(\sigma\mathbf{y}) = \sigma\phi_\tau(\mathbf{y})$ $\forall \tau \in J(\mathbf{y})$. This can be seen in the following way. Given $\mathbf{y} \in \mathbb{R}^3$, let $\mathbf{y}(\tau) = \phi_\tau(\mathbf{y})$ $\forall \tau \in J(\mathbf{y})$. Then $\mathbf{y}(\tau)$ solves $\dot{\mathbf{y}} = \mathbf{X}(\mathbf{y})$ on $J(\mathbf{y})$ with $\mathbf{y}(0) = \mathbf{y}$. It follows that $\sigma\mathbf{y}(\tau)$ solves $\dot{\mathbf{y}} = \mathbf{X}(\mathbf{y})$ on $J(\mathbf{y})$ with $\sigma\mathbf{y}(0) = \sigma\mathbf{y}$. Hence, $J(\mathbf{y}) \subseteq J(\sigma\mathbf{y})$ and $\forall\tau \in J(\mathbf{y})$, $\phi_\tau(\sigma\mathbf{y}) = \sigma\mathbf{y}(\tau) = \sigma\phi_\tau(\mathbf{y})$. Also, since $\sigma\mathbf{y}(\tau)$ solves $\dot{\mathbf{y}} = \mathbf{X}(\mathbf{y})$ on $J(\sigma\mathbf{y})$, $\sigma^2\mathbf{y}(\tau) = \mathbf{y}(\tau)$ must solve $\dot{\mathbf{y}} = \mathbf{X}(\mathbf{y})$ on $J(\sigma\mathbf{y})$, implying that $J(\sigma\mathbf{y}) \subseteq J(\mathbf{y})$. Thus, $J(\sigma\mathbf{y}) = J(\mathbf{y})$. σ is therefore a symmetry of the vector field $\mathbf{X}$ (cf. section 1.2.5). Moreover, as $\sigma^2 = \mathbf{1}_3$, the symmetry group G_σ generated by σ is $G_\sigma = \{\mathbf{1}_3, \sigma\}$, which is isomorphic to $\mathbb{Z}_2$.

Define the plane D by:

$$D = \left\{(x, x, \varepsilon)^T \in \mathbb{R}^3 : x, \varepsilon \in \mathbb{R}\right\} \tag{3.22}$$

Then in terms of the state space, σ is equivalent to reflection in D followed by reflection in P. The symmetry of the vector field under σ simplifies the analysis of the burster system. In particular, since $\dot{\mathbf{y}} = \mathbf{X}(\mathbf{y})$ is eventually compact, it follows from the discussion at the end of section 1.2.5 that $\dot{\mathbf{y}} = \mathbf{X}(\mathbf{y})$ has the following properties:

1. $\forall\tau \geq 0$

$$\phi_\tau \circ \sigma = \sigma \circ \phi_\tau \tag{3.23}$$

2. $\forall i \in I_B$, $\sigma\omega(\mathbf{y}_i) = \omega(\sigma\mathbf{y}_i)$ and $[\sigma\mathbf{y}_i] = \sigma[\mathbf{y}_i]$.

3. $\bar{\mathbf{y}}$ is a fixed point of $\dot{\mathbf{y}} = \mathbf{X}(\mathbf{y})$ iff $\sigma\bar{\mathbf{y}}$ is a fixed point. Also, $\bar{\mathbf{y}}$ is stable iff $\sigma\bar{\mathbf{y}}$ is stable, while $\bar{\mathbf{y}}$ is unstable iff $\sigma\bar{\mathbf{y}}$ is unstable.

4. $\mathcal{C}$ is a limit cycle of $\dot{\mathbf{y}} = \mathbf{X}(\mathbf{y})$ of period T iff $\sigma\mathcal{C}$ is a limit cycle of period T. Also, $\mathcal{C}$ is stable iff $\sigma\mathcal{C}$ is stable and $\mathcal{C}$ is unstable iff $\sigma\mathcal{C}$ is unstable.

5. $\mathcal{A} = \omega(\mathbf{y}_i)$ is an attractor of $\dot{\mathbf{y}} = \mathbf{X}(\mathbf{y})$ with basin of attraction $\mathcal{B}(\mathcal{A})$ iff $\sigma(\mathcal{A}) = \omega(\sigma\mathbf{y}_i)$ is an attractor with basin of attraction $\sigma(\mathcal{B}(\mathcal{A}))$.

6. The set $\digamma(\sigma)$ defined by

$$\digamma(\sigma) = \left\{\mathbf{y} \in \mathbb{R}^3 : \sigma\mathbf{y} = \mathbf{y}\right\}$$

is positively invariant.

Note that properties 3-5 imply fixed points, limit cycles and attractors of $\dot{\mathbf{y}} = \mathbf{X}(\mathbf{y})$ are either symmetry invariant, or come in symmetry-related pairs. Explicitly, $\digamma(\sigma)$ is given by

$$\digamma(\sigma) = \left\{(r,l,\varepsilon)^T : (l,r,-\varepsilon)^T = (r,l,\varepsilon)^T\right\}$$

from which it follows that $\digamma(\sigma)$ is the line L_0 where:

$$L_0 = \{(x,x,0)^T : x \in \mathbb{R}\} \tag{3.24}$$

On L_0 the dynamics are described by:

$$\dot{x} = -(1+\gamma x^2)x \tag{3.25}$$

The system (3.25) has the unique fixed point $x = 0$. Additionally, $\dot{x} > 0$ for $x < 0$ and $\dot{x} < 0$ for $x > 0$ and so $x = 0$ is globally attracting. In terms of the full system $\dot{\mathbf{y}} = \mathbf{X}(\mathbf{y})$, it can be concluded that L_0 is a stable 1-dimensional manifold of the origin $\mathbf{0}$. Since L_0 is a consequence of the symmetry of the system, its existence and form do not depend on the choice of $\boldsymbol{\alpha}$.

Equations (3.16), (3.17) and (3.20) imply that for each $\mathbf{y} = (r,l,\varepsilon)^T \in \mathbb{R}^3$:

$$\mathbf{X}_+(\sigma\mathbf{y}) = \mathbf{X}_+(l,r,-\varepsilon) = \begin{pmatrix} -l-\gamma lr^2 + f(-\varepsilon) \\ -r-\gamma rl^2 + h(\varepsilon) \\ -\epsilon(l-r) \end{pmatrix} = \sigma \begin{pmatrix} -r-\gamma rl^2 + h(\varepsilon) \\ -l-\gamma lr^2 + f(-\varepsilon) \\ -\epsilon(r-l) \end{pmatrix} = \sigma\mathbf{X}_-(\mathbf{y})$$

Hence:

$$\mathbf{X}_+ \circ \sigma = \sigma \circ \mathbf{X}_- \tag{3.26}$$

In addition to conjugating the vector field $\mathbf{X}$, the map σ therefore also conjugates the extended vector fields $\mathbf{X}_+$ and $\mathbf{X}_-$. Using a similar argument to the one above which showed that σ is a symmetry of $\mathbf{X}$, it follows from the conjugacy (3.26) that for each $\mathbf{y} \in \mathbb{R}^3$, $J_-(\sigma\mathbf{y}) = J_+(\mathbf{y})$ with $\phi_\tau^-(\sigma\mathbf{y}) = \sigma\phi_\tau^+(\mathbf{y})\ \forall\tau \in J_+(\mathbf{y})$. Recall from section 3.1.3 that if $\mathbf{y} \in \mathbb{R}^3$ such that $(\tau_1,\tau_2) \subseteq J(\mathbf{y})$ with $\phi_\tau(\mathbf{y}) \in N_\pm\ \forall\tau \in (\tau_1,\tau_2)$, then $(\tau_1,\tau_2) \subseteq J_\pm(\mathbf{y})$ with $\phi_\tau^\pm(\mathbf{y}) = \phi_\tau(\mathbf{y})\ \forall\tau \in (\tau_1,\tau_2)$. Hence, since L_0 is positively invariant and $L_0 \subseteq N_+ \cap N_-$, this means that for each $\mathbf{y} \in L_0$, $[0,\infty) \subset J_\pm(\mathbf{y})$ with $\phi_\tau^\pm(\mathbf{y}) = \phi_\tau(\mathbf{y})\ \forall\tau \in [0,\infty)$. L_0 is therefore a stable 1-dimensional manifold of $\mathbf{0}$ in the extended systems $\dot{\mathbf{y}} = \mathbf{X}_+(\mathbf{y})$ and

$\dot{\mathbf{y}} = \mathbf{X}_- (\mathbf{y})$ also. Moreover, the dynamics of both $\dot{\mathbf{y}} = \mathbf{X}_+ (\mathbf{y})$ and $\dot{\mathbf{y}} = \mathbf{X}_- (\mathbf{y})$ on L_0 are given by (3.25).[1]

3.4 The slow manifold

Equations (3.2)-(3.4) indicate that for small ϵ, the burster equations are a slow-fast system with a slow manifold S_M given by the intersection of the r and l nullclines (cf. section 2.3). Equations (3.2) and (3.3) imply that the r and l nullclines are the surfaces I_r and I_l defined below:

$$I_r = \left\{ \left(\tfrac{F(\varepsilon;\alpha,\beta)}{1+\gamma l^2}, l, \varepsilon \right)^T : l, \varepsilon \in \mathbb{R} \right\} \tag{3.27}$$

$$I_l = \left\{ \left(r, \tfrac{F(-\varepsilon;\alpha,\beta)}{1+\gamma r^2}, \varepsilon \right)^T : r, \varepsilon \in \mathbb{R} \right\} \tag{3.28}$$

(3.27) and (3.28) show that $\sigma I_r = I_l$. It follows that S_M is invariant under the symmetry since $\sigma S_M = \sigma(I_r \cap I_l) = (\sigma I_r) \cap (\sigma I_l) = I_l \cap I_r = S_M$. As S_M is an intersection of two surfaces, it is a union of curves. Also, since S_M is an intersection of nullclines, it must contain all fixed points of the burster system. By (3.4), a given fixed point $(r_*, l_*, \varepsilon_*)^T$ of $\dot{\mathbf{y}} = \mathbf{X}(\mathbf{y})$ will have $r_* = l_*$. Fixed points will therefore lie on the intersection of S_M with the plane $r = l$ (i.e. the plane D).

The discussion of slow-fast systems in section 2.3 implies that trajectories of the burster system outside the neighbourhood of S_M will contract very rapidly onto it parallel to the (r, l) plane. On S_M the dynamics are governed by the equation for $\dot{\varepsilon}$: trajectories therefore move along S_M in the positive ε direction for $r < l$ and in the negative ε direction for $r > l$. As ϵ is decreased, the contraction onto S_M becomes more rapid and trajectories follow S_M more closely. As ϵ is increased, the contraction becomes less rapid and trajectories no longer follow S_M. Note from the forms of I_r and I_l that S_M is a function of α and β only; that is $S_M = S_M(\alpha, \beta)$.

For each choice of (α, β) in the range $(0, \infty) \times (0, \infty)$, the slow manifold can be computed in the following way. For a given value of ε_M, the points on S_M with ε coordinate equal

[1]Note that since L_0 is a positively invariant set of $\dot{\mathbf{y}} = \mathbf{X}_\pm(\mathbf{y})$, $T_\pm = \mathbb{R}$.

to ε_M have the form $(r_M, l_M, \varepsilon_M)^T$, where r_M and l_M satisfy the pair of equations:

$$r_M(1+\gamma l_M^2) - F(\varepsilon_M;\alpha,\beta) = 0 \tag{3.29}$$

$$l_M(1+\gamma r_M^2) - F(-\varepsilon_M;\alpha,\beta) = 0 \tag{3.30}$$

Let $F_1 = F(\varepsilon_M;\alpha,\beta)$ and $F_2 = F(-\varepsilon_M;\alpha,\beta)$. Rearranging (3.29) for r_M, substituting into (3.30) and then rearranging for l_M gives:

$$l_M^5 - F_2 l_M^4 + \frac{2}{\gamma} l_M^3 - \frac{2F_2}{\gamma} l_M^2 + \frac{1}{\gamma}\left(F_1^2 + \frac{1}{\gamma}\right) l_M - \frac{F_2}{\gamma^2} = 0 \tag{3.31}$$

For a real solution of (3.31), the corresponding value of r_M is then obtained from:

$$r_M = \frac{F_1}{1+\gamma l_M^2} \tag{3.32}$$

By varying ε_M over an ε range of interest, and performing this calculation for each choice of ε_M, it is therefore possible to calculate all the points of the slow manifold over the range. Since $\sigma S_M = S_M$, if $\mathbf{y}_1, ..., \mathbf{y}_k$ are the points on S_M with ε coordinate $= \varepsilon_M$, the corresponding points on S_M with ε coordinate $= -\varepsilon_M$ are $\sigma\mathbf{y}_1, ..., \sigma\mathbf{y}_k$. In computing S_M over an ε range symmetric about $\varepsilon = 0$, it is therefore only necessary to calculate the points lying in N_+ or N_-: the remaining points can be obtained by applying σ.

Note from (3.32) that for each choice of ε_M, $r_M \geq 0$ since $F_1 \geq 0$. The symmetry therefore implies that $l_M \geq 0$ also. The slow manifold must therefore lie in the physiological state space S.

3.4.1 Geometry

It has been shown above that for a given choice of α and β, the points $(r_M, l_M, \varepsilon_M)^T$ of S_M lying in N_+ can be obtained by considering the solutions of (3.31) for nonnegative values of ε_M. For $\varepsilon_M \geq 0$, $F_1 = F(\varepsilon_M;\alpha,\beta) = f(\varepsilon_M)$ and $F_2 = F(-\varepsilon_M;\alpha,\beta) = h(-\varepsilon_M;\alpha,\beta)$. A solution of (3.31) is therefore a root of the quintic polynomial $G_M(l_M;\varepsilon_M,\alpha,\beta) = 0$ where:

$$\begin{aligned} G_M(l_M;\varepsilon_M,\alpha,\beta) &= l_M^5 - h(-\varepsilon_M;\alpha,\beta)\, l_M^4 + \frac{2}{\gamma} l_M^3 - \frac{2h(-\varepsilon_M;\alpha,\beta)}{\gamma} l_M^2 \\ &\quad + \frac{1}{\gamma}\left(f(\varepsilon_M)^2 + \frac{1}{\gamma}\right) l_M - \frac{h(-\varepsilon_M;\alpha,\beta)}{\gamma^2} \end{aligned} \tag{3.33}$$

For each $\varepsilon_M \geq 0$, $G_M(l_M; \varepsilon_M, \alpha, \beta)$ has 1, 3 or 5 real roots, as the complex solutions to a general polynomial equation come in conjugate pairs. S_M therefore intersects the plane $\varepsilon = \varepsilon_M$ at 1, 3 or 5 points. Moreover, $G_M(l_M; \varepsilon_M, \alpha, \beta)$ always has at least 1 real root, and so $S_M \cap N_+$ must extend infinitely into $S \cap N_+$ in the positive ε direction. As $\varepsilon_M \to 0+$, both $f(\varepsilon_M)$ and $h(-\varepsilon_M; \alpha, \beta) \to 0$ and so $G_M(l_M; \varepsilon_M, \alpha, \beta) \to G_M(l_M; 0, \alpha, \beta)$ uniformly over bounded $|l_M|$, where from (3.33):

$$G_M(l_M; 0, \alpha, \beta) = l_M \left(l_M^4 + \frac{2}{\gamma} l_M^2 + \frac{1}{\gamma^2} \right)$$

The only real root of $G_M(l_M; 0, \alpha, \beta)$ is 0. Substituting $l_M = 0$ into (3.32) gives $r_M = 0$. For $\varepsilon_M \geq 0$ small, there is therefore only one point on S_M. This point is approximated by $\mathbf{0}$; the error in the approximation approaches zero as $\varepsilon_M \to 0+$, and equals zero at $\varepsilon_M = 0$. For $\varepsilon_M \geq 0$ small, S_M is therefore a single curve which intersects P at $\mathbf{0}$.

As $\varepsilon_M \to \infty$, $h(-\varepsilon_M; \alpha, \beta) \to 0$ and so $G_M(l_M; \varepsilon_M, \alpha, \beta) \to \bar{G}_M(l_M; \varepsilon_M, \alpha, \beta)$ uniformly over bounded $|l_M|$, where:

$$\bar{G}_M(l_M; \varepsilon_M, \alpha, \beta) = l_M \left(l_M^4 + \frac{2}{\gamma} l_M^2 + \frac{1}{\gamma} \left(f(\varepsilon_M)^2 + \frac{1}{\gamma} \right) \right) \tag{3.34}$$

The only real root of $\bar{G}_M(l_M; \varepsilon_M, \alpha, \beta)$ is $l_M = 0$. Substituting $l_M = 0$ into (3.32) gives $r_M = f(\varepsilon_M)$. For $\varepsilon_M \geq 0$ large, there is therefore only one point on S_M. This point is approximated by $(f(\varepsilon_M), 0, \varepsilon_M)^T$, with the error in the approximation approaching zero as $\varepsilon_M \to \infty$. For large $\varepsilon_M \geq 0$, S_M is thus a single curve C_1^+, which converges to the curve $\hat{C}_1^+ \stackrel{def}{=} \left\{ (f(\varepsilon_M), 0, \varepsilon_M)^T : \varepsilon_M \geq 0 \right\}$ as $\varepsilon_M \to \infty$. As ε_M is decreased from a large positive value to 0, additional roots of $G_M(l_M; \varepsilon_M, \alpha, \beta)$ may be created or destroyed as local maxima and minima of $G_M(l_M; \varepsilon_M, \alpha, \beta)$ cross the l_M-axis. Such events will correspond to turning points in the corresponding curves that comprise S_M. It follows that C_1^+ will extend to the plane P from above, and may have turning points between P and $\varepsilon_M \geq 0$ large. The fact that C_1^+ extends to the plane P identifies it as the single curve which comprises S_M for $\varepsilon_M \geq 0$ small, and intersects P at $\mathbf{0}$. Hence, $S_M = C_1^+$ for $\varepsilon_M \geq 0$ small as well as $\varepsilon_M \geq 0$ large. For intermediate values of $\varepsilon_M \geq 0$, S_M may contain other curves in addition to C_1^+. Moreover, as roots of $G_M(l_M; \varepsilon_M, \alpha, \beta)$ are created or destroyed in pairs, any such curves will be closed loops.

By the symmetry of the slow manifold under σ it can be deduced that $S_M \cap N_-$ always contains the curve C_1^- defined by $C_1^- = \sigma C_1^+$. C_1^- intersects the origin, and converges to the curve $\hat{C}_1^- \overset{def}{=} \sigma\hat{C}_1^+ = \left\{(0, f(\varepsilon_M), -\varepsilon_M)^T : \varepsilon_M \geq 0\right\}$ as $\varepsilon_M \to -\infty$. Additionally, $S_M = C_1^-$ for $\varepsilon_M \leq 0$ with $|\varepsilon_M|$ small and $\varepsilon_M \leq 0$ with $|\varepsilon_M|$ large, while for intermediate values of $\varepsilon_M \leq 0$, C_1^- may have turning points, and S_M may contain additional closed loops to C_1^-. Any additional loops will map to corresponding ones in $S_M \cap N_+$.

The existence of S_M places a strong restriction on the behaviour of the burster system for small ϵ. One important restriction is that trajectories cannot cross the plane P. This follows from the fact that for $|\varepsilon_M|$ small, S_M is the single curve $C_1^+ \cup C_1^-$. Consequently, a trajectory which crosses P must do so on $C_1^+ \cup C_1^-$. This cannot happen as $C_1^+ = \sigma C_1^-$ and thus $\dot{\varepsilon}$ has opposite signs on C_1^+ and C_1^-. Another important restriction pertains to the attractors of the system. Fix $\boldsymbol{\alpha}$ with ϵ small, and assume that the burster system has an attractor which is not a fixed point. Consider a trajectory on this attractor. Portions of the trajectory must lie on S_M. As S_M is a union of curves, this suggests that the attractor is a limit cycle or a homoclinic orbit. Thus, for generic choices of $\boldsymbol{\alpha}$ with ϵ small, the only attractors that the burster system may have are fixed points and limit cycles. In particular, for sufficiently small α, it is possible to deduce that the unique attractor of the burster system is the origin. To see this, note that as $\alpha \to 0$ for a fixed β, $h(-\varepsilon_M; \alpha, \beta) \to 0$ uniformly in $\varepsilon_M \geq 0$. This implies that as $\alpha \to 0$, $G_M(l_M; \varepsilon_M, \alpha, \beta) \to \bar{G}_M(l_M; \varepsilon_M, \alpha, \beta)$ uniformly in ε_M and l_M for $\varepsilon_M \geq 0$ and $|l_M|$ bounded, where $\bar{G}_M(l_M; \varepsilon_M, \alpha, \beta)$ is defined in (3.34). It was shown above that for each $\varepsilon_M \geq 0$, the only real root of $\bar{G}_M(l_M; \varepsilon_M, \alpha, \beta)$ is $l_M = 0$, giving the point $(f(\varepsilon_M), 0, \varepsilon_M)^T$ on S_M. It follows that for small α, $S_M = C_1^+$ in N_+ where C_1^+ is approximated by the curve $\hat{C}_1^+$ defined above, with the error in the approximation tending to zero as $\alpha \to 0$. The symmetry of the system then implies that for small α, $S_M = C_1^-$ in N_- where C_1^- is approximated by the curve $\hat{C}_1^-$ defined above, with the error in the approximation tending to 0 as $\alpha \to 0$. Note that since f is independent of α and β, $\hat{C}_1^{\pm}$ is also independent of α and β. Figures (3-1)-(3-2) show S_M together with the curves $\hat{C}_1^+$ and $\hat{C}_1^-$ for $\{\alpha = 20, \beta = 2.25\}$ and $\{\alpha = 200, \beta = 22.5\}$. It can be seen in both cases that $S_M \cap N_{\pm} = C_1^{\pm}$, and that $C_1^{\pm}$ is well approximated by $\hat{C}_1^{\pm}$. Now consider what happens to trajectories $\mathbf{y}(\tau) = (r(\tau), l(\tau), \varepsilon(\tau))^T$ of the burster system for α small when ϵ is small. First consider trajectories with initial condition in $\varepsilon \neq 0$. If $\varepsilon(0) > 0$, $\mathbf{y}(\tau)$ will contract to S_M at C_1^+. As C_1^+ is approximated by $\hat{C}_1^+$, $C_1^+ \backslash \{\mathbf{0}\}$ will lie entirely in $r > l$. This implies that $\dot{\varepsilon} < 0$ on $C_1^+ \backslash \{\mathbf{0}\}$ and so $\mathbf{y}(\tau)$ will contract to the origin along C_1^+. All trajectories with initial condition in $\varepsilon > 0$ will thus converge to the origin in N_+. By symmetry, this implies that all trajectories with initial condition in $\varepsilon < 0$ will

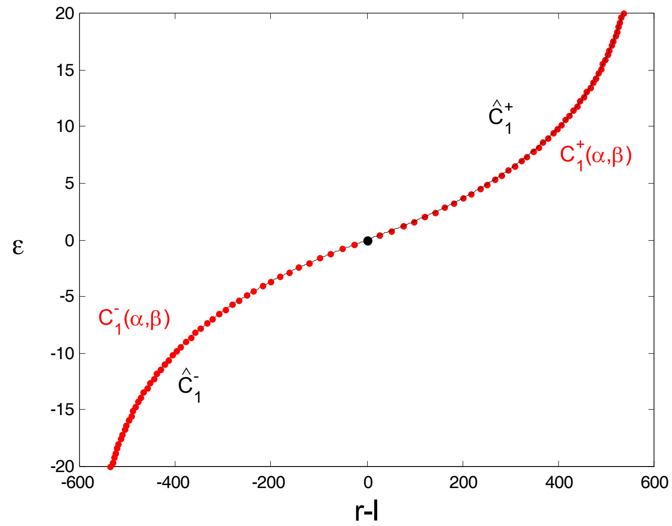

Figure 3-1: Projection of $S_M(\alpha, \beta)$ (red dots) and the curves $\hat{C}_1^{\pm}$ (black lines) onto the $(r-l, \varepsilon)$ plane for $\alpha = 20$, $\beta = 2.25$.

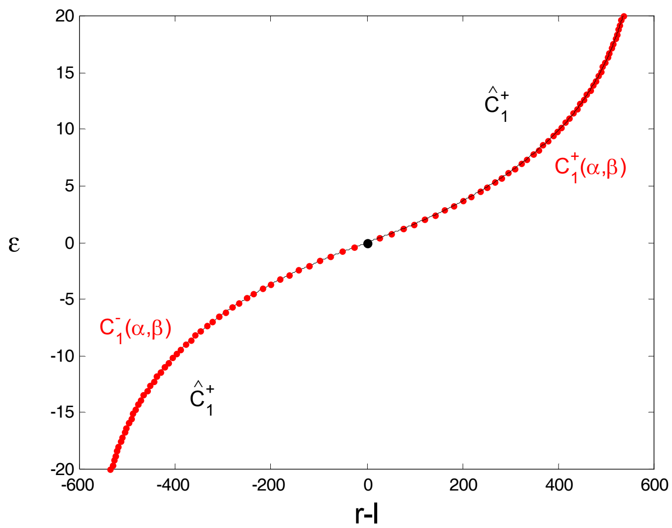

Figure 3-2: Projection of $S_M(\alpha, \beta)$ (red dots) and the curves $\hat{C}_1^{\pm}$ (black lines) onto the $(r-l, \varepsilon)$ plane for $\alpha = 200$, $\beta = 22.5$.

converge to the origin in N_-. Now consider trajectories with initial condition in $\varepsilon = 0$. If $r(0) > l(0)$, $\dot{\varepsilon}(0) < 0$ and so $\mathbf{y}(\tau)$ will move into $\varepsilon < 0$, from where it will converge to $\mathbf{0}$ in N_-, as argued above. By symmetry, if $r(0) < l(0)$, $\mathbf{y}(\tau)$ will converge to $\mathbf{0}$ in N_+. If $\varepsilon(0) = 0$ and $r(0) = l(0)$, $\mathbf{y}(0) \in L_0$ and so $\mathbf{y}(\tau)$ will converge to $\mathbf{0}$ along L_0. All trajectories with initial condition on $\varepsilon = 0$ will therefore also converge to the origin. It has thus been shown that all trajectories will converge to the origin, implying that the origin is globally attracting in this case.

3.4.2 An example of the form of S_M

The projection of S_M onto the $(\varepsilon, r), (\varepsilon, l)$ and $(r - l, \varepsilon)$ planes is plotted for the choice of parameters $\{\alpha = 98, \beta = 1.5\}$ in figures (3-3)-(3-6). Also plotted are the trajectories of the burster system generated by the initial condition $\{r(0) = l(0) = 0, \varepsilon(0) = 2\}$ for $\epsilon = 0.001$ and $\epsilon = 0.005$. Note that this initial condition corresponds to a rightward saccade of $2°$. S_M is seen in this case to be composed of the curves $C_1^{\pm}$ together with two closed loops $C_2^{\pm} \subset N_{\pm}$, that map into each other under the symmetry. Also C_1^+ lies entirely in $r > l$ while C_1^- lies entirely in $r < l$. Since $\varepsilon(0) = 2$ and $S_M = C_1^+$ for $\varepsilon = 2$, both trajectories initially contract onto C_1^+. As C_1^+ lies in $r > l$, the trajectories then slowly move down this curve in the ε direction towards the origin, which is a stable fixed point in this case. The trajectory generated with the smaller value of ϵ is seen to follow C_1^+ more closely.

3.5 Fixed points

3.5.1 Conditions for existence

Equations (3.2)-(3.4) show that fixed points of $\dot{\mathbf{y}} = \mathbf{X}(\mathbf{y})$ have the form $(x_*, x_*, \varepsilon_*)^T$, where x_* and ε_* solve the pair of equations:

$$\gamma x_*^3 + x_* = F(\varepsilon_*) \tag{3.35}$$

$$\gamma x_*^3 + x_* = F(-\varepsilon_*) \tag{3.36}$$

Subtracting (3.35) from (3.36) gives:

$$F(\varepsilon_*) = F(-\varepsilon_*) \tag{3.37}$$

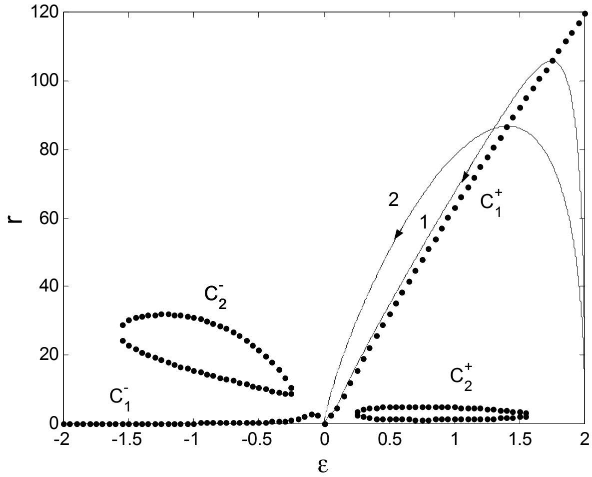

Figure 3-3: Projection of the slow manifold S_M onto the (ε, r) plane for $\alpha = 98$, $\beta = 1.5$ (dotted lines). The trajectories generated by the initial condition $r(0) = l(0) = 0$, $\varepsilon(0) = 2$ for $\epsilon = 0.001$ and $\epsilon = 0.005$ are shown by the solid lines 1 and 2 respectively. Arrows indicate the direction of time.

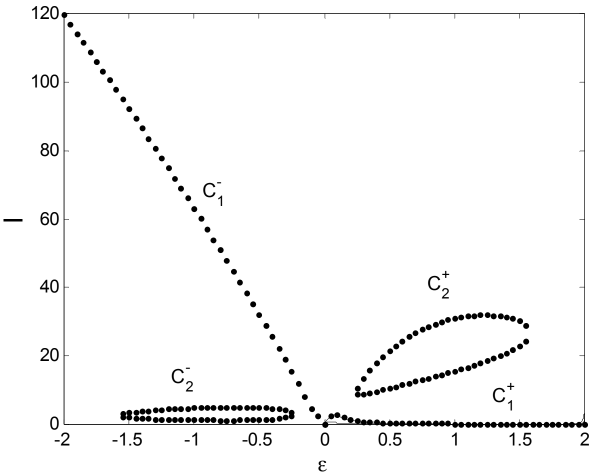

Figure 3-4: Projection of the slow manifold S_M onto the (ε, l) plane for $\alpha = 98$, $\beta = 1.5$ (dotted lines). The trajectories generated by the initial condition $r(0) = l(0) = 0$, $\varepsilon(0) = 2$ for $\epsilon = 0.001$ and $\epsilon = 0.005$ are shown by the solid lines 1 and 2 respectively. Arrows indicate the direction of time. See figure (3-5) for details of trajectories.

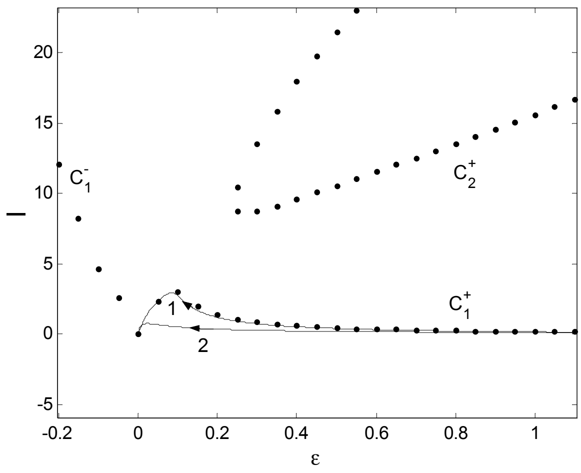

Figure 3-5: An expanded portion of figure (3-4) about the origin.

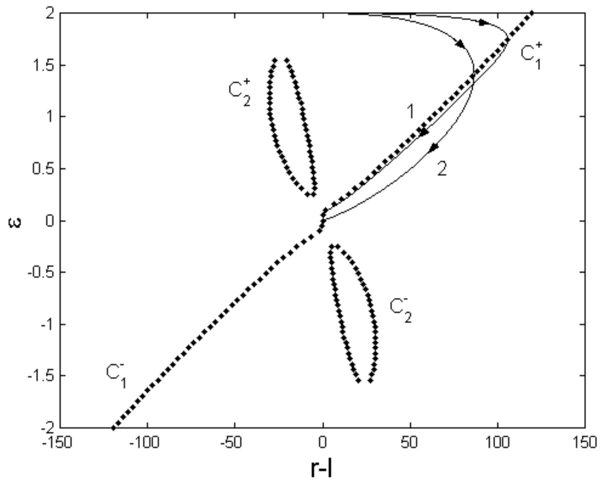

Figure 3-6: Projection of the slow manifold S_M onto the $(r - l, \varepsilon)$ plane for $\alpha = 98$, $\beta = 1.5$ (dotted lines). The trajectories generated by the initial condition $r(0) = l(0) = 0$, $\varepsilon(0) = 2$ for $\epsilon = 0.001$ and $\epsilon = 0.005$ are shown by the solid lines 1 and 2 respectively. Arrows indicate the direction of time.

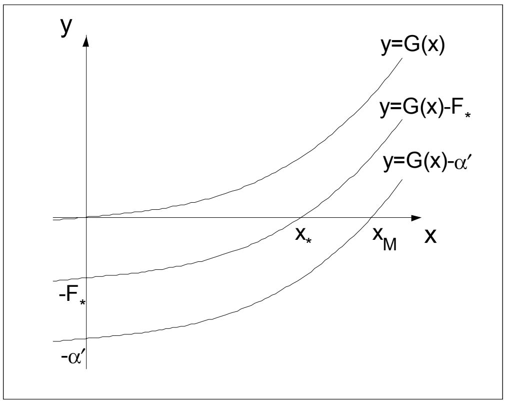

Figure 3-7: The curves $y = G(x)$, $y = G(x) - F_*$ and $y = G(x) - \alpha'$, where $G(x) = x(\gamma x^2 + 1)$.

ε_* must therefore satisfy (3.37). Since equation (3.37) is symmetric in ε_*, it can be assumed that ε_* is nonnegative. Using the definition of F given in (3.7), equation (3.37) can be rewritten for nonnegative ε_* as:

$$f(\varepsilon_*) = h(-\varepsilon_*) \tag{3.38}$$

Writing $F_* = F(\varepsilon_*)$ results in the following equation for x_*:

$$\gamma x_*^3 + x_* - F_* = 0 \tag{3.39}$$

Define $G(x)$ by $G(x) = \gamma x^3 + x = x(\gamma x^2 + 1)$. Real solutions to (3.39) are then real zeros of $G(x) - F_*$, and correspond geometrically to intersections of the curve $y = G(x) - F_*$ with the x axis. This curve is obtained by displacing the curve $y = G(x)$ by $-F_*$ parallel to the y axis. Thus, since G is a strictly increasing function of x and $F_* \geq 0$ (F is a nonnegative function), $y = G(x) - F_*$ crosses the x axis once in $x \geq 0$ (cf. figure (3-7)). Each solution ε_* of (3.38) therefore gives rise to a single real nonnegative solution x_* of (3.39). x_* can therefore be considered a function of ε_*, $x_*(\varepsilon_*)$. Note that $x_*(\varepsilon_*)$ will be a continuous function of ε_* on $[0, \infty)$. Moreover, since F_* is a strictly increasing function of ε_*, figure (3-7) shows that x_* is a strictly increasing function of ε_* on $[0, \infty)$ with $x_*(0) = 0$. Also, $F_* < \alpha'$ with $F_* \to \alpha'$ as $\varepsilon_* \to \infty$ and so $x_* < x_M$ with $x_* \to x_M$ as $\varepsilon_* \to \infty$, where x_M is the single real root of $G(x) - \alpha'$ (cf. figure (3-7) again).

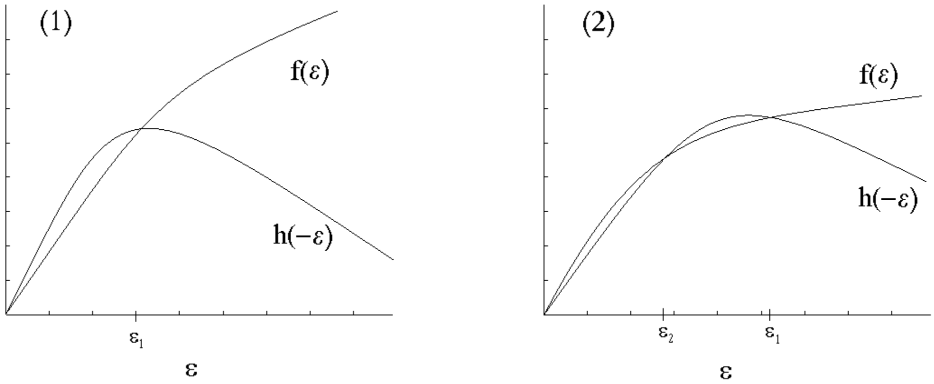

Figure 3-8: Intersections of $f(\varepsilon)$ and $h(-\varepsilon)$ on the positive real line.

For a given fixed point $(x_*, x_*, \varepsilon_*)^T$, $(x_*, x_*, -\varepsilon_*)^T = \sigma(x_*, x_*, \varepsilon_*)^T$ is also a fixed point, as mentioned in section 3.3. Since $f(0) = h(0) = 0$, equation (3.38) always has the trivial solution $\varepsilon_* = 0$. $x_*(0) = 0$ and so this trivial solution gives rise to the fixed point at the origin, which maps to itself under σ. A nontrivial solution $\varepsilon_* > 0$ of (3.38) will give rise to the pair of distinct fixed points $(x_*, x_*, \varepsilon_*)^T$ and $(x_*, x_*, -\varepsilon_*)^T$, with $x_* > 0$ ($x_*(\varepsilon_*) > 0$ for $\varepsilon_* > 0$).

Note that equation (3.38) implicitly involves the parameters α, β, α' and β' while equation (3.39) involves the parameter γ. Since it is assumed that α', β' and γ are fixed, this implies that when ε_* and x_* are considered as functions of the system parameters, ε_* and x_* are functions of α and β only, $\varepsilon_*(\alpha, \beta)$ and $x_*(\alpha, \beta)$; they are independent of ϵ.

3.5.2 Nontrivial fixed points

Geometrically, a nontrivial solution of (3.38) corresponds to an intersection of the graph of $f(\varepsilon)$ with the graph of $h(-\varepsilon)$ on the positive real line. Intuitively, such an intersection can occur in two ways, as illustrated in figure (3-8). Since α' and β' are fixed, $f(\varepsilon)$ is fixed. By varying α and β, intersections of $f(\varepsilon)$ and $h(-\varepsilon)$ are obtained by varying the shape of $h(-\varepsilon)$. In the case where there is a single nontrivial intersection, the nontrivial solution of (3.38) will be written as ε_1. In the case where there is a double intersection, the nontrivial solutions will be written as ε_1 and ε_2 with $\varepsilon_2 < \varepsilon_1$. The two fixed points associated with a given nontrivial solution ε_i can be written as $\mathbf{y}_i^{\pm}$ where $\mathbf{y}_i^{\pm} = (x_i, x_i, \pm\varepsilon_i)^T$ and x_i satisfies

$$\gamma x_i^3 + x_i - F_i = 0 \tag{3.40}$$

with $F_i = F(\varepsilon_i) = f(\varepsilon_i)$. Note that when $\mathbf{y}_i^{\pm}$ is considered as a function of $\boldsymbol{\alpha}$, $\mathbf{y}_i^{\pm} = \mathbf{y}_i^{\pm}(\alpha, \beta)$, as $\varepsilon_i = \varepsilon_i(\alpha, \beta)$ and $x_i = x_i(\alpha, \beta)$. From equation (3.6) it can be seen that for a fixed β and $\varepsilon > 0$, $h(-\varepsilon)$ is a strictly increasing function of α. Since $f(\varepsilon)$ is fixed, the geometry of $f(\varepsilon)$ and $h(-\varepsilon)$ then implies that for a fixed β, ε_1 is a strictly increasing function of α, while ε_2 is a strictly decreasing function of α (cf. figure (3-8)). As x_i is a strictly increasing function of ε_i, this in turn implies that for a fixed β, x_1 is a strictly increasing function of α, while x_2 is a strictly decreasing function of α.

The intersections of the graphs of $f(\varepsilon)$ and $h(-\varepsilon)$ on the positive real line can be understood by considering the corresponding tangents at $0, \varepsilon_1$ and ε_2. Recall from section 3.1.1 that the right derivative of $f(\varepsilon)$ at 0 is Λ_+ and the left derivative of $h(\varepsilon)$ at 0 is Λ_-. Λ_+ therefore represents the tangent to the graph of $f(\varepsilon)$ at 0, while $-\Lambda_-$ represents the tangent to the graph of $h(-\varepsilon)$ at 0. Also, the tangents to $f(\varepsilon)$ and $h(-\varepsilon)$ at ε_i are represented by Γ_i^+ and $-\Gamma_i^-$ respectively where $\Gamma_i^+ = Df(\varepsilon_i)$ and $\Gamma_i^- = Dh(-\varepsilon_i)$. Using (3.9) and (3.10) gives the following explicit forms for Γ_i^+ and Γ_i^-:

$$\Gamma_i^+ = \frac{\alpha'}{\beta'} e^{-\varepsilon_i/\beta'} = \Lambda_+ e^{-\varepsilon_i/\beta'} \tag{3.41}$$

$$\Gamma_i^- = -\frac{\alpha}{\beta}\left(1 - \frac{1}{\beta}\varepsilon_i\right) e^{-\varepsilon_i/\beta} = \Lambda_-\left(1 - \frac{1}{\beta}\varepsilon_i\right) e^{-\varepsilon_i/\beta} \tag{3.42}$$

Note that when Γ_i^+ and Γ_i^- are considered as functions of $\boldsymbol{\alpha}$,

$$\Gamma_i^+ = \Gamma_i^+(\alpha, \beta) = D_\varepsilon f(\varepsilon_i(\alpha, \beta))$$

and:

$$\Gamma_i^- = \Gamma_i^-(\alpha, \beta) = D_\varepsilon h(-\varepsilon_i(\alpha, \beta); \alpha, \beta)$$

$\Lambda_\pm$ and $\Gamma_1^\pm$ are illustrated in figure (3-9) together with the graphs of $f(\varepsilon)$ and $h(-\varepsilon)$ on the positive real line for the choice of parameters $\{\alpha = 200, \beta = 1.5\}$. Figures (3-8) and (3-9) suggest that the intersection behaviour of $f(\varepsilon)$ and $h(-\varepsilon)$ changes with the sign of $\Lambda_+ + \Lambda_-$. Noting from (3.13) that $\Lambda_+ = -\Lambda_-$ is equivalent to $\alpha = \Lambda_+\beta$, the 3 cases $\alpha > \Lambda_+\beta$, $\alpha = \Lambda_+\beta$ and $\alpha < \Lambda_+\beta$ are now considered in turn.

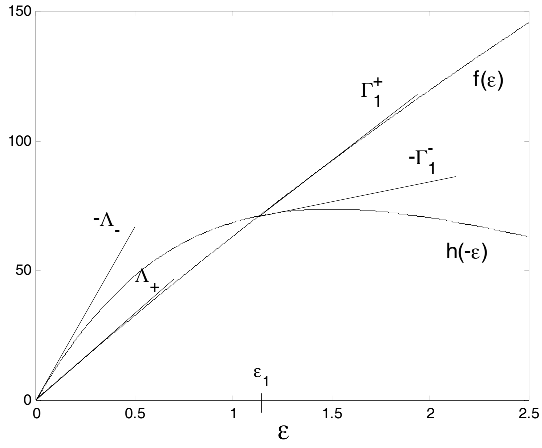

Figure 3-9: The tangents to $f(\varepsilon)$ and $h(-\varepsilon)$ at 0 and ε_1 for the choice of parameters $\alpha = 200$, $\beta = 1.5$.

1. $\alpha > \Lambda_+\beta$ $(\Lambda_+ < -\Lambda_-)$

Case (1) of figure (3-8) suggests that in this range there is only one nontrivial solution to (3.38), ε_1.

2. $\alpha < \Lambda_+\beta$ $(\Lambda_+ > -\Lambda_-)$

Case (2) of figure (3-8) suggests that in this range it is possible to have 2 nontrivial solutions of (3.38). By a continuity argument, these solutions must be created through a tangency of $f(\varepsilon)$ and $h(-\varepsilon)$. For a given β, let the value of α at which the graphs of $f(\varepsilon)$ and $h(-\varepsilon)$ are tangent at a point on the positive real line be $T(\beta)$. Then since $f(\varepsilon)$ is fixed, and $h(-\varepsilon)$ is a strictly increasing function of α for a fixed β and $\varepsilon > 0$, the geometry of $f(\varepsilon)$ and $h(-\varepsilon)$ implies that for $\alpha > T(\beta)$ there are 2 nontrivial solutions $\{\varepsilon_1, \varepsilon_2\}$ to (3.38), while for $\alpha < T(\beta)$ there are no nontrivial solutions. At the point of tangency, there is one nontrivial solution ε_1 which satisfies the pair of equations below:

$$f(\varepsilon_1) = h(-\varepsilon_1) \tag{3.43}$$

$$\Gamma_1^+ = -\Gamma_1^- \tag{3.44}$$

Using (3.43) and (3.44) it is possible to obtain a parametric representation of the curve $\alpha = T(\beta)$. For a given $\varepsilon_1 = \theta > 0$, let the corresponding values of β and α for which the curves are tangent at θ be $\beta_T(\theta)$ and $\alpha_T(\theta)$ respectively. (Note that with this notation, for $\beta = \beta_T(\theta), T(\beta) = \alpha_T(\theta)$). Substituting into equations (3.43) and (3.44) gives the following pair of equations for $\theta, \beta_T(\theta)$ and $\alpha_T(\theta)$:

$$\alpha'\left(1-e^{-\theta/\beta'}\right) = \frac{\alpha_T}{\beta_T}\theta e^{-\theta/\beta_T} \tag{3.45}$$

$$\Lambda_+ e^{-\theta/\beta'} = \frac{\alpha_T}{\beta_T}\left(1-\frac{\theta}{\beta_T}\right)e^{-\theta/\beta_T} \tag{3.46}$$

$e^{-\theta/\beta'}$ can be eliminated from (3.45) and (3.46), resulting in the following expression for $e^{-\theta/\beta_T}$:

$$e^{-\theta/\beta_T} = \frac{\beta_T\Lambda_+}{\alpha_T}\left(\left(1-\frac{\theta}{\beta_T}\right)+\frac{\theta}{\beta'}\right)^{-1} \tag{3.47}$$

Substituting (3.47) into (3.46) and rearranging for β_T yields:

$$\beta_T(\theta) = \frac{\beta'\theta\left(1-e^{\theta/\beta'}\right)}{\beta'\left(1-e^{\theta/\beta'}\right)+\theta} \tag{3.48}$$

Substituting (3.48) into (3.47) and rearranging for α_T gives:

$$\alpha_T(\theta) = \frac{\alpha'\beta_T(\theta)e^{\theta/\beta_T(\theta)}}{\beta'+\theta\left(1-\frac{\beta'}{\beta_T(\theta)}\right)} \tag{3.49}$$

Equations (3.48) and (3.49) give the curve $\alpha = T(\beta)$ in terms of the parameter θ. Note that $\beta_T(\theta)$ and $\alpha_T(\theta)$ are smooth functions of θ for $\theta > 0$, the range of interest. Differentiating $\beta_T(\theta)$ and $\alpha_T(\theta)$ in $\theta > 0$ gives

$$D\beta_T(\theta) = \frac{P(\theta)}{\left(\beta'\left(1-e^{\theta/\beta'}\right)+\theta\right)^2} \tag{3.50}$$

and

$$D\alpha_T(\theta) = \Lambda_+ e^{\theta\left(\frac{1}{\beta_T(\theta)}-\frac{1}{\beta'}\right)} D\beta_T(\theta) \tag{3.51}$$

where:

$$P(\theta) = \left(\beta'\right)^2 e^{2\theta/\beta'} - \left(2\left(\beta'\right)^2+\theta^2\right)e^{\theta/\beta'} + \left(\beta'\right)^2$$

Fix $\theta > 0$ and consider the inequality $P(\theta) > 0$:

$$P(\theta) \quad > \quad 0$$

$$\begin{aligned}
\iff (\beta')^2\left(1+e^{2\theta/\beta'}\right) &> \left(2(\beta')^2+\theta^2\right)e^{\theta/\beta'}\\
\iff (\beta')^2\left(e^{-\theta/\beta'}+e^{\theta/\beta'}\right) &> 2(\beta')^2+\theta^2\\
\iff 2(\beta')^2\left(\cosh\tfrac{\theta}{\beta'}-1\right) &> \theta^2\\
\iff \cosh\tfrac{\theta}{\beta'}-1 &> \tfrac{\theta^2}{2(\beta')^2}
\end{aligned}$$

By Taylor's Theorem, $\cosh\frac{\theta}{\beta'} = 1+\frac{\theta^2}{2(\beta')^2}+\frac{1}{6}\sinh\frac{\xi}{\beta'}\left(\frac{\theta}{\beta'}\right)^3$ for some $\xi\in(0,\theta)$. It follows from the above that $P(\theta)>0 \iff \sinh\frac{\xi}{\beta'}\left(\frac{\theta}{\beta'}\right)^3>0$. As $\theta,\xi>0$, $\sinh\frac{\xi}{\beta'}\left(\frac{\theta}{\beta'}\right)^3>0$ and so $P(\theta)>0$. Hence, $P(\theta)>0\ \forall\theta>0$. Equations (3.50) and (3.51) then imply that $D\alpha_T(\theta), D\beta_T(\theta)>0\ \forall\theta>0$. Both $\beta_T(\theta)$ and $\alpha_T(\theta)$ are thus increasing functions of θ on $(0,\infty)$.

This information can be used to understand the shape of the curve $\alpha=T(\beta)$ in the (β,α) plane. Begin by considering what happens to $\beta_T(\theta),\alpha_T(\theta)$ as $\theta\to 0$. At $\theta=0$, $\beta_T(\theta)$ is of the form $\frac{0}{0}$. It can be shown using L'Hôpital's rule that $\lim_{\theta\to 0+}\beta_T(\theta)=2\beta'$. Substituting into (3.49) implies that $\lim_{\theta\to 0+}\alpha_T(\theta)=2\alpha'$. As $\beta_T(\theta)$ and $\alpha_T(\theta)$ are increasing functions of θ, it follows that $\forall\theta>0$, $\beta_T(\theta)>2\beta'$ and $\alpha_T(\theta)>2\alpha'$. In the (β,α) plane, the curve $\alpha=T(\beta)$ therefore lies in the region $\left\{(\beta,\alpha)^T:\beta>2\beta',\alpha>2\alpha'\right\}$ with $T(\beta)\to 2\alpha'$ as $\beta\to 2\beta'+$. Since $\left(2\beta',2\alpha'\right)$ lies on the line $\alpha=\Lambda_+\beta$, this means that the curve $\alpha=T(\beta)$ converges to $\alpha=\Lambda_+\beta$ at this point.

The shape of the curve $\alpha=T(\beta)$ can be further understood by considering the derivative of $T(\beta)$. As $\beta_T(\theta)$ and $\alpha_T(\theta)$ are smooth functions of θ for $\theta>0$, $T(\beta)$ is a smooth function of β for $\beta>2\beta'$ with $DT(\beta)=\frac{D\alpha_T(\theta)}{D\beta_T(\theta)}$. Substituting (3.50) and (3.51) into this expression gives

$$DT(\beta)=\Lambda_+ e^{\theta\left(\frac{1}{\beta}-\frac{1}{\beta'}\right)} \tag{3.52}$$

where $\beta=\beta_T(\theta)$. Note that $\beta>2\beta'\Rightarrow\frac{1}{\beta}-\frac{1}{\beta'}<0\Rightarrow 0<e^{\theta\left(\frac{1}{\beta}-\frac{1}{\beta'}\right)}<1\Rightarrow 0<DT(\beta)<\Lambda_+$. Also $\lim_{\theta\to 0+}\beta_T(\theta)=2\beta'$ implies $\lim_{\beta\to 2\beta'+}DT(\beta)=\Lambda_+$. The curve $\alpha=T(\beta)$ therefore lies below the line $\alpha=\Lambda_+\beta$, converging to it tangentially at $\left(2\beta',2\alpha'\right)$ as $\beta\to 2\beta'+$. Finally, the behaviour of $T(\beta)$ as $\beta\to\infty$ can be understood by noting from (3.48) that for $\theta\gg 0$, $\beta_T(\theta)\sim\theta$. Substituting into (3.49) gives $\alpha_T(\theta)\sim\alpha' e$. Hence, as $\beta\to\infty$, $\theta\to\infty$ and so $T(\beta)\to\alpha' e$. Since $T(\beta)$ is an increasing function of β, it can be concluded that the curve $\alpha=T(\beta)$ asymptotes to the line $\alpha=\alpha' e$ from below as $\beta\to\infty$. Figure (3-10) shows the form of the curve $\alpha=T(\beta)$ together with the line $\alpha=\Lambda_+\beta$. It

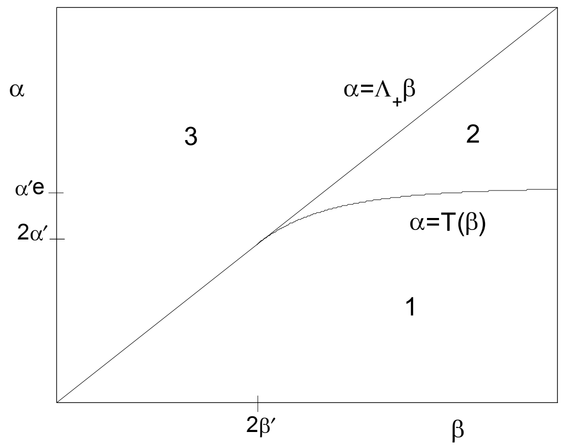

Figure 3-10: Plots of $\alpha = T(\beta)$ and $\alpha = \Lambda_+\beta$ in the (β, α) plane. These curves partition the (β, α) plane into the regions labelled 1-3 above.

should be noted that $\alpha = T(\beta)$ and $\alpha = \Lambda_+\beta$ divide the (β, α) plane into 3 sectors. These are numbered for future reference in figure (3-10).

3. $\alpha = \Lambda_+\beta$ $(\Lambda_+ = -\Lambda_-)$

For $\beta \leq 2\beta'$ cases 1 and 2 imply that there is one nontrivial solution ε_1 to (3.38) for $\alpha > \Lambda_+\beta$ and no nontrivial solutions for $\alpha < \Lambda_+\beta$. Thus, since ε_1 is a strictly increasing function of α, as $\alpha \to (\Lambda_+\beta)+$, the nontrivial solution $\varepsilon_1 \to 0+$ and at $\alpha = \Lambda_+\beta$ there are no nontrivial solutions. For $\beta > 2\beta'$ there is one nontrivial solution ε_1 for $\alpha > \Lambda_+\beta$ and two nontrivial solutions $\varepsilon_1, \varepsilon_2$ for $\alpha < \Lambda_+\beta$. Thus, since ε_2 is a strictly decreasing function of α, as $\alpha \to (\Lambda_+\beta)-$, the nontrivial solution $\varepsilon_2 \to 0+$ and at $\alpha = \Lambda_+\beta$ there is one nontrivial solution ε_1.

3.5.3 Classification in the (β, α) plane

Recall from above that a nontrivial solution ε_i of (3.38) corresponds to two nontrivial fixed points $\{\mathbf{y}_i^+, \mathbf{y}_i^-\}$ of $\dot{\mathbf{y}} = \mathbf{X}(\mathbf{y})$. Using the analysis of section 3.5.2 it is therefore possible to determine the fixed points of the burster system for each choice of α and β. The classification of the fixed points is given in table 3.1. The sector numbers refer to figure (3-10).

(β, α) range	Fixed points
Sector 1	$\mathbf{0}$
$\alpha = T(\beta)$	$\mathbf{0}, \mathbf{y}_1^+, \mathbf{y}_1^-$
Sector 2	$\mathbf{0}, \mathbf{y}_1^+, \mathbf{y}_1^-, \mathbf{y}_2^+, \mathbf{y}_2^-$
$\alpha = \Lambda_+\beta, \beta > 2\beta'$	$\mathbf{0}, \mathbf{y}_1^+, \mathbf{y}_1^-$
$\alpha = \Lambda_+\beta, \beta \leq 2\beta'$	$\mathbf{0}$
Sector 3	$\mathbf{0}, \mathbf{y}_1^+, \mathbf{y}_1^-$

Table 3.1: Fixed points of the burster system.

3.5.4 Smoothness of ε_i, x_i, $\mathbf{y}_i^{\pm}$, $\Gamma_i^{\pm}$ as functions of α and β

It was shown in the previous section that for $i = 1$ and 2, the quantities ε_i, x_i, $\mathbf{y}_i^{\pm}$, $\Gamma_i^{\pm}$ are independent of ϵ. In this section, it will be shown that these quantities are C^∞ functions of α and β in the regions R_1 and R_2 defined below:

$$\begin{aligned} R_1 &= \left\{(\alpha, \beta) : \beta \leq 2\beta', \alpha > \Lambda_+\beta\right\} \cup \left\{(\alpha, \beta) : \beta > 2\beta', \alpha > T(\beta)\right\} \\ R_2 &= \left\{(\alpha, \beta) : \beta > 2\beta', T(\beta) < \alpha < \Lambda_+\beta\right\} \end{aligned}$$

With reference to figure (3-10), R_1 is the union of sectors 2 and 3 with the line

$$\left\{(\alpha, \beta) : \beta > 2\beta', \alpha = \Lambda_+\beta\right\}$$

and R_2 is sector 2.

Consider the case $i = 1$. For $(\alpha, \beta) \in R_1$, $\varepsilon_1(\alpha, \beta)$ solves the equation $G(\varepsilon_1(\alpha, \beta); \alpha, \beta) = 0$ where $G : (0, \infty) \times R_1 \to (0, \infty)$ is defined by $G(\varepsilon; \alpha, \beta) = f(\varepsilon) - h(-\varepsilon; \alpha, \beta)$ (cf. section 3.5.1). As f and h are C^∞ on $\mathbb{R}$ and $\mathbb{R} \times (0, \infty) \times (0, \infty)$ respectively, G is C^∞ on $(0, \infty) \times R_1$. Also, $D_\varepsilon G(\varepsilon_1(\alpha, \beta); \alpha, \beta) = \Gamma_1^+(\alpha, \beta) + \Gamma_1^-(\alpha, \beta)$ and so $D_\varepsilon G(\varepsilon_1(\alpha, \beta); \alpha, \beta) > 0$ for $(\alpha, \beta) \in R_1$. It follows from the Implicit Function Theorem that $\varepsilon_1(\alpha, \beta)$ is C^∞ on R_1 [4]. Similarly, for $(\alpha, \beta) \in R_1$, $x_1(\alpha, \beta)$ solves the equation $H(x_1(\alpha, \beta); \alpha, \beta) = 0$ where $H : (0, \infty) \times R_1 \to (0, \infty)$ is defined by $H_1(x; \alpha, \beta) = \gamma x^3 + x - f(\varepsilon_1(\alpha, \beta))$ (cf. section 3.5.2). As $\varepsilon_1(\alpha, \beta)$ is C^∞ on R_1, it follows that H_1 is C^∞ on $(0, \infty) \times R_1$. Also, $D_x H_1(x_1(\alpha, \beta); \alpha, \beta) = 3\gamma x_1(\alpha, \beta)^2 + 1$ and so $D_x H_1(x_1(\alpha, \beta); \alpha, \beta) > 0$ for $(\alpha, \beta) \in R_1$. The Implicit Function Theorem then implies that $x_1(\alpha, \beta)$ is C^∞ on R_1. As both $\varepsilon_1(\alpha, \beta)$ and $x_1(\alpha, \beta)$ are C^∞ on R_1, $\mathbf{y}_i^{\pm}(\alpha, \beta) = (x_1(\alpha, \beta), x_1(\alpha, \beta), \varepsilon_1(\alpha, \beta))^T$ is also C^∞ on R_1. Moreover since $\Gamma_1^+(\alpha, \beta) = D_\varepsilon f(\varepsilon_1(\alpha, \beta))$ and $\Gamma_1^-(\alpha, \beta) = D_\varepsilon h(-\varepsilon_1(\alpha, \beta); \alpha, \beta)$, it follows from the fact that $D_\varepsilon f(\varepsilon)$ and $D_\varepsilon h(\varepsilon; \alpha, \beta)$ are C^∞ on $\mathbb{R}$ and $\mathbb{R} \times (0, \infty) \times (0, \infty)$ respectively that $\Gamma_1^+(\alpha, \beta)$ and $\Gamma_1^-(\alpha, \beta)$ are C^∞ on R_1. The case of $i = 2$ is similar.

3.5.5 Invariant lines

Recall from section 3.3 that the line $L_0 = \{(x, x, 0)^T : x \in \mathbb{R}\}$ is a stable manifold of the origin which is invariant under the symmetry. It is possible to show that every fixed point of the burster system has such a stable manifold associated with it. For a given fixed point $\mathbf{y}_* = (x_*, x_*, \varepsilon_*)^T$, define the line L_{ε_*} by $L_{\varepsilon_*} = \{(x, x, \varepsilon_*)^T : x \in \mathbb{R}\}$. Since $F(\varepsilon_*) = F(-\varepsilon_*) = F_*$ on L_{ε_*}, the equations of motion (3.2)-(3.4) can be written as $\frac{d}{d\tau}(r - l) = 0$ and $\dot{\varepsilon} = 0$. Thus for each $\mathbf{y} \in L_{\varepsilon_*}$, $\phi_\tau(\mathbf{y}) \in L_{\varepsilon_*}$ $\forall \tau \in J(\mathbf{y})$. As $[0, \infty) \subset J(\mathbf{y})$ for all $\mathbf{y} \in \mathbb{R}^3$, it follows that L_{ε_*} is positively invariant. Restricting the dynamics to L_{ε_*} gives the 1-D system:

$$\dot{x} = -(1 + \gamma x^2)x + F_* \tag{3.53}$$

This has the unique fixed point $x = x_*$. Moreover, $\dot{x} > 0$ for $x < x_*$ and $\dot{x} < 0$ for $x > x_*$, and so this fixed point is globally attracting. In terms of the whole system, it can be concluded that L_{ε_*} is a stable 1-dimensional manifold of $\mathbf{y}_*$. In particular, taking $\mathbf{y}_* = \mathbf{0}$ gives the line L_0 (setting $F_* = 0$ in (3.53) yields (3.25)), and taking $\mathbf{y}_* = \mathbf{y}_i^+$ shows that $\mathbf{y}_i^+$ has the stable manifold $L_{\varepsilon_i}^+ = \{(x, x, \varepsilon_i)^T : x \in \mathbb{R}\}$. For brevity, write $L_{\varepsilon_i}^+$ as L_i^+. Then by the symmetry, $\mathbf{y}_i^- = \sigma \mathbf{y}_i^+$ has the stable manifold $L_i^- = \sigma L_i^+ = \{(x, x, -\varepsilon_i)^T : x \in \mathbb{R}\}$. From (3.53), the dynamics on $L_i^\pm$ are given by

$$\dot{x} = -(1 + \gamma x^2)x + F_i \tag{3.54}$$

where $F_i = F(\varepsilon_i)$. Figure (3-11) shows the position of the invariant lines in the physiological state space S.

3.6 Stability of the fixed points

It has been shown in this chapter that the vector field $\mathbf{X}$ of the burster system is C^∞ smooth in an open neighbourhood of the general nontrivial fixed point $\mathbf{y}_i^\pm$. The discussion of section 1.2.3 therefore implies that if $\mathbf{y}_i^\pm$ is hyperbolic, there is a homeomorphism $H_i^\pm$ which maps an open neighbourhood $V_\mathbf{0}^\pm$ of $\mathbf{0}$ to an open neighbourhood $U_{\mathbf{y}_i^\pm}$ of $\mathbf{y}_i^\pm$ such that (i) $H_i^\pm(\mathbf{0}) = \mathbf{y}_i^\pm$, and (ii) $H_i^\pm$ maps trajectories of the linearised system $\dot{\mathbf{z}} = D\mathbf{X}(\mathbf{y}_i^\pm)\mathbf{z}$ in $V_\mathbf{0}^\pm$ to trajectories of $\dot{\mathbf{y}} = \mathbf{X}(\mathbf{y})$ in $U_{\mathbf{y}_i^\pm}$ in such a way as to preserve the parameterisation

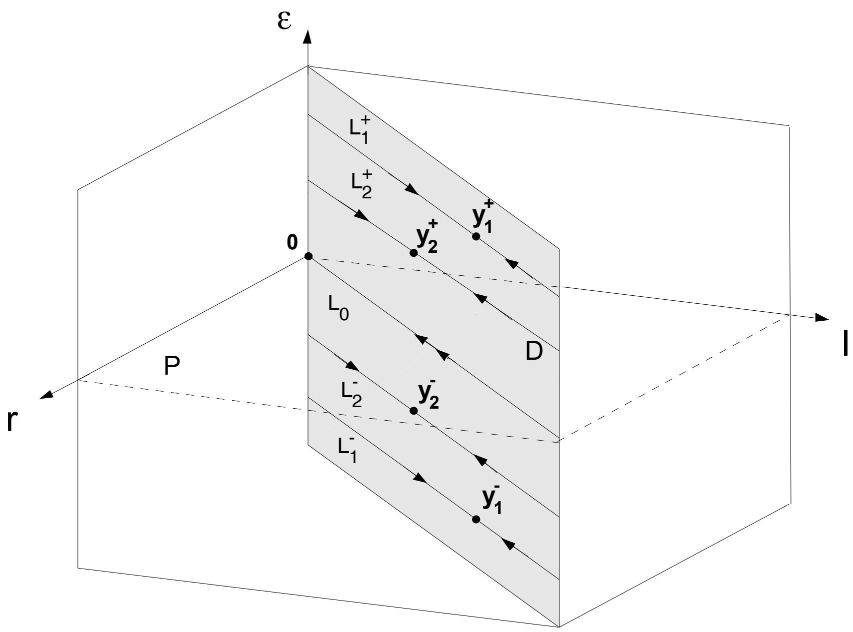

Figure 3-11: Restriction to the physiological state space S of the invariant lines $L_0, L_1^{\pm}$ and $L_2^{\pm}$ associated with the fixed points $\mathbf{0}, \mathbf{y}_1^{\pm}$ and $\mathbf{y}_2^{\pm}$ respectively. The planes D (shaded) and P and are also shown.

of trajectories with time. The stability of $\mathbf{y}_i^{\pm}$ is therefore determined by the eigenvalue spectrum of $D\mathbf{X}(\mathbf{y}_i^{\pm})$, when $\mathbf{y}_i^{\pm}$ is hyperbolic. Additionally, as long as the eigenvalues of $D\mathbf{X}(\mathbf{y}_i^{\pm})$ have no resonances of order r for any $r \geq 2$, $H_i^{\pm}$ is a C^{∞} diffeomorphism with $DH_i^{\pm}(\mathbf{0}) = \mathbf{1}_3$. In the case where $H_i^{\pm}$ is C^{∞}, a given k-dimensional invariant set $A_k^{\pm}$ of $\dot{\mathbf{z}} = D\mathbf{X}(\mathbf{y}_i^{\pm})\mathbf{z}$ containing $\mathbf{0}$ is mapped by $H_i^{\pm}$ to a k-dimensional C^{∞} local invariant manifold $M_k^{\pm}$ of $\mathbf{y}_i^{\pm}$ in $\dot{\mathbf{y}} = \mathbf{X}(\mathbf{y})$ which is tangential to $A_k^{\pm}$ at $\mathbf{y}_i^{\pm}$. The stability analysis of the fixed point at the origin is more subtle because the origin lies in the plane P where $\mathbf{X}$ is not smooth. In view of this, the stability of the nontrivial fixed points $\mathbf{y}_i^{\pm}$ is examined first.

3.6.1 Stability of the nontrivial fixed points

Recall from section 3.1.1 that $\mathbf{X}|_{N_+} = \mathbf{X}_+|_{N_+}$ and $\mathbf{X}|_{N_-} = \mathbf{X}_-|_{N_-}$. Thus, since $\mathbf{y}_i^+ \in N_+$ and $\mathbf{y}_i^- \in N_-$, $D\mathbf{X}\left(\mathbf{y}_i^{\pm}\right) = D\mathbf{X}_{\pm}\left(\mathbf{y}_i^{\pm}\right)$. Additionally, it was shown in section 3.3 that $\mathbf{X}_- \circ \sigma = \sigma \circ \mathbf{X}_+$. Applying the chain rule to both sides of this expression at $\mathbf{y} \in \mathbb{R}^3$

gives:

$$D\mathbf{X}_{-}(\sigma\mathbf{y})\sigma = \sigma D\mathbf{X}_{+}(\mathbf{y}) \tag{3.55}$$

Setting $\mathbf{y} = \mathbf{y}_i^+$ in the above and using the relation $D\mathbf{X}\left(\mathbf{y}_i^{\pm}\right) = D\mathbf{X}_{\pm}\left(\mathbf{y}_i^{\pm}\right)$ then implies:

$$D\mathbf{X}(\mathbf{y}_i^-)\sigma = \sigma D\mathbf{X}(\mathbf{y}_i^+) \tag{3.56}$$

The symmetry therefore implies a similarity relation between $D\mathbf{X}\left(\mathbf{y}_i^+\right)$ and $D\mathbf{X}(\mathbf{y}_i^-)$. The stability of the pair $\left\{\mathbf{y}_i^+, \mathbf{y}_i^-\right\}$ is therefore determined in the hyperbolic case by the eigenvalue spectrum of $D\mathbf{X}(\mathbf{y}_i^+)$.

From (3.16), given $\mathbf{y} = (r, l, \varepsilon)^T$, $D\mathbf{X}_+(\mathbf{y})$ is given by:

$$D\mathbf{X}_{+}(\mathbf{y}) = \begin{pmatrix} -\left(1+\gamma l^2\right) & -2\gamma rl & Df(\varepsilon) \\ -2\gamma lr & -\left(1+\gamma r^2\right) & -Dh(-\varepsilon) \\ -\epsilon & \epsilon & 0 \end{pmatrix} \tag{3.57}$$

Substituting $\mathbf{y}_i^+$ for $\mathbf{y}$ in (3.57) leads to the following expression for $D\mathbf{X}(\mathbf{y}_i^+)$

$$D\mathbf{X}(\mathbf{y}_i^+) = \begin{pmatrix} -\left(1+\gamma x_i^2\right) & -2\gamma x_i^2 & \Gamma_i^+ \\ -2\gamma x_i^2 & -\left(1+\gamma x_i^2\right) & -\Gamma_i^- \\ -\epsilon & \epsilon & 0 \end{pmatrix} \tag{3.58}$$

Recall that Γ_i^+ and Γ_i^- are given explicitly by:

$$\begin{aligned} \Gamma_i^+ &= \frac{\alpha'}{\beta'} e^{-\varepsilon_i/\beta'} \\ \Gamma_i^- &= -\frac{\alpha}{\beta}\left(1 - \frac{1}{\beta}\varepsilon_i\right) e^{-\varepsilon_i/\beta} \end{aligned}$$

Write $\{\mu_{i1}, \mu_{i2}, \mu_{i3}\}$ for the eigenvalues of $D\mathbf{X}(\mathbf{y}_i^+)$. It was shown above that the restriction of the dynamics to the positively invariant manifold $L_i^{\pm} = \mathbf{y}_i^{\pm} + \mathrm{Sp}\left\{(1,1,0)^T\right\}$ is

$$\dot{x} = -(1+\gamma x^2)x + F_i$$

where $F_i = F(\varepsilon_i)$ (cf. (3.53)). Linearising this about x_i gives an eigenvalue (written μ_{i1} below) of the full system with corresponding eigenvector $\mathbf{v}_{i1}^+ = (1,1,0)^T$. By factoring out

μ_{i1}, the remaining eigenvalues can easily be calculated as

$$\begin{aligned}
\mu_{i1} &= -\left(1+3\gamma x_i^2\right) \\
\mu_{i2} &= \tfrac{1}{2}\left(\Delta_i + \sqrt{\Delta_i^2 - 4\epsilon\left(\Gamma_i^+ + \Gamma_i^-\right)}\right) \\
\mu_{i3} &= \tfrac{1}{2}\left(\Delta_i - \sqrt{\Delta_i^2 - 4\epsilon\left(\Gamma_i^+ + \Gamma_i^-\right)}\right)
\end{aligned} \tag{3.59}$$

where $\Delta_i = \gamma x_i^2 - 1$. Let $\left\{\mathbf{v}_{i1}^+, \mathbf{v}_{i2}^+, \mathbf{v}_{i3}^+\right\}$ be the corresponding eigenvectors. ($\left\{\mathbf{v}_{i1}^+, \mathbf{v}_{i2}^+, \mathbf{v}_{i3}^+\right\}$ are taken to be the generalised eigenvectors of $D\mathbf{X}\left(\mathbf{y}_i^+\right)$ when the eigenvalues are not distinct). Similarly, write $\left\{\mathbf{v}_{i1}^-, \mathbf{v}_{i2}^-, \mathbf{v}_{i3}^-\right\}$ for the eigenvectors of $D\mathbf{X}\left(\mathbf{y}_i^-\right)$ corresponding to $\{\mu_{i1}, \mu_{i2}, \mu_{i3}\}$. (Again, $\left\{\mathbf{v}_{i1}^-, \mathbf{v}_{i2}^-, \mathbf{v}_{i3}^-\right\}$ are taken to be generalised eigenvectors when the eigenvalues are not distinct). The relation (3.56) implies that it is possible to choose $\left\{\mathbf{v}_{i1}^-, \mathbf{v}_{i2}^-, \mathbf{v}_{i3}^-\right\}$ so that $\mathbf{v}_{ik}^- = \sigma\mathbf{v}_{ik}^+$ $\forall 1 \le k \le 3$. This can be seen by noting that

$$\sigma\left(D\mathbf{X}(\mathbf{y}_i^+) - \mu I_3\right) = \left(D\mathbf{X}(\mathbf{y}_i^-) - \mu I_3\right)\sigma$$

from which it follows that

$$\sigma\left(D\mathbf{X}(\mathbf{y}_i^+) - \mu I_3\right)^k = \left(D\mathbf{X}(\mathbf{y}_i^-) - \mu I_3\right)^k\sigma$$

$\forall k \ge 1$. So assume $\mathbf{v}$ is a generalised eigenvector of $D\mathbf{X}(\mathbf{y}_i^+)$ corresponding to the eigenvalue μ with multiplicity $1 \le m \le 3$. $\mathbf{v}$ then satisfies:

$$\begin{gathered}
\left(D\mathbf{X}(\mathbf{y}_i^+) - \mu I_3\right)^m \mathbf{v} = \mathbf{0} \\
\Longrightarrow \sigma\left(D\mathbf{X}(\mathbf{y}_i^+) - \mu I_3\right)^m \mathbf{v} = \mathbf{0} \\
\Longrightarrow \left(D\mathbf{X}(\mathbf{y}_i^-) - \mu I_3\right)^m \sigma\mathbf{v} = \mathbf{0}
\end{gathered}$$

$\sigma\mathbf{v}$ is thus an eigenvector of $D\mathbf{X}(\mathbf{y}_i^-)$ corresponding to μ. $\left\{\mathbf{v}_{i1}^-, \mathbf{v}_{i2}^-, \mathbf{v}_{i3}^-\right\}$ can therefore be chosen to satisfy $\left[\mathbf{v}_{i1}^- \ \mathbf{v}_{i2}^- \ \mathbf{v}_{i3}^-\right] = \sigma\left[\mathbf{v}_{i1}^+ \ \mathbf{v}_{i2}^+ \ \mathbf{v}_{i3}^+\right]$ as claimed. In particular, $\mathbf{v}_{i1}^-$ can be set equal to $\sigma\mathbf{v}_{i1}^+ = (1,1,0)^T$. For the generic case when the eigenvalues are distinct, the other two eigenvectors $\mathbf{v}_{i2}^+$ and $\mathbf{v}_{i3}^+$ of $D\mathbf{X}\left(\mathbf{y}_i^+\right)$ are as below:

$$
\begin{aligned}
\mathbf{v}_{i2}^{+} &= \begin{pmatrix} \left(\Gamma_i^{+}-\Gamma_i^{-}\right)\mu_{i3}-\left(\Gamma_i^{+}+\Gamma_i^{-}\right)\left(\mu_{i2}-\mu_{i1}\right) \\ \left(\Gamma_i^{+}-\Gamma_i^{-}\right)\mu_{i3}+\left(\Gamma_i^{+}+\Gamma_i^{-}\right)\left(\mu_{i2}-\mu_{i1}\right) \\ 2\mu_{i3}\left(\mu_{i2}-\mu_{i1}\right) \end{pmatrix} \\
\mathbf{v}_{i3}^{+} &= \begin{pmatrix} \left(\Gamma_i^{+}-\Gamma_i^{-}\right)\mu_{i2}-\left(\Gamma_i^{+}+\Gamma_i^{-}\right)\left(\mu_{i3}-\mu_{i1}\right) \\ \left(\Gamma_i^{+}-\Gamma_i^{-}\right)\mu_{i2}+\left(\Gamma_i^{+}+\Gamma_i^{-}\right)\left(\mu_{i3}-\mu_{i1}\right) \\ 2\mu_{i2}\left(\mu_{i3}-\mu_{i1}\right) \end{pmatrix}
\end{aligned}
\tag{3.60}
$$

[It should be noted that when the dependence of $\mathbf{X}$ on the parameter vector $\boldsymbol{\alpha}$ is being explicitly considered, the Jacobian matrix $D\mathbf{X}(\mathbf{y}_i^{\pm})$ is $D_{\mathbf{y}}\mathbf{X}(\mathbf{y}_i^{\pm}(\alpha,\beta);\boldsymbol{\alpha})$, while the eigenvalues and eigenvectors of the Jacobian are functions of $\boldsymbol{\alpha}$, $\mu_{ij}=\mu_{ij}(\boldsymbol{\alpha})$, $\mathbf{v}_{ij}^{\pm}=\mathbf{v}_{ij}^{\pm}(\boldsymbol{\alpha})$, $1\leq i\leq 2$, $1\leq j\leq 3$. Also, as x_i is a function of α and β, $\Delta_i=\gamma x_i^2-1$ will be a function of α and β, $\Delta_i=\Delta_i(\alpha,\beta)$].

Returning to the eigenvalue spectrum of $D\mathbf{X}(\mathbf{y}_i^{+})$, since μ_{i1} is always <0, it follows that $\mathbf{y}_i^{\pm}$ is stable if $\mathrm{Re}(\mu_{i2}),\mathrm{Re}(\mu_{i3})<0$ and unstable if $\mathrm{Re}\{\mu_{i2}\}\,\mathrm{Re}\{\mu_{i3}\}\neq 0$ with $\mathrm{Re}\{\mu_{i2}\}>0$ or $\mathrm{Re}\{\mu_{i3}\}>0$. If for a given $\boldsymbol{\alpha}$ one or both of $\{\mu_{i2},\mu_{i3}\}$ have real part equal to 0, $\mathbf{y}_i^{\pm}$ is nonhyperbolic and so the burster system undergoes a local bifurcation at this choice of parameters [4]. The stability of the fixed points $\mathbf{y}_2^{\pm}$ and $\mathbf{y}_1^{\pm}$ will now be examined by consideration of the pairs $\{\mu_{22},\mu_{23}\}$ and $\{\mu_{12},\mu_{13}\}$ respectively.

The stability of $\mathbf{y}_2^{\pm}$

From (3.59), μ_{22} and μ_{23} are given by

$$
\begin{aligned}
\mu_{22} &= \tfrac{1}{2}\left(\Delta_2+\sqrt{\Delta_2^2-4\epsilon\left(\Gamma_2^{+}+\Gamma_2^{-}\right)}\right) \\
\mu_{23} &= \tfrac{1}{2}\left(\Delta_2-\sqrt{\Delta_2^2-4\epsilon\left(\Gamma_2^{+}+\Gamma_2^{-}\right)}\right)
\end{aligned}
\tag{3.61}
$$

where $\Delta_2=\gamma x_2^2-1$. Consideration of the forms of $f(\varepsilon)$ and $h(-\varepsilon)$ on $\varepsilon>0$ indicates that $\Gamma_2^{+}<-\Gamma_2^{-}$ (cf. figures (3-8) and (3-9)). μ_{22} and μ_{23} are therefore both real. Moreover, $\sqrt{\Delta_2^2-4\epsilon\left(\Gamma_2^{+}+\Gamma_2^{-}\right)}>|\Delta_2|$, and so $\mu_{22}>0$ and $\mu_{23}<0$. It follows that $\mathbf{y}_2^{\pm}$ is always unstable.

The stability of $\mathbf{y}_1^{\pm}$

From (3.59), μ_{12} and μ_{13} are given by

$$\begin{array}{rcl}\mu_{12} & = & \frac{1}{2}\left(\Delta_1 + \sqrt{\Delta_1^2 - 4\epsilon\left(\Gamma_1^+ + \Gamma_1^-\right)}\right) \\ \mu_{13} & = & \frac{1}{2}\left(\Delta_1 - \sqrt{\Delta_1^2 - 4\epsilon\left(\Gamma_1^+ + \Gamma_1^-\right)}\right)\end{array} \tag{3.62}$$

where $\Delta_1 = \gamma x_1^2 - 1$. Consideration of the forms of $f(\varepsilon)$ and $h(-\varepsilon)$ on $\varepsilon > 0$ indicates that $\Gamma_1^+ + \Gamma_1^- > 0$, except on the curve $\alpha = T(\beta)$ where $\Gamma_1^+ + \Gamma_1^- = 0$ (cf. figures (3-8) and (3-9)). The stability of $\mathbf{y}_1^{\pm}$ therefore depends the sign of Δ_1. In view of this, the sign of Δ_1 in the regions of the (β, α) plane where $\mathbf{y}_1^{\pm}$ exists is now found.

- The sign of Δ_1

Recall from section 3.5.3 that $\mathbf{y}_1^{\pm} = (x_1, x_1, \pm\varepsilon_1)^T$ exists in the ranges $\{\alpha > \Lambda_+\beta\}$ and $\{\alpha \leq \Lambda_+\beta, \alpha \geq T(\beta)\}$ (sectors 2 and 3 of figure (3-10) together with the line $\alpha = \Lambda_+\beta$ for $\beta > 2\beta'$ and the curve $\alpha = T(\beta)$). Also recall from section 3.5.1 that ε_1 and x_1 satisfy the pair of equations

$$f(\varepsilon_1) = h(-\varepsilon_1) \tag{3.63}$$

$$\gamma x_1^3 + x_1 - f(\varepsilon_1) = 0 \tag{3.64}$$

and that x_1 is a strictly increasing function of ε_1 with $x_1 < x_M$, where x_M is the real root of the polynomial $\gamma x^3 + x - \alpha'$. Since $\Delta_1 = \gamma x_1^2 - 1$, this means that $\operatorname{sign}\{\Delta_1\} = \operatorname{sign}\left\{x_1 - \frac{1}{\sqrt{\gamma}}\right\}$.

When $\alpha' = \frac{2}{\sqrt{\gamma}}$, $x_M = \frac{1}{\sqrt{\gamma}}$. Since x_M is an increasing function of α' (cf. figure (3-7)), $x_M \leq \frac{1}{\sqrt{\gamma}}$ for $\alpha' \leq \frac{2}{\sqrt{\gamma}}$, in which case $\Delta_1 < 0$. Conversely, for Δ_1 to exceed zero, it is necessary to have $\alpha'\sqrt{\gamma} > 2$. This is certainly possible since $\alpha' = 600$ and $\gamma = 0.05$, giving $\alpha'\sqrt{\gamma} = 134.16$. Let the value of ε_1 when $x_1 = \frac{1}{\sqrt{\gamma}}$ be ε_H. Then as x_1 is a strictly increasing function of ε_1, $\operatorname{sign}\{\Delta_1\} = \operatorname{sign}\{\varepsilon_1 - \varepsilon_H\}$. Consideration of (3.64) shows that ε_H depends only on the fixed parameters α', β' and γ. It is possible to find ε_H explicitly. Setting $x_1 = \frac{1}{\sqrt{\gamma}}$ and $\varepsilon_1 = \varepsilon_H$ in (3.64) gives $f(\varepsilon_H) = \frac{2}{\sqrt{\gamma}}$. Using (3.5) this can be written as:

$$\alpha'(1 - e^{-\varepsilon_H/\beta'}) = \frac{2}{\sqrt{\gamma}}$$

Solving for ε_H then gives

$$\varepsilon_H = \ln\left(\frac{\alpha'\sqrt{\gamma}}{\alpha'\sqrt{\gamma}-2}\right)^{\beta'} \tag{3.65}$$

which has the approximate numerical value 0.13517413.

In analysing the sign of Δ_1, it is useful to consider the cases $\beta \leq 2\beta'$ and $\beta > 2\beta'$ separately.

1. $\beta > 2\beta'$.

When $\beta > 2\beta'$, $\mathbf{y}_1^+$ exists for $\alpha \geq T(\beta)$. Recall from section 3.5.2 that on the curve $\alpha = T(\beta)$, $f(\varepsilon)$ and $h(-\varepsilon)$ intersect tangentially on the positive real line at $\varepsilon_1 = \theta$, and that β is a strictly increasing function of θ with $\beta \to 2\beta'+$ as $\theta \to 0+$. It follows that there is some value of β, β_2 say, with $\beta_2 > 2\beta'$ at which $\theta = \varepsilon_H$. Let $\alpha_2 = T(\beta_2)$. Then, since ε_1 is a strictly increasing function of α for a fixed β, it follows that for $\beta \geq \beta_2$, $\varepsilon_1 > \varepsilon_H$ except for at $\{\beta = \beta_2, \alpha = \alpha_2\}$ where $\varepsilon_1 = \varepsilon_H$. Hence, for $\beta \geq \beta_2$, $\Delta_1 > 0$ except for at $\beta = \beta_2, \alpha = \alpha_2$ where $\Delta_1 = 0$. β_2 and α_2 can be found explicitly by substituting $\theta = \varepsilon_H$ into (3.48) and (3.49) giving

$$\beta_2 = \frac{2\beta'\varepsilon_H}{2\beta' - \varepsilon_H\left(\alpha'\sqrt{\gamma}-2\right)} \tag{3.66}$$

and:

$$\alpha_2 = \frac{2\beta_2 e^{\varepsilon_H/\beta_2}}{\varepsilon_H\sqrt{\gamma}} \tag{3.67}$$

Note that α', β', γ and ε_H are all fixed and so β_2 and α_2 are constants. β_2 and α_2 have the approximate numerical values $\beta_2 = 18.045171$ and $\alpha_2 = 1203$. For $2\beta' < \beta < \beta_2$, $\varepsilon_1 < \varepsilon_H$ on $\alpha = T(\beta)$. Thus, since ε_1 is a strictly increasing function of α for a fixed β, given a value of β in this range there is a value of α, $\alpha_H(\beta)$ with $\alpha_H(\beta) > T(\beta)$ for which $\varepsilon_1 = \varepsilon_H$. Hence, for $2\beta' < \beta < \beta_2$, $\operatorname{sign}\{\Delta_1\} = \operatorname{sign}\{\alpha - \alpha_H(\beta)\}$.

2. $\beta \leq 2\beta'$

In this range, $\mathbf{y}_1^\pm$ exists for $\alpha > \Lambda_+\beta$, with $\varepsilon_1 \to 0+$ as $\alpha \to (\Lambda_+\beta)+$. Hence, since ε_1 is a strictly increasing function of α for a fixed β, for each value of β in this range there is a value of α, $\alpha_H(\beta)$, for which $\varepsilon_1 = \varepsilon_H$, as in the case $2\beta' < \beta < \beta_2$ above. Also, as for $2\beta' < \beta < \beta_2$, $\operatorname{sign}\{\Delta_1\} = \operatorname{sign}\{\alpha - \alpha_H(\beta)\}$.

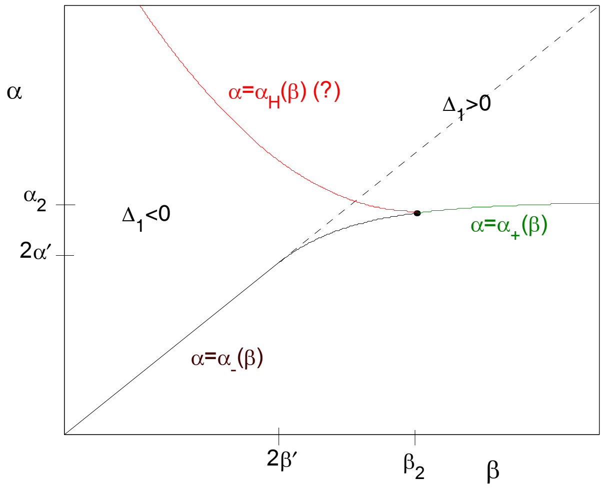

Figure 3-12: The sign of Δ_1.

In conclusion, it has been shown that for $\beta \geq \beta_2$, $\Delta_1 > 0$ except at $\{\beta = \beta_2, \alpha = \alpha_2\}$ where $\Delta_1 = 0$. For $\beta < \beta_2$, sign $\{\Delta_1\} =$ sign $\{\alpha - \alpha_H(\beta)\}$, where $\alpha_H(\beta) > \Lambda_+\beta$ for $\beta \leq 2\beta'$ and $\alpha_H(\beta) > T(\beta)$ for $2\beta' < \beta < \beta_2$. The results on the sign of Δ_1 can be expressed in a simple form by introducing the function $\alpha_- : (0, \beta_2] \to \mathbb{R}^+$ defined by

$$\alpha_-(\beta) = \begin{cases} \Lambda_+\beta & \text{if} \quad \beta \leq 2\beta' \\ T(\beta) & \text{if} \quad 2\beta' < \beta \leq \beta_2 \end{cases}$$

and the function $\alpha_+ : [\beta_2, \infty) \to \mathbb{R}^+$ defined by $\alpha_+(\beta) = T(\beta)\ \forall \beta \geq \beta_2$. The curves $\alpha = \alpha_-(\beta)$ and $\alpha = \alpha_+(\beta)$ intersect at the point (β_2, α_2) in the (β, α) plane. The curve $\alpha = \alpha_H(\beta)$ lies between these, in the sense that a continuous clockwise path about (β_2, α_2) from a point on $\alpha = \alpha_-(\beta)$ to a point on $\alpha = \alpha_+(\beta)$ passes through $\alpha = \alpha_H(\beta)$. It has been shown that $\Delta_1 < 0$ for (β, α) lying between $\alpha = \alpha_-(\beta)$ and $\alpha = \alpha_H(\beta)$, while $\Delta_1 > 0$ for (β, α) lying between $\alpha = \alpha_+(\beta)$ and $\alpha = \alpha_H(\beta)$. This is illustrated in figure (3-12).

An expression for $\alpha_H(\beta)$ can be found explicitly, enabling the precise form of the curve $\alpha = \alpha_H(\beta)$ to be established.

- The function $\alpha = \alpha_H(\beta)$

Setting $\varepsilon_1 = \varepsilon_H$ in (3.63) and using the fact that $f(\varepsilon_H) = \frac{2}{\sqrt{\gamma}}$ together with expression (3.6) for $h(\varepsilon)$ leads to the following equation involving α_H, β and ε_H:

$$\frac{2}{\sqrt{\gamma}} = \frac{\alpha_H}{\beta} \varepsilon_H e^{-\varepsilon_H/\beta}$$

Rearranging for α_H gives:

$$\alpha_H(\beta) = \frac{2}{\varepsilon_H \sqrt{\gamma}} \beta e^{\varepsilon_H/\beta} \tag{3.68}$$

Clearly $\alpha_H(\beta)$ is smooth on $(0, \beta_2)$, the range of interest. The derivative $D\alpha_H(\beta)$ of $\alpha_H(\beta)$ is given by:

$$D\alpha_H(\beta) = \frac{2}{\varepsilon_H \sqrt{\gamma}} \left(1 - \frac{\varepsilon_H}{\beta}\right) e^{\varepsilon_H/\beta} \tag{3.69}$$

This implies that $D\alpha_H(\varepsilon_H) = 0$ with $D\alpha_H(\beta) < 0$ for $\beta < \varepsilon_H$ and $D\alpha_H(\beta) > 0$ for $\beta > \varepsilon_H$. The graph of $\alpha_H(\beta)$ thus has a global minimum at $\beta = \varepsilon_H$ and no other extrema. Setting $\beta = \varepsilon_H$ in (3.68) gives $\alpha_H(\varepsilon_H) = \frac{2e}{\sqrt{\gamma}}$, which has the approximate numerical value 24.3131. So consider the form of the curve $\alpha = \alpha_H(\beta)$ in the (β, α) plane. It can be seen from (3.68) that $\lim_{\beta \to \beta_2 -} \alpha_H(\beta) = \alpha_2$ (cf. (3.67)), and so $\alpha = \alpha_H(\beta)$ converges to the curve $\alpha = T(\beta)$ from above as $\beta \to \beta_2-$. Also, it can be shown using (3.66) and (3.69) that $\lim_{\beta \to \beta_2 -} D\alpha_H(\beta) = \Lambda_+ e^{\varepsilon_H\left(\frac{1}{\beta_2} - \frac{1}{\beta'}\right)}$. Setting $\beta = \beta_2$ in (3.52) gives $DT(\beta_2) = \Lambda_+ e^{\varepsilon_H\left(\frac{1}{\beta_2} - \frac{1}{\beta'}\right)}$ implying that $\alpha = \alpha_H(\beta)$ becomes tangential to $\alpha = T(\beta)$ as $\beta \to \beta_2-$. Additionally, since $\alpha = \alpha_H(\beta)$ converges to the curve $\alpha = T(\beta)$ from above as $\beta \to \beta_2-$, and $T(\beta) < \Lambda_+\beta$ for $\beta > 2\beta'$, $\alpha = \alpha_H(\beta)$ must intersect the line $\alpha = \Lambda_+\beta$ at some value of β, β_1 say, with $2\beta' < \beta_1 < \beta_2$. From (3.68), $\alpha_H(\beta_1) = \Lambda_+\beta_1$ is equivalent to:

$$\frac{2}{\varepsilon_H \sqrt{\gamma}} \beta_1 e^{\varepsilon_H/\beta_1} = \Lambda_+ \beta_1$$

Dividing through by β_1 and rearranging gives:

$$\beta_1 = \frac{\varepsilon_H}{\ln\left(\frac{\Lambda_+ \sqrt{\gamma} \varepsilon_H}{2}\right)} \tag{3.70}$$

Write α_1 for the corresponding value of α, so $\alpha_1 = \Lambda_+\beta_1$. β_1 and α_1 have the approximate numerical values $\beta_1 = 18.022557$ and $\alpha_1 = 1201.5$. Note that $\alpha_1 < \alpha_2$. Finally, (3.68) shows that $\alpha_H(\beta) \to \infty$ as $\beta \to 0+$, implying that $\alpha = \alpha_H(\beta)$ asymptotes to the α axis

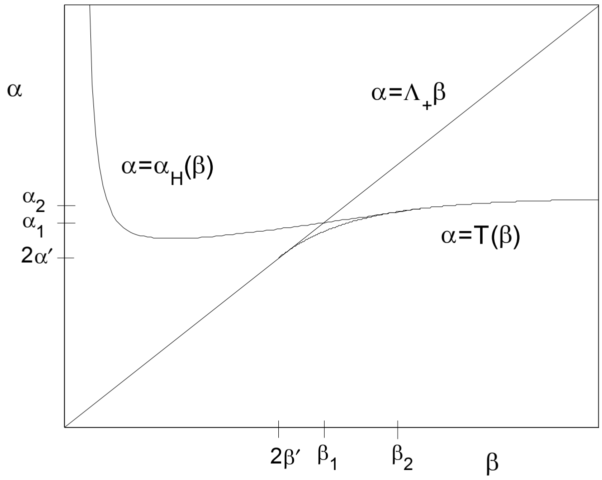

Figure 3-13: Plots of $\alpha = \alpha_H(\beta)$, $\alpha = T(\beta)$ and $\alpha = \Lambda_+\beta$ in the (β, α) plane.

as $\beta \to 0+$. The form of the curve $\alpha = \alpha_H(\beta)$ is shown in figure (3-13) together with $\alpha = T(\beta)$ and $\alpha = \Lambda_+\beta$.

It will be necessary when discussing bifurcations of the burster system in Chapter 4 to use the values of Γ_1^+ and Γ_1^- when $\alpha = \alpha_H(\beta)$. Denote these values by $\left(\Gamma_1^+\right)_H$ and $\left(\Gamma_1^-\right)_H$ respectively. Then from (3.41), (3.42) and (3.65), $\left(\Gamma_1^+\right)_H$ and $\left(\Gamma_1^-\right)_H$ are given explicitly by:

$$\left(\Gamma_1^+\right)_H = \Lambda_+\left(1 - \frac{2}{\alpha'\sqrt{\gamma}}\right) \tag{3.71}$$

$$\left(\Gamma_1^-\right)_H = \frac{2}{\sqrt{\gamma}}\left(\frac{1}{\beta} - \frac{1}{\varepsilon_H}\right) \tag{3.72}$$

Note that since α', β', γ and ε_H are fixed, when $\left(\Gamma_1^+\right)_H$ and $\left(\Gamma_1^-\right)_H$ are considered as functions of $\boldsymbol{\alpha}$, $\left(\Gamma_1^+\right)_H$ is a constant while $\left(\Gamma_1^-\right)_H$ is a function of β, $\left(\Gamma_1^-\right)_H = \left(\Gamma_1^-\right)_H(\beta)$. $\left(\Gamma_1^+\right)_H$ has the approximate numerical value 65.6728.

- Stability

The stability of $\mathbf{y}_1^{\pm}$ can now be fully addressed. Recall the expressions for μ_{12} and μ_{13} given at the beginning of this section:

$$\begin{aligned} \mu_{12} &= \tfrac{1}{2}\left(\Delta_1 + \sqrt{\Delta_1^2 - 4\epsilon\left(\Gamma_1^+ + \Gamma_1^-\right)}\right) \\ \mu_{13} &= \tfrac{1}{2}\left(\Delta_1 - \sqrt{\Delta_1^2 - 4\epsilon\left(\Gamma_1^+ + \Gamma_1^-\right)}\right) \end{aligned} \tag{3.73}$$

It has been argued above that $\Gamma_1^+ + \Gamma_1^- = 0$ for $\alpha = T(\beta)$ and $\Gamma_1^+ + \Gamma_1^- > 0$ everywhere else. Also, $\Delta_1 < 0$ for (β, α) lying between $\alpha = \alpha_- (\beta)$ and $\alpha = \alpha_H (\beta)$, $\Delta_1 = 0$ on $\alpha = \alpha_H (\beta)$, and $\Delta_1 > 0$ for α lying between $\alpha = \alpha_H (\beta)$ and $\alpha = \alpha_+ (\beta)$. In view of this, the pair $\{\mu_{12}, \mu_{13}\}$ is now considered in turn for (β, α) lying between $\alpha = \alpha_- (\beta)$ and $\alpha = \alpha_+ (\beta)$ with $\alpha \neq \alpha_H(\beta)$, for $\alpha = \alpha_H (\beta)$ and for $\alpha = T (\beta)$.

1. (β, α) lying between $\alpha = \alpha_- (\beta)$ and $\alpha = \alpha_+ (\beta)$ with $\alpha \neq \alpha_H(\beta)$

In order to establish the forms of μ_{12} and μ_{13} in this range, it is necessary to determine the sign of the quantity $\Delta_1^2 - 4\epsilon \left(\Gamma_1^+ + \Gamma_1^-\right)$. Fix $\epsilon > 0$, and assume (β, α) lies between $\alpha = \alpha_- (\beta)$ and $\alpha = \alpha_H (\beta)$. As $\alpha \to \alpha_H (\beta) -$, $\Delta_1 \to 0$ and $\Gamma_1^+ + \Gamma_1^- \to \left(\Gamma_1^+\right)_H + \left(\Gamma_1^-\right)_H > 0$. Thus, $\Delta_1^2 - 4\epsilon \left(\Gamma_1^+ + \Gamma_1^-\right) < 0$ for $\alpha - \alpha_H (\beta) < 0$ sufficiently small. Now as $\alpha \to (\Lambda_+ \beta) +$ in $\beta \leq 2\beta'$, $\varepsilon_1 \to 0$. This implies that $\Gamma_1^+ + \Gamma_1^- \to \Lambda_+ + \Lambda_-$ as $\alpha \to (\Lambda_+ \beta) +$. However at $\alpha = \Lambda_+ \beta$, $\Lambda_+ + \Lambda_- = 0$ and so $\Gamma_1^+ + \Gamma_1^- \to 0$ as $\alpha \to (\Lambda_+ \beta) +$. Thus, since $\Delta_1 \to -1$ as $\alpha \to (\Lambda_+ \beta) +$, it follows that $\Delta_1^2 - 4\epsilon \left(\Gamma_1^+ + \Gamma_1^-\right) > 0$ for $\alpha - \Lambda_+ \beta > 0$ sufficiently small in $\beta \leq 2\beta'$. Also, $\Gamma_1^+ + \Gamma_1^- \to 0$ as $\alpha \to T (\beta) +$ in $2\beta' < \beta < \beta_2$. Let the value of Δ_1 when $\alpha = T (\beta)$ be $\bar{\Delta}_1$. Then $\bar{\Delta}_1 < 0$ and so as $\alpha \to T (\beta) +$, $\Delta_1^2 \to \bar{\Delta}_1^2$ with $\bar{\Delta}_1^2 > 0$. It follows that for $\alpha - T (\beta) > 0$ sufficiently small in $2\beta' < \beta < \beta_2$, $\Delta_1^2 - 4\epsilon \left(\Gamma_1^+ + \Gamma_1^-\right) > 0$. Combining these last two results implies that $\Delta_1^2 - 4\epsilon \left(\Gamma_1^+ + \Gamma_1^-\right) > 0$ for $\alpha - \alpha_- (\beta) > 0$ sufficiently small.

It has been argued thus far that for a fixed $\epsilon > 0$, given (β, α) lying between $\alpha = \alpha_- (\beta)$ and $\alpha = \alpha_H (\beta)$, $\Delta_1^2 - 4\epsilon \left(\Gamma_1^+ + \Gamma_1^-\right) < 0$ for $\alpha - \alpha_H (\beta) < 0$ sufficiently small and $\Delta_1^2 - 4\epsilon \left(\Gamma_1^+ + \Gamma_1^-\right) > 0$ for $\alpha - \alpha_- (\beta) > 0$ sufficiently small. This fact, together with the standard trace/determinant stability picture of linear systems in the plane, suggests that for each $\epsilon > 0$, there is a single curve $\alpha = R_- (\beta, \epsilon)$ in the (β, α) plane lying between $\alpha = \alpha_- (\beta)$ and $\alpha = \alpha_H (\beta)$ on which $\Delta_1^2 - 4\epsilon \left(\Gamma_1^+ + \Gamma_1^-\right) = 0$ [4]. Hence, for (β, α) lying between $\alpha = \alpha_- (\beta)$ and $\alpha = R_- (\beta, \epsilon)$, $\Delta_1^2 - 4\epsilon \left(\Gamma_1^+ + \Gamma_1^-\right) > 0$. μ_{12} and μ_{13} are therefore real. Moreover since $\Delta_1 < 0$ and $\Gamma_1^+ + \Gamma_1^- > 0$ in this range, $\mu_{13} < \mu_{12} < 0$. For (β, α) lying between $\alpha = R_- (\beta, \epsilon)$ and $\alpha = \alpha_H (\beta)$, $\Delta_1^2 - 4\epsilon \left(\Gamma_1^+ + \Gamma_1^-\right) < 0$. μ_{12} and μ_{13} are therefore complex conjugate with $\mathrm{Re}\{\mu_{12}\} = \mathrm{Re}\{\mu_{13}\} = \frac{1}{2}\Delta_1 < 0$. For $\alpha = R_- (\beta, \epsilon)$, $\Delta_1^2 - 4\epsilon \left(\Gamma_1^+ + \Gamma_1^-\right) = 0$, implying that $\mu_{12} = \mu_{13} = \frac{1}{2}\Delta_1 < 0$.

Now assume that (β, α) lies between $\alpha = \alpha_H (\beta)$ and $\alpha = \alpha_+ (\beta)$. A similar argument to the one above implies that for each $\epsilon > 0$, there is a single curve $\alpha = R_+ (\beta, \epsilon)$ in the (β, α) plane lying between $\alpha = \alpha_H (\beta)$ and $\alpha = \alpha_+ (\beta)$ on which $\Delta_1^2 - 4\epsilon \left(\Gamma_1^+ + \Gamma_1^-\right) = 0$. For (β, α) lying

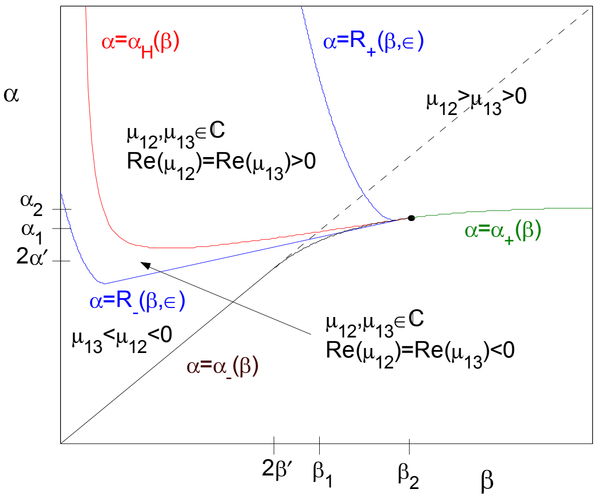

Figure 3-14: The signs of μ_{12} and μ_{13} in the (β, α) plane.

between $\alpha = \alpha_+(\beta)$ and $\alpha = R_+(\beta, \epsilon)$, $\Delta_1^2 - 4\epsilon\left(\Gamma_1^+ + \Gamma_1^-\right) > 0$. μ_{12} and μ_{13} are therefore real. Moreover, since Δ_1 and $\Gamma_1^+ + \Gamma_1^-$ are both greater than zero in this range, $\mu_{12} > \mu_{13} > 0$. For (β, α) lying between $\alpha = R_+(\beta, \epsilon)$ and $\alpha = \alpha_H(\beta)$, $\Delta_1^2 - 4\epsilon\left(\Gamma_1^+ + \Gamma_1^-\right) < 0$. μ_{12} and μ_{13} are therefore complex conjugate with $\mathrm{Re}\{\mu_{12}\} = \mathrm{Re}\{\mu_{13}\} = \frac{1}{2}\Delta_1 > 0$. For $\alpha = R_+(\beta, \epsilon)$, $\Delta_1^2 - 4\epsilon\left(\Gamma_1^+ + \Gamma_1^-\right) = 0$, implying that $\mu_{12} = \mu_{13} = \frac{1}{2}\Delta_1 > 0$.

The signs of μ_{12} and μ_{13} in the (β, α) plane are summarised in figure (3-14). The analysis above implies that in the range of interest, $\mathbf{y}_1^{\pm}$ is stable for (β, α) lying between $\alpha = \alpha_-(\beta)$ and $\alpha = \alpha_H(\beta)$ and unstable for (β, α) lying between $\alpha = \alpha_H(\beta)$ and $\alpha = \alpha_+(\beta)$.

It is useful to consider what happens to the curves $\alpha = R_-(\beta, \epsilon)$ and $\alpha = R_+(\beta, \epsilon)$ as $\epsilon \to 0$ and $\epsilon \to \infty$. So fix (β, α) lying between $\alpha = R_-(\beta, \epsilon)$ and $\alpha = \alpha_H(\beta)$. In this range $\Delta_1^2 - 4\epsilon\left(\Gamma_1^+ + \Gamma_1^-\right) < 0$. Since Δ_1 and $\Gamma_1^+ + \Gamma_1^-$ are functions of α and β only, they are fixed. By decreasing ϵ it is therefore possible to make $\Delta_1^2 - 4\epsilon\left(\Gamma_1^+ + \Gamma_1^-\right) > 0$, and hence for the curve $\alpha = R_-(\beta, \epsilon)$ to lie above (β, α). This can be done for (β, α) lying arbitrarily close to $\alpha = \alpha_H(\beta)$, implying that the curve $\alpha = R_-(\beta, \epsilon)$ converges to the curve $\alpha = \alpha_H(\beta)$ as $\epsilon \to 0$. Now fix (β, α) lying between $\alpha = \alpha_-(\beta)$ and $\alpha = R_-(\beta, \epsilon)$. In this range $\Delta_1^2 - 4\epsilon\left(\Gamma_1^+ + \Gamma_1^-\right) > 0$. By increasing ϵ it is possible to make $\Delta_1^2 - 4\epsilon\left(\Gamma_1^+ + \Gamma_1^+\right) < 0$, and hence for the curve $\alpha = R_-(\beta, \epsilon)$ to lie below (β, α). This can be done for (β, α) lying arbitrarily close to $\alpha = \alpha_-(\beta)$, implying that the curve $\alpha = R_-(\beta, \epsilon)$ converges to the curve $\alpha = \alpha_-(\beta)$ as $\epsilon \to \infty$. Similar arguments show that $\alpha = R_+(\beta, \epsilon)$ converges to $\alpha = \alpha_H(\beta)$ as $\epsilon \to 0$ and to $\alpha = \alpha_+(\beta)$ as $\epsilon \to \infty$.

2. $\alpha = \alpha_H(\beta)$

Setting $\Delta_1 = 0$ in (3.73) gives $\mu_{12} = -\mu_{13} = i\sqrt{\epsilon\left(\Gamma_1^+ + \Gamma_1^-\right)}$. $\mathbf{y}_1^{\pm}$ is thus nonhyperbolic for this choice of parameters. The burster system will undergo a codimension 1 bifurcation at $\mathbf{y}_1^{\pm}$ when $\alpha = \alpha_H(\beta)$, which is generically a Hopf bifurcation [4].

3. $\alpha = T(\beta)$

Setting $\Gamma_1^+ + \Gamma_1^- = 0$ in (3.62) gives $\mu_{12} = \frac{1}{2}(\Delta_1 + |\Delta_1|)$ and $\mu_{13} = \frac{1}{2}(\Delta_1 - |\Delta_1|)$. For $\beta < \beta_2$, $\Delta_1 < 0$ giving $\mu_{12} = 0$ and $\mu_{13} = \Delta_1 < 0$. For $\beta > \beta_2$, $\Delta_1 > 0$ giving $\mu_{12} = \Delta_1 > 0$ and $\mu_{13} = 0$. $\mathbf{y}_1^{\pm}$ is thus nonhyperbolic on $\alpha = T(\beta)$ for $\beta \neq \beta_2$. In this range, the burster system will undergo a codimension 1 bifurcation at $\mathbf{y}_1^{\pm}$, which is generically a saddlenode bifurcation [4]. For $\beta = \beta_2$ on $\alpha = T(\beta)$, $\alpha = \alpha_2$ and so $\Delta_1 = 0$, giving $\mu_{12} = \mu_{13} = 0$. For $\{\beta = \beta_2, \alpha = \alpha_2\}$, $\mathbf{y}_1^{\pm}$ is therefore nonhyperbolic. At this point, the burster system undergoes a codimension 2 bifurcation at $\mathbf{y}_1^{\pm}$.

Note that both the stabilities of $\left\{\mathbf{y}_1^{\pm}, \mathbf{y}_2^{\pm}\right\}$, and the values of the parameters at which local bifurcations occur are dependent only on α and β: they are independent of ϵ.

The results concerning the stability of $\mathbf{y}_i^{\pm}$ obtained so far in this section have used the fact that the linearising map $H_i^{\pm} : V_{\mathbf{0}}^{\pm} \to U_{\mathbf{y}_i^{\pm}}$ is a homeomorphism. This has enabled the stability of $\mathbf{y}_i^{\pm}$ to be determined by the signs of the real parts of the eigenvalues of $D\mathbf{X}(\mathbf{y}_i^{\pm})$, in regions of the (β, α) plane where it is hyperbolic. It has been shown in this way that $\mathbf{y}_2^{\pm}$ is always unstable, while $\mathbf{y}_1^{\pm}$ is stable for (β, α) lying between $\alpha = \alpha_-(\beta)$ and $\alpha = \alpha_H(\beta)$ and unstable for (β, α) lying between $\alpha = \alpha_H(\beta)$ and $\alpha = \alpha_+(\beta)$. By using the fact that $H_i^{\pm}$ is generically a C^∞ diffeomorphism with $DH_i^{\pm}(\mathbf{0}) = \mathbf{1}_3$, a more detailed picture of the local dynamics of the burster system at the fixed points can now be obtained. This analysis will come in useful when discussing bifurcations in Chapter 4.[2]

Local dynamics at $\mathbf{y}_2^{\pm}$

It was shown above that $\mu_{23} < 0$ and $\mu_{22} > 0$. Hence, given $\boldsymbol{\alpha}$ such that $\mathbf{y}_2^{\pm}$ exists, the origin is a saddle node of $\dot{\mathbf{z}} = D\mathbf{X}(\mathbf{y}_2^{\pm})\mathbf{z}$, with an unstable invariant line $\mathrm{Sp}\left\{\mathbf{v}_{22}^{\pm}\right\}$,

[2] It should be kept in mind during the following analysis that if the dependence of $\mathbf{X}$ on $\boldsymbol{\alpha}$ were being explicitly considered, all local invariant manifolds of $\mathbf{y}_i^{\pm}$ in $\dot{\mathbf{y}} = \mathbf{X}(\mathbf{y})$ would be functions of $\boldsymbol{\alpha}$, as would all eigenvectors.

and a stable invariant plane $\mathrm{Sp}\left\{(1,1,0)^T, \mathbf{v}_{23}^{\pm}\right\}$ on which the origin is a stable node [27]. Typical trajectories $\mathbf{z}(\tau)$ of $\dot{\mathbf{z}} = D\mathbf{X}(\mathbf{y}_2^{\pm})\mathbf{z}$ with $\mathbf{z}(0) \in \mathrm{Sp}\left\{(1,1,0)^T, \mathbf{v}_{23}^{\pm}\right\}$ will contract to the origin tangential to either $\mathrm{Sp}\left\{\mathbf{v}_{23}^{\pm}\right\}$ if $|\mu_{21}| > |\mu_{23}|$, or $\mathrm{Sp}\left\{(1,1,0)^T\right\}$ if $|\mu_{23}| \geq |\mu_{21}|$. Trajectories $\mathbf{z}(\tau)$ with $\mathbf{z}(0) \notin \mathrm{Sp}\left\{(1,1,0)^T, \mathbf{v}_{23}^{\pm}\right\}$ will diverge to ∞ in the direction of $\mathrm{Sp}\left\{\mathbf{v}_{22}^{\pm}\right\}$.

As $H_2^{\pm}$ is C^{∞}, it therefore follows that $\mathbf{y}_2^{\pm}$ is a nonlinear saddle node of $\dot{\mathbf{y}} = \mathbf{X}(\mathbf{y})$ with a 1-dimensional C^{∞} local unstable manifold $W_{2\pm}^{U} \stackrel{def}{=} H_2^{\pm}\left(\mathrm{Sp}\left\{\mathbf{v}_{22}^{\pm}\right\}\right)$ which is tangential to $\mathrm{Sp}\left\{\mathbf{v}_{22}^{\pm}\right\}$ at $\mathbf{y}_2^{\pm}$, and a 2-dimensional C^{∞} local stable manifold $W_{2\pm}^{SN} \stackrel{def}{=} H_2^{\pm}\left(\mathrm{Sp}\left\{(1,1,0)^T, \mathbf{v}_{23}^{\pm}\right\}\right)$ which is tangential to $\mathrm{Sp}\left\{(1,1,0)^T, \mathbf{v}_{23}^{\pm}\right\}$ at $\mathbf{y}_2^{\pm}$, on which $\mathbf{y}_2^{\pm}$ is a nonlinear stable node. Moreover, by the Stable Manifold Theorem, $W_{2\pm}^{U}$ and $W_{2\pm}^{SN}$ are unique [4]. Typical trajectories $\mathbf{y}(\tau)$ of $\dot{\mathbf{y}} = \mathbf{X}(\mathbf{y})$ with $\left\|\mathbf{y}(0) - \mathbf{y}_2^{\pm}\right\|$ small and $\mathbf{y}(0) \in W_{2\pm}^{SN}$ will contract to $\mathbf{y}_2^{\pm}$ tangential to either $\mathrm{Sp}\left\{\mathbf{v}_{23}^{\pm}\right\}$ if $|\mu_{21}| > |\mu_{23}|$, or $L_2^{\pm}$ if $|\mu_{23}| \geq |\mu_{21}|$. Trajectories $\mathbf{y}(\tau)$ with $\left\|\mathbf{y}(0) - \mathbf{y}_2^{\pm}\right\|$ small and $\mathbf{y}(0) \notin W_{2\pm}^{SN}$ will diverge away from $\mathbf{y}_2^{\pm}$ in the direction of $\mathrm{Sp}\left\{\mathbf{v}_{22}^{\pm}\right\}$.

Local dynamics at $\mathbf{y}_1^{\pm}$

For a given choice of $\boldsymbol{\alpha}$ such that $\mathbf{y}_1^{\pm}$ exists, there are four generic possibilities for the local dynamics at $\mathbf{y}_1^{\pm}$ depending upon where the point (β, α) lies relative to the curves $\alpha = \alpha_{\pm}(\beta), \alpha = R_{\pm}(\beta)$ and $\alpha = \alpha_H(\beta)$ in the (β, α) plane (cf. figure (3-14)). Each of these possibilities will now be examined in turn for a fixed ϵ.

1. (β, α) lying between $\alpha = \alpha_{-}(\beta)$ and $\alpha = R_{-}(\beta, \epsilon)$

In this range $\mu_{11} < \mu_{13} < \mu_{12} < 0$ (see section A.1.3 for a proof that $\mu_{11} < \mu_{13}$). The origin is therefore a stable node of $\dot{\mathbf{z}} = D\mathbf{X}(\mathbf{y}_1^{\pm})\mathbf{z}$ [27]. Typical trajectories $\mathbf{z}(\tau)$ of $\dot{\mathbf{z}} = D\mathbf{X}(\mathbf{y}_1^{\pm})\mathbf{z}$ contract to the origin tangential to $\mathrm{Sp}\left\{\mathbf{v}_{12}^{\pm}\right\}$. As $H_1^{\pm}$ is C^{∞}, it therefore follows that $\mathbf{y}_1^{\pm}$ is a nonlinear stable node of $\dot{\mathbf{y}} = \mathbf{X}(\mathbf{y})$. Moreover, typical trajectories $\mathbf{y}(\tau)$ of $\dot{\mathbf{y}} = \mathbf{X}(\mathbf{y})$ with $\left\|\mathbf{y}(0) - \mathbf{y}_1^{\pm}\right\|$ small contract onto $\mathbf{y}_1^{\pm}$ tangential to $\mathrm{Sp}\left\{\mathbf{v}_{12}^{\pm}\right\}$. Figure (3-15) shows the projection onto the $(r-l, \varepsilon)$ plane of some typical trajectories $\mathbf{y}(\tau)$ of the burster system with $\left\|\mathbf{y}(0) - \mathbf{y}_1^{+}\right\|$ small obtained for $\{\alpha = 106, \beta = 1.5, \epsilon = 0.0005\}$.[3] Also shown are the sets $\mathrm{Sp}\left\{\mathbf{v}_{12}^{+}\right\}$ and $\mathrm{Sp}\left\{\mathbf{v}_{13}^{+}\right\}$ together with the slow manifold S_M. For this choice

[3] This projection is a convenient one to use-particularly when discussing the local dynamics at the fixed points-because the $(r-l, \varepsilon)$ plane is orthogonal to the parameter-independent stable manifolds of the fixed points.

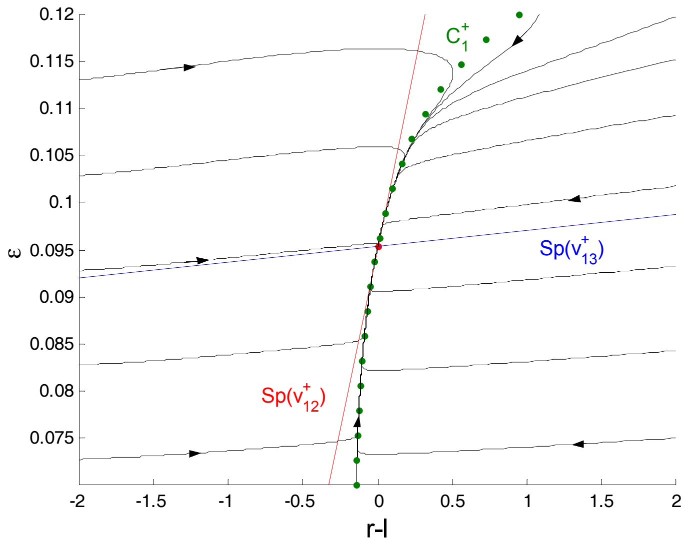

Figure 3-15: Projection onto the $(r-l,\varepsilon)$ plane of some trajectories $\mathbf{y}(\tau)$ of the burster system with $\left\|\mathbf{y}(0)-\mathbf{y}_1^+\right\|$ small obtained for $\alpha=106$, $\beta=1.5$, $\epsilon=0.0005$. The dotted lines indicate the slow manifold S_M. Arrows indicate the direction of trajectories with time.

of parameters (β,α) lies between $\alpha=\alpha_-(\beta)$ and $\alpha=R_-(\beta,\epsilon)$. It can be seen that the trajectories shown contract onto $\mathbf{y}_1^+$ tangential to $\mathrm{Sp}\left\{\mathbf{v}_{12}^+\right\}$, as expected.

2. (β,α) lying between $\alpha=R_-(\beta,\epsilon)$ and $\alpha=\alpha_H(\beta)$

In this range $\mu_{12},\mu_{13}\in\mathbb{C}$ with $\mathrm{Re}(\mu_{12})=\mathrm{Re}(\mu_{13})<0$. The origin is therefore a stable fixed point of $\dot{\mathbf{z}}=D\mathbf{X}(\mathbf{y}_1^\pm)\mathbf{z}$ with the stable invariant line $\mathrm{Sp}\left\{(1,1,0)^T\right\}$ and the stable invariant plane $\mathrm{Sp}\left\{\mathrm{Re}\left(\mathbf{v}_{12}^\pm\right),\mathrm{Im}\left(\mathbf{v}_{12}^\pm\right)\right\}$, on which the origin is a stable focus [27]. Trajectories $\mathbf{z}(\tau)$ of $\dot{\mathbf{z}}=D\mathbf{X}(\mathbf{y}_1^\pm)\mathbf{z}$ with $\mathbf{z}(0)\notin\mathrm{Sp}\left\{(1,1,0)^T\right\}$ spiral around $\mathrm{Sp}\left\{(1,1,0)^T\right\}$ as they contract onto the origin. As $H_1^\pm$ is C^∞, it follows that $\mathbf{y}_1^\pm$ is a stable fixed point of $\dot{\mathbf{y}}=\mathbf{X}(\mathbf{y})$, and that trajectories $\mathbf{y}(\tau)$ of $\dot{\mathbf{y}}=\mathbf{X}(\mathbf{y})$ with $\left\|\mathbf{y}(0)-\mathbf{y}_1^\pm\right\|$ small and $\mathbf{y}(0)\notin L_1^\pm$ spiral around $L_1^\pm$ as they contract onto $\mathbf{y}_1^\pm$. Figure (3-16) shows the projection onto the $(r-l,\varepsilon)$ plane of some trajectories $\mathbf{y}(\tau)$ of the burster system with $\left\|\mathbf{y}(0)-\mathbf{y}_1^+\right\|$ small and $\mathbf{y}(0)\notin L_1^+$ obtained for $\{\alpha=256,\beta=3.75,\epsilon=0.05\}$. Also shown is the slow manifold S_M. For this choice of parameters, (β,α) lies between $\alpha=R_-(\beta,\epsilon)$ and $\alpha=\alpha_H(\beta)$. It can be seen that the trajectories shown spiral around L_1^+ as they contract onto $\mathbf{y}_1^+$, as expected.

3. (β,α) lying between $\alpha=\alpha_H(\beta)$ and $\alpha=R_+(\beta,\epsilon)$

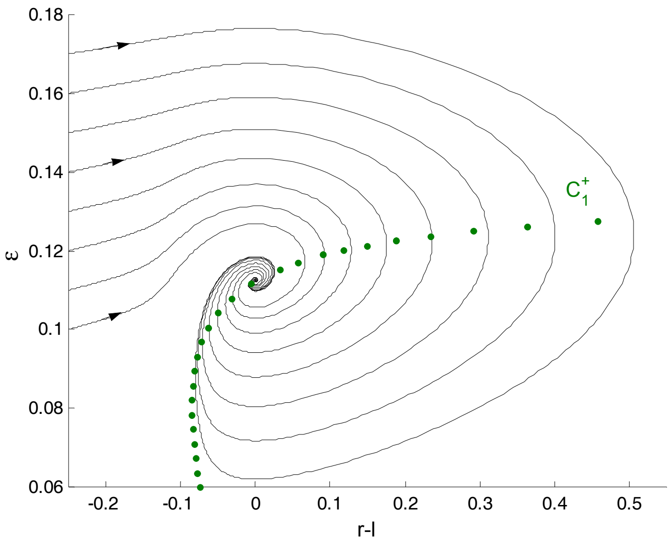

Figure 3-16: Projection onto the $(r-l, \varepsilon)$ plane of some trajectories $\mathbf{y}(\tau)$ of the burster system with $\left\|\mathbf{y}(0)-\mathbf{y}_1^+\right\|$ small obtained for $\alpha = 256$, $\beta = 3.75$, $\epsilon = 0.05$. The dotted lines indicates the slow manifold S_M. Arrows indicate the direction of trajectories with time.

In this range $\mu_{12}, \mu_{13} \in \mathbb{C}$ with $\operatorname{Re}(\mu_{12}) = \operatorname{Re}(\mu_{13}) > 0$. The origin is therefore a saddle focus of $\dot{\mathbf{z}} = D\mathbf{X}(\mathbf{y}_1^{\pm})\mathbf{z}$, with the stable invariant line $\operatorname{Sp}\left\{(1,1,0)^T\right\}$, and the unstable invariant plane $\operatorname{Sp}\left\{\operatorname{Re}\left(\mathbf{v}_{12}^{\pm}\right), \operatorname{Im}\left(\mathbf{v}_{12}^{\pm}\right)\right\}$ on which the origin is an unstable focus [27]. Trajectories $\mathbf{z}(\tau)$ of $\dot{\mathbf{z}} = D\mathbf{X}(\mathbf{y}_1^{\pm})\mathbf{z}$ with $\mathbf{z}(0) \notin \operatorname{Sp}\left\{(1,1,0)^T\right\}$ spiral around $\operatorname{Sp}\left\{(1,1,0)^T\right\}$ as they diverge away from the origin to ∞. As $H_1^{\pm}$ is C^{∞}, it therefore follows that $\mathbf{y}_1^{\pm}$ is a nonlinear saddle focus of $\dot{\mathbf{y}} = \mathbf{X}(\mathbf{y})$, with a 1-dimensional C^{∞} local stable manifold $H_1^{\pm}\left(\operatorname{Sp}\left\{(1,1,0)^T\right\}\right)$ which is tangential to $L_1^{\pm}$ at $\mathbf{y}_1^{\pm}$, and a 2-dimensional C^{∞} local unstable manifold $W_{1\pm}^{UF} \overset{def}{=} H_1^{\pm}\left(\operatorname{Sp}\left\{\operatorname{Re}\left(\mathbf{v}_{12}^{\pm}\right), \operatorname{Im}\left(\mathbf{v}_{12}^{\pm}\right)\right\}\right)$ which is tangential to $\operatorname{Sp}\left\{\operatorname{Re}\left(\mathbf{v}_{12}^{\pm}\right), \operatorname{Im}\left(\mathbf{v}_{12}^{\pm}\right)\right\}$ at $\mathbf{y}_1^{\pm}$, on which $\mathbf{y}_1^{\pm}$ is a nonlinear unstable focus. By the Stable Manifold Theorem, these local manifolds are unique; in particular $H_1^{\pm}\left(\operatorname{Sp}\left\{(1,1,0)^T\right\}\right)$ can be identified with $L_1^{\pm}$. Trajectories $\mathbf{y}(\tau)$ of $\dot{\mathbf{y}} = \mathbf{X}(\mathbf{y})$ with $\left\|\mathbf{y}(0)-\mathbf{y}_1^{\pm}\right\|$ small and $\mathbf{y}(0) \notin L_1^{\pm}$ spiral around $L_1^{\pm}$ as they diverge away from $\mathbf{y}_1^{\pm}$.

4. (β, α) lying between $\alpha = R_+(\beta, \epsilon)$ and $\alpha = \alpha_+(\beta)$

In this range, $\mu_{12} > \mu_{13} > 0$. The origin is therefore a saddle node of $\dot{\mathbf{z}} = D\mathbf{X}(\mathbf{y}_1^{\pm})\mathbf{z}$, with the stable invariant line $\operatorname{Sp}\left\{(1,1,0)^T\right\}$, and the unstable invariant plane $\operatorname{Sp}\left\{\mathbf{v}_{12}^{\pm}, \mathbf{v}_{13}^{\pm}\right\}$ on which the origin is an unstable node [27]. Typical trajectories $\mathbf{z}(\tau)$ of $\dot{\mathbf{z}} = D\mathbf{X}(\mathbf{y}_1^{\pm})\mathbf{z}$ with $\mathbf{z}(0) \notin \operatorname{Sp}\left\{(1,1,0)^T\right\}$ diverge to ∞ in the direction of $\operatorname{Sp}\left\{\mathbf{v}_{12}^{\pm}\right\}$. As $H_1^{\pm}$ is C^{∞}, it therefore follows that $\mathbf{y}_1^{\pm}$ is a nonlinear saddle node of $\dot{\mathbf{y}} = \mathbf{X}(\mathbf{y})$, with a 1-dimensional

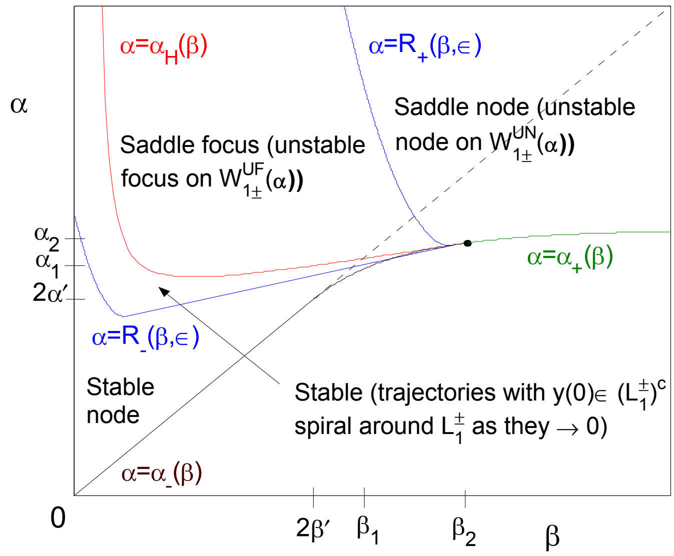

Figure 3-17: The stability of $\mathbf{y}_1^{\pm}$.

C^{∞} local stable manifold $H_1^{\pm}\left(\mathrm{Sp}\left\{(1,1,0)^T\right\}\right)$ which is tangential to $L_1^{\pm}$ at $\mathbf{y}_1^{\pm}$, and a 2-dimensional C^{∞} local unstable manifold $W_{1\pm}^{UN} = H_1^{\pm}\left(\mathrm{Sp}\left\{\mathbf{v}_{12}^{\pm}, \mathbf{v}_{13}^{\pm}\right\}\right)$ which is tangential to $\mathrm{Sp}\left\{\mathbf{v}_{12}^{\pm}, \mathbf{v}_{13}^{\pm}\right\}$ at $\mathbf{y}_1^{\pm}$, on which $\mathbf{y}_1^{\pm}$ is a nonlinear unstable node. Again, by the Stable Manifold Theorem, these local manifolds are unique; in particular $H_1^{\pm}\left(\mathrm{Sp}\left\{(1,1,0)^T\right\}\right)$ can be identified with $L_1^{\pm}$. Typical trajectories $\mathbf{y}(\tau)$ of $\dot{\mathbf{y}} = \mathbf{X}(\mathbf{y})$ with $\left\|\mathbf{y}(0) - \mathbf{y}_1^{\pm}\right\|$ small and $\mathbf{y}(0) \notin L_1^{\pm}$ will diverge away from the origin in the direction of $\mathrm{Sp}\left\{\mathbf{v}_{12}^{\pm}\right\}$.

Figures (3-17) and (3-18) summarise the results obtained in this section concerning the stabilities of $\mathbf{y}_1^{\pm}$ and $\mathbf{y}_2^{\pm}$.

3.6.2 Approximation to $\varepsilon(\tau)$ for large $\tau \geq 0$ for initial conditions in $\mathcal{B}\left(\mathbf{y}_1^{+}\right) \cup \mathcal{B}\left(\mathbf{y}_1^{-}\right)$ with $\alpha_{-}(\beta) < \alpha < R_{-}(\beta, \epsilon)$

Assume that $\alpha_{-}(\beta) < \alpha < R_{-}(\beta,\epsilon)$, so that $\mathbf{y}_1^{+}$ and $\mathbf{y}_1^{-}$ are stable nodes of $\dot{\mathbf{y}} = \mathbf{X}(\mathbf{y})$, and let $\mathbf{y}_0$ lie in the basin of attraction $\mathcal{B}(\mathbf{y}_*)$ of $\mathbf{y}_* = (x_1, x_1, \varepsilon_*)^T$, where $\mathbf{y}_* = \mathbf{y}_1^{+}$ or $\mathbf{y}_1^{-}$. Define $\mathbf{y}(\tau) = (r(\tau), l(\tau), \varepsilon(\tau))^T = \phi_\tau(\mathbf{y}_0)\ \forall \tau \geq 0$. In this section, an approximate expression for $\varepsilon(\tau)$ is obtained for τ large, based on the fact that sufficiently close to $\mathbf{y}_*$, the nonlinear dynamics are well approximated by the linearised dynamics. This expression will come in useful when discussing the modelling of saccades in chapter 6.

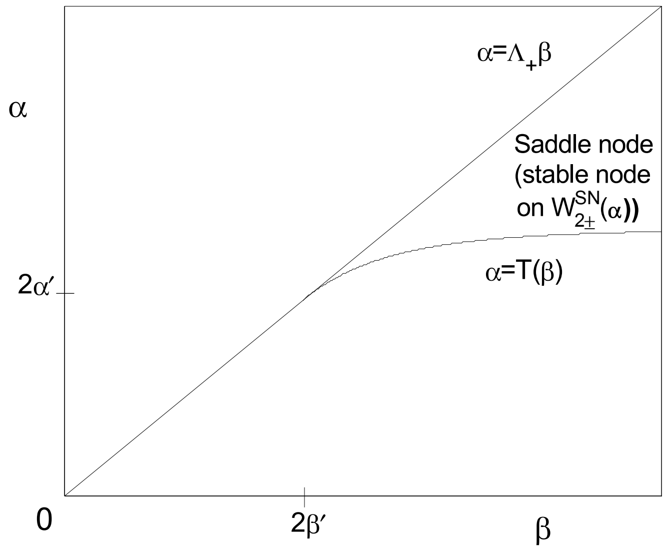

Figure 3-18: The stability of $\mathbf{y}_2^{\pm}$.

Write L_τ for the flow associated with the linearised dynamics $\dot{\mathbf{z}} = D\mathbf{X}(\mathbf{y}_*)\,\mathbf{z}$, and fix μ with $\max_{1\leq j\leq 3}\mathrm{Re}\left\{\mu_{1j}\right\} < \mu < 0$. It then follows from section 1.2.3 that there is $\delta > 0$ and $K > 0$ such that if $\|\mathbf{y} - \mathbf{y}_*\| < \delta$, then $\forall\tau \geq 0$

$$\phi_\tau(\mathbf{y}) - \mathbf{y}_* = L_\tau(\mathbf{y} - \mathbf{y}_*) + \mathbf{S}(\tau) \tag{3.74}$$

where:

$$\|\mathbf{S}(\tau)\| \leq K\delta^2 e^{\mu\tau} \tag{3.75}$$

Choose τ_L for which $\left\|\phi_{\tau_L}(\mathbf{y}_0) - \mathbf{y}_*\right\| < \delta$. By (3.74), $\forall\tau \geq 0$:

$$\phi_\tau\left(\phi_{\tau_L}(\mathbf{y}_0)\right) - \mathbf{y}_* = L_\tau\left(\phi_{\tau_L}(\mathbf{y}_0) - \mathbf{y}_*\right) + \mathbf{S}(\tau)$$

Write $\mathbf{y}_L = \phi_{\tau_L}(\mathbf{y}_0) - \mathbf{y}_*$, and define $\mathbf{z}_L(\tau) = (u_L(\tau), v_L(\tau), w_L(\tau))^T = L_\tau(\mathbf{y}_L)\ \forall\tau \geq 0$. $\mathbf{z}_L(\tau)$ solves the linearised system $\dot{\mathbf{z}} = D\mathbf{X}(\mathbf{y}_*)\,\mathbf{z}$ with initial condition $\mathbf{z}_L(0) = \mathbf{y}_L$. Moreover, the above expression implies that $\forall\tau \geq 0$:

$$\mathbf{y}(\tau + \tau_L) = \mathbf{y}_* + \mathbf{z}_L(\tau) + \mathbf{S}(\tau)$$

It follows that $\forall\tau \geq \tau_L$

$$\mathbf{y}(\tau) = \mathbf{y}_* + \mathbf{z}_L(\tau - \tau_L) + \mathbf{S}(\tau - \tau_L) \tag{3.76}$$

where by (3.75):

$$\|\mathbf{S}(\tau - \tau_L)\| \leq K\delta^2 e^{\mu(\tau - \tau_L)}$$

Write $\mathbf{S}(\tau) = (S_r(\tau), S_l(\tau), S_\varepsilon(\tau))^T$ $\forall \tau \geq 0$. (3.76) implies that $\forall \tau \geq \tau_L$:

$$\varepsilon(\tau) = \varepsilon_* + w_L(\tau - \tau_L) + S_\varepsilon(\tau - \tau_L) \tag{3.77}$$

By the equivalence of norms on $\mathbb{R}^3$, there is a constant $L > 0$ such that $\|\mathbf{y}\|_1 \leq L\|\mathbf{y}\|$ $\forall \mathbf{y} \in \mathbb{R}^3$. Thus, $\forall \tau \geq \tau_L$:

$$|S_\varepsilon(\tau - \tau_L)| \leq KL\delta^2 e^{\mu(\tau - \tau_L)} \tag{3.78}$$

(3.77) and (3.78) together show that for $\tau - \tau_L > 0$ sufficiently large:

$$\varepsilon(\tau) \approx \varepsilon_* + w_L(\tau - \tau_L) \tag{3.79}$$

So far, it has been argued that $\exists \tau_L > 0$ such that $\varepsilon(\tau)$ satisfies the approximation (3.79) for $\tau - \tau_L > 0$ sufficiently large. This is equivalent to the statement that given $\tau_L > 0$ sufficiently large, $\varepsilon(\tau)$ satisfies (3.79) $\forall \tau \geq \tau_L$.

It is shown in section A.1.5 of the Appendix that $w_L(\tau)$ satisfies

$$\ddot{w}_L - \Delta_1 \dot{w}_L + \epsilon\left(\Gamma_1^+ + \Gamma_1^-\right) w_L = 0$$

and

$$\dot{w}_L = -\epsilon\left(u_L - v_L\right)$$

on $\mathbb{R}$. The first equation implies that $w_L(\tau)$ solves the general linear harmonic oscillator equation $\ddot{X} + a\dot{X} + bX = 0$ with $a = -\Delta_1$ and $b = \epsilon\left(\Gamma_1^+ + \Gamma_1^-\right)$. Since $\mathbf{y}_L = \phi_{\tau_L}(\mathbf{y}_0) - \mathbf{y}_*$, $u_L(0) = r(\tau_L) - x_1$, $v_L(0) = l(\tau_L) - x_1$ and $w_L(0) = \varepsilon(\tau_L) - \varepsilon_*$. The second equation thus implies that $\dot{w}_L(0) = -\epsilon b(\tau_L)$ where $b(\tau_L) = r(\tau_L) - l(\tau_L)$. As $\Delta_1^2 - 4\epsilon\left(\Gamma_1^+ + \Gamma_1^-\right) > 0$

for the parameter range considered here, it then follows from the discussion of the equation $\ddot{X} + a\dot{X} + bX = 0$ in section A.1.4 of the Appendix that $\forall \tau \geq 0$

$$w_L(\tau) = Ae^{\mu_{12}\tau} + Be^{\mu_{13}\tau} \tag{3.80}$$

where:

$$\begin{aligned} d &= \sqrt{\Delta_1^2 - 4\epsilon\left(\Gamma_1^+ + \Gamma_1^-\right)} \\ A &= -\tfrac{1}{d}\left(\mu_{13}\left(\varepsilon\left(\tau_L\right) - \varepsilon_*\right) + \epsilon b\left(\tau_L\right)\right) \\ B &= \tfrac{1}{d}\left(\mu_{12}\left(\varepsilon\left(\tau_L\right) - \varepsilon_*\right) + \epsilon b\left(\tau_L\right)\right) \end{aligned} \tag{3.81}$$

In conclusion, it has been argued here that given $\tau_L > 0$ sufficiently large, $\varepsilon(\tau)$ satisfies the approximation (3.79) $\forall \tau \geq \tau_L$, where $w_L(\tau)$ is defined by (3.80)-(3.81).

3.6.3 Stability of the origin

As mentioned previously, the stability analysis of the origin is complicated by the fact that $\mathbf{X}$ is not smooth at $\mathbf{0}$. In understanding the stability of $\mathbf{0}$ as a fixed point of $\dot{\mathbf{y}} = \mathbf{X}(\mathbf{y})$ it is useful to first examine the stability of $\mathbf{0}$ as a fixed point of the extended systems $\dot{\mathbf{y}} = \mathbf{X}_+(\mathbf{y})$ and $\dot{\mathbf{y}} = \mathbf{X}_-(\mathbf{y})$ introduced in section 3.1.3.

Stability of the origin in $\dot{\mathbf{y}} = \mathbf{X}_\pm(\mathbf{y})$

Recall from section 3.1.3 that $\mathbf{X}_+$ and $\mathbf{X}_-$ are C^∞ smooth. It therefore follows that if $\mathbf{0}$ is hyperbolic in $\dot{\mathbf{y}} = \mathbf{X}_\pm(\mathbf{y})$, there is a homeomorphism $H_0^\pm$ which maps an open neighbourhood $V_\mathbf{0}^\pm$ of $\mathbf{0}$ to an open neighbourhood $U_\mathbf{0}^\pm$ of $\mathbf{0}$ such that (i) $H_0^\pm(\mathbf{0}) = \mathbf{0}$, and (ii) $H_0^\pm$ maps trajectories of $\dot{\mathbf{z}} = D\mathbf{X}_\pm(\mathbf{0})\,\mathbf{z}$ to trajectories of $\dot{\mathbf{y}} = \mathbf{X}_\pm(\mathbf{y})$ in such a way as to preserve the parameterisation of trajectories with time. In this case, the stability of $\mathbf{0}$ in $\dot{\mathbf{y}} = \mathbf{X}_\pm(\mathbf{y})$ is determined by the eigenvalue spectrum of $D\mathbf{X}_\pm(\mathbf{0})$. Setting $\mathbf{y} = \mathbf{0}$ in equation (3.55) gives

$$D\mathbf{X}_-(\mathbf{0})\,\sigma = \sigma D\mathbf{X}_+(\mathbf{0}) \tag{3.82}$$

which implies that $D\mathbf{X}_+(\mathbf{0})$ and $D\mathbf{X}_-(\mathbf{0})$ have the same eigenvalue spectrum. The stability of $\mathbf{0}$ as a fixed point of both $\dot{\mathbf{y}} = \mathbf{X}_+(\mathbf{y})$ and $\dot{\mathbf{y}} = \mathbf{X}_-(\mathbf{y})$ is therefore determined by the eigenvalue spectrum of $D\mathbf{X}_+(\mathbf{0})$ in the hyperbolic case. Setting $\mathbf{y} = \mathbf{0}$ in (3.57) gives:

$$D\mathbf{X}_+(\mathbf{0}) = \begin{pmatrix} -1 & 0 & \Lambda_+ \\ 0 & -1 & -\Lambda_- \\ -\epsilon & \epsilon & 0 \end{pmatrix} \tag{3.83}$$

The eigenvalues $\{\lambda_1, \lambda_2, \lambda_3\}$ of $D\mathbf{X}_+(\mathbf{0})$ are then

$$\begin{aligned} \lambda_1 &= -1 \\ \lambda_2 &= \tfrac{1}{2}(-1 + \Delta) \\ \lambda_3 &= \tfrac{1}{2}(-1 - \Delta) \end{aligned} \tag{3.84}$$

where $\Delta = \sqrt{1 - 4\epsilon(\Lambda_+ + \Lambda_-)}$. Note that $\Lambda_+ + \Lambda_- \neq 0$ corresponds to the hyperbolic case. Also note that $\lambda_1 = \lambda_2 + \lambda_3$. $\{\lambda_1, \lambda_2, \lambda_3\}$ therefore have a resonance of order 2, and so by Sternberg's Theorem, $H_0^{\pm}$ is at most a C^1 diffeomorphism when $\Lambda_+ + \Lambda_- \neq 0$.

Let $\left\{\mathbf{w}_1^+, \mathbf{w}_2^+, \mathbf{w}_3^+\right\}$ be the corresponding eigenvectors of $D\mathbf{X}_+(\mathbf{0})$ corresponding to $\{\lambda_1, \lambda_2, \lambda_3\}$. ($\left\{\mathbf{w}_1^+, \mathbf{w}_2^+, \mathbf{w}_3^+\right\}$ are taken to be the generalised eigenvectors of $D\mathbf{X}_+(\mathbf{0})$ when the eigenvalues are not distinct). Similarly, write $\left\{\mathbf{w}_1^-, \mathbf{w}_2^-, \mathbf{w}_3^-\right\}$ for the eigenvectors of $D\mathbf{X}_-(\mathbf{0})$ corresponding to $\{\lambda_1, \lambda_2, \lambda_3\}$. (Again, $\left\{\mathbf{w}_1^-, \mathbf{w}_2^-, \mathbf{w}_3^-\right\}$ are taken to be the generalised eigenvectors of $D\mathbf{X}_-(\mathbf{0})$ when the eigenvalues are not distinct). Using (3.82), it can be shown that it is possible to choose $\left\{\mathbf{w}_1^-, \mathbf{w}_2^-, \mathbf{w}_3^-\right\}$ so that $\left[\mathbf{w}_1^- \ \mathbf{w}_2^- \ \mathbf{w}_3^-\right] = \sigma\left[\mathbf{w}_1^+ \ \mathbf{w}_2^+ \ \mathbf{w}_3^+\right]$ (cf. the proof that $\left\{\mathbf{v}_{i1}^-, \mathbf{v}_{i2}^-, \mathbf{v}_{i3}^-\right\}$ can be chosen to satisfy $\left[\mathbf{v}_{i1}^- \ \mathbf{v}_{i2}^- \ \mathbf{v}_{i3}^-\right] = \sigma\left[\mathbf{v}_{i1}^+ \ \mathbf{v}_{i2}^+ \ \mathbf{v}_{i3}^+\right]$ in section 3.6.1). It can be seen from (3.83) that $(1,1,0)^T$ is an eigenvector of $D\mathbf{X}_+(\mathbf{0})$ corresponding to the eigenvalue -1. $\mathbf{w}_1^+$ can therefore be set equal to $(1,1,0)^T$. Since $\sigma(1,1,0)^T = (1,1,0)^T$, $\mathbf{w}_1^-$ can also be set equal to $(1,1,0)^T$. The fact that $(1,1,0)^T$ is an eigenvector of $D\mathbf{X}_\pm(\mathbf{0})$ corresponding to -1 means that $L_0 = \mathrm{Sp}\left\{(1,1,0)^T\right\}$ is always a stable 1-dimensional manifold of the linearised system $\dot{\mathbf{z}} = D\mathbf{X}_\pm(\mathbf{0})\mathbf{z}$. Moreover, the dynamics of $\dot{\mathbf{z}} = D\mathbf{X}_\pm(\mathbf{0})\mathbf{z}$ on L_0 is given by

$$\dot{x} = -x \tag{3.85}$$

which is consistent with the linearisation of (3.25) about $x = 0$ (recall that (3.25) describes the nonlinear dynamics of $\dot{\mathbf{y}} = \mathbf{X}_\pm(\mathbf{y})$ on the invariant line L_0). For the generic case when the eigenvalues $\{\lambda_1, \lambda_2, \lambda_3\}$ are distinct, the other two eigenvectors $\mathbf{w}_2^+$ and $\mathbf{w}_3^+$ of $D\mathbf{X}_+(\mathbf{0})$ are as below:

$$\mathbf{w}_2^+ = \begin{pmatrix} \Lambda_+ \\ -\Lambda_- \\ \frac{1}{2}(1+\Delta) \end{pmatrix}, \mathbf{w}_3^+ = \begin{pmatrix} \Lambda_+ \\ -\Lambda_- \\ \frac{1}{2}(1-\Delta) \end{pmatrix} \tag{3.86}$$

It should be noted that when the dependence of $\mathbf{X}_+$ on $\boldsymbol{\alpha}$ is being explicitly considered, the Jacobian matrix $D\mathbf{X}_+(\mathbf{0})$ is $D_{\mathbf{y}}\mathbf{X}_+(\mathbf{0};\boldsymbol{\alpha})$, while the eigenvalues and eigenvectors of the Jacobian are functions of $\boldsymbol{\alpha}$, $\lambda_i = \lambda_i(\boldsymbol{\alpha})$ and $\mathbf{w}_i^+ = \mathbf{w}_i^+(\boldsymbol{\alpha})$ for $1 \leq i \leq 3$. Similarly for $\mathbf{X}_-$.

Returning to the eigenvalue spectrum of $D\mathbf{X}_+(\mathbf{0})$, recall from (3.13) that $\Lambda_- = -\frac{\alpha}{\beta}$. It follows that $\alpha \neq \Lambda_+\beta$ corresponds to the hyperbolic case $\Lambda_+ + \Lambda_- \neq 0$. Thus, since $\lambda_1 < 0$, the stability of $\mathbf{0}$ in $\dot{\mathbf{y}} = \mathbf{X}_\pm(\mathbf{y})$ when $\alpha \neq \Lambda_+\beta$ is determined by the signs of $\mathrm{Re}(\lambda_2)$ and $\mathrm{Re}(\lambda_3)$. For $\alpha < \Lambda_+\beta$, $\Lambda_+ + \Lambda_- > 0$ and so Δ is either complex or is less than 1. This means that $\mathrm{Re}(\lambda_2), \mathrm{Re}(\lambda_3) < 0$ and hence the origin is a stable fixed point of $\dot{\mathbf{y}} = \mathbf{X}_\pm(\mathbf{y})$. For $\alpha > \Lambda_+\beta$, $\Lambda_+ + \Lambda_- < 0$ implying that $\Delta > 1$, and so $\lambda_2 > 0, \lambda_3 < 0$. In this range the origin is therefore an unstable fixed point of $\dot{\mathbf{y}} = \mathbf{X}_\pm(\mathbf{y})$. The origin thus changes from being a stable fixed point of $\dot{\mathbf{y}} = \mathbf{X}_\pm(\mathbf{y})$ to an unstable fixed point as $\alpha - \Lambda_+\beta$ increases through 0. Note that the stability of $\mathbf{0}$ as a fixed point of $\dot{\mathbf{y}} = \mathbf{X}_\pm(\mathbf{y})$ is a function of α and β: it is independent of ϵ. Also, the extended version of the Hartman-Grobman Theorem stated in section 1.2.3 implies that $H_0^\pm$ is a diffeomorphism for $\alpha < \Lambda_+\beta$, since $\mathrm{Re}\{\lambda_i\} < 0$ for $1 \leq i \leq 3$ in this range. For $\alpha > \Lambda_+\beta$, $\lambda_1 = \lambda_2 + \lambda_3$ with $\mathrm{Re}(\lambda_2), -\mathrm{Re}(\lambda_3) > 0$, and so $H_0^\pm$ may not be a diffeomorphism.

Stability of the origin in $\dot{\mathbf{y}} = \mathbf{X}(\mathbf{y})$

A useful expression for the dynamics of $\dot{\mathbf{y}} = \mathbf{X}(\mathbf{y})$ about the origin can be obtained by utilising the extended vector fields $\{\mathbf{X}_+, \mathbf{X}_-\}$. Since $\mathbf{X}_+$ is smooth, $\mathbf{X}_+$ can be expanded as a Taylor series about $\mathbf{0}$ giving

$$\mathbf{X}_+(\mathbf{y}) = D\mathbf{X}_+(\mathbf{0})\,\mathbf{y} + \mathbf{R}_+(\mathbf{y})$$

where $\mathbf{R}_+(\mathbf{y})$ is $O\left(\|\mathbf{y}\|^2\right)$. Similarly, $\mathbf{X}_-$ can be written as

$$\mathbf{X}_-(\mathbf{y}) = D\mathbf{X}_-(\mathbf{0})\,\mathbf{y} + \mathbf{R}_-(\mathbf{y})$$

where $\mathbf{R}_-(\mathbf{y})$ is $O\left(\|\mathbf{y}\|^2\right)$. Hence, as $\mathbf{X}_\pm|_{N_\pm} = \mathbf{X}|_{N_\pm}$, $\mathbf{X}$ can be written in the form

$$\mathbf{X}(\mathbf{y}) = \mathbf{L}_\mathbf{X}(\mathbf{y}) + \mathbf{R}(\mathbf{y}) \tag{3.87}$$

where $\mathbf{L}_\mathbf{X}, \mathbf{R} : \mathbb{R}^3 \to \mathbb{R}^3$ are defined by

$$\mathbf{L}_\mathbf{X}(\mathbf{y}) = \begin{cases} D\mathbf{X}_+(\mathbf{0})\,\mathbf{y} & \text{if} \quad \mathbf{y} \in N_+ \\ D\mathbf{X}_-(\mathbf{0})\,\mathbf{y} & \text{if} \quad \mathbf{y} \in N_- \end{cases} \tag{3.88}$$

and:

$$\mathbf{R}(\mathbf{y}) = \begin{cases} \mathbf{R}_+(\mathbf{y}) & \text{if} \quad \mathbf{y} \in N_+ \\ \mathbf{R}_-(\mathbf{y}) & \text{if} \quad \mathbf{y} \in N_- \end{cases} \tag{3.89}$$

Note that $\mathbf{R}(\mathbf{y})$ is $O\left(\|\mathbf{y}\|^2\right)$ with $\mathbf{R}(\mathbf{0}) = \mathbf{0}$. Using (3.87), the burster dynamics about the origin can therefore be written as below:

$$\dot{\mathbf{y}} = \mathbf{L}_\mathbf{X}(\mathbf{y}) + \mathbf{R}(\mathbf{y}) \tag{3.90}$$

The piecewise linear system $\dot{\mathbf{z}} = \mathbf{L}_\mathbf{X}(\mathbf{z})$ will be referred to in what follows as the linearisation of the burster system about the origin. Using the expression for $D\mathbf{X}_+(\mathbf{0})$ given in (3.83) and the fact that $\sigma D\mathbf{X}_-(\mathbf{0}) = D\mathbf{X}_+(\mathbf{0})\,\sigma$, $\dot{\mathbf{z}} = \mathbf{L}_\mathbf{X}(\mathbf{z})$ can be written as:

$$\dot{\mathbf{z}} = \begin{cases} \begin{pmatrix} -1 & 0 & \Lambda_+ \\ 0 & -1 & -\Lambda_- \\ -\epsilon & \epsilon & 0 \end{pmatrix} \mathbf{z} & \text{if} \quad \mathbf{z} \in N_+ \\ \begin{pmatrix} -1 & 0 & \Lambda_- \\ 0 & -1 & -\Lambda_+ \\ -\epsilon & \epsilon & 0 \end{pmatrix} \mathbf{z} & \text{if} \quad \mathbf{z} \in N_- \end{cases} \tag{3.91}$$

Writing $\mathbf{z} = (u, v, w)^T$, the equations are given explicitly by:

$$\dot{u} = -u + L(w)\,|w| \tag{3.92}$$

$$\dot{v} = -v + L(-w)\,|w| \tag{3.93}$$

$$\dot{w} = -\epsilon\,(u - v) \tag{3.94}$$

where $L : \mathbb{R}^3 \to \mathbb{R}^3$ is defined as follows:

$$L(w) = \begin{cases} \Lambda_+ & \text{if} \quad w > 0 \\ -\Lambda_- & \text{if} \quad w < 0 \end{cases} \tag{3.95}$$

It can be shown that solutions of the linearised system $\dot{\mathbf{z}} = \mathbf{L_X}(\mathbf{z})$ exist and can be extended infinitely far forward in time. Proofs are given in section A.1.6. Note from the definition of $\mathbf{L_X}$ that $\mathbf{L_X}|_{N_\pm} = D\mathbf{X}_\pm(\mathbf{0})|_{N_\pm}$. Hence if $\mathbf{z}(\tau)$ is a solution of $\dot{\mathbf{z}} = D\mathbf{X}_\pm(\mathbf{0})\mathbf{z}$ with $\mathbf{z}(\tau) \in N_\pm$ on some interval (τ_1, τ_2), then $\mathbf{z}(\tau)$ solves $\dot{\mathbf{z}} = \mathbf{L_X}(\mathbf{z})$ on (τ_1, τ_2) also. In particular this means that the line $L_0 = \text{Sp}\left\{(1,1,0)^T\right\}$ will be a stable 1-dimensional manifold of the fixed point at the origin in $\dot{\mathbf{z}} = \mathbf{L_X}(\mathbf{z})$. It is easy to see that $\sigma \circ \mathbf{L_X} = \mathbf{L_X} \circ \sigma$; that is σ conjugates both the nonlinear and linearised vector fields of the burster system. [Let $\mathbf{z} \in N_+$. Then $\sigma \mathbf{L_X}(\mathbf{z}) = \sigma D\mathbf{X}_+(\mathbf{0})\mathbf{z} = D\mathbf{X}_-(\mathbf{0})(\sigma\mathbf{z})$. Now $\sigma\mathbf{z} \in N_-$ and so $\mathbf{L_X}(\sigma\mathbf{z}) = D\mathbf{X}_-(\mathbf{0})(\sigma\mathbf{z})$. Thus, $\sigma\mathbf{L_X}(\mathbf{z}) = \mathbf{L_X}(\sigma\mathbf{z})$. A similar argument proves the case $\mathbf{z} \in N_-$]. The conjugacy implies that if $\mathbf{z}(\tau)$ is a solution of the linearised system, then $\sigma\mathbf{z}(\tau)$ is also a solution (cf. section 3.3).

As $\mathbf{R}(\mathbf{y}) = O\left(\|\mathbf{y}\|^2\right)$, $\mathbf{X}(\mathbf{y})$ is approximated by $\mathbf{L_X}(\mathbf{y})$ for small $\|\mathbf{y}\|$. This suggests that trajectories $\mathbf{y}(\tau)$ of the burster system with $\|\mathbf{y}(\tau)\|$ small may be well approximated by corresponding trajectories of the linearised burster system. In particular, it follows that the stability properties of the origin in the nonlinear system may be determined by the stability properties of the origin in the linearised system. This claim is supported by extensive numerical evidence. However, as the vector field of the burster system is not smooth at $\mathbf{0}$, there is no obvious general result, such as the Hartman-Grobman Theorem, which can be used to prove this statement.

For $\alpha > \Lambda_+\beta$, $\lambda_1, \lambda_3 < 0$ and $\lambda_2 > 0$. The 1-dimensional set $E^U_{0\pm} \overset{def}{=} \text{Sp}\left\{\mathbf{w}_2^\pm\right\}$ is therefore the unstable manifold of the origin in the system $\dot{\mathbf{z}} = D\mathbf{X}_\pm(\mathbf{0})\mathbf{z}$. Since $\mathbf{L_X}|_{N_\pm} = D\mathbf{X}_\pm(\mathbf{0})|_{N_\pm}$, it follows that E^U_0 defined by $E^U_0 = \left(E^U_{0+} \cap N_+\right) \cup \left(E^U_{0-} \cap N_-\right)$ is a 1-dimensional unstable invariant set of the origin in the linearised system $\dot{\mathbf{z}} = \mathbf{L_X}(\mathbf{z})$ which maps into itself under σ. The origin is therefore unstable in $\dot{\mathbf{z}} = \mathbf{L_X}(\mathbf{z})$ for $\alpha > \Lambda_+\beta$. By considering the explicit form of the linearised equations, it can be shown that the origin is a stable fixed point of $\dot{\mathbf{z}} = \mathbf{L_X}(\mathbf{z})$ for $\alpha < \Lambda_+\beta$. A proof is given in section A.1.7.

The claim that trajectories of the nonlinear system lying close to $\mathbf{0}$ may be well approximated by corresponding trajectories of the linearised system would therefore seem to suggest that the origin will be unstable in the nonlinear system for $\alpha > \Lambda_+\beta$ and stable for $\alpha < \Lambda_+\beta$. The Stable Manifold Theorem implies that for $\alpha > \Lambda_+\beta$, the origin has a unique local unstable manifold $W^U_{0\pm}$ in the extended system $\dot{\mathbf{y}} = \mathbf{X}_\pm(\mathbf{y})$ such that $W^U_{0\pm}$ is 1-dimensional, C^∞ smooth and tangential to $E^U_{0\pm}$ at $\mathbf{0}$ [4]. Since $\mathbf{X}|_{N_\pm} = \mathbf{X}_\pm|_{N_\pm}$, it follows that W^U_0 defined by $W^U_0 = \left(W^U_{0+} \cap N_+\right) \cup \left(W^U_{0-} \cap N_-\right)$ is a 1-dimensional local unstable invariant set of the origin in $\dot{\mathbf{y}} = \mathbf{X}(\mathbf{y})$. Moreover, W^U_0 is (i) piecewise tangential to E^U_0 at $\mathbf{0}$ about $\mathbf{0}$, (ii) piecewise C^∞ smooth about $\mathbf{0}$ and (iii) maps into itself under σ. The existence of W^U_0 implies that the origin is unstable in the burster system for $\alpha > \Lambda_+\beta$. Numerical results suggest that for $\alpha < \Lambda_+\beta$ the origin is stable, as predicted. This will be assumed true in what follows. The fact that the origin changes stability with the sign of $\alpha - \Lambda_+\beta$ suggests that the burster system undergoes a nonsmooth codimension 1 bifurcation at the origin when $\alpha = \Lambda_+\beta$.

The hypothesis that trajectories $\mathbf{y}(\tau)$ of the burster system with $\|\mathbf{y}(\tau)\|$ small may be well approximated by corresponding trajectories of the linearised burster system can be used to obtain a more detailed insight into the stability properties of the origin in the burster system, by examining the behaviour of the linearised system $\dot{\mathbf{z}} = \mathbf{L}_\mathbf{X}(\mathbf{z})$. This will be of use when discussing saccades in chapter 6. There are 3 generic cases to consider: $\alpha > \Lambda_+\beta$, $\left(\Lambda_+ - \frac{1}{4\epsilon}\right)\beta < \alpha < \Lambda_+\beta$, and $\alpha < \left(\Lambda_+ - \frac{1}{4\epsilon}\right)\beta$. These are now analysed in turn.[4]

1. $\alpha > \Lambda_+\beta$

In this range $\lambda_1, \lambda_3 < 0$ and $\lambda_2 > 0$ with $|\lambda_3| > |\lambda_1|$ (cf. (3.84)). The origin is therefore a saddle node of $\dot{\mathbf{z}} = \mathbf{DX}_\pm(\mathbf{0})\,\mathbf{z}$, with the stable invariant plane $E^S_{0\pm} = \mathrm{Sp}\left\{L_0, \mathbf{w}_3^\pm\right\}$ and the unstable invariant line $E^U_{0\pm} = \mathrm{Sp}\left\{\mathbf{w}_2^\pm\right\}$. Since $|\lambda_3| > |\lambda_1|$, typical trajectories $\mathbf{z}(\tau)$ of $\dot{\mathbf{z}} = \mathbf{DX}_\pm(\mathbf{0})\,\mathbf{z}$ with $\mathbf{z}(0) \in E^S_{0\pm}$ contract onto the origin tangential to L_0. Trajectories with $\mathbf{z}(0) \notin E^S_{0\pm}$ diverge to ∞ in the direction of $E^U_{0\pm}$. Note that as L_0 is always a stable manifold of $\dot{\mathbf{z}} = \mathbf{DX}_+(\mathbf{0})\,\mathbf{z}$, trajectories of this system with initial condition in $E^S_{0+} \cap N_+$ will be confined to $E^S_{0+} \cap N_+$ for all $\tau \geq 0$, as they cannot cross L_0. Typical trajectories with initial condition in $E^S_{0+} \cap N_+$ will therefore contract to the origin tangential to L_0 confined to N_+. It follows that $E^S_{0+} \cap N_+$ is a stable invariant half-plane of $\mathbf{0}$ in $\dot{\mathbf{z}} = \mathbf{DX}_+(\mathbf{0})\,\mathbf{z}$. By symmetry, $E^S_{0-} \cap N_-$ is a stable invariant half-plane of $\mathbf{0}$ in $\dot{\mathbf{z}} = \mathbf{DX}_-(\mathbf{0})\,\mathbf{z}$. Since $\mathbf{L}_\mathbf{X}|_{N_\pm} = D\mathbf{X}_\pm(\mathbf{0})\,|_{N_\pm}$, it follows that the set E^S_0 defined by $E^S_0 = \left\{E^S_{0+} \cap N_+\right\} \cup \left\{E^S_{0-} \cap N_-\right\}$ is a local 2 dimensional invariant stable set of the origin in the linearised system $\dot{\mathbf{z}} = \mathbf{L}_\mathbf{X}(\mathbf{z})$,

[4] During the following analysis, it should be kept in mind that if the explicit dependence of $\mathbf{X}$ on $\boldsymbol{\alpha}$ were being considered, all local invariant sets of $\mathbf{0}$ in $\dot{\mathbf{y}} = \mathbf{X}(\mathbf{y})$ would be functions of $\boldsymbol{\alpha}$, as would all eigenvectors.

which maps into itself under σ. Typical trajectories $\mathbf{z}(\tau)$ of $\dot{\mathbf{z}} = \mathbf{L_X}(\mathbf{z})$ with $\mathbf{z}(0) \in E_0^S$ will contract to the origin tangential to L_0, confined to either N_+ or N_-.

It can be shown that trajectories of $\dot{\mathbf{z}} = \mathbf{L_X}(\mathbf{z})$ can only cross the plane P an infinite number of times if $1 - 4\epsilon(\Lambda_+ + \Lambda_-) < 0$ (cf. the remark at the end of section A.1.7). In the range of interest, $\Lambda_+ + \Lambda_- < 0$, implying that trajectories cross P a finite number of times. So let $\mathbf{z}(\tau)$ be a trajectory of the linearised system with $\mathbf{z}(0) \notin E_0^S$. The relation $\mathbf{L_X}|_{N_\pm} = D\mathbf{X}_\pm(\mathbf{0})|_{N_\pm}$ then implies that after crossing P for the final time, $\mathbf{z}(\tau)$ will be a trajectory of either $\dot{\mathbf{z}} = \mathbf{DX}_+(\mathbf{0})\,\mathbf{z}$ in N_+ or $\dot{\mathbf{z}} = \mathbf{DX}_-(\mathbf{0})\,\mathbf{z}$ in N_- for all subsequent time, and so will diverge to ∞ in the direction of either $E_{0+}^U \cap N_+$ or $E_{0-}^U \cap N_-$. Recalling the 1-dimensional unstable invariant set $E_0^U = \left(E_{0+}^U \cap N_+\right) \cup \left(E_{0-}^U \cap N_-\right)$ defined previously, it can be concluded that $\mathbf{z}(\tau)$ will cross P a finite number of times before diverging to ∞ in the direction of E_0^U.

Thus far, it has been argued that for $\alpha > \Lambda_+\beta$, the origin is a 'saddle node' of $\dot{\mathbf{z}} = \mathbf{L_X}(\mathbf{z})$, in that it has a 2-dimensional stable invariant set E_0^S and a 1-dimensional unstable invariant set E_0^U. Both these sets map into themselves under σ. It can be shown by applying the Stable Manifold Theorem to $\mathbf{0}$ in $\dot{\mathbf{z}} = \mathbf{DX}_\pm(\mathbf{0})\,\mathbf{z}$ and using the relation $\mathbf{X}|_{N_\pm} = \mathbf{X}_\pm|_{N_\pm}$ that in $\dot{\mathbf{y}} = \mathbf{X}(\mathbf{y})$, the origin has a 2-dimensional local stable invariant set W_0^S containing L_0. Moreover, W_0^S is (i) piecewise tangential to E_0^S at $\mathbf{0}$ about L_0, (ii) piecewise C^∞ smooth about L_0 and (iii) maps into itself under σ. For $\alpha > \Lambda_+\beta$, the origin is therefore a nonlinear 'saddle node' of the burster system, in that it has both stable and unstable local invariant sets, which are tangential to corresponding invariant sets of the linearised system at $\mathbf{0}$. Also, the conjecture that trajectories $\mathbf{y}(\tau)$ of the burster system with $\|\mathbf{y}(\tau)\|$ sufficiently small are well approximated by corresponding trajectories of the linearised burster system suggests that for $\mathbf{y}(0) \notin W_0^S$ with $\|\mathbf{y}(0)\|$ sufficiently small, $\mathbf{y}(\tau)$ crosses P a finite number of times before diverging away from the origin in the direction of E_0^U.

Figure (3-19) shows the projection onto the $(r - l, \varepsilon)$ plane of some trajectories of the burster system with $\mathbf{y}(0) \notin W_0^S$ and $\|\mathbf{y}(0)\|$ small obtained for $\{\alpha = 600, \beta = 7.5, \epsilon = 0.001\}$. For this choice of parameters, $\alpha > \Lambda_+\beta$. Also shown in figure (3-19) is the set E_0^U. It can be seen that trajectories cross the plane P a finite number of times before diverging away from the origin in the direction of E_0^U, as predicted.

2. $\left(\Lambda_+ - \frac{1}{4\epsilon}\right)\beta < \alpha < \Lambda_+\beta$

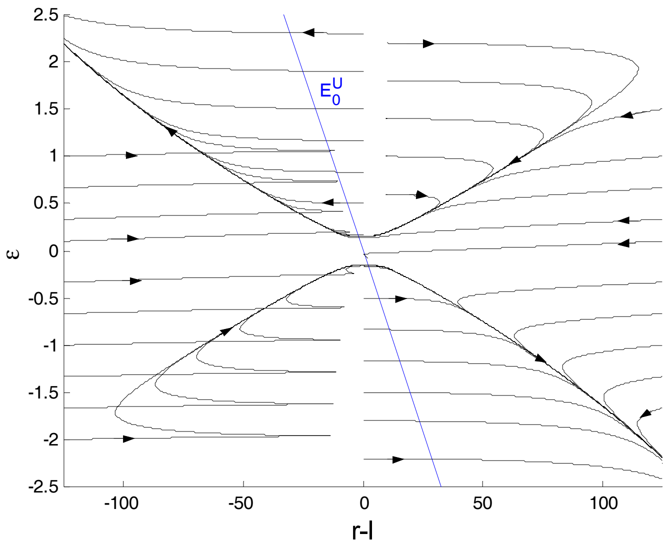

Figure 3-19: Projection onto the $(r-l,\varepsilon)$ plane of some trajectories $\mathbf{y}(\tau)$ of the burster system with $\|\mathbf{y}(0)\|$ small obtained for $\alpha = 600$, $\beta = 7.5$, $\epsilon = 0.001$. Arrows indicate the direction of trajectories with time.

In this range, $1 - 4\epsilon(\Lambda_+ + \Lambda_-) > 0$ and so $0 < \Delta < 1$, implying that λ_2 and λ_3 are real with $\lambda_2, \lambda_3 < 0$ and $|\lambda_1| > |\lambda_3| > |\lambda_2|$ (cf. (3.84)). The origin is therefore a stable node of $\dot{\mathbf{z}} = \mathbf{DX}_\pm(\mathbf{0})\,\mathbf{z}$, with the stable invariant lines L_0, $\mathrm{Sp}\left\{\mathbf{w}_2^\pm\right\}$ and $\mathrm{Sp}\left\{\mathbf{w}_3^\pm\right\}$. As $|\lambda_1| > |\lambda_3| > |\lambda_2|$, trajectories $\mathbf{z}(\tau)$ of $\dot{\mathbf{z}} = \mathbf{DX}_\pm(\mathbf{0})\,\mathbf{z}$ with $\mathbf{z}(0) \notin L_0 \cup \mathrm{Sp}\left\{\mathbf{w}_3^\pm\right\}$ contract onto the origin tangential to $\mathrm{Sp}\left\{\mathbf{w}_2^\pm\right\}$. Since $\mathbf{L_X}|_{N_\pm} = D\mathbf{X}_\pm(\mathbf{0})\,|_{N_\pm}$, it follows that in $\dot{\mathbf{z}} = \mathbf{L_X}(\mathbf{z})$, the origin will have the stable invariant lines L_0, E_2^S, E_3^S where $E_i^S = \left\{\mathrm{Sp}\left\{\mathbf{w}_i^+\right\} \cap N_+\right\} \cup \left\{\mathrm{Sp}\left\{\mathbf{w}_i^-\right\} \cap N_-\right\}$ for $2 \le i \le 3$. Note that E_2^S and E_3^S map into themselves under σ. For $\left(\Lambda_+ - \frac{1}{4\epsilon}\right)\beta < \alpha < \Lambda_+\beta$, the origin is therefore a 'stable node' of $\dot{\mathbf{z}} = \mathbf{L_X}(\mathbf{z})$ in that it is stable, with the 3 symmetric stable invariant lines, L_0, E_2^S and E_3^S defined above. Since $1 - 4\epsilon(\Lambda_+ + \Lambda_-) > 0$ in the range of interest, a given trajectory $\mathbf{z}(\tau)$ of $\dot{\mathbf{z}} = \mathbf{L_X}(\mathbf{z})$ will cross the plane P a finite number of times before being confined to N_+ or N_-. i.e. there will exist $s > 0$ such that $\mathbf{z}(\tau) \in N_+\ \forall \tau \ge s$ or $\mathbf{z}(\tau) \in N_-\ \forall \tau \ge s$. So assume $\mathbf{z}(0) \notin L_0 \cup E_3^S$. Then as $L_0 \cup E_3^S$ is invariant, $\mathbf{z}(s) \notin L_0 \cup E_3^S$. If $\mathbf{z}(s) \in N_+$, $\mathbf{z}(\tau)$ will be a solution of $\dot{\mathbf{z}} = \mathbf{DX}_+(\mathbf{0})\,\mathbf{z}$ on $[s, \infty)$ with $\mathbf{z}(s) \notin L_0 \cup \mathrm{Sp}\left\{\mathbf{w}_3^+\right\}$. The discussion of the system $\dot{\mathbf{z}} = \mathbf{DX}_+(\mathbf{0})\,\mathbf{z}$ above then implies that $\mathbf{z}(\tau)$ will contract to the origin tangential to $\mathrm{Sp}\left\{\mathbf{w}_2^+\right\}$ as $\tau \to \infty$ from s. A similar argument shows that if $\mathbf{z}(s) \in N_-$, $\mathbf{z}(\tau)$ will contract to the origin tangential to $\mathrm{Sp}\left\{\mathbf{w}_2^-\right\}$ as $\tau \to \infty$ from s. It has thus been argued that trajectories $\mathbf{z}(\tau)$ of the linearised system with $\mathbf{z}(0) \notin L_0 \cup E_3^S$ will cross P a finite number of times before contracting to the origin tangential to E_2^S. This suggests that

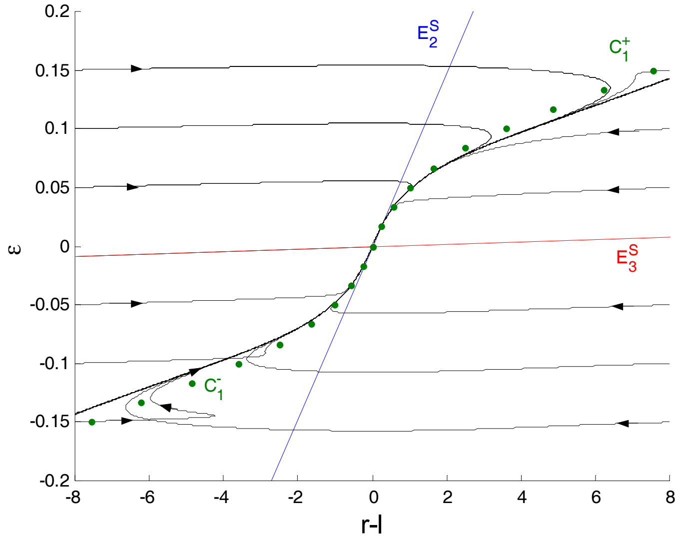

Figure 3-20: Projection onto the $(r-l, \varepsilon)$ plane of some trajectories $\mathbf{y}(\tau)$ of the burster system with $\|\mathbf{y}(0)\|$ small obtained for $\alpha = 80$, $\beta = 1.5$, $\epsilon = 0.001$. The dotted line indicates the slow manifold S_M. Arrows indicate the direction of trajectories with time.

typical trajectories $\mathbf{y}(\tau)$ of the nonlinear system with $\|\mathbf{y}(0)\|$ sufficiently small will cross P a finite number of times before contracting to the origin tangential to E_2^S.

Figure (3-20) shows the projection onto the $(r-l, \varepsilon)$ plane of some typical trajectories of the burster system with $\|\mathbf{y}(0)\|$ small obtained for $\{\alpha = 80, \beta = 1.5, \epsilon = 0.001\}$. For this choice of parameters, $\left(\Lambda_+ - \frac{1}{4\epsilon}\right)\beta < \alpha < \Lambda_+\beta$. Also shown in figure (3-20) are the sets E_2^S and E_3^S together with the slow manifold S_M. It can be seen that the trajectories shown cross the plane P a finite number of times before contracting to the origin tangential to E_2^S, as predicted. For $\left(\Lambda_+ - \frac{1}{4\epsilon}\right)\beta < \alpha < \Lambda_+\beta$, the origin is a nonlinear 'stable node' of $\dot{\mathbf{y}} = \mathbf{X}(\mathbf{y})$, in that its local behaviour appears to be determined by the dynamics of the linearised system $\dot{\mathbf{z}} = \mathbf{L}_{\mathbf{X}}(\mathbf{z})$, for which the origin is a 'stable node' in the sense described above.

3. $\alpha < \left(\Lambda_+ - \frac{1}{4\epsilon}\right)\beta$

For $\alpha < \left(\Lambda_+ - \frac{1}{4\epsilon}\right)\beta$, $1 - 4\epsilon(\Lambda_+ + \Lambda_-) < 0$ and so $\lambda_2 = \frac{1}{2}(-1 + \omega i), \lambda_3 = \frac{1}{2}(-1 - \omega i)$ where $\omega = \sqrt{4\epsilon(\Lambda_+ + \Lambda_-) - 1}$ (cf. (3.84)). It follows that the origin is a stable fixed point of $\dot{\mathbf{z}} = \mathbf{DX}_\pm(\mathbf{0})\,\mathbf{z}$ with invariant directions L_0 and $\mathrm{Sp}\left\{\mathrm{Re}\left\{\mathbf{w}_2^\pm\right\}, \mathrm{Im}\left\{\mathbf{w}_2^\pm\right\}\right\}$, such that on $\mathrm{Sp}\left\{\mathrm{Re}\left\{\mathbf{w}_2^\pm\right\}, \mathrm{Im}\left\{\mathbf{w}_2^\pm\right\}\right\}$ the origin is a stable focus. Trajectories $\mathbf{z}(\tau) = (u(\tau), v(\tau), w(\tau))^T$ of $\dot{\mathbf{z}} = \mathbf{DX}_\pm(\mathbf{0})\,\mathbf{z}$ with $\mathbf{z}(0) \notin L_0$ spiral around L_0 as they converge to the origin. More-

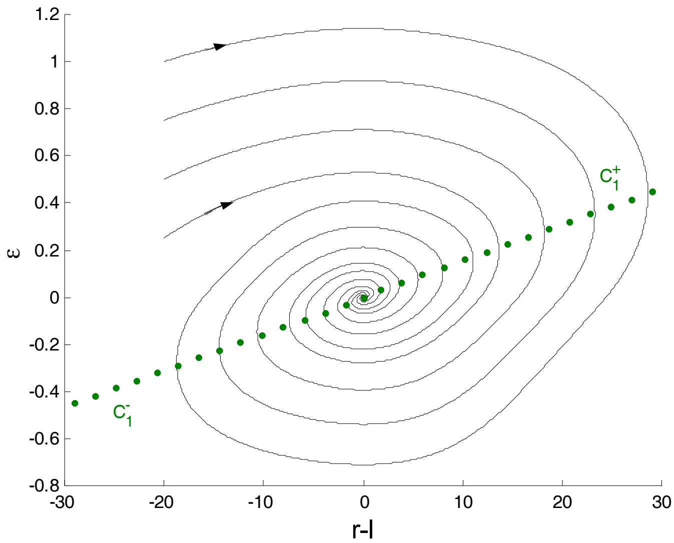

Figure 3-21: Projection onto the $(r-l,\varepsilon)$ plane of some trajectories $\mathbf{y}(\tau)$ of the burster system with $\|\mathbf{y}(0)\|$ small for $\alpha = 200$, $\beta = 15$, $\epsilon = 0.05$. The dotted line indicates the slow manifold S_M. Arrows indicate the direction of trajectories with time.

over, since $\dot{w} = -\epsilon(u-v)$ in $\dot{\mathbf{z}} = \mathbf{DX}_+(\mathbf{0})\,\mathbf{z}$ and $\dot{\mathbf{z}} = \mathbf{DX}_-(\mathbf{0})\,\mathbf{z}$, the spiralling direction is the same in both linear systems. As $\mathbf{L_X}|_{N_\pm} = D\mathbf{X}_\pm(\mathbf{0})\,|_{N_\pm}$, it follows that trajectories $\mathbf{z}(\tau)$ of $\dot{\mathbf{z}} = \mathbf{L_X}(\mathbf{z})$ with $\mathbf{z}(0) \notin L_0$ will spiral around L_0 as they approach the origin. This suggests that trajectories $\mathbf{y}(\tau)$ of the burster system with $\|\mathbf{y}(0)\|$ sufficiently small and $\mathbf{y}(0) \notin L_0$ will spiral around L_0 as they converge to the origin.

Figure (3-21) shows the projection onto the $(r-l,\varepsilon)$ plane of some trajectories $\mathbf{y}(\tau)$ of the burster system with $\|\mathbf{y}(0)\|$ small and $\mathbf{y}(0) \notin L_0$ obtained for $\{\alpha = 200, \beta = 15, \epsilon = 0.05\}$. For this choice of parameters, $\alpha < \left(\Lambda_+ - \frac{1}{4\epsilon}\right)\beta$. Also shown in figure (3-21) is the slow manifold S_M. The behaviour of the trajectories is as expected.

Figure (3-22) summarises the work on the stability of the origin in the burster system given above. It is instructive to consider the effect on the stability of $\mathbf{0}$ of increasing ϵ for a fixed α and β with $\alpha < \Lambda_+\beta$. This will be useful when discussing saccades in Chapter 6. Figure (3-22) shows that as ϵ is increased for such a choice of (β,α), the origin changes from a stable node to a stable fixed point for which trajectories $\mathbf{y}(\tau)$ with $\mathbf{y}(0) \notin L_0$ spiral around L_0 as they contract to the origin. This change can be interpreted in terms of the slow manifold S_M. For ϵ small, trajectories with $\mathbf{y}(0) \notin L_0$ and $\|\mathbf{y}(0)\|$ small contract onto S_M and converge along it to $\mathbf{0}$ (cf. figure (3-20)). Increasing ϵ causes these trajectories

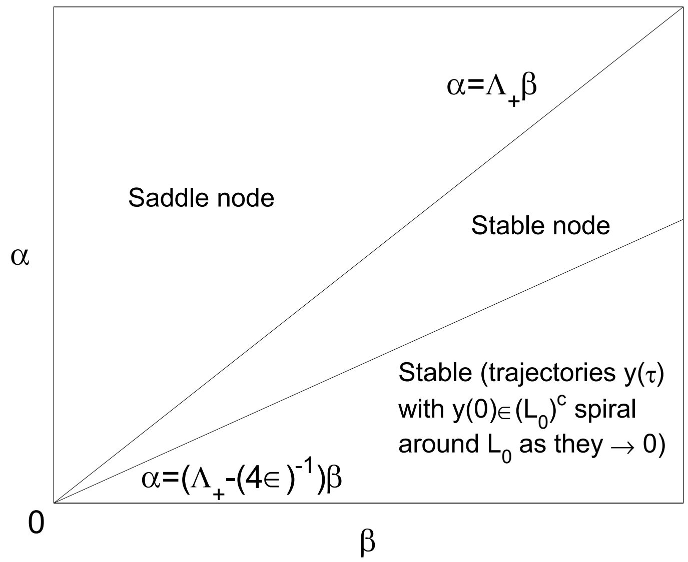

Figure 3-22: Stability of the origin as a fixed point of $\dot{\mathbf{y}} = \mathbf{X}(\mathbf{y})$.

to contract onto S_M more slowly and follow it less closely, until they eventually begin to spiral around L_0 as they approach the origin (cf. figure (3-21)).

3.6.4 Approximation to $\varepsilon(\tau)$ for large $\tau \geq 0$ for initial conditions in $\mathcal{B}(\mathbf{0})$ with $\left(\Lambda_+ - \frac{1}{4\epsilon}\right)\beta < \alpha < \Lambda_+\beta$ or $0 < \alpha < \left(\Lambda_+ - \frac{1}{4\epsilon}\right)\beta$

Assume that $\left(\Lambda_+ - \frac{1}{4\epsilon}\right)\beta < \alpha < \Lambda_+\beta$, so that $\mathbf{0}$ is a stable node of $\dot{\mathbf{y}} = \mathbf{X}(\mathbf{y})$, or $0 < \alpha < \left(\Lambda_+ - \frac{1}{4\epsilon}\right)\beta$, so that $\mathbf{0}$ is a stable fixed point for which trajectories spiral around L_0 as they approach $\mathbf{0}$. Let $\mathbf{y}_0$ lie in $\mathcal{B}(\mathbf{0})$ and define $\mathbf{y}(\tau) = (r(\tau), l(\tau), \varepsilon(\tau))^T = \phi_\tau(\mathbf{y}_0)$ $\forall \tau \geq 0$. In this section, an approximate expression for $\varepsilon(\tau)$ is obtained for large τ, based on the assumption that sufficiently close to $\mathbf{0}$, the nonlinear dynamics are well approximated by the linearised dynamics (cf. the similar analysis of section 3.6.2). This expression will be used when discussing the modelling of saccades in chapter 6. Write $L_\tau^{\mathbf{0}}$ for the flow associated with the linearised dynamics $\dot{\mathbf{z}} = \mathbf{L}_{\mathbf{x}}(\mathbf{z})$. Then by assumption, given $\|\mathbf{y}\|$ sufficiently small, for all sufficiently large $\tau > 0$:

$$\phi_\tau(\mathbf{y}) \approx L_\tau^{\mathbf{0}}(\mathbf{y})$$

Choose τ_L for which $\left\|\phi_{\tau_L}(\mathbf{y}_0)\right\|$ is sufficiently small. The expression above then implies that for sufficiently large $\tau > 0$:

$$\phi_\tau\left(\phi_{\tau_L}(\mathbf{y}_0)\right) \approx L_\tau^{\mathbf{0}}\left(\phi_{\tau_L}(\mathbf{y}_0)\right)$$

Write $\mathbf{y}_L = \phi_{\tau_L}(\mathbf{y}_0)$, and define $\mathbf{z}_L(\tau) = (u_L(\tau), v_L(\tau), w_L(\tau))^T = L_\tau^{\mathbf{0}}\mathbf{y}_L\ \forall\tau \geq 0$. $\mathbf{z}_L(\tau)$ solves the linearised system $\dot{\mathbf{z}} = \mathbf{L}_{\mathbf{X}}(\mathbf{z})$ with initial condition $\mathbf{z}_L(0) = \mathbf{y}_L$. Moreover, the expression above implies that for sufficiently large $\tau > 0$:

$$\mathbf{y}(\tau + \tau_L) \approx \mathbf{z}_L(\tau)$$

It follows that for sufficiently large $\tau - \tau_L > 0$

$$\mathbf{y}(\tau) \approx \mathbf{z}_L(\tau - \tau_L)$$

which suggests:

$$\varepsilon(\tau) \approx w_L(\tau - \tau_L) \tag{3.96}$$

Thus far, it has been shown that $\exists\tau_L > 0$ such that $\varepsilon(\tau)$ satisfies the approximation (3.96) for sufficiently large $\tau - \tau_L > 0$. This is equivalent to the statement that for sufficiently large $\tau_L > 0$, $\varepsilon(\tau)$ satisfies (3.96) $\forall\tau \geq \tau_L$.

Section A.1.7 of the Appendix implies that $w_L(\tau)$ satisfies

$$\ddot{w}_L + \dot{w}_L + \epsilon(\Lambda_+ + \Lambda_-)w_L = 0$$

and

$$\dot{w}_L = -\epsilon(u_L - v_L)$$

on $[0, \infty)$. The first equation in this pair shows that $w_L(\tau)$ solves the general linear harmonic oscillator equation $\ddot{X} + a\dot{X} + bX = 0$ on $[0, \infty)$ with $a = 1$ and $b = \epsilon(\Lambda_+ + \Lambda_-)$. Since $\mathbf{y}_L = \phi_{\tau_L}(\mathbf{y}_0)$, $u_L(0) = r(\tau_L)$, $v_L(0) = l(\tau_L)$ and $w_L(0) = \varepsilon(\tau_L)$. The second equation therefore implies that $\dot{w}_L(0) = -\epsilon b(\tau_L)$, where $b(\tau_L) = r(\tau_L) - l(\tau_L)$. The discussion of the equation $\ddot{X} + a\dot{X} + bX = 0$ in section A.1.4 of the Appendix leads to the following expressions for $w_L(\tau)$ on $[0, \infty)$ in the ranges $\left(\Lambda_+ - \frac{1}{4\epsilon}\right)\beta < \alpha < \Lambda_+\beta$ and $0 < \alpha < \left(\Lambda_+ - \frac{1}{4\epsilon}\right)\beta$:

1. $\left(\Lambda_+ - \frac{1}{4\epsilon}\right)\beta < \alpha < \Lambda_+\beta$. In this range, $1 - 4\epsilon\left(\Lambda_+ + \Lambda_-\right) > 0$. Thus, $\forall\tau \geq 0$

$$w_L(\tau) = Ae^{\lambda_2\tau} + Be^{\lambda_3\tau} \tag{3.97}$$

where:

$$\begin{aligned} d &= \sqrt{1 - 4\epsilon\left(\Lambda_+ + \Lambda_-\right)} \\ A &= -\tfrac{1}{d}\left(\lambda_3\varepsilon\left(\tau_L\right) + \epsilon b\left(\tau_L\right)\right) \\ B &= \tfrac{1}{d}\left(\lambda_2\varepsilon\left(\tau_L\right) + \epsilon b\left(\tau_L\right)\right) \end{aligned} \tag{3.98}$$

2. $0 < \alpha < \left(\Lambda_+ - \frac{1}{4\epsilon}\right)\beta$. In this range, $1 - 4\epsilon\left(\Lambda_+ + \Lambda_-\right) < 0$. Thus, $\forall\tau \geq 0$

$$w_L(\tau) = Ae^{-\frac{\tau}{2}}\cos\left(d\tau + B\right) \tag{3.99}$$

where:

$$\begin{aligned} d &= \tfrac{1}{2}\sqrt{4\epsilon\left(\Lambda_+ + \Lambda_-\right) - 1} \\ A &= \tfrac{1}{d}\sqrt{\left(\tfrac{1}{4} + d^2\right)\varepsilon\left(\tau_L\right)^2 - \epsilon\varepsilon\left(\tau_L\right)b\left(\tau_L\right) + \epsilon^2 b\left(\tau_L\right)^2} \\ B &= -\arctan\left(\tfrac{\varepsilon(\tau_L) - 2\epsilon b(\tau_L)}{2d\varepsilon(\tau_L)}\right) \end{aligned} \tag{3.100}$$

In conclusion, it has been argued here that for sufficiently large $\tau_L > 0$, $\varepsilon(\tau)$ satisfies the approximation (3.96) $\forall\tau \geq \tau_L$, where $w_L(\tau)$ is defined by either (3.97)-(3.98) or (3.99)-(3.100).

3.6.5 Stability of the fixed points in the (β, α) plane

Using the analysis of sections 3.6.1 and 3.6.3, the stability of the fixed points in each region of the (β, α) plane is summarised in figure (3-23).

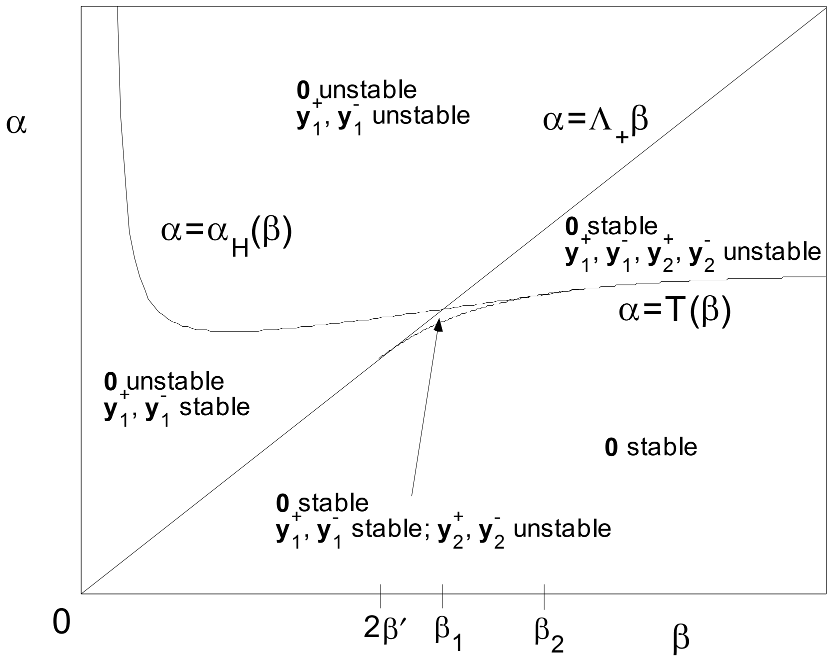

Figure 3-23: Stability of the fixed points of the burster system in the (β, α) plane. Codimension 1 bifurcations occur on the curves $\alpha = \Lambda_+\beta$, $\alpha = \alpha_H(\beta)$ and $\alpha = T(\beta)$.

Chapter 4

Analysis of the burster equations II: Bifurcations

In this chapter, the bifurcations and attractors of the burster equations $\dot{\mathbf{y}} = \mathbf{X}(\mathbf{y}; \boldsymbol{\alpha})$ are investigated. Consequently, the vector field $\mathbf{X}$ will be explicitly considered as a function of the parameter vector $\boldsymbol{\alpha}$ in the following analysis. To begin with, each of the instabilities proposed in the previous chapter is analysed. The results of this analysis together with the restriction on the behaviour of trajectories imposed by the existence of the slow manifold $S_M(\alpha, \beta)$ will then enable a full picture of the bifurcations and attractors of $\dot{\mathbf{y}} = \mathbf{X}(\mathbf{y}; \boldsymbol{\alpha})$ to be proposed for ϵ small. Finally, the effect on the attractors of $\dot{\mathbf{y}} = \mathbf{X}(\mathbf{y}; \boldsymbol{\alpha})$ of increasing ϵ will be discussed. This will enable a full classification of the bifurcations and attractors of the burster equations to be proposed for $\boldsymbol{\alpha}$ in a range $\hat{\Pi}_P$ containing the physiological range Π_P. During this work, several parameter regions will be located in which the error time series associated with limit cycle attractors of the burster equations resemble congenital nystagmus waveforms.

Recall from section 3.6 that the burster system $\dot{\mathbf{y}} = \mathbf{X}(\mathbf{y}; \boldsymbol{\alpha})$ undergoes a codimension 2 bifurcation at $\mathbf{y}_1^{\pm}$ when $\{\alpha = \alpha_2, \beta = \beta_2\}$, a codimension 1 bifurcation at $\mathbf{y}_1^{\pm}$ when $\alpha = \alpha_H(\beta)$, a codimension 1 bifurcation at $\mathbf{y}_1^{\pm}$ when $\{\alpha = T(\beta), \beta \neq \beta_2\}$ and a codimension 1 bifurcation at the origin when $\alpha = \Lambda_+\beta$. Each of these bifurcations is examined in greater detail during this section. The bifurcation at the origin is perhaps the most interesting, since it occurs in a region of the state space where the vector field is not smooth. This will be examined first.

4.1 The bifurcation at the origin when $\alpha = \Lambda_+\beta$

Set $\mu = -(\Lambda_+ + \Lambda_-)$. For simplicity μ will be used as the bifurcation parameter during this section, so that the bifurcation at the origin occurs at $\mu = 0$. It is important to note that the bifurcation must change type at $\beta = 2\beta'$, since as μ increases through 0 in $\beta \leq 2\beta'$, the origin becomes unstable and a pair of stable fixed points $\{\mathbf{y}_1^+, \mathbf{y}_1^-\}$ are created, while as μ increases through 0 in $\beta > 2\beta'$ the origin becomes unstable and a pair of unstable fixed points $\{\mathbf{y}_2^+, \mathbf{y}_2^-\}$ are destroyed (cf. fig (3-23)). The bifurcation which occurs at $\mu = 0$ can be understood in both these cases by examining the properties of the extended system $\dot{\mathbf{y}} = \mathbf{X}_+(\mathbf{y}; \boldsymbol{\alpha})$ in the neighbourhood of the origin for small μ. It is first shown that given ϵ, for small μ the origin has a 1-dimensional local invariant set $W_0^C(\boldsymbol{\alpha})$ in $\dot{\mathbf{y}} = \mathbf{X}(\mathbf{y}; \boldsymbol{\alpha})$. $W_0^C(\boldsymbol{\alpha})$ is obtained by gluing together the sets $W_{0+}^C(\boldsymbol{\alpha}) \cap N_+$ and $\sigma W_{0+}^C(\boldsymbol{\alpha}) \cap N_-$, where $W_{0+}^C(\boldsymbol{\alpha})$ is a 1-dimensional C^∞ local invariant manifold of the origin in $\dot{\mathbf{y}} = \mathbf{X}_+(\mathbf{y}; \boldsymbol{\alpha})$. The dynamics on $W_0^C(\boldsymbol{\alpha})$ are then derived from the smooth dynamics on $W_{0+}^C(\boldsymbol{\alpha})$. It is found that as μ increases through 0 in $\beta \leq 2\beta'$, $\mathbf{y}_1^+$ and $\mathbf{y}_1^-$ are created in a supercritical pitchfork-type bifurcation on $W_0^C(\boldsymbol{\alpha})$, while as μ increases through 0 in $\beta > 2\beta'$, $\mathbf{y}_2^+$ and $\mathbf{y}_2^-$ are destroyed in a subcritical pitchfork-type bifurcation on $W_0^C(\boldsymbol{\alpha})$. For $\beta \neq 2\beta'$, this 'pitchfork-type' bifurcation can be attributed to a transcritical bifurcation on $W_{0+}^C(\boldsymbol{\alpha})$, while for $\beta = 2\beta'$, it can be attributed to a pitchfork bifurcation on $W_{0+}^C(\boldsymbol{\alpha})$. Finally, the flow on $W_0^C(\boldsymbol{\alpha})$ in the immediate neighbourhood of the origin for μ small is characterised.

For simplicity, it will be assumed throughout the following analysis that β is fixed, and α is being implicitly varied by varying μ.

4.1.1 Derivation of the dynamics on $W_0^C(\boldsymbol{\alpha})$ for small μ

Fix $\epsilon, \beta > 0$ and consider the extended system $\dot{\mathbf{y}} = \mathbf{X}_+(\mathbf{y};\alpha, \beta, \epsilon)$. From equations (3.12)-(3.13), μ is given in terms of α and β by:

$$\mu = \frac{\alpha}{\beta} - \Lambda_+$$

Rearranging for α gives:

$$\alpha = \beta(\mu + \Lambda_+)$$

Write $\dot{\mathbf{y}} = \mathbf{X}_+(\mathbf{y};\alpha,\beta,\epsilon)$ in the μ parameter coordinates as $\dot{\mathbf{y}} = \mathbf{X}_+(\mathbf{y};\mu,\beta,\epsilon)$, and the burster system $\dot{\mathbf{y}} = \mathbf{X}(\mathbf{y};\alpha,\beta,\epsilon)$ as $\dot{\mathbf{y}} = \mathbf{X}(\mathbf{y};\mu,\beta,\epsilon)$. Then since $\mathbf{X}_+(\mathbf{y};\alpha,\beta,\epsilon)$ is a C^∞ function of $\mathbf{y}$ and α for $\mathbf{y} \in \mathbb{R}^3$, $\alpha \in (0,\infty)$, it follows that $\mathbf{X}_+(\mathbf{y};\mu,\beta,\epsilon)$ is a C^∞ function of $\mathbf{y}$ and μ for $\mathbf{y} \in \mathbb{R}^3$, $\mu \in (-\Lambda_+,\infty)$ (cf. section 3.1.3). Expanding each of the components of $\mathbf{X}_+(\mathbf{y};\mu,\beta,\epsilon)$ as power series in r, l and ε about $\mathbf{0}$ leads to the following expression for $\mathbf{X}_+(\mathbf{y};\mu,\beta,\epsilon)$:

$$\mathbf{X}_+(\mathbf{y};\mu,\beta,\epsilon) = D_{\mathbf{y}}\mathbf{X}_+(\mathbf{0};\mu,\beta,\epsilon)\,\mathbf{y} + \mathbf{R}(\mathbf{y};\mu,\beta,\epsilon) \tag{4.1}$$

Here the components of $\mathbf{R}(\mathbf{y};\mu,\beta,\epsilon)$ contain terms of the form $f(\mu,\beta,\epsilon)\,r^{k_1}l^{k_2}\varepsilon^{k_3}$, where $k_i \geq 0$ for $1 \leq i \leq 3$ with $k_1+k_2+k_3 \geq 2$, and $f(\mu,\beta,\epsilon)$ is a C^∞ function of μ on $(-\Lambda_+,\infty)$. Explicitly, $\dot{\mathbf{y}} = \mathbf{X}_+(\mathbf{y};\mu,\beta,\epsilon)$ is:

$$\begin{aligned}
\dot{r} &= -r + \Lambda_+\varepsilon - \gamma r l^2 - \frac{\Lambda_+}{2\beta'}\varepsilon^2 + \frac{\Lambda_+}{6\left(\beta'\right)^2}\varepsilon^3 + O\left(\varepsilon^4\right) && (4.2)\\
\dot{l} &= -l + (\mu+\Lambda_+)\,\varepsilon - \gamma l r^2 - \frac{(\mu+\Lambda_+)}{\beta}\varepsilon^2 + \frac{(\mu+\Lambda_+)}{2\beta^2}\varepsilon^3 + O\left(\varepsilon^4\right) && (4.3)\\
\dot{\varepsilon} &= -\epsilon r + \epsilon l && (4.4)
\end{aligned}$$

At $\mu = 0$, the derivative of $\mathbf{X}_+$ with respect to $\mathbf{y}$ evaluated at $\mathbf{0}$, $D_{\mathbf{y}}\mathbf{X}_+(\mathbf{0};0,\beta,\epsilon)$, is given by:

$$D_{\mathbf{y}}\mathbf{X}_+(\mathbf{0};0,\beta,\epsilon) = \begin{pmatrix} -1 & 0 & \Lambda_+ \\ 0 & -1 & \Lambda_+ \\ -\epsilon & \epsilon & 0 \end{pmatrix}$$

(cf. (3.83)). This has eigenvalues -1 with multiplicity 2 and 0 with multiplicity 1. The eigenvector corresponding to 0 is $\mathbf{w}_P = (\Lambda_+,\Lambda_+,1)^T$. The generalised eigenvectors of $D_{\mathbf{y}}\mathbf{X}_+(\mathbf{0};0,\beta,\epsilon)$ corresponding to -1 can be taken to be $(1,1,0)^T$ and $\mathbf{v}_P = \left(\frac{1}{\epsilon\Lambda_+}, 0, \frac{1}{\Lambda_+}\right)^T$.

Define the 3×3 matrix $P_+(\epsilon)$ by $P_+(\epsilon) = \left[(1,1,0)^T\ \mathbf{v}_P\ \mathbf{w}_P\right]$. Then the matrix

$$P_+(\epsilon)^{-1}\,D_{\mathbf{y}}\mathbf{X}_+(\mathbf{0};0,\beta,\epsilon)\,P_+(\epsilon)$$

is a normal form for $D_{\mathbf{y}}\mathbf{X}_+(\mathbf{0};0,\beta,\epsilon)$. Explicitly:

$$P_+(\epsilon)^{-1} D_{\mathbf{y}}\mathbf{X}_+(\mathbf{0};0,\beta,\epsilon)\,P_+(\epsilon) = \begin{pmatrix} -1 & 1 & 0 \\ 0 & -1 & 0 \\ 0 & 0 & 0 \end{pmatrix} \tag{4.5}$$

Perform the change of coordinates $\mathbf{y} \to \mathbf{x}_+$ given by $\mathbf{x}_+ = (x_+, y_+, z_+)^T = P_+(\epsilon)^{-1}\mathbf{y}$. The coordinate transformations $\mathbf{x}_+ \to \mathbf{y}$ and $\mathbf{y} \to \mathbf{x}_+$ are given by

$$x_+ = \epsilon\Lambda_+ r + (1 - \epsilon\Lambda_+)\,l - \Lambda_+\varepsilon \tag{4.6}$$

$$y_+ = \epsilon\Lambda_+ r - \epsilon\Lambda_+ l \tag{4.7}$$

$$z_+ = -\epsilon r + \epsilon l + \varepsilon \tag{4.8}$$

and:

$$r = x_+ + \frac{1}{\epsilon\Lambda_+}y_+ + \Lambda_+ z_+ \tag{4.9}$$

$$l = x_+ + \Lambda_+ z_+ \tag{4.10}$$

$$\varepsilon = \frac{1}{\Lambda_+}y_+ + z_+ \tag{4.11}$$

In the new coordinates, the dynamics are $\dot{\mathbf{x}}_+ = \mathbf{G}(\mathbf{x}_+;\mu,\beta,\epsilon)$ where:

$$\mathbf{G}(\mathbf{x}_+;\mu,\beta,\epsilon) = P_+(\epsilon)^{-1}\mathbf{X}_+(P_+(\epsilon)\,\mathbf{x}_+;\mu,\beta,\epsilon) \tag{4.12}$$

Since $\mathbf{X}_+(\mathbf{y};\mu,\beta,\epsilon)$ is C^∞ in $\mathbf{y}$ and μ for $\mathbf{y} \in \mathbb{R}^3$, $\mu \in (-\Lambda_+, \infty)$, it follows that $\mathbf{G}(\mathbf{x}_+;\mu,\beta,\epsilon)$ is C^∞ in $\mathbf{x}_+$ and μ over this range. Write:

$$\mathbf{G}(\mathbf{x}_+;\mu,\beta,\epsilon) = (G_1(\mathbf{x}_+;\mu,\beta,\epsilon), G_2(\mathbf{x}_+;\mu,\beta,\epsilon), G_3(\mathbf{x}_+;\mu,\beta,\epsilon))^T$$

Then for each $1 \le i \le 3$, $G_i(\mathbf{x}_+;\mu,\beta,\epsilon)$ is also C^∞ in $\mathbf{x}_+$ and μ for $\mathbf{y} \in \mathbb{R}^3$, $\mu \in (-\Lambda_+, \infty)$. Substituting $\mathbf{y} = P_+(\epsilon)\,\mathbf{x}_+$ into (4.1) and then substituting into (4.12) gives

$$\mathbf{G}(\mathbf{x}_+;\mu,\beta,\epsilon) = A(\mu,\beta,\epsilon)\,\mathbf{x}_+ + \mathbf{S}(\mathbf{x}_+;\mu,\beta,\epsilon) \tag{4.13}$$

where

$$A(\mu,\beta,\epsilon) = P_+(\epsilon)^{-1} D_{\mathbf{y}}\mathbf{X}_+(\mathbf{0};\mu,\beta,\epsilon)\,P_+(\epsilon) \tag{4.14}$$

and:

$$\mathbf{S}\left(\mathbf{x}_+;\mu,\beta,\epsilon\right) = P_+\left(\epsilon\right)^{-1}\mathbf{R}\left(P_+\left(\epsilon\right)\mathbf{x}_+;\mu,\beta,\epsilon\right)$$

Here the components of $\mathbf{S}\left(\mathbf{x}_+;\mu,\beta,\epsilon\right)$ contain terms of the form $g\left(\mu,\beta,\epsilon\right)x_+^{k_1}y_+^{k_2}z_+^{k_3}$ where $k_i \geq 0$ for $1 \leq i \leq 3$ with $k_1 + k_2 + k_3 \geq 2$, and $g\left(\mu,\beta,\epsilon\right)$ is a C^∞ function of μ on $(-\Lambda_+,\infty)$. Note that this implies $\mathbf{G}\left(\mathbf{0};\mu,\beta,\epsilon\right) = \mathbf{0}$ $\forall\mu \in (-\Lambda_+,\infty)$.

Consider the system composed of $\dot{\mathbf{x}}_+ = \mathbf{G}\left(\mathbf{x}_+,\mu;\beta,\epsilon\right)$ together with the trivial equation $\dot{\mu} = 0$:

$$\dot{\mathbf{x}}_+ = \mathbf{G}\left(\mathbf{x}_+,\mu;\beta,\epsilon\right) \tag{4.15}$$

$$\dot{\mu} = 0 \tag{4.16}$$

$(\mathbf{0},\mu)^T$ is a fixed point of this augmented system $\forall\mu \in (-\Lambda_+,\infty)$. Moreover, as $\mathbf{G}\left(\mathbf{x}_+,\mu;\beta,\epsilon\right)$ is a C^∞ function of $(\mathbf{x}_+,\mu)^T$ for $\mathbf{x}_+ \in \mathbb{R}^3$, $\mu \in (-\Lambda_+,\infty)$, the vector field of this augmented system is a C^∞ function of $(\mathbf{x}_+,\mu)^T$ over this range. In particular, the vector field is C^∞ in a neighbourhood of $(\mathbf{0},0)^T$.

The derivative of the vector field of the augmented system evaluated at $(\mathbf{0},0)^T$ is:

$$\begin{pmatrix} D_{\mathbf{x}_+}\mathbf{G}\left(\mathbf{0},0;\beta,\epsilon\right) & D_\mu\mathbf{G}\left(\mathbf{0},0;\beta,\epsilon\right) \\ 0 & 0 \end{pmatrix}$$

(4.13) and (4.14) imply that:

$$\begin{aligned} D_{\mathbf{x}_+}\mathbf{G}\left(\mathbf{0},0;\beta,\epsilon\right) &= P_+\left(\epsilon\right)^{-1}D_{\mathbf{y}}\mathbf{X}_+\left(\mathbf{0};0,\beta,\epsilon\right)P_+\left(\epsilon\right) \\ D_\mu\mathbf{G}\left(\mathbf{0},0;\beta,\epsilon\right) &= \mathbf{0} \end{aligned}$$

Thus, from (4.5), the derivative at $(\mathbf{0},0)^T$ is:

$$\begin{pmatrix} -1 & 1 & 0 & 0 \\ 0 & -1 & 0 & 0 \\ 0 & 0 & 0 & 0 \\ 0 & 0 & 0 & 0 \end{pmatrix} \tag{4.17}$$

Explicitly the equations for the augmented system (4.15)-(4.16) are

$$
\begin{aligned}
\dot{x}_+ &= -x_+ + y_+ + \frac{a}{\Lambda_+}\mu y_+ + a\mu z_+ + 2\epsilon\Lambda_+ d y_+ z_+ + \epsilon d y_+^2 + \epsilon\Lambda_+^2 d z_+^2 \\
&\quad +\Lambda_+ f z_+^3 + \hat{O}\left(3\right) &\quad (4.18)\\
\dot{y}_+ &= -y_+ - \epsilon\mu y_+ - \epsilon\Lambda_+\mu z_+ + 2\epsilon\Lambda_+ b y_+ z_+ + \epsilon b y_+^2 + \epsilon\Lambda_+^2 b z_+^2 + \epsilon\Lambda_+^2 e z_+^3 \\
&\quad +\hat{O}\left(3\right) &\quad (4.19)\\
\dot{z}_+ &= \epsilon\mu z_+ + \frac{\epsilon}{\Lambda_+}\mu y_+ - 2\epsilon b y_+ z_+ - \frac{\epsilon}{\Lambda_+} b y_+^2 - \epsilon\Lambda_+ b z_+^2 - \epsilon\Lambda_+ e z_+^3 + \hat{O}\left(3\right) &\quad (4.20)\\
\dot{\mu} &= 0 &\quad (4.21)
\end{aligned}
$$

where a, b, c, d and e are constants given by

$$
\begin{aligned}
a &= 1 - \epsilon\Lambda_+ \\
b &= \tfrac{1}{\beta} - \tfrac{1}{2\beta'} \\
c &= \tfrac{\epsilon}{6(\beta')^2} - \gamma\Lambda_+ \\
d &= b - \tfrac{1}{\epsilon\beta\Lambda_+} \\
e &= \tfrac{1}{6(\beta')^2} - \tfrac{1}{2\beta^2} \\
f &= \tfrac{1}{2\beta^2} a + \Lambda_+ c
\end{aligned}
\qquad (4.22)
$$

and $\hat{O}\left(3\right)$ denotes terms of order 3 in x_+, y_+, z_+ and μ, excluding z_+^3. (4.17) implies that in the linearised augmented system, the origin $(\mathbf{0}, 0)^T$ has a 2-dimensional stable manifold

$$E_{0+}^S = \left\{(x_+, y_+, z_+, \mu)^T : z_+, \mu = 0\right\}$$

and a 2-dimensional centre manifold:

$$E_{0+}^C = \left\{(x_+, y_+, z_+, \mu)^T : x_+, y_+ = 0\right\}$$

It follows from the Centre Manifold Theorem that in the nonlinear augmented system, the origin has a 2-dimensional C^∞ local stable manifold $W_{0+}^S(\beta, \epsilon)$ tangential to E_{0+}^S at $(\mathbf{0}, 0)^T$, and a 2-dimensional C^∞ local centre manifold $W_{0+}^C(\beta, \epsilon)$ tangential to E_{0+}^C at $(\mathbf{0}, 0)^T$ [4]. Moreover, as $(\mathbf{0}, \mu)^T$ is a fixed point of the system $\forall \mu \in (-\Lambda_+, \infty)$, $(\mathbf{0}, \mu)^T \in W_{0+}^C(\beta, \epsilon)$ for sufficiently small μ. Now as $W_{0+}^C(\beta, \epsilon)$ is tangential to E_{0+}^C at $(\mathbf{0}, 0)^T$, $W_{0+}^C(\beta, \epsilon)$ can be considered as a graph

$$\left\{\left(h_1\left(z_+, \mu; \beta, \epsilon\right), h_2\left(z_+, \mu; \beta, \epsilon\right), z_+, \mu\right)^T\right\}$$

over z_+ and μ for small $\left\|(z_+,\mu)^T\right\|$, where h_1 and h_2 are C^∞ functions of z_+ and μ with $h_i(0,\mu;\beta,\epsilon)=0$, and $\frac{\partial h_i}{\partial z_+}(0,0;\beta,\epsilon)=\frac{\partial h_i}{\partial \mu}(0,0;\beta,\epsilon)=0$ for $i=1,2$. The centre manifold dynamics can be found up to terms of order 2 and z_+^3 by calculating $h_2(z_+,\mu;\beta,\epsilon)$ up to these terms, and then substituting $x_+=h_1(z_+,\mu;\beta,\epsilon)$, $y_+=h_2(z_+,\mu;\beta,\epsilon)$ into equation (4.20).

So write $h_2(z_+,\mu;\beta,\epsilon)$ as

$$h_2(z_+,\mu;\beta,\epsilon)=k_1z_+^2+k_2\mu z_++k_3\mu^2+k_4z_+^3+\hat{O}(3) \tag{4.23}$$

where, as above, $\hat{O}(3)$ represents terms of order 3 in y_+, z_+ and μ, excluding z_+^3. The constants $k_1\to k_4$ can be found by obtaining two different expressions for $\dot{y}_+$, equating these expressions and then comparing coefficients. On the centre manifold, $y_+=h_2(z_+,\mu;\beta,\epsilon)$. Differentiating gives

$$\begin{aligned}\dot{y}_+ &= \frac{\partial h_2}{\partial z_+}(z_+,\mu;\beta,\epsilon)\,\dot{z}_++\frac{\partial h_2}{\partial \mu}(z_+,\mu;\beta,\epsilon)\,\dot{\mu}=\frac{\partial h_2}{\partial z_+}(z_+,\mu;\beta,\epsilon)\,\dot{z}_+\\ &= \left(2k_1z_++k_2\mu+3k_4z_+^2+\hat{O}(2)\right)\dot{z}_+\end{aligned}$$

where $\hat{O}(2)$ represents terms of order 2 in y_+, z_+ and μ, excluding z_+^2. Substituting (4.23) for y_+, and $h_1(z_+,\mu;\beta,\epsilon)$ for x_+ in (4.20), and then substituting the resulting expression into the above leads to the first expression for $\dot{y}_+$ on the centre manifold:

$$\dot{y}_+=-2\epsilon\Lambda_+k_1bz_+^3+\hat{O}(3) \tag{4.24}$$

Setting $y_+=h_2(z_+,\mu;\beta,\epsilon)$, $x_+=h_1(z_+,\mu;\beta,\epsilon)$ in equation (4.19) and rearranging gives another expression for $\dot{y}_+$ on the centre manifold:

$$\dot{y}_+=\left(\epsilon\Lambda_+^2b-k_1\right)z_+^2-\left(\epsilon\Lambda_++k_2\right)\mu z_+-k_3\mu^2+\left(2\epsilon\Lambda_+k_1b+\epsilon\Lambda_+^2e-k_4\right)z_+^3+\hat{O}(3) \tag{4.25}$$

Equating (4.24) and (4.25) and comparing the coefficients of z_+^2, μz_+, μ^2 and z_+^3 gives $k_1=\epsilon\Lambda_+^2b$, $k_2=-\epsilon\Lambda_+$, $k_3=0$ and $k_4=\epsilon\Lambda_+^2e+4\epsilon\Lambda_+k_1b$. Thus, up to terms of order 2 and z_+^3, $h_2(z_+,\mu;\beta,\epsilon)$ is given by:

$$h_2(z_+,\mu;\beta,\epsilon)=\epsilon\Lambda_+^2bz_+^2-\epsilon\Lambda_+\mu z_++\epsilon\Lambda_+^2\left(e+4\epsilon\Lambda_+b^2\right)z_+^3+\hat{O}(3) \tag{4.26}$$

Substituting the above for y_+ and substituting $h_1(z_+,\mu;\beta,\epsilon)$ for x_+ in (4.20) then gives the flow on the centre manifold up to terms of order 2 and z_+^3:

$$\begin{aligned} \dot{z}_+ &= \epsilon\mu z_+ - \epsilon\Lambda_+ b z_+^2 - \epsilon\Lambda_+\left(2\epsilon\Lambda_+ b^2 + e\right)z_+^3 + \hat{O}(3) && (4.27) \\ \dot{\mu} &= 0 && (4.28) \end{aligned}$$

Note that the $\dot{z}_+$ equation can be written as $\dot{z}_+ = G(z_+,\mu;\beta,\epsilon)$ where:

$$G(z_+,\mu;\beta,\epsilon) = G_3\left(h_1(z_+,\mu;\beta,\epsilon), h_2(z_+,\mu;\beta,\epsilon), z_+,\mu;\beta,\epsilon\right)$$

Since $G_3(x_+,y_+,z_+,\mu;\beta,\epsilon)$ is a C^∞ function of $(x_+,y_+,z_+,\mu)^T$ for $(x_+,y_+,z_+)^T \in \mathbb{R}^3$, $\mu \in (-\Lambda_+,\beta)$, it follows that $G(z_+,\mu;\beta,\epsilon)$ is a C^∞ function of $(z_+,\mu)^T$ for small $\left\|(z_+,\mu)^T\right\|$.

It follows from the analysis of the augmented system (4.15)-(4.16) above that given μ small, in the 3-dimensional system $\dot{\mathbf{y}} = \mathbf{X}_+(\mathbf{y};\mu,\beta,\epsilon)$, the origin has a 1-dimensional C^∞ local invariant manifold $W_{0+}^C(\mu,\beta,\epsilon)$ defined by

$$W_{0+}^C(\mu,\beta,\epsilon) = \left\{\mathbf{y}\in\mathbb{R}^3 : (\mathbf{y},\mu)^T \in W_{0+}^C(\beta,\epsilon)\right\}$$

which is tangential to the vector $(\Lambda_+,\Lambda_+,1)^T$ at $\mathbf{0}$ when $\mu = 0$. In the normal form coordinates $(x_+,y_+,z_+)^T$, the dynamics on $W_{0+}^C(\mu,\beta,\epsilon)$ is $\dot{z}_+ = G(z_+;\mu,\beta,\epsilon)$, where G is given by:

$$G(z_+;\mu,\beta,\epsilon) = \epsilon\mu z_+ - \epsilon\Lambda_+ b z_+^2 - \epsilon\Lambda_+\left(2\epsilon\Lambda_+ b^2 + e\right)z_+^3 + \hat{O}(3) \qquad (4.29)$$

For a given μ small, each fixed point z_* of $\dot{z}_+ = G(z_+;\mu,\beta,\epsilon)$ will correspond to a fixed point $\mathbf{y}_*$ of $\dot{\mathbf{y}} = \mathbf{X}_+(\mathbf{y};\mu,\beta,\epsilon)$ lying on $W_{0+}^C(\mu,\beta,\epsilon)$ close to the origin. If $\mathbf{y}_* \in W_{0+}^C(\mu,\beta,\epsilon)\cap N_+$, $\mathbf{y}_*$ is a fixed point of the burster system $\dot{\mathbf{y}} = \mathbf{X}(\mathbf{y};\mu,\beta,\epsilon)$ with the form $\mathbf{y}_* = (x_*,x_*,\varepsilon_*)^T$, and so (4.8) implies $z_* = \varepsilon_*$. In particular, as $G(0;\mu,\beta,\epsilon) = 0$, 0 is a fixed point of $\dot{z}_+ = G(z_+;\mu,\beta,\epsilon)$, corresponding to the fixed point of the burster system at the origin.[1] Write $\boldsymbol{\mu} = (\mu,\beta,\epsilon)^T$ for brevity. By using the fact that the burster system is symmetric under σ, it can be inferred that given μ small, the set $W_0^C(\boldsymbol{\mu})$ defined by

$$W_0^C(\boldsymbol{\mu}) = \left(W_{0+}^C(\boldsymbol{\mu})\cap N_+\right)\cup\left(\sigma W_{0+}^C(\boldsymbol{\mu})\cap N_-\right)$$

[1] z_*, x_*, ε_* and $\mathbf{y}_*$ are all explicitly functions of μ and β (c.f. section 3.5.2). Their (μ,β) dependence is in general supressed throughout this chapter for simplicity.

is a 1-dimensional local invariant set of the burster system containing the origin, which is piecewise C^{∞} smooth about the origin, and tangential to $(\Lambda_+, \Lambda_+, 1)^T$ in N_+ when $\mu = 0$. The $W_{0+}^{C}(\boldsymbol{\mu})$ dynamics induce piecewise dynamics on $W_0^C(\boldsymbol{\mu})$ about the origin. Moreover, using ε as a coordinate for fixed points of the $W_0^C(\boldsymbol{\mu})$ dynamics, a fixed point ε_* of $\dot{z}_+ = G(z_+; \boldsymbol{\mu})$ with $\varepsilon_* \geq 0$ will correspond to a pair of fixed points $\{\varepsilon_*, -\varepsilon_*\}$ of the $W_0^C(\boldsymbol{\mu})$ dynamics, with $\pm\varepsilon_*$ stable (resp. unstable) according to whether ε_* is stable (resp. unstable) in $\dot{z}_+ = G(z_+; \boldsymbol{\mu})$. The pair $\{\varepsilon_*, -\varepsilon_*\}$ themselves correspond to a pair of symmetry-related fixed points $\mathbf{y}_* = (x_*, x_*, \varepsilon_*)^T$ and $\mathbf{y}_* = (x_*, x_*, -\varepsilon_*)^T$ of $\dot{\mathbf{y}} = \mathbf{X}(\mathbf{y}; \boldsymbol{\mu})$ lying on $W_0^C(\boldsymbol{\mu})$ close to the origin.

Using the observations above, the bifurcation of the burster system that occurs on $W_0^C(\boldsymbol{\mu})$ at $\mu = 0$ is now characterised.

4.1.2 Bifurcation on the invariant line $W_0^C(\boldsymbol{\alpha})$ at $\mu = 0$

Assume μ is small, and let ε_* be a fixed point of the $W_{0+}^C(\boldsymbol{\mu})$ dynamics $\dot{z}_+ = G(z_+; \boldsymbol{\mu})$. ε_* satisfies $G(\varepsilon_*; \boldsymbol{\mu}) = 0$, which by (4.29) has the form

$$\epsilon\mu\varepsilon_* - \epsilon\Lambda_+ b\varepsilon_*^2 - \epsilon\Lambda_+ \left(2\epsilon\Lambda_+ b^2 + e\right)\varepsilon_*^3 + \hat{O}(3) = 0 \tag{4.30}$$

where now $\hat{O}(3)$ denotes terms of order 3 in ε_* and μ, excluding ε_*^3. The stability of ε_* is dependent on the sign of $D_{z_+}G(\varepsilon_*; \boldsymbol{\mu})$ [4]. Differentiating (4.29) w.r.t. z_+ and evaluating at ε_* leads to

$$D_{z_+}G(\varepsilon_*; \boldsymbol{\mu}) = \epsilon\mu - 2\epsilon\Lambda_+ b\varepsilon_* - 3\epsilon\Lambda_+ \left(2\epsilon\Lambda_+ b^2 + e\right)\varepsilon_*^2 + \hat{O}(2) \tag{4.31}$$

where $\hat{O}(2)$ denotes terms of order 2 in ε_* and μ, excluding ε_*^2. There are 2 cases to consider in solving $G(\varepsilon_*; \boldsymbol{\mu}) = 0$: $\beta \neq 2\beta'$ and $\beta = 2\beta'$.

1. $\beta \neq 2\beta'$

Since $b = \frac{1}{\beta} - \frac{1}{2\beta'}$, this case corresponds to $b \neq 0$. Equation (4.30) suggests trying a power series solution of $G(\varepsilon_*; \boldsymbol{\mu}) = 0$ of the form $\varepsilon_* = a_1\mu + a_2\mu^2 + ...$ Substituting into (4.30) gives:

$$a_1\epsilon(1 - \Lambda_+ b a_1)\mu^2 + O\left(\mu^3\right) = 0$$

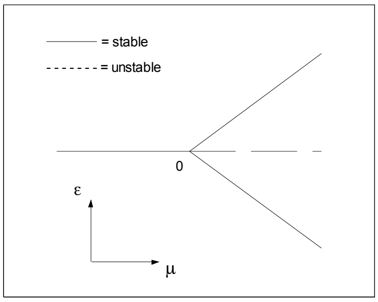

Figure 4-1: Schematic of the supercritical pitchfork-type bifurcation which occurs in the $W_0^C(\boldsymbol{\mu})$ dynamics for $\beta < 2\beta'$ as $\mu = -(\Lambda_+ + \Lambda_-)$ increases through 0.

Comparing terms of order μ^2 implies $a_1\epsilon(1 - \Lambda_+ b a_1) = 0$. There are thus two possible values of a_1: $a_1 = 0$ and $a_1 = \frac{1}{b\Lambda_+} = \frac{2\beta'\beta}{\Lambda_+(2\beta'-\beta)}$. The first case gives the trivial solution, $\varepsilon_* = 0$. The second case gives a nontrivial solution $\hat{\varepsilon}$ of the form:

$$\hat{\varepsilon} = \frac{2(\beta')^2\beta}{\alpha'(2\beta' - \beta)}\mu + O(\mu^2)$$

From (4.31):

$$\begin{aligned} D_{z_+}G(0;\boldsymbol{\mu}) &= \epsilon\mu + O(\mu^2) \\ D_{z_+}G(\hat{\varepsilon};\boldsymbol{\mu}) &= -\epsilon\mu + O(\mu^2) \end{aligned}$$

For $\mu < 0$, 0 is stable and $\hat{\varepsilon}$ is unstable, while for $\mu > 0$, 0 is unstable and $\hat{\varepsilon}$ is stable. Moreover, $\hat{\varepsilon}$ scales linearly with μ. As μ increases through 0, 0 therefore loses stability in $\dot{z}_+ = G(z_+;\boldsymbol{\mu})$ through a transcritical bifurcation [4].

If $\beta < 2\beta'$, $\hat{\varepsilon} < 0$ for $\mu < 0$ and $\hat{\varepsilon} > 0$ for $\mu > 0$. It follows that for $\mu < 0$, the only fixed point of the $W_0^C(\boldsymbol{\mu})$ dynamics is 0, which is stable, while for $\mu > 0$, the fixed points are $\{0, \hat{\varepsilon}, -\hat{\varepsilon}\}$, with 0 unstable and $\{\hat{\varepsilon}, -\hat{\varepsilon}\}$ stable. Given $\beta < 2\beta'$, the fixed points of the burster system are $\mathbf{0}$ for $\mu < 0$ and $\{\mathbf{0}, \mathbf{y}_1^+, \mathbf{y}_1^-\}$ for $\mu > 0$. The correspondence between fixed points of the $W_0^C(\boldsymbol{\mu})$ dynamics and fixed points of the burster system therefore implies that $\hat{\varepsilon}$ can be identified with ε_1 in this range. As μ increases through 0, the transcritical bifurcation in $\dot{z}_+ = G(z_+;\boldsymbol{\mu})$ thus induces a supercritical pitchfork-type bifurcation in the $W_0^C(\boldsymbol{\mu})$ dynamics, in which 0 loses stability creating the stable pair $\{\varepsilon_1, -\varepsilon_1\}$, where ε_1 scales linearly with μ. A schematic of this bifurcation is given in figure (4-1). The values of

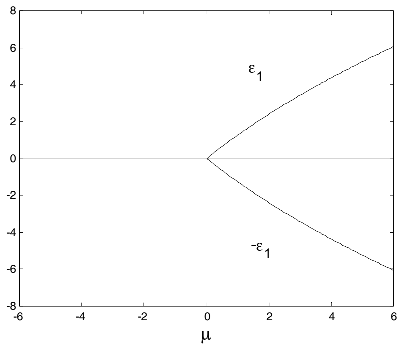

Figure 4-2: Scaling of ε_1 and $-\varepsilon_1$ with μ for $\beta = 15$. $\beta < 2\beta'$, so this choice of β corresponds to the supercritical linear pitchfork-type bifurcation (cf. fig (4-1)).

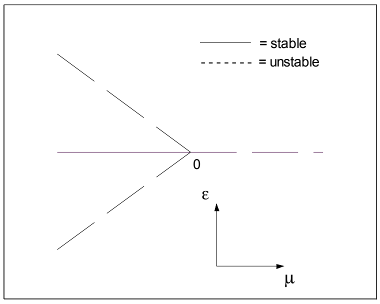

Figure 4-3: Schematic of the subcritical pitchfork-type bifurcation which occurs in the $W_0^C(\boldsymbol{\mu})$ dynamics for $\beta > 2\beta'$ as μ increases through 0.

ε_1 and $-\varepsilon_1$ as a function of μ are shown in figure (4-2) for $\beta = 15$. These were obtained by varying α over an appropriate range and numerically solving the equation $f(\varepsilon_*) = h(-\varepsilon_*)$ for $\varepsilon_* > 0$. The scaling of ε_1 with μ seems to agree with the analysis.

If $\beta > 2\beta'$, $\hat{\varepsilon} > 0$ for $\mu < 0$ and $\hat{\varepsilon} < 0$ for $\mu > 0$. It follows that for $\mu < 0$, the fixed points of the $W_0^C(\boldsymbol{\mu})$ dynamics are 0, $\hat{\varepsilon}$ and $-\hat{\varepsilon}$, with 0 stable and $\{\hat{\varepsilon}, -\hat{\varepsilon}\}$ unstable, while for $\mu > 0$, the only fixed point is 0, which is unstable. Given $\beta > 2\beta'$, the fixed points of $\dot{\mathbf{y}} = \mathbf{X}(\mathbf{y}; \boldsymbol{\mu})$ lying close to $\mathbf{0}$ are $\{\mathbf{0}, \mathbf{y}_2^+, \mathbf{y}_2^-\}$ for $\mu < 0$ and $\mathbf{0}$ for $\mu > 0$. The correspondence between fixed points of the $W_0^C(\boldsymbol{\mu})$ dynamics and fixed points of $\dot{\mathbf{y}} = \mathbf{X}(\mathbf{y}; \boldsymbol{\mu})$ therefore implies that $\hat{\varepsilon}$ can be identified with ε_2 in this range. As μ increases through 0, the transcritical bifurcation in $\dot{z}_+ = G(z_+; \boldsymbol{\mu})$ thus induces a subcritical pitchfork-type bifurcation in the $W_0^C(\boldsymbol{\mu})$ dynamics, in which 0 loses stability destroying the unstable pair $\{\varepsilon_2, -\varepsilon_2\}$, where ε_2 scales linearly with μ. A schematic of this bifurcation is given in figure (4-3). The values

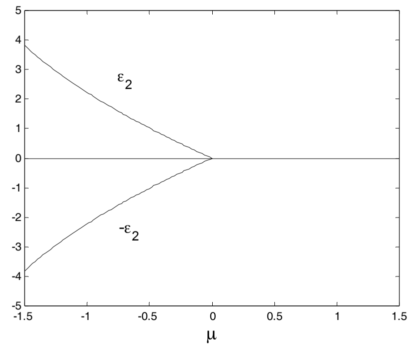

Figure 4-4: Scaling of ε_2 and $-\varepsilon_2$ with μ for $\beta = 21$. $\beta > 2\beta'$, so this choice of β corresponds to the subcritical linear pitchfork-type bifurcation (cf. fig (4-3)).

of ε_2 and $-\varepsilon_2$ as a function of μ are shown in figure (4-4) for $\beta = 21$. Again, the scaling of ε_2 with μ agrees with the analysis.

2. $\beta = 2\beta'$

In this case, $b = 0$. $G(\varepsilon_*; \boldsymbol{\mu}) = 0$ becomes:

$$\epsilon\mu\varepsilon_* - \epsilon\Lambda_+ e\varepsilon_*^3 + \hat{O}(3) = 0 \tag{4.32}$$

(4.32) suggests trying a power series solution of the form $\varepsilon_* = a_1\mu^{\frac{1}{2}} + a_2\mu + ...$ with $\mu > 0$ to obtain a nontrivial solution. Substituting into (4.32) gives:

$$\epsilon a_1 \left(1 - \Lambda_+ e a_1^2\right) \mu^{\frac{3}{2}} + O\left(\mu^2\right) = 0$$

Comparing terms of order $\mu^{\frac{3}{2}}$ implies $\epsilon a_1 \left(1 - \Lambda_+ e a_1^2\right) = 0$. Thus, $a_1 = 0$ or $a_1 = \pm\frac{1}{\sqrt{\Lambda_+ e}} = \pm 2\sqrt{\frac{6(\beta')^3}{\alpha'}}$. The first case corresponds to the trivial solution $\varepsilon_* = 0$. The second case gives a pair of nontrivial solutions $\{\hat{\varepsilon}, -\hat{\varepsilon}\}$ with:

$$\hat{\varepsilon} = 2\left(\sqrt{\frac{6\left(\beta'\right)^3}{\alpha'}}\right)\mu^{\frac{1}{2}} + O\left(\mu\right)$$

Setting $b = 0$ in (4.31) gives

$$D_{z_+} G(\varepsilon_*; \boldsymbol{\mu}) = \epsilon\mu - 3\epsilon\Lambda_+ e\varepsilon_*^2 + \hat{O}(2)$$

which leads to:

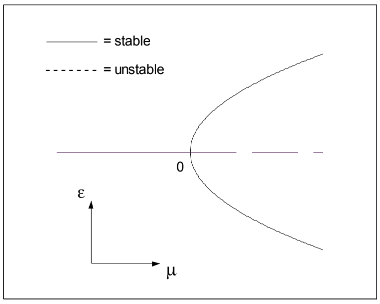

Figure 4-5: Schematic of the supercritical pitchfork-type bifurcation which occurs in the $W_0^C(\boldsymbol{\mu})$ dynamics for $\beta = 2\beta'$ as μ increases through 0.

$$
\begin{aligned}
D_{z_+}G(0;\boldsymbol{\mu}) &= \epsilon\mu + O\left(\mu^2\right) \\
D_{z_+}G(\hat{\varepsilon};\boldsymbol{\mu}) &= -2\epsilon\mu + O\left(\mu^{\frac{3}{2}}\right)
\end{aligned}
$$

$\hat{\varepsilon}$ is stable, while 0 is stable for $\mu < 0$ and unstable for $\mu > 0$. Moreover, $\hat{\varepsilon}$ scales like $\mu^{\frac{1}{2}}$. As μ increases through 0, 0 therefore loses stability in $\dot{z}_+ = G(z_+;\boldsymbol{\mu})$ through a supercritical pitchfork bifurcation [4].

$\hat{\varepsilon}$ exists for $\mu > 0$, where it is greater than 0. It follows that for $\mu < 0$, the only fixed point of the $W_0^C(\boldsymbol{\mu})$ dynamics is 0, which is stable, while for $\mu > 0$, the fixed points are $\{0, \hat{\varepsilon}, -\hat{\varepsilon}\}$, with 0 unstable and $\{\hat{\varepsilon}, -\hat{\varepsilon}\}$ stable. Given $\beta = 2\beta'$, the fixed points of the burster system are $\mathbf{0}$ for $\mu < 0$ and $\left\{\mathbf{0}, \mathbf{y}_1^+, \mathbf{y}_1^-\right\}$ for $\mu > 0$. The correspondence between fixed points of the $W_0^C(\boldsymbol{\mu})$ dynamics and fixed points of the burster system therefore implies that $\hat{\varepsilon}$ can be identified with ε_1 for $\beta = 2\beta'$. As μ increases through 0, the supercritical pitchfork bifurcation in $\dot{z}_+ = G(z_+;\boldsymbol{\mu})$ thus induces a supercritical pitchfork-type bifurcation in the $W_0^C(\boldsymbol{\mu})$ dynamics, in which 0 loses stability creating the stable pair $\{\varepsilon_1, -\varepsilon_1\}$, where ε_1 scales like $\mu^{\frac{1}{2}}$. A schematic of this bifurcation is shown in figure (4-5). The values of ε_1 and $-\varepsilon_1$ as a function of μ are shown in figure (4-6) for $\beta = 18$. The scaling of ε_1 with μ is seen to agree with the analysis.

In conclusion it has been shown during this section that given ϵ, for $|\alpha - \Lambda_+\beta|$ small, the origin of the burster system $\dot{\mathbf{y}} = \mathbf{X}(\mathbf{y}, \boldsymbol{\alpha})$ has a local 1-dimensional invariant set $W_0^C(\boldsymbol{\alpha})$ which maps into itself under the symmetry operator σ, and is tangential to $(\Lambda_+, \Lambda_+, 1)^T$

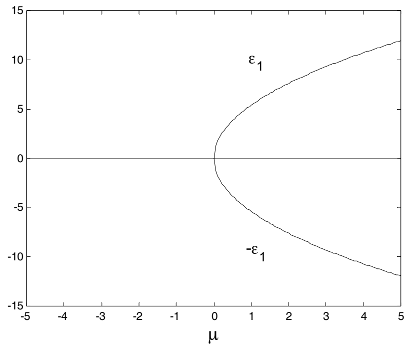

Figure 4-6: Scaling of ε_1 and $-\varepsilon_1$ with μ for $\beta = 18$. $\beta = 2\beta'$, so this choice of β corresponds to the supercritical square-root pitchfork-type bifurcation (cf. fig (4-5)).

at $\mathbf{0}$ in N_+ when $\alpha = \Lambda_+\beta$. As α increases through $\Lambda_+\beta$ in $\beta \leq 2\beta'$, $\mathbf{0}$ goes unstable and $\{\mathbf{y}_1^+, \mathbf{y}_1^-\}$ are created on $W_0^C(\boldsymbol{\alpha})$, via the fixed point 0 of the $W_0^C(\boldsymbol{\alpha})$ dynamics going unstable in a supercritical pitchfork-type bifurcation, which creates the stable fixed points $\{\varepsilon_1, -\varepsilon_1\}$. As α increases through $\Lambda_+\beta$ in $\beta > 2\beta'$, $\mathbf{0}$ goes unstable and $\{\mathbf{y}_2^+, \mathbf{y}_2^-\}$ are destroyed on $W_0^C(\boldsymbol{\alpha})$, via the fixed point 0 of the $W_0^C(\boldsymbol{\alpha})$ dynamics going unstable in a subcritical pitchfork-type bifurcation, which destroys the unstable fixed points $\{\varepsilon_2, -\varepsilon_2\}$. For $\beta \neq 2\beta'$, the pitchfork-type bifurcation can be attributed to a transcritical bifurcation in the $W_{0+}^C(\boldsymbol{\alpha})$ dynamics, while for $\beta = 2\beta'$, it can be attributed to a supercritical pitchfork bifurcation in the $W_{0+}^C(\boldsymbol{\alpha})$ dynamics.

4.1.3 Local dynamics on $W_0^C(\boldsymbol{\alpha})$

In order to obtain a fuller understanding of the bifurcation at the origin, it is useful to have a more detailed picture of the local dynamics on $W_0^C(\boldsymbol{\alpha})$ in the immediate neighbourhood of the origin for $|\alpha - \Lambda_+\beta|$ small.

First consider the dynamics for $\beta > 2\beta'$ and $|\alpha - \Lambda_+\beta|$ small. For $\beta > 2\beta'$ and $\alpha - \Lambda_+\beta < 0$ small, the fixed points of the burster system in the immediate neighbourhood of $\mathbf{0}$ are $\mathbf{0}$, $\mathbf{y}_2^+$ and $\mathbf{y}_2^-$. 0 is stable in the $W_0^C(\boldsymbol{\alpha})$ dynamics and so as $\mathbf{y}_2^\pm$ lies on $W_0^C(\boldsymbol{\alpha})$, this means that $W_0^C(\boldsymbol{\alpha})$ must contain a 1-dimensional local unstable manifold of $\mathbf{y}_2^\pm$ in $N_\pm$. Recall from section 3.6.1 that $\mathbf{y}_2^\pm$ is a saddle node with a unique 1-dimensional C^∞ local unstable manifold $W_{2\pm}^U(\boldsymbol{\alpha})$, which is tangential to $\mathrm{Sp}\{\mathbf{v}_{22}^\pm(\boldsymbol{\alpha})\}$ at $\mathbf{y}_2^\pm$. If follows that in the parameter range of interest, $W_0^C(\boldsymbol{\alpha})$ must contain $W_{2\pm}^U(\boldsymbol{\alpha})$ in $N_\pm$. Moreover, as $W_0^C(\boldsymbol{\alpha})$ contains a unique invariant manifold in both N_+ and N_-, it is also unique.

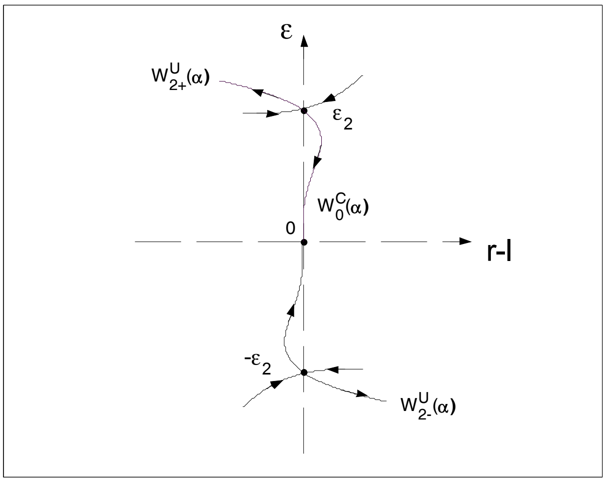

Figure 4-7: Projection of the flow on $W_0^C(\boldsymbol{\alpha})$ in the neighbourhood of $\mathbf{0}$ onto the $(r-l, \varepsilon)$ plane for $\beta > 2\beta'$ and $\alpha - \Lambda_+\beta < 0$ small.

For $\beta > 2\beta'$ and $\alpha - \Lambda_+\beta > 0$ small, the only fixed point in the immediate neighbourhood of $\mathbf{0}$ is $\mathbf{0}$. 0 is unstable in the $W_0^C(\boldsymbol{\alpha})$ dynamics, and so $W_0^C(\boldsymbol{\alpha})$ must contain a 1-dimensional local unstable invariant set of the origin in the burster system. As the unique such unstable invariant set of $\mathbf{0}$ in the parameter range of interest is the set $W_0^U(\boldsymbol{\alpha})$ introduced in section 3.6.3, $W_0^C(\boldsymbol{\alpha})$ must contain $W_0^U(\boldsymbol{\alpha})$. Also, as $W_0^C(\boldsymbol{\alpha})$ contains a unique invariant set, it must itself be unique. Figures (4-7)-(4-8) are schematics of the projection of the flow on $W_0^C(\boldsymbol{\alpha})$ in the neighbourhood of $\mathbf{0}$ onto the $(r-l, \varepsilon)$ plane for $\beta > 2\beta'$ and $|\alpha - \Lambda_+\beta|$ small, based on these arguments.

Now consider the dynamics for $\beta \leq 2\beta'$ and $|\alpha - \Lambda_+\beta|$ small. For $\beta \leq 2\beta'$ and $\alpha - \Lambda_+\beta < 0$ small, the only fixed point of the burster system is $\mathbf{0}$. 0 is stable in the $W_0^C(\boldsymbol{\alpha})$ dynamics and so $W_0^C(\boldsymbol{\alpha})$ is a 1-dimensional local stable invariant set of the origin in the burster system. For $\beta \leq 2\beta'$ and $\alpha - \Lambda_+\beta > 0$ small, the fixed points are $\mathbf{0}$, $\mathbf{y}_1^+$ and $\mathbf{y}_1^-$. 0 is unstable in the $W_0^C(\boldsymbol{\alpha})$ dynamics and so $W_0^C(\boldsymbol{\alpha})$ contains a 1-dimensional local unstable invariant set of the origin in the burster system. Again, the unique such set in the parameter range of interest is $W_0^U(\boldsymbol{\alpha})$, implying that $W_0^C(\boldsymbol{\alpha})$ contains $W_0^U(\boldsymbol{\alpha})$, and is therefore unique. Also, since $W_0^C(\boldsymbol{\alpha})$ contains $\mathbf{y}_1^\pm$, $W_0^C(\boldsymbol{\alpha})$ must intersect a local stable manifold of $\mathbf{y}_1^\pm$ in $N_\pm$. Figures (4-9)-(4-10) are schematics of the projection of the flow on $W_0^C(\boldsymbol{\alpha})$ in the neighbourhood of $\mathbf{0}$ onto the $(r-l, \varepsilon)$ plane for $\beta \leq 2\beta'$ and $|\alpha - \Lambda_+\beta|$ small, based on these arguments.

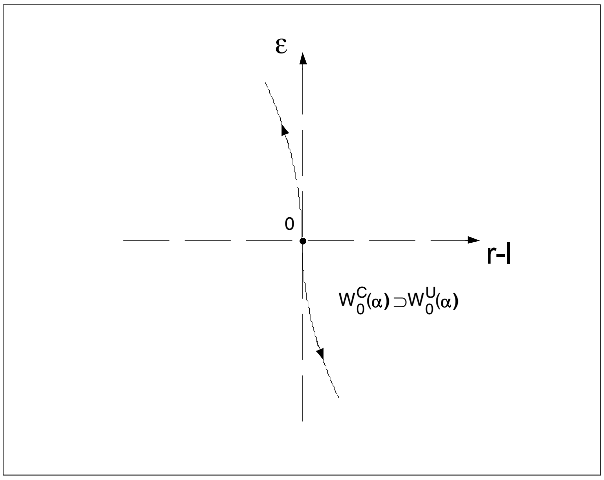

Figure 4-8: Projection of the flow on $W_0^C(\boldsymbol{\alpha})$ in the neighbourhood of $\mathbf{0}$ onto the $(r-l, \varepsilon)$ plane for $\beta > 2\beta'$ and $\alpha - \Lambda_+\beta > 0$ small.

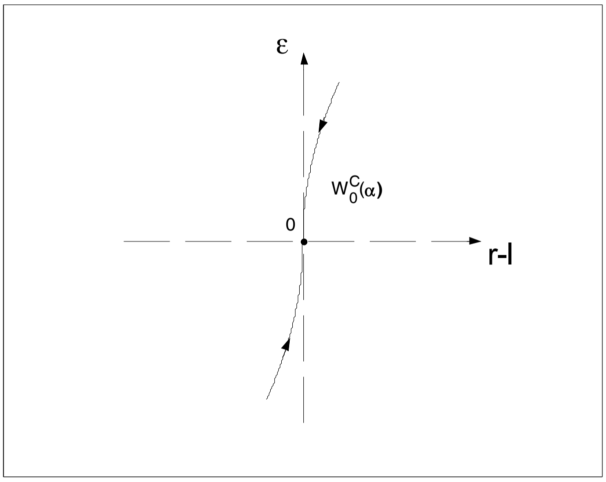

Figure 4-9: Projection of the flow on $W_0^C(\boldsymbol{\alpha})$ in the neighbourhood of $\mathbf{0}$ onto the $(r-l, \varepsilon)$ plane for $\beta \leq 2\beta'$ and $\alpha - \Lambda_+\beta < 0$ small.

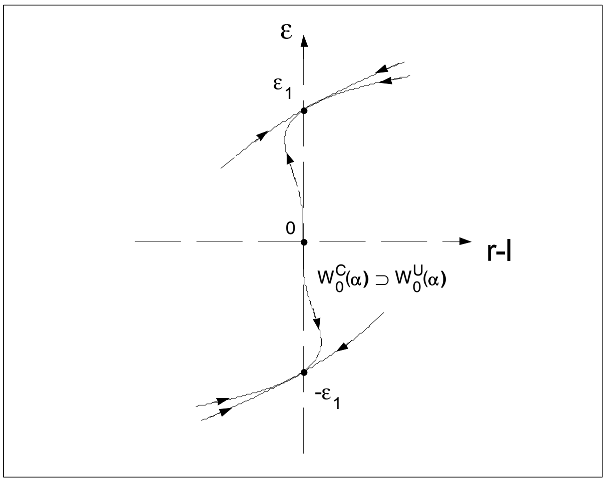

Figure 4-10: Projection of the flow on $W_0^C(\boldsymbol{\alpha})$ in the neighbourhood of $\mathbf{0}$ onto the $(r-l,\varepsilon)$ plane for $\beta \leq 2\beta'$ and $\alpha - \Lambda_+\beta > 0$ small.

Using the analysis of this section together with the work of the previous chapter, the provisional local bifurcation scheme for the burster system in the (β, α) plane shown in figure (4-11) can be obtained. Also indicated on the figure are the fixed points of the burster system, together with their stabilities.

4.2 The codimension 2 bifurcation at $\alpha = \alpha_2, \beta = \beta_2$

The bifurcation which occurs in the burster system $\dot{\mathbf{y}} = \mathbf{X}(\mathbf{y};\alpha,\beta,\epsilon)$ at $\mathbf{y}_1^{\pm}$ when $(\alpha,\beta) = (\alpha_2,\beta_2)$ will be examined in this section. Although this occurs in a region of the state space where the vector field is smooth, and so is amenable to standard centre manifold theory, it will be analysed fully in this case for completeness. The bifurcation at $\mathbf{y}_1^+$ will be examined first. The nature of the bifurcation at $\mathbf{y}_1^-$ can then be inferred from the symmetry of the system.[2]

Fix $\epsilon > 0$. Also fix an open set $\bar{R}_P$ of the (α,β) plane containing (α_2,β_2), and consider the burster system $\dot{\mathbf{y}} = \mathbf{X}(\mathbf{y};\alpha,\beta,\epsilon)$ for $\mathbf{y} \in N_+\backslash P$, $(\alpha,\beta)^T \in \bar{R}_P$. $\mathbf{X}$ is a C^∞ function of both $\mathbf{y}$ and $(\alpha,\beta)^T$ in this range. Let $\bar{\mathbf{y}}_1^+ = \mathbf{y}_1^+(\alpha_2,\beta_2)$. Explicitly, $\bar{\mathbf{y}}_1^+$ is given by

[2] As in the disussion of the pitchfork-type bifurcation in the previous section, the dependence of $\mathbf{y}_i^{\pm}$ on α and β will be generally supressed throughout this section.

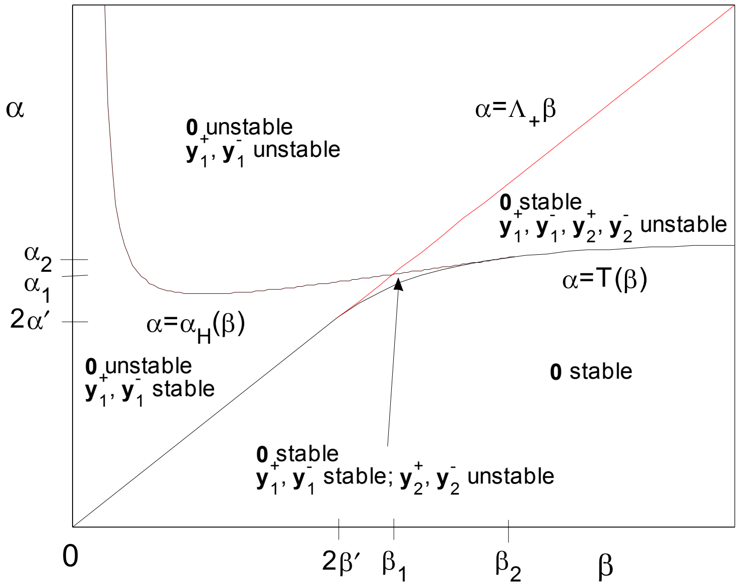

Figure 4-11: Provisional local bifurcation scheme for the burster system. $\alpha = \alpha_H(\beta)$ is a line of Hopf bifurcations at $\mathbf{y}_1^{\pm}$, $\alpha = T(\beta)$ is a line of saddlenode bifurcations at $\mathbf{y}_1^{\pm}$, $\alpha = \Lambda_+\beta$ is a line of pitchfork-type bifurcations at the origin. The pitchfork-type bifurcation is supercritical for $\beta \leq 2\beta'$ and subcritical for $\beta > 2\beta'$ (red line). Also shown are the fixed points of the system.

$\bar{\mathbf{y}}_1^+ = \left(\frac{1}{\sqrt{\gamma}}, \frac{1}{\sqrt{\gamma}}, \varepsilon_H\right)^T$. Change to local parameter coordinates by setting $a = \alpha - \alpha_2$ and $b = \beta - \beta_2$, and let

$$\bar{\mathbf{X}}(\mathbf{y};a,b,\epsilon) = \mathbf{X}(\mathbf{y};\alpha_2 + a, \beta_2 + b, \epsilon)$$

so that the burster system is $\dot{\mathbf{y}} = \bar{\mathbf{X}}(\mathbf{y};a,b,\epsilon)$ in the new coordinates. In these coordinates, the bifurcation at $\bar{\mathbf{y}}_1^+$ occurs when $(a,b)^T = (0,0)^T$. Also, $\bar{\mathbf{X}}(\mathbf{y};a,b,\epsilon)$ is a C^∞ function of $\mathbf{y}$ and $(a,b)^T$ for $\mathbf{y} \in N_+ \backslash P$, $(a,b)^T \in R_P$ where $R_P = \bar{R}_P - (\alpha_2, \beta_2)$. At $(a,b)^T = (0,0)^T$, the derivative of $\bar{\mathbf{X}}$ evaluated at $\bar{\mathbf{y}}_1^+$, $D_{\mathbf{y}}\bar{\mathbf{X}}\left(\bar{\mathbf{y}}_1^+;0,0,\epsilon\right)$, is given by

$$D_{\mathbf{y}}\bar{\mathbf{X}}\left(\bar{\mathbf{y}}_1^+;0,0,\epsilon\right) = D_{\mathbf{y}}\mathbf{X}\left(\bar{\mathbf{y}}_1^+;\alpha_2,\beta_2,\epsilon\right) = \begin{pmatrix} -2 & -2 & \left(\Gamma_1^+\right)_H \\ -2 & -2 & \left(\Gamma_1^+\right)_H \\ -\epsilon & \epsilon & 0 \end{pmatrix}$$

where $\left(\Gamma_1^+\right)_H = \Gamma_1^+(\alpha_H(\beta), \beta)$ (cf. (3.71)). The eigenvalues of this matrix are -4 with multiplicity 1, and 0 with multiplicity 2. The eigenvector corresponding to -4 is $(1,1,0)^T$.

The generalised eigenvectors corresponding to 0 can be taken as $\mathbf{v}_C(\epsilon)$ and $\mathbf{w}_C(\epsilon)$ where:

$$\mathbf{v}_C(\epsilon) = \begin{pmatrix} \left(\Gamma_1^+\right)_H \\ \left(\Gamma_1^+\right)_H \\ 4 \end{pmatrix}, \mathbf{w}_C(\epsilon) = \begin{pmatrix} 0 \\ 4 \\ \frac{8}{\left(\Gamma_1^+\right)_H} + \epsilon \end{pmatrix} \tag{4.33}$$

Define the 3×3 matrix $P(\epsilon)$ by $P(\epsilon) = \left[(1,1,0)^T \ \mathbf{v}_C(\epsilon) \ \mathbf{w}_C(\epsilon)\right]$. Then the matrix

$$A(\epsilon) = P(\epsilon)^{-1} D_{\mathbf{y}}\bar{\mathbf{X}}\left(\bar{\mathbf{y}}_1^+; 0, 0, \epsilon\right) P(\epsilon)$$

is a normal form for $D_{\mathbf{y}}\bar{\mathbf{X}}\left(\bar{\mathbf{y}}_1^+; 0, 0, \epsilon\right)$. Explicitly:

$$A(\epsilon) = \begin{pmatrix} -4 & 0 & 0 \\ 0 & 0 & 1 \\ 0 & 0 & 0 \end{pmatrix} \tag{4.34}$$

Now with the change of coordinates $\mathbf{y} \to \mathbf{y}' = (r', l', \varepsilon')^T$ defined by $\mathbf{y}' = \mathbf{y} - \bar{\mathbf{y}}_1^+$, the burster system can be written as

$$\dot{\mathbf{y}}' = \mathbf{F}\left(\mathbf{y}'; a, b, \epsilon\right)$$

where:

$$\mathbf{F}\left(\mathbf{y}'; a, b, \epsilon\right) = \bar{\mathbf{X}}\left(\mathbf{y}' + \bar{\mathbf{y}}_1^+; a, b, \epsilon\right) \tag{4.35}$$

(Note that since $\bar{\mathbf{X}}(\mathbf{y}; a, b, \epsilon)$ is a C^∞ function of $\mathbf{y}$ and $(a,b)^T$ for $\mathbf{y} \in N_+ \backslash P$, $(a,b)^T \in R_P$, $\mathbf{F}(\mathbf{y}'; a, b, \epsilon)$ is a C^∞ function of $\mathbf{y}'$ and $(a,b)^T$ for $\mathbf{y}' \in N_+ \backslash P - \bar{\mathbf{y}}_1^+$, $(a,b)^T \in R_P$.) A final change of coordinates $\mathbf{y}' \to \mathbf{x}$ defined by

$$\mathbf{x} = (x, y, z)^T = P(\epsilon)^{-1} \mathbf{y}' + P(\epsilon)^{-1} D_1(\epsilon)^{-1} D_2(\epsilon)\,\mathbf{a} \tag{4.36}$$

where $\mathbf{a} = (a,b)^T$, $D_1(\epsilon) = D_{\mathbf{y}}\bar{\mathbf{X}}\left(\bar{\mathbf{y}}_1^+; 0, 0, \epsilon\right)$ and $D_2(\epsilon) = D_{\mathbf{a}}\mathbf{F}(\mathbf{0}; 0, 0, \epsilon)$ brings the burster system into the following useful form

$$\dot{\mathbf{x}} = \mathbf{G}(\mathbf{x}; a, b, \epsilon) \tag{4.37}$$

with:

$$\mathbf{G}\left(\mathbf{x};a,b,\epsilon\right)=P\left(\epsilon\right)^{-1}\mathbf{F}\left(P\left(\epsilon\right)\mathbf{x}-D_1\left(\epsilon\right)^{-1}D_2\left(\epsilon\right)\mathbf{a};a,b,\epsilon\right)$$

Since $\mathbf{F}\left(\mathbf{y}';a,b,\epsilon\right)$ is a C^{∞} function of $\mathbf{y}'$ and $(a,b)^T$ for $\mathbf{y}'\in N_+\backslash P-\bar{\mathbf{y}}_1^+$, $(a,b)^T\in R_P$, there is an open set R_C of $\mathbb{R}^3$ containing $\mathbf{0}=(0,0,0)^T$ such that $\mathbf{G}\left(\mathbf{x};a,b,\epsilon\right)$ is a C^{∞} function of $\mathbf{x}$ and $(a,b)^T$ for $\mathbf{x}\in R_C$, $(a,b)^T\in R_P$. For $(a,b)^T=(0,0)^T$, the change of coordinates $\mathbf{y}'\to\mathbf{x}$ is $\mathbf{x}=P\left(\epsilon\right)^{-1}\mathbf{y}'$, and so $\mathbf{0}$ is a fixed point of (4.37) corresponding to the fixed point $\bar{\mathbf{y}}_1^+$ in the $\mathbf{y}$ coordinates. Write:

$$\mathbf{G}\left(\mathbf{x};a,b,\epsilon\right)=\left(G_1\left(\mathbf{x};a,b,\epsilon\right),G_2\left(\mathbf{x};a,b,\epsilon\right),G_3\left(\mathbf{x};a,b,\epsilon\right)\right)^T$$

Then as $\mathbf{G}\left(\mathbf{x};a,b,\epsilon\right)$ is C^{∞} in $\mathbf{x}$ and $(a,b)^T$ for $\mathbf{x}\in R_C$, $(a,b)^T\in R_P$, $G_i\left(\mathbf{x};a,b,\epsilon\right)$ is also C^{∞} over this range for $1\le i\le 3$.

Now consider the 5-dimensional system composed of $\dot{\mathbf{x}}=\mathbf{G}\left(\mathbf{x},a,b;\epsilon\right)$ together with the trivial equations $\dot{a}=0$ and $\dot{b}=0$:

$$\begin{aligned}
&\dot{\mathbf{x}}=\mathbf{G}\left(\mathbf{x},a,b;\epsilon\right)\\
&\dot{a}=0\\
&\dot{b}=0
\end{aligned}\tag{4.38}$$

$(\mathbf{0},0,0)^T$ is a fixed point of this augmented system. Also, the vector field of the system is a C^{∞} function of $(\mathbf{x},a,b)^T$ for $\mathbf{x}\in R_C$, $(a,b)^T\in R_P$. In particular, the vector field is C^{∞} in a neighbourhood of $(\mathbf{0},0,0)^T$. Using (4.35), it can be shown that in the $(\mathbf{y}',a,b)^T$ coordinates, the derivative of the vector field of the augmented system evaluated at $(\mathbf{0},0,0)^T$ is:

$$\begin{pmatrix} D_1\left(\epsilon\right) & D_2\left(\epsilon\right)\\ \mathbf{0}_{2\times 3} & \mathbf{0}_{2\times 2}\end{pmatrix}$$

It follows that the derivative of the vector field of (4.38) evaluated at $(\mathbf{0},0,0)^T$ has the form:

$$\begin{pmatrix} P\left(\epsilon\right)^{-1} & P\left(\epsilon\right)^{-1}D_1\left(\epsilon\right)^{-1}D_2\left(\epsilon\right)\\ \mathbf{0}_{2\times 3} & \mathbf{1}_{2\times 2}\end{pmatrix}\begin{pmatrix} D_1\left(\epsilon\right) & D_2\left(\epsilon\right)\\ \mathbf{0}_{2\times 3} & \mathbf{0}_{2\times 2}\end{pmatrix}\begin{pmatrix} P\left(\epsilon\right) & -D_1\left(\epsilon\right)^{-1}D_2\left(\epsilon\right)\\ \mathbf{0}_{2\times 3} & \mathbf{1}_{2\times 2}\end{pmatrix}$$

Evaluating this product and using (4.34) leads to the following expression for the derivative:

$$\begin{pmatrix} -4 & 0 & 0 & 0 & 0 \\ 0 & 0 & 1 & 0 & 0 \\ 0 & 0 & 0 & 0 & 0 \\ 0 & 0 & 0 & 0 & 0 \\ 0 & 0 & 0 & 0 & 0 \end{pmatrix}$$

In the $\mathbf{x}$ coordinates, the linearised augmented system thus has a 1-dimensional stable manifold

$$E^S_{1+} = \left\{ (x, y, z, a, b)^T : y = z = a = b = 0 \right\}$$

and a 4-dimensional centre manifold:

$$E^C_{1+} = \left\{ (x, y, z, a, b)^T : x = 0 \right\}$$

It therefore follows from the Centre Manifold Theorem that in the nonlinear augmented system, $(\mathbf{0},0,0)^T$ has a C^∞ 1-dimensional local stable manifold $W^S_{1+}(\epsilon)$ tangential to E^S_{1+} at $(\mathbf{0},0,0)^T$ and a C^∞ 4-dimensional local centre manifold $W^C_{1+}(\epsilon)$ tangential to E^C_{1+} at $(\mathbf{0},0,0)^T$ [4]. Also, since the nonzero eigenvalue is negative, $W^C_{1+}(\epsilon)$ will be attracting.

Now as $W^C_{1+}(\epsilon)$ is tangential to E^C_{1+} at $(\mathbf{0},0,0)^T$, it can be considered as a graph

$$\left\{ (h(y, z, a, b; \epsilon), y, z, a, b)^T \right\}$$

over y, z, a and b, for $\left\| (y, z, a, b)^T \right\|$ small, where h is a C^∞ function of $(y, z, a, b)^T$ with $h(0, 0, 0, 0; \epsilon) = 0$, and $\frac{\partial h}{\partial u}(0, 0, 0, 0; \epsilon) = 0$ for $u = y$, z, a and b. Setting $x = h(y, z, a, b; \epsilon)$ in the equations for $\dot{y}$ and $\dot{z}$ in (4.38) gives the following expression for the dynamics on $W^C_{1+}(\epsilon)$:

$$\begin{aligned} \dot{y} &= G_2(h(y, z, a, b; \epsilon), y, z, a, b; \epsilon) \\ \dot{z} &= G_3(h(y, z, a, b; \epsilon), y, z, a, b; \epsilon) \\ \dot{a} &= 0 \\ \dot{b} &= 0 \end{aligned}$$

Define $\mathbf{z} = (y, z)^T$. Then the y and z equations can be written as $\dot{\mathbf{z}} = \mathbf{H}(\mathbf{z}, a, b; \epsilon)$ where

$$\mathbf{H}(y, z, a, b; \epsilon) = \begin{pmatrix} G_2(h(y, z, a, b; \epsilon), y, z, a, b; \epsilon) \\ G_3(h(y, z, a, b; \epsilon), y, z, a, b; \epsilon) \end{pmatrix}$$

Note that since $G_2(\mathbf{x}, a, b; \epsilon)$ and $G_3(\mathbf{x}, a, b; \epsilon)$ are C^∞ functions of $(\mathbf{x}, a, b)^T$ for $\mathbf{x} \in R_C, (a, b)^T \in R_P$, $\mathbf{H}(\mathbf{z}, a, b; \epsilon)$ is a C^∞ function of $(\mathbf{z}, a, b)^T$ for $\left\|(\mathbf{z}, a, b)^T\right\|$ small. Also $\mathbf{H}(0, 0, 0, 0; \epsilon) = \begin{pmatrix} 0 \\ 0 \end{pmatrix}$ and $D_{\mathbf{z}}\mathbf{H}(0, 0, 0, 0; \epsilon) = \begin{pmatrix} 0 & 1 \\ 0 & 0 \end{pmatrix}$.

The analysis of the augmented system (4.38) implies that given a fixed $(a, b)^T$ with $\left\|(a, b)^T\right\|$ small, for $\|\mathbf{x}\|$ small, the nonaugmented system (4.37) has an attracting 2-dimensional C^∞ invariant manifold $W^C_{1+}(a, b, \epsilon)$ defined by:

$$W^C_{1+}(a, b, \epsilon) = \left\{\mathbf{x} \in \mathbb{R}^3 : (\mathbf{x}, a, b)^T \in W^C_{1+}(\epsilon)\right\}$$

Moreover, $(0, 0)^T \in W^C_{1+}(0, 0, \epsilon)$ and $W^C_{1+}(0, 0, \epsilon)$ is tangential to the plane $\left\{(x, y, z)^T : x = 0\right\}$ at $(0, 0)^T$. On $W^C_{1+}(a, b, \epsilon)$, the dynamics is given by $\dot{\mathbf{z}} = \mathbf{H}(\mathbf{z}; a, b, \epsilon)$, where $\mathbf{H}$ is defined above. For $(a, b)^T$ with $\left\|(a, b)^T\right\|$ small, $\dot{\mathbf{z}} = \mathbf{H}(\mathbf{z}; a, b, \epsilon)$ can be considered a small perturbation of the system $\dot{\mathbf{z}} = \mathbf{H}(\mathbf{z}; 0, 0, \epsilon)$, the linear part of which is $\begin{pmatrix} 0 & 1 \\ 0 & 0 \end{pmatrix}$. The dynamics of systems with this linear part have been analysed in detail by both Takens and Bogadanov independently. The discussion here follows the summary of their results given in Chapter 7.3 of [25].

It is shown in [25] that the following 2-parameter families of 2-dimensional systems provide a universal unfolding of $\dot{\mathbf{z}} = \mathbf{H}(\mathbf{z}; 0, 0, \epsilon)$

$$\begin{aligned} \dot{Y} &= Z \\ \dot{Z} &= -\mu_2 - \mu_1 Z + Y^2 \pm YZ \end{aligned} \tag{4.39}$$

in the sense that either the (+) or the (-) family provides a family of vector fields whose local flows contain all possible small perturbations of the degenerate flow of $\dot{\mathbf{z}} = \mathbf{H}(\mathbf{z}; 0, 0, \epsilon)$, up to a smooth change of coordinates. It is necessary to establish which of these families is relevant to the given problem. This family will be referred to as the canonical family. It follows that given $(a, b)^T$ with $\left\|(a, b)^T\right\|$ small, there will exist $\mu_1 = \mu_1(a, b)$ and $\mu_2 = \mu_2(a, b)$ such that the flow of $\dot{\mathbf{z}} = \mathbf{H}(\mathbf{z}; a, b, \epsilon)$ local to $(0, 0)^T$ will be equivalent to the flow of the canonical family local to $(0,0)^T$, up to a smooth change of coordinates. Hence, for a and b with $\left\|(a,b)^T\right\|$ small, one would expect to find a 1 to 1 correspondence between curves in the (b,a) plane of bifurcations of $\dot{\mathbf{z}} = \mathbf{H}(\mathbf{z};a,b,\epsilon)$, and curves in the (μ_1,μ_2) plane of bifurcations of the canonical family.

Recall that system (4.37) represents the dynamics of the burster system $\dot{\mathbf{y}} = \mathbf{X}(\mathbf{y};\alpha,\beta,\epsilon)$ in the local spatial coordinates $\mathbf{x}$ and the local parameter coordinates $(a,b)^T$. The analysis of system (4.37) above therefore implies that given α and β with $\left\|(\alpha,\beta)^T - (\alpha_2,\beta_2)^T\right\|$ small, for $\left\|\mathbf{y} - \bar{\mathbf{y}}_1^+\right\|$ small the burster system has an attracting 2-dimensional C^∞ invariant manifold $W_{1+}^C(\boldsymbol{\alpha})$ in N_+, such that $\bar{\mathbf{y}}_1^+ \in W_{1+}^C(\alpha_2,\beta_2,\epsilon)$ and $W_{1+}^C(\alpha_2,\beta_2,\epsilon)$ is tangential to the plane $\mathrm{Sp}\{\mathbf{v}_C(\epsilon),\mathbf{w}_C(\epsilon)\}$ at $\bar{\mathbf{y}}_1^+$, where $\mathbf{v}_C(\epsilon)$ and $\mathbf{w}_C(\epsilon)$ are defined in (4.33). Moreover, given α and β with $\left\|(\alpha,\beta)^T - (\alpha_2,\beta_2)^T\right\|$ small, there will exist $\mu_1 = \mu_1(\alpha,\beta)$ and $\mu_2 = \mu_2(\alpha,\beta)$ for which the flow on $W_{1+}^C(\boldsymbol{\alpha})$ local to $\bar{\mathbf{y}}_1^+$ will be equivalent to the flow of the canonical family local to $(0,0)^T$, up to a smooth change of coordinates. This implies that there will be a 1 to 1 correspondence between curves in the (β,α) plane of bifurcations of $\dot{\mathbf{y}} = \mathbf{X}(\mathbf{y};\boldsymbol{\alpha})$ which occur on $W_{1+}^C(\boldsymbol{\alpha})$, and curves in the (μ_1,μ_2) plane of bifurcations of the canonical family. Note that in the parameter range of interest, fixed points $\mathbf{y}_*(\alpha,\beta)$ of the burster system with $\left\|\mathbf{y}_*(\alpha,\beta) - \bar{\mathbf{y}}_1^+\right\|$ small will lie on $W_{1+}^C(\boldsymbol{\alpha})$ and correspond to fixed points of the $W_{1+}^C(\boldsymbol{\alpha})$ dynamics. It follows that there will be a 1 to 1 correspondence between such fixed points of the burster system and fixed points of the canonical family close to $(0,0)^T$. Moreover as $W_{1+}^C(\boldsymbol{\alpha})$ is locally attracting, a fixed point of the canonical system corresponding to a fixed point $\mathbf{y}_*(\alpha,\beta)$ of the burster system will be stable (resp. unstable) according to whether $\mathbf{y}_*(\alpha,\beta)$ is stable (resp. unstable).

The bifurcation set and local phase portraits of the (-) family of (4.39) is shown in figure (4-12). In the (-) family, as μ_2 increases through 0, a pair of fixed points $\mathbf{r}_1 = \left(-\sqrt{\mu_2},0\right)$ and $\mathbf{r}_2 = \left(\sqrt{\mu_2},0\right)$ are created in a saddlenode bifurcation. $\mathbf{r}_2$ is a saddle while $\mathbf{r}_1$ is created stable in $\mu_1 < 0$ and unstable in $\mu_1 > 0$. The curve $\mu_2 = \mu_1^2$ in $\mu_1 < 0$ is a line of supercritical Hopf bifurcations. As μ_2 increases through μ_1^2 in $\mu_1 < 0$, $\mathbf{r}_1$ goes unstable and a stable limit cycle enclosing $\mathbf{r}_1$ is created. The curve $\mu_2 = H_{SC}(\mu_1) = \frac{49}{25}\mu_1 + O\left(\mu_1^3\right)$ in $\mu_1 < 0$ is a line of homoclinic bifurcations. As μ_2 increases from μ_1^2 to $H_{SC}(\mu_1)$ in $\mu_1 < 0$, the limit cycle increases in size and its period tends to infinity. At $\mu_2 = H_{SC}(\mu_1)$, there is an orbit homoclinic to $\mathbf{r}_2$. For $\mu_2 > H_{SC}(\mu_1)$, the limit cycle does not exist. The bifurcation set and local phase portraits of the (+) family can be obtained from the (-) family by what amounts to a time reversal. Hence, in the (+) family, $\mu_2 = \mu_1^2$ will be

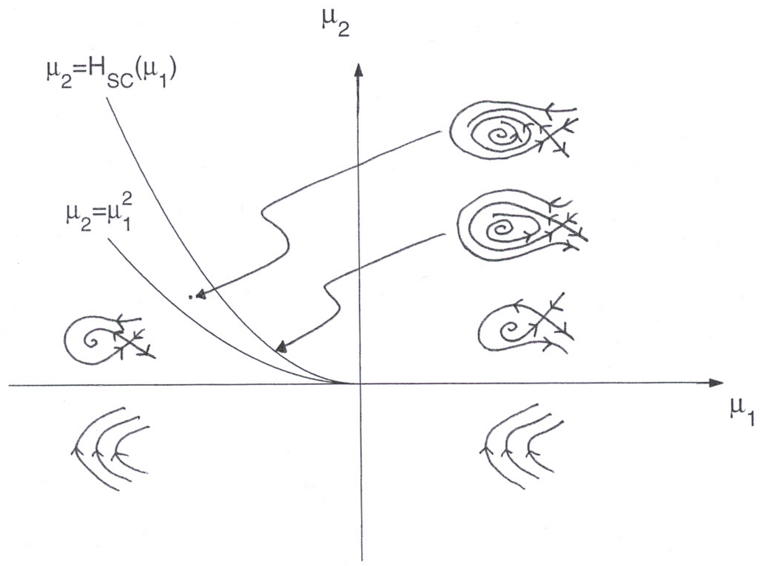

Figure 4-12: The bifurcation set and local phase portraits of the (-) family of (4.39).

a curve of subcritical Hopf bifurcations with $\mathbf{r}_1$ changing from unstable to stable as μ_2 increases through μ_1^2.

The fixed points and bifurcation curves of the burster system for α and β with $\left\|(\alpha,\beta)^T - (\alpha_2,\beta_2)^T\right\|$ small can now be matched up with those of the canonical system. The fact that $\mathbf{y}_1^+$ and $\mathbf{y}_2^+$ are created in a saddlenode bifurcation at $\alpha = T(\beta)$ means that the pair $\{\mathbf{y}_1^+, \mathbf{y}_2^+\}$ can be identified with the pair $\{\mathbf{r}_1, \mathbf{r}_2\}$, while $\alpha = T(\beta)$ can be identified with the μ_1 axis (see figure (4-11)). Moreover, since $\mathbf{y}_1^+$ undergoes a Hopf bifurcation at $\alpha = \alpha_H(\beta)$, $\mathbf{y}_1^+$ can be identified with $\mathbf{r}_1$ and $\mathbf{y}_2^+$ with $\mathbf{r}_2$, while $\alpha = \alpha_H(\beta)$ can be identified with $\mu_2 = \mu_1^2$. Also, since $\mathbf{y}_1^+$ can be identified with $\mathbf{r}_1$, it follows that, for α and β such that $\mathbf{y}_1^+$ exists, $\mathbf{y}_1^+ \in W_{1+}^C(\boldsymbol{\alpha})$, and thus $W_{1+}^C(\boldsymbol{\alpha})$ is a local invariant manifold of $\mathbf{y}_1^+$. It was argued above that $\mathbf{r}_1$ is stable (resp. unstable) in the canonical family when $\mathbf{y}_1^+$ is stable (resp. unstable) in the burster system. Hence, since $\mathbf{y}_1^+$ changes from stable to unstable as α increases through $\alpha_H(\beta)$, it follows that in the canonical family, $\mathbf{r}_1$ must change from stable to unstable as μ_2 increases through μ_1^2 . This identifies the canonical system as the (-) family. $\alpha = \alpha_H(\beta)$ is therefore a curve of supercritical Hopf bifurcations of the $W_{1+}^C(\boldsymbol{\alpha})$ dynamics. Hence, as $W_{1+}^C(\boldsymbol{\alpha})$ is locally attracting, the supercritical Hopf bifurcation at $\alpha = \alpha_H(\beta)$ will create a limit cycle which is stable in the full 3-D system. This limit cycle will be referred to in what follows as $\mathcal{C}_+$.

The existence in the (μ_1, μ_2) plane of the curve $\mu_2 = H_{SC}(\mu_1)$ of homoclinic bifurcations of the canonical family at $\mathbf{r}_2$ implies that there will be a corresponding curve $\alpha = \alpha_h(\beta, \epsilon)$ in the (β, α) plane of homoclinic bifurcations of the $W^C_{1+}(\boldsymbol{\alpha})$ dynamics at $\mathbf{y}^+_2$. Moreover since $\mathbf{y}^+_2$ exists for (β, α) between $\alpha = \Lambda_+\beta$ and $\alpha = T(\beta)$, $\alpha = \alpha_h(\beta, \epsilon)$ will lie between the line $\alpha = \Lambda_+\beta$ in $\beta \geq \beta_1$ and the union of the two curves $\alpha = \alpha_H(\beta)$ and $\alpha = \alpha_+(\beta)$ in $\beta \geq \beta_1$.[3] As (β, α) approaches $\alpha = \alpha_h(\beta, \epsilon)$ from the left, $\mathcal{C}_+$ will increase in size and approach $\mathbf{y}^+_2$. At $\alpha = \alpha_h(\beta, \epsilon)$, $\mathcal{C}_+$ will be homoclinic to $\mathbf{y}^+_2$ on $W^C_{1+}(\boldsymbol{\alpha})$, while for (β, α) to the right of $\alpha = \alpha_h(\beta, \epsilon)$, $\mathcal{C}_+$ will no longer exist. Finally, note that as the saddlenode bifurcation at $\alpha = T(\beta)$ which creates $\mathbf{y}^+_1$ and $\mathbf{y}^+_2$ is a 1-dimensional bifurcation, it will occur on a 1-dimensional invariant manifold of the burster system lying in $W^C_{1+}(\boldsymbol{\alpha})$. Also, since $\mathbf{y}^+_1$ is unstable for (β, α) lying between $\alpha = \alpha_H(\beta)$ and $\alpha = \alpha_+(\beta)$, $W^C_{1+}(\boldsymbol{\alpha})$ will contain a 2-dimensional local unstable manifold of $\mathbf{y}^+_1$ in this range. This manifold can be identified as $W^{UF}_{1+}(\boldsymbol{\alpha})$ for (β, α) between $\alpha = \alpha_H(\beta)$ and $\alpha = R_+(\beta, \epsilon)$, and as $W^{UN}_{1+}(\boldsymbol{\alpha})$ for (β, α) between $\alpha = R_+(\beta, \epsilon)$ and $\alpha = \alpha_+(\beta)$, where $W^{UF}_{1+}(\boldsymbol{\alpha})$ and $W^{UN}_{1+}(\boldsymbol{\alpha})$ are the unique 2-dimensional local manifolds of $\mathbf{y}^+_1$ defined in section 3.6.1 (cf. figure (3-17)). $W^C_{1+}(\boldsymbol{\alpha})$ thus contains a unique 2-dimensional manifold for (β, α) lying between $\alpha = \alpha_H(\beta)$ and $\alpha = \alpha_+(\beta)$, and so will itself be unique in this range.

To conclude-and by way of a summary-the symmetry of the system under σ implies that the following will hold for a given ϵ:

1. For α and β with $\left\|(\alpha, \beta)^T - (\alpha_2, \beta_2)^T\right\|$ small, the burster system $\dot{\mathbf{y}} = \mathbf{X}(\mathbf{y}, \boldsymbol{\alpha})$ has an attracting 2-dimensional C^∞ local invariant manifold $W^C_{1-}(\boldsymbol{\alpha})$ in N_-, which can be considered to be the image of $W^C_{1+}(\boldsymbol{\alpha})$ under σ. For (β, α) lying between $\alpha = \alpha_-(\beta)$ and $\alpha = \alpha_+(\beta)$, $W^C_{1-}(\boldsymbol{\alpha})$ contains $\mathbf{y}^-_1$, while for $\{\alpha = \alpha_2, \beta = \beta_2\}$, $W^C_{1-}(\boldsymbol{\alpha})$ is tangential to the plane $\sigma\,\mathrm{Sp}\{\mathbf{v}_C(\epsilon), \mathbf{w}_C(\epsilon)\}$ at $\mathbf{y}^-_1$. Also, $W^C_{1-}(\boldsymbol{\alpha})$ is unique for (β, α) lying between $\alpha = \alpha_H(\beta)$ and $\alpha = \alpha_+(\beta)$.

2. As α increases through $T(\beta)$, $\mathbf{y}^-_1$ and $\mathbf{y}^-_2$ are created in a saddlenode bifurcation on a 1-dimensional invariant manifold of the system lying in $W^C_{1-}(\boldsymbol{\alpha})$. This can be considered to be the image under σ of a corresponding invariant manifold in $W^C_{1+}(\boldsymbol{\alpha})$.

3. As α increases through $\alpha_H(\beta)$, $\mathbf{y}^-_1$ goes unstable in a supercritical Hopf bifurcation on $W^C_{1-}(\boldsymbol{\alpha})$, creating a stable limit cycle $\mathcal{C}_-$ where $\mathcal{C}_- \stackrel{def}{=} \sigma\mathcal{C}_+$.

[3]The curve $\alpha = \alpha_+(\beta)$ was defined in section 3.6.1 as the restriction of the curve $\alpha = T(\beta)$ to the range (β_2, ∞).

4. As (β, α) crosses $\alpha = \alpha_h(\beta, \epsilon)$ from left to right, $\mathcal{C}_-$ is destroyed in a homoclinic bifurcation on $W^C_{1-}(\boldsymbol{\alpha})$ at $\mathbf{y}_2^-$.

The Takens-Bogadanov analysis thus enables a full description of the bifurcations of the burster system close to the codimension 2 point (α_2, β_2) to be proposed for a fixed ϵ. In order to construct a picture of the bifurcations of the system away from this point, the Hopf, saddlenode and homoclinic bifurcations will now be examined in greater detail. This will enable a full bifurcation diagram to be suggested for $\boldsymbol{\alpha}$ with ϵ small.

4.3 The Hopf bifurcation at $\alpha = \alpha_H(\beta)$

The Hopf bifurcation which occurs at $\mathbf{y}_1^+$ when $\alpha = \alpha_H(\beta)$ for a given ϵ will be examined in this section. The properties of the bifurcation which occurs at $\mathbf{y}_1^-$ for $\alpha = \alpha_H(\beta)$ can then be understood by using the symmetry of the system under σ.

Fix $\epsilon, \beta > 0$. Also fix α_m and α_M with $\alpha_-(\beta) < \alpha_m < \alpha_H(\beta) < \alpha_M$ and consider the burster system $\dot{\mathbf{y}} = \mathbf{X}(\mathbf{y}; \alpha, \beta, \epsilon)$ for $\mathbf{y} \in N_+ \backslash P$, $\alpha \in (\alpha_m, \alpha_M)$. At $\alpha = \alpha_H(\beta)$, $\mathbf{y}_1^+ = \left(\frac{1}{\sqrt{\gamma}}, \frac{1}{\sqrt{\gamma}}, \varepsilon_H\right)^T$, which is independent of $\boldsymbol{\alpha}$. In keeping with section 4.2, write this as $\bar{\mathbf{y}}_1^+$. Recall from (3.59) that the eigenvalues $\{\mu_{11}(\boldsymbol{\alpha}), \mu_{12}(\boldsymbol{\alpha}), \mu_{13}(\boldsymbol{\alpha})\}$ of $D_{\mathbf{y}}\mathbf{X}(\mathbf{y}_1^+; \boldsymbol{\alpha})$ are

$$\begin{aligned} \mu_{11}(\boldsymbol{\alpha}) &= -(1 + 3(\Delta_1(\alpha, \beta) + 1)) \\ \mu_{12}(\boldsymbol{\alpha}) &= \tfrac{1}{2}\left(\Delta_1(\alpha, \beta) + \sqrt{\Delta_1(\alpha, \beta)^2 - 4\epsilon\left(\Gamma_1^+(\alpha, \beta) + \Gamma_1^-(\alpha, \beta)\right)}\right) \\ \mu_{13}(\boldsymbol{\alpha}) &= \tfrac{1}{2}\left(\Delta_1(\alpha, \beta) - \sqrt{\Delta_1(\alpha, \beta)^2 - 4\epsilon\left(\Gamma_1^+(\alpha, \beta) + \Gamma_1^-(\alpha, \beta)\right)}\right) \end{aligned} \tag{4.40}$$

where $\Delta_1(\alpha, \beta) = \gamma x_1(\alpha, \beta)^2 - 1$. Also recall that the corresponding eigenvectors are

$$\left\{(1, 1, 0)^T, \mathbf{v}_{12}(\boldsymbol{\alpha}), \mathbf{v}_{13}(\boldsymbol{\alpha})\right\}$$

where $\mathbf{v}_{12}(\boldsymbol{\alpha})$ and $\mathbf{v}_{13}(\boldsymbol{\alpha})$ are given by:

$$\mathbf{v}_{12}^{+}(\boldsymbol{\alpha}) = \begin{pmatrix} \left(\Gamma_1^{+}(\alpha,\beta) - \Gamma_1^{-}(\alpha,\beta)\right)\mu_{13}(\boldsymbol{\alpha}) - \left(\Gamma_1^{+}(\alpha,\beta) + \Gamma_1^{-}(\alpha,\beta)\right)\left(\mu_{12}(\boldsymbol{\alpha}) - \mu_{11}(\boldsymbol{\alpha})\right) \\ \left(\Gamma_1^{+}(\alpha,\beta) - \Gamma_1^{-}(\alpha,\beta)\right)\mu_{13}(\boldsymbol{\alpha}) + \left(\Gamma_1^{+}(\alpha,\beta) + \Gamma_1^{-}(\alpha,\beta)\right)\left(\mu_{12}(\boldsymbol{\alpha}) - \mu_{11}(\boldsymbol{\alpha})\right) \\ 2\mu_{13}(\boldsymbol{\alpha})\left(\mu_{12}(\boldsymbol{\alpha}) - \mu_{11}(\boldsymbol{\alpha})\right) \end{pmatrix}$$

$$\mathbf{v}_{13}^{+}(\boldsymbol{\alpha}) = \begin{pmatrix} \left(\Gamma_1^{+}(\alpha,\beta) - \Gamma_1^{-}(\alpha,\beta)\right)\mu_{12}(\boldsymbol{\alpha}) - \left(\Gamma_1^{+}(\alpha,\beta) + \Gamma_1^{+}(\alpha,\beta)\right)\left(\mu_{13}(\boldsymbol{\alpha}) - \mu_{11}(\boldsymbol{\alpha})\right) \\ \left(\Gamma_1^{+}(\alpha,\beta) - \Gamma_1^{-}(\alpha,\beta)\right)\mu_{12}(\boldsymbol{\alpha}) + \left(\Gamma_1^{+}(\alpha,\beta) + \Gamma_1^{-}(\alpha,\beta)\right)\left(\mu_{13}(\boldsymbol{\alpha}) - \mu_{11}(\boldsymbol{\alpha})\right) \\ 2\mu_{12}(\boldsymbol{\alpha})\left(\mu_{13}(\boldsymbol{\alpha}) - \mu_{11}(\boldsymbol{\alpha})\right) \end{pmatrix} \tag{4.41}$$

Let $\left(\mu_j\right)_H(\beta,\epsilon) = \mu_{1j}\left(\alpha_H(\beta),\beta,\epsilon\right)$ for $1 \leq j \leq 3$. On the curve $\alpha = \alpha_H(\beta)$, $\Delta_1 = 0$, and so (4.40) implies

$$\begin{aligned} (\mu_1)_H(\beta,\epsilon) &= -4 \\ (\mu_2)_H(\beta,\epsilon) &= i\sqrt{\epsilon\left(\left(\Gamma_1^{+}\right)_H + \left(\Gamma_1^{-}\right)_H(\beta)\right)} \\ (\mu_3)_H(\beta,\epsilon) &= -i\sqrt{\epsilon\left(\left(\Gamma_1^{+}\right)_H + \left(\Gamma_1^{-}\right)_H(\beta)\right)} \end{aligned}$$

where $\left(\Gamma_1^{+}\right)_H = \Gamma_1^{+}\left(\alpha_H(\beta),\beta\right)$ and $\left(\Gamma_1^{-}\right)_H(\beta) = \Gamma_1^{-}\left(\alpha_H(\beta),\beta\right)$ (cf. (3.71) and (3.72)). Introduce the vectors $\mathbf{v}_H(\beta,\epsilon) = \operatorname{Re}\left\{\mathbf{v}_{12}^{+}\left(\alpha_H(\beta),\beta,\epsilon\right)\right\}$ and $\mathbf{w}_H(\beta,\epsilon) = \operatorname{Im}\left\{\mathbf{v}_{12}^{+}\left(\alpha_H(\beta),\beta,\epsilon\right)\right\}$. Setting $\alpha = \alpha_H(\beta)$ in (4.41) gives:

$$\mathbf{v}_H(\beta,\epsilon) = \sqrt{\frac{\left(\Gamma_1^{+}\right)_H + \left(\Gamma_1^{-}\right)_H(\beta)}{\epsilon}}\begin{pmatrix} 2 \\ -2 \\ -\epsilon \end{pmatrix}, \mathbf{w}_H(\beta,\epsilon) = \begin{pmatrix} \left(\Gamma_1^{+}\right)_H \\ -\left(\Gamma_1^{-}\right)_H(\beta) \\ 4 \end{pmatrix} \tag{4.42}$$

These quantities allow the reduction of $D_{\mathbf{y}}\mathbf{X}\left(\bar{\mathbf{y}}_1^{+};\alpha_H(\beta),\beta,\epsilon\right)$ to its Jordan normal form. Define the 3×3 matrix $P(\beta,\epsilon)$ by $P(\beta,\epsilon) = \left[(1,1,0)^T\ \mathbf{v}_H(\beta,\epsilon)\ \mathbf{w}_H(\beta,\epsilon)\right]$ and write $A(\beta,\epsilon)$ for the real 3×3 matrix $P(\beta,\epsilon)^{-1} D_{\mathbf{y}}\mathbf{X}\left(\bar{\mathbf{y}}_1^{+};\alpha_H(\beta),\beta,\epsilon\right) P(\beta,\epsilon)$. By construction, $A(\beta,\epsilon)$ has the form:

$$A(\beta,\epsilon) = \begin{pmatrix} -4 & 0 & 0 \\ 0 & 0 & \sqrt{\epsilon\left(\left(\Gamma_1^{+}\right)_H + \left(\Gamma_1^{-}\right)_H(\beta)\right)} \\ 0 & -\sqrt{\epsilon\left(\left(\Gamma_1^{+}\right)_H + \left(\Gamma_1^{-}\right)_H(\beta)\right)} & 0 \end{pmatrix}$$

Bringing these results together, it is now possible to analyse the bifurcation that occurs on $\alpha = \alpha_H(\beta)$. Change to local coordinates $\mathbf{y}'$ by setting $\mathbf{y}' = \mathbf{y} - \mathbf{y}_1^{+}(\alpha,\beta)$, and then perform the normal form change of coordinates $\mathbf{y}' \to \mathbf{x}$ defined by $\mathbf{x} = (x, y, z)^T = P(\beta, \epsilon)^{-1} \mathbf{y}'$. Using a similar analysis to that of section 4.1, it can be shown that the following hold for $|\alpha - \alpha_H(\beta)|$ small:

1. $\mathbf{y}_1^+$ has an attracting 2-dimensional C^∞ local invariant manifold $W_{1+}^H(\boldsymbol{\alpha})$ in $\dot{\mathbf{y}} = \mathbf{X}(\mathbf{y}; \boldsymbol{\alpha})$, such that $W_{1+}^H(\boldsymbol{\alpha})$ is tangential to the plane $\mathrm{Sp}\{\mathbf{v}_H(\beta, \epsilon), \mathbf{w}_H(\beta, \epsilon)\}$ at $\mathbf{y}_1^+$ when $\alpha = \alpha_H(\beta)$. Also, in the normal form coordinates $\mathbf{x} = (x, y, z)^T$, $W_{1+}^H(\boldsymbol{\alpha})$ can be considered as a graph

$$\left\{(h(y, z; \boldsymbol{\alpha}), y, z)^T\right\}$$

over y and z for $\left\|(y, z)^T\right\|$ small, where h is a C^∞ function of y and z such that (i) $h(0, 0; \boldsymbol{\alpha}) = 0 \ \forall \alpha$ and (ii) $\frac{\partial h}{\partial y}(0, 0; \alpha_H(\beta), \beta, \epsilon) = \frac{\partial h}{\partial z}(0, 0; \alpha_H(\beta), \beta, \epsilon) = 0$.

2. The dynamics on $W_{1+}^H(\boldsymbol{\alpha})$ has the form $\left\{\dot{\mathbf{z}} = \mathbf{G}(\mathbf{z}; \boldsymbol{\alpha}) : \mathbf{z} = (y, z)^T\right\}$, where $\mathbf{G}(\mathbf{z}; \boldsymbol{\alpha})$ is a C^∞ function of $\mathbf{z}$ and α such that (i) $\mathbf{G}(0, 0; \boldsymbol{\alpha}) = \begin{pmatrix} 0 \\ 0 \end{pmatrix} \forall \alpha$ and (ii) $D_{\mathbf{z}}\mathbf{G}(0, 0; \alpha_H(\beta), \beta, \epsilon)$ is given by:

$$D_{\mathbf{z}}\mathbf{G}(0, 0; \alpha_H(\beta), \beta, \epsilon) = \begin{pmatrix} 0 & \sqrt{\epsilon\left(\left(\Gamma_1^+\right)_H + \left(\Gamma_1^-\right)_H(\beta)\right)} \\ -\sqrt{\epsilon\left(\left(\Gamma_1^+\right)_H + \left(\Gamma_1^-\right)_H(\beta)\right)} & 0 \end{pmatrix} \tag{4.43}$$

The fixed point $(0, 0)^T$ of the $W_{1+}^H(\boldsymbol{\alpha})$ dynamics corresponds to the fixed point $\mathbf{y}_1^+$ of the burster dynamics.

It was shown in 3.6.1 that $\mathbf{y}_1^+$ is stable in the burster system for $\alpha < \alpha_H(\beta)$. This implies that $(0, 0)^T$ is a stable fixed point of $\dot{\mathbf{z}} = \mathbf{G}(\mathbf{z}; \boldsymbol{\alpha})$ for $\alpha - \alpha_H(\beta) < 0$ small. It was also shown that for $\alpha - \alpha_H(\beta) > 0$ small, $\mathbf{y}_1^+$ has a unique 2-dimensional C^∞ local unstable manifold $W_{1+}^{UF}(\boldsymbol{\alpha})$ (cf. figure (3-17)). In this range $W_{1+}^H(\boldsymbol{\alpha})$ must therefore contain $W_{1+}^{UF}(\boldsymbol{\alpha})$, and so is itself unique. Moreover, $(0, 0)^T$ will be an unstable fixed point of $\dot{\mathbf{z}} = \mathbf{G}(\mathbf{z}; \boldsymbol{\alpha})$. As $D_{\mathbf{z}}\mathbf{G}(0, 0; \alpha_H(\beta), \beta, \epsilon)$ has the form shown in (4.43), and $(0, 0)^T$ becomes unstable in $\dot{\mathbf{z}} = \mathbf{G}(\mathbf{z}; \boldsymbol{\alpha})$ as α increases through $\alpha_H(\beta)$, it follows from the Hopf Bifurcation Theorem that generically, there are two possibilities for the $W_{1+}^H(\boldsymbol{\alpha})$ dynamics [4]:

1. $(0, 0)^T$ is a stable focus for $\alpha < \alpha_H(\beta)$, and an unstable focus surrounded by a stable limit cycle for $\alpha > \alpha_H(\beta)$ (supercritical Hopf).

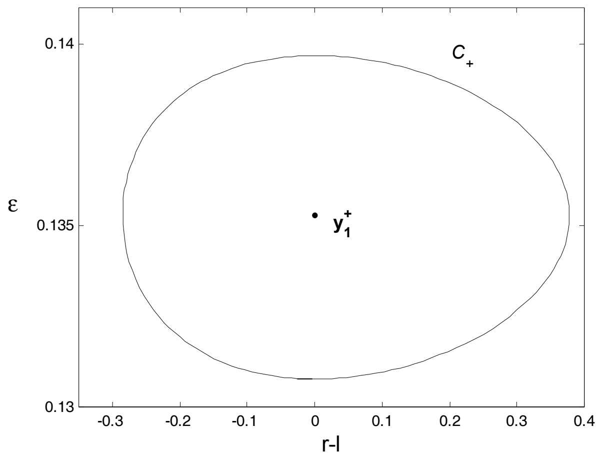

Figure 4-13: Projection of the stable limit cycle $\mathcal{C}_+$ onto the $(r-l, \varepsilon)$ plane for $\alpha = 108.62$, $\beta = 1.5$, $\epsilon = 0.001$. This choice of parameters corresponds to $\alpha - \alpha_H(\beta) \approx 0.008$.

2. $(0,0)^T$ is a stable focus surrounded by an unstable limit cycle for $\alpha < \alpha_H(\beta)$, and an unstable focus for $\alpha > \alpha_H(\beta)$ (subcritical Hopf).

In both cases, for $|\alpha - \alpha_H(\beta)|$ small, the limit cycle is approximately harmonic, and its amplitude grows like $\sqrt{|\alpha - \alpha_H(\beta)|}$ [4], [27]. In keeping with section 4.2, the limit cycle created by the Hopf will be referred to in what follows as $\mathcal{C}_+$. The Takens-Bogadanov analysis of section 4.2 showed that the Hopf is supercritical for $\beta - \beta_2 < 0$ small. Numerical results suggest that the Hopf is in fact supercritical for all $\beta > 0$. As $W_{1+}^H(\boldsymbol{\alpha})$ is attracting, this implies that $\forall \beta > 0$, $\mathcal{C}_+$ will be stable in the full burster system for $\alpha - \alpha_H(\beta) > 0$ small. Figure (4-13) shows the projection of $\mathcal{C}_+$ onto the $(r-l, \varepsilon)$ plane for $\{\alpha = 108.62, \beta = 1.5, \epsilon = 0.001\}$. This choice of parameters is equivalent to $\alpha - \alpha_H(\beta) \approx 0.008$, close to the bifurcation point. It can be seen that $\mathcal{C}_+$ is an approximate ellipse in this case, as predicted by the Hopf Bifurcation Theorem. Figure (4-14) shows the projection of $\mathcal{C}_+$ onto the $(r-l, \varepsilon)$ plane for $\{\alpha = 110, \beta = 1.5, \epsilon = 0.001\}$. This choice of parameters is equivalent to $\alpha - \alpha_H(\beta) \approx 1.39 \gg 0.008$. It can be seen that $\mathcal{C}_+$ has increased significantly in size and is now anharmonic.

In summary, given a fixed ϵ, for $|\alpha - \alpha_H(\beta)|$ small, $\mathbf{y}_1^+$ has a 2-dimensional C^∞ local invariant manifold $W_{1+}^H(\boldsymbol{\alpha})$. $W_{1+}^H(\boldsymbol{\alpha})$ is tangential to the plane $\mathrm{Sp}\{\mathbf{v}_H(\beta,\epsilon), \mathbf{w}_H(\beta,\epsilon)\}$ at $\mathbf{y}_1^+$ when $\alpha = \alpha_H(\beta)$, where $\mathbf{v}_H(\beta,\epsilon)$ and $\mathbf{w}_H(\beta,\epsilon)$ are given by (4.42). Also, $W_{1+}^H(\boldsymbol{\alpha})$ is unique for $\alpha > \alpha_H(\beta)$. Finally, as α increases through $\alpha_H(\beta)$, $\mathbf{y}_1^+$ loses stability in a supercritical Hopf bifurcation on $W_{1+}^H(\boldsymbol{\alpha})$, creating a stable limit cycle $\mathcal{C}_+$. Note that the

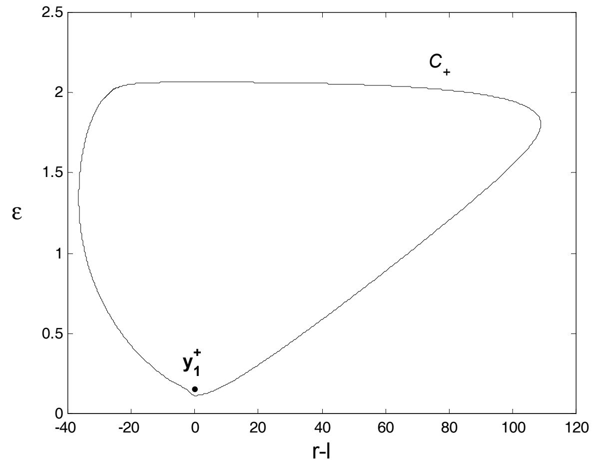

Figure 4-14: Projection of the stable limit cycle $\mathcal{C}_+$ onto the $(r-l, \varepsilon)$ plane for $\alpha = 110$, $\beta = 1.5$, $\epsilon = 0.001$. This choice of parameters corresponds to $\alpha - \alpha_H(\beta) \approx 1.39$.

uniqueness of $W_{1+}^H(\boldsymbol{\alpha})$ for $\alpha > \alpha_H(\beta)$ means that for $\beta - \beta_2 < 0$ small in this range, it can be thought of as a subset of the invariant manifold $W_{1+}^C(\boldsymbol{\alpha})$ introduced in section 4.2. The symmetry of the system under σ implies that the following holds for a given ϵ:

1. For $|\alpha - \alpha_H(\beta)|$ small, $\mathbf{y}_1^-$ has a 2-dimensional C^∞ local invariant manifold $W_{1-}^H(\boldsymbol{\alpha})$, which can be considered to be the image of $W_{1+}^H(\boldsymbol{\alpha})$ under σ. $W_{1-}^H(\boldsymbol{\alpha})$ is tangential to the plane $\sigma\,\mathrm{Sp}\{\mathbf{v}_H(\beta,\epsilon), \mathbf{w}_H(\beta,\epsilon)\}$ at $\mathbf{y}_1^-$ when $\alpha = \alpha_H(\beta)$. Also, $W_{1-}^H(\boldsymbol{\alpha})$ is unique for $\alpha > \alpha_H(\beta)$, and can be thought of as a subset of $W_{1-}^C(\boldsymbol{\alpha})$ for $\beta - \beta_2 < 0$ small in this range.

2. As α increases through $\alpha_H(\beta)$, $\mathbf{y}_1^-$ loses stability in a supercritical Hopf bifurcation on $W_{1-}^H(\boldsymbol{\alpha})$, creating a stable limit cycle $\mathcal{C}_-$, where $\mathcal{C}_- = \sigma\mathcal{C}_+$.

It was argued at the end of section 3.4.1 that for small ϵ, trajectories of the burster system cannot cross the plane P. As limit cycles are trajectories, it follows that for small ϵ, $\mathcal{C}_+$ lies entirely in N_+ and $\mathcal{C}_-$ lies entirely in N_-.

4.4 The saddlenode bifurcation

The bifurcation which occurs at $\mathbf{y}_1^+$ when $\alpha = T(\beta)$, $\beta \neq \beta_2$ will be examined in this section. Again, the properties of the bifurcation at $\mathbf{y}_1^-$ when $\alpha = T(\beta)$, $\beta \neq \beta_2$ can then be inferred by the symmetry of the system under σ.

$2\beta' < \beta < \beta_2$	$\beta > \beta_2$
$(\mu_1)_T(\beta,\epsilon) = -(1+3((\Delta_1)_T(\beta)+1)) < 0$ $(\mu_2)_T(\beta,\epsilon) = 0$ $(\mu_3)_T(\beta,\epsilon) = (\Delta_1)_T(\beta) < 0$	$(\mu_1)_T(\beta,\epsilon) = -(1+3((\Delta_1)_T(\beta)+1)) < 0$ $(\mu_2)_T(\beta,\epsilon) = (\Delta_1)_T(\beta) > 0$ $(\mu_3)_T(\beta,\epsilon) = 0$

Table 4.1: Values and signs of $\{(\mu_1)_T(\beta,\epsilon), (\mu_2)_T(\beta,\epsilon), (\mu_3)_T(\beta,\epsilon)\}$.

Fix $\epsilon > 0$ and $\beta > 2\beta'$. Also fix α_m and α_M with $0 < \alpha_m < T(\beta) < \alpha_M < \Lambda_+\beta$ and consider the burster system $\dot{\mathbf{y}} = \mathbf{X}(\mathbf{y};\alpha,\beta,\epsilon)$ for $\mathbf{y} \in N_+\backslash P$, $\alpha \in (\alpha_m, \alpha_M)$. It was shown in section 3.6.1 that the eigenvalues $\{\mu_{21}(\boldsymbol{\alpha}), \mu_{22}(\boldsymbol{\alpha}), \mu_{23}(\boldsymbol{\alpha})\}$ of $D_{\mathbf{y}}\mathbf{X}(\mathbf{y}_2^+;\boldsymbol{\alpha})$ are always real and have the signs below:

$$\{\mu_{21}(\boldsymbol{\alpha}) < 0, \mu_{22}(\boldsymbol{\alpha}) > 0, \mu_{23}(\boldsymbol{\alpha}) < 0\}$$

Following the notation of 3.6.1, let $\left\{(1,1,0)^T, \mathbf{v}_{22}^+(\boldsymbol{\alpha}), \mathbf{v}_{23}^+(\boldsymbol{\alpha})\right\}$ be the eigenvectors of $D_{\mathbf{y}}\mathbf{X}(\mathbf{y}_2^+;\boldsymbol{\alpha})$ corresponding to $\{\mu_{21}(\boldsymbol{\alpha}), \mu_{22}(\boldsymbol{\alpha}), \mu_{23}(\boldsymbol{\alpha})\}$. As was stated in 3.6.1, $\mathbf{y}_2^+$ has a unique 1-dimensional C^∞ local unstable manifold $W_{2+}^U(\boldsymbol{\alpha})$ which is tangential to $\mathbf{v}_{22}^+(\boldsymbol{\alpha})$ at $\mathbf{y}_2^+$. $\mathbf{y}_2^+$ also has a unique 2-dimensional C^∞ local stable manifold $W_{2+}^{SN}(\boldsymbol{\alpha})$ which is tangential to the plane $\mathrm{Sp}\left\{(1,1,0)^T, \mathbf{v}_{23}^+(\boldsymbol{\alpha})\right\}$ at $\mathbf{y}_2^+$, on which it is a stable node.

Write $\hat{\mathbf{y}}_1^+(\beta) = (x_T(\beta), x_T(\beta), \varepsilon_T(\beta))^T$ for $\mathbf{y}_1^+(T(\beta),\beta)$ and let the eigenvalues of $D_{\mathbf{y}}\mathbf{X}(\hat{\mathbf{y}}_1^+(\beta); T(\beta), \beta, \epsilon)$ be $\{(\mu_1)_T(\beta,\epsilon), (\mu_2)_T(\beta,\epsilon), (\mu_3)_T(\beta,\epsilon)\}$. It then follows from the stability analysis of $\mathbf{y}_1^+(\alpha,\beta)$ in section 3.6.1 that $\{(\mu_1)_T(\beta,\epsilon), (\mu_2)_T(\beta,\epsilon), (\mu_3)_T(\beta,\epsilon)\}$ have the values and signs shown in table (4.1), where $(\Delta_1)_T(\beta) = \gamma x_T(\beta)^2 - 1$. Let the generalised eigenvectors of $D_{\mathbf{y}}\mathbf{X}(\hat{\mathbf{y}}_1^+(\beta); T(\beta), \beta, \epsilon)$ corresponding to the eigenvalues $\{(\mu_1)_T(\beta,\epsilon), (\mu_2)_T(\beta,\epsilon), (\mu_3)_T(\beta,\epsilon)\}$ be $\left\{(1,1,0)^T, \mathbf{v}_T(\beta,\epsilon), \mathbf{w}_T(\beta,\epsilon)\right\}$. It can be shown that $\mathbf{v}_T(\beta,\epsilon)$ and $\mathbf{w}_T(\beta,\epsilon)$ are given by

$$\begin{aligned} \mathbf{v}_T(\beta,\epsilon) &= \begin{cases} \mathbf{a}_T(\beta,\epsilon) & \text{if} \quad 2\beta' < \beta < \beta_2 \\ \mathbf{b}_T(\beta,\epsilon) & \text{if} \quad \beta > \beta_2 \end{cases} \\ \mathbf{w}_T(\beta,\epsilon) &= \begin{cases} \mathbf{b}_T(\beta,\epsilon) & \text{if} \quad 2\beta' < \beta < \beta_2 \\ \mathbf{a}_T(\beta,\epsilon) & \text{if} \quad \beta > \beta_2 \end{cases} \end{aligned}$$

where

$$\mathbf{a}_T(\beta,\epsilon) = \begin{pmatrix} 1 \\ 1 \\ -\frac{(\mu_1)_T(\beta,\epsilon)}{\left(\Gamma_1^+\right)_T(\beta)} \end{pmatrix}, \mathbf{b}_T(\beta,\epsilon) = \begin{pmatrix} \frac{\epsilon\left(\Gamma_1^+\right)_T(\beta) - 2\gamma x_T(\beta)^2(\Delta_1)_T(\beta)}{4\epsilon\gamma x_T(\beta)^2} \\ \frac{\epsilon\left(\Gamma_1^+\right)_T(\beta) + 2\gamma x_T(\beta)^2(\Delta_1)_T(\beta)}{4\epsilon\gamma x_T(\beta)^2} \\ 1 \end{pmatrix} \tag{4.44}$$

and $\left(\Gamma_1^+\right)_T(\beta) = \Gamma_1^+(T(\beta), \beta)$. Define the 3×3 matrix $P(\beta, \epsilon)$ by

$$P(\beta, \epsilon) = \left[(1,1,0)^T \, \mathbf{v}_T(\beta, \epsilon) \, \mathbf{w}_T(\beta, \epsilon)\right]$$

and the 3×3 normal form matrix $A(\beta, \epsilon)$ by:

$$A(\beta, \epsilon) = P(\beta, \epsilon)^{-1} D_{\mathbf{y}} \mathbf{X}\left(\hat{\mathbf{y}}_1^+(\beta); T(\beta), \beta, \epsilon\right) P(\beta, \epsilon)$$

Table (4.1) then implies that $A(\beta, \epsilon)$ has the form:

$$A(\beta, \epsilon) = \begin{cases} \begin{pmatrix} -\left(1 + 3\left((\Delta_1)_T(\beta) + 1\right)\right) & 0 & 0 \\ 0 & 0 & 0 \\ 0 & 0 & (\Delta_1)_T(\beta) \end{pmatrix} & \text{if } \; 2\beta' < \beta < \beta_2 \\ \begin{pmatrix} -\left(1 + 3\left((\Delta_1)_T(\beta) + 1\right)\right) & 0 & 0 \\ 0 & (\Delta_1)_T(\beta) & 0 \\ 0 & 0 & 0 \end{pmatrix} & \text{if } \; \beta > \beta_2 \end{cases} \tag{4.45}$$

Perform the change of coordinates $\mathbf{y} \to \mathbf{y}'$ defined by $\mathbf{y}' = \mathbf{y} - \hat{\mathbf{y}}_1^+(\beta)$. Next perform the normal form change of coordinates $\mathbf{y}' \to \mathbf{x}$ defined by

$$\mathbf{x} = P(\beta, \epsilon)^{-1} \mathbf{y}' + P(\beta, \epsilon)^{-1} D_{\mathbf{y}} \mathbf{X}\left(\hat{\mathbf{y}}_1^+(\beta); T(\beta), \beta, \epsilon\right)^{-1} D_{\alpha} \mathbf{F}(\mathbf{0}; T(\beta), \beta, \epsilon)(\alpha - T(\beta))$$

where

$$\mathbf{F}\left(\mathbf{y}'; \alpha, \beta, \epsilon\right) = \mathbf{X}\left(\mathbf{y}' + \hat{\mathbf{y}}_1^+(\beta); \alpha, \beta, \epsilon\right)$$

and

$$\mathbf{x} = \begin{cases} (x, z, y)^T & \text{if } \; 2\beta' < \beta < \beta_2 \\ (x, y, z)^T & \text{if } \; \beta > \beta_2 \end{cases}$$

Using a similar analysis to that of section 4.2, it can be shown that the following hold for $|\alpha - T(\beta)|$ small, $\beta \neq \beta_2$:

1. $\dot{\mathbf{y}} = \mathbf{X}(\mathbf{y}; \boldsymbol{\alpha})$ has a 1-dimensional C^∞ invariant manifold $W_{1+}^{SD}(\boldsymbol{\alpha})$ such that $\hat{\mathbf{y}}_1^+(\beta) \in W_{1+}^{SD}(T(\beta), \beta, \epsilon)$ and $W_{1+}^{SD}(T(\beta), \beta, \epsilon)$ is tangential to the vector $\mathbf{a}_T(\beta, \epsilon)$ at $\hat{\mathbf{y}}_1^+(\beta)$.

Also, in the normal form coordinates $\mathbf{x}$, $W_{1+}^{SD}(\boldsymbol{\alpha})$ can be considered as a graph

$$\left\{(h_1(z;\boldsymbol{\alpha}), h_2(z,\boldsymbol{\alpha}), z)^T\right\}$$

over z for $|z|$ small, where for $i = 1, 2$, h_i is a C^∞ function of z such that(i) $h_i(0; T(\beta), \beta, \epsilon) = 0$ and (ii) $\frac{\partial h_i}{\partial z}(0; T(\beta), \beta, \epsilon) = 0$.

2. The dynamics on $W_{1+}^{SD}(\boldsymbol{\alpha})$ have the form $\dot{z} = G(z;\boldsymbol{\alpha})$, where $G(z;\boldsymbol{\alpha})$ is a C^∞ function of both z and α with $G(0; T(\beta), \beta, \epsilon) = 0$ and $D_z G(0; T(\beta), \beta, \epsilon) = 0$. At $\alpha = T(\beta)$ the fixed point 0 of the $W_{1+}^{SD}(\boldsymbol{\alpha})$ dynamics corresponds to the fixed point $\hat{\mathbf{y}}_1^+(\beta)$ of the burster dynamics.

Since $D_z G(0; T(\beta), \beta, \epsilon) = 0$, it follows from the Saddlenode Bifurcation Theorem that, generically, there are two possibilities for the $W_{1+}^{SD}(\boldsymbol{\alpha})$ dynamics.

1. There is a pair of fixed points of opposite stability in $\alpha < T(\beta)$ and no fixed points in $\alpha > T(\beta)$.

2. There are no fixed points in $\alpha < T(\beta)$ and a pair of fixed points of opposite stability in $\alpha > T(\beta)$.

[4].

The burster system has the fixed point $\mathbf{0}$ for $\alpha < T(\beta)$ and the fixed points $\{\mathbf{0}, \mathbf{y}_1^+, \mathbf{y}_1^-, \mathbf{y}_2^+, \mathbf{y}_2^-\}$ for $\alpha > T(\beta)$ (cf. figure (3-23)). Thus, since fixed points of the $G(z;\boldsymbol{\alpha})$ dynamics will correspond to nontrivial fixed points of $\dot{\mathbf{y}} = \mathbf{X}(\mathbf{y};\boldsymbol{\alpha})$ close to $\hat{\mathbf{y}}_1^+(\beta)$, this suggests that case 2 above holds: as α increases through $T(\beta)$, two fixed points of the $W_{1+}^{SD}(\boldsymbol{\alpha})$ dynamics of opposite stability are created, corresponding to the fixed points $\mathbf{y}_1^+$ and $\mathbf{y}_2^+$ of the burster system. Moreover, as the positions of $\mathbf{y}_1^+$ and $\mathbf{y}_2^+$ in the $r = l$ plane are determined by ε_1 and ε_2 respectively, ε can be used as a coordinate for the fixed points of the $W_{1+}^{SD}(\boldsymbol{\alpha})$ dynamics.

The stability of ε_1 and ε_2 as fixed points of the $W_{1+}^{SD}(\boldsymbol{\alpha})$ dynamics for $\alpha - T(\beta) > 0$ small can be determined by noting that since $W_{1+}^{SD}(\boldsymbol{\alpha})$ contains $\mathbf{y}_1^+$ and $\mathbf{y}_2^+$, $W_{1+}^{SD}(\boldsymbol{\alpha})$ is a local invariant manifold of both $\mathbf{y}_1^+$ and $\mathbf{y}_2^+$. i.e. it is a heteroclinic connection of the two fixed points [27]. Thus, since ε_1 and ε_2 have opposite stability, if $W_{1+}^{SD}(\boldsymbol{\alpha})$ is a local stable manifold of $\mathbf{y}_1^+$, ε_1 is stable and ε_2 is unstable. Conversely, if $W_{1+}^{SD}(\boldsymbol{\alpha})$ is a local unstable manifold of $\mathbf{y}_1^+$, ε_1 is unstable and ε_2 is stable. Now when $2\beta' < \beta < \beta_2$, $\mathbf{y}_1^+$ is a stable

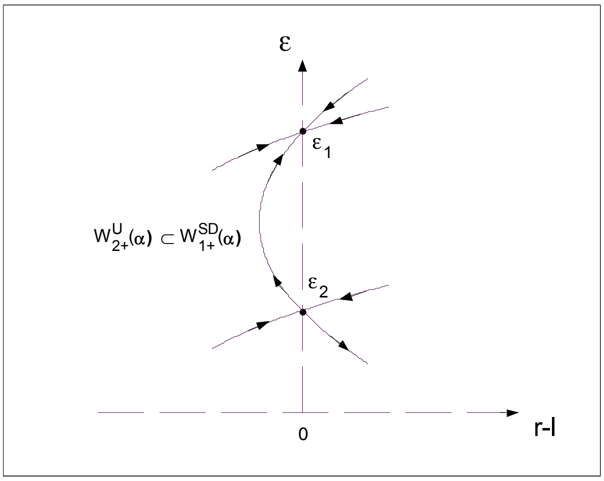

Figure 4-15: Schematic of the projection of the flow on W_{1+}^{SD} onto the $(r-l,\varepsilon)$ plane for small $\alpha - T(\beta) > 0$ in the case $2\beta' < \beta < \beta_2$.

node for small $\alpha - T(\beta) > 0$ (cf. figure (3-17)). In this range, $W_{1+}^{SD}(\boldsymbol{\alpha})$ is therefore a local stable manifold of $\mathbf{y}_1^+$, and so ε_1 is stable in the $W_{1+}^{SD}(\boldsymbol{\alpha})$ dynamics. [Also, $W_{1+}^{SD}(\boldsymbol{\alpha})$ is a local unstable manifold of $\mathbf{y}_2^+$, and so must contain the unique such manifold $W_{2+}^{U}(\boldsymbol{\alpha})$. Moreover, as $W_{1+}^{SD}(\boldsymbol{\alpha})$ contains a unique set, it is itself unique in this range]. For $\beta > \beta_2$, $\mathbf{y}_1^+$ is a saddle node for small $\alpha - T(\beta) > 0$ (cf. figure (3-17) again). It is possible to argue-by contradiction-that $W_{1+}^{SD}(\boldsymbol{\alpha})$ is an unstable local manifold of $\mathbf{y}_1^+$, and hence that ε_1 is unstable in the $W_{1+}^{SD}(\boldsymbol{\alpha})$ dynamics. Assume that $W_{1+}^{SD}(\boldsymbol{\alpha})$ is a local stable manifold of $\mathbf{y}_1^+$. It is then a local unstable manifold of $\mathbf{y}_2^+$, and must therefore contain $W_{2+}^{U}(\boldsymbol{\alpha})$. Now as $\alpha \to T(\beta)+$, $\mathbf{y}_2^+ \to \mathbf{y}_1^+$. Thus, since $W_{2+}^{U}(\boldsymbol{\alpha})$ is tangential to $\mathbf{v}_{22}^+(\boldsymbol{\alpha})$ at $\mathbf{y}_2^+$ and $W_{1+}^{SD}(\boldsymbol{\alpha})$ is tangential to $\mathbf{a}_T(\beta,\epsilon)$ at $\mathbf{y}_1^+$ when $\alpha = T(\beta)$, it would be expected that $\mathbf{v}_{22}^+ \to \mathbf{a}_T(\beta,\epsilon)$ as $\alpha \to T(\beta)+$, implying that $\mathbf{v}_T(\beta,\epsilon) = \mathbf{a}_T(\beta,\epsilon)$. By (4.44), $\mathbf{v}_T(\beta,\epsilon) = \mathbf{b}_T(\beta,\epsilon)$ for $\beta > \beta_2$, giving the contradiction.

Figures (4-15) and (4-16) are schematics of the projection of the flow on $W_{1+}^{SD}(\boldsymbol{\alpha})$ onto the $(r-l,\varepsilon)$ plane for small $\alpha - T(\beta) > 0$ in the cases $2\beta' < \beta < \beta_2$ and $\beta > \beta_2$, based on this analysis. The exact values of ε_1 and ε_2 as a function of $\alpha - T(\beta)$ for $\beta = 21$ and $\beta = 30$ are shown in figures (4-17) and (4-18) respectively. These are obtained in each case by varying α over an appropriate range and numerically solving the equation $f(\varepsilon_*) = h(-\varepsilon_*)$ for $\varepsilon_* > 0$. It can be seen from figures (4-17) and (4-18) that ε_1 and ε_2 scale like $\sqrt{\alpha - T(\beta)}$ for small $\alpha - T(\beta) > 0$, which is consistent with the existence of a saddlenode bifurcation

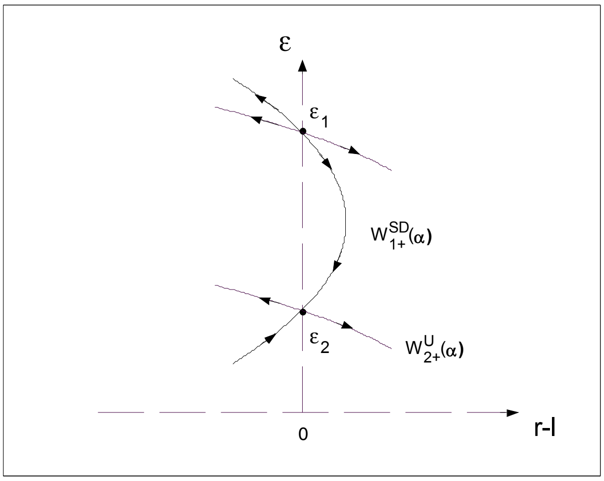

Figure 4-16: Schematic of the projection of the flow on W_{1+}^{SD} onto the $(r-l,\varepsilon)$ plane for small $\alpha - T\left(\beta\right) > 0$ in the case $\beta > \beta_2$.

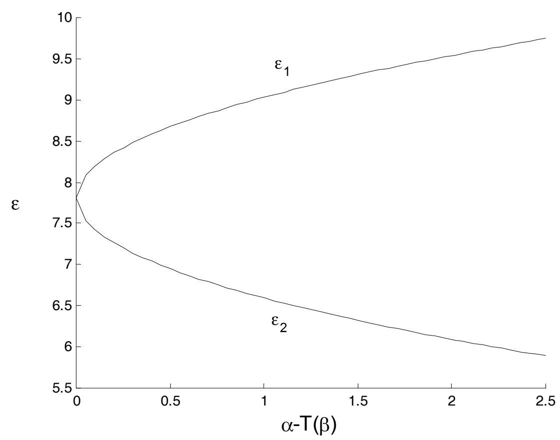

Figure 4-17: Scaling of ε_1 and ε_2 with $\alpha - T\left(\beta\right)$ for $\beta = 21$.

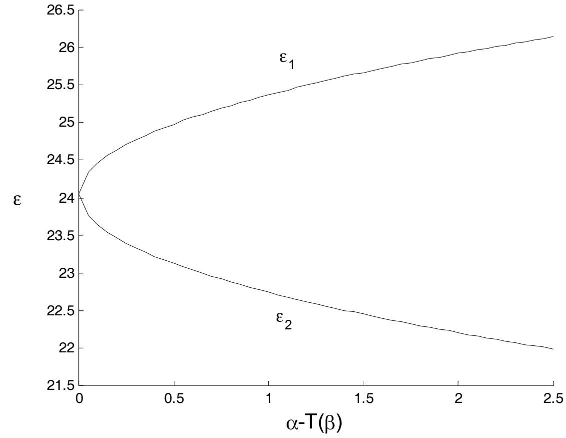

Figure 4-18: Scaling of ε_1 and ε_2 with $\alpha - T(\beta)$ for $\beta = 30$.

at $\alpha = T(\beta)$ [4]. Note that for $|\beta - \beta_2|$ small, $W_{1+}^{SD}(\boldsymbol{\alpha})$ can be thought of as a subset of the local invariant manifold $W_{1+}^{C}(\boldsymbol{\alpha})$ of $\mathbf{y}_1^+$ introduced in section 4.2.

Using the results of this section together with the symmetry of the burster system under σ leads to the following conclusions about $\mathbf{y}_1^-$:

1. For $|\alpha - T(\beta)|$ small, $\dot{\mathbf{y}} = \mathbf{X}(\mathbf{y}; \boldsymbol{\alpha})$ has a 1-dimensional C^∞ invariant manifold $W_{1-}^{SD}(\boldsymbol{\alpha})$, which can be considered as the image of $W_{1+}^{SD}(\boldsymbol{\alpha})$ under σ. $W_{1-}^{SD}(\boldsymbol{\alpha})$ is tangential to the vector $\sigma \mathbf{a}_T(\beta, \epsilon)$ at $\mathbf{y}_1^-$ for $\alpha = T(\beta)$. Also, $W_{1-}^{SD}(\boldsymbol{\alpha})$ is unique for $2\beta' < \beta < \beta_2$, and can be thought of as a subset of $W_{1-}^{C}(\boldsymbol{\alpha})$ for $|\beta - \beta_2|$ small.

2. As α increases through $T(\beta)$, $\mathbf{y}_1^-$ and $\mathbf{y}_2^-$ are created on $W_{1-}^{C}(\boldsymbol{\alpha})$ via a saddlenode bifurcation in the $W_{1-}^{C}(\boldsymbol{\alpha})$ dynamics which creates the fixed points $\{-\varepsilon_1, -\varepsilon_2\}$. For $2\beta' < \beta < \beta_2$, $-\varepsilon_1$ is stable and $-\varepsilon_2$ is unstable while for $\beta > \beta_2$ the stabilities are reversed.

4.5 The homoclinic bifurcation

Using the Takens-Bogadanov analysis, it was argued in section 4.2 that given $\epsilon > 0$, for α and β with $\left\| (\alpha, \beta)^T - (\alpha_2, \beta_2)^T \right\|$ small, there exists a line of homoclinic bifurcations $\alpha = \alpha_h(\beta, \epsilon)$ in the (β, α) plane between the line $\alpha = \Lambda_+ \beta$ in $\beta \geq \beta_1$ and the union of the two curves $\alpha = \alpha_H(\beta)$ and $\alpha = \alpha_+(\beta)$ in $\beta \geq \beta_1$, such that as (β, α) crosses $\alpha = \alpha_h(\beta, \epsilon)$ from left to right, $\mathcal{C}_\pm$ is destroyed in a homoclinic bifurcation on $W_{1\pm}^{C}(\boldsymbol{\alpha})$ at $\mathbf{y}_2^\pm$. The fact that the curves of Hopf and saddlenode bifurcations extend out away from the point

(β_2, α_2) in the (β, α) plane suggests that the curve of homoclinic bifurcations may do the same. Before addressing this issue, it will be useful to briefly summarise some results concerning homoclinic bifurcations in smooth systems.

4.5.1 Homoclinic bifurcations of smooth systems

Consider the general 1-parameter family of systems $\dot{\mathbf{x}} = \mathbf{F}(\mathbf{x};\mu)$, with $\mathbf{x} \in W$ where W is an open subset of $\mathbb{R}^n$ for some $n \geq 2$, $\mu \in (\mu_1, \mu_2)$ with $-\infty \leq \mu_1 < \mu_2 < \infty$, and $\mathbf{F} : W \times (\mu_1, \mu_2) \to \mathbb{R}^n$ is a C^∞ function of $\mathbf{x}$ and μ. Assume that for each $\mu \in (\mu_1, \mu_2)$, $\mathbf{y}(\mu)$ is a hyperbolic saddle of $\dot{\mathbf{x}} = \mathbf{F}(\mathbf{x};\mu)$, and that for some $\mu = \bar{\mu}$, $\dot{\mathbf{x}} = \mathbf{F}(\mathbf{x};\mu)$ has an orbit Γ homoclinic to $\mathbf{y}(\mu)$ which is bounded away from any other fixed points, and has no homoclinic orbits for $\mu \in (\mu_1, \mu_2) \backslash \bar{\mu}$. Further assume that $\mathbf{y}(\mu)$ is C^1 linearisable in $\dot{\mathbf{x}} = \mathbf{F}(\mathbf{x};\mu)$ $\forall \mu \in (\mu_1, \mu_2)$, and that the eigenvalues of $D_{\mathbf{x}}\mathbf{F}(\mathbf{y}(\bar{\mu});\bar{\mu})$ are distinct. Homoclinic bifurcations in systems of this type will henceforth be referred to as **regular homoclinic bifurcations.** Since the eigenvalues of $D_{\mathbf{x}}\mathbf{F}(\mathbf{y}(\bar{\mu});\bar{\mu})$ are distinct, they can be divided into two sets $\{l_i : 1 \leq i \leq d_u\}$ and $\{m_j : 1 \leq j \leq d_s\}$, such that $0 < \mathrm{Re}\{l_i\} \leq \mathrm{Re}\{l_{i+1}\}$ for $1 \leq i < d_u$ and $0 < -\mathrm{Re}\{m_j\} \leq -\mathrm{Re}\{m_{j+1}\}$ for $1 \leq j < d_s$. In $\dot{\mathbf{x}} = \mathbf{F}(\mathbf{x};\bar{\mu})$, typical trajectories which approach $\mathbf{y}(\bar{\mu})$ as $t \to \infty$ do so tangential to the eigenspace corresponding to eigenvalues with $\mathrm{Re}\{m_j\} = \mathrm{Re}\{m_1\}$. Similarly, typical trajectories which approach $\mathbf{y}(\bar{\mu})$ as $t \to -\infty$ do so tangential to the eigenspace corresponding to the eigenvalues with $\mathrm{Re}\{l_i\} = \mathrm{Re}\{l_1\}$ [4], [32]. There are then 3 possibilities for the behaviour of solutions of $\dot{\mathbf{x}} = \mathbf{F}(\mathbf{x};\bar{\mu})$ close to Γ according to the dimensions of these eigenspaces: 1) Both of the eigenspaces are 1-dimensional, in which case the behaviour is typically 2-dimensional (a saddle homoclinic orbit). 2) One of the eigenspaces is 1-dimensional and the other is 2-dimensional, in which case the behaviour is 3-dimensional (a saddle-focus homoclinic orbit). 3) Both of the eigenspaces are 2-dimensional, in which case the behaviour is 4 dimensional (a bi-focus homoclinic orbit). In each case, the behaviour of $\dot{\mathbf{x}} = \mathbf{F}(\mathbf{x};\mu)$ in a tubular neighbourhood of Γ for $|\mu - \bar{\mu}|$ small is determined by a quantity known as the **saddle index** [4], [32]. If the homoclinic orbit is of the saddle type, the saddle index δ is defined as $\delta = -\frac{m_1}{l_1}$. If the orbit is a saddle-focus, the saddle index is defined as $\delta = -\frac{\mathrm{Re}\{m_1\}}{l_1}$ if m_1 is complex and $\delta = -\frac{m_1}{\mathrm{Re}\{l_1\}}$ if l_1 is complex. If the orbit is a bi-focus, the saddle index is defined as $\delta = -\frac{\mathrm{Re}\{m_1\}}{\mathrm{Re}\{l_1\}}$. The case that will be of interest in the following analysis is the bifurcation associated with a saddle homoclinic orbit. For the saddle homoclinic bifurcation, a single limit cycle is created at $\bar{\mu}$ which exists in either $\mu < \bar{\mu}$ or

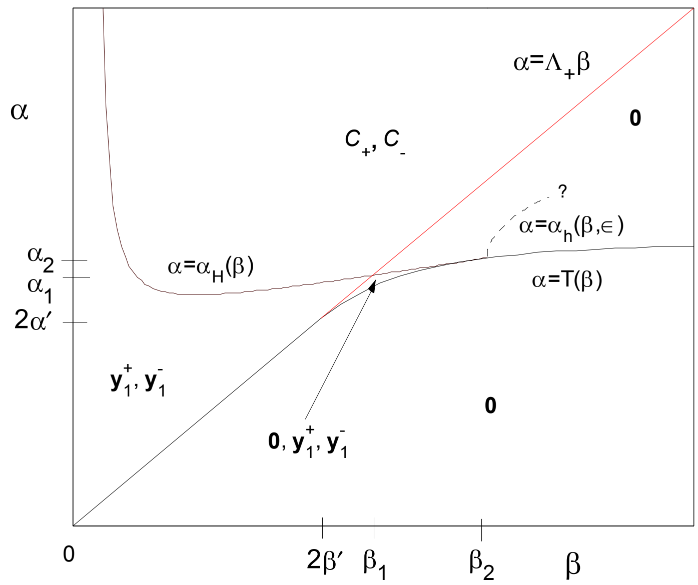

Figure 4-19: Putative bifurcation diagram for small ϵ. $\alpha = \Lambda_+\beta$ is a line of nonsmooth pitchfork bifurcations at $\mathbf{0}$. The bifurcations are supercritical for $\beta \leq 2\beta'$ (black line) and subcritical for $\beta > 2\beta'$ (red line). $\alpha = \alpha_H(\beta)$ is a line of supercritical Hopf bifurcations at $\mathbf{y}_1^{\pm}$. $\alpha = T(\beta)$ is a line of saddlenode bifurcations at $\mathbf{y}_1^{\pm}$. $\alpha = \alpha_h(\beta, \epsilon)$ is a line of homoclinic bifurcations at $\mathbf{y}_2^{\pm}$. Identified attractors of the system are also shown.

$\mu > \bar{\mu}$. If $d_u = 1$, the limit cycle is stable for $\delta > 1$ and is a saddle for $\delta < 1$ [4], [32].

4.5.2 Homoclinic bifurcation of $\dot{\mathbf{y}} = \mathbf{X}(\mathbf{y}; \boldsymbol{\alpha})$ at $\alpha = \alpha_h(\beta, \epsilon)$

In section 3.4, it was argued on the basis of the existence of the slow manifold that for small ϵ, the only possible attractors of the burster system are limit cycles and fixed points. For (β, α) lying between $\alpha = \alpha_H(\beta)$ in $\beta \leq \beta_1$ and the line $\alpha = \Lambda_+\beta$ in $\beta \geq \beta_1$, the burster system has no stable fixed points (cf. figure (4-11)). This suggests that $\mathcal{C}_+$ and $\mathcal{C}_-$ will exist in this range, where they are the attractors. Incorporating this observation leads to figure (4-19) which shows the bifurcations and attractors of the burster system identified thus far. It was also argued in section 3.4 that for a given β, if α is sufficiently small, the origin is the unique attractor. This implies that for a fixed $\beta > \beta_2$ and ϵ small, $\mathcal{C}_\pm$ is destroyed in a bifurcation as α is decreased (cf. figure (4-19)). The bifurcation that destroys $\mathcal{C}_\pm$ must be the homoclinic bifurcation at $\mathbf{y}_2^{\pm}$ for $\beta - \beta_2 > 0$ small. Hence, since $\mathcal{C}_\pm$ was argued to be confined to $N_\pm$ for ϵ small at the end of section 4.3, it seems reasonable to suggest that the bifurcation will continue to be a homoclinic bifurcation at $\mathbf{y}_2^{\pm}$ as β is increased from

β_2. This argument thus suggests that for a given small ϵ, in the (β, α) plane the curve $\alpha = \alpha_h(\beta, \epsilon)$ will extend out from (β_2, α_2) in the positive β direction between $\alpha = T(\beta)$ and $\alpha = \Lambda_+\beta$, and that the limit cycles $\mathcal{C}_+$ and $\mathcal{C}_-$ will exist for (β, α) lying between $\alpha = \alpha_H(\beta)$ and $\alpha = \alpha_h(\beta, \epsilon)$. Numerical evidence supports this hypothesis. Additionally, numerics indicate that for each ϵ small, $\alpha_h(\beta, \epsilon)$ converges quickly to $\Lambda_+\beta$ as $\beta \to \infty$. This makes the homoclinic bifurcation difficult to resolve accurately for large values of β. Additionally, $\beta_2 - \beta_1$ is very small (≈ 0.022614) which makes it hard to ascertain whether the curve $\alpha = \alpha_h(\beta, \epsilon)$ extends out into (β_1, β_2) or not. Write $\beta_H(\epsilon)$ for the minimum β value of the curve in the (β, α) plane. Then for $\beta < \beta_H(\epsilon)$, $\mathcal{C}_\pm$ is destroyed by the Hopf bifurcation as α is decreased to 0, while for $\beta > \beta_H(\epsilon)$, $\mathcal{C}_\pm$ is destroyed by the homoclinic bifurcation as α is decreased to 0.[4]

Since $\mathbf{X}(\mathbf{y}; \boldsymbol{\alpha})$ is a C^∞ function of $(\mathbf{y}, \boldsymbol{\alpha})^T$ on $\mathbb{R}^3 \backslash P \times \Pi$ and $\mathbf{y}_2^\pm, \mathcal{C}_\pm \subset N_\pm \backslash P$, the homoclinic bifurcation at $\mathbf{y}_2^\pm$ for ϵ small and $\beta > \beta_1$ is regular, and so the analysis of section 4.5.1 can be used to determine some properties of the bifurcation. Keeping with the notation of 3.6.1, let $\{\mu_{21}(\boldsymbol{\alpha}), \mu_{22}(\boldsymbol{\alpha}), \mu_{23}(\boldsymbol{\alpha})\}$ be the eigenvalues of $D_{\mathbf{y}}\mathbf{X}\left(\mathbf{y}_2^\pm(\alpha, \beta); \boldsymbol{\alpha}\right)$, and $\left\{(1,1,0)^T, \mathbf{v}_{22}^\pm(\boldsymbol{\alpha}), \mathbf{v}_{23}^\pm(\boldsymbol{\alpha})\right\}$ be the corresponding eigenvectors. Also, denote the orbit of $\dot{\mathbf{y}} = \mathbf{X}(\mathbf{y}; \alpha_h(\beta, \epsilon), \beta, \epsilon)$ homoclinic to $\mathbf{y}_2^\pm(\alpha_h(\beta, \epsilon), \beta)$ by $H_\pm(\beta, \epsilon)$. Note that by the symmetry, $H_-(\beta, \epsilon) = \sigma H_+(\beta, \epsilon)$. It was shown in section 3.6.1 that $\mu_{21}(\boldsymbol{\alpha}), \mu_{23}(\boldsymbol{\alpha}) < 0$ and $\mu_{22}(\boldsymbol{\alpha}) > 0$. The homoclinic bifurcation is therefore of the saddle type, with $d_u = 1$. As was stated in section 3.6.1, the eigenvalue spectrum of $D_{\mathbf{y}}\mathbf{X}\left(\mathbf{y}_2^\pm(\alpha, \beta); \boldsymbol{\alpha}\right)$ implies that $\mathbf{y}_2^\pm(\alpha, \beta)$ has a unique 1-dimensional C^∞ local unstable manifold $W_{2\pm}^U(\boldsymbol{\alpha})$ which is tangential to $\mathrm{Sp}\left\{\mathbf{v}_{22}^\pm(\boldsymbol{\alpha})\right\}$ at $\mathbf{y}_2^\pm(\alpha, \beta)$. $H_\pm(\beta, \epsilon)$ must therefore intersect $W_{2\pm}^U(\alpha_h(\beta, \epsilon), \beta, \epsilon)$ in the system $\dot{\mathbf{y}} = \mathbf{X}(\mathbf{y}; \alpha_h(\beta, \epsilon), \beta, \epsilon)$, and so converges to $\mathbf{y}_2^\pm(\alpha_h(\beta, \epsilon), \beta)$ tangentially to $\mathrm{Sp}\left\{\mathbf{v}_{22}^\pm(\alpha_h(\beta, \epsilon), \beta, \epsilon)\right\}$ as $\tau \to -\infty$. Additionally, if $\mu_{21}(\alpha_h(\beta, \epsilon), \beta, \epsilon) < \mu_{23}(\alpha_h(\beta, \epsilon), \beta, \epsilon)$, $H_\pm(\beta, \epsilon)$ will converge to $\mathbf{y}_2^\pm(\alpha_h(\beta, \epsilon), \beta)$ tangential to $\mathrm{Sp}\left\{\mathbf{v}_{23}^\pm(\alpha_h(\beta, \epsilon), \beta, \epsilon)\right\}$ as $\tau \to \infty$, while if $\mu_{23}(\alpha_h(\beta, \epsilon), \beta, \epsilon) < \mu_{21}(\alpha_h(\beta, \epsilon), \beta, \epsilon)$, $H_\pm(\beta, \epsilon)$ will converge to $\mathbf{y}_2^\pm(\alpha_h(\beta, \epsilon), \beta)$ tangential to $\mathrm{Sp}\left\{(1,1,0)^T\right\}$ as $\tau \to \infty$.

Figures (4-20) and (4-21) are plots of $H_+(\beta, \epsilon)$ for $\{\beta = 18.6375, \epsilon = 0.001\}$. For this choice of parameters, $\mu_{21}(\alpha_h(\beta, \epsilon), \beta, \epsilon) < \mu_{23}(\alpha_h(\beta, \epsilon), \beta, \epsilon)$. It can be seen that the convergence of $H_+(\beta, \epsilon)$ to $\mathbf{y}_2^+(\alpha_h(\beta, \epsilon), \beta)$ is tangential to $\mathrm{Sp}\left\{\mathbf{v}_{23}^+(\alpha_h(\beta, \epsilon), \beta, \epsilon)\right\}$ as $\tau \to \infty$, and is tangential to $\mathrm{Sp}\left\{\mathbf{v}_{22}^+(\alpha_h(\beta, \epsilon), \beta, \epsilon)\right\}$ as $\tau \to -\infty$.

[4] It is being assumed here that there are no other bifurcations of the system for $\beta_1 < \beta < \beta_2$ other than those predicted by the Takens-Bogadanov analysis.

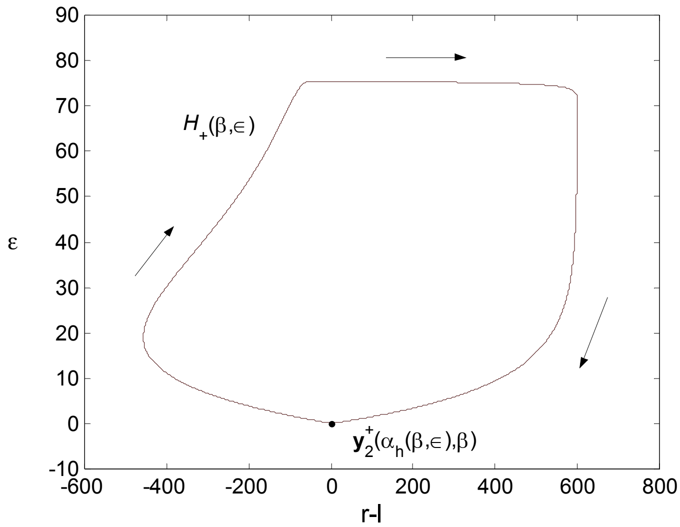

Figure 4-20: Projection onto the $(r-l,\varepsilon)$ plane of $H_+(\beta,\epsilon)$ for $\beta = 18.6375$, $\epsilon = 0.001$. Arrows indicate the direction of motion with time. $\alpha_h(\beta,\epsilon) \approx 1242.26$ for this choice of β and ϵ.

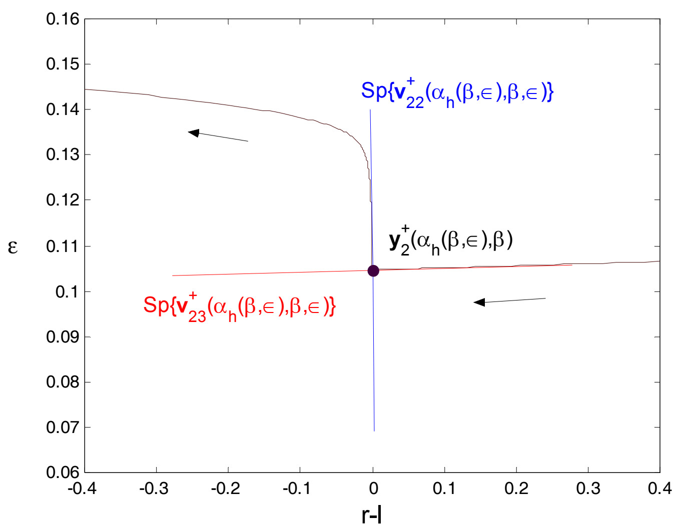

Figure 4-21: Close up of figure (4-20) about $\mathbf{y}_2^+$. The projections of $\mathrm{Sp}\left\{\mathbf{v}_{22}^+(\alpha_h(\beta,\epsilon),\beta,\epsilon)\right\}$ and $\mathrm{Sp}\left\{\mathbf{v}_{23}^+(\alpha_h(\beta,\epsilon),\beta,\epsilon)\right\}$ onto the $(r-l,\varepsilon)$ plane are also shown (coloured lines).

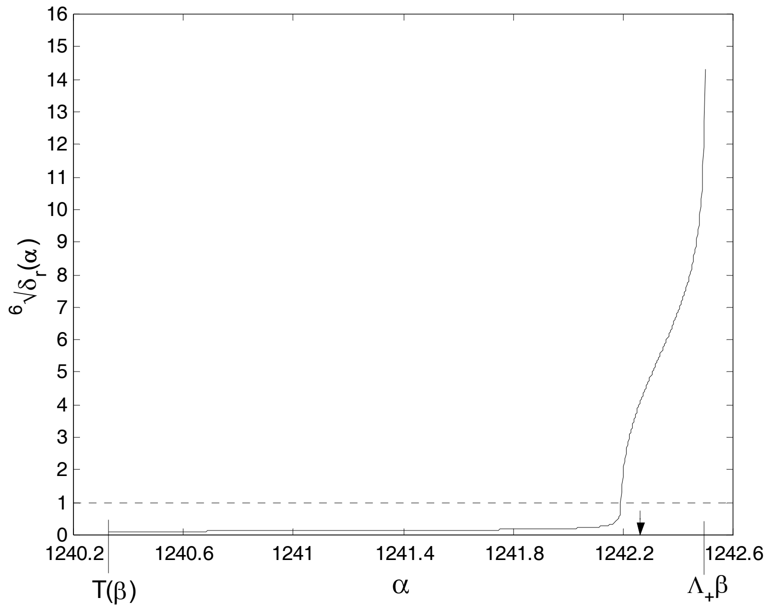

Figure 4-22: Plot of $\sqrt[6]{\delta_r(\boldsymbol{\alpha})}$ against α on the interval $(T(\beta), \Lambda_+\beta)$ for $\beta = 18.6375$, $\epsilon = 0.001$. The dotted line indicates $\delta_r(\boldsymbol{\alpha}) = 1$. The arrow indicates the numerical approximation to $\alpha_h(\beta, \epsilon)$. [The quantity $\sqrt[6]{\delta_r(\boldsymbol{\alpha})}$ is plotted instead of $\delta_r(\boldsymbol{\alpha})$ so that the point at which $\delta_r(\boldsymbol{\alpha})$ increases through 1 can be seen].

Since the homoclinic bifurcation involves the destruction of the stable limit cycle $\mathcal{C}_\pm$, the saddle index $\delta(\beta, \epsilon)$ must be greater than 1. Given a fixed ϵ small and $\beta > \beta_H(\epsilon)$, this restriction enables a range of existence of $\alpha_h(\beta, \epsilon)$ to be constructed, thereby reducing the amount of numerical work necessary to approximate $\alpha_h(\beta, \epsilon)$. More explicitly, for each $T(\beta) < \alpha < \Lambda_+\beta$, define the quantity $\delta_r(\boldsymbol{\alpha})$ as below:

$$\delta_r(\boldsymbol{\alpha}) = \begin{cases} -\frac{\mu_{23}(\boldsymbol{\alpha})}{\mu_{22}(\boldsymbol{\alpha})} & \text{if} \quad \mu_{21}(\boldsymbol{\alpha}) < \mu_{23}(\boldsymbol{\alpha}) \\ -\frac{\mu_{21}(\boldsymbol{\alpha})}{\mu_{22}(\boldsymbol{\alpha})} & \text{if} \quad \mu_{23}(\boldsymbol{\alpha}) < \mu_{21}(\boldsymbol{\alpha}) \end{cases} \tag{4.46}$$

Then $\alpha_h(\beta, \epsilon)$ must lie in a subinterval of $(T(\beta), \Lambda_+\beta)$ where $\delta_r(\boldsymbol{\alpha})$ is greater than 1. The union of these subintervals gives the possible range of existence of $\alpha_h(\beta, \epsilon)$. Figure (4-22) is a plot of $\sqrt[6]{\delta_r(\boldsymbol{\alpha})}$ against α on the interval $(T(\beta), \Lambda_+\beta)$ for the choice of β and ϵ used to generate figures (4-20) and (4-21). $\alpha_h(\beta, \epsilon)$ is seen to lie in a small subinterval of $(T(\beta), \Lambda_+\beta)$ close to $\Lambda_+\beta$ on which $\delta_r(\boldsymbol{\alpha}) > 1$.

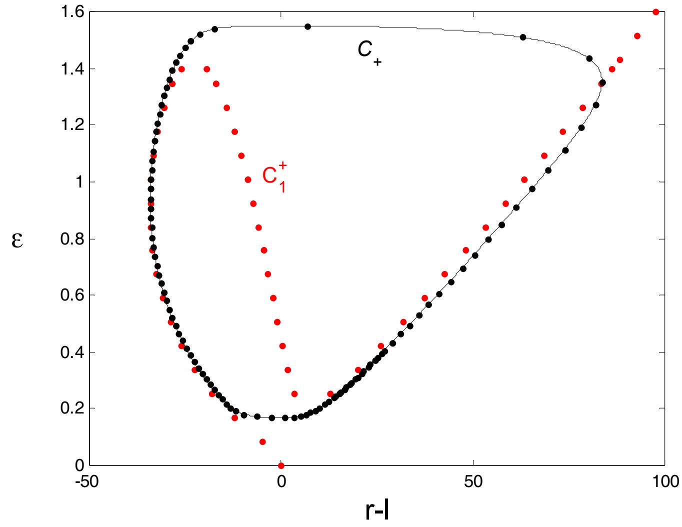

Figure 4-23: Projections of $\mathcal{C}_+$ and S_M onto the $(r-l,\varepsilon)$ plane for $\alpha = 100$, $\beta = 1$, $\epsilon = 0.001$. $\mathcal{C}_+$ is in black, with the dots representing points spaced equally in time. S_M is in red.

4.6 Relaxation oscillations and canards

Given $\boldsymbol{\alpha} \in \Pi$ with (β, α) lying between $\alpha = \alpha_H(\beta)$ and $\alpha_h(\beta, \epsilon)$, define $\rho_\varepsilon(\boldsymbol{\alpha})$ by:

$$\rho_\varepsilon(\boldsymbol{\alpha}) = \max_{\mathbf{y}\in\mathcal{C}_+(\boldsymbol{\alpha})}\{\varepsilon\} - \min_{\mathbf{y}\in\mathcal{C}_+(\boldsymbol{\alpha})}\{\varepsilon\} \tag{4.47}$$

$\rho_\varepsilon(\boldsymbol{\alpha})$ can be taken as a measure of the amplitude of $\mathcal{C}_\pm(\boldsymbol{\alpha})$. Numerical results indicate that for small ϵ, $\rho_\varepsilon(\boldsymbol{\alpha})$ is a monotonically increasing function of α for fixed $\{\beta, \epsilon\}$. Assume ϵ is small. Then the existence of the slow manifold, S_M, suggests the possibility that for sufficiently large $\rho_\varepsilon(\boldsymbol{\alpha})$, $\mathcal{C}_\pm$ can consist of parts lying on S_M (on which the dynamics is slow motion along S_M) together with parts parallel to the (r,l) plane which connect different regions of S_M (on which the dynamics is rapid motion in one direction). Figure (4-23) is a plot of the projection of $\mathcal{C}_+$ and the slow manifold S_M onto the $(r-l,\varepsilon)$ plane for $\{\alpha = 100, \beta = 1, \epsilon = 0.001\}$, while figure (4-24) is a plot of a corresponding burster time series, $\{b(\tau) = r(\tau) - l(\tau) : \tau \geq 0\}$. Figures (4-25) and (4-26) are similar plots for $\{\alpha = 2000, \beta = 27, \epsilon = 0.002\}$. The figures show that for both parameter choices, $\rho_\varepsilon(\boldsymbol{\alpha})$ is sufficiently large for $\mathcal{C}_+$ to have the anticipated form. The rapid contractions onto S_M are manifested as large jumps in the corresponding burster time series, as can be observed in figures (4-24) and (4-26). The existence of the slow manifold thus means that for ϵ sufficiently small and α sufficiently large, $\dot{\mathbf{y}} = \mathbf{X}(\mathbf{y};\boldsymbol{\alpha})$ is a relaxation oscillator [4]. In

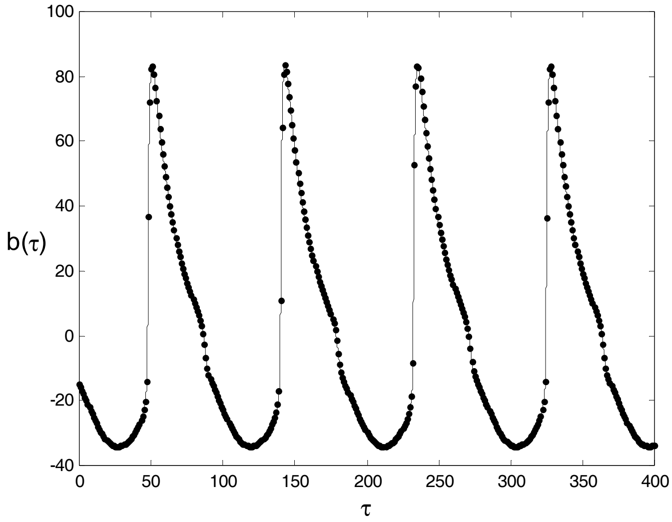

Figure 4-24: Plot of a burster time series $\{b(\tau) : \tau \geq 0\}$ associated with $\mathcal{C}_+$ for $\alpha = 100$, $\beta = 1$, $\epsilon = 0.001$. Dots indicate points spaced equally in time.

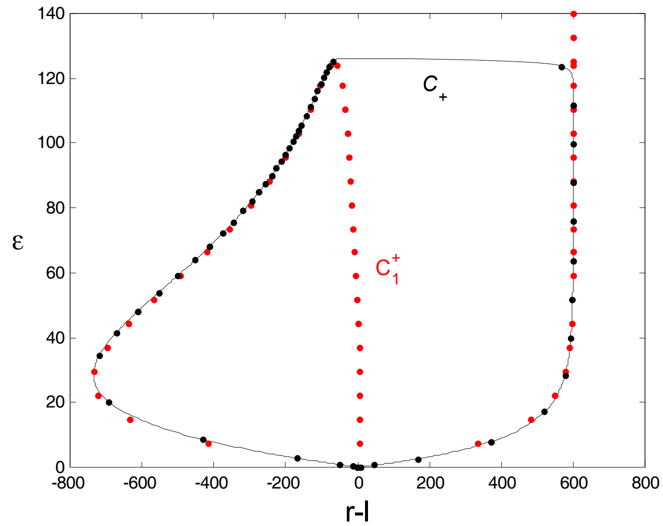

Figure 4-25: Projections of $\mathcal{C}_+$ and S_M onto the $(r - l, \varepsilon)$ plane for $\alpha = 2000$, $\beta = 27$, $\epsilon = 0.002$. $\mathcal{C}_+$ is in black, with the dots representing points spaced equally in time. S_M is in red.

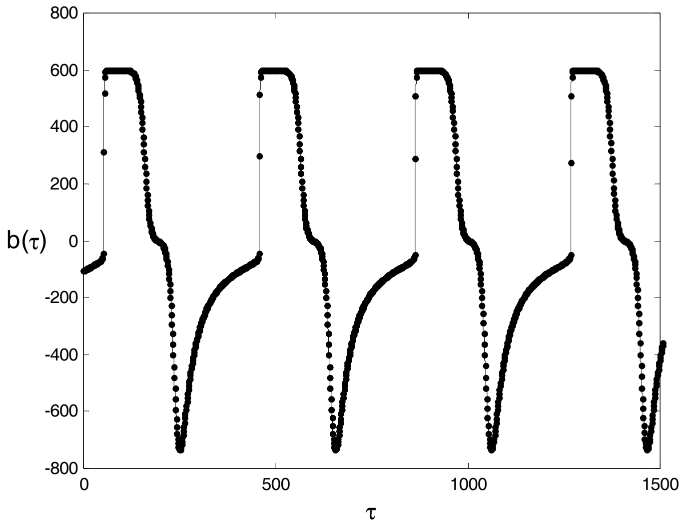

Figure 4-26: Plot of a burster time series $\{b(\tau) : \tau \geq 0\}$ associated with $\mathcal{C}_+$ for $\alpha = 2000$, $\beta = 27$, $\epsilon = 0.002$. Dots indicate points spaced equally in time.

such parameter ranges, the limit cycle $\mathcal{C}_\pm(\boldsymbol{\alpha})$ is a relaxation oscillation with 2 time scales: a 'fast' time scale corresponding to rapid contraction onto $S_M(\alpha, \beta)$ and a 'slow' time scale corresponding to motion along $S_M(\alpha, \beta)$.

Numerical work indicates that given ϵ small, for $\beta > \beta_2$, $\mathcal{C}_\pm$ is always a relaxation oscillation, while for small β, $\rho_\varepsilon(\boldsymbol{\alpha})$ increases steadily with α, generating a steady transition to a relaxation oscillation. This steady transition can be seen in figures (4-27) and (4-28). Figure (4-27) shows a plot of $\rho_\varepsilon(\boldsymbol{\alpha})$ against $\alpha - \alpha_H(\beta)$ for $\{\beta = 0.15, \epsilon = 0.001\}$. In figure (4-28), a plot of a numerical estimate $\hat{D}_\alpha \rho_\varepsilon(\boldsymbol{\alpha})$ of $D_\alpha \rho_\varepsilon(\boldsymbol{\alpha})$ against $\alpha - \alpha_H(\beta)$ is shown for the same choice of β and ϵ.[5] The steady increase in $\rho_\varepsilon(\boldsymbol{\alpha})$ with α is characterised by the monotonicity of the derivative $D_\alpha \rho_\varepsilon(\boldsymbol{\alpha})$.

The transition to a relaxation oscillation for intermediate values of β is more interesting. Figures (4-29) and (4-30) are plots of $\rho_\varepsilon(\boldsymbol{\alpha})$ and $\hat{D}_\alpha \rho_\varepsilon(\boldsymbol{\alpha})$ against $\alpha - \alpha_H(\beta)$ for $\{\beta = 0.75, \epsilon = 0.001\}$. For this choice of parameters, $\rho_\varepsilon(\boldsymbol{\alpha})$ increases steadily with α until

[5] Given the set of points

$$\{\rho_\varepsilon(\alpha_1, \beta, \epsilon), \rho_\varepsilon(\alpha_1 + h, \beta, \epsilon), \ldots, \rho_\varepsilon(\alpha_1 + Nh, \beta, \epsilon)\}$$

the numerical estimate $\hat{D}_\alpha \rho_\varepsilon(\alpha_1 + kh, \beta, \epsilon)$ to $D_\alpha \rho_\varepsilon(\alpha_1 + kh, \beta, \epsilon)$ is defined by

$$\hat{D}_\alpha \rho_\varepsilon(\alpha_1 + kh, \beta, \epsilon) = \frac{\rho_\varepsilon(\alpha_1 + (k+1)h, \beta, \epsilon) - \rho_\varepsilon(\alpha_1 + kh, \beta, \epsilon)}{h}$$

for all $0 \leq k \leq N - 1$.

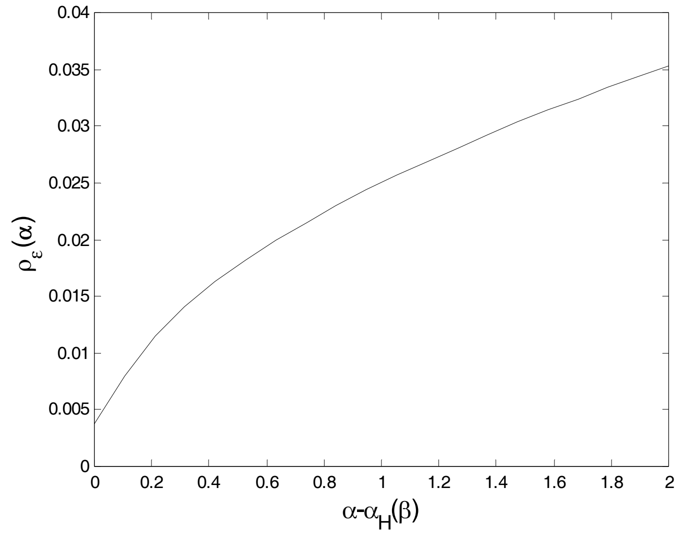

Figure 4-27: Plot of $\rho_{\varepsilon}\left(\boldsymbol{\alpha}\right)$ against $\alpha - \alpha_H\left(\beta\right)$ for $\beta = 0.15$, $\epsilon = 0.001$.

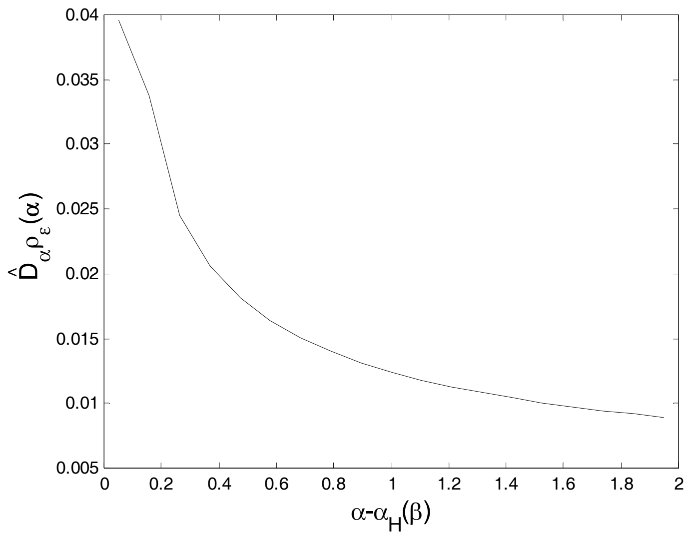

Figure 4-28: Plot of a numerical estimate $\hat{D}_{\alpha}\rho_{\varepsilon}\left(\boldsymbol{\alpha}\right)$ of the derivative $D_{\alpha}\rho_{\varepsilon}\left(\boldsymbol{\alpha}\right)$ against $\alpha - \alpha_H\left(\beta\right)$ for $\beta = 0.15$, $\epsilon = 0.001$.

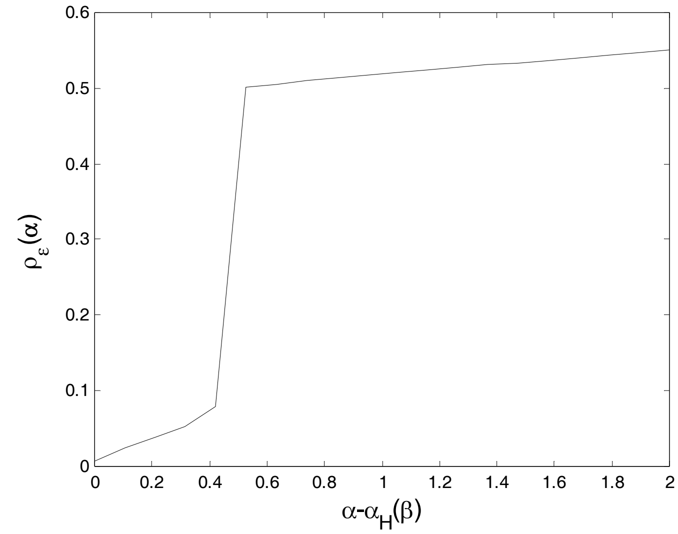

Figure 4-29: Plot of $\rho_\varepsilon(\boldsymbol{\alpha})$ against $\alpha - \alpha_H(\beta)$ for $\beta = 0.75$, $\epsilon = 0.001$.

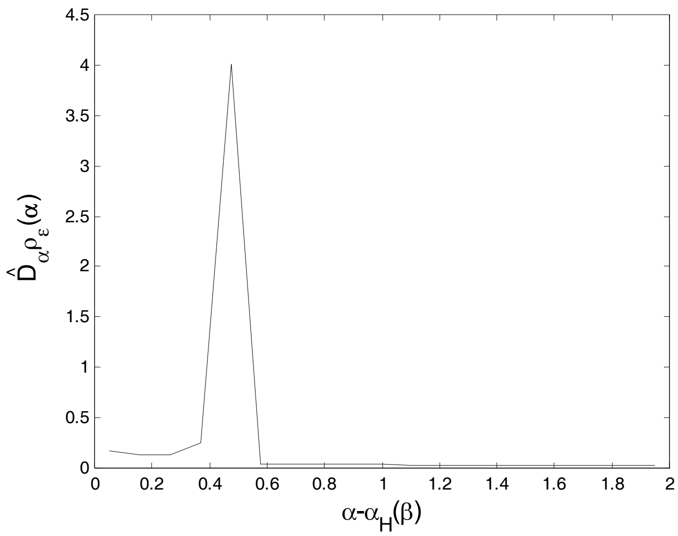

Figure 4-30: Plot of a numerical estimate $\hat{D}_\alpha \rho_\varepsilon(\boldsymbol{\alpha})$ of the derivative $D_\alpha \rho_\varepsilon(\boldsymbol{\alpha})$ against $\alpha - \alpha_H(\beta)$ for $\beta = 0.75$, $\epsilon = 0.001$.

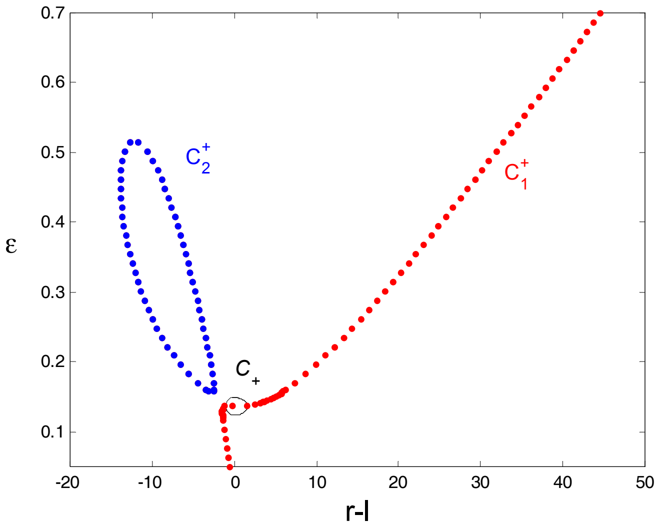

Figure 4-31: Projection of $\mathcal{C}_+$ (black) and S_M (coloured dots) onto the $(r-l, \varepsilon)$ plane for $\alpha = 59.5328$, $\beta = 0.75$, $\epsilon = 0.001$.

at a critical value $\alpha_C(\beta, \epsilon)$ of α, $\rho_\varepsilon(\boldsymbol{\alpha})$ suddenly jumps to a larger value. The sudden increase in $\rho_\varepsilon(\boldsymbol{\alpha})$ at $\alpha_C(\beta, \epsilon)$ can be seen to correspond to a local maximum of $D_\alpha \rho_\varepsilon(\boldsymbol{\alpha})$. For $\alpha > \alpha_C(\beta, \epsilon)$, the rate of increase of $\rho_\varepsilon(\boldsymbol{\alpha})$ is comparable to the rate of increase for $\alpha < \alpha_C(\beta, \epsilon)$. The sudden jump in the increase of the amplitude of $\mathcal{C}_\pm$ is referred to as a canard. Canards are associated with relaxation oscillators in which limit cycles can interact with the slow manifold as a parameter of the system is varied [4], [30]. For the purposes of this discussion, canards will be identified with local maxima of $D_\alpha \rho_\varepsilon(\boldsymbol{\alpha})$.

In the burster system, the canard can be understood by observing the evolution of the slow manifold S_M as α increases through the critical value. Figures (4-31)-(4-33) show how both $\mathcal{C}_+$ and S_M vary as α increases through $\alpha_C(\beta, \epsilon)$ for $\{\beta = 0.75, \epsilon = 0.001\}$. Figure (4-31) is a plot of $\mathcal{C}_+$ and S_M for $\alpha = 59.5328$. This corresponds to $\alpha - \alpha_H(\beta) \approx 0.105$, just after the Hopf bifurcation. It can be seen that $S_M \cap N_+$ comprises C_1^+, together with a closed curve C_2^+. For this value of α, $\mathcal{C}_+$ is confined entirely to C_1^+. Figure (4-32) is a plot of $\mathcal{C}_+$ and S_M for $\alpha = 59.8486$. This corresponds to $\alpha - \alpha_H(\beta) \approx 0.42$, just before the critical value. $S_M \cap N_+$ now consists solely of C_1^+, where C_1^+ has a double loop for intermediate values of $\varepsilon \geq 0$, and is asymmetric about the plane $r = l$. The change in the shape of S_M has occurred through the curve C_2^+ intersecting C_1^+ as α is increased through some value $\bar{\alpha}_C(\beta)$. The double loop form of C_1^+ means that for $\alpha > \bar{\alpha}_C(\beta)$, C_1^+ can be subdivided into 2 portions $\left(C_1^+\right)_L$ and $\left(C_1^+\right)_R$, on the basis of the projections of the loops

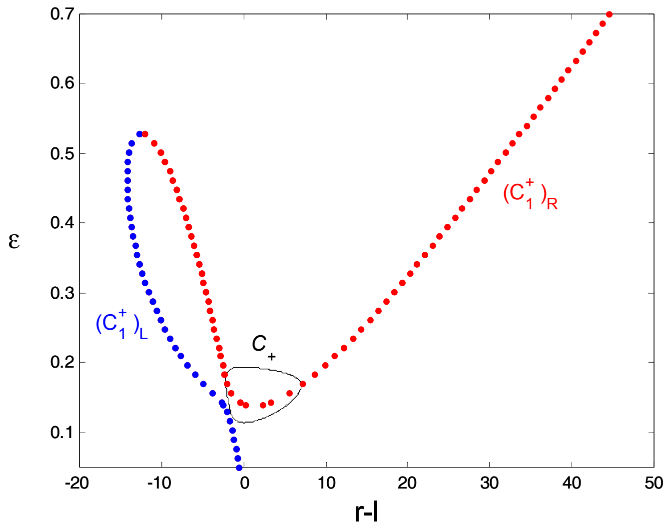

Figure 4-32: Projection of $\mathcal{C}_+$ (black) and S_M (coloured dots) onto the $(r-l, \varepsilon)$ plane for $\alpha = 59.8486$, $\beta = 0.75$, $\epsilon = 0.001$.

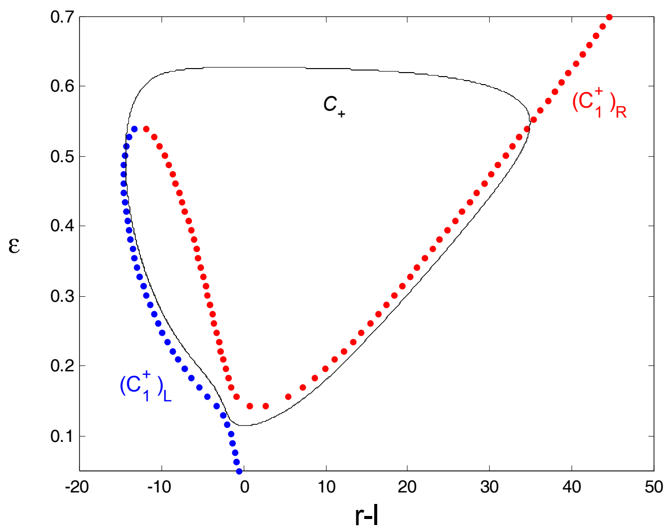

Figure 4-33: Projection of $\mathcal{C}_+$ (black) and S_M (coloured dots) onto the $(r-l, \varepsilon)$ plane for $\alpha = 59.9539$, $\beta = 0.75$, $\epsilon = 0.001$.

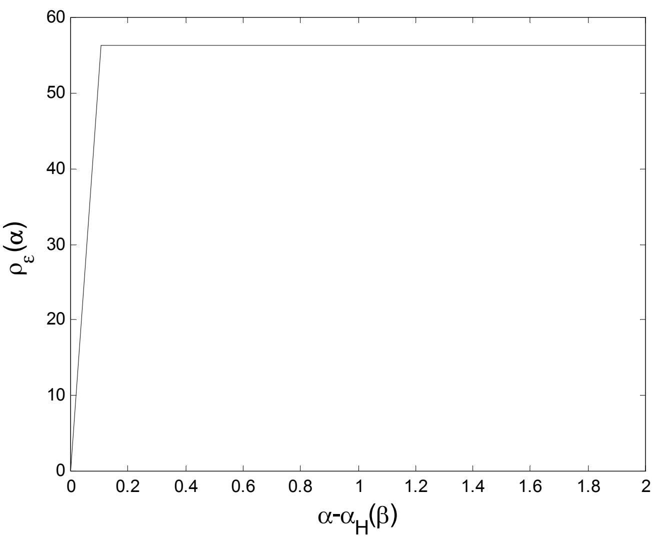

Figure 4-34: Plot of $\rho_\varepsilon(\boldsymbol{\alpha})$ against $\alpha - \alpha_H(\beta)$ for $\beta = 15$, $\epsilon = 0.002$.

onto the $(r-l, \varepsilon)$ plane. $\left(C_1^+\right)_L$ is defined to be the part of C_1^+ connecting the origin to the maximum of the leftmost loop, and $\left(C_1^+\right)_R$ is defined as $C_1^+ \setminus \left(C_1^+\right)_L$. For the value of α corresponding to figure (4-32), only the region of $\left(C_1^+\right)_L$ closest to $\left(C_1^+\right)_R$ is attracting, thereby limiting the extent of $\mathcal{C}_+$ in the ε direction. Figure (4-33) is a plot of $\mathcal{C}_+$ and S_M for $\alpha = 59.9539$. This corresponds to $\alpha - \alpha_H(\beta) \approx 0.52$, just after the critical value. It can be seen from the figure that all of $\left(C_1^+\right)_L$ has now become attracting, resulting in a sudden jump in the extent of $\mathcal{C}_+$ in the ε direction.

Numerical results indicate that for all values of β lying between β_2 and some cut-off value $\beta_C \approx 0.615$, $S_M \cap N_+$ comprises the two curves C_1^+ and C_2^+ for $\alpha - \alpha_H(\beta) > 0$ sufficiently small. Moreover, there is some value $\bar{\alpha}_C(\beta) > \alpha_H(\beta)$ at which C_1^+ and C_2^+ coalesce to form the asymmetric double loop form of C_1^+. Additionally, given $\beta_C < \beta < \beta_2$, for each small ϵ there is a value $\alpha_C(\beta, \epsilon) > \bar{\alpha}_C(\beta)$ of α such that $\alpha_C(\beta, \epsilon)$ is a local maximum of $D_\alpha \rho_\varepsilon(\boldsymbol{\alpha})$, corresponding to a sudden jump in $\rho_\varepsilon(\boldsymbol{\alpha})$. This jump appears to be attributable to $\left(C_1^+\right)_L$ becoming attracting, as in the example above. Figures (4-34)-(4-36) are plots showing the canard for $\{\beta = 15, \epsilon = 0.002\}$.

For $\beta_C < \beta < \beta_2$ and ϵ small, as α is increased from $\alpha_H(\beta)$, $\mathcal{C}_\pm$ thus becomes a relaxation oscillation through a canard at $\alpha = \alpha_C(\beta, \epsilon)$. Numerics suggest that for a fixed $\beta_C < \beta < \beta_2$, $\alpha_C(\beta, \epsilon)$ is an increasing function of ϵ with $\alpha_C(\beta, \epsilon) \to \bar{\alpha}_C(\beta)$ as $\epsilon \to 0$. Additionally, numerics indicate that $\bar{\alpha}_C(\beta) - \alpha_H(\beta)$ is a decreasing function of β on (β_C, β_2) with

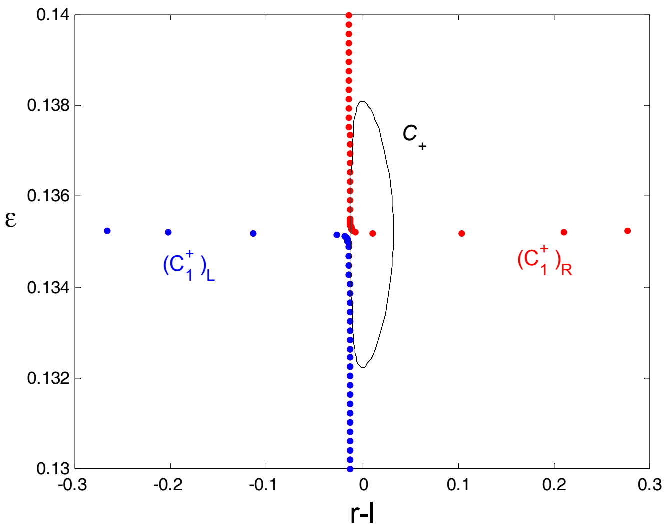

Figure 4-35: Projection of $\mathcal{C}_+$ (black) and S_M (coloured dots) onto the $(r-l, \varepsilon)$ plane for $\alpha = 1001.51$, $\beta = 15$, $\epsilon = 0.002$. This choice of parameters corresponds to α just before the critical value $\alpha_C(\beta, \epsilon)$.

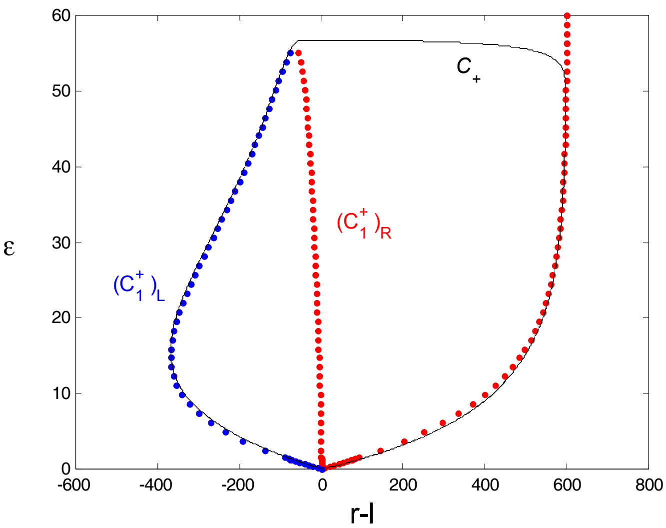

Figure 4-36: Projection of $\mathcal{C}_+$ (black) and S_M (coloured dots) onto the $(r-l, \varepsilon)$ plane for $\alpha = 1001.62$, $\beta = 15$, $\epsilon = 0.002$. This choice of parameters corresponds to α just after the critical value $\alpha_C(\beta, \epsilon)$.

$\bar{\alpha}_C(\beta) - \alpha_H(\beta) \to 0$ as $\beta \to \beta_2$. Also, for each fixed value of ϵ, $\alpha_C(\beta,\epsilon) - \alpha_H(\beta)$ is a decreasing function of β on (β_C, β_2) with $\alpha_C(\beta,\epsilon) - \alpha_H(\beta) \to 0$ as $\beta \to \beta_2$. In terms of curves in the (β,α) plane, $\alpha = \bar{\alpha}_C(\beta)$ and $\alpha = \alpha_C(\beta,\epsilon)$ intersect at the codimension 2 point, and $\alpha = \alpha_C(\beta,\epsilon)$ converges to $\alpha = \bar{\alpha}_C(\beta)$ from above as $\epsilon \to 0$.

4.6.1 Error time series associated with relaxation oscillations for $\beta_C < \beta < \beta_2$, $\alpha_C(\beta,\epsilon) < \alpha < 2.5\alpha'$ and ϵ small

Given $\beta_C < \beta < \beta_2$, for $\bar{\alpha}_C(\beta) < \alpha < 2.5\alpha'$, the slow manifold curves $C_1^+(\alpha,\beta)$ and $C_1^-(\alpha,\beta)$ appear to have the asymmetric double-loop form of figure (4-23), where in the $(r-l,\varepsilon)$ plane, C_1^+ has greater extension in the positive $r-l$ direction than in the negative $r-l$ direction, and by symmetry, C_1^- has greater extension in the negative $r-l$ direction than in the positive $r-l$ direction. This configuration of C_1^+ and C_1^- has an important effect on the error time series $\{\varepsilon(\tau) : \tau \geq 0\}$ corresponding to the post-canard limit cycles which are observed for α and β in this range with ϵ small. Since $\dot{\varepsilon} = -\epsilon(r-l)$, the contraction of $\mathcal{C}_+$ onto C_1^+ parallel to the (r,l) plane results in $\dot{\varepsilon}$ changing rapidly from small and positive to large and negative. By symmetry, the contraction of $\mathcal{C}_-$ onto C_1^- parallel to the (r,l) plane results in $\dot{\varepsilon}$ changing rapidly from small and negative to large and positive. This means that the error time series associated with $\mathcal{C}_+$ and $\mathcal{C}_-$ for such parameter choices in the range of interest consist of a slow drift away from $\varepsilon = 0$ followed by a sudden switch to a faster return towards $\varepsilon = 0$. Figures (4-37) and (4-38) show two such error time series associated with $\mathcal{C}_+$ while figure (4-39) shows a time series of this form associated with $\mathcal{C}_-$. The error time series are seen to have a 'slow-fast' form which resembles jerk nystagmus (cf. section 1.1.3).

4.7 Bifurcations and attractors for small ϵ

The results of this chapter and the previous chapter suggest the bifurcation diagram of the burster system for small ϵ given in figure (4-40). Also shown in this figure are the attractors of the system. It can be seen from the figure that the dynamics of $\dot{\mathbf{y}} = \mathbf{X}(\mathbf{y};\boldsymbol{\alpha})$ for small ϵ are organised by the codimension 2 points $(2\beta', 2\alpha')$ and (β_2, α_2). The point (β_1, α_1) is not a codimension 2 point, as may be inferred from the diagram. At (β_1, α_1), three separate bifurcations occur simultaneously: a nonsmooth subcritical pitchfork bifurcation occurs at

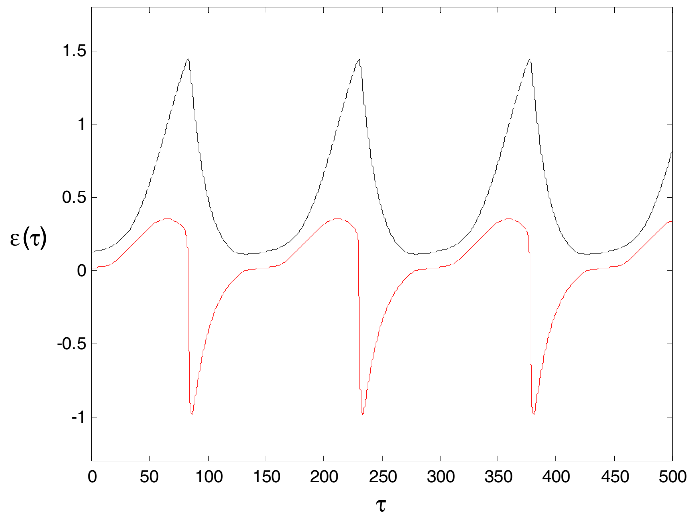

Figure 4-37: Plot of an error time series $\{\varepsilon(\tau) : \tau \geq 0\}$ associated with $\mathcal{C}_+$ for $\alpha = 90$, $\beta = 1.2$, $\epsilon = 0.001$ (black). The corresponding velocity time series $\{\dot{\varepsilon}(\tau) : \tau \geq 0\}$ is also shown (red). $\dot{\varepsilon}(\tau)$ has been rescaled to enable it to be compared with $\varepsilon(\tau)$ on the same plot.

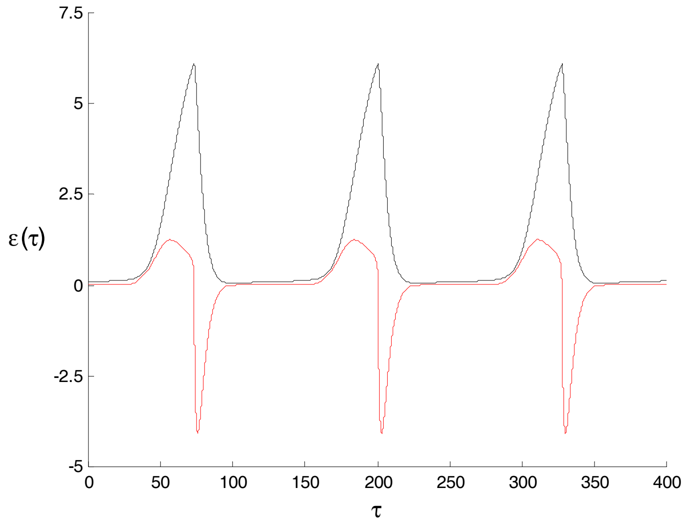

Figure 4-38: Plot of an error time series $\{\varepsilon(\tau) : \tau \geq 0\}$ associated with $\mathcal{C}_+$ for $\alpha = 210$, $\beta = 3$, $\epsilon = 0.003$ (black). The corresponding velocity time series $\{\dot{\varepsilon}(\tau) : \tau \geq 0\}$ is also shown (red). $\dot{\varepsilon}(\tau)$ has been rescaled to enable it to be compared with $\{\varepsilon(\tau)\}$ on the same plot.

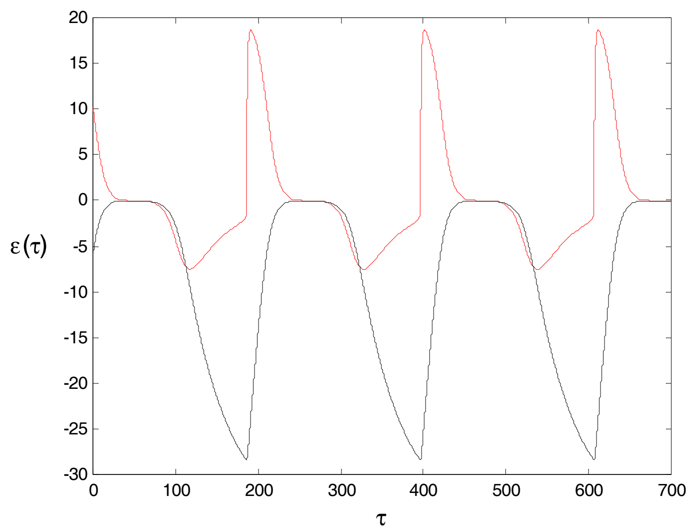

Figure 4-39: Plot of an error time series $\{\varepsilon(\tau) : \tau \geq 0\}$ associated with $\mathcal{C}_-$ for $\alpha = 620$, $\beta = 9$, $\epsilon = 0.002$ (black). The corresponding velocity time series $\{\dot{\varepsilon}(\tau) : \tau \geq 0\}$ is also shown (red). $\dot{\varepsilon}(\tau)$ has been rescaled to enable it to be compared with $\varepsilon(\tau)$ on the same plot.

the origin together with a pair of symmetry related supercritical Hopfs at $\mathbf{y}_1^{\pm}$. It should be noted that since $\mathbf{X}(\mathbf{y};\boldsymbol{\alpha}) = \mathbf{X}_{\pm}(\mathbf{y};\boldsymbol{\alpha})\ \forall\mathbf{y} \in N_{\pm}$, the saddlenode and Hopf bifurcations at $\mathbf{y}_1^{\pm}$, and the homoclinic bifurcation at $\mathbf{y}_2^{\pm}$ can be thought of as occurring in the smooth system $\dot{\mathbf{y}} = \mathbf{X}_{\pm}(\mathbf{y};\boldsymbol{\alpha})$. The nonsmooth pitchfork bifurcation at $\alpha = \Lambda_+\beta$, however, is specific to the piecewise smooth system $\dot{\mathbf{y}} = \mathbf{X}(\mathbf{y};\boldsymbol{\alpha})$.

Figures (4-42)-(4-44) are schematic bifurcation diagrams showing how the ω-limit sets of the burster system evolve as the parameter $\boldsymbol{\alpha}$ describes three representative closed curves in the (β, α) plane for a fixed small ϵ, shown in figure (4-41). In the bifurcation diagrams, for each choice of $\boldsymbol{\alpha}$, the corresponding values on the vertical axis are the minimum and maximum ε values of the ω-limit sets which exist for that $\boldsymbol{\alpha}$. Attractors are indicated by solid lines and nonattractors by dotted lines. The saddlenode bifurcation in $\beta < \beta_2$ is labelled 'a', the homoclinic bifurcation is labelled 'b', 'c' labels the Hopf, 'd' labels the saddlenode bifurcation in $\beta > \beta_2$, 'e' labels the nonsmooth subcritical pitchfork bifurcation and 'f' labels the nonsmooth supercritical pitchfork bifurcation.

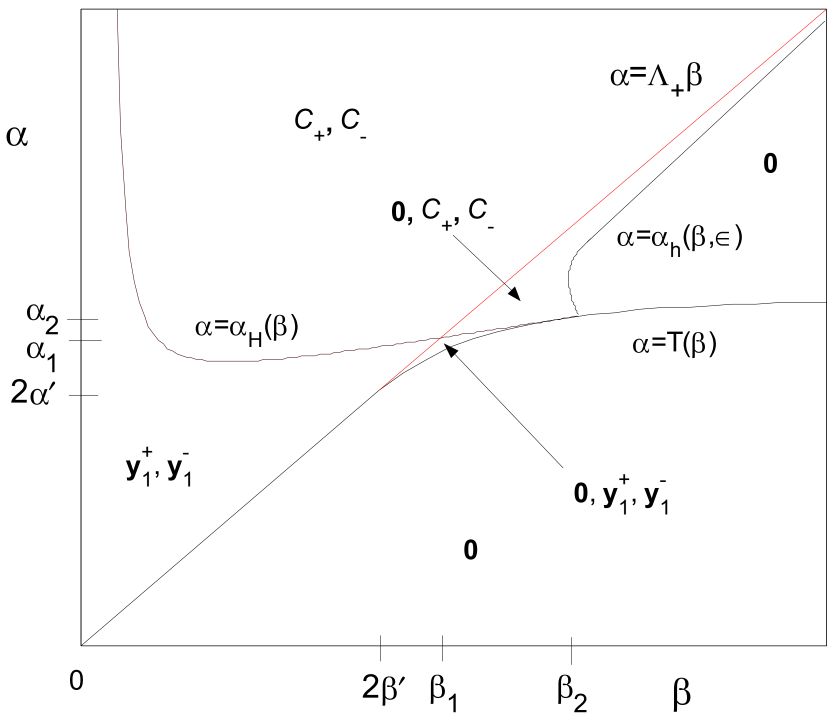

Figure 4-40: Bifurcations and attractors of the burster system for small ϵ. $\alpha = \Lambda_+\beta$ is a line of nonsmooth pitchfork bifurcations at $\mathbf{0}$. The bifurcations are supercritical for $\beta \leq 2\beta'$ (black line) and subcritical for $\beta > 2\beta'$ (red line). $\alpha = \alpha_H(\beta)$ is a line of supercritical Hopf bifurcations at $\mathbf{y}_1^{\pm}$. $\alpha = T(\beta)$ is a line of saddlenode bifurcations at $\mathbf{y}_1^{\pm}$. $\alpha = \alpha_h(\beta, \epsilon)$ is a line of homoclinic bifurcations at $\mathbf{y}_2^{\pm}$.

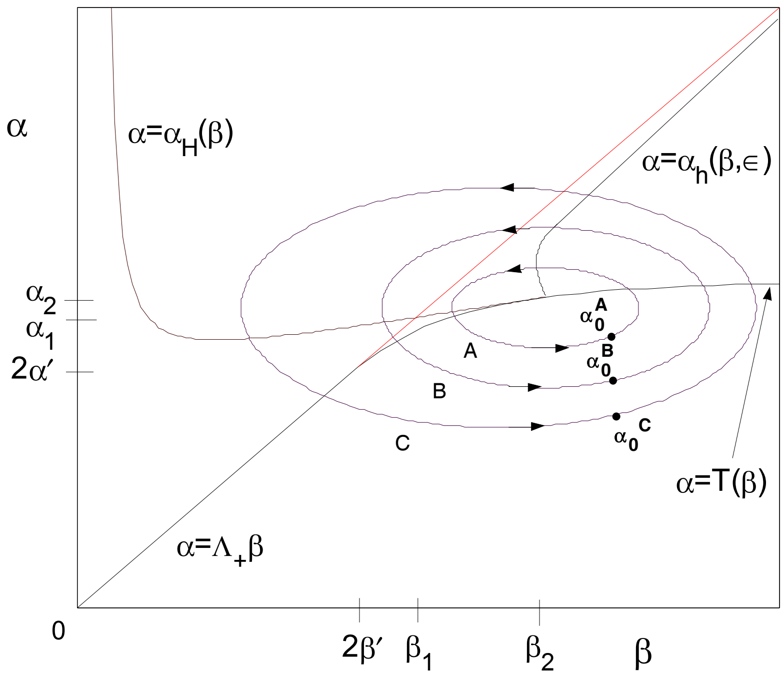

Figure 4-41: Three representative closed parameter paths in the (β, α) plane for a fixed small ϵ.

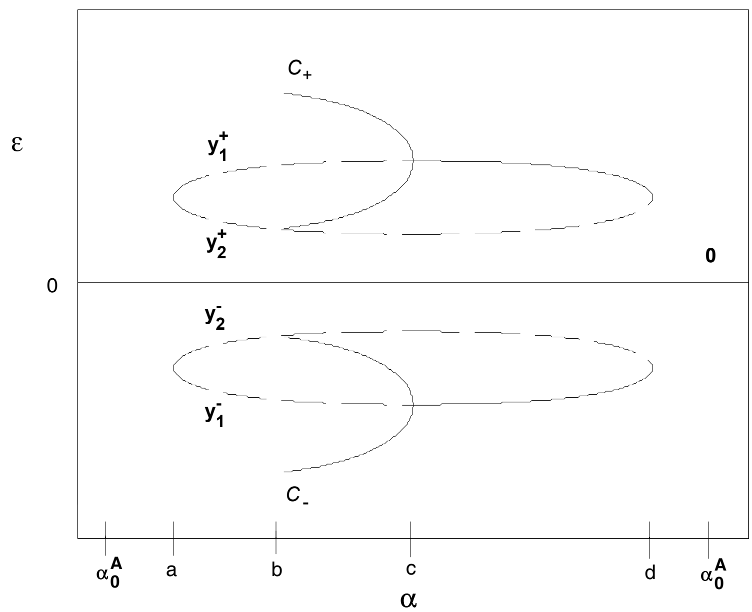

Figure 4-42: Bifurcation diagram corresponding to parameter path A in figure (4-41).

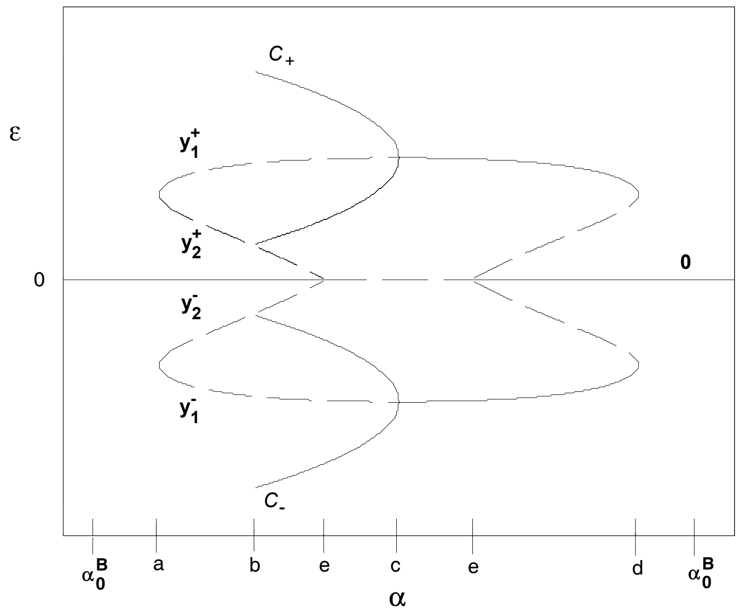

Figure 4-43: Bifurcation diagram corresponding to parameter path B in figure (4-41).

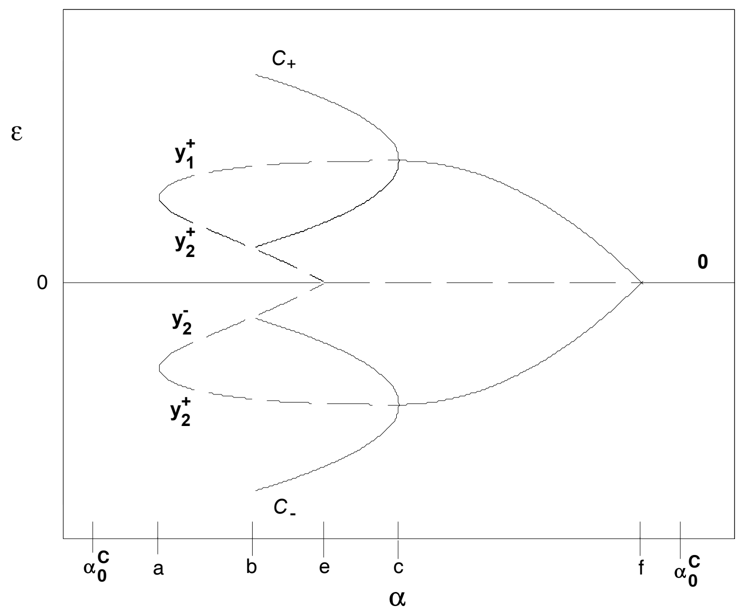

Figure 4-44: Bifurcation diagram corresponding to parameter path C in figure (4-41).

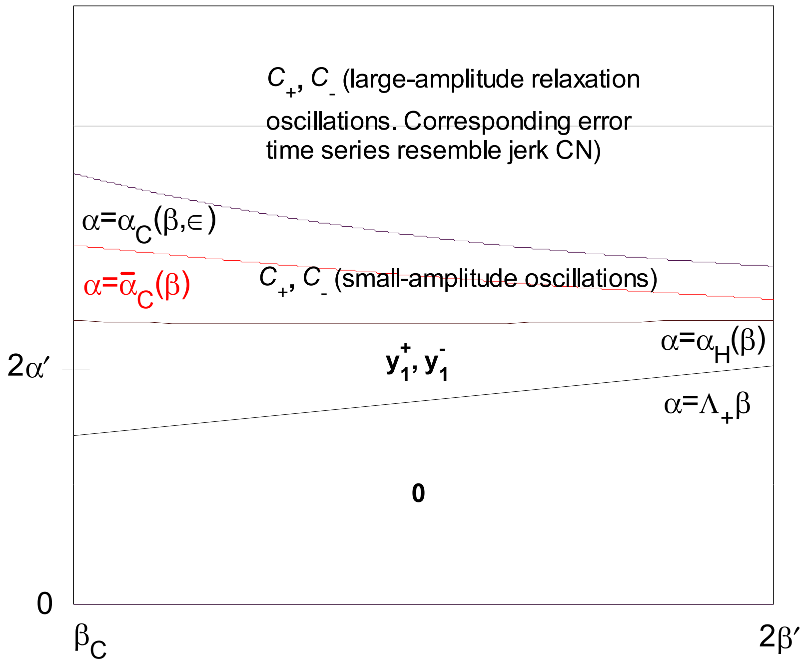

Figure 4-45: Bifurcations and attractors of the burster system for small ϵ and $\beta_C < \beta < 2\beta'$. $\alpha = \Lambda_+\beta$ is a line of supercritical pitchfork-type bifurcations. $\alpha = \alpha_H(\beta)$ is a line of supercritical Hopfs. $\alpha = \alpha_C(\beta, \epsilon)$ is a line of canards. $\alpha = \bar{\alpha}_C(\beta)$ is the limiting curve of $\alpha = \alpha_C(\beta, \epsilon)$ as $\epsilon \to 0$.

4.8 The effect of increasing ϵ from 0 to 0.05 for $\beta_C < \beta < 2\beta'$

In this section the effect on the burster dynamics of increasing ϵ from 0 to 0.05 in the reduced range $\beta_C < \beta < 2\beta'$ is discussed. The findings of this section will be used to propose a description of the bifurcations and attractors of the burster system in an $\boldsymbol{\alpha}$ range $\hat{\Pi}_P$ containing the physiological range Π_P.

Figure (4-45) is a proposed picture of the bifurcations and attractors of the burster system for ϵ small and $\beta_C < \beta < 2\beta'$, including the canard, based on the findings of this chapter thus far. Figure (4-45) was obtained by combining local analysis of the system with the global information that can be inferred from the observation that trajectories are constrained by the slow manifold for small ϵ. As ϵ is increased, trajectories are no longer constrained by the slow manifold, creating the possibility of bifurcations and attractors other than those shown in figure (4-45). In particular, the restriction that limit cycles cannot cross the plane P no longer holds. The effect of increasing ϵ for $\alpha > \alpha_H(\beta)$ is discussed first, followed by the effect of increasing ϵ for $\alpha < \alpha_H(\beta)$.

4.8.1 The effect of increasing ϵ from 0 to 0.05 in $\beta_C < \beta < 2\beta'$, $\alpha > \alpha_H(\beta)$

For small ϵ, the attractors of the system in this range are the pair of symmetry related limit cycles $\mathcal{C}_\pm(\boldsymbol{\alpha})$ (cf. figure (4-45)). An important consequence of increasing ϵ in this range is that eventually $\mathcal{C}_\pm$ stops undergoing a canard as α is increased from 0 for a fixed β. Recall from section 4.6 that given ϵ small, for each $\beta_C < \beta < 2\beta'$, $\mathcal{C}_\pm$ undergoes a canard at $\alpha_C(\beta,\epsilon) > \bar{\alpha}_C(\beta)$, characterised by a local maximum of $D_\alpha\rho_\varepsilon(\boldsymbol{\alpha})$ on $(\bar{\alpha}_C(\beta), \infty)$. The natural objects of interest in section 4.6 were the curves of canards $\alpha = \alpha_C(\beta,\epsilon)$ in the (β,α) plane. Since the idea in this section is to consider the effect of increasing ϵ, the natural object of interest is the surface of canards in (α,β,ϵ) space. This will be thought of as the graph of a function $\epsilon_C(\alpha,\beta)$.

Properties of the surface $\epsilon = \epsilon_C(\alpha,\beta)$

Given $\beta_C < \beta < 2\beta'$ and $\epsilon > 0$, define $\alpha_L(\beta,\epsilon)$ to be the maximum value of α such that $\mathcal{C}_\pm(\boldsymbol{\alpha})$ exists on $(\bar{\alpha}_C(\beta), \alpha)$. (For ϵ small, $\alpha_L(\beta,\epsilon) = \infty$). Numerics indicate that for $\beta - \beta_C > 0$ small, $D_\alpha\rho_\varepsilon(\alpha_C(\beta,\epsilon), \beta, \epsilon)$ decreases with increasing ϵ until at some critical value $\hat{\epsilon}(\beta)$ of ϵ, $D_\alpha\rho_\varepsilon(\boldsymbol{\alpha})$ no longer has a local maximum on $(\bar{\alpha}_C(\beta), \alpha_L(\beta,\epsilon))$. For $\epsilon > \hat{\epsilon}(\beta)$, no canards are observed to occur as α is increased from $\alpha = \bar{\alpha}_C(\beta)$. Figures (4-46) and (4-47) illustrate the termination of the canard through this mechanism for $\beta = 0.75$. The decrease in $D_\alpha\rho_\varepsilon(\alpha_C(\beta,\epsilon), \beta, \epsilon)$ as ϵ is increased can be clearly seen.

For β greater than some cut-off $\hat{\beta}_C \approx 0.9$, the situation is different. $D_\alpha\rho_\varepsilon(\boldsymbol{\alpha})$ does not evolve into a monotonic function on $(\bar{\alpha}_C(\beta), \alpha_L(\beta,\epsilon))$ as ϵ is increased. Instead, the canard keeps occurring until at some sufficiently large value of ϵ, a bifurcation appears in which $\mathcal{C}_\pm$ is destroyed as α is increased from $\bar{\alpha}_C(\beta)$. In addition to the destruction of $\mathcal{C}_+$ and $\mathcal{C}_-$, this bifurcation also involves the creation of a σ-invariant limit cycle. In keeping with the notation above, write $\hat{\epsilon}(\beta)$ for the critical value of ϵ at which the bifurcation begins to occur. It follows that for all $\beta_C < \beta < 2\beta'$, no canards occur for $\epsilon > \hat{\epsilon}(\beta)$. Given β with $\beta_C < \beta < 2\beta'$, write $\hat{\alpha}_C(\beta)$ for $\lim_{\epsilon\to\hat{\epsilon}(\beta)-} \alpha_C(\beta,\epsilon)$. The findings of this section can then be summarised as below:

1. For a given $\epsilon' \in \left(0, \max_{(\beta_c, 2\beta')} \hat{\epsilon}(\beta)\right)$, the curve $\alpha = \alpha_C(\beta,\epsilon')$ is the projection onto the

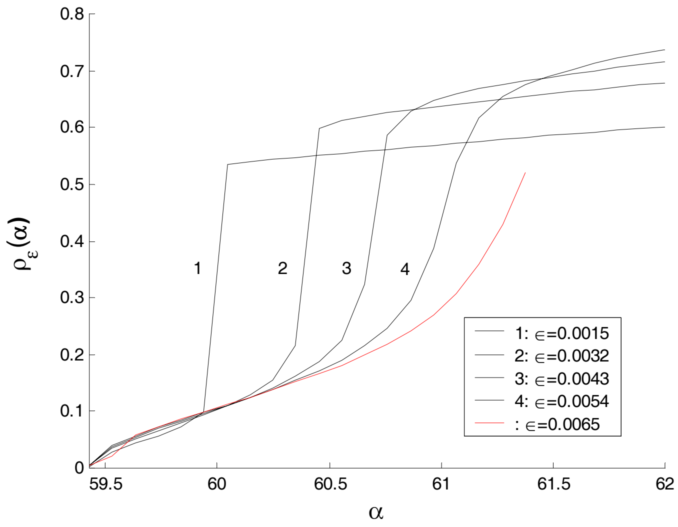

Figure 4-46: Plots of $\rho_\varepsilon(\boldsymbol{\alpha})$ against α on $(\bar{\alpha}_C(\beta), \alpha_L(\beta,\epsilon))$ when $\beta = 0.75$. The red line corresponds to a value of ϵ greater than $\hat{\epsilon}(\beta)$.

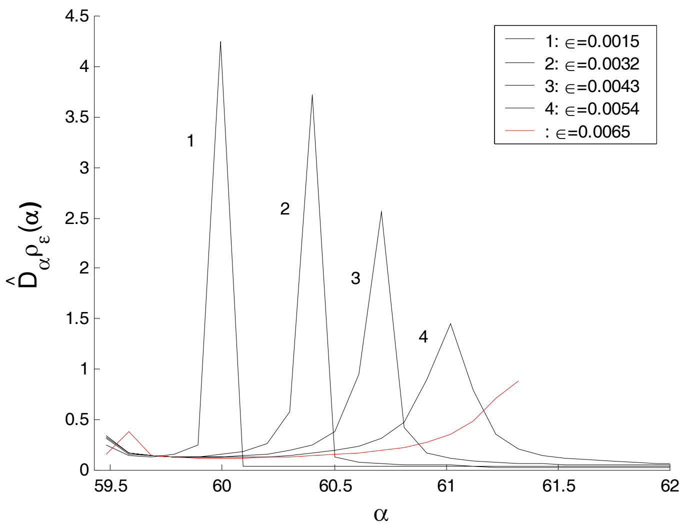

Figure 4-47: Plots of a numerical estimate $\hat{D}_\alpha\rho_\varepsilon(\boldsymbol{\alpha})$ of the derivative $D_\alpha\rho_\varepsilon(\boldsymbol{\alpha})$ against α on $(\bar{\alpha}_C(\beta), \alpha_L(\beta,\epsilon))$ when $\beta = 0.75$. The red line corresponds to a value of ϵ greater than $\hat{\epsilon}(\beta)$.

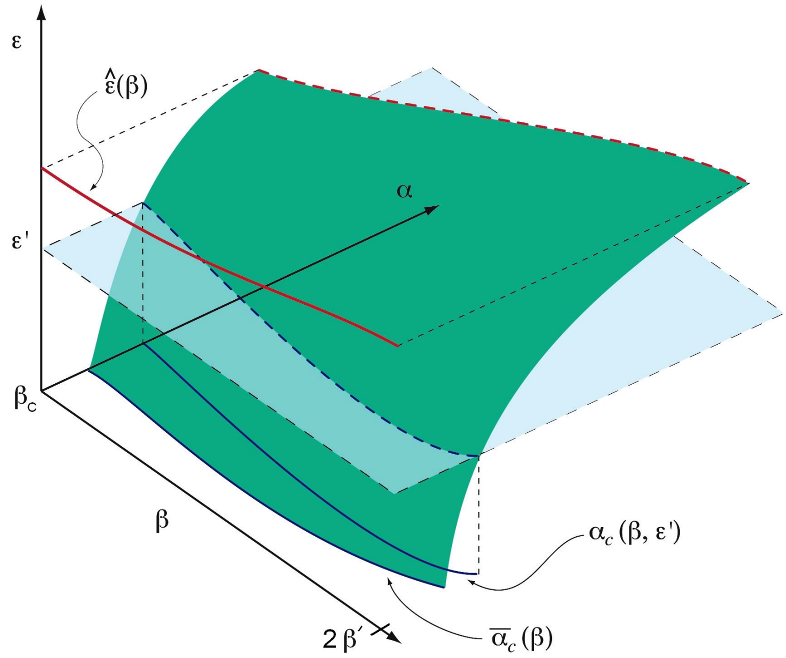

Figure 4-48: Schematic of the canard surface $\epsilon = \epsilon_C(\alpha, \beta)$ (see text for details).

(β, α) plane of the intersection of $\epsilon = \epsilon_C(\alpha, \beta)$ with the plane $\epsilon = \epsilon'$.

2. $\epsilon = \epsilon_C(\alpha, \beta)$ is bounded above by the curve $E_C = \left\{(\hat{\alpha}_C(\beta), \beta, \hat{\epsilon}(\beta))^T : \beta_C < \beta < 2\beta'\right\}$. The projection of this line onto the (β, α) plane is the curve $\alpha = \hat{\alpha}_C(\beta)$.

3. $\epsilon = \epsilon_C(\alpha, \beta)$ is bounded below on the (β, α) plane by the curve $\alpha = \bar{\alpha}_C(\beta)$.

4. For $\hat{\beta}_C < \beta < 2\beta'$, the canard surface intersects a surface of bifurcations on the curve E_C. As α increases through $\hat{\alpha}_C(\beta)$ from $\bar{\alpha}_C(\beta)$ for $\epsilon > \hat{\epsilon}(\beta)$, this bifurcation simultaneously destroys $\{\mathcal{C}_+(\boldsymbol{\alpha}), \mathcal{C}_-(\boldsymbol{\alpha})\}$ and creates a symmetric limit cycle.

Figure (4-48) is a schematic of the surface $\epsilon = \epsilon_C(\alpha, \beta)$, while (4-49) is a schematic of a cross-section through $\epsilon = \epsilon_C(\alpha, \beta)$ for a fixed $\beta_C < \beta < 2\beta'$, to aid visualisation of the surface.

Bifurcations in the range $\beta_C < \beta < 2\beta'$, $\alpha > \alpha_H(\beta)$, $0 < \epsilon < 0.05$

The discussion of the surface $\epsilon = \epsilon_C(\alpha, \beta)$ in the previous section implies that any parameter path in $(\alpha, \beta, \epsilon)$ space which crosses $\epsilon = \epsilon_C(\alpha, \beta)$ will involve a canard. In particular, for a fixed α and β with $\beta_C < \beta < 2\beta'$ and $\bar{\alpha}_C(\beta) < \alpha < \hat{\alpha}_C(\beta)$, increasing ϵ through

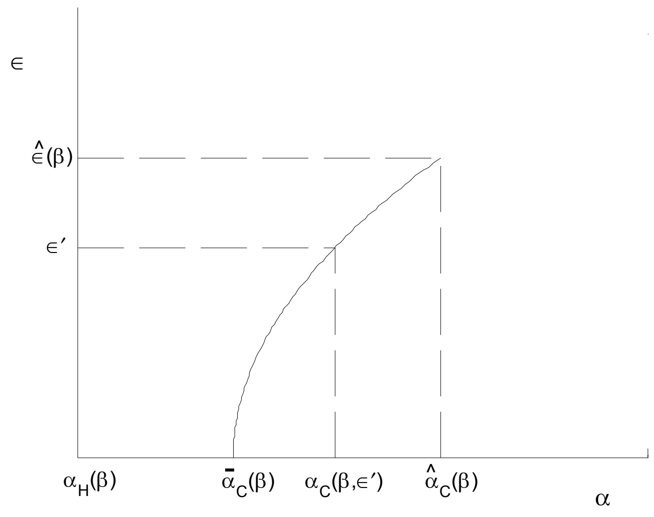

Figure 4-49: Schematic of a cross-section through the canard surface $\epsilon = \epsilon_C(\alpha, \beta)$ for a fixed $\beta_C < \beta < 2\beta'$.

$\epsilon_C(\alpha, \beta)$ will cause $\mathcal{C}_\pm$ to go through the canard 'backwards'. For $\epsilon > \epsilon_C(\alpha, \beta)$, $\mathcal{C}_\pm$ will no longer be a relaxation oscillation (cf. fig (4-45)). Figures (4-50)-(4-52) illustrate such a parameter path for the case $\{\alpha = 59.9539, \beta = 0.75\}$.

For a fixed α and β with $\beta_C < \beta < 2\beta'$ and $\alpha - \hat{\alpha}_C(\beta) > 0$ small, $\mathcal{C}_\pm(\boldsymbol{\alpha})$ does not go through the canard backwards as ϵ is increased from 0. In fact, numerics indicate that for such a choice of α and β, the distance $d(\mathcal{C}_\pm(\boldsymbol{\alpha}), \mathbf{0})$ between $\mathcal{C}_\pm(\boldsymbol{\alpha})$ and the origin $\mathbf{0}$ decreases as ϵ is increased, until $\mathcal{C}_\pm(\boldsymbol{\alpha})$ becomes homoclinic to the origin at some value $\epsilon_G(\alpha, \beta)$. Since $\mathbf{X}(\mathbf{y}; \boldsymbol{\alpha}) = \mathbf{X}_\pm(\mathbf{y}; \boldsymbol{\alpha})\ \forall \mathbf{y} \in N_\pm$, and $\mathcal{C}_\pm(\boldsymbol{\alpha}) \subset N_\pm$, $\mathcal{C}_\pm(\boldsymbol{\alpha})$ is homoclinic to $\mathbf{0}$ in the C^∞ system $\dot{\mathbf{y}} = \mathbf{X}_\pm(\mathbf{y}; \boldsymbol{\alpha})$when $\epsilon = \epsilon_G(\alpha, \beta)$. Assuming that $\mathbf{0}$ is C^1 linearisable in $\dot{\mathbf{y}} = \mathbf{X}_\pm(\mathbf{y}; \boldsymbol{\alpha})$ for $|\epsilon - \epsilon_G(\alpha, \beta)|$ small, the homoclinic bifurcation of $\dot{\mathbf{y}} = \mathbf{X}_\pm(\mathbf{y}; \boldsymbol{\alpha})$ at $\mathbf{0}$ when $\epsilon = \epsilon_G(\alpha, \beta)$ is regular, and so the analysis of 4.5.1 can be used to determine some properties of the bifurcation.[6]. It was shown in 3.6.3 that the eigenvalues $\{\lambda_1(\boldsymbol{\alpha}), \lambda_2(\boldsymbol{\alpha}), \lambda_3(\boldsymbol{\alpha})\}$ of $D_{\mathbf{y}}\mathbf{X}_\pm(\mathbf{0}; \boldsymbol{\alpha})$ are

$$\begin{aligned} \lambda_1(\boldsymbol{\alpha}) &= -1 \\ \lambda_2(\boldsymbol{\alpha}) &= \frac{1}{2}(-1 + \Delta(\boldsymbol{\alpha})) \\ \lambda_3(\boldsymbol{\alpha}) &= \frac{1}{2}(-1 - \Delta(\boldsymbol{\alpha})) \end{aligned}$$

[6]Recall from section 3.6.3 that for $\alpha > \Lambda_+\beta$, the C^1 linearisability of the origin in $\dot{\mathbf{y}} = \mathbf{X}_\pm(\mathbf{y}; \boldsymbol{\alpha})$ cannot be assumed from the extended version of Hartman's Theorem.

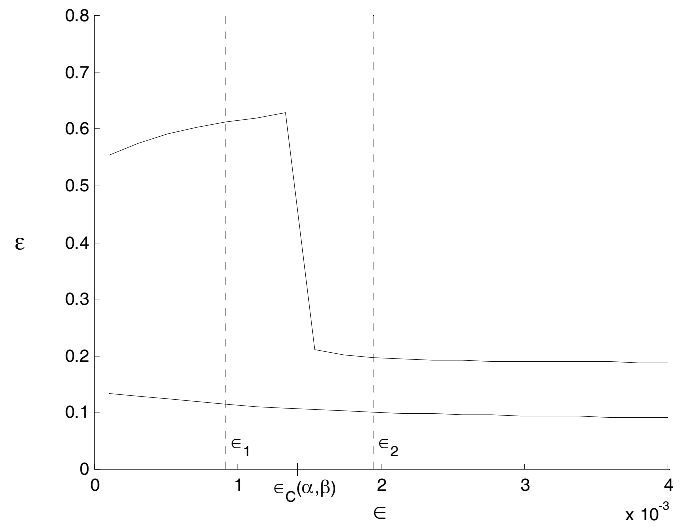

Figure 4-50: Plot of the minimum and maximum ε values of the limit cycle $\mathcal{C}_+$ against ϵ for $\alpha = 59.9539$, $\beta = 0.75$. For this choice of α and β, $\bar{\alpha}_C(\beta) < \alpha < \hat{\alpha}_C(\beta)$. $\mathcal{C}_+$ can be seen to go through the canard backwards as ϵ increases through $\epsilon_C(\alpha, \beta)$.

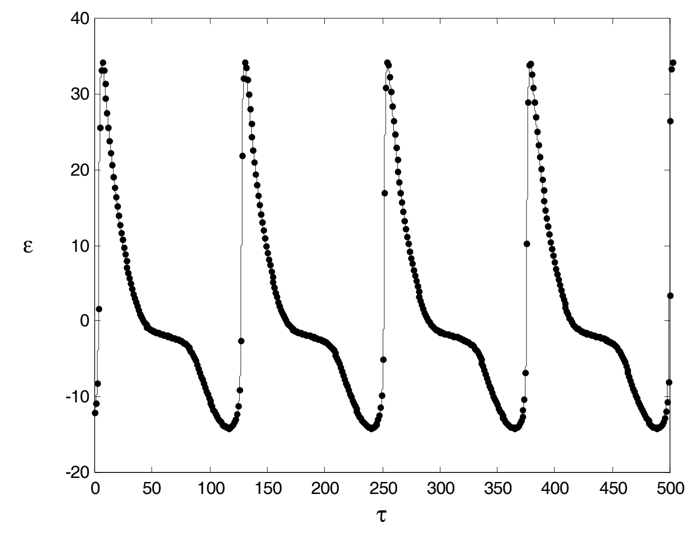

Figure 4-51: Plot of a burster time series $\{b(\tau) : \tau \geq 0\}$ associated with $\mathcal{C}_+$ for $\alpha = 59.9539$, $\beta = 0.75$ and $\epsilon = \epsilon_1 = 0.0092$. Dots represent points spaced equally in time. $\epsilon_1 < \epsilon_C(\alpha, \beta)$ for these values of α and β, as can be seen in figure (4-50) on which ϵ_1 is indicated. The time series shows that $\mathcal{C}_+$ is a relaxation oscillation for this choice of parameters.

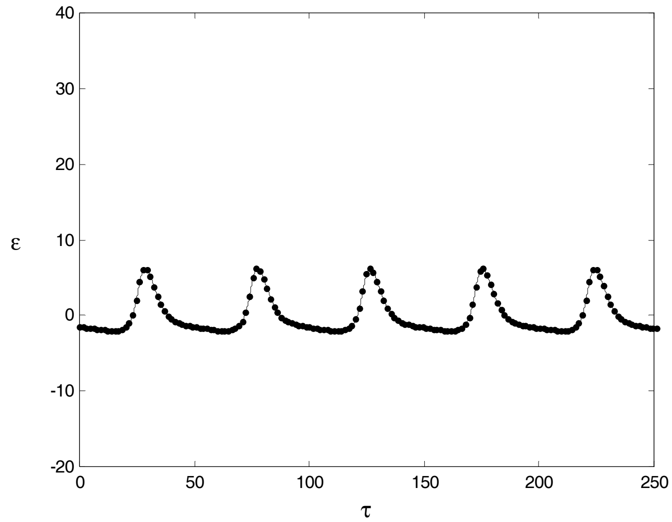

Figure 4-52: Plot of a burster time series $\{b(\tau) : \tau \geq 0\}$ associated with $\mathcal{C}_+$ for $\alpha = 59.9539$, $\beta = 0.75$ and $\epsilon = \epsilon_2 = 0.0195$. Dots represent points spaced equally in time. $\epsilon_2 > \epsilon_C(\alpha, \beta)$ for these values of α and β, as can be seen in figure (4-50) on which ϵ_2 is indicated. The time series shows that $\mathcal{C}_+$ is not a relaxation oscillation for this choice of parameters.

where $\Delta(\boldsymbol{\alpha}) = \sqrt{1 - 4\epsilon(\Lambda_+ + \Lambda_-(\alpha, \beta))}$ (cf. (3.84)). Recalling the notation of 3.6.3, write the corresponding eigenvectors of $D_{\mathbf{y}}\mathbf{X}_\pm(\mathbf{0}; \boldsymbol{\alpha})$ as $\left\{(1,1,0)^T, \mathbf{w}_2^\pm(\boldsymbol{\alpha}), \mathbf{w}_3^\pm(\boldsymbol{\alpha})\right\}$. Writing $G_\pm(\alpha, \beta)$ for the homoclinic orbit of the system $\dot{\mathbf{y}} = \mathbf{X}_\pm(\mathbf{y}; \alpha, \beta, \epsilon_G(\alpha, \beta))$, the effect of the symmetry can be expressed as $G_-(\alpha, \beta) = \sigma G_+(\alpha, \beta)$. For $\alpha > \Lambda_+\beta$, $\lambda_2(\boldsymbol{\alpha}) > 0$ and $\lambda_3(\boldsymbol{\alpha}) < \lambda_1(\boldsymbol{\alpha}) < 0$. The homoclinic bifurcation at $\epsilon = \epsilon_G(\alpha, \beta)$ is therefore of the saddle type, with $d_u = 1$ (cf. section 4.5.1). As was stated in section 3.6.3, the eigenvalue spectrum of $D_{\mathbf{y}}\mathbf{X}_\pm(\mathbf{0}; \boldsymbol{\alpha})$ for $\alpha > \Lambda_+\beta$ implies that in this parameter range, the origin has a unique 1-dimensional C^∞ local unstable manifold $W_{0\pm}^U(\boldsymbol{\alpha})$ in the system $\dot{\mathbf{y}} = \mathbf{X}_\pm(\mathbf{y}; \boldsymbol{\alpha})$, which is tangential to $\mathrm{Sp}\left\{\mathbf{w}_2^\pm(\boldsymbol{\alpha})\right\}$ at the origin. $G_\pm(\alpha, \beta)$ must therefore intersect $W_{0\pm}^U(\alpha, \beta, \epsilon_G(\alpha, \beta))$ in the system $\dot{\mathbf{y}} = \mathbf{X}_\pm(\mathbf{y}; \alpha, \beta, \epsilon_G(\alpha, \beta))$. In $\dot{\mathbf{y}} = \mathbf{X}_\pm(\mathbf{y}; \alpha, \beta, \epsilon_G(\alpha, \beta))$, $G_\pm(\alpha, \beta)$ thus converges to the origin tangential to $\mathrm{Sp}\left\{\mathbf{w}_2^\pm(\alpha, \beta, \epsilon_G(\alpha, \beta))\right\}$ as $\tau \to -\infty$. Also, since $\lambda_3(\boldsymbol{\alpha}) < \lambda_1(\boldsymbol{\alpha})$, $G_\pm(\alpha, \beta)$ converges to the origin tangentially to the stable manifold L_0 as $\tau \to \infty$. It follows from these observations that in the system $\dot{\mathbf{y}} = \mathbf{X}(\mathbf{y}; \alpha, \beta, \epsilon_G(\alpha, \beta))$, both $G_+(\alpha, \beta)$ and $G_-(\alpha, \beta)$ intersect the 1-dimensional local unstable invariant set $W_0^U(\alpha, \beta, \epsilon_G(\alpha, \beta))$ of the origin, defined by:

$$W_0^U(\alpha, \beta, \epsilon_G(\alpha, \beta)) = \left\{W_{0+}^U(\alpha, \beta, \epsilon_G(\alpha, \beta)) \cap N_+\right\} \cup \left\{W_{0-}^U(\alpha, \beta, \epsilon_G(\alpha, \beta)) \cap N_-\right\}$$

(cf. section 3.6.3). Additionally, as $\tau \to -\infty$, $G_+(\alpha, \beta)$ will converge to $\mathbf{0}$ tangential to

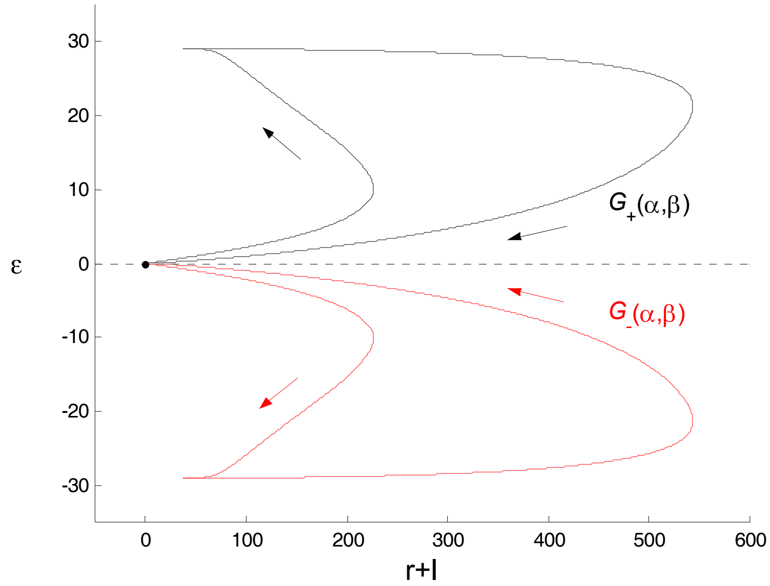

Figure 4-53: Projection onto the $(r + l, \varepsilon)$ plane of $G_+(\alpha, \beta)$ (black line) and $G_-(\alpha, \beta)$ (red line) for $\alpha = 620$, $\beta = 9$. Arrows indicate the direction of motion with time. $\epsilon_G(\alpha, \beta) \approx 0.004823385$ for this choice of α and β.

$\mathrm{Sp}\left\{\mathbf{w}_2^+(\alpha, \beta, \epsilon_G(\alpha, \beta))\right\} \cap N_+$ and $G_-(\alpha, \beta)$ will converge to $\mathbf{0}$ tangential to $\mathrm{Sp}\left\{\mathbf{w}_2^-(\alpha, \beta, \epsilon_G(\alpha, \beta))\right\} \cap N_-$, while as $\tau \to \infty$, both $G_+(\alpha, \beta)$ and $G_-(\alpha, \beta)$ will converge to $\mathbf{0}$ tangential to L_0. Figures (4-53) and (4-54) are plots of $G_+(\alpha, \beta)$ and $G_-(\alpha, \beta)$ for $\{\alpha = 620, \beta = 9\}$. It can be seen that the behaviour of the homoclinic orbits close to the origin is consistent with these arguments.

Since the homoclinic bifurcation in $\dot{\mathbf{y}} = \mathbf{X}_\pm(\mathbf{y}; \boldsymbol{\alpha})$ at $\epsilon = \epsilon_G(\alpha, \beta)$ involves a stable limit cycle, the discussion of section 4.5.1 implies that $\dot{\mathbf{y}} = \mathbf{X}_\pm(\mathbf{y}; \boldsymbol{\alpha})$ has no stable limit cycles passing close to the origin for small $\epsilon - \epsilon_G(\alpha, \beta) > 0$, and that the saddle index $\delta(\alpha, \beta)$ is greater than 1. This means that for small $\epsilon - \epsilon_G(\alpha, \beta) > 0$, the piecewise smooth system $\dot{\mathbf{y}} = \mathbf{X}(\mathbf{y}; \boldsymbol{\alpha})$ has no limit cycles passing close to the origin which are attributable to the existence of corresponding limit cycles in the smooth systems $\dot{\mathbf{y}} = \mathbf{X}_+(\mathbf{y}; \boldsymbol{\alpha})$ and $\dot{\mathbf{y}} = \mathbf{X}_-(\mathbf{y}; \boldsymbol{\alpha})$. However, numerical work does indicate that for small $\epsilon - \epsilon_G(\alpha, \beta) > 0$, the piecewise smooth system $\dot{\mathbf{y}} = \mathbf{X}(\mathbf{y}; \boldsymbol{\alpha})$ has a σ-invariant limit cycle which passes close to the origin, and that this is produced by the 'gluing' together of $\mathcal{C}_+(\boldsymbol{\alpha})$ and $\mathcal{C}_-(\boldsymbol{\alpha})$. Figures (4-55)-(4-57) illustrate the gluing process for $\{\alpha = 110, \beta = 1.5\}$.

The simultaneous homoclinic bifurcations of the asymmetric limit cycles $\mathcal{C}_+$ and $\mathcal{C}_-$ at the origin to form a symmetric limit cycle is very similar to a smooth bifurcation known as the

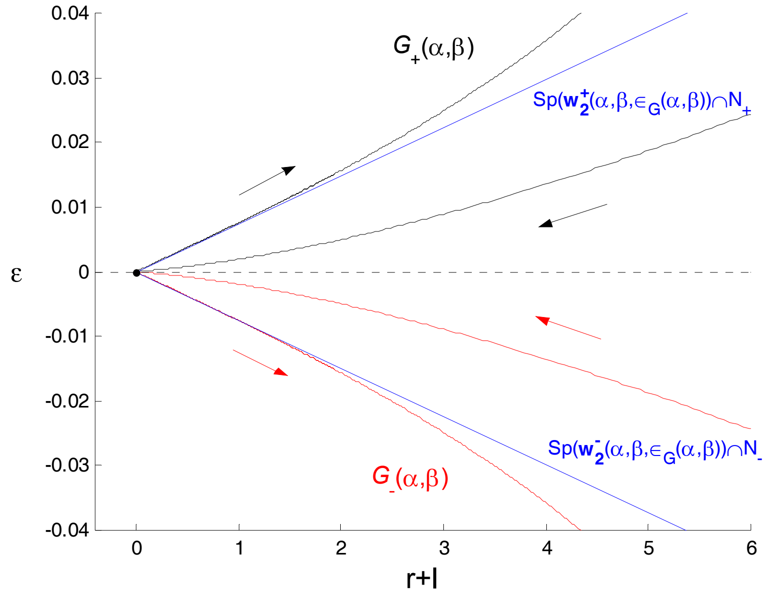

Figure 4-54: Close up of figure (4-53) about $\mathbf{0}$. The projections of $\mathrm{Sp}\left\{\mathbf{w}_2^+\left(\alpha,\beta,\epsilon_G\left(\alpha,\beta\right)\right)\right\}\cap N_+$ and $\mathrm{Sp}\left\{\mathbf{w}_2^-\left(\alpha,\beta,\epsilon_G\left(\alpha,\beta\right)\right)\right\}\cap N_-$ onto the $(r+l,\varepsilon)$ plane are also shown (coloured lines).

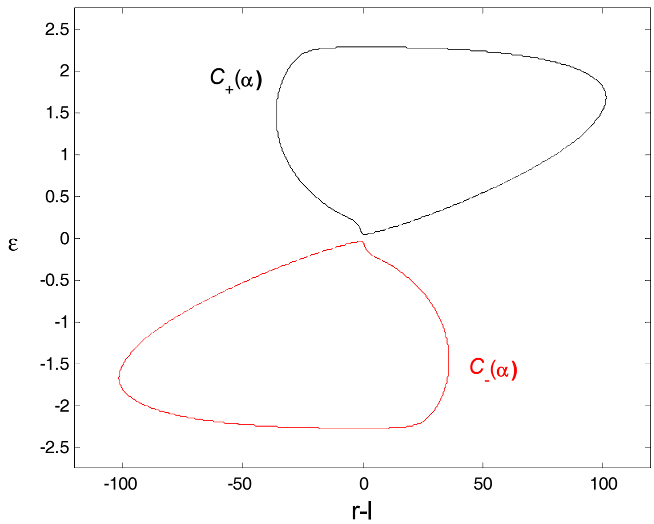

Figure 4-55: Projection onto the $(r-l,\varepsilon)$ plane of the pre-gluing asymmetric limit cycles $\mathcal{C}_+\left(\boldsymbol{\alpha}\right)$ (black) and $\mathcal{C}_-\left(\boldsymbol{\alpha}\right)$ (red) for $\alpha=110$, $\beta=1.5$, $\epsilon=0.004$.

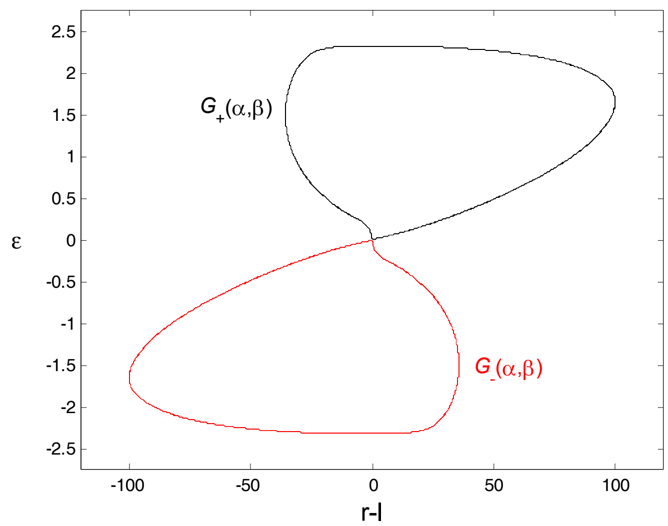

Figure 4-56: Projection onto the $(r-l,\varepsilon)$ plane of the symmetry-related homoclinic orbits $G_+(\alpha,\beta)$ (black) and $G_-(\alpha,\beta)$ (red) for $\alpha = 110$, $\beta = 1.5$, $\epsilon = \epsilon_G(\alpha,\beta) \approx 0.005076305$.

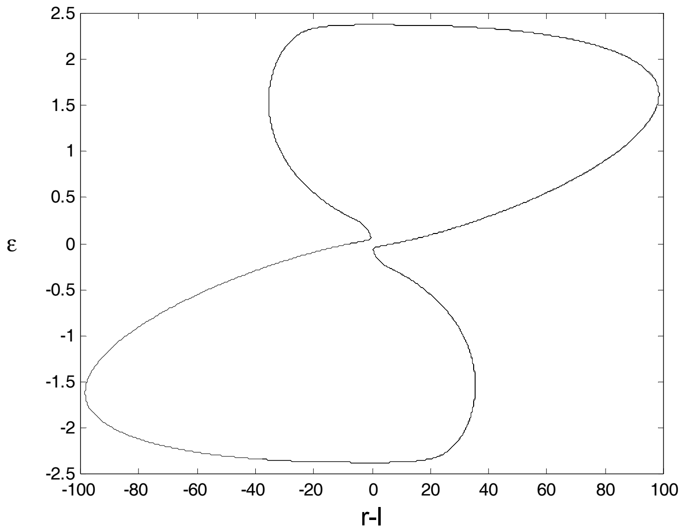

Figure 4-57: Projection onto the $(r-l,\varepsilon)$ plane of the post-gluing symmetric limit cycle for $\alpha = 110$, $\beta = 1.5$, $\epsilon = 0.006$.

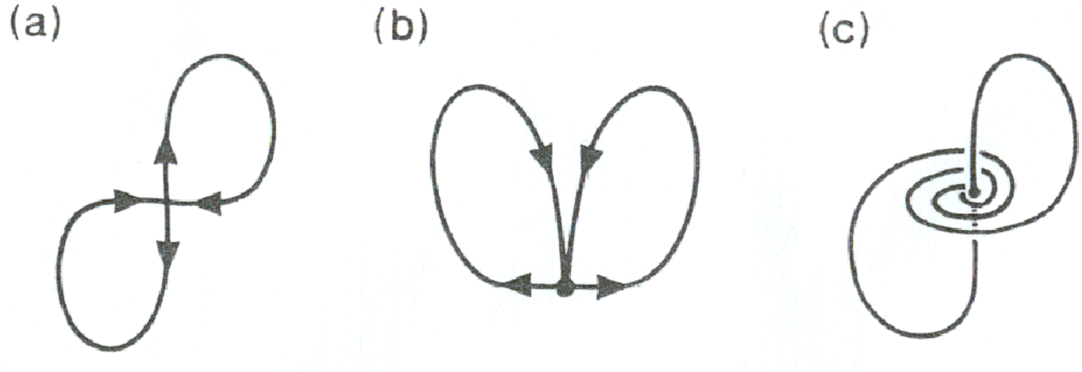

Figure 4-58: Possible configurations of the gluing bifurcation in 3-D. (a) the figure-eight; (b) the butterfly; (c) the saddle focus. (Reproduced from figure 12.6 of [4]).

gluing bifurcation. Gluing bifurcations are homoclinic bifurcations of smooth systems in which a pair of limit cycles merge at a saddle point which has a single unstable eigenvalue to form a large limit cycle [4], [33], [34], [35]. These bifurcations are typically observed in systems possessing a reflection symmetry that maps a saddle point onto itself. For such systems, the existence of an orbit homoclinic to the saddle point implies the existence of another, which is the image of the first under the reflection. In 3 dimensions, the gluing bifurcation can occur in one of three configurations. Two of these-the 'butterfly' and 'figure-of-eight' configurations-are associated with a saddle homoclinic bifurcation, while the third is associated with a saddle-focus homoclinic bifurcation (cf. section 4.5.1). Schematics of the 3 possible configurations are given in figure (4-58).

As may be expected, the value of the saddle index δ is significant in determining the dynamics for each of the configurations. If $\delta > 1$ gluing bifurcations occur in all 3 configurations and the limit cycles involved are stable. If $\delta < 1$, a gluing bifurcation occurs for the figure-of-eight configuration, but the limit cycles involved are unstable. No gluing bifurcation occurs for the butterfly configuration for $\delta < 1$. Instead a pair of homoclinic orbits arise through a homoclinic explosion and no large-amplitude limit cycles exist beyond the bifurcation point. No gluing bifurcation occurs for the saddle-focus configuration either for $\delta < 1$ [4], [33], [34], [35]. The bifurcation which occurs in the burster system $\dot{\mathbf{y}} = \mathbf{X}\left(\mathbf{y};\boldsymbol{\alpha}\right)$ as ϵ passes through $\epsilon_G\left(\alpha,\beta\right)$ appears to be qualitatively equivalent to a smooth gluing bifurcation of the saddle type with saddle index $\delta > 1$.

The observation that the saddle index $\delta\left(\alpha,\beta\right) > 1$ for the homoclinic bifurcation of $\dot{\mathbf{y}} = \mathbf{X}_{\pm}\left(\mathbf{y};\boldsymbol{\alpha}\right)$ at the origin can be used to obtain a restriction on the value of $\epsilon_G\left(\alpha,\beta\right)$ for a given α and β. Since $\lambda_3(\boldsymbol{\alpha}) < \lambda_1(\boldsymbol{\alpha}) < 0$, $\delta(\alpha, \beta)$ is given by:

$$\delta(\alpha,\beta) = -\frac{\lambda_1(\alpha,\beta,\epsilon_G(\alpha,\beta))}{\lambda_2(\alpha,\beta,\epsilon_G(\alpha,\beta))} = \frac{2}{-1+\sqrt{1-4\epsilon_G(\alpha,\beta)(\Lambda_+ + \Lambda_-(\alpha,\beta))}} \tag{4.48}$$

It follows from (4.48) and $\Lambda_-(\alpha,\beta) = -\frac{\alpha}{\beta}$ that $\delta(\alpha,\beta) > 1$ is equivalent to $\epsilon_G(\alpha,\beta) < \hat{\epsilon}_G(\alpha,\beta)$ where:

$$\hat{\epsilon}_G(\alpha,\beta) = \frac{2\beta}{\alpha - \Lambda_+\beta} \tag{4.49}$$

This implies that in (α,β,ϵ) space, the surface of gluing bifurcations $\epsilon = \epsilon_G(\alpha,\beta)$ lies below the surface $\epsilon = \hat{\epsilon}_G(\alpha,\beta)$. The relation $\epsilon_G(\alpha,\beta) < \hat{\epsilon}_G(\alpha,\beta)$ reduces the amount of numerical work necessary to approximate $\epsilon_G(\alpha,\beta)$.

In addition to the gluing bifurcation and the canard, there is a further global bifurcation which occurs in the burster system as ϵ is increased from 0 to 0.05 for a fixed α and β with $\beta_C < \beta < 2\beta'$ and $\alpha > \bar{\alpha}_C(\beta)$. This bifurcation has only been observed numerically. It also produces a stable symmetric limit cycle, although the mechanism by which this occurs is unclear and-unlike the gluing bifurcation-does not seem related to any global bifurcations which occur in the smooth systems $\dot{\mathbf{y}} = \mathbf{X}_+(\mathbf{y};\boldsymbol{\alpha})$ and $\dot{\mathbf{y}} = \mathbf{X}_-(\mathbf{y};\boldsymbol{\alpha})$. The bifurcation will be henceforth referred to as the **hard oscillation bifurcation**, or **H-bifurcation** for short. Actually, it appears that there are two different bifurcations which might sensibly be designated ‘H-type’. In addition to the basic creation of a symmetric limit cycle, the simultaneous destruction of the symmetry-related pair $\{\mathcal{C}_+(\boldsymbol{\alpha}), \mathcal{C}_-(\boldsymbol{\alpha})\}$ can also occur. The H-bifurcation which only involves the creation of the symmetric limit cycle will be referred to as the **type I H-bifurcation**, while the H-bifurcation which also involves the destruction of the asymmetric limit cycles will be referred to as the **type II H-bifurcation**.

For a given α and β in the range of interest, the value of ϵ at which a type I H-bifurcation occurs will be denoted $\epsilon_S(\alpha,\beta)$, and the value of ϵ at which a type II H-bifurcation occurs will be denoted $\bar{\epsilon}_S(\alpha,\beta)$. The existence of the gluing and H-bifurcations means that there are choices of $\boldsymbol{\alpha}$ for which the burster system has 2 distinct symmetric limit cycles. For such parameter choices, the limit cycle with the greatest amplitude in the ε direction will be labelled $\mathcal{C}_2$ and the other limit cycle $\mathcal{C}_1$. More specifically, $\mathcal{C}_1$ and $\mathcal{C}_2$ are labelled so as to satisfy:

$$\max_{\mathbf{y}\in\mathcal{C}_2}\{\varepsilon\}-\min_{\mathbf{y}\in\mathcal{C}_2}\{\varepsilon\}>\max_{\mathbf{y}\in\mathcal{C}_1}\{\varepsilon\}-\min_{\mathbf{y}\in\mathcal{C}_1}\{\varepsilon\}$$

For parameter choices for which there is only one symmetric limit cycle, this will usually be labelled $\mathcal{C}_2$, unless convenience dictates otherwise.

A natural question to ask is what happens to the surfaces of gluing and H-bifurcations as α is varied for a fixed $\beta_C<\beta<2\beta'$. Numerical work seems to indicate that the type I H-bifurcation exists for all $0<\alpha<\hat{\alpha}_C(\beta)$, with $\epsilon_S(\alpha,\beta)$ increasing without bound as $\alpha\to 0+$. Numerics also indicate that as α is increased from $\hat{\alpha}_C(\beta)$, the type I H-bifurcation and gluing bifurcation both persist, with $\epsilon_G(\alpha,\beta)$ a decreasing function of α, and $\epsilon=\epsilon_S(\alpha,\beta)$ an eventually increasing function of α. Both bifurcations certainly exist for $\hat{\alpha}_C(\beta)<\alpha<2.5\alpha'$. For a fixed β with $\beta_C<\beta<\hat{\beta}_C$, the type II H-bifurcation does not occur. Also, as $\alpha\to\alpha_H(\beta)+$, $\epsilon_G(\alpha,\beta)$ increases without bound. Figure (4-59) is a schematic of the surfaces $\epsilon=\epsilon_C(\alpha,\beta)$, $\epsilon=\epsilon_G(\alpha,\beta)$, $\epsilon=\hat{\epsilon}_G(\alpha,\beta)$ and $\epsilon=\epsilon_S(\alpha,\beta)$ for $\beta=0.75$, $\alpha_H(\beta)<\alpha<2.5\alpha'$, $0<\epsilon<0.05$, based on numerics. Also shown are the attractors in this range. Figure (4-60) is a bifurcation diagram obtained numerically for a closed parameter path in the (α,ϵ) plane for $\beta=0.75$. Figure (4-59) is the typical bifurcation picture observed in the (α,ϵ) plane for a fixed β with $\beta_C<\beta<\hat{\beta}_C$, and $\alpha_H(\beta)<\alpha<2.5\alpha'$, $0<\epsilon<0.05$.

For a fixed β with $\hat{\beta}_C<\beta<2\beta'$, both the type I and type II H-bifurcations occur. Figure (4-61) is a schematic of the surfaces $\epsilon=\epsilon_C(\alpha,\beta)$, $\epsilon=\epsilon_G(\alpha,\beta)$, $\epsilon=\hat{\epsilon}_G(\alpha,\beta)$, $\epsilon=\epsilon_S(\alpha,\beta)$ and $\epsilon=\bar{\epsilon}_S(\alpha,\beta)$ for $\beta=3$, $\alpha_H(\beta)<\alpha<2.5\alpha'$, $0<\epsilon<0.05$, based on numerics. Also shown are the attractors in this range. Figures (4-62)-(4-65) are bifurcation diagrams obtained numerically for parameter paths in the (α,ϵ) plane for $\beta=3$. Figure (4-61) is the typical bifurcation picture observed in the (α,ϵ) plane for a fixed β with $\hat{\beta}_C<\beta<2\beta'$, and $\alpha_H(\beta)<\alpha<2.5\alpha'$, $0<\epsilon<0.05$. In this range, numerics suggest that the surface of gluing bifurcations $\epsilon=\epsilon_G(\alpha,\beta)$ and the surface of type II H-bifurcations $\epsilon=\bar{\epsilon}_S(\alpha,\beta)$ both intersect the canard surface $\epsilon=\epsilon_C(\alpha,\beta)$ at the point $(\hat{\alpha}_C(\beta),\hat{\epsilon}(\beta))$ in the (α,ϵ) plane. It is the surface of type II H-bifurcations which terminates the canards for $\hat{\beta}_C<\beta<2\beta'$ (cf. section 4.8.1). The surfaces $\epsilon=\epsilon_G(\alpha,\beta)$ and $\epsilon=\bar{\epsilon}_S(\alpha,\beta)$ also intersect the surface of type I H-bifurcations $\epsilon=\epsilon_S(\alpha,\beta)$ at a point $(\bar{\alpha}(\beta),\epsilon_S(\bar{\alpha}(\beta),\beta))$ in the (α,ϵ) plane with $\alpha_H(\beta)<\bar{\alpha}(\beta)<\hat{\alpha}_C(\beta)$. The surface $\epsilon=\bar{\epsilon}_S(\alpha,\beta)$ exists between

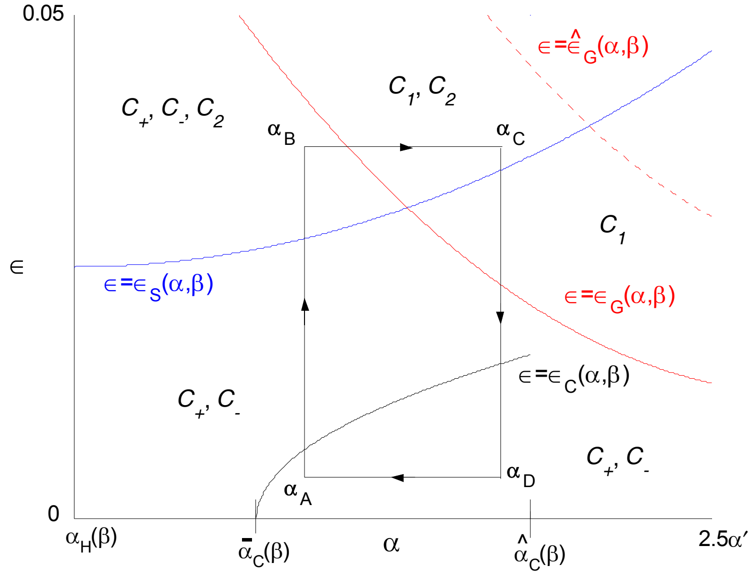

Figure 4-59: Schematic of the global bifurcation surfaces for $\beta = 0.75$, $\alpha_H(\beta) < \alpha < 2.5\alpha'$, $0 < \epsilon < 0.05$, based on numerical results. Also shown are the attractors for this parameter range, the parameter path used to generate figure (4-60), and the limiting surface $\epsilon = \hat{\epsilon}_G(\alpha, \beta)$ of $\epsilon = \epsilon_G(\alpha, \beta)$.

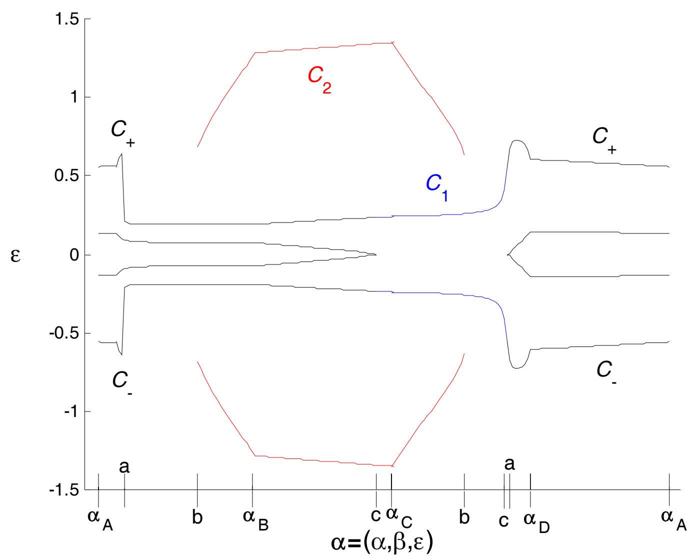

Figure 4-60: Bifurcation diagram obtained numerically for a closed parameter path in the (α, ϵ) plane for $\beta = 0.75$. A schematic of the parameter path is shown in figure (4-59). $\alpha = 60.0591$ at $\boldsymbol{\alpha}_A$, $\alpha = 61.4275$ at $\boldsymbol{\alpha}_D$, $\epsilon = 0.0001$ at $\boldsymbol{\alpha}_A$, $\epsilon = 0.04$ at $\boldsymbol{\alpha}_B$. For each choice of $\boldsymbol{\alpha}$, the corresponding values shown on the vertical axis are the minimum and maximum ε values of the attractors which exist for that $\boldsymbol{\alpha}$. 'a' denotes the canard, 'b' denotes the type I H-bifurcation and 'c' denotes the nonsmooth gluing bifurcation.

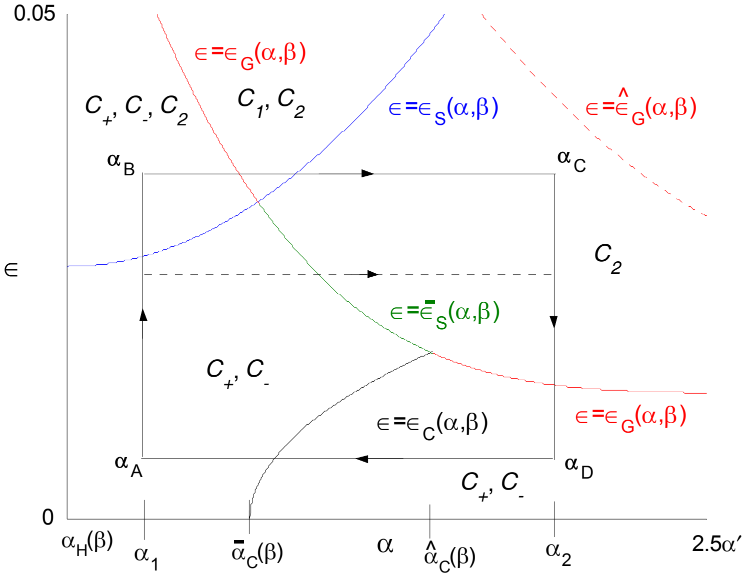

Figure 4-61: Schematic of the global bifurcation surfaces for $\beta = 3$, $\alpha_H(\beta) < \alpha < 2.5\alpha'$, $0 < \epsilon < 0.05$, based on numerical results. Also shown are the attractors for this parameter range, the parameter paths used to generate figures (4-62)-(4-64), and the limiting surface $\epsilon = \hat{\epsilon}_G(\alpha, \beta)$ of $\epsilon = \epsilon_G(\alpha, \beta)$

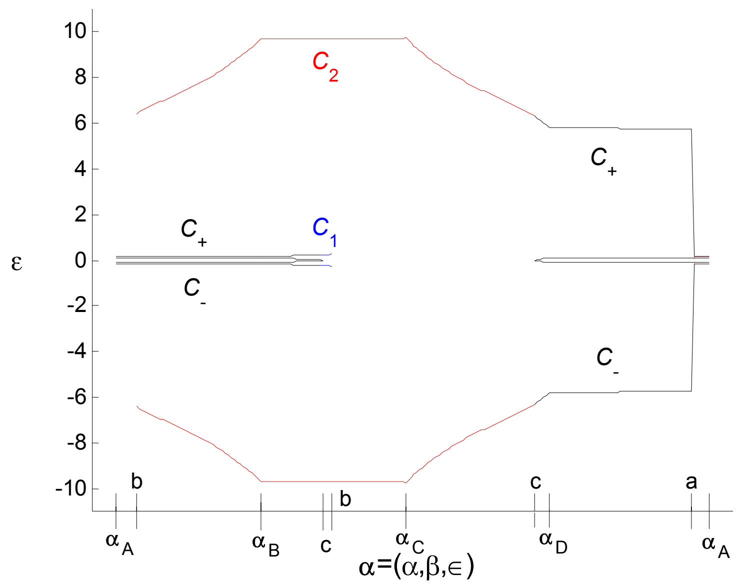

Figure 4-62: Bifurcation diagram obtained numerically for a closed parameter path in the (α, ϵ) plane for $\beta = 3$. A schematic of the parameter path is shown in figure (4-61) (solid line). $\alpha = \alpha_1 = 207.6744$ at $\boldsymbol{\alpha}_A$, $\alpha = \alpha_2 = 209.6544$ at $\boldsymbol{\alpha}_D$, $\epsilon = 0.001$ at $\boldsymbol{\alpha}_A$, $\epsilon = 0.04$ at $\boldsymbol{\alpha}_B$. For each choice of $\boldsymbol{\alpha}$, the corresponding values shown on the vertical axis are the minimum and maximum ε values of the attractors which exist for that $\boldsymbol{\alpha}$. 'a' denotes the canard, 'b' denotes the type I H-bifurcation and 'c' denotes the nonsmooth gluing bifurcation.

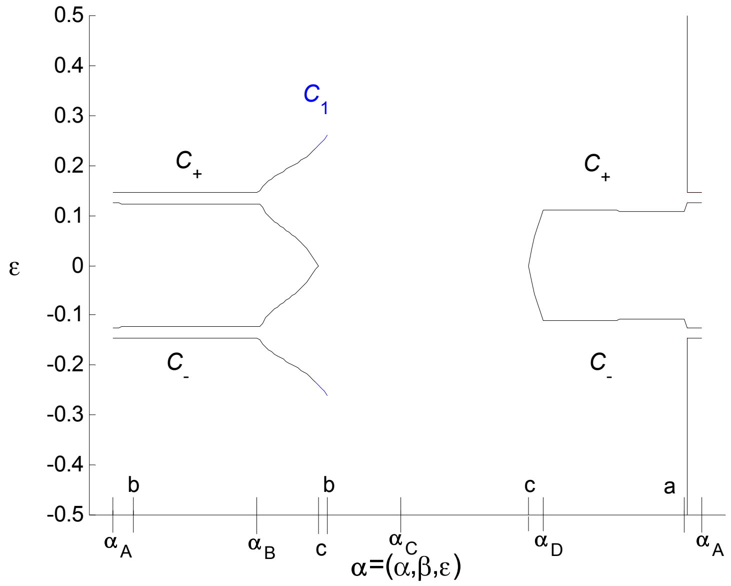

Figure 4-63: Close up of figure (4-62) to reveal the details of the canard and the type I H-bifurcation which occurs between $\boldsymbol{\alpha}_B$ and $\boldsymbol{\alpha}_C$.

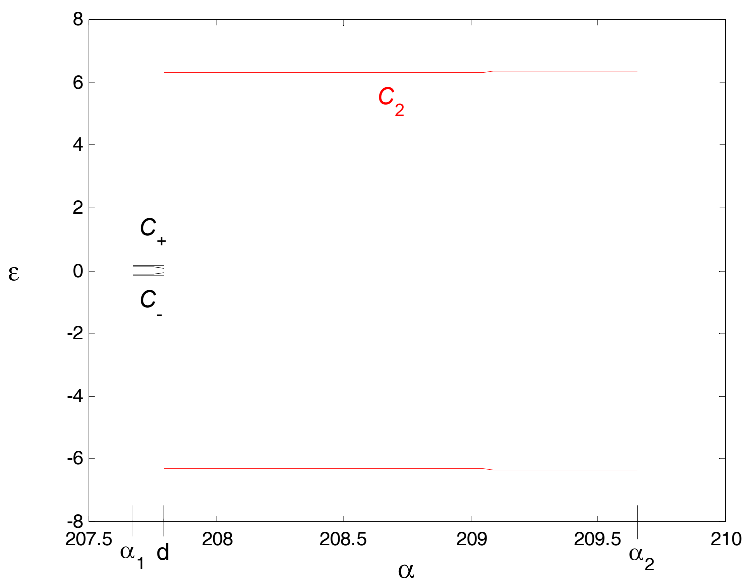

Figure 4-64: Bifurcation diagram obtained numerically by varying α between $\alpha_1 = 207.6744$ and $\alpha_2 = 209.6544$ for $\beta = 3$, $\epsilon = 0.0054$. A schematic of this parameter path is shown in figure (4-69) (dotted line). For each choice of α, the corresponding values shown on the vertical axis are the minimum and maximum ε values of the attractors which exist for that α. 'd' denotes the type II H-bifurcation.

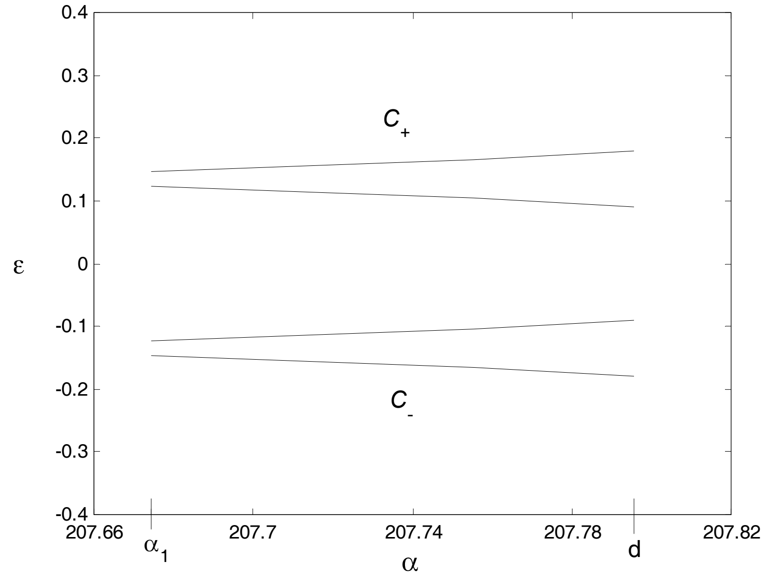

Figure 4-65: Close up of figure (4-64) to reveal the details of the type II H-bifurcation which simultaneously destroys the asymmetric pair $\{\mathcal{C}_+(\boldsymbol{\alpha}), \mathcal{C}_-(\boldsymbol{\alpha})\}$ and creates the symmetric limit cycle $\mathcal{C}_2(\boldsymbol{\alpha})$.

the two points of intersection $(\bar{\alpha}(\beta), \epsilon_S(\bar{\alpha}(\beta), \beta))$ and $(\hat{\alpha}_C(\beta), \hat{\epsilon}(\beta))$, while $\epsilon = \epsilon_G(\alpha, \beta)$ exists for $\alpha < \bar{\alpha}(\beta)$ and $\alpha > \hat{\alpha}_C(\beta)$. Numerics also indicate that as $\alpha \to \alpha_H(\beta)+$, $\epsilon_G(\alpha, \beta)$ increases without bound. Note that in both the β ranges considered above, the curves $\epsilon = \epsilon_G(\alpha, \beta)$ and $\epsilon = \epsilon_S(\alpha, \beta)$ can intersect, meaning that there are regions of the (α, ϵ) plane where $\mathcal{C}_1$ and $\mathcal{C}_2$ both exist, and regions where $\mathcal{C}_+$ and $\mathcal{C}_-$ coexist with $\mathcal{C}_2$. Figures (4-66) and (4-67) are plots of the attractors of the burster system corresponding to both these situations. It should also be noted that the bifurcation picture of the burster equations in the range $\beta_C < \beta < 2\beta'$, $\alpha_H(\beta) < \alpha < 2.5\alpha'$, $0 < \epsilon < 0.05$ proposed here seems to suggest that the surface of type II H-bifurcations is created by the surface of gluing bifurcations intersecting the canard surface as β increases through $\hat{\beta}_C$ (cf. figures (4-59) and (4-61)).

Numerics indicate that for β greater than some value $\bar{\beta}_C \approx 1.35$, $\epsilon_S(\alpha, \beta) > 0.05$ for $\alpha > \hat{\alpha}_C(\beta)$. Consequently for a fixed α and β with $\bar{\beta}_C < \beta < 2\beta'$, $\alpha > \hat{\alpha}_C(\beta)$, only the gluing bifurcation occurs as ϵ is increased from 0 to 0.05: the canard and H-bifurcation do not occur.

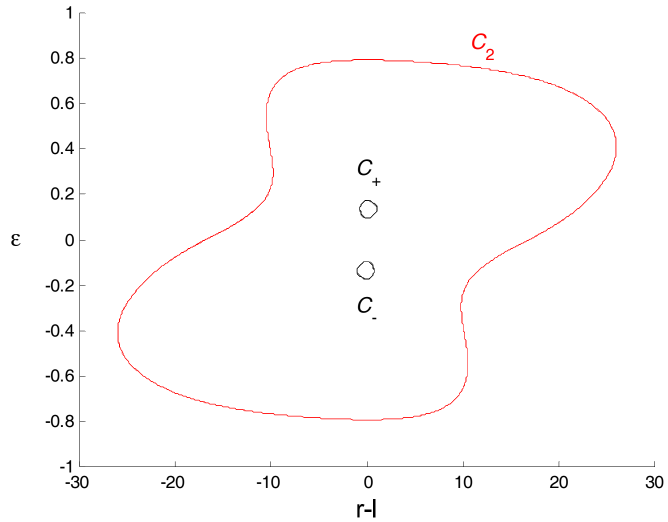

Figure 4-66: Attractors of the burster system for $\alpha = 64.6$, $\beta = 0.825$ and $\epsilon = 0.02$. This choice of parameters corresponds to $\beta_C < \beta < \hat{\beta}_C$, $\alpha < \hat{\alpha}_C(\beta)$, $\epsilon_S(\alpha, \beta) < \epsilon < \epsilon_G(\alpha, \beta)$. The attractors are the pair of asymmetric limit cycles $\mathcal{C}_+$ and $\mathcal{C}_-$ (black) produced by the Hopf bifurcation at $\alpha = \alpha_H(\beta)$, and the symmetric limit cycle $\mathcal{C}_2$ (red) produced by the type I H-bifurcation at $\epsilon = \epsilon_S(\alpha, \beta)$.

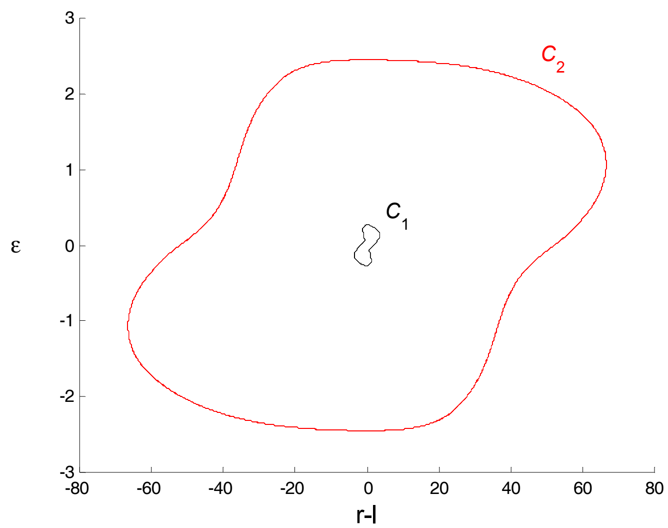

Figure 4-67: Attractors of the burster system for $\alpha = 88.1822$, $\beta = 1.1591$ and $\epsilon = 0.0338$. This choice of parameters corresponds to $\hat{\beta}_C < \beta < 2\beta'$, $\alpha > \hat{\alpha}_C(\beta)$, $\epsilon > \epsilon_G(\alpha, \beta) > \epsilon_S(\alpha, \beta)$. The attractors are the symmetric limit cycle $\mathcal{C}_1$ (black) produced by the nonsmooth gluing bifurcation at $\epsilon = \epsilon_G(\alpha, \beta)$, and the symmetric limit cycle $\mathcal{C}_2$ (red) produced by the type I H-bifurcation at $\epsilon = \epsilon_S(\alpha, \beta)$.

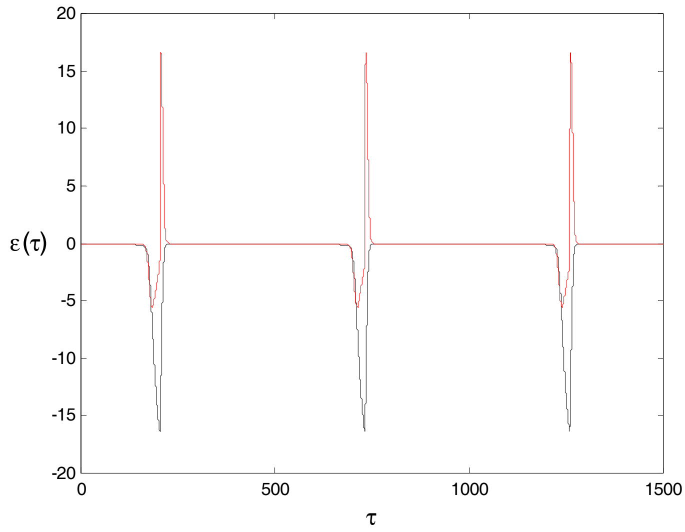

Figure 4-68: Plot of an error time series $\{\varepsilon(\tau) : \tau \geq 0\}$ associated with $\mathcal{C}_-$ for $\alpha = 408.0569$, $\beta = 6$, $\epsilon = 0.0047$ (black). The corresponding velocity time series $\{\dot{\varepsilon}(\tau) : \tau \geq 0\}$ is also shown (red). $\dot{\varepsilon}(\tau)$ has been rescaled to enable it to be compared with $\varepsilon(\tau)$ on the same plot.

4.8.2 Error time series for $\bar{\beta}_C < \beta < 2\beta'$, $\hat{\alpha}_C(\beta) < \alpha < 2.5\alpha'$ and $\epsilon < 0.05$

For $\epsilon < \epsilon_G(\alpha, \beta)$ in this range, the attractors are $\mathcal{C}_+$ and $\mathcal{C}_-$. Thus since $\alpha > \hat{\alpha}_C(\beta)$, if $\epsilon_G(\alpha, \beta)$ is not too large, then for $\epsilon < \epsilon_G(\alpha, \beta)$, $\mathcal{C}_+$ and $\mathcal{C}_-$ lie close to the slow manifold S_M, and so are large-amplitude relaxation oscillations. Moreover, S_M has the asymmetric double-loop form discussed in section 4.6.1, and therefore the corresponding error time series $\{\varepsilon(\tau) : \tau \geq 0\}$ will have the associated slow-fast form, which resembles jerk nystagmus. As $\epsilon \to \epsilon_G(\alpha, \beta)-$, the period of $\mathcal{C}_\pm$ goes to ∞ as it becomes homoclinic to the origin. The effect of this on $\{\varepsilon(\tau) : \tau \geq 0\}$ is that the waveform develops longer and longer intervals on which $\varepsilon(\tau) \approx 0$. This effect can be seen in figure (4-68) which shows a plot of an error time series corresponding to $\mathcal{C}_-$ for a choice of $\boldsymbol{\alpha}$ in the range of interest at which $\mathcal{C}_-$ is near-homoclinic. $\varepsilon(\tau)$ can be seen to resemble a jerk nystagmus waveform with an extended foveation period (cf. section 1.1.3).

For $\epsilon - \epsilon_G(\alpha, \beta) > 0$ small, the symmetric limit cycle $\mathcal{C}_2$ created by the gluing of $\mathcal{C}_+$ and $\mathcal{C}_-$ has the form of a relaxation oscillation, as parts of it still lie close to S_M. Moreover, the asymmetric double-loop form of S_M means that the error time series associated with $\mathcal{C}_2$ are of slow-fast form, consisting of a slow drift away from $\varepsilon = 0$ in the positive ε direction followed by a faster motion back towards $\varepsilon = 0$ in the negative ε direction, and then a slow

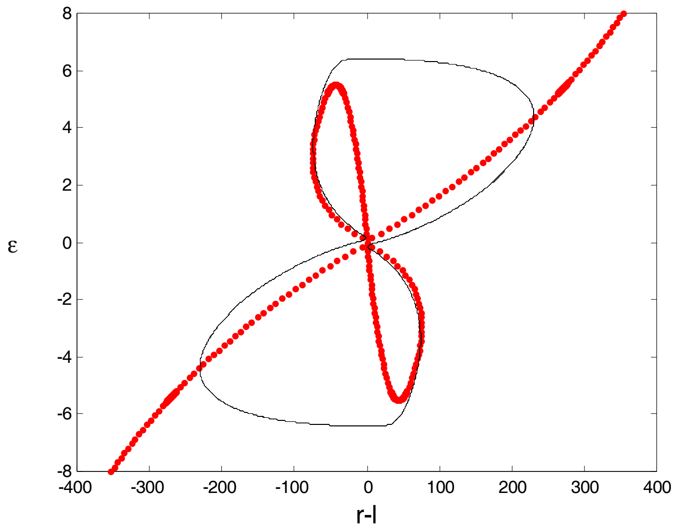

Figure 4-69: Projections of $\mathcal{C}_2$ (black line) and S_M (red dots) onto the $(r-l, \varepsilon)$ plane for $\alpha = 209.6544$, $\beta = 3$, $\epsilon = 0.006$.

drift away from $\varepsilon = 0$ in the negative ε direction followed by a faster motion back towards $\varepsilon = 0$ in the positive ε direction. Figures (4-69) and (4-71) show projections of $\mathcal{C}_2$ and S_M onto the $(r-l, \varepsilon)$ plane for two choices of $\boldsymbol{\alpha}$ in the range of interest, while figures (4-70) and (4-72) are plots of error time series associated with $\mathcal{C}_2$ for these parameter choices. In both cases, $\varepsilon(\tau)$ resembles a bilateral jerk nystagmus waveform (cf. section 1.1.3). As $\epsilon \to \epsilon_G(\alpha, \beta)+$, the period of $\mathcal{C}_2$ goes to ∞ as it becomes homoclinic to the origin. This causes the same effect on $\{\varepsilon(\tau) : \tau \geq 0\}$ as the homoclinicity of $\mathcal{C}_{\pm}$, with the waveform developing increasingly long intervals on which $\varepsilon(\tau) \approx 0$. Figure (4-73) illustrates this effect, showing a plot of an error time series corresponding to $\mathcal{C}_2$ for a choice of $\boldsymbol{\alpha}$ in the range of interest, at which $\mathcal{C}_2$ is near-homoclinic. It can be seen that $\varepsilon(\tau)$ resembles a bilateral jerk waveform with an extended foveation period.

As ϵ is increased to 0.05 from $\epsilon_G(\alpha, \beta)$, $\mathcal{C}_2$ is progressively less confined to S_M, and so no longer has the form of a relaxation oscillation. Consequently, the corresponding error time series $\{\varepsilon(\tau) : \tau \geq 0\}$ lose the slow-fast form, and become increasingly sinusoidal. This transition is illustrated in figures (4-74)-(4-77) which show the effect of increasing ϵ for $\{\alpha = 408.0569, \beta = 6\}$. The figures indicate that increasing ϵ seems to generate error time series which resemble pendular nystagmus (cf. section 1.1.3).

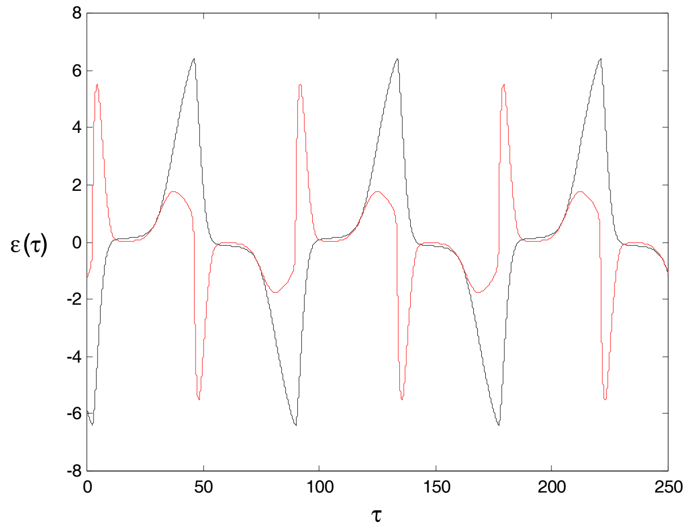

Figure 4-70: Plot of an error time series $\{\varepsilon(\tau) : \tau \geq 0\}$ associated with $\mathcal{C}_2$ for $\alpha = 209.6544$, $\beta = 3$, $\epsilon = 0.006$ (black). The corresponding velocity time series $\{\dot{\varepsilon}(\tau) : \tau \geq 0\}$ is also shown (red). $\dot{\varepsilon}(\tau)$ has been rescaled to enable it to be compared with $\varepsilon(\tau)$ on the same plot.

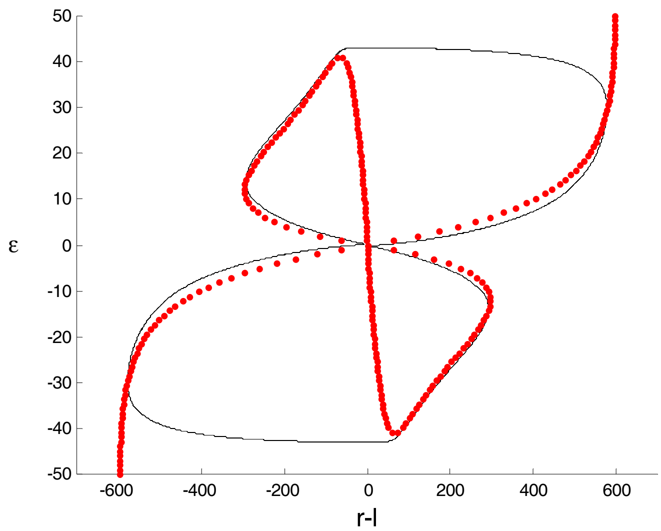

Figure 4-71: Projections of $\mathcal{C}_2$ (black line) and S_M (red dots) onto the $(r-l, \varepsilon)$ plane for $\alpha = 805.0171$, $\beta = 12$, $\epsilon = 0.0065$.

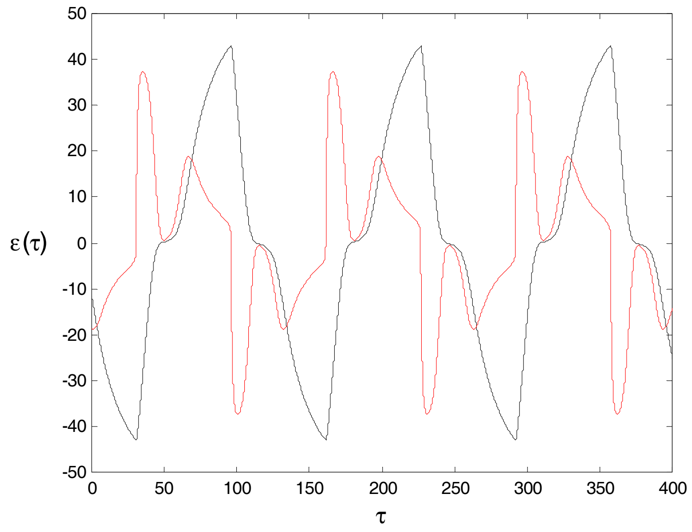

Figure 4-72: Plot of an error time series $\{\varepsilon(\tau) : \tau \geq 0\}$ associated with $\mathcal{C}_2$ for $\alpha = 805.0171$, $\beta = 12$, $\epsilon = 0.0065$ (black). The corresponding velocity time series $\{\dot{\varepsilon}(\tau) : \tau \geq 0\}$ is also shown (red). $\dot{\varepsilon}(\tau)$ has been rescaled to enable it to be compared with $\varepsilon(\tau)$ on the same plot.

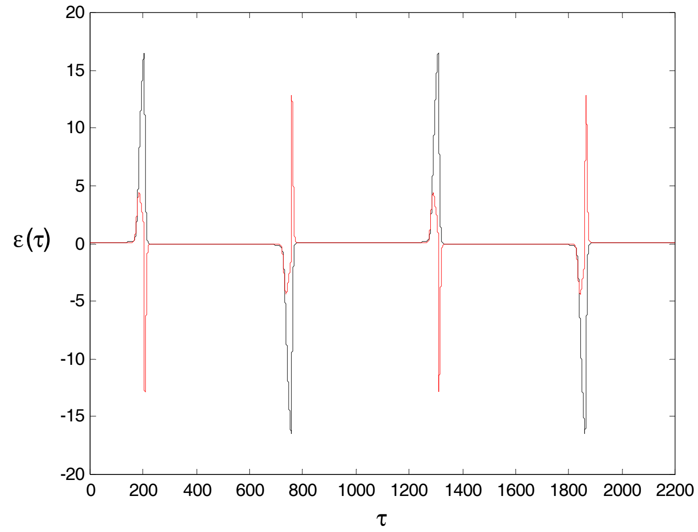

Figure 4-73: Plot of an error time series $\{\varepsilon(\tau) : \tau \geq 0\}$ associated with $\mathcal{C}_+$ for $\alpha = 408.0569$, $\beta = 6$, $\epsilon = 0.0049$ (black). The corresponding velocity time series $\{\dot{\varepsilon}(\tau) : \tau \geq 0\}$ is also shown (red). $\dot{\varepsilon}(\tau)$ has been rescaled to enable it to be compared with $\varepsilon(\tau)$ on the same plot.

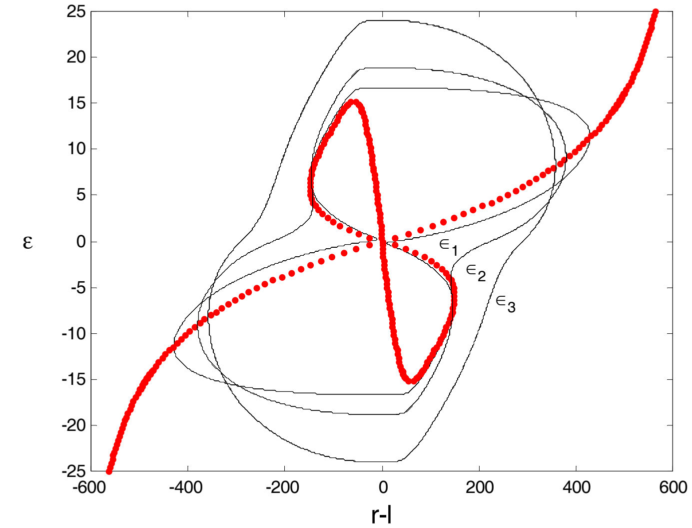

Figure 4-74: Plots of $\mathcal{C}_2$ in the $(r-l,\varepsilon)$ plane for increasing values of $\epsilon > \epsilon_G(\alpha,\beta)$, given α and β fixed at the values $\alpha = 408.0569$, $\beta = 6$. The slow manifold S_M is also shown (red dots). $\epsilon_1 = 0.065$, $\epsilon_2 = 0.0214$, $\epsilon_3 = 0.05$.

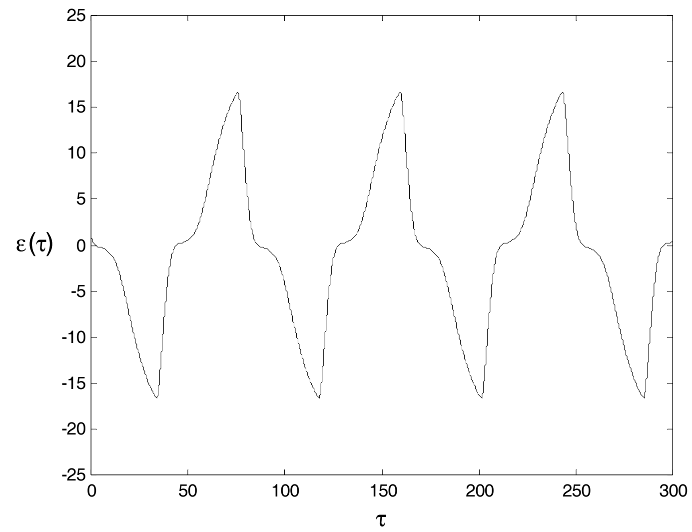

Figure 4-75: Plot of an error time series $\{\varepsilon(\tau) : \tau \geq 0\}$ associated with $\mathcal{C}_2$ for $\alpha = 408.0569$, $\beta = 6$, $\epsilon = \epsilon_1 = 0.0065$ (cf. figure (4-74)).

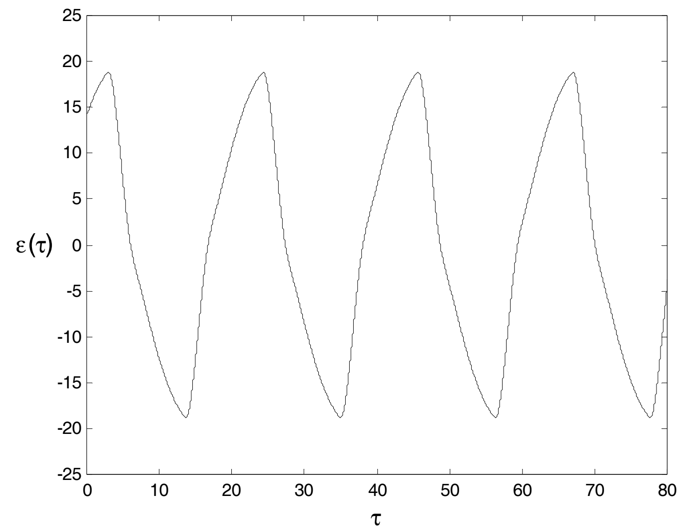

Figure 4-76: Plot of an error time series $\{\varepsilon(\tau) : \tau \geq 0\}$ associated with $\mathcal{C}_2$ for $\alpha = 408.0569$, $\beta = 6$, $\epsilon = \epsilon_2 = 0.0214$ (cf. figure (4-74)).

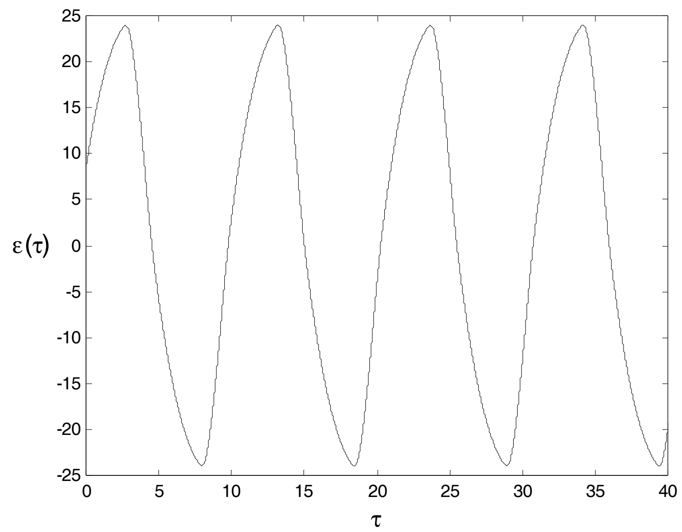

Figure 4-77: Plot of an error time series $\{\varepsilon(\tau) : \tau \geq 0\}$ associated with $\mathcal{C}_2$ for $\alpha = 408.0569$, $\beta = 6$, $\epsilon = \epsilon_3 = 0.05$ (cf. figure (4-74)).

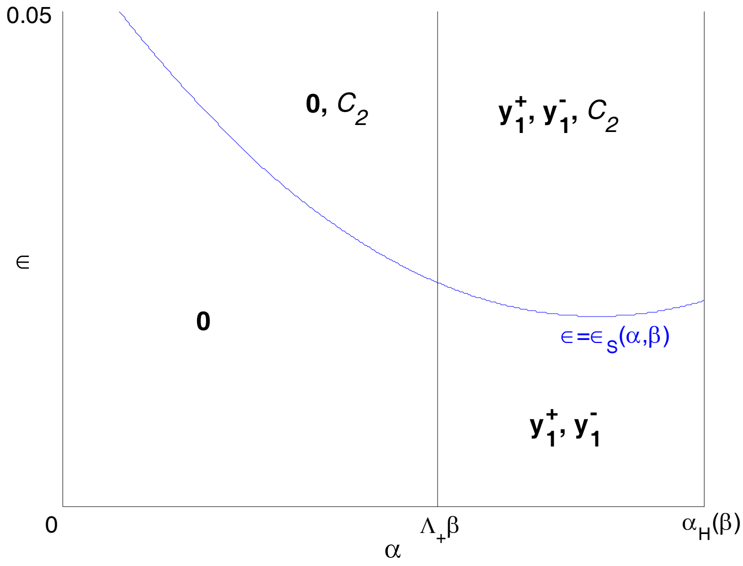

Figure 4-78: Bifurcations and attractors of the burster equations for $\beta_C < \beta < 2\beta'$, $0 < \alpha < \alpha_H(\beta)$, $0 < \epsilon < 0.05$.

4.8.3 The effect of increasing ϵ from 0 to 0.05 in $\beta_C < \beta < 2\beta'$, $0 < \alpha < \alpha_H(\beta)$

As mentioned above, numerics suggest that for a fixed β with $\beta_C < \beta < 2\beta'$, the surface of gluing bifurcations $\epsilon = \epsilon_G(\alpha, \beta)$ and the surface of type II H-bifurcations $\epsilon = \bar{\epsilon}_S(a, \beta)$ do not exist in $\alpha < \alpha_H(\beta)$, while the surface of type I H-bifurcations $\epsilon = \epsilon_S(\alpha, \beta)$ does exist in $\alpha < \alpha_H(\beta)$, with $\epsilon_S(\alpha, \beta)$ becoming unbounded as $\alpha \to 0+$. Assume that α and β are fixed with $\beta_C < \beta < 2\beta'$, $0 < \alpha < \Lambda_+\beta$. In this range, the attractor of the system is the origin $\mathbf{0}$ for ϵ small (cf. figure (4-45)). If $\epsilon_S(\alpha, \beta) > 0.05$, no bifurcation occurs as ϵ is increased from 0 to 0.05, while if $\epsilon_S(\alpha, \beta) < 0.05$, the type I H-bifurcation occurs, and so $\mathcal{C}_2$ coexists with $\mathbf{0}$ for $\epsilon_S(\alpha, \beta) < \epsilon < 0.05$. Now assume α and β are fixed with $\beta_C < \beta < 2\beta'$, $\Lambda_+\beta < \alpha < \alpha_H(\beta)$. In this range, the attractors of the system are the pair of symmetry-related nontrivial fixed points $\mathbf{y}_1^+$ and $\mathbf{y}_1^-$ for ϵ small (cf. figure (4-45) again). If $\epsilon_S(\alpha, \beta) > 0.05$, no bifurcation occurs as ϵ is increased from 0 to 0.05, while if $\epsilon_S(\alpha, \beta) < 0.05$, the type I H-bifurcation occurs, and so $\mathcal{C}_2$ coexists with $\mathbf{y}_1^+$ and $\mathbf{y}_1^-$ for $\epsilon_S(\alpha, \beta) < \epsilon < 0.05$. This discussion is summarised in figure (4-78).

4.9 Bifurcations and attractors for $\boldsymbol{\alpha} \in \hat{\Pi}_P$

The work of the previous section suggests the bifurcation diagram of the burster system for $\boldsymbol{\alpha}$ in the range $\hat{\Pi}_P$ defined by

$$\hat{\Pi}_P = \left\{\bar{\beta}_C < \beta < 2\beta', 0 < \alpha < 2.5\alpha', 0 < \epsilon < 0.05\right\}$$

given in figure (4-79) (cf. figures (4-61) and (4-78)). Also shown in this figure are the attractors of the system, and the corresponding modelled nystagmus waveforms, where applicable. $\hat{\Pi}_P$ contains the physiological range Π_P defined in (2.17). The bifurcation diagram has been split into sectors labelled A-J for future reference. In the following, these labels will be taken to represent the corresponding subsets of $\hat{\Pi}_P$ in $(\alpha, \beta, \epsilon)$ space. For example, A will be taken to represent the range:

$$\left\{\bar{\beta}_C < \beta < 2\beta', 0 < \alpha < \Lambda_+\beta, 0 < \epsilon < \min\left\{0.05, \epsilon_S\left(\alpha, \beta\right)\right\}\right\}$$

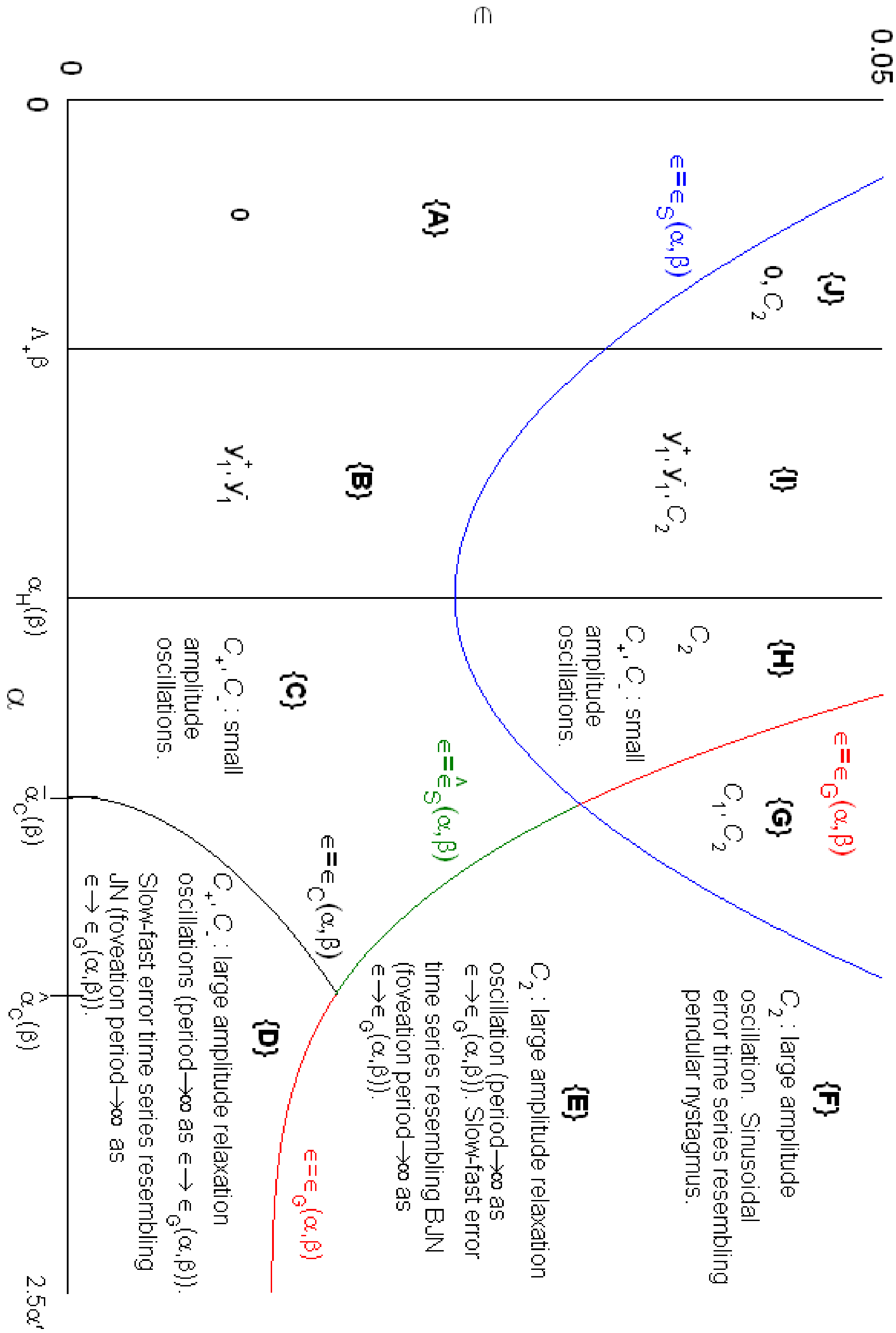

Figure 4-79: Bifurcations and attractors of the burster equations for $\boldsymbol{\alpha}$ in $\hat{\Pi}_P$. Here JN=jerk nystagmus and BJN=bilateral jerk nystagmus.

Chapter 5

Analysis of the saccadic equations

This chapter is an analysis of the saccadic equations $\dot{\mathbf{z}} = \mathbf{Z}(\mathbf{z})$. The results described here are based on knowledge of the behaviour of the burster equations $\dot{\mathbf{y}} = \mathbf{Y}(\mathbf{y})$ obtained in the previous two chapters.[1] The first part of this chapter is similar to the first part of chapter 3, examining the existence and uniqueness of solutions, symmetry and fixed points. It is then shown that there is a one-to-one correspondence between attractors of $\dot{\mathbf{y}} = \mathbf{Y}(\mathbf{y})$ and $\dot{\mathbf{z}} = \mathbf{Z}(\mathbf{z})$ for the parameter ranges considered in chapter 4, where the attractors of $\dot{\mathbf{y}} = \mathbf{Y}(\mathbf{y})$ were found to be stable fixed points and stable limit cycles. Next it is argued that the gluing bifurcation of the burster equations described in chapter 4 induces a gluing bifurcation in the full saccadic equations. Following this, Fourier analysis is used to approximate a relationship between the gaze and error time series associated with limit cycles of $\dot{\mathbf{z}} = \mathbf{Z}(\mathbf{z})$. The approximation is in turn used to describe the morphology of the gaze time series associated with stable limit cycles of $\dot{\mathbf{z}} = \mathbf{Z}(\mathbf{z})$ in the parameter range $\hat{\Pi}_P$. In particular, it is found that error time series resembling congenital nystagmus waveforms correspond to gaze time series resembling the same type of waveform. The chapter finishes with a suggested description of the attractors of $\dot{\mathbf{z}} = \mathbf{Z}(\mathbf{z})$ in the range $\hat{\Pi}_P$, analogous to that obtained in chapter 4 (cf. figure (4-79)).

During the analysis of the saccadic equations in this chapter, much use will be made of the projection operator $\pi : \mathbb{R}^6 \to \mathbb{R}^3$ defined through the 3×6 matrix:

[1] Recall that the equations $\frac{d\mathbf{y}}{d\tau} = \mathbf{X}(\mathbf{y})$ analysed in chapters 3 and 4 are obtained from $\dot{\mathbf{y}} = \mathbf{Y}(\mathbf{y})$ by setting $\tau = \frac{t}{\epsilon}$.

$$\pi = \begin{pmatrix} \mathbf{0}_{3\times 3} & \mathbf{1}_3 \end{pmatrix} \tag{5.1}$$

Clearly $\forall \mathbf{x}, \mathbf{y} \in \mathbb{R}^3$, $\pi(\mathbf{x}, \mathbf{y}) = \mathbf{y}$. It can be shown that π is linear, continuous and maps open sets of $\mathbb{R}^6$ to open sets of $\mathbb{R}^3$. Proofs are given in section A.2.1.

5.1 Vector field

Recall from chapter 2 that the vector field $\mathbf{Z} : \mathbb{R}^6 \to \mathbb{R}^6$ of the saccadic equations is defined by

$$\mathbf{Z}(\mathbf{z}) = \begin{pmatrix} A\mathbf{x}+B\mathbf{y} \\ \mathbf{Y}(\mathbf{y}) \end{pmatrix} \tag{5.2}$$

where

$$\mathbf{Y}(\mathbf{y}) = \frac{1}{\epsilon}\mathbf{X}(\mathbf{y}) = \begin{pmatrix} \frac{1}{\epsilon}\left(-r - \gamma r l^2 + F(\varepsilon)\right) \\ \frac{1}{\epsilon}\left(-l - \gamma l r^2 + F(-\varepsilon)\right) \\ -(r-l) \end{pmatrix} \tag{5.3}$$

and:

$$A = \begin{pmatrix} 0 & 1 & 0 \\ -P_2 & -P_1 & P_2 \\ 0 & 0 & -\frac{1}{T_N} \end{pmatrix} \tag{5.4}$$

$$B = \begin{pmatrix} 0 & 0 & 0 \\ P_1 & -P_1 & 0 \\ 1 & -1 & 0 \end{pmatrix} \tag{5.5}$$

$$P_1 = \frac{1}{T_1} + \frac{1}{T_2} \tag{5.6}$$

$$P_2 = \frac{1}{T_1 T_2} \tag{5.7}$$

(Here $\mathbf{x} = (g, v, n)^T$, $\mathbf{y} = (r, l, \varepsilon)^T$ and $\mathbf{z} = (\mathbf{x}, \mathbf{y})^T$ are the state vectors. Also, $P_1 = 90$ and $P_2 = 555\frac{5}{9}$). The saccadic equations $\dot{\mathbf{z}} = \mathbf{Z}(\mathbf{z})$ can thus be expressed as the skew product

$$\dot{\mathbf{x}} = A\mathbf{x}+B\mathbf{y} \tag{5.8}$$

$$\dot{\mathbf{y}} = \mathbf{Y}(\mathbf{y}) \tag{5.9}$$

where (5.8) are the plant equations. Written explicitly, the full saccadic equations are:

$$\dot{g} = v \tag{5.10}$$

$$\dot{v} = -P_1 v - P_2 g + P_2 n + P_1 (r-l) \tag{5.11}$$

$$\dot{n} = -\frac{1}{T_N} n + r - l \tag{5.12}$$

$$\dot{r} = \frac{1}{\epsilon}\left(-r - \gamma r l^2 + F(\varepsilon)\right) \tag{5.13}$$

$$\dot{l} = \frac{1}{\epsilon}\left(-l - \gamma l r^2 + F(-\varepsilon)\right) \tag{5.14}$$

$$\dot{\varepsilon} = -(r-l) \tag{5.15}$$

It should be noted that as $\mathbf{X}$ is continuous on $\mathbb{R}^3$, $\mathbf{Y}$ is continuous on $\mathbb{R}^3$ and so the form of $\mathbf{Z}$ implies that $\mathbf{Z}$ is continuous on $\mathbb{R}^6$. Also, as $\mathbf{X}(\mathbf{0}) = \mathbf{0}$ where $\mathbf{0} = (0,0,0)^T$, $\mathbf{Y}(\mathbf{0}) = \mathbf{0}$. Setting $\mathbf{x} = \mathbf{y} = \mathbf{0}$ in (5.2) therefore gives $\mathbf{Z}(\mathbf{0},\mathbf{0}) = (\mathbf{0},\mathbf{0})^T$. The origin $(\mathbf{0},\mathbf{0})^T = (0,0,0,0,0,0)^T$ is thus always a fixed point of the saccadic system $\dot{\mathbf{z}} = \mathbf{Z}(\mathbf{z})$. This fixed point corresponds to a gaze angle and gaze velocity equal to zero. i.e. to the eye being at rest in its natural resting position.

5.1.1 Smoothness of the vector field

It was established in section 3.1.1 that $\mathbf{X}$ is C^∞ on $\mathbb{R}^3\backslash P$ where $P \subset \mathbb{R}^3$ is the plane defined by $P = \left\{(r,l,\varepsilon)^T \in \mathbb{R}^3 :, r,l \in \mathbb{R}, \varepsilon = 0\right\}$. As $\mathbf{Y} = \frac{1}{\epsilon}\mathbf{X}$, $\mathbf{Y}$ is also C^∞ on $\mathbb{R}^3\backslash P$. Define the hyperplane $\hat{P} \subset \mathbb{R}^6$ by:

$$\hat{P} = \left\{(g,v,n,r,l,\varepsilon)^T \in \mathbb{R}^6 : g,v,n,r,l \in \mathbb{R}, \varepsilon = 0\right\} = \mathbb{R}^3 \times P$$

The form of $\mathbf{Z}$ then implies that $\mathbf{Z}$ is C^∞ on the set $\mathbb{R}^6\backslash\hat{P}$. $\mathbf{Z}$ is however not differentiable at $\hat{P}$ since, as was shown in section 3.1.1, F is not differentiable at 0. $\mathbf{Z}$ is therefore not smooth at $\hat{P}$, and so is a piecewise C^∞ function about $\hat{P}$. Note that $\pi\hat{P} = P$.

Smoothness of the vector field as a function of z and $\boldsymbol{\alpha}$

It can be seen from the form of the saccadic vector field $\mathbf{Z}$ that the dependence of $\mathbf{Z}$ on the parameter vector $\boldsymbol{\alpha}$ comes from the dependence of the burster vector field $\mathbf{Y}$ on $\boldsymbol{\alpha}$. When considered as a function of both $\mathbf{z}$ and $\boldsymbol{\alpha}$, $\mathbf{Z} : \mathbb{R}^6 \times \Pi \to \mathbb{R}^6$, $\mathbf{Z}(\mathbf{z};\boldsymbol{\alpha})$ can be written as below:

$$\mathbf{Z}(\mathbf{z};\boldsymbol{\alpha}) = \begin{pmatrix} A\mathbf{x}+B\mathbf{y} \\ \mathbf{Y}(\mathbf{y};\boldsymbol{\alpha}) \end{pmatrix}$$

It was shown in section 3.1.3 that $\mathbf{X}(\mathbf{y};\boldsymbol{\alpha})$ is C^∞ on $\mathbb{R}^3\backslash P \times \Pi$. Since $\mathbf{Y} = \frac{1}{\epsilon}\mathbf{X}$, it follows that $\mathbf{Y}(\mathbf{y};\boldsymbol{\alpha})$ is also C^∞ on $\mathbb{R}^3\backslash P \times \Pi$. The form of $\mathbf{Z}(\mathbf{z};\boldsymbol{\alpha})$ then implies that $\mathbf{Z}(\mathbf{z};\boldsymbol{\alpha})$ is C^∞ on $\mathbb{R}^6\backslash \hat{P} \times \Pi$.

5.1.2 Existence and uniqueness of solutions of the saccadic system

It can be shown that the vector field $\mathbf{Z}$ is locally Lipschitz. A proof is given in section A.2.2 of the appendix. Solutions of $\dot{\mathbf{z}} = \mathbf{Z}(\mathbf{z})$ therefore exist and are unique (cf. section 1.2). Additionally, solutions can be extended infinitely far forward in time. To show this, it is first necessary to establish some notation relating to solutions of the unscaled burster system $\dot{\mathbf{y}} = \mathbf{Y}(\mathbf{y})$. Given $\mathbf{y} \in \mathbb{R}^3$, the maximal open interval on which the unique solution $\mathbf{y}(t)$ of $\dot{\mathbf{y}} = \mathbf{Y}(\mathbf{y})$ with $\mathbf{y}(0) = \mathbf{y}$ exists will be written as $J_B(\mathbf{y})$. Also, the flow of $\dot{\mathbf{y}} = \mathbf{Y}(\mathbf{y})$ will be denoted by φ. The relation $\tau = \frac{t}{\epsilon}$ therefore implies that given $\mathbf{y} \in \mathbb{R}^3$, $J_B(\mathbf{y}) = \epsilon J(\mathbf{y})$ and $\varphi(\mathbf{y}{,}t) = \phi\left(\mathbf{y}, \frac{t}{\epsilon}\right)$ $\forall t \in J_B(\mathbf{y})$.

Returning to solutions of the saccadic system, for each $\mathbf{z} \in \mathbb{R}^6$, write $J_S(\mathbf{z})$ for the maximal open interval on which the unique solution $\mathbf{z}(t)$ of $\dot{\mathbf{z}} = \mathbf{Z}(\mathbf{z})$ with $\mathbf{z}(0) = \mathbf{z}$ exists. Further, denote the flow of $\dot{\mathbf{z}} = \mathbf{Z}(\mathbf{z})$ by ψ, the time set by $\hat{T}$, and the t set by $\hat{U}_t$ for each $t \in \hat{T}$. It is now shown that $\forall \mathbf{z} \in \mathbb{R}^6$, $J_S(\mathbf{z}) = J_B(\pi\mathbf{z})$. Since $[0,\infty) \subset J_B(\mathbf{y})$ $\forall \mathbf{y} \in \mathbb{R}^3$, this implies that solutions of $\dot{\mathbf{z}} = \mathbf{Z}(\mathbf{z})$ can be extended infinitely far forward in time. i.e. $[0,\infty) \subset J_S(\mathbf{z})$ $\forall \mathbf{z} \in \mathbb{R}^6$.

Let $\mathbf{z}_0 = (\mathbf{x}_0, \mathbf{y}_0)^T \in \mathbb{R}^6$, and define $\mathbf{y}_R(t)$ by $\mathbf{y}_R(t) = \varphi_t(\mathbf{y}_0)$ $\forall t \in J_B(\mathbf{y}_0)$. Then $\mathbf{y}_R(t)$ solves $\dot{\mathbf{y}} = \mathbf{Y}(\mathbf{y})$ on $J_B(\mathbf{y}_0)$ with $\mathbf{y}_R(0) = \mathbf{y}_0$. Now it can be shown that if $\mathbf{r}(t)$ is a C^1 function defined on some open interval (t_1, t_2) containing 0 (t_1 may be $-\infty$ and t_2 may be ∞), then the unique solution of the initial value problem $\{\dot{\mathbf{x}} = A\mathbf{x}+B\mathbf{r}(t) : \mathbf{x}(0) = \hat{\mathbf{x}}\}$ on

(t_1, t_2) is $\mathbf{x}_r(t)$, where $\forall t \in (t_1, t_2)$:

$$\mathbf{x}_r(t) = e^{At}\hat{\mathbf{x}} + \int_0^t e^{A(t-s)} B\mathbf{r}(s)\, ds$$

Moreover, there is a constant $P_C \geq 1$ such that $\forall t \in [0, t_2)$:

$$\|\mathbf{x}_r(t)\|_1 \leq P_C \left(e^{-\frac{t}{T_N}} \|\hat{\mathbf{x}}\|_1 + \int_0^t e^{-\frac{(t-s)}{T_N}} \|B\mathbf{r}(s)\|_1 \, ds \right)$$

A proof of this can be found in the appendix in section A.2.3. Since $\mathbf{y}_R(t)$ is C^1, this means that the function $\mathbf{x}_R(t)$ defined $\forall t \in J_B(\mathbf{y}_0)$ by

$$\mathbf{x}_R(t) = e^{At}\mathbf{x}_0 + \int_0^t e^{A(t-s)} B\mathbf{y}_R(s)\, ds$$

solves $\dot{\mathbf{x}} = A\mathbf{x} + B\mathbf{y}_R(t)$ on $J_B(\mathbf{y}_0)$ with $\mathbf{x}_R(0) = \mathbf{x}_0$. Also, as $[0, \infty) \subset J_B(\mathbf{y}_0)$, $\forall t \geq 0$:

$$\|\mathbf{x}_R(t)\|_1 \leq P_C \left(e^{-\frac{t}{T_N}} \|\mathbf{x}_0\|_1 + \int_0^t e^{-\frac{(t-s)}{T_N}} \|B\mathbf{y}_R(s)\|_1 \, ds \right)$$

Define $\mathbf{z}_R(t)$ by $\mathbf{z}_R(t) = (\mathbf{x}_R(t), \mathbf{y}_R(t))^T$ $\forall t \in J_B(\mathbf{y}_0)$. It then follows from the fact that the saccadic equations can be written as the skew product (5.8)-(5.9) that $\mathbf{z}_R(t)$ solves $\dot{\mathbf{z}} = \mathbf{Z}(\mathbf{z})$ on $J_B(\mathbf{y}_0)$ with $\mathbf{z}_R(t) = \mathbf{z}_0$. Hence $J_B(\mathbf{y}_0) \subseteq J_S(\mathbf{z}_0)$ and $\mathbf{z}_R(t) = \psi_t(\mathbf{z}_0)$ $\forall t \in J_B(\mathbf{y}_0)$. Extend $\mathbf{z}_R(t)$ to $J_S(\mathbf{z}_0)$ by setting $\mathbf{z}_R(t) = (\mathbf{x}_R(t), \mathbf{y}_R(t))^T = \psi_t(\mathbf{z}_0)$ $\forall t \in J_S(\mathbf{z}_0)$. The skew product form of $\dot{\mathbf{z}} = \mathbf{Z}(\mathbf{z})$ implies that $\mathbf{y}_R(t)$ solves $\dot{\mathbf{y}} = \mathbf{Y}(\mathbf{y})$ on $J_S(\mathbf{z}_0)$ with $\mathbf{y}_R(0) = \mathbf{y}_0$. Hence $J_S(\mathbf{z}_0) \subseteq J_B(\mathbf{y}_0)$ and so $J_B(\mathbf{y}_0) = J_S(\mathbf{z}_0)$. This holds for each $\mathbf{z}_0 = (\mathbf{x}_0, \mathbf{y}_0)^T \in \mathbb{R}^6$, showing that $J_S(\mathbf{z}) = J_B(\pi\mathbf{z})$ $\forall \mathbf{z} \in \mathbb{R}^6$, as claimed.

Using the analysis of the saccadic system thus far, the following facts can be easily established:

1. ψ is continuous.

2. $\hat{T} = \mathbb{R}$.

3. $\forall t \in \mathbb{R}$, $\hat{U}_t = \mathbb{R}^3 \times U_{\frac{t}{\epsilon}}$ and $\psi_t : \hat{U}_t \to \psi_t\left(\hat{U}_t\right)$ is a homeomorphism with $\psi_t^{-1} = \psi_{-t}$.

4. $\forall t \geq 0$, $\hat{U}_t = \mathbb{R}^6$.

5. For $\mathbf{z} \in \mathbb{R}^6$ and $t_1, t_2 \in \mathbb{R}$ such that $\psi_{t_2}(\mathbf{z}), \psi_{t_1}\left(\psi_{t_2}(\mathbf{z})\right)$ and $\psi_{t_1+t_2}(\mathbf{z})$ all exist, $\psi_{t_1}\left(\psi_{t_2}(\mathbf{z})\right) = \psi_{t_1+t_2}(\mathbf{z})$. In particular, given $\mathbf{z} \in \mathbb{R}^6$, $\psi_{t_1}\left(\psi_{t_2}(\mathbf{z})\right) = \psi_{t_1+t_2}(\mathbf{z})$ $\forall t_1, t_2 \geq 0$.

6. If $\mathbf{z}(t)$ is a solution of $\dot{\mathbf{z}} = \mathbf{Z}(\mathbf{z})$, $\mathbf{z}(t)$ is C^1 on $J_B(\pi\mathbf{z}(0))$.

7. Given $t \in \mathbb{R}$ and $\mathbf{z} = (\mathbf{x}, \mathbf{y})^T \in \hat{U}_t$, $\psi_t(\mathbf{z})$ is defined by

$$\psi_t(\mathbf{z}) = \begin{pmatrix} L_t(\mathbf{x}, \mathbf{y}) \\ \varphi_t(\mathbf{y}) \end{pmatrix} \tag{5.16}$$

where:

$$L_t(\mathbf{x}, \mathbf{y}) = e^{At}\mathbf{x} + \int_0^t e^{A(t-s)} B\varphi_s(\mathbf{y})\, ds \tag{5.17}$$

Also, given $\mathbf{z} = (\mathbf{x}, \mathbf{y})^T \in \mathbb{R}^6$, $\forall t \geq 0$:

$$\|L_t(\mathbf{x}, \mathbf{y})\|_1 \leq P_C\left(e^{-\frac{t}{T_N}} \|\mathbf{x}\|_1 + \int_0^t e^{-\frac{(t-s)}{T_N}} \|B\varphi_s(\mathbf{y})\|_1\, ds\right) \tag{5.18}$$

The form of ψ_t implies that for each $t \in \mathbb{R}$, $\pi \circ \psi_t(\mathbf{z}) = \varphi_t \circ \pi(\mathbf{z})$ $\forall \mathbf{z} \in \hat{U}_t$ (or equivalently for each $\mathbf{z} \in \mathbb{R}^6$, $\pi \circ \psi_t(\mathbf{z}) = \varphi_t \circ \pi(\mathbf{z})$ $\forall t \in J_B(\pi\mathbf{z})$). The projection operator π thus semi-conjugates the time t maps of $\dot{\mathbf{z}} = \mathbf{Z}(\mathbf{z})$ and $\dot{\mathbf{y}} = \mathbf{Y}(\mathbf{y})$. In particular:

$$\pi \circ \psi_t = \varphi_t \circ \pi : t \geq 0 \tag{5.19}$$

5.1.3 C^∞ extensions of the vector field

Define the sets $\hat{N}_+, \hat{N}_- \subset \mathbb{R}^6$ by:

$$\begin{aligned} \hat{N}_+ &= \left\{(g, v, n, r, l, \varepsilon)^T \in \mathbb{R}^6 : g, v, n, r, l \in \mathbb{R}, \varepsilon \geq 0\right\} = \mathbb{R}^3 \times N_+ && (5.20) \\ \hat{N}_- &= \left\{(g, v, n, r, l, \varepsilon)^T \in \mathbb{R}^6 : g, v, n, r, l \in \mathbb{R}, \varepsilon \leq 0\right\} = \mathbb{R}^3 \times N_- && (5.21) \end{aligned}$$

Then $\mathbb{R}^6 = \hat{N}_+ \cup \hat{N}_-$ and $\hat{N}_+ \cap \hat{N}_- = \hat{P}$. Also $\pi\hat{N}_\pm = N_\pm$. It will be useful in the analysis of the saccadic system to extend $\mathbf{Z}|_{\hat{N}_+}$ out into $\hat{N}_-$ and $\mathbf{Z}|_{\hat{N}_-}$ out into $\hat{N}_+$ in such a way as to generate two C^∞ vector fields $\mathbf{Z}_+$ and $\mathbf{Z}_-$ which agree with $\mathbf{Z}$ in $\hat{N}_+$ and $\hat{N}_-$ respectively. This can be done easily by using the extended vector fields $\mathbf{X}_+, \mathbf{X}_- : \mathbb{R}^3 \to \mathbb{R}^3$. Define $\mathbf{Z}_+, \mathbf{Z}_- : \mathbb{R}^6 \to \mathbb{R}^6$ by

$$\mathbf{Z}_+(\mathbf{z}) = \begin{pmatrix} A\mathbf{x} + B\mathbf{y} \\ \mathbf{Y}_+(\mathbf{y}) \end{pmatrix} \tag{5.22}$$

$$\mathbf{Z}_-(\mathbf{z}) = \begin{pmatrix} A\mathbf{x} + B\mathbf{y} \\ \mathbf{Y}_-(\mathbf{y}) \end{pmatrix} \tag{5.23}$$

where $\mathbf{Y}_\pm(\mathbf{y}) = \frac{1}{\epsilon}\mathbf{X}_\pm(\mathbf{y})$. The relation $\mathbf{X}|_{N_\pm} = \mathbf{X}_\pm|_{N_\pm}$ implies $\mathbf{Y}|_{N_\pm} = \mathbf{Y}_\pm|_{N_\pm}$. Let $\mathbf{z} = (\mathbf{x},\mathbf{y})^T \in \hat{N}_+$. Then $\mathbf{y} \in N_+$ and so $\mathbf{Z}(\mathbf{z}) = (A\mathbf{x} + B\mathbf{y}, \mathbf{Y}(\mathbf{y}))^T = (A\mathbf{x} + B\mathbf{y}, \mathbf{Y}_+(\mathbf{y}))^T = \mathbf{Z}_+(\mathbf{z})$. This holds $\forall \mathbf{z} \in \hat{N}_+$, and so $\mathbf{Z}|_{\hat{N}_+} = \mathbf{Z}_+|_{\hat{N}_+}$. A similar argument implies that $\mathbf{Z}|_{\hat{N}_-} = \mathbf{Z}_-|_{\hat{N}_-}$. As $\mathbf{X}_\pm$ is C^∞ on $\mathbb{R}^3$, $\mathbf{Y}_\pm$ is C^∞ on $\mathbb{R}^3$. The form of $\mathbf{Z}_\pm$ therefore implies that $\mathbf{Z}_\pm$ is C^∞ on $\mathbb{R}^6$.

Smoothness of the extended vector fields as functions of y and $\boldsymbol{\alpha}$

Equations (5.22) and (5.23) show that the dependence of the extended saccadic vector field $\mathbf{Z}_\pm$ on the parameter vector $\boldsymbol{\alpha}$ comes from the dependence of the extended burster vector field $\mathbf{Y}_\pm$ on $\boldsymbol{\alpha}$. When considered as a function of both $\mathbf{z}$ and $\boldsymbol{\alpha}$, $\mathbf{Z}_\pm : \mathbb{R}^6 \times \Pi \to \mathbb{R}^6$, $\mathbf{Z}_\pm(\mathbf{z};\boldsymbol{\alpha})$ can be written as below:

$$\mathbf{Z}_\pm(\mathbf{z};\boldsymbol{\alpha}) = \begin{pmatrix} A\mathbf{x}+B\mathbf{y} \\ \mathbf{Y}_\pm(\mathbf{y};\boldsymbol{\alpha}) \end{pmatrix}$$

Recall from section 3.1.3 that $\mathbf{X}_\pm(\mathbf{y};\boldsymbol{\alpha})$ is C^∞ on $\mathbb{R}^3 \times \Pi$. Since $\mathbf{Y}_\pm = \frac{1}{\epsilon}\mathbf{X}_\pm$, it follows that $\mathbf{Y}_\pm(\mathbf{y};\boldsymbol{\alpha})$ is also C^∞ on $\mathbb{R}^3 \times \Pi$. The form of $\mathbf{Z}_\pm(\mathbf{z};\boldsymbol{\alpha})$ then implies that $\mathbf{Z}_\pm(\mathbf{z};\boldsymbol{\alpha})$ is C^∞ on $\mathbb{R}^6 \times \Pi$.

5.1.4 Existence and uniqueness of solutions of the extended systems $\dot{\mathbf{z}} = \mathbf{Z}_+(\mathbf{z})$ and $\dot{\mathbf{z}} = \mathbf{Z}_-(\mathbf{y})$

As the extended vector field $\mathbf{Z}_\pm$ is C^∞, it is Lipschitz, and so solutions of $\dot{\mathbf{z}} = \mathbf{Z}_\pm(\mathbf{z})$ exist and are unique (cf. section 1.2.1). Given $\mathbf{z} \in \mathbb{R}^6$, denote the maximal open interval on which the unique solution $\mathbf{z}_\pm(t)$ of $\dot{\mathbf{z}} = \mathbf{Z}_\pm(\mathbf{z})$ with $\mathbf{z}_\pm(0) = \mathbf{z}$ exists by $J_S^\pm(\mathbf{z})$. Additionally, denote the flow of $\dot{\mathbf{z}} = \mathbf{Z}_\pm(\mathbf{z})$ by $\psi^\pm$, the time set by $\hat{T}_\pm$ and the t set by $\hat{U}_t^\pm$ for each $t \in \hat{T}_\pm$. Rescaling time in the extended burster system $\dot{\mathbf{y}} = \mathbf{Y}_\pm(\mathbf{y})$ via $\tau = \frac{t}{\epsilon}$ gives the system $\frac{d\mathbf{y}}{d\tau} = \mathbf{X}_{\pm}(\mathbf{y})$ discussed in section 3.1.4. Given $\mathbf{y} \in \mathbb{R}^3$, write the maximal open interval on which the unique solution $\mathbf{y}(t)$ of $\dot{\mathbf{y}} = \mathbf{Y}_{\pm}(\mathbf{y})$ with $\mathbf{y}(0) = \mathbf{y}$ exists as $J_B^{\pm}(\mathbf{y})$. Also, denote the flow of $\dot{\mathbf{y}} = \mathbf{Y}_{\pm}(\mathbf{y})$ by $\varphi^{\pm}$. The relation $\tau = \frac{t}{\epsilon}$ therefore implies that given $\mathbf{y} \in \mathbb{R}^3$, $J_B^{\pm}(\mathbf{y}) = \epsilon J_{\pm}(\mathbf{y})$ and $\varphi^{\pm}(\mathbf{y},t) = \phi^{\pm}\left(\mathbf{y}, \frac{t}{\epsilon}\right)$ $\forall t \in J_B^{\pm}(\mathbf{y})$. Similar arguments to those used in the discussion of the existence and uniqueness of solutions of $\dot{\mathbf{z}} = \mathbf{Z}(\mathbf{z})$ together with the fact that $\mathbf{Z}_{\pm}$ is C^{∞} on $\mathbb{R}^6$ and $T_{\pm} = \mathbb{R}$ then allow the following facts to be established:

1. $\forall \mathbf{z} \in \mathbb{R}^6$, $J_S^{\pm}(\mathbf{z}) = J_B^{\pm}(\pi\mathbf{z})$.

2. $\psi^{\pm}$ is C^{∞}.

3. $\hat{T}_{\pm} = \mathbb{R}$.

4. For each $t \in \hat{T}_{\pm}$, $\hat{U}_t^{\pm} = \mathbb{R}^3 \times U_{\frac{t}{\epsilon}}^{\pm}$ and $\psi_t^{\pm} : U_t^{\pm} \to \psi_t^{\pm}\left(U_t^{\pm}\right)$ is a C^{∞} diffeomorphism with $\left(\psi_t^{\pm}\right)^{-1} = \psi_{-t}^{\pm}$.

5. Given $t \in \hat{T}_{\pm}$ and $\mathbf{z} = (\mathbf{x}, \mathbf{y})^T \in \hat{U}_t^{\pm}$, $\psi_t^{\pm}(\mathbf{z})$ is defined by

$$\psi_t^{\pm}(\mathbf{z}) = \begin{pmatrix} L_t^{\pm}(\mathbf{x}, \mathbf{y}) \\ \varphi_t^{\pm}(\mathbf{y}) \end{pmatrix} \tag{5.24}$$

where:

$$L_t^{\pm}(\mathbf{x}, \mathbf{y}) = e^{At}\mathbf{x} + \int_0^t e^{A(t-s)} B\varphi_s^{\pm}(\mathbf{y})\, ds \tag{5.25}$$

Also, given $\mathbf{z} = (\mathbf{x}, \mathbf{y})^T \in \mathbb{R}^6$, $\forall t \in J_S^{\pm}(\mathbf{z}) \cap [0, \infty)$:

$$\left\|L_t^{\pm}(\mathbf{x}, \mathbf{y})\right\|_1 \le P_C \left(e^{-\frac{t}{T_N}} \|\mathbf{x}\|_1 + \int_0^t e^{-\frac{(t-s)}{T_N}} \left\|B\varphi_s^{\pm}(\mathbf{y})\right\|_1 ds\right) \tag{5.26}$$

6. For $\mathbf{z} \in \mathbb{R}^6$ and $t_1, t_2 \in \mathbb{R}$ such that $\psi_{t_2}^{\pm}(\mathbf{z}), \psi_{t_1}^{\pm}\left(\psi_{t_2}^{\pm}(\mathbf{z})\right)$ and $\psi_{t_1+t_2}^{\pm}(\mathbf{z})$ all exist, $\psi_{t_1}^{\pm}\left(\psi_{t_2}^{\pm}(\mathbf{z})\right) = \psi_{t_1+t_2}^{\pm}(\mathbf{z})$.

The form of $\psi_t^{\pm}$ implies that for each $t \in T_{\pm}$, $\pi \circ \psi_t^{\pm}(\mathbf{z}) = \varphi_t^{\pm} \circ \pi(\mathbf{z})$ $\forall \mathbf{z} \in \hat{U}_t^{\pm}$ (or equivalently, for each $\mathbf{z} \in \mathbb{R}^6$, $\pi \circ \psi_t^{\pm}(\mathbf{z}) = \varphi_t^{\pm} \circ \pi(\mathbf{z})$ $\forall t \in J_S^{\pm}(\mathbf{z})$). The projection operator π thus semi-conjugates the time t maps of $\dot{\mathbf{z}} = \mathbf{Z}_{\pm}(\mathbf{z})$ and $\dot{\mathbf{y}} = \mathbf{Y}_{\pm}(\mathbf{y})$. Also, note that $\mathbf{Z}_{\pm}(\mathbf{0}, \mathbf{0}) = (\mathbf{0}, \mathbf{0})^T$ and so the origin $(\mathbf{0}, \mathbf{0})^T$ is a fixed point of $\dot{\mathbf{z}} = \mathbf{Z}_{\pm}(\mathbf{z})$.

The relation between the vector fields $\mathbf{Z}_{\pm}$ and $\mathbf{Z}$ can be translated into a relation between the associated flows $\psi_t^{\pm}$ and ψ_t. Using a similar argument to that at the end of section 3.1.4, it can be shown that if $\mathbf{z} \in \mathbb{R}^6$ such that $(t_1, t_2) \subseteq J_S(\mathbf{z})$ with $\psi_t(\mathbf{z}) \in \hat{N}_{\pm}$ $\forall t \in (t_1, t_2)$, then $(t_1, t_2) \subseteq J_S^{\pm}(\mathbf{z})$ with $\psi_t^{\pm}(\mathbf{z}) = \psi_t(\mathbf{z})$ $\forall t \in (t_1, t_2)$.

5.2 Physiological state space and attractors

The state space of the saccadic system $\dot{\mathbf{z}} = \mathbf{Z}(\mathbf{z})$ is $\mathbb{R}^6$. However, since r and l are nonnegative quantities, all biologically feasible trajectories of $\dot{\mathbf{z}} = \mathbf{Z}(\mathbf{z})$ must be confined to the set $\hat{S} \subset \mathbb{R}^6$ defined by

$$\hat{S} = \mathbb{R}^3 \times S$$

where

$$S = \left\{ (r, l, \varepsilon)^T \in \mathbb{R}^3 : r, l \geq 0, \varepsilon \in \mathbb{R} \right\}$$

is the physiological state space of the burster system $\dot{\mathbf{y}} = \mathbf{Y}(\mathbf{y})$ introduced in section 3.2 (cf. 3.18). $\hat{S}$ will be referred to as the physiological state space of the saccadic system. As S is a positively invariant set of $\dot{\mathbf{y}} = \mathbf{Y}(\mathbf{y})$, $\hat{S}$ is a positively invariant set of the saccadic system. Hence, since the trajectories of interest have initial conditions of the form $(g(0), 0, 0, 0, 0, \Delta g)^T$, these are confined to $\hat{S}$ for all $t \geq 0$. This limits the possibility of biologically unrealistic behaviour in the saccadic equations.

Recall from section 3.2 that-by assumption-all trajectories of the burster system $\dot{\mathbf{y}} = \mathbf{Y}(\mathbf{y})$ are eventually confined to a compact set $C = C(\boldsymbol{\alpha}) \subset S$ of the form:

$$C = \left\{ (r, l, \varepsilon)^T \in \mathbb{R}^3 : 0 \leq r, l \leq \alpha_M, |\varepsilon| \leq \varepsilon_M \right\} \tag{5.27}$$

(cf. (3.19)). It is possible to show that this implies the existence of an $M_{\bar{\varepsilon}} = M_{\bar{\varepsilon}}(\boldsymbol{\alpha}) > 0$, such that all trajectories of the saccadic system $\dot{\mathbf{z}} = \mathbf{Z}(\mathbf{z})$ are eventually confined to the compact set $\hat{C} = \hat{C}(\boldsymbol{\alpha}) \subset \hat{S}$, defined by

$$\hat{C} = \bar{B}_{M_{\bar{\varepsilon}}}(\mathbf{0}) \times C$$

where:

$$\bar{B}_{M_{\bar{\varepsilon}}}(\mathbf{0}) = \left\{\mathbf{x} \in \mathbb{R}^3 : \|\mathbf{x}\|_1 \leq M_{\bar{\varepsilon}}\right\}$$

A proof of this can be found in the appendix in section A.2.4. Since solutions of the saccadic system $\dot{\mathbf{z}} = \mathbf{Z}(\mathbf{z})$ can be extended infinitely forward in time, and are by assumption eventually confined to the compact subset $\hat{C}$ of the state space $\mathbb{R}^6$, $\dot{\mathbf{z}} = \mathbf{Z}(\mathbf{z})$ is eventually compact. Given $\mathbf{z} \in \mathbb{R}^6$, denote the ω-limit set of $\mathbf{z}$ in $\dot{\mathbf{z}} = \mathbf{Z}(\mathbf{z})$ by $\omega(\mathbf{z})$. Then as discussed in section 1.2.4, there is an index set I_S and a set of points $\left\{\mathbf{z}_i = (\mathbf{x}_i, \mathbf{y}_i)^T : i \in I_S\right\}$ in $\mathbb{R}^6$ such that $\mathbb{R}^6$ can be written as the disjoint union $\bigcup_{i \in I_S} [\mathbf{z}_i]$, and the ω-limit sets as the distinct collection $\{\omega(\mathbf{z}_i) : i \in I_S\}$ where for each $i \in I_S$:

$$[\mathbf{z}_i] = \left\{\mathbf{z} \in \mathbb{R}^6 : \omega(\mathbf{z}) = \omega(\mathbf{z}_i)\right\}$$

Moreover, $\forall i \in I_S$, $\omega(\mathbf{z}_i)$ is a compact, invariant set lying in $\hat{C}$ such that all points in $[\mathbf{z}_i]$ converge to $\omega(\mathbf{z}_i)$ as $t \to \infty$. Conveniently, I_S can be chosen to be equal to I_B, where I_B is the index set of the ω-limit sets of the burster equations $\dot{\mathbf{y}} = \mathbf{Y}(\mathbf{y})$, as will now be demonstrated.

It can be shown that given $\mathbf{y} \in \mathbb{R}^3$, $\omega\left((\mathbf{x}_1, \mathbf{y})^T\right) = \omega\left((\mathbf{x}_2, \mathbf{y})^T\right)$ $\forall \mathbf{x}_1, \mathbf{x}_2 \in \mathbb{R}^3$. Consequently, for each $i \in J_S$, $[\mathbf{z}_i] = \left[(\mathbf{0}, \mathbf{y}_i)^T\right]$. $\mathbb{R}^6$ can therefore be written as the disjoint union $\bigcup_{i \in I_S}\left[(\mathbf{0}, \mathbf{y}_i)^T\right]$, and the ω-limit sets as the distinct collection $\left\{\omega\left((\mathbf{0}, \mathbf{y}_i)^T\right) : i \in I_S\right\}$. It can also be proven that $\pi\omega(\mathbf{z}) = \omega(\pi\mathbf{z})$ $\forall \mathbf{z} \in \mathbb{R}^6$. This in turn can be used to demonstrate that given $i_1, i_2 \in I_B$, $\left[(\mathbf{0}, \mathbf{y}_{i_1})^T\right] \cap \left[(\mathbf{0}, \mathbf{y}_{i_2})^T\right] = \phi$ if $i_1 \neq i_2$. The latter implies that I_S can be chosen so that $I_B \subseteq I_S$. Choose such an I_S. Then it can be shown that $\forall i \in I_S$, $\left[(\mathbf{0}, \mathbf{y}_i)^T\right] = \mathbb{R}^3 \times [\mathbf{y}_i]$. Thus, $\left[(\mathbf{0}, \mathbf{y}_i)^T\right] = \mathbb{R}^3 \times [\mathbf{y}_i]$ $\forall i \in I_B$ and so:

$$\bigcup_{i \in I_B}\left[(\mathbf{0}, \mathbf{y}_i)^T\right] = \bigcup_{i \in I_B} \mathbb{R}^3 \times [\mathbf{y}_i] = \mathbb{R}^3 \times \bigcup_{i \in I_B} [\mathbf{y}_i] = \mathbb{R}^3 \times \mathbb{R}^3 = \mathbb{R}^6$$

Since $\mathbb{R}^6 = \bigcup_{i \in I_S}\left[(\mathbf{0}, \mathbf{y}_i)^T\right]$ is a disjoint union, this implies $I_S = I_B$, as claimed.

In conclusion, $\mathbb{R}^6$ can be written as the disjoint union $\bigcup_{i \in I_B}\left[(\mathbf{0}, \mathbf{y}_i)^T\right]$, and the ω-limit sets as the distinct collection $\left\{\omega\left((\mathbf{0}, \mathbf{y}_i)^T\right) : i \in I_B\right\}$, where for each $i \in I_B$:

$$\left[(\mathbf{0}, \mathbf{y}_i)^T\right] = \mathbb{R}^3 \times [\mathbf{y}_i]$$

Moreover, since $\pi\omega\left(\left(\mathbf{0},\mathbf{y}_i\right)^T\right) = \omega\left(\mathbf{y}_i\right)\ \forall i \in I_B$, the projection operator π provides a bijection from the set of ω-limit sets of the saccadic system $\dot{\mathbf{z}} = \mathbf{Z}\left(\mathbf{z}\right)$ to the set of ω-limit sets of the burster system $\dot{\mathbf{y}} = \mathbf{Y}\left(\mathbf{y}\right)$.

Note that since the ω-limit sets of $\dot{\mathbf{z}} = \mathbf{Z}\left(\mathbf{z}\right)$ all lie in $\hat{C}$, they must all lie in $\hat{S}$. Thus all fixed points, limit cycles and attractors of the saccadic equations lie in the physiological state space.

Using the results concerning the ω-limit sets of the saccadic system that have been stated so far, it is straightforward to prove that if $\hat{\mathcal{A}} = \omega\left(\left(\mathbf{0},\mathbf{y}_i\right)^T\right)$ is an attractor of $\dot{\mathbf{z}} = \mathbf{Z}\left(\mathbf{z}\right)$ then $\pi\hat{\mathcal{A}} = \omega\left(\mathbf{y}_i\right)$ is an attractor of $\dot{\mathbf{y}} = \mathbf{Y}\left(\mathbf{y}\right)$. The proof of this and the other results stated here without proof can be found in section A.2.5 of the appendix.

5.3 Symmetry

Recall from section 3.3 that the map $\sigma : \mathbb{R}^3 \to \mathbb{R}^3$ defined through the 3×3 matrix

$$\sigma = \begin{pmatrix} 0 & 1 & 0 \\ 1 & 0 & 0 \\ 0 & 0 & -1 \end{pmatrix}$$

is a symmetry of the rescaled burster system vector field $\mathbf{X}$. The equivalence of the solutions of $\frac{d\mathbf{y}}{d\tau} = \mathbf{X}\left(\mathbf{y}\right)$ and $\dot{\mathbf{y}} = \mathbf{Y}\left(\mathbf{y}\right)$ under the rescaling of time $\tau \to t$ implies that σ is also a symmetry of the vector field $\mathbf{Y}$. This symmetry can be regarded as a consequence of a corresponding symmetry of the saccadic vector field $\mathbf{Z}$. Define the map $\Sigma : \mathbb{R}^6 \to \mathbb{R}^6$ through the 6×6 matrix below:

$$\Sigma = \begin{pmatrix} -\mathbf{1}_3 & \mathbf{0}_{3\times 3} \\ \mathbf{0}_{3\times 3} & \sigma \end{pmatrix} \tag{5.28}$$

Note that the form of Σ implies $\pi \circ \Sigma = \sigma \circ \pi$. Given $\mathbf{z} = \left(\mathbf{x},\mathbf{y}\right)^T \in \mathbb{R}^6$, $\Sigma\mathbf{z} = \left(-\mathbf{x},\sigma\mathbf{y}\right)^T$. Hence, by (5.2):

$$\mathbf{Z}\left(\Sigma\mathbf{z}\right) = \mathbf{Z}\left(-\mathbf{x},\sigma\mathbf{y}\right) = \begin{pmatrix} -A\mathbf{x} + B\sigma\mathbf{y} \\ \mathbf{Y}\left(\sigma\mathbf{y}\right) \end{pmatrix} \tag{5.29}$$

It was shown in section 3.3 that $\mathbf{X} \circ \sigma = \sigma \circ \mathbf{X}$. Thus, since $\mathbf{Y}(\mathbf{y}) = \frac{1}{\epsilon}\mathbf{X}(\mathbf{y})$, $\mathbf{Y} \circ \sigma = \sigma \circ \mathbf{Y}$. Also, by (5.5):

$$B\sigma = \begin{pmatrix} 0 & 0 & 0 \\ P_1 & -P_1 & 0 \\ 1 & -1 & 0 \end{pmatrix} \begin{pmatrix} 0 & 1 & 0 \\ 1 & 0 & 0 \\ 0 & 0 & -1 \end{pmatrix} = \begin{pmatrix} 0 & 0 & 0 \\ -P_1 & P_1 & 0 \\ -1 & 1 & 0 \end{pmatrix} = -B$$

Setting $\mathbf{Y}(\sigma\mathbf{y}) = \sigma\mathbf{Y}(\mathbf{y})$ and $B\sigma = -B$ in (5.29) gives:

$$\mathbf{Z}(\Sigma\mathbf{z}) = \begin{pmatrix} -(A\mathbf{x} + B\mathbf{y}) \\ \sigma\mathbf{Y}(\mathbf{y}) \end{pmatrix} = \Sigma\mathbf{Z}(\mathbf{z})$$

This holds $\forall \mathbf{z} \in \mathbb{R}^6$, and so:

$$\mathbf{Z} \circ \Sigma = \Sigma \circ \mathbf{Z} \tag{5.30}$$

Σ thus conjugates the vector field $\mathbf{Z}$. Also, as $\sigma^2 = \mathbf{1}_3$, $\Sigma^2 = \mathbf{1}_6$. A similar argument to that which showed σ is a symmetry of $\mathbf{X}$ in section 3.3 therefore implies that Σ is a symmetry of $\mathbf{Z}$. Moreover, since $\Sigma^2 = \mathbf{1}_6$, the symmetry group G_Σ generated by Σ is $G_\Sigma = \{\mathbf{1}_6, \Sigma\}$, which is isomorphic to $\mathbb{Z}_2$. The symmetry of $\mathbf{Z}$ under Σ simplifies the analysis of the saccadic equations. In particular since $\dot{\mathbf{z}} = \mathbf{Z}(\mathbf{z})$ is eventually compact, the discussion at the end of section 1.2.5 implies that $\dot{\mathbf{z}} = \mathbf{Z}(\mathbf{z})$ has the following properties:

1. $\forall t \geq 0$

$$\psi_t \circ \Sigma = \Sigma \circ \psi_t : t \geq 0 \tag{5.31}$$

2. $\forall i \in I_B$, $\Sigma\omega\left((0, \mathbf{y}_i)^T\right) = \omega\left(\Sigma(0, \mathbf{y}_i)^T\right)$ and $\left[\Sigma(0, \mathbf{y}_i)^T\right] = \Sigma\left[(0, \mathbf{y}_i)^T\right]$.

3. $\bar{\mathbf{z}}$ is a fixed point of $\dot{\mathbf{z}} = \mathbf{Z}(\mathbf{z})$ iff $\Sigma\bar{\mathbf{z}}$ is a fixed point. Also, $\bar{\mathbf{z}}$ is stable iff $\Sigma\bar{\mathbf{z}}$ is stable, while $\bar{\mathbf{z}}$ is unstable iff $\Sigma\bar{\mathbf{z}}$ is unstable.

4. $\hat{\mathcal{C}}$ is a limit cycle of $\dot{\mathbf{z}} = \mathbf{Z}(\mathbf{z})$ of period T iff $\Sigma\hat{\mathcal{C}}$ is a limit cycle of period T. Also, $\hat{\mathcal{C}}$ is stable iff $\Sigma\hat{\mathcal{C}}$ is stable and $\hat{\mathcal{C}}$ is unstable iff $\Sigma\hat{\mathcal{C}}$ is unstable.

5. $\hat{\mathcal{A}} = \omega\left((0, \mathbf{y}_i)^T\right)$ is an attractor of $\dot{\mathbf{z}} = \mathbf{Z}(\mathbf{z})$ with basin of attraction $\mathcal{B}\left(\hat{\mathcal{A}}\right)$ iff $\Sigma\left(\hat{\mathcal{A}}\right) = \omega\left(\Sigma(0, \mathbf{y}_i)^T\right)$ is an attractor with basin of attraction $\Sigma\left(\mathcal{B}\left(\hat{\mathcal{A}}\right)\right)$.

6. The set $\hat{F}(\Sigma)$ defined by

$$\hat{F}(\Sigma) = \left\{\mathbf{z} \in \mathbb{R}^6 : \Sigma\mathbf{z} = \mathbf{z}\right\}$$

is positively invariant.

(cf. the similar list in section 3.3). Properties 3-5 imply fixed points, limit cycles and attractors of $\dot{\mathbf{z}} = \mathbf{Z}(\mathbf{z})$ are either symmetry invariant, or come in symmetry-related pairs. Explicitly, the positively invariant set $\hat{F}(\Sigma)$ is given by

$$\hat{F}(\Sigma) = \left\{(x, y, z, r, l, \varepsilon)^T : (-x, -y, -z, l, r, -\varepsilon)^T = (x, y, z, r, l, \varepsilon)^T\right\}$$

from which it follows that $\hat{F}(\Sigma)$ is the line $\hat{L}_0$ where:

$$\hat{L}_0 = \{(0, 0, 0, x, x, 0)^T : x \in \mathbb{R}\} \tag{5.32}$$

Thus, $\hat{L}_0 = \mathbf{0} \times L_0$ where L_0 is the stable invariant line of $\mathbf{0}$ in $\dot{\mathbf{y}} = \mathbf{Y}(\mathbf{y})$. On $\hat{L}_0$ the dynamics are described by:

$$\dot{x} = -\frac{1}{\epsilon}(1 + \gamma x^2)x \tag{5.33}$$

The system (5.33) has the unique fixed point $x = 0$. Additionally, $\dot{x} > 0$ for $x < 0$ and $\dot{x} < 0$ for $x > 0$ and so $x = 0$ is globally attracting. In terms of the full system $\dot{\mathbf{z}} = \mathbf{Z}(\mathbf{z})$, it can be concluded that $\hat{L}_0$ is a stable 1-dimensional manifold of the origin $(\mathbf{0}, \mathbf{0})^T$.

In addition to conjugating the vector field $\mathbf{Z}$, the symmetry map Σ also conjugates the extended vector fields $\mathbf{Z}_+$ and $\mathbf{Z}_-$ introduced in section 5.1.3. To see this, let $\mathbf{z} = (\mathbf{x}, \mathbf{y})^T \in \mathbb{R}^6$. Then by (5.22):

$$\mathbf{Z}_+(\Sigma\mathbf{z}) = \mathbf{Z}_+(-\mathbf{x}, \sigma\mathbf{y}) = \begin{pmatrix} -A\mathbf{x} + B\sigma\mathbf{y} \\ \mathbf{Y}_+(\sigma\mathbf{y}) \end{pmatrix} = \begin{pmatrix} -A\mathbf{x} - B\mathbf{y} \\ \mathbf{Y}_+(\sigma\mathbf{y}) \end{pmatrix}$$

It was shown in section 3.3 that $\mathbf{X}_+ \circ \sigma = \sigma \circ \mathbf{X}_-$. Thus, since $\mathbf{Y}_\pm(\mathbf{y}) = \frac{1}{\epsilon}\mathbf{X}_\pm(\mathbf{y})$, $\mathbf{Y}_+ \circ \sigma = \sigma \circ \mathbf{Y}_-$. Substituting this into the above yields:

$$\mathbf{Z}_{+}\left(\Sigma\mathbf{z}\right)=\left(\begin{array}{c}-A\mathbf{x}-B\mathbf{y}\\ \sigma\mathbf{Y}_{-}\left(\mathbf{y}\right)\end{array}\right)=\Sigma\left(\begin{array}{c}A\mathbf{x}+B\mathbf{y}\\ \mathbf{Y}_{-}\left(\mathbf{y}\right)\end{array}\right)$$

(5.23) therefore implies that $\mathbf{Z}_{+}\left(\Sigma\mathbf{z}\right)=\Sigma\mathbf{Z}_{-}\left(\mathbf{z}\right)$. This holds $\forall\mathbf{z}\in\mathbb{R}^{6}$, and so

$$\mathbf{Z}_{+}\circ\Sigma=\Sigma\circ\mathbf{Z}_{-} \tag{5.34}$$

as claimed. This conjugacy implies that for each $\mathbf{z}\in\mathbb{R}^{6}$, $J_{S}^{-}\left(\Sigma\mathbf{z}\right)=J_{S}^{+}\left(\mathbf{z}\right)$ with $\psi_{t}^{-}\left(\Sigma\mathbf{z}\right)=\Sigma\psi_{t}^{+}\left(\mathbf{z}\right)$ $\forall t\in J_{S}^{+}\left(\mathbf{z}\right)$.

Finally, the relation between the flows of $\dot{\mathbf{z}}=\mathbf{Z}_{\pm}(\mathbf{z})$ and $\dot{\mathbf{z}}=\mathbf{Z}\left(\mathbf{z}\right)$ can be used to show that $\hat{L}_{0}$ is a stable 1-dimensional manifold of the origin $\left(\mathbf{0},\mathbf{0}\right)^{T}$ in $\dot{\mathbf{z}}=\mathbf{Z}_{\pm}(\mathbf{z})$, with the dynamics of $\dot{\mathbf{z}}=\mathbf{Z}_{\pm}(\mathbf{z})$ given by (5.33) (cf. the similar discussion at the end of section 3.3).

5.4 Fixed points

In this section the fixed points of the saccadic equations are characterised. Let $\mathbf{z}_{*}=\left(\mathbf{x}_{*},\mathbf{y}_{*}\right)^{T}$ be a fixed point of $\dot{\mathbf{z}}=\mathbf{Z}\left(\mathbf{z}\right)$. Then (5.2) implies that $\mathbf{x}_{*}$ and $\mathbf{y}_{*}$ satisfy:

$$\begin{aligned} A\mathbf{x}_{*}+B\mathbf{y}_{*} &= 0 &\quad (5.35)\\ \mathbf{Y}\left(\mathbf{y}_{*}\right) &= 0 &\quad (5.36)\end{aligned}$$

(5.36) shows that $\mathbf{y}_{*}$ is a fixed point of the burster system $\dot{\mathbf{y}}=\mathbf{Y}\left(\mathbf{y}\right)$. $\mathbf{y}_{*}$ thus has the form $\mathbf{y}_{*}=\left(x_{*},x_{*},\varepsilon_{*}\right)^{T}$ (cf. section 3.5). (5.4) implies that $\det\left(A\right)=-\frac{P_{2}}{T_{N}}=-\frac{1}{T_{1}T_{2}T_{N}}\neq 0$. A is therefore invertible and so (5.36) implies $\mathbf{x}_{*}=-A^{-1}B\mathbf{y}_{*}$. By (5.5):

$$B\mathbf{y}_{*}=\left(\begin{array}{ccc}0&0&0\\ P_{1}&-P_{1}&0\\ 1&-1&0\end{array}\right)\left(\begin{array}{c}x_{*}\\ x_{*}\\ \varepsilon_{*}\end{array}\right)=\mathbf{0}$$

Hence, $\mathbf{x}_{*}=\mathbf{0}$. Fixed points $\mathbf{z}_{*}$ of $\dot{\mathbf{z}}=\mathbf{Z}\left(\mathbf{z}\right)$ therefore have the form $\mathbf{z}_{*}=\left(\mathbf{0},\mathbf{y}_{*}\right)^{T}$ where $\mathbf{y}_{*}$ is a fixed point of the burster system $\dot{\mathbf{y}}=\mathbf{Y}\left(\mathbf{y}\right)$. (In terms of the projection operator π, $\mathbf{z}_{*}$ is a fixed point of $\dot{\mathbf{z}}=\mathbf{Z}\left(\mathbf{z}\right)$ iff $\pi\mathbf{z}_{*}$ is a fixed point of $\dot{\mathbf{y}}=\mathbf{Y}\left(\mathbf{y}\right)$). The analysis of section 3.5 therefore implies that the possible fixed points of $\dot{\mathbf{z}}=\mathbf{Z}\left(\mathbf{z}\right)$ are $\left(\mathbf{0},\mathbf{0}\right)^{T}$ and

$\mathbf{z}_i^{\pm} \overset{def}{=} \left(\mathbf{0}, \mathbf{y}_i^{\pm}\right)^T$, for $1 \leq i \leq 2$. By the definition of Σ, for $1 \leq i \leq 2$, $\mathbf{z}_i^{-} = \left(\mathbf{0}, \mathbf{y}_i^{-}\right)^T = \left(-\mathbf{0}, \sigma \mathbf{y}_{-}^{+}\right)^T = \Sigma \left(\mathbf{0}, \mathbf{y}_{-}^{+}\right)^T = \Sigma \mathbf{z}_i^{+}$.

Note that when $\mathbf{z}_i^{\pm}$ is considered as a function of $\boldsymbol{\alpha}$, $\mathbf{z}_i^{\pm} = \mathbf{z}_i^{\pm}(\alpha, \beta)$ as $\mathbf{y}_i^{\pm} = \mathbf{y}_i^{\pm}(\alpha, \beta)$. Moreover, the region of existence of $\mathbf{z}_i^{\pm}$ in the (β, α) plane is the same as that of $\mathbf{y}_i^{\pm}$.

5.5 Stability of the fixed points

During the first part of this section, the skew product nature of the saccadic equations is used to relate the stability of a given fixed point $\mathbf{z}_* = (\mathbf{0}, \mathbf{y}_*)^T$ of $\dot{\mathbf{z}} = \mathbf{Z}(\mathbf{z})$ to the stability of the corresponding fixed point $\mathbf{y}_*$ of $\dot{\mathbf{y}} = \mathbf{Y}(\mathbf{y})$. This analysis is used in the next section, when discussing the relation between attractors of the burster and saccadic systems. Next, the eigenvalues and eigenvectors of $D\mathbf{Z}_{\pm}(\mathbf{0})$ are examined, showing that $(\mathbf{0}, \mathbf{0})^T$ is a hyperbolic fixed point of $\dot{\mathbf{z}} = \mathbf{Z}_{\pm}(\mathbf{z})$ iff $\mathbf{0}$ is a hyperbolic fixed point of $\dot{\mathbf{y}} = \mathbf{Y}_{\pm}(\mathbf{y})$. Finally, it is demonstrated that π maps the local stable and unstable manifolds of $\dot{\mathbf{z}} = \mathbf{Z}_{\pm}(\mathbf{z})$ at $(\mathbf{0}, \mathbf{0})^T$ to the local stable and unstable manifolds of $\dot{\mathbf{y}} = \mathbf{Y}_{\pm}(\mathbf{y})$ at $\mathbf{0}$, when $(\mathbf{0}, \mathbf{0})^T$ is hyperbolic. This fact is used later on in the chapter when discussing gluing bifurcations of the saccadic system.

5.5.1 Using the stability of $\mathbf{y}_*$ to determine the stability of $\mathbf{z}_* = (\mathbf{0}, \mathbf{y}_*)^T$

It is shown here that the stability of a given fixed point $\mathbf{z}_* = (\mathbf{0}, \mathbf{y}_*)^T$ of the saccadic equations $\dot{\mathbf{z}} = \mathbf{Z}(\mathbf{z})$ is determined by the stability of the corresponding fixed point $\mathbf{y}_*$ of the burster equations $\dot{\mathbf{y}} = \mathbf{Y}(\mathbf{y})$. i.e. $\mathbf{z}_*$ is stable (resp. unstable) according to whether $\mathbf{y}_*$ is stable (resp. unstable). The proof that $\mathbf{z}_*$ is stable when $\mathbf{y}_*$ is stable is presented first.

Proof that $\mathbf{y}_*$ stable implies $\mathbf{z}_*$ stable

Assume that $\mathbf{y}_* = (x_*, x_*, \varepsilon_*)^T$ is stable. To prove that $\mathbf{z}_*$ is stable, it is necessary to demonstrate that it is both Liapunov stable and quasi-asymptotically stable. It is first shown that $\mathbf{z}_*$ is Liapunov stable.

To prove that $\mathbf{z}_*$ is Liapunov stable, it is required to show that for any $\epsilon > 0$, there is a $\delta > 0$ such that $\forall \mathbf{z} \in B_\delta(\mathbf{z}_*)$, $\psi_t(\mathbf{z}) \in B_\epsilon(\mathbf{z}_*)$ $\forall t \geq 0$. Let $\epsilon > 0$ be given. Since $\mathbf{y}_*$ is stable, it is Liapunov stable. Hence, $\exists\delta' > 0$ such that $\forall \mathbf{y} \in B_{\delta'}(\mathbf{y}_*)$, $\varphi_t(\mathbf{y}) \in B_{\frac{\epsilon}{2P_C T_N \|B\|_1}}(\mathbf{y}_*)$ $\forall t \geq 0$. So fix $\delta > 0$ with $\delta < \min\left\{\delta', \frac{\epsilon}{2P_C}\right\}$. Let $\mathbf{z} = (\mathbf{x}, \mathbf{y})^T \in B_\delta(\mathbf{z}_*)$. Then $\|\mathbf{z} - \mathbf{z}_*\|_1 = \left\|(\mathbf{x}, \mathbf{y} - \mathbf{y}_*)^T\right\|_1 = \|\mathbf{x}\|_1 + \|\mathbf{y} - \mathbf{y}_*\|_1$. Thus, as $\|\mathbf{z} - \mathbf{z}_*\|_1 < \delta$, $\|\mathbf{x}\|_1 < \delta$ and $\|\mathbf{y} - \mathbf{y}_*\|_1 < \delta$. The latter implies that $\mathbf{y} \in B_\delta(\mathbf{y}_*) \subset B_{\delta'}(\mathbf{y}_*)$, and so $\varphi_t(\mathbf{y}) \in B_{\frac{\epsilon}{2P_C T_N \|B\|_1}}(\mathbf{y}_*)$ $\forall t \geq 0$. Hence, for each $t \geq 0$:

$$\begin{aligned}
\|\psi_t(\mathbf{z}) - \mathbf{z}_*\|_1 &= \left\|(L_t(\mathbf{x}, \mathbf{y}), \varphi_t(\mathbf{y}))^T - (\mathbf{0}, \mathbf{y}_*)^T\right\|_1 \\
&= \left\|(L_t(\mathbf{x}, \mathbf{y}), \varphi_t(\mathbf{y}) - \mathbf{y}_*)^T\right\|_1 \\
&= \|L_t(\mathbf{x}, \mathbf{y})\|_1 + \|\varphi_t(\mathbf{y}) - \mathbf{y}_*\|_1 \\
&< \|L_t(\mathbf{x}, \mathbf{y})\|_1 + \frac{\epsilon}{2P_C T_N \|B\|_1}
\end{aligned}$$

Now $P_C, T_N \geq 1$. Also, $\|B\|_1 = 2P_1 \geq 1$. Thus, $\frac{\epsilon}{2P_C T_N \|B\|_1} \leq \frac{\epsilon}{2}$, and so the expression above implies that for all $t \geq 0$:

$$\|\psi_t(\mathbf{z}) - \mathbf{z}_*\|_1 < \|L_t(\mathbf{x}, \mathbf{y})\|_1 + \frac{\epsilon}{2} \tag{5.37}$$

Consider $\|L_t(\mathbf{x}, \mathbf{y})\|_1$. (5.18) implies that for all $t \geq 0$:

$$\begin{aligned}
\|L_t(\mathbf{x}, \mathbf{y})\|_1 &\leq P_C\left(e^{-\frac{t}{T_N}}\|\mathbf{x}\|_1 + \int_0^t e^{-\frac{(t-s)}{T_N}}\|B\varphi_s(\mathbf{y})\|_1\, ds\right) \\
&\leq P_C e^{-\frac{t}{T_N}}\left(\delta + \int_0^t e^{\frac{s}{T_N}}\|B\varphi_s(\mathbf{y})\|_1\, ds\right) \\
&< e^{-\frac{t}{T_N}}\left(\frac{\epsilon}{2} + P_C\int_0^t e^{\frac{s}{T_N}}\|B\varphi_s(\mathbf{y})\|_1\, ds\right)
\end{aligned} \tag{5.38}$$

Define $\mathbf{y}_T(t)$ by $\mathbf{y}_T(t) = \varphi_t(\mathbf{y}) - \mathbf{y}_*$ $\forall t \geq 0$. Then for each $t \geq 0$:

$$B\varphi_t(\mathbf{y}) = B\mathbf{y}_T(t) + B\mathbf{y}_* = B\mathbf{y}_T(t)$$

Hence $\forall t \geq 0$, $\|B\varphi_t(\mathbf{y})\|_1 = \|B\mathbf{y}_T(t)\|_1 \leq \|B\|_1\|\mathbf{y}_T(t)\|_1 < \frac{\epsilon}{2P_C T_N}$. It follows from (5.38) that for all $t \geq 0$:

$$\begin{aligned}
\|L_t(\mathbf{x}, \mathbf{y})\|_1 &< \frac{\epsilon}{2}e^{-\frac{t}{T_N}}\left(1 + \frac{1}{T_N}\int_0^t e^{\frac{s}{T_N}}\, ds\right) \\
&= \frac{\epsilon}{2}e^{-\frac{t}{T_N}}\left(1 + \frac{1}{T_N}\left(T_N e^{\frac{t}{T_N}} - T_N\right)\right) \\
&= \frac{\epsilon}{2}
\end{aligned}$$

Substituting into (5.37) implies that for all $t \geq 0$, $\|\psi_t(\mathbf{z}) - \mathbf{z}_*\|_1 < \epsilon$ and so $\psi_t(\mathbf{z}) \in B_\epsilon(\mathbf{z}_*)$, as claimed. This holds for all $\mathbf{z} \in B_\delta(\mathbf{z}_*)$, completing the proof that $\mathbf{z}_*$ is Liapunov stable.

It is now shown that $\mathbf{z}_* = (\mathbf{0}, \mathbf{y}_*)^T$ is quasi-asymptotically stable. To prove this, it is necessary to show that there is a $\delta > 0$ such that $\forall \mathbf{z} \in B_\delta(\mathbf{z}_*)$, $\psi_t(\mathbf{z}) \to \mathbf{z}_*$ as $t \to \infty$. Since $\mathbf{y}_*$ is stable, it is quasi-asymptotically stable, and so there is a $\delta > 0$ such that $\forall \mathbf{y} \in B_\delta(\mathbf{y}_*)$, $\varphi_t(\mathbf{y}) \to \mathbf{y}_*$ as $t \to \infty$. Fix such a δ, and let $\mathbf{z} = (\mathbf{x}, \mathbf{y})^T \in B_\delta(\mathbf{z}_*)$. Then as was established in the previous proof, $\|\mathbf{y} - \mathbf{y}_*\|_1 < \delta$ implying that $\varphi_t(\mathbf{y}) \to \mathbf{y}_*$ as $t \to \infty$. Define $\mathbf{z}(t) = (\mathbf{x}(t), \mathbf{y}(t))^T$ by $\mathbf{z}(t) = \psi_t(\mathbf{z})$ $\forall t \in J_B(\mathbf{y})$. Also set $\mathbf{z}_T(t) = (\mathbf{x}_T(t), \mathbf{y}_T(t))^T = \mathbf{z}(t) - \mathbf{z}_*$ $\forall t \in J_B(\mathbf{y})$. Then if it can be shown that $\mathbf{z}_T(t) \to (\mathbf{0}, \mathbf{0})^T$ as $t \to \infty$, this will imply that $\psi_t(\mathbf{z}) \to \mathbf{z}_*$ as $t \to \infty$. Since $\mathbf{z}(t)$ solves $\dot{\mathbf{z}} = \mathbf{Z}(\mathbf{z})$ on $J_B(\mathbf{y})$, $\forall t \in J_B(\mathbf{y})$, $\mathbf{x}(t)$ and $\mathbf{y}(t)$ satisfy:

$$\dot{\mathbf{x}}(t) = A\mathbf{x}(t) + B\mathbf{y}(t)$$

Hence, $\forall t \in J_B(\mathbf{y})$:

$$\dot{\mathbf{x}}_T(t) = A\mathbf{x}_T(t) + B\mathbf{y}_T(t) + B\mathbf{y}_*$$

But $B\mathbf{y}_* = \mathbf{0}$, and so $\forall t \in J_B(\mathbf{y})$:

$$\dot{\mathbf{x}}_T(t) = A\mathbf{x}_T(t) + B\mathbf{y}_T(t)$$

The discussion of the initial value problem $\{\dot{\mathbf{x}} = A\mathbf{x} + B\mathbf{r}(t) : \mathbf{x}(0) = \hat{\mathbf{x}}\}$ in section 5.1.2 therefore implies that $\forall t \geq 0$:

$$\|\mathbf{x}_T(t)\|_1 \leq P_C\left(e^{-\frac{t}{T_N}}\|\mathbf{x}\|_1 + \int_0^t e^{-\frac{(t-s)}{T_N}}\|B\mathbf{y}_T(s)\|_1\, ds\right)$$

Define $U_B(t)$ by $U_B(t) = \|B\mathbf{y}_T(t)\|_1$ $\forall t \geq 0$, and $U_E(t)$ by $U_E(t) = e^{-\frac{t}{T_N}}$ $\forall t \geq 0$. It then follows from the inequality above that for all $t \geq 0$

$$\|\mathbf{x}_T(t)\|_1 \leq P_C\left(e^{-\frac{t}{T_N}}\|\mathbf{x}\|_1 + (U_B * U_E)(t)\right) \tag{5.39}$$

where $U_B * U_E$ represents the convolution of U_B and U_E [36]. Now $\forall t \geq 0$, $\mathbf{y}_T(t) = \mathbf{y}(t) - \mathbf{y}_*$. Hence since $\varphi_t(\mathbf{y}) \to \mathbf{y}_*$ as $t \to \infty$, $\mathbf{y}_T(t) \to \mathbf{0}$ as $t \to \infty$ implying that $U_B(t) \to 0$ as $t \to \infty$. Also, $U_E(t)$ converges to 0 exponentially fast as $t \to \infty$, and thus $(U_B * U_E)(t) \to 0$ as $t \to \infty$ (cf. section A.2.6). (5.39) therefore implies that $\mathbf{x}_T(t) \to \mathbf{0}$ as $t \to \infty$, and so

$\mathbf{z}_T(t) \to (\mathbf{0},\mathbf{0})^T$ as $t \to \infty$. Hence, $\psi_t(\mathbf{z}) \to \mathbf{z}_*$ as $t \to \infty$. This holds for all $\mathbf{z} \in B_\delta(\mathbf{z}_*)$, completing the proof that $\mathbf{z}_*$ is quasi-asymptotically stable.

It has been shown that $\mathbf{y}_*$ stable implies that $\mathbf{z}_*$ is both Liapunov stable and quasi-asymptotically stable, and therefore that $\mathbf{z}_*$ is stable. In particular $\mathbf{0}$ stable implies that $(\mathbf{0},\mathbf{0})^T$ is stable.

Proof that $\mathbf{y}_*$ unstable implies $\mathbf{z}_*$ unstable

Assume that $\mathbf{y}_*$ is unstable. To prove that $\mathbf{z}_*$ is unstable, it is necessary to demonstrate that it is not Liapunov stable. i.e. that there is an $\epsilon > 0$ such that $\forall \delta > 0$, $\mathbf{z} \in B_\delta(\mathbf{z}_*)$ and $t' \geq 0$ can be found for which $\psi_{t'}(\mathbf{z}) \notin B_\epsilon(\mathbf{z}_*)$. Now since $\mathbf{y}_*$ is unstable, it is not Liapunov stable. Fix $\epsilon > 0$ such that $\forall \delta > 0$, $\mathbf{y} \in B_\delta(\mathbf{y}_*)$ and $t' \geq 0$ can be found for which $\varphi_{t'}(\mathbf{y}) \notin B_\epsilon(\mathbf{y}_*)$. Let $\delta > 0$ be given. Choose $\mathbf{y} \in B_\delta(\mathbf{y}_*)$ and $t' \geq 0$ for which $\varphi_{t'}(\mathbf{y}) \notin B_\epsilon(\mathbf{y}_*)$, and define $\mathbf{z} \in \mathbb{R}^6$ by $\mathbf{z} = (\mathbf{0},\mathbf{y})^T$. Then:

$$
\begin{aligned}
\|\psi_{t'}(\mathbf{z}) - \mathbf{z}_*\|_1 &= \left\|(L_{t'}(\mathbf{0},\mathbf{y}), \varphi_{t'}(\mathbf{y}))^T - (\mathbf{0},\mathbf{y}_*)^T\right\|_1 \\
&= \left\|(L_{t'}(\mathbf{0},\mathbf{y}), \varphi_{t'}(\mathbf{y}) - \mathbf{y}_*)^T\right\|_1 \\
&= \|L_{t'}(\mathbf{0},\mathbf{y})\|_1 + \|\varphi_{t'}(\mathbf{y}) - \mathbf{y}_*\|_1
\end{aligned}
$$

Since $\varphi_{t'}(\mathbf{y}) \notin B_\epsilon(\mathbf{y}_*)$, $\|\varphi_{t'}(\mathbf{y}) - \mathbf{y}_*\|_1 > \epsilon$. Thus from the expression for $\|\psi_{t'}(\mathbf{z}) - \mathbf{z}_*\|_1$ above, $\|\psi_{t'}(\mathbf{z}) - \mathbf{z}_*\|_1 > \epsilon$, implying that $\psi_{t'}(\mathbf{z}) \notin B_\epsilon(\mathbf{z}_*)$. Such a $\mathbf{z} \in B_\delta(\mathbf{z}_*)$ and $t' \geq 0$ can be found for all $\delta > 0$, completing the proof that $\mathbf{z}_*$ is unstable.

It has been shown that $\mathbf{y}_*$ unstable implies $\mathbf{z}_*$ is unstable. In particular, $\mathbf{0}$ unstable implies that $(\mathbf{0},\mathbf{0})^T$ is unstable.

5.5.2 Eigenvalues and eigenvectors of $D\mathbf{Z}_\pm(\mathbf{0},\mathbf{0})$

In section 5.3 it was shown that $\mathbf{Z}_- \circ \Sigma = \Sigma \circ \mathbf{Z}_+$. Applying the chain rule to both sides of this expression at $\mathbf{z} \in \mathbb{R}^6$ yields:

$$D\mathbf{Z}_-(\Sigma\mathbf{z})\Sigma = \Sigma D\mathbf{Z}_+(\mathbf{z})$$

Setting $\mathbf{z} = (\mathbf{0},\mathbf{0})^T$ in the above gives

$$D\mathbf{Z}_{-}\left(\mathbf{0},\mathbf{0}\right)\Sigma = \Sigma D\mathbf{Z}_{+}\left(\mathbf{0},\mathbf{0}\right) \tag{5.40}$$

which implies that $D\mathbf{Z}_{+}\left(\mathbf{0},\mathbf{0}\right)$ and $D\mathbf{Z}_{-}\left(\mathbf{0},\mathbf{0}\right)$ have the same eigenvalue spectrum. From (5.22), given $\mathbf{z} \in \mathbb{R}^6$, $D\mathbf{Z}_{+}(\mathbf{z})$ has the form:

$$D\mathbf{Z}_{+}(\mathbf{z}) = \begin{pmatrix} A & B \\ \mathbf{0}_{3\times 3} & D\mathbf{Y}_{+}\left(\pi\mathbf{z}\right) \end{pmatrix}$$

Setting $\mathbf{z} = \left(\mathbf{0},\mathbf{0}\right)^T$ in the above gives:

$$D\mathbf{Z}_{+}(\mathbf{0},\mathbf{0}) = \begin{pmatrix} A & B \\ \mathbf{0}_{3\times 3} & D\mathbf{Y}_{+}\left(\mathbf{0}\right) \end{pmatrix} \tag{5.41}$$

Write $\{p_1, p_2, p_3\}$ for the eigenvalues of A and $\{\mathbf{p}_1, \mathbf{p}_2, \mathbf{p}_3\}$ for the corresponding eigenvectors. It can be shown that $p_1 = -\frac{1}{T_1}$, $p_2 = -\frac{1}{T_2}$, $p_3 = -\frac{1}{T_N}$ and:

$$\mathbf{p}_1 = \begin{pmatrix} -T_1 \\ 1 \\ 0 \end{pmatrix}, \mathbf{p}_2 = \begin{pmatrix} -T_2 \\ 1 \\ 0 \end{pmatrix}, \mathbf{p}_3 = \begin{pmatrix} -T_N \\ 1 \\ -\frac{(T_1-T_N)(T_2-T_N)}{T_N} \end{pmatrix} \tag{5.42}$$

($\{p_1, p_2, p_3\}$ have the following values: $p_1 = -6\frac{2}{3}, p_2 = -83\frac{1}{3}$ and $p_3 = -0.04$). Also, for $1 \le i \le 3$ define $\hat{\lambda}_i$ by $\hat{\lambda}_i = \frac{1}{\epsilon}\lambda_i$ where $\{\lambda_1, \lambda_2, \lambda_3\}$ are the eigenvalues of $D\mathbf{X}_{+}\left(\mathbf{0}\right)$ (cf. section 3.6.3). $\left\{\hat{\lambda}_1, \hat{\lambda}_2, \hat{\lambda}_3\right\}$ are then the eigenvalues of $D\mathbf{Y}_{+}\left(\mathbf{0}\right)$, with corresponding eigenvectors $\left\{\mathbf{w}_1^+, \mathbf{w}_2^+, \mathbf{w}_3^+\right\}$. (5.41) thus implies that the eigenvalues of $D\mathbf{Z}_{+}(\mathbf{0},\mathbf{0})$ are:

$$\left\{p_1, p_2, p_3, \hat{\lambda}_1, \hat{\lambda}_2, \hat{\lambda}_3\right\}$$

[37]. Since p_1, p_2, $p_3 < 0$, this means $\left(\mathbf{0},\mathbf{0}\right)^T$ is hyperbolic in $\dot{\mathbf{z}} = \mathbf{Z}_{\pm}\left(\mathbf{z}\right)$ iff $\mathbf{0}$ is hyperbolic in $\dot{\mathbf{y}} = \mathbf{Y}_{\pm}\left(\mathbf{y}\right)$. Thus $\left(\mathbf{0},\mathbf{0}\right)^T$ is hyperbolic iff $\alpha \neq \Lambda_{+}\beta$. Also note that since $\lambda_1 = \lambda_2 + \lambda_3$, $\hat{\lambda}_1 = \hat{\lambda}_2 + \hat{\lambda}_3$. The eigenvalues of $D\mathbf{Z}_{+}(\mathbf{0},\mathbf{0})$ thus have a resonance of order 2 and so Sternberg's Theorem implies that the origin is at most C^1 linearisable. Moreover, the extended Hartman-Grobman Theorem mentioned in section 1.2.3 cannot be used to show that the origin is C^1 linearisable when $\alpha > \Lambda_{+}\beta$, as $\hat{\lambda}_2 > 0$ and $\hat{\lambda}_3 < 0$ in this range.

Let $\left\{\hat{\mathbf{p}}_1^{\pm}, \hat{\mathbf{p}}_2^{\pm}, \hat{\mathbf{p}}_3^{\pm}, \hat{\mathbf{w}}_1^{\pm}, \hat{\mathbf{w}}_2^{\pm}, \hat{\mathbf{w}}_3^{\pm}\right\}$ be the eigenvectors of $D\mathbf{Z}_{\pm}(\mathbf{0},\mathbf{0})$ corresponding to:

$$\left\{p_1, p_2, p_3, \hat{\lambda}_1, \hat{\lambda}_2, \hat{\lambda}_3\right\}$$

($\{\hat{\mathbf{p}}_1^{\pm}, \hat{\mathbf{p}}_2^{\pm}, \hat{\mathbf{p}}_3^{\pm}, \hat{\mathbf{w}}_1^{\pm}, \hat{\mathbf{w}}_2^{\pm}, \hat{\mathbf{w}}_3^{\pm}\}$ are taken to be the generalised eigenvectors when the eigenvalues are not distinct). By (5.41):

$$D\mathbf{Z}_+(\mathbf{0},\mathbf{0})\begin{pmatrix}\mathbf{p}_j\\ \mathbf{0}\end{pmatrix} = \begin{pmatrix}A\mathbf{p}_j\\ \mathbf{0}\end{pmatrix} = \begin{pmatrix}p_j\mathbf{p}_j\\ \mathbf{0}\end{pmatrix} = p_j\begin{pmatrix}\mathbf{p}_j\\ \mathbf{0}\end{pmatrix}$$

Thus, $\hat{\mathbf{p}}_j^+$ can be set equal to $\hat{\mathbf{p}}_j \overset{def}{=} (\mathbf{p}_j, \mathbf{0})^T$ for $1 \le j \le 3$. It was shown in section 3.6.3 that $\mathbf{w}_1^+ = (1,1,0)^T$. Hence:

$$D\mathbf{Z}_+(\mathbf{0},\mathbf{0})\begin{pmatrix}\mathbf{0}\\ \mathbf{w}_1^+\end{pmatrix} = \begin{pmatrix}B\mathbf{w}_1^+\\ D\mathbf{Y}_+(\mathbf{0})\,\mathbf{w}_1^+\end{pmatrix} = \begin{pmatrix}B\mathbf{w}_1^+\\ \hat{\lambda}_1\mathbf{w}_1^+\end{pmatrix} \tag{5.43}$$

By (5.5):

$$B\mathbf{w}_1^+ = \begin{pmatrix}0 & 0 & 0\\ P_1 & -P_1 & 0\\ 1 & -1 & 0\end{pmatrix}\begin{pmatrix}1\\ 1\\ 0\end{pmatrix} = \mathbf{0}$$

Substituting $\mathbf{0}$ for $B\mathbf{w}_1^+$ in (5.43) gives:

$$D\mathbf{Z}_+(\mathbf{0},\mathbf{0})\begin{pmatrix}\mathbf{0}\\ \mathbf{w}_1^+\end{pmatrix} = \begin{pmatrix}\mathbf{0}\\ \hat{\lambda}_1\mathbf{w}_1^+\end{pmatrix} = \hat{\lambda}_1\begin{pmatrix}\mathbf{0}\\ \mathbf{w}_1^+\end{pmatrix}$$

$\hat{\mathbf{w}}_1^+$ can therefore be set equal to $\left(\mathbf{0}, \mathbf{w}_1^+\right)^T = (0,0,0,1,1,0)^T$. Note that the form of $\hat{\mathbf{w}}_1^+$ implies $\pi\hat{\mathbf{w}}_1^+ = \mathbf{w}_1^+$. In the generic case when $\left\{p_1, p_2, p_3, \hat{\lambda}_1, \hat{\lambda}_2, \hat{\lambda}_3\right\}$ are all distinct, the other eigenvectors $\left\{\hat{\mathbf{w}}_2^+, \hat{\mathbf{w}}_3^+\right\}$ are given by

$$\hat{\mathbf{w}}_2^+ = \begin{pmatrix}-\left(A - \hat{\lambda}_2\mathbf{1}_3\right)^{-1}B\mathbf{w}_2^+\\ \mathbf{w}_2^+\end{pmatrix}, \hat{\mathbf{w}}_3^+ = \begin{pmatrix}-\left(A - \hat{\lambda}_3\mathbf{1}_3\right)^{-1}B\mathbf{w}_3^+\\ \mathbf{w}_3^+\end{pmatrix}$$

where $\mathbf{w}_2^+$ and $\mathbf{w}_3^+$ are defined in (3.86). The forms of $\hat{\mathbf{w}}_2^+$ and $\hat{\mathbf{w}}_3^+$ imply that $\pi\hat{\mathbf{w}}_j^+ = \mathbf{w}_j^+$ for $2 \le j \le 3$.

Let $1 \le j \le 3$. (5.40) implies:

$$
\begin{aligned}
D\mathbf{Z}_{-}(\mathbf{0},\mathbf{0})\,\Sigma\hat{\mathbf{p}}_j &= \Sigma D\mathbf{Z}_{+}(\mathbf{0},\mathbf{0})\,\hat{\mathbf{p}}_j\\
\Rightarrow D\mathbf{Z}_{-}(\mathbf{0},\mathbf{0})\begin{pmatrix}-\mathbf{p}_j\\ \mathbf{0}\end{pmatrix} &= p_j\Sigma\hat{\mathbf{p}}_j\\
\Rightarrow D\mathbf{Z}_{-}(\mathbf{0},\mathbf{0})\begin{pmatrix}-\mathbf{p}_j\\ \mathbf{0}\end{pmatrix} &= p_j\begin{pmatrix}-\mathbf{p}_j\\ \mathbf{0}\end{pmatrix}\\
\Rightarrow D\mathbf{Z}_{-}(\mathbf{0},\mathbf{0})\,\hat{\mathbf{p}}_j &= p_j\hat{\mathbf{p}}_j
\end{aligned}
$$

$\hat{\mathbf{p}}_j^-$ can therefore be set equal to $\hat{\mathbf{p}}_j$ for each $1 \le j \le 3$. By using (5.40), it is possible to show that $\left\{\hat{\mathbf{w}}_1^-, \hat{\mathbf{w}}_2^-, \hat{\mathbf{w}}_3^-\right\}$ can be chosen to satisfy $\left[\hat{\mathbf{w}}_1^-\ \hat{\mathbf{w}}_2^-\ \hat{\mathbf{w}}_3^-\right] = \Sigma\left[\hat{\mathbf{w}}_1^+\ \hat{\mathbf{w}}_2^+\ \hat{\mathbf{w}}_3^+\right]$ (cf. the discussion of $\left\{\mathbf{w}_1^-, \mathbf{w}_2^-, \mathbf{w}_3^-\right\}$ in section 3.6.1). In particular, $\hat{\mathbf{w}}_1^-$ can be set equal to $\left(\mathbf{0},\sigma\mathbf{w}_1^+\right)^T = \left(\mathbf{0}, \mathbf{w}_1^-\right)^T = (0,0,0,1,1,0)^T$. Note that $\pi\hat{\mathbf{w}}_1^- = \mathbf{w}_1^-$. Also, since $\pi\circ\Sigma = \sigma\circ\pi$, in the generic case when $\left\{p_1, p_2, p_3, \hat{\lambda}_1, \hat{\lambda}_2, \hat{\lambda}_3\right\}$ are all distinct, for each $2 \le j \le 3$, $\pi\hat{\mathbf{w}}_j^- = \pi\left(\Sigma\hat{\mathbf{w}}_j^+\right) = \sigma\left(\pi\hat{\mathbf{w}}_j^+\right) = \sigma\mathbf{w}_j^+ = \mathbf{w}_j^-$.

It should be observed that when the dependence of $\mathbf{Z}_\pm$ on $\boldsymbol{\alpha}$ is being explicitly considered, the Jacobian matrix $D\mathbf{Z}_\pm(\mathbf{0},\mathbf{0})$ is $D_{\mathbf{z}}\mathbf{Z}_\pm(\mathbf{0},\mathbf{0};\boldsymbol{\alpha})$, while the eigenvalues and eigenvectors of the Jacobian attributable to the burster equations are functions of $\boldsymbol{\alpha}$, $\hat{\lambda}_i = \hat{\lambda}_i(\boldsymbol{\alpha})$, $\hat{\mathbf{w}}_i^\pm = \hat{\mathbf{w}}_i^\pm(\boldsymbol{\alpha})$, $1 \le i \le 3$.

5.5.3 Local stable and unstable manifolds of $\dot{\mathbf{z}} = \mathbf{Z}_\pm(\mathbf{z})$ at $(\mathbf{0},\mathbf{0})^T$

Assume that $\alpha \ne \Lambda_+\beta$, so $(\mathbf{0},\mathbf{0})^T$ is a hyperbolic fixed point of $\dot{\mathbf{z}} = \mathbf{Z}_\pm(\mathbf{z})$. The semi-conjugation of the time t maps of $\dot{\mathbf{z}} = \mathbf{Z}_\pm(\mathbf{z})$ and $\dot{\mathbf{y}} = \mathbf{Y}_\pm(\mathbf{y})$ by the projection operator π can be used to show that the local stable and unstable manifolds $W_S^\pm$ and $W_U^\pm$ of $\dot{\mathbf{y}} = \mathbf{Y}_\pm(\mathbf{y})$ at $\mathbf{0}$ are the images of the local stable and unstable manifolds $\hat{W}_S^\pm$ and $\hat{W}_U^\pm$ of $\dot{\mathbf{z}} = \mathbf{Z}_\pm(\mathbf{z})$ at $(\mathbf{0},\mathbf{0})^T$ under π. It is proved here that $W_S^+ = \pi\hat{W}_S^+$. Using a very similar argument, it can be shown that $W_U^+ = \pi\hat{W}_U^+$. The conjugacies $\mathbf{Z}_+\circ\Sigma = \Sigma\circ\mathbf{Z}_-$ and $\pi\circ\Sigma = \sigma\circ\pi$ then imply that $W_S^- = \pi\hat{W}_S^-$ and $W_U^- = \pi\hat{W}_U^-$.

To prove $W_S^+ = \pi\hat{W}_S^+$, it is sufficient by the uniqueness of W_S^+ to demonstrate that $\pi\hat{W}_S^+$ is a local stable manifold of $\mathbf{0}$ in $\dot{\mathbf{y}} = \mathbf{Y}_+(\mathbf{y})$. i.e. that $\pi\hat{W}_S^+$ is positively invariant with $\varphi_t^+(\mathbf{y}) \to \mathbf{0}$ as $t \to \infty$ $\forall\mathbf{y} \in \pi\hat{W}_S^+$. So let $\mathbf{y} \in \pi\hat{W}_S^+$. Then there is an $\mathbf{x} \in \mathbb{R}^3$ such that $\mathbf{z} = (\mathbf{x},\mathbf{y})^T \in \hat{W}_S^+$. Hence, $J_B^+(\mathbf{y}) = J_S^+(\mathbf{z}) \supset [0,\infty)$. Now, as $\hat{W}_S^+$ is positively invariant, for all $t \geq 0$:

$$\begin{aligned} &\psi_t^+ (\mathbf{z}) \in \hat{W}_S^+ \\ &\Rightarrow \pi \psi_t^+ (\mathbf{z}) \in \pi \hat{W}_S^+ \\ &\Rightarrow \varphi_t^+ (\mathbf{y}) \in \pi \hat{W}_S^+ \end{aligned}$$

Also, since $\hat{W}_S^+$ is a stable manifold of $(\mathbf{0}, \mathbf{0})^T$:

$$\psi_t^+ (\mathbf{z}) \to (\mathbf{0}, \mathbf{0})^T \text{ as } t \to \infty$$

However, π is continuous and so:

$$\begin{aligned} &\pi \psi_t^+ (\mathbf{z}) \to \pi (\mathbf{0}, \mathbf{0})^T \text{ as } t \to \infty \\ &\Rightarrow \varphi_t^+ (\mathbf{y}) \to \mathbf{0} \text{ as } t \to \infty \end{aligned}$$

It has been shown that given $\mathbf{y} \in \pi \hat{W}_S^+$, $\varphi_t^+ (\mathbf{y}) \in \pi \hat{W}_S^+$ $\forall t \geq 0$, and $\varphi_t^+ (\mathbf{y}) \to \mathbf{0}$ as $t \to \infty$. $\pi \hat{W}_S^+$ is therefore a local stable manifold of $\mathbf{0}$, as claimed.

5.6 The relationship between the attractors of the burster and saccadic systems

Recall from section 5.2 that the projection map π provides a bijection between the set of ω-limit sets of $\dot{\mathbf{z}} = \mathbf{Z}(\mathbf{z})$, $\left\{\omega\left((\mathbf{0}, \mathbf{y}_i)^T\right) : i \in I_B\right\}$, and the set of ω-limit sets of $\dot{\mathbf{y}} = \mathbf{Y}(\mathbf{y})$, $\{\omega(\mathbf{y}_i) : i \in I_B\}$. It was stated at the end of section 5.2 that if $\hat{\mathcal{A}}$ is an attractor of $\dot{\mathbf{z}} = \mathbf{Z}(\mathbf{z})$ then, $\pi \hat{\mathcal{A}}$ is an attractor of $\dot{\mathbf{y}} = \mathbf{Y}(\mathbf{y})$. It follows that if to each attractor $\mathcal{A}$ of $\dot{\mathbf{y}} = \mathbf{Y}(\mathbf{y})$ there corresponds an attractor $\hat{\mathcal{A}}$ of $\dot{\mathbf{z}} = \mathbf{Z}(\mathbf{z})$ with $\pi \hat{\mathcal{A}} = \mathcal{A}$, then π provides a bijection between the set of attractors of $\dot{\mathbf{z}} = \mathbf{Z}(\mathbf{z})$ and the set of attractors of $\dot{\mathbf{y}} = \mathbf{Y}(\mathbf{y})$. The attractors of $\dot{\mathbf{z}} = \mathbf{Z}(\mathbf{z})$ can then be written as $\left\{\hat{\mathcal{A}}_i = \omega\left((\mathbf{0}, \mathbf{y}_i)^T\right) : i \in I_A\right\}$ and the attractors of $\dot{\mathbf{y}} = \mathbf{Y}(\mathbf{y})$ as $\{\mathcal{A}_i = \omega(\mathbf{y}_i) : i \in I_A\}$, where $I_A \subseteq I_B$.

Let $\boldsymbol{\alpha}$ lie in a region of Π where the attractors of $\dot{\mathbf{y}} = \mathbf{Y}(\mathbf{y})$ are either stable fixed points or stable limit cycles. It was shown in section 5.5.1 that if $\mathbf{y}_*$ is a stable fixed point of $\dot{\mathbf{y}} = \mathbf{Y}(\mathbf{y})$ then $\mathbf{z}_* = (\mathbf{0}, \mathbf{y}_*)^T$ is a stable fixed point of $\dot{\mathbf{z}} = \mathbf{Z}(\mathbf{z})$. It is demonstrated in this section that for each stable limit cycle $\mathcal{C}$ of $\dot{\mathbf{y}} = \mathbf{Y}(\mathbf{y})$, there is a corresponding stable limit cycle $\hat{\mathcal{C}}$ of $\dot{\mathbf{z}} = \mathbf{Z}(\mathbf{z})$ of the same period as $\mathcal{C}$, with $\pi\hat{\mathcal{C}} = \mathcal{C}$. For $\boldsymbol{\alpha}$ lying in the regions of Π discussed in chapter 4 (ϵ small and $\hat{\Pi}_P$), the attractors of $\dot{\mathbf{y}} = \mathbf{Y}(\mathbf{y})$ are stable fixed points and stable limit cycles, and so the argument above implies that π provides a bijection between the sets of attractors of $\dot{\mathbf{y}} = \mathbf{Y}(\mathbf{y})$ and $\dot{\mathbf{z}} = \mathbf{Z}(\mathbf{z})$ in these ranges. Consequently, the attractors of the saccadic system for such choices of $\boldsymbol{\alpha}$ can be inferred from the attractors of the burster system.

In the regions of Π discussed in chapter 4, each stable limit cycle of $\dot{\mathbf{y}} = \mathbf{Y}(\mathbf{y})$ is labelled $\mathcal{C}_+$, $\mathcal{C}_-$, $\mathcal{C}_1$ or $\mathcal{C}_2$. In the following, the corresponding limit cycle of $\dot{\mathbf{z}} = \mathbf{Z}(\mathbf{z})$ will be labelled $\hat{\mathcal{C}}_+$, $\hat{\mathcal{C}}_-$, $\hat{\mathcal{C}}_1$ or $\hat{\mathcal{C}}_2$ respectively.

Remark: Recall from section 5.3 that $\hat{\mathcal{C}}$ is a stable limit cycle of $\dot{\mathbf{z}} = \mathbf{Z}(\mathbf{z})$ with period T iff $\Sigma\hat{\mathcal{C}}$ is a stable limit cycle of the same period. The relations $\sigma\mathcal{C}_+ = \mathcal{C}_-, \sigma\mathcal{C}_1 = \mathcal{C}_1$, and $\sigma\mathcal{C}_2 = \mathcal{C}_2$ therefore imply that $\Sigma\hat{\mathcal{C}}_+ = \hat{\mathcal{C}}_-, \Sigma\hat{\mathcal{C}}_1 = \hat{\mathcal{C}}_1$, and $\Sigma\hat{\mathcal{C}}_2 = \hat{\mathcal{C}}_2$. To see that $\Sigma\hat{\mathcal{C}}_+ = \hat{\mathcal{C}}_-$, assume $\Sigma\hat{\mathcal{C}}_+ \neq \hat{\mathcal{C}}_-$. It is shown that this gives a contradiction. Since $\hat{\mathcal{C}}_+$ is a stable limit cycle of $\dot{\mathbf{z}} = \mathbf{Z}(\mathbf{z})$, $\Sigma\hat{\mathcal{C}}_+$ is also a stable limit cycle and so $\Sigma\hat{\mathcal{C}}_+ \in \left\{\hat{\mathcal{C}}_+, \hat{\mathcal{C}}_1, \hat{\mathcal{C}}_2\right\}$. Hence, $\pi\Sigma\hat{\mathcal{C}}_+ \in \left\{\pi\hat{\mathcal{C}}_+, \pi\hat{\mathcal{C}}_1, \pi\hat{\mathcal{C}}_2\right\} = \{\mathcal{C}_+, \mathcal{C}_1, \mathcal{C}_2\}$. Now $\pi \circ \Sigma = \sigma \circ \pi$, and so $\pi\Sigma\hat{\mathcal{C}}_+ = \sigma\pi\hat{\mathcal{C}}_+ = \sigma\mathcal{C}_+ = \mathcal{C}_-$. This implies $\mathcal{C}_- \in \{\mathcal{C}_+, \mathcal{C}_1, \mathcal{C}_2\}$, giving a contradiction. Thus, $\Sigma\hat{\mathcal{C}}_+ = \hat{\mathcal{C}}_-$ as claimed. The other relations can be proved by using a similar argument.

5.6.1 Proof that stable limit cycles of $\dot{\mathbf{y}} = \mathbf{Y}(\mathbf{y})$ correspond to stable limit cycles of $\dot{\mathbf{z}} = \mathbf{Z}(\mathbf{z})$

Let $\mathcal{C}$ be a stable limit cycle of $\dot{\mathbf{y}} = \mathbf{Y}(\mathbf{y})$ of period T. It is demonstrated here that there is a stable limit cycle $\hat{\mathcal{C}}$ of $\dot{\mathbf{z}} = \mathbf{Z}(\mathbf{z})$ of period T such that $\pi\hat{\mathcal{C}} = \mathcal{C}$.

The first step is to show that if $\mathcal{C}$ is a limit cycle of $\dot{\mathbf{y}} = \mathbf{Y}(\mathbf{y})$ of period T, then there is a corresponding periodic orbit $\hat{\mathcal{C}}$ of $\dot{\mathbf{z}} = \mathbf{Z}(\mathbf{z})$ of period T with $\pi\hat{\mathcal{C}} = \mathcal{C}$. To do this , fix some $\mathbf{y}_0 \in \mathcal{C}$, and define $\mathbf{y}_S(t) = (r_S(t), l_S(t), \varepsilon_S(t))^T$ by $\mathbf{y}_S(t) = \varphi_t(\mathbf{y}_0)$ for all $t \in \mathbb{R}$. Then $\mathbf{y}_S(t)$ is a periodic solution of $\dot{\mathbf{y}} = \mathbf{Y}(\mathbf{y})$ with period T. As $\mathbf{y}_S(t)$ is C^1, this means it can be expressed as a vectorised complex Fourier series

$$\mathbf{y}_S(t) = \sum_{k=-\infty}^{\infty} \mathbf{y}_k^S e^{ik\omega_T t} \tag{5.44}$$

where the $\mathbf{y}_k^S$s are the Fourier coefficients, and $\omega_T = \frac{2\pi}{T}$ is the fundamental frequency [36],

[38]. For each $k \in \mathbb{Z}$, write $\mathbf{y}_k^S$ as:

$$\mathbf{y}_k^S = \begin{pmatrix} r_k^S \\ l_k^S \\ \varepsilon_k^S \end{pmatrix} \tag{5.45}$$

Define $b_S(t)$ by $b_S(t) = r_S(t) - l_S(t)\ \forall t \in \mathbb{R}$. Then by (5.44) and (5.45), $b_S(t)$ has the Fourier series

$$b_S(t) = \sum_{k=-\infty}^{\infty} b_k^S e^{ik\omega_T t} \tag{5.46}$$

where:

$$b_k^S = r_k^S - l_k^S \tag{5.47}$$

So consider the 1st order system below:

$$\dot{n}(t) + \frac{1}{T_N} n(t) = b_S(t) \tag{5.48}$$

The transfer function of this system is $H_n(s)$ where:

$$H_n(s) = \frac{1}{s + \frac{1}{T_N}} \tag{5.49}$$

It therefore follows from linear systems theory that the function $n_S(t)$ defined on $\mathbb{R}$ by the Fourier series

$$n_S(t) = \sum_{k=-\infty}^{\infty} H_n(ik\omega_T)\, b_k^S e^{ik\omega_T t} \tag{5.50}$$

solves (5.48) on $\mathbb{R}$ [36]. Thus, $\forall t \in \mathbb{R}$:

$$\dot{n}_S(t) = -\frac{1}{T_N} n_S(t) + r_S(t) - l_S(t) \tag{5.51}$$

Next, consider the 2nd order system:

$$\ddot{g}(t) + P_1 \dot{g}(t) + P_2 g(t) = P_2 n_S(t) + P_1 b_S(t) \tag{5.52}$$

The transfer function of this system is $H_g(s)$ where:

$$H_g(s) = \frac{1}{\left(s + \frac{1}{T_1}\right)\left(s + \frac{1}{T_2}\right)} \tag{5.53}$$

Additionally, (5.46) and (5.50) imply that the right-hand side of (5.52) has the Fourier series expansion below:

$$P_2 n_S(t) + P_1 b_S(t) = \sum_{k=-\infty}^{\infty} \left(P_1 + P_2 H_n(ik\omega_T)\right) b_k^S e^{ik\omega_T t}$$

Consequently, it follows from linear systems theory again that the function $g_S(t)$ defined on $\mathbb{R}$ by the Fourier series:

$$g_S(t) = \sum_{k=-\infty}^{\infty} H_g(ik\omega_T)\left(P_1 + P_2 H_n(ik\omega_T)\right) b_k^S e^{ik\omega_T t} \tag{5.54}$$

solves (5.52) on $\mathbb{R}$. Thus $\forall t \in \mathbb{R}$:

$$\ddot{g}_S(t) = -P_1 \dot{g}_S(t) - P_2 g_S(t) + P_2 n_S(t) + P_1\left(r_S(t) - l_S(t)\right) \tag{5.55}$$

Define the function $v_S(t)$ by:

$$\dot{g}_S(t) = v_S(t) \tag{5.56}$$

(5.54) implies that this has the Fourier series expansion:

$$v_S(t) = \sum_{k=-\infty}^{\infty} (ik\omega_T) H_g(ik\omega_T)\left(P_1 + P_2 H_n(ik\omega_T)\right) b_k^S e^{ik\omega_T t} \tag{5.57}$$

Also, (5.55) implies that $\forall t \in \mathbb{R}$:

$$\dot{v}_S(t) = -P_1 v_S(t) - P_2 g_S(t) + P_2 n_S(t) + P_1\left(r_S(t) - l_S(t)\right) \tag{5.58}$$

Finally, define $\mathbf{x}_S(t)$ by $\mathbf{x}_S(t) = (g_S(t), v_S(t), n_S(t))^T$ $\forall t \in \mathbb{R}$, and $\mathbf{z}_S(t)$ by $\mathbf{z}_S(t) = (\mathbf{x}_S(t), \mathbf{y}_S(t))^T$ $\forall t \in \mathbb{R}$, and set $\mathbf{x}_0 = \mathbf{x}_S(0)$ and $\mathbf{z}_0 = \mathbf{z}_S(0) = (\mathbf{x}_0, \mathbf{y}_0)^T$. Then since $\mathbf{y}_S(t)$ solves $\dot{\mathbf{y}} = \mathbf{Y}(\mathbf{y})$ on $\mathbb{R}$, and the elements of $\mathbf{x}_S(t)$ satisfy (5.51), (5.56) and (5.58) on $\mathbb{R}$, $\mathbf{z}_S(t)$ solves the saccadic equations $\dot{\mathbf{z}} = \mathbf{Z}(\mathbf{z})$ on $\mathbb{R}$, with $\mathbf{z}_S(0) = \mathbf{z}_0$ (cf. (5.10)-(5.12)).

Moreover, $\mathbf{x}_S(t)$ can be expressed as the vectorised complex Fourier series

$$\mathbf{x}_S(t) = \sum_{k=-\infty}^{\infty} \mathbf{x}_k^S e^{ik\omega_T t} \tag{5.59}$$

where for each $k \in \mathbb{Z}$:

$$\mathbf{x}_k^S = \begin{pmatrix} H_g(ik\omega_T)(P_1 + P_2 H_n(ik\omega_T)) \\ (ik\omega_T) H_g(ik\omega_T)(P_1 + P_2 H_n(ik\omega_T)) \\ H_n(ik\omega_T) \end{pmatrix} b_k^S \tag{5.60}$$

(5.59) implies that $\mathbf{x}_S(t)$ is periodic with period T, from which it follows that $\mathbf{z}_S(t)$ is periodic with period T. Since $\mathbf{z}_S(t)$ solves $\dot{\mathbf{z}} = \mathbf{Z}(\mathbf{z})$ on $\mathbb{R}$ with $\mathbf{z}_S(0) = \mathbf{z}_0$, $\mathbf{z}_S(t) = \psi_t(\mathbf{z}_0)$ $\forall t \in \mathbb{R}$. Hence, $\psi_T(\mathbf{z}_0) = \mathbf{z}_S(T) = \mathbf{z}_S(0) = \mathbf{z}_0$. Also, $\psi_t(\mathbf{z}_0) \neq \mathbf{z}_0$ for all $0 < t < T$. [Assume that there is some $0 < t' < T$ with $\psi_{t'}(\mathbf{z}_0) = \mathbf{z}_0$. Then $\pi\psi_{t'}(\mathbf{z}_0) = \pi\mathbf{z}_0 \Rightarrow \varphi_{t'}(\mathbf{y}_0) = \mathbf{y}_0$. But $\mathbf{y}_0 \in \mathcal{C}$, which is a periodic orbit of period T, so this gives a contradiction.]. It follows that the set $\hat{\mathcal{C}} \subset \mathbb{R}^6$ defined by

$$\hat{\mathcal{C}} = \{\psi_t(\mathbf{z}_0) : 0 \leq t < T\}$$

is a periodic orbit of $\dot{\mathbf{z}} = \mathbf{Z}(\mathbf{z})$ with period T. Also:

$$\pi\hat{\mathcal{C}} = \{\pi\psi_t(\mathbf{z}_0) : 0 \leq t < T\} = \{\varphi_t(\mathbf{y}_0) : 0 \leq t < T\} = \mathcal{C}$$

This completes the first part of the proof.

It will be useful later on to be able to express the Fourier coefficients $\mathbf{x}_k^S$ of $\mathbf{x}_S(t)$ in a slightly different way. As $\mathbf{y}_S(t)$ solves $\dot{\mathbf{y}} = \mathbf{Y}(\mathbf{y})$ on $\mathbb{R}$, $\forall t \in \mathbb{R}$:

$$\dot{\varepsilon}_S(t) = -b_S(t) \tag{5.61}$$

(5.44) and (5.45) imply that $\varepsilon_S(t)$ has the Fourier series expansion:

$$\varepsilon_S(t) = \sum_{k=-\infty}^{\infty} \varepsilon_k^S e^{ik\omega_T t}$$

Hence by (5.61), $b_S(t)$ has the Fourier series expansion:

$$b_S(t) = -\sum_{k=-\infty}^{\infty} (ik\omega_T)\,\varepsilon_k^S e^{ik\omega_T t}$$

Comparing this expression with (5.46) implies that $\forall k \in \mathbb{Z}$, $b_k^S = -(ik\omega_T)\,\varepsilon_k^S$. It is convenient to introduce the functions $T_g(s)$ and $T_n(s)$

$$T_g(s) = -sH_g(s)\,(P_1 + P_2 H_n(s)) \tag{5.62}$$

$$T_n(s) = -sH_n(s) \tag{5.63}$$

because it then follows from (5.60) that $\forall k \in \mathbb{Z}$:

$$\mathbf{x}_k^S = \begin{pmatrix} T_g(ik\omega_T) \\ (ik\omega_T)\,T_g(ik\omega_T) \\ T_n(ik\omega_T) \end{pmatrix} \varepsilon_k^S \tag{5.64}$$

In conclusion, $\mathbf{z}_S(t)$ can be written as the Fourier series

$$\mathbf{z}_S(t) = \sum_{k=-\infty}^{\infty} \begin{pmatrix} \mathbf{x}_k^S \\ \mathbf{y}_k^S \end{pmatrix} e^{ik\omega_T t}$$

where for each $k \in \mathbb{Z}$, $\mathbf{x}_k^S \in \mathbb{R}^3$ is given by (5.64) and $\mathbf{y}_k^S \in \mathbb{R}^3$ is given by (5.45).

It is now shown that $\exists\delta > 0$ such that for each $\mathbf{z} \in N\left(\hat{\mathcal{C}},\delta\right)$, there is a $\mathbf{z}' \in \hat{\mathcal{C}}$ with $\psi_t(\mathbf{z}) \to \psi_t(\mathbf{z}')$ as $t \to \infty$. This implies that $\hat{\mathcal{C}}$ is a stable limit cycle. Since $\mathcal{C}$ is stable, $\exists\delta > 0$ such that for all $\mathbf{y} \in N(\mathcal{C},\delta)$ there is a $\mathbf{y}' \in \mathcal{C}$ with $\varphi_t(\mathbf{y}) \to \varphi_t(\mathbf{y}')$ as $t \to \infty$. Fix this δ. Let $\mathbf{z} = (\mathbf{x},\mathbf{y})^T \in N\left(\hat{\mathcal{C}},\delta\right)$, and define $\mathbf{z}(t) = (\mathbf{x}(t),\mathbf{y}(t))^T$ by $\mathbf{z}(t) = \psi_t(\mathbf{z})$ $\forall t \in J_S(\mathbf{z})$. As $\mathbf{z} \in N\left(\hat{\mathcal{C}},\delta\right)$, there is a $\hat{\mathbf{z}} \in \hat{\mathcal{C}}$ with $\|\mathbf{z} - \hat{\mathbf{z}}\|_1 < \delta$. Thus, $\|\pi(\mathbf{z} - \hat{\mathbf{z}})\|_1 < \delta \Rightarrow \|\mathbf{y} - \pi\hat{\mathbf{z}}\|_1 < \delta$ (cf. section A.2.1). $\pi\hat{\mathbf{z}} \in \mathcal{C}$, and so this implies $\mathbf{y} \in N(\mathcal{C},\delta)$. Hence, $\exists\mathbf{y}' \in \mathcal{C}$ with $\varphi_t(\mathbf{y}) \to \varphi_t(\mathbf{y}')$ as $t \to \infty$. Choose $\mathbf{x}' \in \mathbb{R}^3$ such that $\mathbf{z}' = (\mathbf{x}',\mathbf{y}')^T \in \hat{\mathcal{C}}$, and define $\mathbf{z}_S(t) = (\mathbf{x}_S(t),\mathbf{y}_S(t))^T$ by $\mathbf{z}_S(t) = \psi_t(\mathbf{z}')$ $\forall t \in \mathbb{R}$. Also set $\mathbf{z}_T(t) = (\mathbf{x}_T(t),\mathbf{y}_T(t))^T = \mathbf{z}(t) - \mathbf{z}_S(t)$ $\forall t \in J_S(\mathbf{z})$. Then $\forall t \in J_S(\mathbf{z})$, $\mathbf{y}_T(t) = \varphi_t(\mathbf{y}) - \varphi_t(\mathbf{y}')$, and so $\mathbf{y}_T(t) \to 0$ as $t \to \infty$. Hence if it can be shown that $\mathbf{x}_T(t) \to \mathbf{0}$ as $t \to \infty$, this will imply that $\psi_t(\mathbf{z}) \to \psi_t(\mathbf{z}')$ as $t \to \infty$.

As $\mathbf{z}(t)$ solves $\dot{\mathbf{z}} = \mathbf{Z}(\mathbf{z})$ on $J_S(\mathbf{z})$, $\forall t \in J_S(\mathbf{z})$, $\mathbf{x}(t)$ and $\mathbf{y}(t)$ satisfy:

$$\dot{\mathbf{x}}(t) = A\mathbf{x}(t) + B\mathbf{y}(t)$$

Hence, $\forall t \in J_S(\mathbf{z})$:

$$\dot{\mathbf{x}}_S(t) + \dot{\mathbf{x}}_T(t) = A\mathbf{x}_S(t) + B\mathbf{y}_S(t) + A\mathbf{x}_T(t) + B\mathbf{y}_T(t)$$

But $\mathbf{z}_S(t)$ also solves $\dot{\mathbf{z}} = \mathbf{Z}(\mathbf{z})$ on $J_S(\mathbf{z})$, and so $\dot{\mathbf{x}}_S(t) = A\mathbf{x}_S(t) + B\mathbf{y}_S(t)$ $\forall t \in J_S(\mathbf{z})$. It follows from above that $\forall t \in J_S(\mathbf{z})$:

$$\dot{\mathbf{x}}_T(t) = A\mathbf{x}_T(t) + B\mathbf{y}_T(t)$$

The discussion regarding solutions of the initial value problem $\{\dot{\mathbf{x}} = A\mathbf{x} + B\mathbf{r}(t) : \mathbf{x}(0) = \hat{\mathbf{x}}\}$ in section 5.1.2 therefore implies that $\forall t \geq 0$:

$$\|\mathbf{x}_T(t)\|_1 \leq P_C\left(e^{-\frac{t}{T_N}}\left\|\mathbf{x} - \mathbf{x}'\right\|_1 + \int_0^t e^{-\frac{(t-s)}{T_N}}\|B\mathbf{y}_T(s)\|_1\, ds\right)$$

Define $U_B(t)$ by $U_B(t) = \|B\mathbf{y}_T(t)\|_1$ $\forall t \geq 0$ and $U_E(t)$ by $U_E(t) = e^{-\frac{t}{T_N}}$ $\forall t \geq 0$, as in section 5.5.1. It then follows from the above inequality that $\forall t \geq 0$:

$$\|\mathbf{x}_T(t)\|_1 \leq P_C\left(e^{-\frac{t}{T_N}}\left\|\mathbf{x} - \mathbf{x}'\right\|_1 + (U_B * U_E)(t)\right) \tag{5.65}$$

$\mathbf{y}_T(t) \to \mathbf{0}$ as $t \to \infty$ implying that $U_B(t) \to 0$ as $t \to \infty$. Also, $U_E(t) \to 0$ exponentially fast as $t \to \infty$ and so $(U_B * U_E)(t)$ must converge to 0 as $t \to \infty$. (5.65) therefore implies that $\mathbf{x}_T(t) \to \mathbf{0}$ as $t \to \infty$. Hence, $\psi_t(\mathbf{z}) \to \psi_t(\mathbf{z}')$ as $t \to \infty$, completing the proof.

5.6.2 Symmetry properties of the coordinate time series associated with symmetric limit cycles

The conjugacy $\psi_t \circ \Sigma = \Sigma \circ \psi_t$ for $t \geq 0$ can be used to obtain some useful properties of the coordinate time series associated with a symmetry invariant limit cycle of the saccadic system. Let $\hat{\mathcal{C}}$ be such a limit cycle of period T. Choose $\mathbf{z}_0 \in \hat{\mathcal{C}}$ and define

$$\mathbf{z}_S(t) = (g_S(t), v_S(t), n_S(t), r_S(t), l_S(t), \varepsilon_S(t))^T$$

by $\mathbf{z}_S(t) = \psi_t(\mathbf{z}_0)\,\forall t \in \mathbb{R}$. Fix $\mathbf{z}_1 \in \hat{\mathcal{C}}$, and set $\mathbf{z}_2 = \Sigma\mathbf{z}_1$. By the Σ-invariance of $\hat{\mathcal{C}}$, $\mathbf{z}_2 \in \hat{\mathcal{C}}$. Moreover, since $\hat{\mathcal{C}} \cap \hat{L}_0 = \phi$, $\mathbf{z}_1 \neq \mathbf{z}_2$. This implies that $\exists 0 < r < T$ with $\psi_r(\mathbf{z}_1) = \mathbf{z}_2$. Applying ψ_r to both sides of this equality and using $\psi_r \circ \Sigma = \Sigma \circ \psi_r$ yields $\psi_{2r}(\mathbf{z}_1) = \mathbf{z}_1$, from which it follows that $2r = kT$ for some $k \geq 1$. As $0 < r < T$, $0 < kT < 2T$, implying that $k = 1$. Thus, $r = \frac{T}{2}$ and so $\psi_{\frac{T}{2}}(\mathbf{z}_1) = \Sigma\mathbf{z}_1$. Let $t \in \mathbb{R}$. Then $\mathbf{z}_S(t) = \psi_{r'}(\mathbf{z}_1)$ for some $0 \leq r' < T$. Hence:

$$\mathbf{z}_S\left(t + \frac{T}{2}\right) = \psi_{\frac{T}{2}}(\mathbf{z}_S(t)) = \psi_{\frac{T}{2}+r'}(\mathbf{z}_1) = \psi_{r'}\left(\psi_{\frac{T}{2}}(\mathbf{z}_1)\right) = \psi_{r'}(\Sigma\mathbf{z}_1) = \Sigma\psi_{r'}(\mathbf{z}_1) = \Sigma\mathbf{z}_S(t)$$

It has been shown that $\mathbf{z}_S\left(t + \frac{T}{2}\right) = \Sigma\mathbf{z}_S(t)\ \forall t \in \mathbb{R}$. By the definition of Σ, the following therefore hold for all $t \in \mathbb{R}$:

$$\begin{array}{lclcl} g_S\left(t + \frac{T}{2}\right) = -g_S(t) & : & v_S\left(t + \frac{T}{2}\right) = -v_S(t) & : & n_S\left(t + \frac{T}{2}\right) = -n_S(t) \\ r_S\left(t + \frac{T}{2}\right) = l_S(t) & : & l_S\left(t + \frac{T}{2}\right) = r_S(t) & : & \varepsilon_S\left(t + \frac{T}{2}\right) = -\varepsilon_S(t) \end{array}$$

$r_S(t)$ is thus simply a delayed version of $l_S(t)$, while $g_S(t), v_S(t), n_S(t)$ and $\varepsilon_S(t)$ have half-wave symmetry [38].

5.7 Gluing bifurcations of the burster and saccadic systems

It is argued in this section that the gluing bifurcation which occurs in the burster system $\dot{\mathbf{y}} = \mathbf{Y}(\mathbf{y};\boldsymbol{\alpha})$ at the origin $\mathbf{0}$ when $\epsilon = \epsilon_G(\alpha,\beta)$ induces a gluing bifurcation of the same type in the saccadic system $\dot{\mathbf{z}} = \mathbf{Z}(\mathbf{z};\boldsymbol{\alpha})$ at the origin $(\mathbf{0},\mathbf{0})^T$.

Following the notation of section 4.8.1, write $G_+(\alpha,\beta)$ and $G_-(\alpha,\beta)$ for the pair of symmetry-related orbits homoclinic to $\mathbf{0}$ in $\dot{\mathbf{y}} = \mathbf{Y}(\mathbf{y};\boldsymbol{\alpha})$ when $\epsilon = \epsilon_G(\alpha,\beta)$. It is first shown that when $\epsilon = \epsilon_G(\alpha,\beta)$, there is a pair of symmetry-related orbits $\hat{G}_+(\alpha,\beta)$ and $\hat{G}_-(\alpha,\beta)$ homoclinic to $(\mathbf{0},\mathbf{0})^T$ in $\dot{\mathbf{z}} = \mathbf{Z}(\mathbf{z};\boldsymbol{\alpha})$ with $\pi\hat{G}_\pm(\alpha,\beta) = G_\pm(\alpha,\beta)$. The existence of these orbits is then used to infer that a gluing bifurcation occurs in $\dot{\mathbf{z}} = \mathbf{Z}(\mathbf{z};\boldsymbol{\alpha})$ when $\epsilon = \epsilon_G(\alpha,\beta)$.

5.7.1 The homoclinic orbits $\hat{G}_+(\alpha,\beta)$ and $\hat{G}_-(\alpha,\beta)$

Recall from section 4.8.1 that $G_\pm(\alpha,\beta) \subset N_\pm$, and so $G_\pm(\alpha,\beta)$ is homoclinic to $\mathbf{0}$ in the smooth system $\dot{\mathbf{y}} = \mathbf{Y}_\pm(\mathbf{y};\boldsymbol{\alpha})$ when $\epsilon = \epsilon_G(\alpha,\beta)$. It is shown here that there is an orbit $\hat{G}_+(\alpha,\beta)$ which is homoclinic to $(\mathbf{0},\mathbf{0})^T$ in the smooth system $\dot{\mathbf{z}} = \mathbf{Z}_+(\mathbf{z};\boldsymbol{\alpha})$ when $\epsilon = \epsilon_G(\alpha,\beta)$, with $\pi\hat{G}_+(\alpha,\beta) = G_+(\alpha,\beta)$. It then follows from the conjugacies $\mathbf{Z}_+\circ\Sigma = \Sigma\circ\mathbf{Z}_-$ and $\pi\circ\Sigma = \sigma\circ\pi$ that $\hat{G}_-(\alpha,\beta) \overset{def}{=} \Sigma\hat{G}_+(\alpha,\beta)$ is homoclinic to $(\mathbf{0},\mathbf{0})^T$ in the smooth system $\dot{\mathbf{z}} = \mathbf{Z}_-(\mathbf{z};\boldsymbol{\alpha})$ when $\epsilon = \epsilon_G(\alpha,\beta)$, with $\pi\hat{G}_-(\alpha,\beta) = G_-(\alpha,\beta)$. As $G_\pm(\alpha,\beta)\subset N_\pm$, $\pi\hat{G}_\pm(\alpha,\beta)\subset N_\pm \Rightarrow \hat{G}_\pm(\alpha,\beta)\subset\hat{N}_\pm$. The relation $\mathbf{Z}(\mathbf{z};\boldsymbol{\alpha}) = \mathbf{Z}_\pm(\mathbf{z};\boldsymbol{\alpha})$ $\forall\mathbf{z}\in\hat{N}_\pm$ therefore implies that when $\epsilon = \epsilon_G(\alpha,\beta)$, $\hat{G}_+(\alpha,\beta)$ and $\hat{G}_-(\alpha,\beta)$ are both simultaneously homoclinic to $(\mathbf{0},\mathbf{0})^T$ in the saccadic system $\dot{\mathbf{z}} = \mathbf{Z}(\mathbf{z};\boldsymbol{\alpha})$.

The existence of $\hat{G}_+(\alpha,\beta)$ is now demonstrated. Recall from section 5.5.2 that the eigenvalues of $D_{\mathbf{z}}\mathbf{Z}_\pm(\mathbf{0},\mathbf{0};\boldsymbol{\alpha})$ are

$$\left\{p_1, p_2, p_3, \hat{\lambda}_1(\boldsymbol{\alpha}), \hat{\lambda}_2(\boldsymbol{\alpha}), \hat{\lambda}_3(\boldsymbol{\alpha})\right\}$$

where $p_1 = -\frac{1}{T_1}$, $p_2 = -\frac{1}{T_2}$, $p_3 = -\frac{1}{T_N}$, and $\left\{\hat{\lambda}_1(\boldsymbol{\alpha}), \hat{\lambda}_2(\boldsymbol{\alpha}), \hat{\lambda}_3(\boldsymbol{\alpha})\right\}$ are the eigenvalues of $D_{\mathbf{y}}\mathbf{Y}_\pm(\mathbf{0};\boldsymbol{\alpha})$. In keeping with the notation of 5.5.2, write $\left\{\hat{\mathbf{p}}_1, \hat{\mathbf{p}}_2, \hat{\mathbf{p}}_3, \hat{\mathbf{w}}_1^\pm(\boldsymbol{\alpha}), \hat{\mathbf{w}}_2^\pm(\boldsymbol{\alpha}), \hat{\mathbf{w}}_3^\pm(\boldsymbol{\alpha})\right\}$ for the corresponding eigenvectors. Since $\hat{\lambda}_i(\boldsymbol{\alpha}) = \frac{1}{\epsilon}\lambda_i(\boldsymbol{\alpha})$ for $1\le i\le 3$, in the range $\alpha > \Lambda_+\beta$, $\lambda_2(\boldsymbol{\alpha}) > 0$ and $\lambda_3(\boldsymbol{\alpha}) < \lambda_1(\boldsymbol{\alpha}) < 0$. It follows that for $\alpha > \Lambda_+\beta$, $(\mathbf{0},\mathbf{0})^T$ has a unique 1-dimensional C^∞ local unstable manifold $\hat{W}^U_{0\pm}(\boldsymbol{\alpha})$ in $\dot{\mathbf{z}} = \mathbf{Z}_\pm(\mathbf{z};\boldsymbol{\alpha})$ which is tangential to $\mathrm{Sp}\left\{\hat{\mathbf{w}}_2^\pm(\boldsymbol{\alpha})\right\}$ at $(\mathbf{0},\mathbf{0})^T$. Also, $\mathbf{0}$ has a unique 1-dimensional C^∞ local unstable manifold $W^U_{0\pm}(\boldsymbol{\alpha})$ in the system $\dot{\mathbf{y}} = \mathbf{Y}_\pm(\mathbf{y};\boldsymbol{\alpha})$ which is tangential to $\mathrm{Sp}\left\{\mathbf{w}_2^\pm(\boldsymbol{\alpha})\right\}$ at $\mathbf{0}$ (cf. section 3.6.3). As was stated in section 4.8.1, $G_+(\alpha,\beta)$ intersects $W^U_{0+}(\alpha,\beta,\epsilon_G(\alpha,\beta))$ in the system $\dot{\mathbf{y}} = \mathbf{Y}_+(\mathbf{y};\alpha,\beta,\epsilon_G(\alpha,\beta))$. The discussion in section 5.5.3 of the relationship between local stable/unstable manifolds of $\dot{\mathbf{z}} = \mathbf{Z}_+(\mathbf{z};\boldsymbol{\alpha})$ at $(\mathbf{0},\mathbf{0})^T$ and local stable/unstable manifolds of $\dot{\mathbf{y}} = \mathbf{Y}_+(\mathbf{y};\boldsymbol{\alpha})$ at $\mathbf{0}$ when $(\mathbf{0},\mathbf{0})^T$ is hyperbolic implies that $\pi\hat{W}^U_{0+}(\alpha,\beta,\epsilon_G(\alpha,\beta)) = W^U_{0+}(\alpha,\beta,\epsilon_G(\alpha,\beta))$. So fix $\mathbf{y}'\in G_+(\alpha,\beta)\cap W^U_{0+}(\alpha,\beta,\epsilon_G(\alpha,\beta))$, and choose $\mathbf{x}'\in\mathbb{R}^3$ so that $\mathbf{z}' = (\mathbf{x}',\mathbf{y}')^T\in\hat{W}^U_{0+}(\alpha,\beta,\epsilon_G(\alpha,\beta))$. As $\mathbf{y}'\in G_+(\alpha,\beta)$ and $G_+(\alpha,\beta)$ is homoclinic to $\mathbf{0}$, $J_B^+(\mathbf{y}') = \mathbb{R}$ and

$$G_+(\alpha,\beta) = \left\{\varphi_t^+(\mathbf{y}') : t\in\mathbb{R}\right\}$$

with $\varphi_t^+(\mathbf{y}')\to\mathbf{0}$ as $t\to\pm\infty$ (cf. section 1.2.2). Since $J_S^+(\mathbf{z}) = J_B^+(\pi\mathbf{z})$ $\forall\mathbf{z}\in\mathbb{R}^6$, $J_S^+(\mathbf{z}') = \mathbb{R}$. Also, $\mathbf{y}'\ne\mathbf{0}$ and thus $\mathbf{z}'\ne(\mathbf{0},\mathbf{0})^T$. Define $\hat{G}_+(\alpha,\beta)$ by:

$$\hat{G}_+(\alpha,\beta) = \left\{\psi_t^+(\mathbf{z}') : t\in\mathbb{R}\right\}$$

The fact that π semi-conjugates φ_t^+ and ψ_t^+ then implies $\pi\hat{G}_+(\alpha,\beta) = G_+(\alpha,\beta)$. If it can be shown that $\psi_t^+(\mathbf{z}') \to (\mathbf{0},\mathbf{0})^T$ as $t \to \pm\infty$, this will imply that $\hat{G}_+(\alpha,\beta)$ is homoclinic to $(\mathbf{0},\mathbf{0})^T$. The fact that $\mathbf{z}' \in \hat{W}_{0+}^U(\alpha,\beta,\epsilon_G(\alpha,\beta))$ means that $\psi_t^+(\mathbf{z}') \to (\mathbf{0},\mathbf{0})^T$ as $t \to -\infty$. For all $t \geq 0$:

$$\psi_t^+(\mathbf{z}') = \left(L_t^+\left(\mathbf{x}',\mathbf{y}'\right), \varphi_t^+(\mathbf{y}')\right)^T$$

where:

$$\left\|L_t^+(\mathbf{x}',\mathbf{y}')\right\|_1 \leq P_C\left(e^{-\frac{t}{T_N}}\left\|\mathbf{x}'\right\|_1 + \int_0^t e^{-\frac{(t-s)}{T_N}}\left\|B\varphi_s^+(\mathbf{y}')\right\|_1 ds\right)$$

(cf. (5.26)). Define $U_B^+(t)$ by $U_B^+(t) = \left\|B\varphi_t^+(\mathbf{y}')\right\|_1$ $\forall t \geq 0$, and $U_E(t)$ by $U_E(t) = e^{-\frac{t}{T_N}}$ $\forall t \geq 0$. It then follows from the inequality above that for all $t \geq 0$:

$$\left\|L_t^+(\mathbf{x}',\mathbf{y}')\right\|_1 \leq P_C\left(e^{-\frac{t}{T_N}}\left\|\mathbf{x}'\right\|_1 + \left(U_B^+ * U_E\right)(t)\right) \tag{5.66}$$

Since $\varphi_t^+(\mathbf{y}') \to \mathbf{0}$ as $t \to \infty$, $U_B^+(t) \to 0$ as $t \to \infty$. Also, $U_E(t)$ converges to 0 exponentially fast as $t \to \infty$, and thus $\left(U_B^+ * U_E\right)(t) \to 0$ as $t \to \infty$ (cf. section A.2.6). Equation (5.66) therefore implies that $L_t^+(\mathbf{x}',\mathbf{y}') \to \mathbf{0}$ as $t \to \infty$. The form of $\psi_t^+(\mathbf{z}')$ then implies $\psi_t^+(\mathbf{z}') \to (\mathbf{0},\mathbf{0})^T$ as $t \to \infty$. $\hat{G}_+(\alpha,\beta)$ is thus homoclinic to $(\mathbf{0},\mathbf{0})^T$ in the smooth system $\dot{\mathbf{z}} = \mathbf{Z}_+(\mathbf{z};\alpha,\beta,\epsilon_G(\alpha,\beta))$, as claimed. Note that $\hat{G}_+(\alpha,\beta)$ intersects $\hat{W}_{0+}^U(\alpha,\beta,\epsilon_G(\alpha,\beta))$ in this system. Thus, the conjugacy $\mathbf{Z}_+ \circ \Sigma = \Sigma \circ \mathbf{Z}_-$ implies $\hat{G}_-(\alpha,\beta)$ intersects $\hat{W}_{0-}^U(\alpha,\beta,\epsilon_G(\alpha,\beta))$ in $\dot{\mathbf{z}} = \mathbf{Z}_-(\mathbf{z};\alpha,\beta,\epsilon_G(\alpha,\beta))$.

Some properties of the homoclinic orbits $\hat{G}_+(\alpha,\beta)$ and $\hat{G}_-(\alpha,\beta)$ in the piecewise smooth system $\dot{\mathbf{z}} = \mathbf{Z}(\mathbf{z};\alpha,\beta,\epsilon_G(\alpha,\beta))$ are now established. Since $\hat{G}_\pm(\alpha,\beta)$ intersects $\hat{W}_{0\pm}^U(\alpha,\beta,\epsilon_G(\alpha,\beta))$ in $\dot{\mathbf{z}} = \mathbf{Z}_\pm(\mathbf{z};\alpha,\beta,\epsilon_G(\alpha,\beta))$, it converges to the origin tangential to $\mathrm{Sp}\left\{\hat{\mathbf{w}}_2^\pm(\alpha,\beta,\epsilon_G(\alpha,\beta))\right\}$ in this system as $t \to -\infty$. Additionally, $\hat{G}_\pm(\alpha,\beta)$ converges to the origin tangential to the eigenvector corresponding to $\max\left\{p_3, \hat{\lambda}_1(\alpha,\beta,\epsilon_G(\alpha,\beta))\right\}$ as $t \to \infty$. Write this eigenvector as $\hat{\mathbf{w}}_{\max}^\pm(\alpha,\beta,\epsilon_G(\alpha,\beta))$. It then follows that in the system $\dot{\mathbf{z}} = \mathbf{Z}(\mathbf{z};\alpha,\beta,\epsilon_G(\alpha,\beta))$, both $\hat{G}_+(\alpha,\beta)$ and $\hat{G}_-(\alpha,\beta)$ intersect the 1-dimensional local unstable invariant set $\hat{W}_0^U(\alpha,\beta,\epsilon_G(\alpha,\beta))$ of the origin, defined by:

$$\hat{W}_0^U(\alpha,\beta,\epsilon_G(\alpha,\beta)) = \left\{\hat{W}_{0+}^U(\alpha,\beta,\epsilon_G(\alpha,\beta)) \cap \hat{N}_+\right\} \cup \left\{\hat{W}_{0-}^U(\alpha,\beta,\epsilon_G(\alpha,\beta)) \cap \hat{N}_-\right\}$$

Moreover, as $t \to -\infty$, $\hat{G}_+(\alpha,\beta)$ will converge to $(\mathbf{0},\mathbf{0})^T$ tangential to $\mathrm{Sp}\left\{\hat{\mathbf{w}}_2^+(\alpha,\beta,\epsilon_G(\alpha,\beta))\right\} \cap \hat{N}_+$ and $\hat{G}_-(\alpha,\beta)$ will converge to $(\mathbf{0},\mathbf{0})^T$ tangential to $\mathrm{Sp}\left\{\hat{\mathbf{w}}_2^-(\alpha,\beta,\epsilon_G(\alpha,\beta))\right\} \cap \hat{N}_-$.

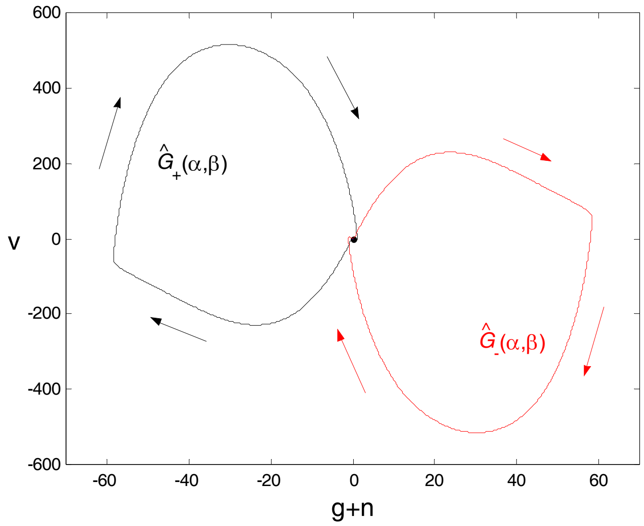

Figure 5-1: Projection onto the $(g+n, v)$ plane of $\hat{G}_{+}(\alpha, \beta)$ (black line) and $\hat{G}_{-}(\alpha, \beta)$ (red line) for $\alpha = 620$, $\beta = 9$. Arrows indicate the direction of motion with time. $\epsilon_G(\alpha, \beta) \approx 0.004823385$ for this choice of α and β.

Also, as $t \to \infty$, $\hat{G}_{+}(\alpha, \beta)$ will converge to $(\mathbf{0}, \mathbf{0})^T$ tangential to $\mathrm{Sp}\{\hat{\mathbf{w}}^{+}_{\max}(\alpha, \beta, \epsilon_G(\alpha, \beta))\} \cap \hat{N}_{+}$, while $\hat{G}_{-}(\alpha, \beta)$ will converge to $(\mathbf{0}, \mathbf{0})^T$ tangential to $\mathrm{Sp}\{\hat{\mathbf{w}}^{-}_{\max}(\alpha, \beta, \epsilon_G(\alpha, \beta))\} \cap \hat{N}_{-}$. Figures (5-1) and (5-2) are plots of $\hat{G}_{+}(\alpha, \beta)$ and $\hat{G}_{-}(\alpha, \beta)$ for $\{\alpha = 620, \beta = 9\}$. This was the choice of parameters used to obtain figures (4-53) and (4-54) in chapter 4. For this choice of α and β, $p_3 > \hat{\lambda}_1(\alpha, \beta, \epsilon_G(\alpha, \beta))$. Thus, $\hat{\mathbf{w}}^{+}_{\max}(\alpha, \beta, \epsilon_G(\alpha, \beta)) = \hat{\mathbf{w}}^{-}_{\max}(\alpha, \beta, \epsilon_G(\alpha, \beta)) = \hat{\mathbf{p}}_3$, and so as $\hat{\mathbf{p}}_3 = (\mathbf{p}_3, \mathbf{0})^T$, $\mathrm{Sp}\{\hat{\mathbf{w}}^{+}_{\max}(\alpha, \beta, \epsilon_G(\alpha, \beta))\} \cap \hat{N}_{+} = \mathrm{Sp}\{\hat{\mathbf{w}}^{-}_{\max}(\alpha, \beta, \epsilon_G(\alpha, \beta))\} \cap \hat{N}_{-} = \mathrm{Sp}\{\hat{\mathbf{p}}_3\}$. It can be seen from figures (5-1) and (5-2) that the behaviour of the homoclinic orbits close to the origin is as expected.

5.7.2 The gluing bifurcation of the saccadic system

The analysis of section 4.8.1 demonstrated that the homoclinic bifurcation of $\dot{\mathbf{y}} = \mathbf{Y}(\mathbf{y}; \boldsymbol{\alpha})$ at $\mathbf{0}$ which occurs when $\epsilon = \epsilon_G(\alpha, \beta)$ involves the destruction of the pair of stable limit cycles $\{\mathcal{C}_{+}(\boldsymbol{\alpha}), \mathcal{C}_{-}(\boldsymbol{\alpha})\}$. The one-to-one correspondence between stable limit cycles of $\dot{\mathbf{z}} = \mathbf{Z}(\mathbf{z}; \boldsymbol{\alpha})$ and $\dot{\mathbf{y}} = \mathbf{Y}(\mathbf{y}; \boldsymbol{\alpha})$ established in section 5.6 therefore implies that the corresponding simultaneous homoclinic bifurcations of $\dot{\mathbf{z}} = \mathbf{Z}(\mathbf{z}; \boldsymbol{\alpha})$ at $(\mathbf{0}, \mathbf{0})^T$ which occur when $\epsilon = \epsilon_G(\alpha, \beta)$ coincide with the destruction of the pair $\left\{\hat{\mathcal{C}}_{+}(\boldsymbol{\alpha}), \hat{\mathcal{C}}_{-}(\boldsymbol{\alpha})\right\}$. Since $\hat{\mathcal{C}}_{\pm}(\boldsymbol{\alpha}) \subset \hat{N}_{\pm}$, it follows that the homoclinic bifurcation in the smooth system $\dot{\mathbf{z}} = \mathbf{Z}_{\pm}(\mathbf{z}; \boldsymbol{\alpha})$ which occurs when $\epsilon = \epsilon_G(\alpha, \beta)$ coincides with the destruction of $\hat{\mathcal{C}}_{\pm}(\boldsymbol{\alpha})$. Assuming that

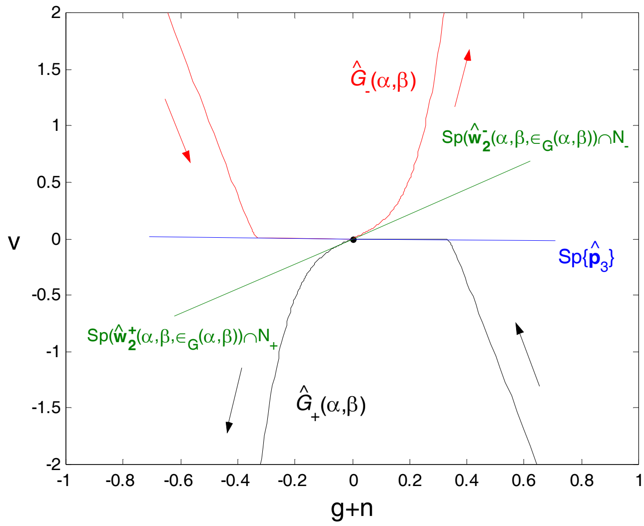

Figure 5-2: Close up of figure (5-1). The projections of Sp $\left\{\hat{\mathbf{w}}_2^+\left(\alpha,\beta,\epsilon_G\left(\alpha,\beta\right)\right)\right\}\cap N_+$, Sp $\left\{\hat{\mathbf{w}}_2^-\left(\alpha,\beta,\epsilon_G\left(\alpha,\beta\right)\right)\right\}\cap N_-$ and Sp $\left\{\hat{\mathbf{p}}_3^+\right\}$ onto the $(g+n,v)$ plane are also shown.

the origin $(\mathbf{0},\mathbf{0})^T$ is C^1 linearisable in $\dot{\mathbf{z}}=\mathbf{Z}_\pm\left(\mathbf{z};\boldsymbol{\alpha}\right)$ for $\left|\epsilon-\epsilon_G\left(\alpha,\beta\right)\right|$ small, this bifurcation is a regular homoclinic bifurcation of the saddle type with $d_u=1$ (cf. section 4.5.1). Since saddle homoclinic bifurcations involve the destruction of a single limit cycle, it is therefore reasonable to assume that $\hat{\mathcal{C}}_\pm\left(\boldsymbol{\alpha}\right)$ becomes homoclinic to $(\mathbf{0},\mathbf{0})^T$ in $\dot{\mathbf{z}}=\mathbf{Z}_\pm\left(\mathbf{z};\boldsymbol{\alpha}\right)$ as $\epsilon\longrightarrow\epsilon_G\left(\alpha,\beta\right)-$. This in turn implies that $\hat{\mathcal{C}}_+\left(\boldsymbol{\alpha}\right)$ and $\hat{\mathcal{C}}_-\left(\boldsymbol{\alpha}\right)$ both become simultaneously homoclinic to $(\mathbf{0},\mathbf{0})^T$ in $\dot{\mathbf{z}}=\mathbf{Z}\left(\mathbf{z};\boldsymbol{\alpha}\right)$ as $\epsilon\longrightarrow\epsilon_G\left(\alpha,\beta\right)-$, which is consistent with the fact that $\mathcal{C}_\pm\left(\boldsymbol{\alpha}\right)$ and $\hat{\mathcal{C}}_\pm\left(\boldsymbol{\alpha}\right)$ have the same period, and hence the period of $\hat{\mathcal{C}}_\pm\left(\boldsymbol{\alpha}\right)$ goes to ∞ as $\epsilon\longrightarrow\epsilon_G\left(\alpha,\beta\right)-$. Note that since the bifurcation in $\dot{\mathbf{z}}=\mathbf{Z}_\pm\left(\mathbf{z};\boldsymbol{\alpha}\right)$ involves a stable limit cycle, the associated saddle index is greater than 1.

The one-to-one correspondence between the stable limit cycles of the burster and saccadic systems also implies that as ϵ increases through $\epsilon_G\left(\alpha,\beta\right)$, the asymmetric pair $\hat{\mathcal{C}}_+\left(\boldsymbol{\alpha}\right)$ and $\hat{\mathcal{C}}_-\left(\boldsymbol{\alpha}\right)$ are destroyed and replaced with the symmetric limit cycle $\hat{\mathcal{C}}_1\left(\boldsymbol{\alpha}\right)$. Since the period of $\hat{\mathcal{C}}_1\left(\boldsymbol{\alpha}\right)$ goes to ∞ as $\epsilon\longrightarrow\epsilon_G\left(\alpha,\beta\right)+$, and the system is symmetric under Σ, it seem reasonable to assert that $\hat{\mathcal{C}}_+\left(\boldsymbol{\alpha}\right)$ and $\hat{\mathcal{C}}_-\left(\boldsymbol{\alpha}\right)$ coalesce in a nonsmooth gluing bifurcation at the origin as ϵ increases through $\epsilon_G\left(\alpha,\beta\right)$, mirroring the gluing of $\mathcal{C}_+\left(\boldsymbol{\alpha}\right)$ and $\mathcal{C}_-\left(\boldsymbol{\alpha}\right)$ in the burster system as ϵ increases through $\epsilon_G\left(\alpha,\beta\right)$. Numerical evidence seems to be in agreement with this argument. Figures (5-3)-(5-5) show this gluing process for $\{\alpha=110,\beta=1.5\}$. This was the choice of parameters used to construct figures (4-55)-(4-57) in chapter 4.

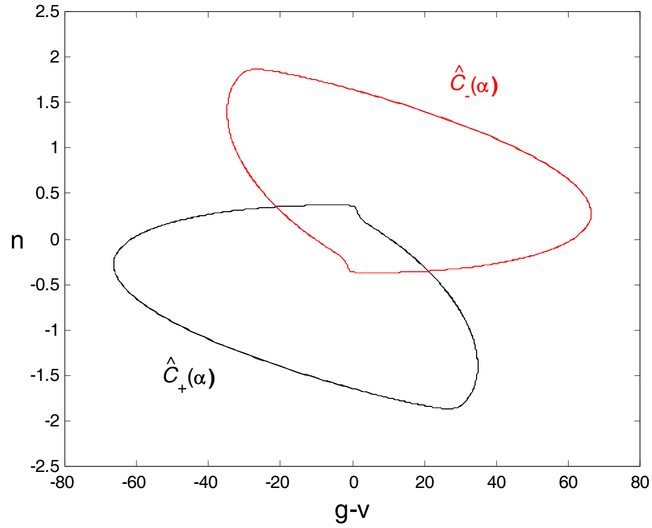

Figure 5-3: Projection onto the $(g - v, n)$ plane of the pre-gluing asymmetric limit cycles $\hat{\mathcal{C}}_+(\boldsymbol{\alpha})$ (black) and $\hat{\mathcal{C}}_-(\boldsymbol{\alpha})$ (red) of $\dot{\mathbf{z}} = \mathbf{Z}(\mathbf{z})$ for $\alpha = 110$, $\beta = 1.5$, $\epsilon = 0.004$ (cf. figure (4-55)).

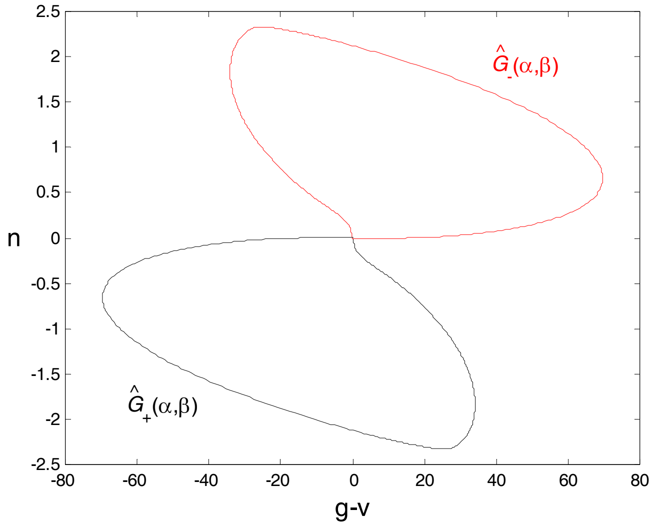

Figure 5-4: Projection onto the $(g - v, n)$ plane of the symmetry-related homoclinic orbits $\hat{G}_+(\alpha, \beta)$ (black) and $\hat{G}_-(\alpha, \beta)$ (red) of $\dot{\mathbf{z}} = \mathbf{Z}(\mathbf{z})$ for $\alpha = 110$, $\beta = 1.5$, $\epsilon \approx 0.005076305$ (cf. figure (4-56)).

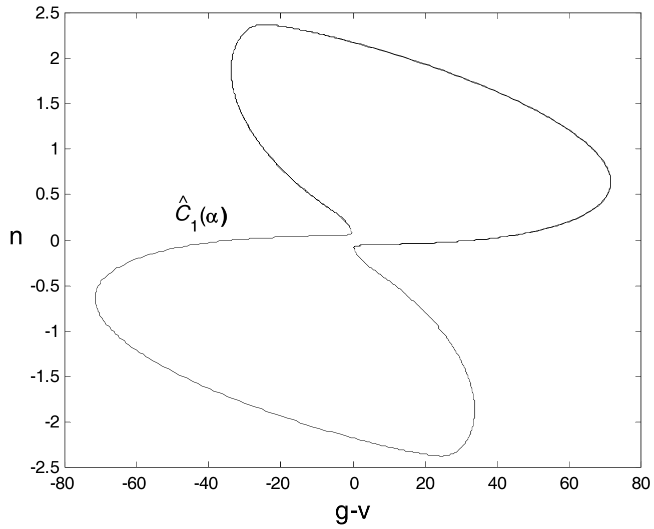

Figure 5-5: Projection onto the $(g-v,n)$ plane of the post-gluing symmetric limit cycle $\hat{\mathcal{C}}_1(\boldsymbol{\alpha})$ for $\alpha = 110$, $\beta = 1.5$, $\epsilon = 0.006$ (cf. figure (4-57)).

The nonsmooth gluing bifurcation discussed in this section appears to be qualitatively equivalent to a smooth gluing bifurcation of the saddle type with saddle index greater than 1 (cf. section 4.8.1). This raises an interesting question regarding the effect on the nonsmooth gluing bifurcation of splitting the symmetry of the saccadic equations which will be addressed in chapter 7.

5.8 Approximation of the gaze time series associated with limit cycles of the saccadic equations

In this section, the Fourier analysis of section 5.6.1 is used to approximate a relationship between the error and gaze time series of limit cycles of $\dot{\mathbf{z}} = \mathbf{Z}(\mathbf{z})$. The approximate relationship is then used to transfer the results of chapter 4 regarding the morphology of the error time series of stable limit cycles in the parameter range $\hat{\Pi}_P$, over to the morphology of the corresponding gaze time series. This analysis, together with the one-to-one relationship between the attractors of $\dot{\mathbf{y}} = \mathbf{Y}(\mathbf{y})$ and $\dot{\mathbf{z}} = \mathbf{Z}(\mathbf{z})$ in $\hat{\Pi}_P$ established earlier, will enable a full description of the attractors of $\dot{\mathbf{z}} = \mathbf{Z}(\mathbf{z})$ in $\hat{\Pi}_P$ to be proposed in the next section.

In the first part of this section, the Fourier analysis of section 5.6.1 is recapped and extended slightly. Following this, the characteristics of a filter which relates the gaze and error time series are examined. Next, the filter characteristics are used to obtain the approximate expression relating the error and gaze time series. In the final part of the section, the morphology of the gaze time series in $\hat{\Pi}_P$ is quantified.

5.8.1 Fourier analysis of the limit cycles

Assume $\hat{\mathcal{C}}$ is a limit cycle of $\dot{\mathbf{z}} = \mathbf{Z}(\mathbf{z})$ of period T. Choose $\mathbf{z}_0 = (\mathbf{x}_0, \mathbf{y}_0)^T \in \hat{\mathcal{C}}$, and define

$$\mathbf{z}_S(t) = (\mathbf{x}_S(t), \mathbf{y}_S(t))^T = (g_S(t), v_S(t), n_S(t), r_S(t), l_S(t), \varepsilon_S(t))^T$$

by $\mathbf{z}_S(t) = \psi_t(\mathbf{z}_0)$. Write $\mathbf{y}_S(t)$ as the vectorised complex Fourier series

$$\mathbf{y}_S(t) = \sum_{k=-\infty}^{\infty} \mathbf{y}_k^S e^{ik\omega_T t} \tag{5.67}$$

where $\omega_T = \frac{2\pi}{T}$ is the fundamental frequency and, for each $k \in \mathbb{Z}$, $\mathbf{y}_k^S$ is given by:

$$\mathbf{y}_k^S = \begin{pmatrix} r_k^S \\ l_k^S \\ \varepsilon_k^S \end{pmatrix} \tag{5.68}$$

It was shown in section 5.6.1 that $\mathbf{x}_S(t)$ can be represented as the vectorised complex Fourier series

$$\mathbf{x}_S(t) = \sum_{k=-\infty}^{\infty} \mathbf{x}_k^S e^{ik\omega_T t} \tag{5.69}$$

where, for each $k \in \mathbb{Z}$, $\mathbf{x}_k^S$ is given by

$$\mathbf{x}_k^S = \begin{pmatrix} T_g(ik\omega_T) \\ (ik\omega_T) T_g(ik\omega_T) \\ T_n(ik\omega_T) \end{pmatrix} \varepsilon_k^S \tag{5.70}$$

with:

$$
\begin{aligned}
T_g(s) &= -sH_g(s)\left(P_1 + P_2 H_n(s)\right) && (5.71)\\
T_n(s) &= -sH_n(s) && (5.72)\\
H_g(s) &= \frac{1}{\left(s+\frac{1}{T_1}\right)\left(s+\frac{1}{T_2}\right)} && (5.73)\\
H_n(s) &= \frac{1}{s+\frac{1}{T_N}} && (5.74)
\end{aligned}
$$

It follows from equations (5.67)-(5.70) that the error and gaze time series $\{\varepsilon_S(t) : t \geq 0\}$ and $\{g_S(t) : t \geq 0\}$ associated with $\hat{\mathcal{C}}$ are given by

$$
\begin{aligned}
\varepsilon_S(t) &= \sum_{k=-\infty}^{\infty} \varepsilon_k^S e^{ik\omega_T t} && (5.75)\\
g_S(t) &= \sum_{k=-\infty}^{\infty} g_k^S e^{ik\omega_T t} && (5.76)
\end{aligned}
$$

where:

$$
g_k^S = T_g(ik\omega_T)\,\varepsilon_k^S : k \in \mathbb{Z} \qquad (5.77)
$$

Equations (5.75)-(5.77) show that $g_S(t)$ is obtained by passing $\varepsilon_S(t)$ through a linear system (or linear filter) with transfer function $T_g(i\omega)$ [38]. It will be useful in what follows to get $T_g(i\omega)$ into polar form. Substituting (5.73) and (5.74) into (5.71) and rearranging yields

$$
T_g(s) = -\frac{P_1 s\,(s+C_1)}{\left(s+\frac{1}{T_1}\right)\left(s+\frac{1}{T_2}\right)\left(s+\frac{1}{T_N}\right)}
$$

where:

$$
C_1 = \frac{1}{T_1+T_2} + \frac{1}{T_N}
$$

Setting $s = i\omega$ in the above expression for $T_g(s)$ and using

$$
\begin{aligned}
a+bi &= \left(\sqrt{a^2+b^2}\right) e^{\arctan\left(\frac{b}{a}\right)i}\\
\frac{1}{a+bi} &= \left(\frac{1}{\sqrt{a^2+b^2}}\right) e^{-\arctan\left(\frac{b}{a}\right)i}
\end{aligned}
$$

leads to the expression

$$T_g(i\omega) = R_g(\omega)\, e^{\theta_g(\omega) i} \tag{5.78}$$

where

$$R_g(\omega) = P_1 |\omega| \sqrt{\frac{\omega^2 + C_1^2}{\left(\omega^2 + \frac{1}{T_1^2}\right)\left(\omega^2 + \frac{1}{T_2^2}\right)\left(\omega^2 + \frac{1}{T_N^2}\right)}} \tag{5.79}$$

and:

$$\theta_g(\omega) = -\left(\arctan(T_1\omega) + \arctan(T_2\omega) + \arctan(T_N\omega) + \arctan\left(\frac{C_1}{\omega}\right)\right) \tag{5.80}$$

The identity

$$\arctan(X) + \arctan(Y) = \begin{cases} \arctan\left(\frac{X+Y}{1-XY}\right) & \text{for} \quad XY < 1 \\ \pi + \arctan\left(\frac{X+Y}{1-XY}\right) & \text{for} \quad X > 0; XY > 1 \\ -\pi + \arctan\left(\frac{X+Y}{1-XY}\right) & \text{for} \quad X < 0; XY > 1 \end{cases}$$

can be used to obtain the alternative expression for $\theta_g(\omega)$ below:

$$\theta_g(\omega) = -\arctan\left(\frac{C_2\omega^4 + C_3\omega^2 - C_1}{\omega\left(C_4\omega^2 + C_5\right)}\right) + \theta_R(\omega) \tag{5.81}$$

Here

$$\theta_R(\omega) = \begin{cases} \pi & \text{for} \quad \omega > 0 \\ -\pi & \text{for} \quad \omega < 0 \end{cases}$$

and:

$$\begin{aligned} C_2 &= T_1 T_2 T_N \\ C_3 &= T_1 T_2 \left(\frac{1}{T_N} + \frac{1}{T_1 + T_2}\right) \\ C_4 &= T_N (T_1 + T_2) - \frac{T_1 T_2 T_N}{T_1 + T_2} \\ C_5 &= \frac{T_1 + T_2 + T_N}{T_1 + T_2} + \frac{T_1 + T_2}{T_N} \end{aligned}$$

(Note that $R_g(0) = 0$, so $\theta_g(\omega)$ does not have to be defined at 0. Also numerics indicate that $C_k > 0 \ \forall 2 \le k \le 5$).

5.8.2 Properties of $R_g(\omega)$ and $\theta_g(\omega)$

The functions $R_g(\omega)$ and $\theta_g(\omega)$ are investigated in this section. $R_g(\omega)$ is analysed first.

Properties of $R_g(\omega)$

The expression (5.79) for $R_g(\omega)$ implies that $R_g(\omega)$ is continuous on $\mathbb{R}$ and C^1 on $\mathbb{R}\backslash\{0\}$. Also, $R_g(\omega)$ is an even function. Consider the right derivative of $R_g(\omega)$ at 0, $D_+R_g(0)$. By definition:

$$\begin{aligned} D_+R_g(0) &= \lim_{h\to 0+} \frac{R_g(h) - R_g(0)}{h} \\ &= \lim_{h\to 0+} P_1 \sqrt{\frac{h^2 + C_1^2}{\left(h^2 + \frac{1}{T_1^2}\right)\left(h^2 + \frac{1}{T_2^2}\right)\left(h^2 + \frac{1}{T_N^2}\right)}} \\ &= P_1 C_1 C_2 \end{aligned}$$

Write $D_-R_g(0)$ for the left derivative of $R_g(\omega)$ at 0. Then as $R_g(\omega)$ is even, $D_-R_g(0) = -D_+R_g(0)$. Thus, since $P_1, C_1, C_2 > 0$, $D_-R_g(0) \neq -D_+R_g(0)$. $R_g(\omega)$ is therefore not differentiable at 0. For $\omega \neq 0$, $DR_g(\omega)$ is given by:

$$DR_g(\omega) = -\frac{P_1 \operatorname{sign}(\omega) R_1(\omega)}{\left(\omega^2 + C_1^2\right)^{\frac{1}{2}} R_2(\omega)^{\frac{3}{2}}} \tag{5.82}$$

where

$$\begin{aligned} R_1(\omega) &= \omega^8 + 2C_1^2\omega^6 + \left(C_6C_1^2 - C_7\right)\omega^4 - 2C_8\omega^2 - C_8C_1^2 && (5.83) \\ R_2(\omega) &= \left(\omega^2 + \frac{1}{T_1^2}\right)\left(\omega^2 + \frac{1}{T_2^2}\right)\left(\omega^2 + \frac{1}{T_N^2}\right) && (5.84) \end{aligned}$$

and:

$$\begin{aligned} C_6 &= \frac{1}{T_1^2} + \frac{1}{T_2^2} + \frac{1}{T_N^2} \\ C_7 &= \frac{1}{(T_1T_2)^2} + \frac{1}{(T_1T_N)^2} + \frac{1}{(T_2T_N)^2} \\ C_8 &= \frac{1}{(T_1T_2T_N)^2} \end{aligned}$$

Equations (5.82)-(5.84) imply that for $\omega > 0$, $\operatorname{sign}(DR_g(\omega)) = -\operatorname{sign}(R_1(\omega))$. It can be seen from (5.83) that $R_1(0) = -C_8C_1^2 < 0$, while $R_1(\omega) \sim \omega^8$ for large ω. $R_1(\omega)$

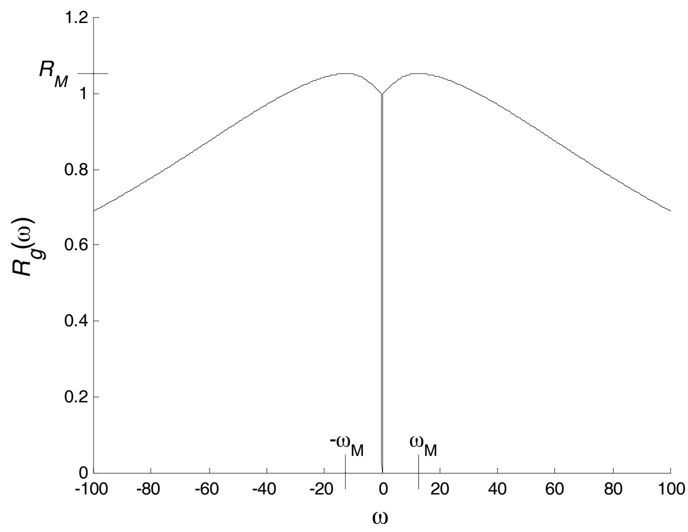

Figure 5-6: Plot of $R_g(\omega)$ in the range $(-100, 100)$. The maxima at ω_M and $-\omega_M$ are indicated.

must therefore have at least one zero on $(0, \infty)$. Numerics indicate that $R_1(\omega)$ has only one zero, ω_M, in this range, with $\omega_M \approx 12.7419$. Define R_M by $R_M = R_g(\omega_M)$. R_M has the approximate numerical value 1.0524. Since $R_1(\omega)$ has only the single zero ω_M on $(0, \infty)$, $R_g(\omega)$ is increasing on $0 < \omega < \omega_M$ and decreasing on $\omega_M < \omega < \infty$, with a maximum at ω_M. As $R_g(\omega)$ is even, this means that $R_g(\omega)$ is increasing on $(-\infty, -\omega_M)$ and decreasing on $(-\omega_M, 0)$, with a maximum at $-\omega_M$. Finally, (5.79) implies that for $\omega \gg 0$, $R_g(\omega) \sim \frac{P_1}{\omega}$. Hence, $R_g(\omega) \to 0+$ as $\omega \to \infty$. Since $R_g(\omega)$ is even, this means $R_g(\omega) \to 0+$ as $t \to -\infty$ also. Figures (5-6) and (5-7) are plots of $R_g(\omega)$, confirming the above analysis. Inspection of figures (5-6) and (5-7) suggests $R_g(\omega) \approx 1$ for ω in the range $0.1 < |\omega| < 35$. This observation will now be made more concrete. As $R_g(\omega)$ has a global maximum on $(0, \infty)$ at ω_M and $R_g(\omega_M) = R_M > 1$, it follows that there are 2 values of ω at which $R_g(\omega) = 1$ on $(0, \infty)$. Write these as ω_1 and ω_2 with $\omega_1 < \omega_2$. By (5.79), ω_1 and ω_2 must satisfy

$$P_1\omega\sqrt{\frac{\omega^2 + C_1^2}{\left(\omega^2 + \frac{1}{T_1^2}\right)\left(\omega^2 + \frac{1}{T_2^2}\right)\left(\omega^2 + \frac{1}{T_N^2}\right)}} = 1$$

Squaring both sides of the above and rearranging yields:

$$\omega^6 + (C_6 - P_1^2)\omega^4 + +(C_7 - P_1^2C_1^2)\omega^2 + C_8 = 0$$

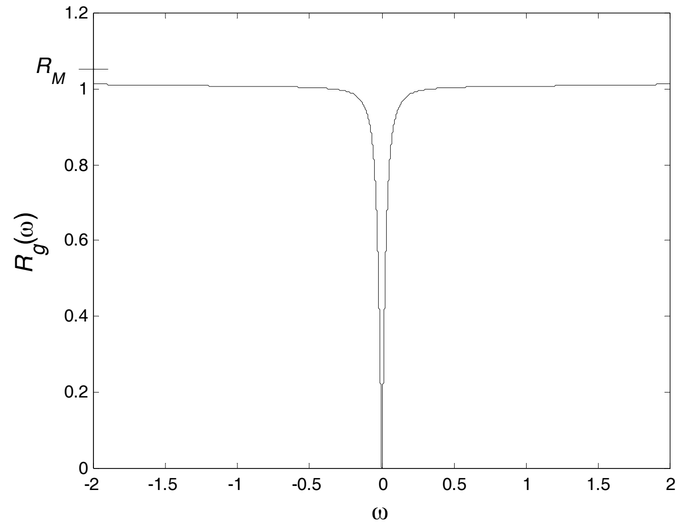

Figure 5-7: Close up of figure (5-6) about $\omega = 0$.

Solving this equation numerically gives $\omega_1 = 0.3456$, $\omega_2 = 33.3871$. For $\omega_1 < |\omega| < \omega_2$, $1 < R_g(\omega) < R_M$ and so $R_g(\omega) \approx 1$. This approximation will be useful later in the section.

Properties of $\theta_g(\omega)$

The function $\theta_g(\omega)$ is now analysed. (5.80) implies that $\theta_g(\omega)$ is C^1 on $\mathbb{R}\backslash\{0\}$. Also, $\theta_g(\omega)$ is an odd function. By, (5.80), $\lim_{\omega\to 0+}\theta_g(\omega) = -\lim_{\omega\to 0+}\arctan\left(\frac{C_1}{\omega}\right)$. As $\omega \to 0+$, $\frac{C_1}{\omega} \to \infty$. Thus, $\lim_{\omega\to 0+}\theta_g(\omega) = \frac{3\pi}{2}$. Since, $\theta_g(\omega)$ is odd, this means that $\lim_{\omega\to 0-}\theta_g(\omega) = -\frac{3\pi}{2}$. $\theta_g(\omega)$ is therefore discontinuous at 0. Using (5.81), the following expression for $D\theta_g(\omega)$ on $\mathbb{R}\backslash\{0\}$ can be derived

$$D\theta_g(\omega) = -\frac{G_3(\omega)}{G_1(\omega)^2 + G_2(\omega)^2} \tag{5.85}$$

where:

$$\begin{aligned} G_1(\omega) &= C_2\omega^4 + C_3\omega^2 - C_1 \\ G_2(\omega) &= \omega\left(C_4\omega^2 + C_5\right) \end{aligned}$$

$$G_3(\omega) = C_2C_4\omega^6 + (3C_2C_5 - C_3C_4)\,\omega^4 + (3C_1C_4 + C_3C_5)\omega^2 + C_1C_5$$

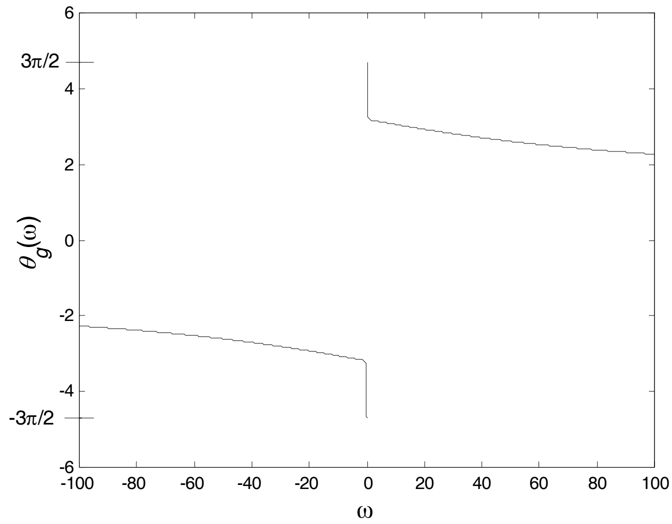

Figure 5-8: Plot of $\theta_g(\omega)$ in the range $(-100, 100)$.

The constant $3C_2C_5 - C_3C_4$ is greater than 0. Thus, $G_3(\omega) > 0 \; \forall\omega \in \mathbb{R}$ and so $\theta_g(\omega)$ is strictly decreasing on $\mathbb{R}\backslash\{0\}$. Finally, it can be seen from (5.81) that for $\omega \gg 0$, $\theta_g(\omega) \sim -\arctan\left(\frac{C_2}{C_4}\omega\right) + \pi$. Hence, as $\omega \to \infty$, $\theta_g(\omega) \to -\frac{\pi}{2} + \pi = \frac{\pi}{2}$. Since $\theta_g(\omega)$ is odd, this means $\theta_g(\omega) \to -\frac{\pi}{2}$ as $\omega \to -\infty$.

Figure (5-8) is a plot of $\theta_g(\omega)$ on the interval $(-100, 100)$, confirming the above analysis. Figure (5-9) shows $\theta_g(\omega)$ restricted to the interval (ω_1, ω_2). It can be seen that $\theta_g(\omega)$ is close to being linear in this range. This suggests that $\theta_g(\omega)$ can be fitted by a linear function on (ω_1, ω_2) (and hence on $(-\omega_2, -\omega_1)$ also). Let $\hat{\theta}_g : \mathbb{R} \to \mathbb{R}$ be defined by

$$\hat{\theta}_g(\omega) = -t_g\omega + \operatorname{sign}(\omega)\, b_g$$

and given $N \geq 1$, set $v_k = \omega_1 + \left(\frac{\omega_2 - \omega_1}{N-1}\right)(k-1) \; \forall 1 \leq k \leq N$. For $N = 10000$, the values of t_g and b_g which minimise the summed square error

$$\sum_{k=1}^{N} \left|\theta_g(v_k) - \hat{\theta}_g(v_k)\right|^2$$

are:

$$t_g = 0.0126 \quad (5.86)$$

$$b_g = 3.1848 \quad (5.87)$$

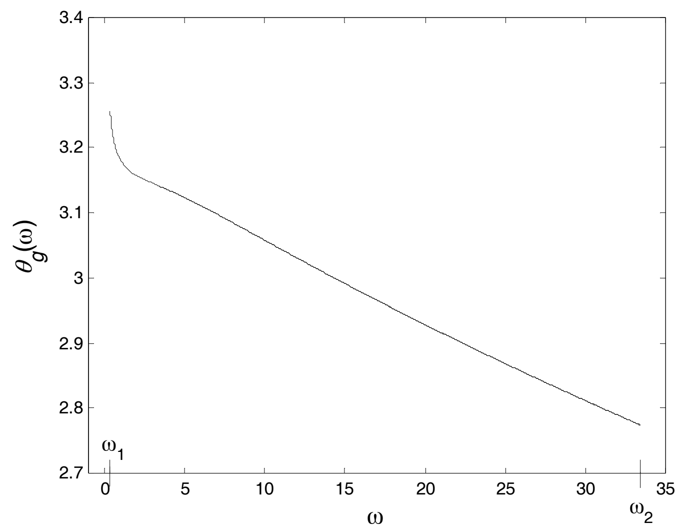

Figure 5-9: Plot of $\theta_g(\omega)$ in the range (ω_1, ω_2)

Figure (5-10) is a plot of both $\theta_g(\omega)$ and $\hat{\theta}_g(\omega)$ on (ω_1, ω_2) for the values of t_g and b_g above. $\hat{\theta}_g(\omega)$ can be seen to be a close approximation to $\theta_g(\omega)$ on (ω_1, ω_2). The mean relative error $E_{MRE} = \frac{1}{N}\sum_{k=1}^{N} \frac{\left|\hat{\theta}_g(v_k) - \theta_g(v_k)\right|}{|\theta_g(v_k)|}$ in the approximation is 0.001219. Since $\hat{\theta}_g(\omega)$ and $\theta_g(\omega)$ are both odd, it follows that $\hat{\theta}_g(\omega)$ is a good approximation to $\theta_g(\omega)$ for $\omega_1 < |\omega| < \omega_2$, with the same mean relative error.

The fact that for $\omega_1 < |\omega| < \omega_2$, $R_g(\omega) \approx 1$ and $\theta_g(\omega)$ is near linear, suggests that the filter $T_g(i\omega)$ will preserve the amplitude of the components of the input signal $\varepsilon_S(t)$ in the frequency range $(-\omega_2, -\omega_1) \cup (\omega_1, \omega_2)$, while introducing a delay. The amplitude of components lying outside this range will be attenuated with the attenuation increasing as $|\omega| \to 0$ and as $|\omega| \to \infty$. In particular, $T_g(0) = 0$, so the output signal $g_S(t)$ will have zero mean. Additionally, the phases of components lying outside the range $(-\omega_2, -\omega_1) \cup (\omega_1, \omega_2)$ will be modified in a nontrivial way. This discussion suggests that provided the input signal does not have significant power outside the frequency range $(-\omega_2, -\omega_1) \cup (\omega_1, \omega_2)$, it may be possible to model $g_S(t)$ as a time-delayed version of $\varepsilon_S(t)$, which has had its mean subtracted. This approach forms the basis of the next part of the analysis.

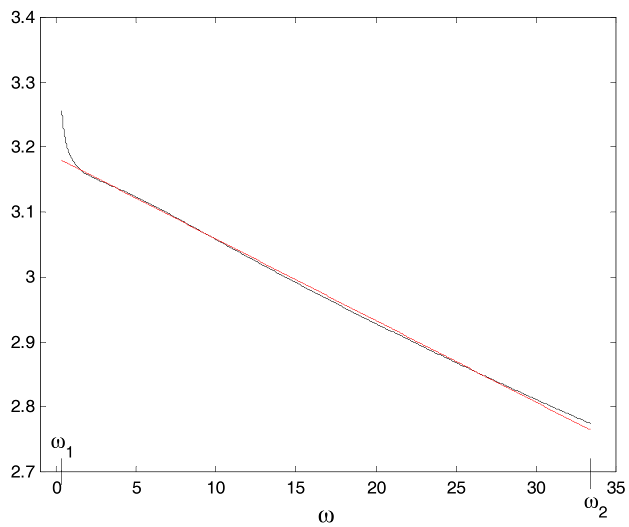

Figure 5-10: Plot of $\theta_g(\omega)$ (black line) and $\hat{\theta}_g(\omega)$ (red line) on (ω_1, ω_2) for the values of t_g and b_g given in (5.86)-(5.87).

5.8.3 Relating $\varepsilon_S(t)$ to $g_S(t)$

It was demonstrated above that for $|\omega| \in (\omega_1, \omega_2)$, $R_g(\omega) \approx 1$ and $\theta_g(\omega) \approx \hat{\theta}_g(\omega)$ where:

$$\hat{\theta}_g(\omega) = \begin{cases} -t_g\omega + b_g & \text{if} \quad \omega_1 < \omega < \omega_2 \\ -t_g\omega - b_g & \text{if} \quad -\omega_2 < \omega < -\omega_1 \end{cases}$$

(Recall, $\omega_1 = 0.3456$, $\omega_2 = 33.3871$, $t_g = 0.0126$, $b_g = 3.1848$). Making the further approximation $b_g \approx \pi$ and using expression (5.78) leads to the approximation $T_g(i\omega) \approx -e^{-it_g\omega}$ for $|\omega| \in (\omega_1, \omega_2)$. Define the set $W_S \subset \mathbb{N}$ by

$$W_S = \{k \geq 1 : k\omega_T \in (\omega_1, \omega_2)\} \tag{5.88}$$

and the set $W_N \subset \mathbb{N}$ by $W_N = \mathbb{N} \backslash W_S$. Then by (5.75):

$$\varepsilon_S(t) = \varepsilon_0^S + \sum_{|k| \in W_S} \varepsilon_k^S e^{ik\omega_T t} + \sum_{|k| \in W_N} \varepsilon_k^S e^{ik\omega_T t}$$

Note that by definition, ε_0^S is equal to the mean $\langle \varepsilon_S(t) \rangle$ of $\varepsilon_S(t)$ over one period, $\langle \varepsilon_S(t) \rangle = \frac{1}{T}\int_0^T \varepsilon_S(t)\, dt$ [38]. Assuming that $\sum_{|k| \in W_S} \left|\varepsilon_k^S\right|^2 \gg \sum_{|k| \in W_N} \left|\varepsilon_k^S\right|^2$ (i.e. that the power of $\varepsilon_S(t)$ in the frequency range (ω_1, ω_2) is greater than the power in the range $(0, \omega_1) \cup$

(ω_2, ∞)), it is possible to make the approximation:

$$\varepsilon_S(t) \approx \langle \varepsilon_S(t) \rangle + \sum_{|k| \in W_S} \varepsilon_k^S e^{ik\omega_T t} \tag{5.89}$$

As mentioned previously, $T_g(0) = 0$, and so $g_0^S = 0$. Hence, by (5.76):

$$g_S(t) = \sum_{|k| \in W_S} g_k^S e^{ik\omega_T t} + \sum_{|k| \in W_N} g_k^S e^{ik\omega_T t}$$

Consider the power of $g_S(t)$ in the frequency range (ω_1, ω_2). Using $g_k^S = T_g(ik\omega_T)\,\varepsilon_k^S$ together with the approximation $T_g(i\omega) \approx -e^{-it_g\omega}$ for $|\omega| \in (\omega_1, \omega_2)$ gives:

$$\sum_{|k| \in W_S} \left|g_k^S\right|^2 \approx \sum_{|k| \in W_S} \left|\varepsilon_k^S\right|^2$$

Thus, since by assumption $\sum_{|k| \in W_S} \left|\varepsilon_k^S\right|^2 \gg \sum_{|k| \in W_N} \left|\varepsilon_k^S\right|^2$, $\sum_{|k| \in W_S} \left|g_k^S\right|^2 \gg \sum_{|k| \in W_N} \left|\varepsilon_k^S\right|^2$. By the definition of W_N, $|T_g(ik\omega_T)| < 1\ \forall\, |k| \in W_N$. Hence:

$$\sum_{|k| \in W_N} \left|\varepsilon_k^S\right|^2 > \sum_{|k| \in W_N} |T_g(ik\omega_T)| \left|\varepsilon_k^S\right|^2 = \sum_{|k| \in W_N} \left|g_k^S\right|^2$$

It follows that $\sum_{|k| \in W_S} \left|g_k^S\right|^2 \gg \sum_{|k| \in W_N} \left|g_k^S\right|^2$ (i.e. the power of $g_S(t)$ in the frequency range (ω_1, ω_2) is greater than the power in the range $(0, \omega_1) \cup (\omega_2, \infty)$). It is therefore possible to make the approximation:

$$g_S(t) \approx \sum_{|k| \in W_S} g_k^S e^{ik\omega_T t}$$

The relation $g_k^S = T_g(ik\omega_T)\,\varepsilon_k^S$ together with the approximation $T_g(i\omega) \approx -e^{-it_g\omega}$ for $|\omega| \in (\omega_1, \omega_2)$ then yields:

$$g_S(t) \approx -\sum_{|k| \in W_S} \varepsilon_k^S e^{ik\omega_T (t - t_g)} \tag{5.90}$$

Comparing (5.89) and (5.90) and using the equality $\langle \varepsilon_S(t - t_g) \rangle = \langle \varepsilon_S(t) \rangle$ leads to the final approximation $g_S(t) \approx \hat{g}_S(t)$ where:

$$\hat{g}_S(t) = -\varepsilon_S(t - t_g) + \langle \varepsilon_S(t) \rangle \tag{5.91}$$

In conclusion, provided that $\varepsilon_S(t)$ does not have significant power in the frequency range $(0, \omega_1) \cup (\omega_2, \infty)$, $g_S(t)$ should be reasonably well modelled as a flipped, time-delayed version of $\varepsilon_S(t)$, with a d.c. shift that zeroes the mean.

If the limit cycle of interest $\hat{\mathcal{C}}$ is symmetric, then as shown in section 5.6.2, $\varepsilon_S\left(t + \frac{T}{2}\right) = -\varepsilon(t)\ \forall t \in \mathbb{R}$, from which it follows that $\langle \varepsilon_S(t) \rangle = 0$. In this case, (5.91) reduces to $\hat{g}_S(t) = -\varepsilon_S(t - t_g)$.

5.8.4 Morphology of $\{g_S(t) : t \geq 0\}$ in the range $\hat{\Pi}_P$

Given $\boldsymbol{\alpha} \in \hat{\Pi}_P$, let

$$\mathbf{z}_S(t) = (g_S(t), v_S(t), n_S(t), r_S(t), l_S(t), \varepsilon_S(t))^T$$

be a periodic solution of $\dot{\mathbf{z}} = \mathbf{Z}(\mathbf{z})$ associated with a stable limit cycle $\hat{\mathcal{C}}$. The approximation $g_S(t) \approx \hat{g}_S(t)$ is now used to relate the morphology of the error time series $\{\varepsilon_S(t) : t \geq 0\}$ to the gaze time series $\{g_S(t) : t \geq 0\}$. By assumption, all limit cycles of the saccadic system lie in the compact set $\hat{C} = \bar{B}_{M_{\bar{\varepsilon}}}(\mathbf{0}) \times C$, where

$$\bar{B}_{M_{\bar{\varepsilon}}}(\mathbf{0}) = \left\{\mathbf{x} \in \mathbb{R}^3 : \|\mathbf{x}\|_1 \leq M_{\bar{\varepsilon}}\right\}$$

and:

$$C = \left\{(r, l, \varepsilon)^T \in \mathbb{R}^3 : 0 \leq r, l \leq \alpha_M, |\varepsilon| \leq \varepsilon_M\right\}$$

(cf. section 5.2). As $\dot{\varepsilon} = -(r - l)$ and $0 \leq r, l \leq \alpha_M$ for $(r, l, \varepsilon)^T \in C$, it follows that $\forall t \geq 0$, $|\dot{\varepsilon}_S(t)| \leq 2\alpha_M$. Moreover (for small ϵ in particular), the extent of $\hat{\mathcal{C}}$ in the $r - l$ direction is limited by the existence of the slow manifold S_M, giving an even tighter bound on $|\dot{\varepsilon}_S(t)|$. The limit on the size of $|\dot{\varepsilon}_S(t)|$ suggests that it is unlikely $\varepsilon_S(t)$ will have significant power in the higher frequencies. Hence, provided $\varepsilon_S(t)$ does not have significant power in the lower frequencies, the function $\hat{g}_S(t)$ defined in (5.91) should provide a good approximation to $g_S(t)$. If, however, $\hat{\mathcal{C}}$ is near-homoclinic, the trajectory $\{\mathbf{z}_S(t) : t \geq 0\}$ spends long periods in the vicinity of the origin $(\mathbf{0}, \mathbf{0})^T$, and so $\varepsilon_S(t)$ may have significant power in the lower frequencies. Consequently, $\hat{g}_S(t)$ may a poorer approximation to $g_S(t)$, at least during the low velocity phases of the waveform. Figures (5-11)-(5-20) are plots of gaze time series $\{g_S(t) : t \geq 0\}$ associated with limit cycle attractors for choices of $\boldsymbol{\alpha}$

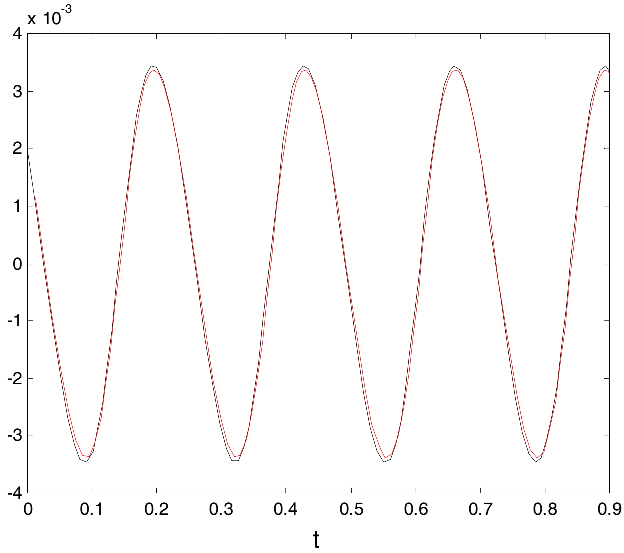

Figure 5-11: Plot of a gaze time series $\{g_S(t) : t \geq 0\}$ associated with $\hat{\mathcal{C}}_+$ for $\alpha = 306.84$, $\beta = 4.5$, $\epsilon = 0.002$ (black line) together with the approximation $\{\hat{g}_S(t) : t \geq 0\}$ (red line). $\boldsymbol{\alpha}$ lies in region C of $\hat{\Pi}_P$. $E_{RE} \approx 0.051535$.

in each of the regions C-J of $\hat{\Pi}_P$, together with plots of the corresponding approximation $\{\hat{g}_S(t) : t \geq 0\}$ in each case. A numerical approximation to the relative error

$$E_{RE} = \frac{\|g_S(t) - \hat{g}_S(t)\|_\infty}{\|g_S(t)\|_\infty} = \frac{\max_{0 \leq t \leq T} |g_S(t) - \hat{g}_S(t)|}{\max_{0 \leq t \leq T} |g_S(t)|}$$

is also included in each figure.[2] For the choices of $\boldsymbol{\alpha}$ used to generate the plots, the limit cycles are far from homoclinicity. It can be seen that in each case $\hat{g}_S(t)$ very closely approximates $g_S(t)$. Indeed, this was found to be the case for all such test choices of $\boldsymbol{\alpha}$ in regions C-J. An important consequence of the accuracy of the approximation $g_S(t) \approx \hat{g}_S(t)$ for far-from homoclinic limit cycles is that the gaze time series $\{g_S(t) : t \geq 0\}$ corresponding to such cycles in regions D and E inherit the slow-fast form of the associated error time series $\{\varepsilon_S(t) : t \geq 0\}$, and therefore resemble the corresponding congenital nystagmus waveforms. This can be seen in figures (5-12) and (5-13): the gaze time series associated with the cycle in D can be seen to have the form of a jerk nystagmus, while the gaze time series associated with the cycle in E has the form of a bilateral jerk nystagmus. Another interesting consequence of the accuracy of the approximation for far from homoclinic limit cycles is that the gaze time series $\{g_S(t) : t \geq 0\}$ corresponding to cycles in region F inherit the si-

[2] E_{RE} is approximated for each function in the fraction by finding the maximum of the absolute value of the function over 10^5 equally spaced points in $\left[0, \hat{T}\right]$, where $\hat{T}$ is a numerical approximation to T obtained through a level crossing method [39].

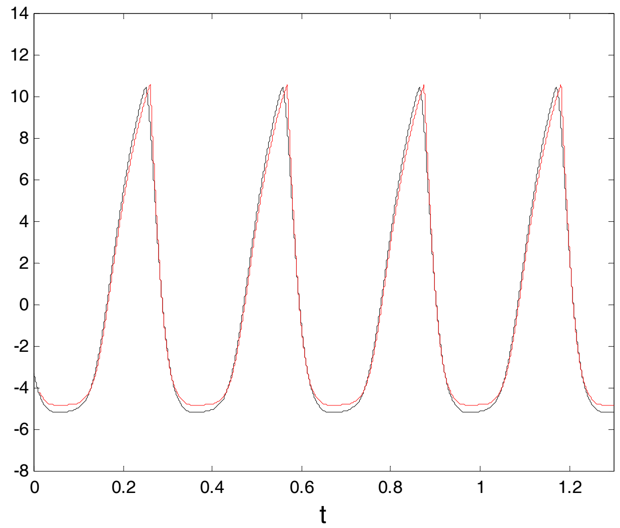

Figure 5-12: Plot of a gaze time series $\{g_S(t) : t \geq 0\}$ associated with $\hat{\mathcal{C}}_-$ for $\alpha = 408.0569$, $\beta = 6$, $\epsilon = 0.0005$ (black line) together with the approximation $\{\hat{g}_S(t) : t \geq 0\}$ (red line). $\boldsymbol{\alpha}$ lies in region D of $\hat{\Pi}_P$. $E_{RE} \approx 0.187591$.

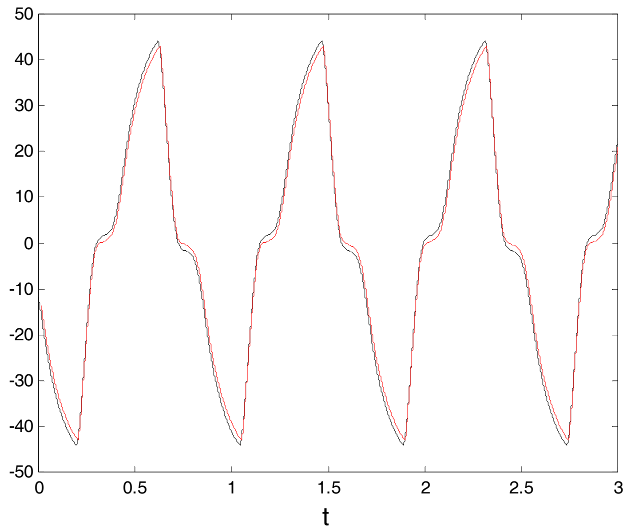

Figure 5-13: Plot of a gaze time series $\{g_S(t) : t \geq 0\}$ associated with $\hat{\mathcal{C}}_2$ for $\alpha = 805.0171$, $\beta = 12$, $\epsilon = 0.0065$ (black line) together with the approximation $\{\hat{g}_S(t) : t \geq 0\}$ (red line). $\boldsymbol{\alpha}$ lies in region E of $\hat{\Pi}_P$. $E_{RE} \approx 0.048727$.

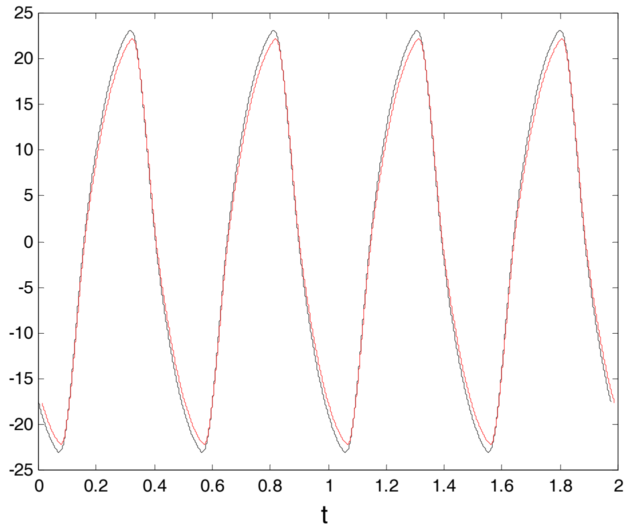

Figure 5-14: Plot of a gaze time series $\{g_S(t) : t \geq 0\}$ associated with $\hat{\mathcal{C}}_2$ for $\alpha = 420$, $\beta = 6$, $\epsilon = 0.04$ (black line) together with the approximation $\{\hat{g}_S(t) : t \geq 0\}$ (red line). $\boldsymbol{\alpha}$ lies in region F of $\hat{\Pi}_P$. $E_{RE} \approx 0.061026$.

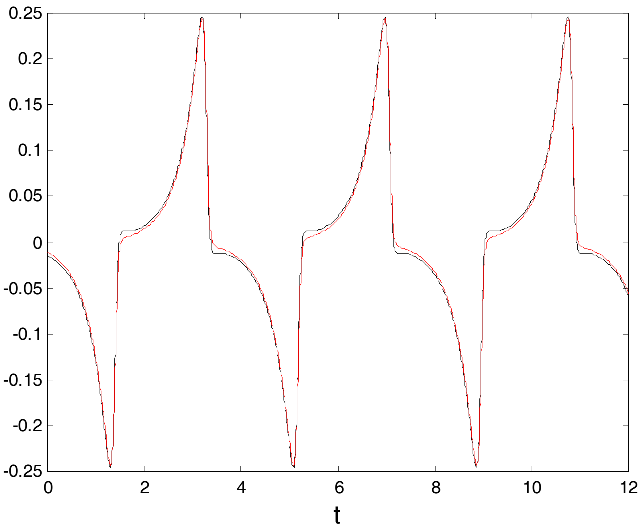

Figure 5-15: Plot of a gaze time series $\{g_S(t) : t \geq 0\}$ associated with $\hat{\mathcal{C}}_1$ for $\alpha = 208.4$, $\beta = 3$, $\epsilon = 0.03$ (black line) together with the approximation $\{\hat{g}_S(t) : t \geq 0\}$ (red line). $\boldsymbol{\alpha}$ lies in region G of $\hat{\Pi}_P$. $E_{RE} \approx 0.041557$.

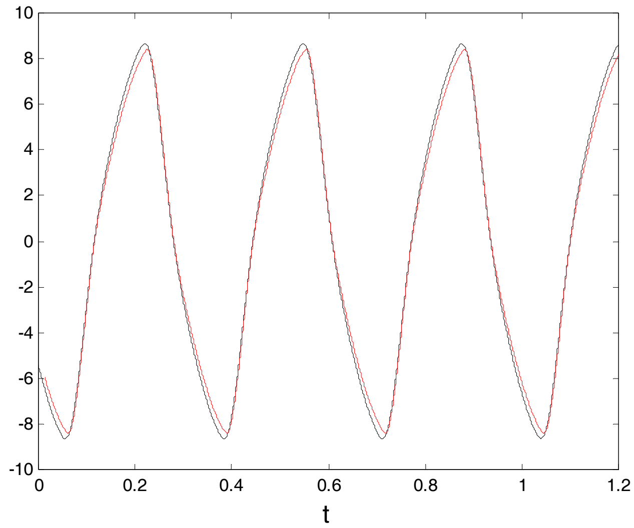

Figure 5-16: Plot of a gaze time series $\{g_S\,(t) : t \geq 0\}$ associated with $\hat{\mathcal{C}}_2$ for $\alpha = 208.4$, $\beta = 3$, $\epsilon = 0.03$ (black line) together with the approximation $\{\hat{g}_S\,(t) : t \geq 0\}$ (red line). $\boldsymbol{\alpha}$ lies in region G of $\hat{\Pi}_P$. $E_{RE} \approx 0.060948$.

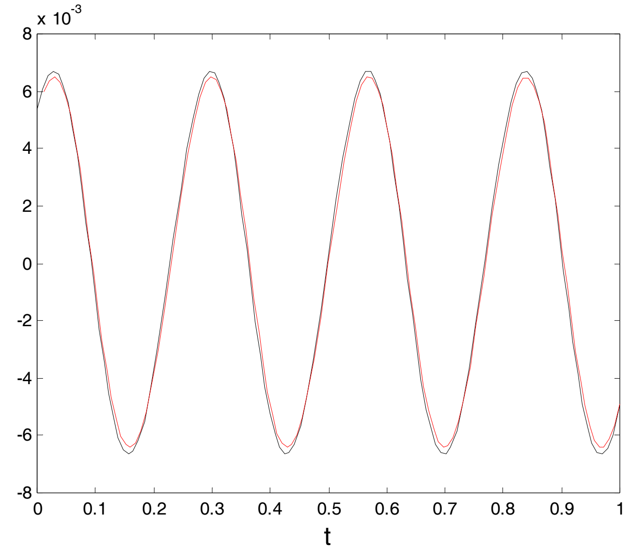

Figure 5-17: Plot of a gaze time series $\{g_S\,(t) : t \geq 0\}$ associated with $\hat{\mathcal{C}}_-$ for $\alpha = 108.62$, $\beta = 1.5$, $\epsilon = 0.01$ (black line) together with the approximation $\{\hat{g}_S\,(t) : t \geq 0\}$ (red line). $\boldsymbol{\alpha}$ lies in region H of $\hat{\Pi}_P$. $E_{RE} \approx 0.051614$.

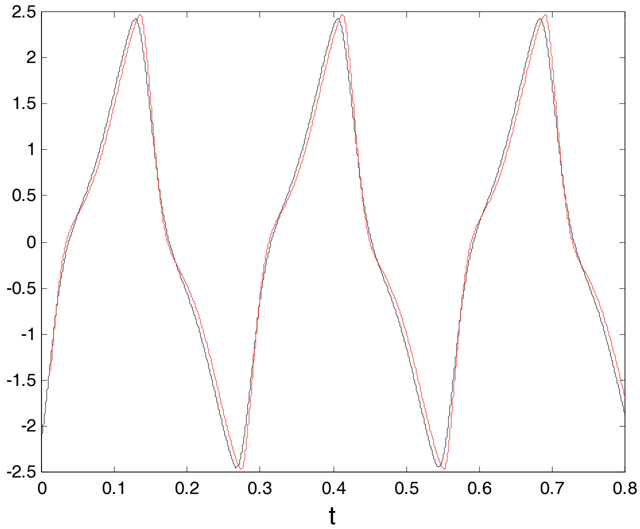

Figure 5-18: Plot of a gaze time series $\{g_S(t) : t \geq 0\}$ associated with $\hat{\mathcal{C}}_2$ for $\alpha = 108.62$, $\beta = 1.5$, $\epsilon = 0.01$ (black line) together with the approximation $\{\hat{g}_S(t) : t \geq 0\}$ (red line). $\boldsymbol{\alpha}$ lies in region H of $\hat{\Pi}_P$. $E_{RE} \approx 0.118728$.

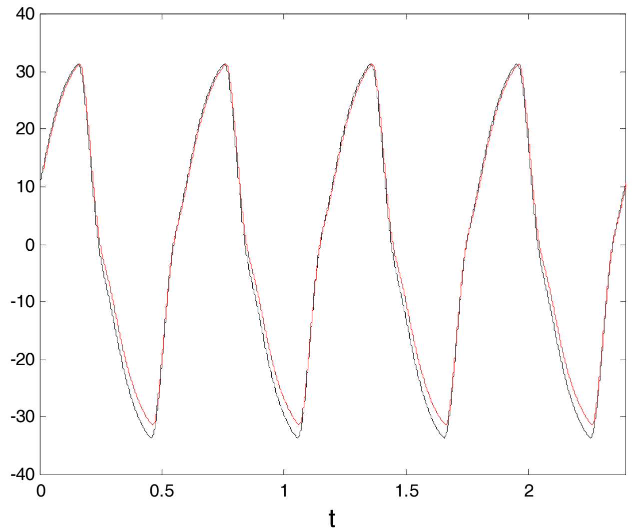

Figure 5-19: Plot of a gaze time series $\{g_S(t) : t \geq 0\}$ associated with $\hat{\mathcal{C}}_2$ for $\alpha = 620$, $\beta = 9$, $\epsilon = 0.02$ (black line) together with the approximation $\{\hat{g}_S(t) : t \geq 0\}$ (red line). $\boldsymbol{\alpha}$ lies in region I of $\hat{\Pi}_P$. $E_{RE} \approx 0.088364$.

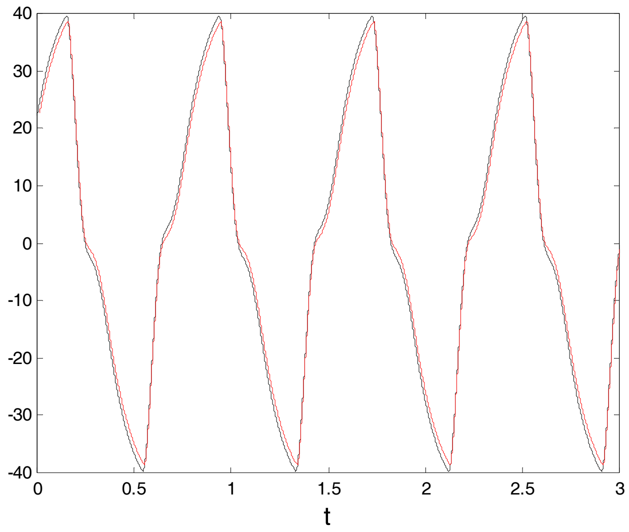

Figure 5-20: Plot of a gaze time series $\{g_S(t) : t \geq 0\}$ associated with $\hat{\mathcal{C}}_2$ for $\alpha = 600$, $\beta = 12$, $\epsilon = 0.01$ (black line) together with the approximation $\{\hat{g}_S(t) : t \geq 0\}$ (red line). $\boldsymbol{\alpha}$ lies in region J of $\hat{\Pi}_P$. $E_{RE} \approx 0.049554$.

nusoidal form of the associated error time series $\{\varepsilon_S(t) : t \geq 0\}$, and consequently resemble pendular nystagmus waveforms. This is illustrated in figure (5-14).

Figures (5-21)-(5-24) are plots of gaze time series $\{g_S(t) : t \geq 0\}$ associated with near-homoclinic limit cycle attractors in regions D, E, G and H of $\hat{\Pi}_P$, together with plots of the corresponding approximation $\{\hat{g}_S(t) : t \geq 0\}$ in each case. The values of α and β used in figures (5-21) and (5-22) are the same as in figures (5-12) and (5-13) respectively, while the values of β and ϵ used in figures (5-23) and (5-24) are the same as in figures (5-15) and (5-17) respectively. Again, a numerical approximation to the relative error E_{RE} is included with each plot.

The figures illustrate that, perhaps surprisingly, $\hat{g}_S(t)$ is still a very good approximation to $g_S(t)$ in each case, despite the near-homoclinicity of the limit cycles. Indeed although $\hat{g}_S(t)$ can be seen to be a poorer approximation to $g_S(t)$ during part of the slow-velocity portions of the waveform, for all test choices of $\boldsymbol{\alpha}$ in regions D, E, G and H, the approximation was found to be sufficiently accurate for the basic morphology of $g_S(t)$ to be determined by that of $\hat{g}_S(t)$. A significant outcome of this is that, as in the far-from homoclinic case, the gaze time series $\{g_S(t) : t \geq 0\}$ corresponding to near-homoclinic limit cycles in regions D and E inherit the slow-fast form of the associated error time series $\{\varepsilon_S(t) : t \geq 0\}$. As a consequence, the gaze time series resemble the corresponding congenital nystagmus

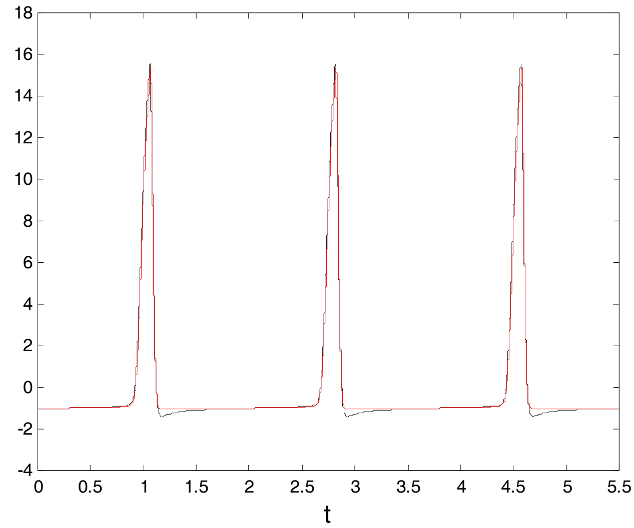

Figure 5-21: Plot of a gaze time series $\{g_S(t) : t \geq 0\}$ associated with $\hat{\mathcal{C}}_-$ for $\alpha = 408.0569$, $\beta = 6$, $\epsilon = 0.0045$ (black line) together with the approximation $\{\hat{g}_S(t) : t \geq 0\}$ (red line). $\boldsymbol{\alpha}$ lies in region D of $\hat{\Pi}_P$. $E_{RE} \approx 0.083806$.

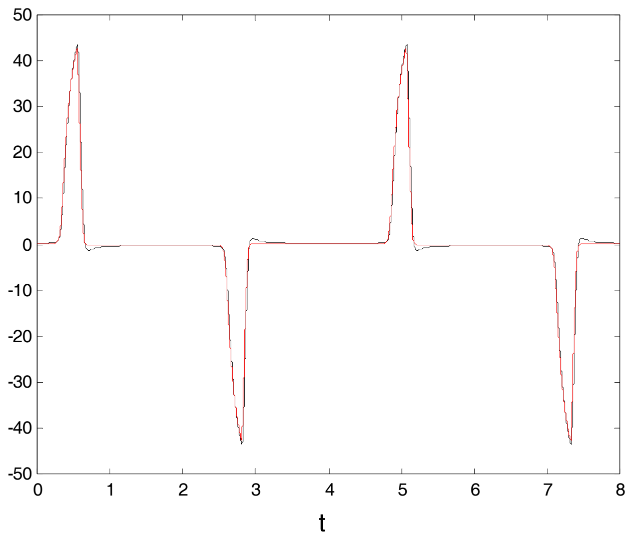

Figure 5-22: Plot of a gaze time series $\{g_S(t) : t \geq 0\}$ associated with $\hat{\mathcal{C}}_2$ for $\alpha = 805.0171$, $\beta = 12$, $\epsilon = 0.0054$ (black line) together with the approximation $\{\hat{g}_S(t) : t \geq 0\}$ (red line). $\boldsymbol{\alpha}$ lies in region E of $\hat{\Pi}_P$. $E_{RE} \approx 0.040183$.

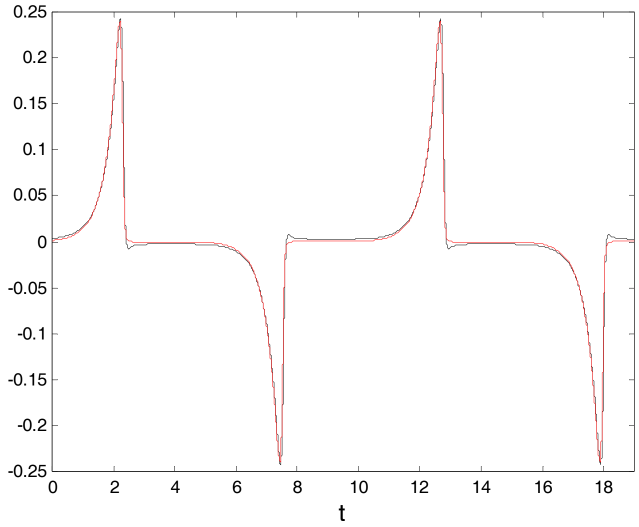

Figure 5-23: Plot of a gaze time series $\{g_S(t) : t \geq 0\}$ associated with $\hat{\mathcal{C}}_1$ for $\alpha = 208.3876$, $\beta = 3$, $\epsilon = 0.03$ (black line) together with the approximation $\{\hat{g}_S(t) : t \geq 0\}$ (red line). $\boldsymbol{\alpha}$ lies in region G of $\hat{\Pi}_P$. $E_{RE} \approx 0.190401$.

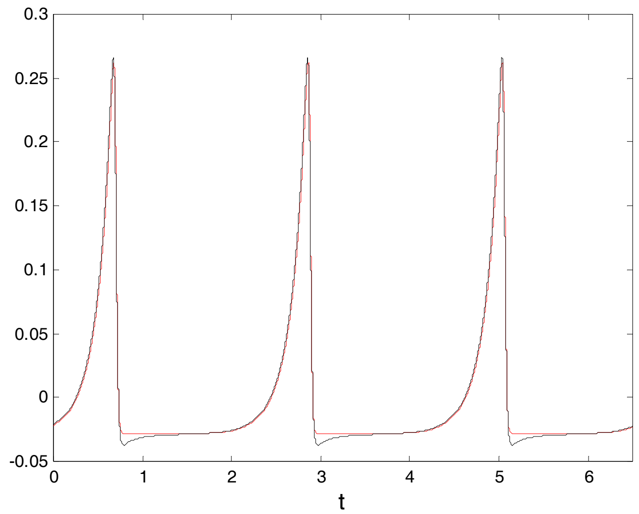

Figure 5-24: Plot of a gaze time series $\{g_S(t) : t \geq 0\}$ associated with $\hat{\mathcal{C}}_-$ for $\alpha = 109.4003$, $\beta = 1.5$, $\epsilon = 0.01$ (black line) together with the approximation $\{\hat{g}_S(t) : t \geq 0\}$ (red line). $\boldsymbol{\alpha}$ lies in region H of $\hat{\Pi}_P$. $E_{RE} \approx 0.218605$.

oscillations. This can be seen in figures (5-21) and (5-22). The gaze time series associated with the limit cycle in D has the form of a jerk nystagmus with an extended foveation period, while the time series associated with the cycle in E has the form of a bilateral jerk nystagmus with an extended foveation period.

5.9 Attractors of the saccadic equations in $\hat{\Pi}_P$

Figure (5-25) is a plot of the attractors of the saccadic system for $\boldsymbol{\alpha} \in \hat{\Pi}_P$, based on the analysis of this chapter (cf. figure (4-79)). Also shown in the figure are the identified modelled nystagmus waveforms, where applicable. The range $\hat{\Pi}_P$ contains the physiological range:

$$\Pi_P = \left\{(\alpha, \beta, \epsilon)^T : 0 < \alpha < \alpha', 1.5 < \beta < 6, 0 < \epsilon < 0.05\right\}$$

Numerics indicate that for $1.5 < \beta < 6$, $\hat{\alpha}_C(\beta) < \alpha'$. The attractor picture for $\boldsymbol{\alpha} \in \Pi_P$ is therefore the same as that in figure (5-25). This figure will form the basis of the classification of the eye movements modelled by the saccadic equations in the following chapter.

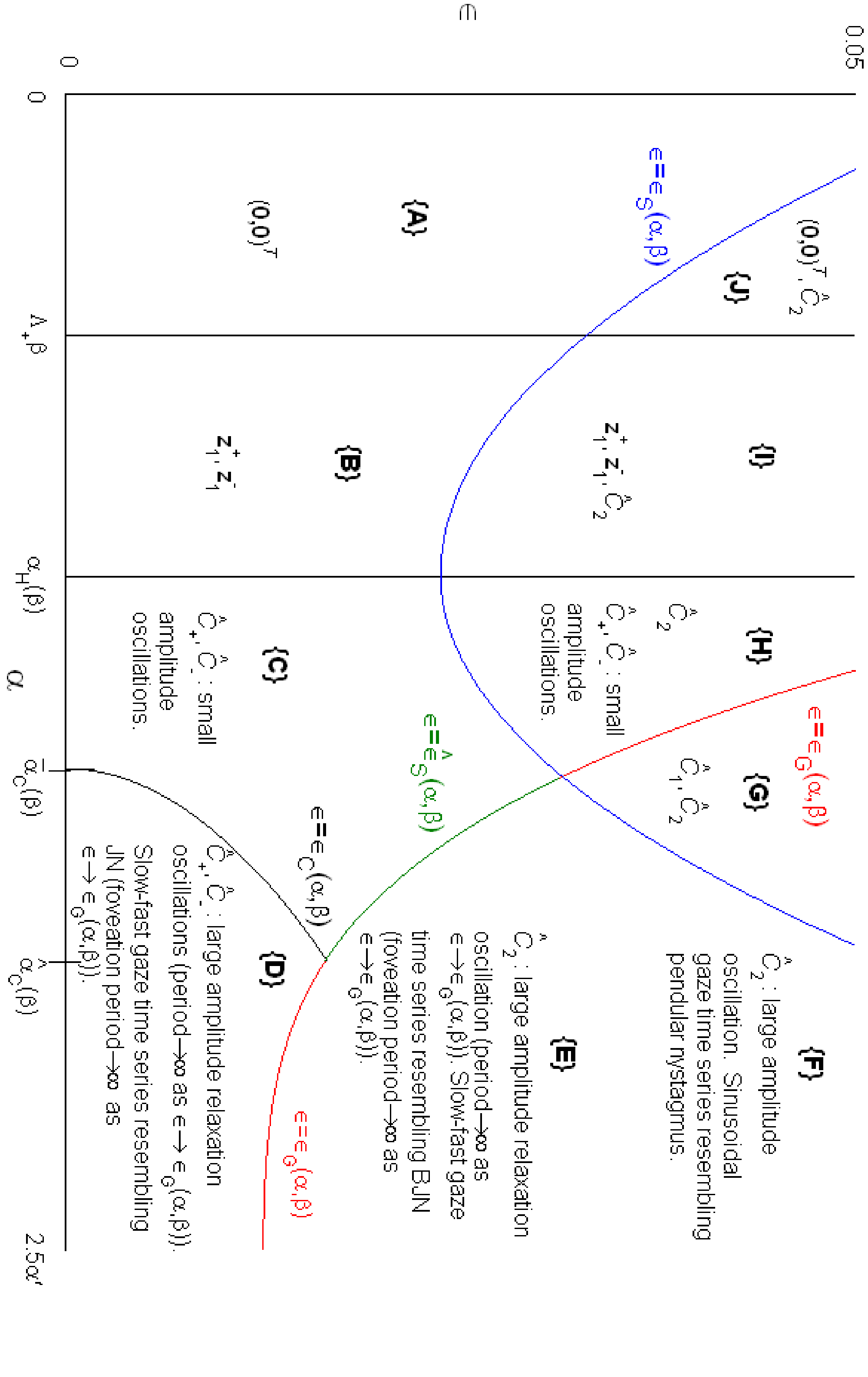

Figure 5-25: Attractors of the saccadic equations for $\boldsymbol{\alpha} \in \hat{\Pi}_P$. Here JN=jerk nystagmus and BJN=bilateral jerk nystagmus.

Chapter 6

Classification of modelled behaviours and biological implications

Recall from chapter 2 that the ultimate objects of interest in the analysis of the saccadic equations $\dot{\mathbf{z}} = \mathbf{Z}(\mathbf{z})$ are the gaze time series of solutions with initial condition

$$\mathbf{z}_0 = (0, 0, 0, 0, 0, \Delta g)^T$$

for choices of $\boldsymbol{\alpha}$ in the physiological range:

$$\Pi_P = \left\{ (\alpha, \beta, \epsilon)^T : 0 < \alpha < \alpha', 1.5 < \beta < 6, 0 < \epsilon < 0.05 \right\} \tag{6.1}$$

As stated in chapter 2, solutions with this initial condition simulate saccades to the gaze angle Δg from an initial gaze angle of 0. In this chapter the morphology of the saccade-modelling solutions generated for $\boldsymbol{\alpha}$ such that $\boldsymbol{\alpha}$ lies in the intersection of Π_P with the union of regions A-F of $\hat{\Pi}_P$ is analysed. It is shown that for such choices of $\boldsymbol{\alpha}$, the solutions can model both accurate saccades, and a range of saccadic instabilities including jerk and pendular nystagmus (cf. section 1.1). Following this, the modelled saccadic behaviours are classified in a diagram based on figure (5-25). The chapter closes with an attempt to interpret some of the biological implications of the modelled behaviour.

For convenience, the analysis of the form of the gaze time series is divided into two sections.

The first section deals with choices of $\boldsymbol{\alpha}$ for which the attractor of the system is a fixed point (regions A-B), and the second with choices of $\boldsymbol{\alpha}$ for which the attractor is a limit cycle (regions C-F). Throughout this chapter, it will be useful to write T_N as T_3.

6.1 The form of the gaze time series for fixed point attractors

Assume that $\boldsymbol{\alpha}$ lies in either region A, where the attractor is the origin $(\mathbf{0},\mathbf{0})^T$, or in B, where the attractors are the nontrivial fixed points $\mathbf{z}_1^+ = \left(\mathbf{0},\mathbf{y}_1^+\right)^T$ and $\mathbf{z}_1^- = \left(\mathbf{0},\mathbf{y}_1^-\right)^T$ (cf. figure (5-25)). Further assume that if $\boldsymbol{\alpha}$ lies in region B, then ϵ is sufficiently small for trajectories of the burster system $\dot{\mathbf{y}} = \mathbf{Y}(\mathbf{y})$ not to cross the plane P, and for $\mathbf{y}_1^\pm$ to be a stable node of $\dot{\mathbf{y}} = \mathbf{Y}(\mathbf{y})$. Fix $\Delta g > 0$ and set $\mathbf{z}_0^\pm = (\mathbf{0},0,0,\pm(\Delta g))^T$. Define $\mathbf{z}_\pm(t)\ \forall t \geq 0$ by:

$$\mathbf{z}_\pm(t) = (\mathbf{x}_\pm(t),\mathbf{y}_\pm(t))^T = (g_\pm(t),v_\pm(t),n_\pm(t),r_\pm(t),l_\pm(t),\varepsilon_\pm(t))^T = \psi_t\left(\mathbf{z}_0^\pm\right)$$

Then $g_+(t)$ simulates a saccade of Δg degrees and $g_-(t)$ simulates a saccade of $-(\Delta g)$ degrees. By the symmetry of the saccadic system under Σ, $\Sigma\mathbf{z}_+(t)$ solves $\dot{\mathbf{z}} = \mathbf{Z}(\mathbf{z})$ on $[0,\infty)$ with initial condition $\Sigma\mathbf{z}_0^+$. Recall from section 5.3 that Σ is given by

$$\Sigma = \begin{pmatrix} -\mathbf{1}_3 & \mathbf{0}_{3\times3} \\ \mathbf{0}_{3\times3} & \sigma \end{pmatrix}$$

where:

$$\sigma = \begin{pmatrix} 0 & 1 & 0 \\ 1 & 0 & 0 \\ 0 & 0 & -1 \end{pmatrix}$$

The above imply that $\mathbf{z}_0^- = \Sigma\mathbf{z}_0^+$. It therefore follows from the uniqueness of trajectories of the saccadic system that $\forall t \geq 0$, $\mathbf{z}_-(t) = \Sigma\mathbf{z}_+(t)$. In particular, the form of Σ implies that $g_-(t) = -g_+(t)\ \forall t \geq 0$. Thus, in order to understand the morphology of both $g_+(t)$ and $g_-(t)$, it is sufficient to understand the morphology of $g_+(t)$.

In this section, the morphology of $g_+(t)$ is analysed by first obtaining an explicit expression for $g_+(t)$ in terms of $\varepsilon_+(t)$ using Laplace transforms. A workable approximation $\hat{g}_+(t)$ to

$g_+(t)$ is then obtained using this expression, and the morphology of $g_+(t)$ is inferred from that of $\hat{g}_+(t)$. Throughout the following, the Laplace and inverse Laplace transform will be denoted by $\mathcal{L}$ and $\mathcal{L}^{-1}$ respectively.

6.1.1 An explicit form for $g_+(t)$

Recall the saccadic equations (2.10)-(2.15):

$$\begin{aligned}
\dot{g} &= v && (6.2)\\
\dot{v} &= -P_1 v - P_2 g + P_2 n + P_1 b && (6.3)\\
\dot{n} &= -\frac{1}{T_3} n + b && (6.4)\\
\dot{r} &= \frac{1}{\epsilon}\left(-r - \gamma r l^2 + F(\varepsilon)\right) && (6.5)\\
\dot{l} &= \frac{1}{\epsilon}\left(-l - \gamma l r^2 + F(-\varepsilon)\right) && (6.6)\\
\dot{\varepsilon} &= -b && (6.7)
\end{aligned}$$

(Here $b = r - l$, $P_1 = \frac{1}{T_1} + \frac{1}{T_2}$ and $P_2 = \frac{1}{T_1 T_2}$). As $\mathbf{z}_+(t)$ satisfies the above, equations (6.2)-(6.3) imply that $\forall t \geq 0$:

$$\ddot{g}_+(t) + P_1 \dot{g}_+(t) + P_2 g_+(t) = P_2 n_+(t) + P_1 b_+(t)$$

Taking Laplace transforms of the above and rearranging using $g_+(0) = \dot{g}_+(0) = 0$ leads to

$$G_+(s) = H_g(s)\left(P_2 N_+(s) + P_1 B_+(s)\right) \tag{6.8}$$

where $G_+(s) = \mathcal{L}(g_+(t))$, $N_+(s) = \mathcal{L}(n_+(t))$, $B_+(s) = \mathcal{L}(b_+(t))$ and

$$H_g(s) = \frac{1}{\left(s + \frac{1}{T_1}\right)\left(s + \frac{1}{T_2}\right)} \tag{6.9}$$

is the transfer function of the system (cf. section 5.6.1). Equation (6.4) implies that $\forall t \geq 0$:

$$\dot{n}_+(t) = -\frac{1}{T_3} n_+(t) + b_+(t)$$

Taking Laplace transforms of the above and rearranging using $n_+(0) = 0$ gives

$$N_+(s) = H_n(s)\, B_+(s) \tag{6.10}$$

where

$$H_n(s) = \frac{1}{s + \frac{1}{T_3}} \tag{6.11}$$

is the transfer function of the system (cf. section 5.6.1). Substituting (6.10) into (6.8) leads to the expression

$$G_+(s) = -\frac{1}{s} T_g(s)\, B_+(s) \tag{6.12}$$

where:

$$T_g(s) = -sH_g(s)\left(P_1 + P_2 H_n(s)\right) \tag{6.13}$$

(cf. section 5.6.1 again). Finally, (6.7) implies that $\forall t \geq 0$:

$$\dot{\varepsilon}_+(t) = -b_+(t)$$

Taking Laplace transforms and rearranging using $\varepsilon_+(0) = \Delta g$ and $b_+(0) = 0$ yields

$$B_+(s) = \Delta g - sE_+(s)$$

where $E_+(s) = \mathcal{L}(\varepsilon_+(t))$. Substituting the above into (6.12) leads to:

$$G_+(s) = -\Delta g \frac{T_g(s)}{s} + T_g(s)\, E_+(s)$$

Write $u_g(t) = \mathcal{L}^{-1}(T_g(s))$. Taking inverse Laplace transforms implies that $\forall t \geq 0$:

$$g_+(t) = (\Delta g)\, g_E(t) + (u_g * \varepsilon_+)(t) \tag{6.14}$$

where:

$$g_E(t) = -\int_0^t u_g(s)\, ds \tag{6.15}$$

(6.14) and (6.15) give $g_+(t)$ explicitly in terms of $\varepsilon_+(t)$.

In order to obtain the approximation $\hat{g}_+(t)$ to $g_+(t)$, it will be necessary to have explicit expressions for $u_g(t)$ and $g_E(t)$. Substituting (6.9) and (6.11) into (6.13), and performing a partial fraction expansion gives:

$$T_g(s) = \frac{K_1}{s + \frac{1}{T_1}} + \frac{K_2}{s + \frac{1}{T_2}} + \frac{K_3}{s + \frac{1}{T_N}} \tag{6.16}$$

where:

$$\begin{aligned} K_1 &= \frac{T_1^2 + T_1 T_2 - T_2 T_3}{T_1 (T_1 - T_2)(T_1 - T_3)} && (6.17) \\ K_2 &= \frac{T_1 T_3 - T_1 T_2 - T_2^2}{T_2 (T_1 - T_2)(T_2 - T_3)} && (6.18) \\ K_3 &= \frac{T_3}{(T_1 - T_3)(T_2 - T_3)} && (6.19) \end{aligned}$$

The constants have the numerical values $K_1 = 0.535970$, $K_2 = -90.576230$, $K_3 = 0.040261$. Taking inverse Laplace Transforms of both sides of (6.16) yields:

$$u_g(t) = \sum_{j=1}^{3} K_j e^{-\frac{t}{T_j}} \tag{6.20}$$

Now consider the function $g_E(t)$. Substituting (6.20) into (6.15) implies that $\forall t \geq 0$

$$g_E(t) = \sum_{j=1}^{3} L_j e^{-\frac{t}{T_j}} - \sum_{j=1}^{3} L_j$$

where $L_j = K_j T_j$ for $1 \leq j \leq 3$. These new constants have the approximate numerical values $L_1 = 0.080395$, $L_2 = -1.086914$, $L_3 = 1.006519$. Using, (6.17)-(6.19), it can be shown that $\sum_{j=1}^{3} L_j = 0$. Hence:

$$g_E(t) = \sum_{j=1}^{3} L_j e^{-\frac{t}{T_j}} \tag{6.21}$$

During the construction of the approximation $\hat{g}_+(t)$, it will be useful to have an understanding of the form of $g_E(t)$ on $[0, \infty)$. (6.15) implies that $g_E(0) = 0$. Moreover, numerics indicate that $g_E(t)$ increases from 0 to a single maximum at $t_E^M \approx 0.065481$, with $g_E(t) \approx L_3 e^{-\frac{t}{T_3}}$ for $t > t_E^M$. Let $g_E^M = g_E\left(t_E^M\right)$. Numerics give $g_E^M \approx 1.051205$. Figure (6-1) is a plot of the function $g_E(t)$ on the interval $[0, 0.5]$ together with a plot of the

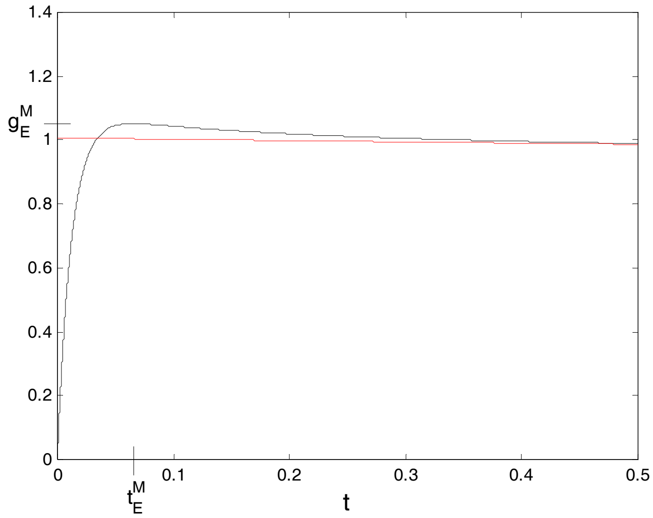

Figure 6-1: The functions $g_E(t)$ (black) and $L_3 e^{-\frac{t}{T_3}}$ (red) for $0 \leq t \leq 0.5$.

function $L_3 e^{-\frac{t}{T_3}}$.

6.1.2 Obtaining the approximation $\hat{g}_+(t)$

In constructing the approximation $\hat{g}_+(t)$ to $g_+(t)$ on $[0, \infty)$, it is first necessary to obtain an approximation $\hat{\varepsilon}_+(t)$ to $\varepsilon_+(t)$ on $[0, \infty)$. Numerics indicate that for sufficiently small t_S, $\varepsilon_+(t)$ is a decreasing function of t on $[0, t_S]$ that can be approximated fairly accurately by the straight line

$$\hat{\varepsilon}_+(t) = \left(\frac{\varepsilon_+(t_S) - \Delta g}{t_S}\right) t + \Delta g \tag{6.22}$$

which interpolates the values of $\varepsilon_+(t)$ at $t = 0$ and $t = t_S$. This gives an approximation to $\varepsilon_+(t)$ for small t. To obtain an approximation to $\varepsilon_+(t)$ for larger t, the results of sections 3.6.2 and 3.6.4 are used. Recall that in these sections, approximations to $\varepsilon(\tau)$ for large $\tau > 0$ were obtained for solutions $\mathbf{y}(\tau) = (r(\tau), l(\tau), \varepsilon(\tau))^T$ of the rescaled burster equations, with initial condition in the basin of attraction of a stable fixed point.

For $\boldsymbol{\alpha}$ in region A, the basin of attraction $\mathcal{B}(\mathbf{0})$ of the origin $\mathbf{0}$ in the burster system is $\mathbb{R}^3$. Hence, the initial condition $\mathbf{y}_+(0) \in \mathcal{B}(\mathbf{0})$. Define the function $\epsilon_F^0(\alpha, \beta)$ by:

$$\epsilon_F^0(\alpha,\beta) = \frac{1}{4\left(\Lambda_+ - \frac{\alpha}{\beta}\right)}$$

For $\epsilon < \epsilon_F^0(\alpha,\beta)$, $\mathbf{0}$ is a stable node, while for $\epsilon > \epsilon_F^0(\alpha,\beta)$, $\mathbf{0}$ is a stable fixed point such that trajectories spiral round the stable invariant line L_0 as they converge to $\mathbf{0}$ (cf. figure (3-22)). Since $\tau = \frac{t}{\epsilon}$, the analysis of section 3.6.4 therefore implies that given sufficiently large $t_L > 0$, $\forall t \geq t_L$

$$\varepsilon_+(t) \approx w_L^+(t - t_L) \tag{6.23}$$

where $w_L^+(0) = \varepsilon_+(t_L)$, and on $[0,\infty)$, $w_L^+(t)$ has one of the two forms below, depending on the sign of $\epsilon - \epsilon_F^0(\alpha,\beta)$:

1. $\epsilon < \epsilon_F^0(\alpha,\beta)$. In this range, $\forall t \geq 0$

$$w_L^+(t) = Ae^{\frac{\lambda_2 t}{\epsilon}} + Be^{\frac{\lambda_3 t}{\epsilon}} \tag{6.24}$$

where

$$\begin{aligned}
d &= \sqrt{1 - 4\epsilon\left(\Lambda_+ - \tfrac{\alpha}{\beta}\right)} \\
\lambda_2 &= \tfrac{1}{2}(-1 + d) \\
\lambda_3 &= \tfrac{1}{2}(-1 - d) \\
A &= -\tfrac{1}{d}\left(\lambda_3\varepsilon_+(t_L) + \epsilon b_+(t_L)\right) \\
B &= \tfrac{1}{d}\left(\lambda_2\varepsilon_+(t_L) + \epsilon b_+(t_L)\right)
\end{aligned} \tag{6.25}$$

and $b_+(t_L) = r_+(t_L) - l_+(t_L)$.

2. $\epsilon > \epsilon_F^0(\alpha,\beta)$. In this range, $\forall t \geq 0$

$$w_L^+(t) = Ae^{-\frac{t}{2\epsilon}}\cos\left(\frac{dt}{\epsilon} + B\right) \tag{6.26}$$

where

$$\begin{aligned}
d &= \tfrac{1}{2}\sqrt{4\epsilon\left(\Lambda_+ - \tfrac{\alpha}{\beta}\right) - 1} \\
A &= \tfrac{1}{d}\sqrt{\left(\tfrac{1}{4} + d^2\right)\varepsilon_+(t_L)^2 - \epsilon\varepsilon_+(t_L)\,b_+(t_L) + \epsilon^2 b_+(t_L)^2} \\
B &= -\arctan\left(\tfrac{\varepsilon_+(t_L) - 2\epsilon b_+(t_L)}{2d\varepsilon_+(t_L)}\right)
\end{aligned} \tag{6.27}$$

and $b_+(t_L) = r_+(t_L) - l_+(t_L)$.

For $\boldsymbol{\alpha}$ in region B, $\Delta g > 0$ implies $\mathbf{y}_+(0) \in \mathcal{B}\left(\mathbf{y}_1^+\right)$, since by assumption ϵ is sufficiently small for trajectories of $\dot{\mathbf{y}} = \mathbf{Y}(\mathbf{y})$ not to cross the plane P. As ϵ is also assumed sufficiently small for $\mathbf{y}_1^+$ to be a stable node, the analysis of section 3.6.2 implies that given sufficiently large $t_L > 0$, $\forall t \geq t_L$

$$\varepsilon_+(t) \approx \varepsilon_1 + w_L^+(t - t_L) \tag{6.28}$$

where $w_L^+(0) = \varepsilon_+(t_L) - \varepsilon_1$, and $w_L^+(t)$ is defined $\forall t \geq 0$ by

$$w_L^+(t) = Ae^{\frac{\mu_{12}t}{\epsilon}} + Be^{\frac{\mu_{13}t}{\epsilon}} \tag{6.29}$$

with

$$\begin{array}{rcl} d & = & \sqrt{\Delta_1(\alpha,\beta)^2 - 4\epsilon\left(\Gamma_1^+(\alpha,\beta) + \Gamma_1^-(\alpha,\beta)\right)} \\ \mu_{12} & = & \frac{1}{2}\left(\Delta_1(\alpha,\beta) + d\right) \\ \mu_{13} & = & \frac{1}{2}\left(\Delta_1(\alpha,\beta) - d\right) \\ A & = & -\frac{1}{d}\left(\mu_{13}\left(\varepsilon_+(t_L) - \varepsilon_1\right) + \epsilon b_+(t_L)\right) \\ B & = & \frac{1}{d}\left(\mu_{12}\left(\varepsilon_+(t_L) - \varepsilon_1\right) + \epsilon b_+(t_L)\right) \end{array} \tag{6.30}$$

and $b_+(t_L) = r_+(t_L) - l_+(t_L)$.

The above analysis implies that for $\boldsymbol{\alpha}$ lying in either region A or B, given sufficiently large $t_L > 0$, $\varepsilon_+(t_L)$ is approximated $\forall t \geq t_L$ by $\hat{\varepsilon}_+(t)$ where

$$\hat{\varepsilon}_+(t) = \varepsilon_* + w_L^+(t - t_L) \tag{6.31}$$

with $\varepsilon_* = 0$ or $\varepsilon_* = \varepsilon_1$, and $w_L^+(t)$ given by (6.24)-(6.25), (6.26)-(6.27) or (6.29)-(6.30).

Assuming that t_L can be chosen to equal t_S, (6.22) and (6.31) together imply that $\varepsilon_+(t_L)$ can be approximated on $[0,\infty)$ by the continuous function $\hat{\varepsilon}_+(t)$ defined by

$$\hat{\varepsilon}_+(t) = \begin{cases} L_+t + \Delta g & \text{if} \quad 0 \leq t \leq t_L \\ \varepsilon_* + w_L^+(t - t_L) & \text{if} \quad t > t_L \end{cases} \tag{6.32}$$

where:

$$L_+ = \frac{\varepsilon_+ (t_L) - \Delta g}{t_L} \tag{6.33}$$

The above approximation together with (6.14) suggests that $g_+ (t)$ can be approximated on $[0, \infty)$ by the continuous function $\hat{g}_+ (t)$ defined by:

$$\hat{g}_+ (t) = (\Delta g)\, g_E (t) + (u_g * \hat{\varepsilon}_+) (t) \tag{6.34}$$

The reminder of this section will deal with analysing the form of the approximation $\hat{g}_+ (t)$ on $[0, \infty)$. Under the assumption that $\hat{g}_+ (t)$ is a good approximation to $g_+ (t)$ in this range, the morphology of $g_+ (t)$ can then be inferred from that of $\hat{g}_+ (t)$. t_L is assumed to take values in the range $[0.01, 0.1]$.

The form of $\hat{g}_+ (t)$ will first be analysed for $0 \leq t \leq t_L$, and then for $t \geq t_L$.

6.1.3 The form of $\hat{g}_+ (t)$ in the range $0 \leq t \leq t_L$

Equations (6.32) and (6.34) imply that for $0 \leq t \leq t_L$:

$$\hat{g}_+ (t) = (\Delta g)\, g_E (t) + (\Delta g) \int_0^t u_g (s)\, ds + L_+ \int_0^t s u_g (t - s)\, ds$$

Note that since, by assumption, $\varepsilon_+ (t)$ is decreasing on $[0, t_L]$, (6.33) implies $L_+ < 0$. The first two terms of this equation cancel (cf. (6.15)). Introducing (6.20) into the remaining convolution term leads to

$$\hat{g}_+ (t) = L_+ g_1 (t)$$

where $g_1 (t)$ is defined $\forall t \geq 0$ by:

$$g_1 (t) = \sum_{j=1}^{3} K_j e^{-\frac{t}{T_j}} \int_0^t s e^{\frac{s}{T_j}}\, ds$$

Evaluating the integrals in the above expression and using $\sum_{j=1}^{3} L_j = 0$ gives:

$$g_1(t) = \sum_{j=1}^{3} L_j T_j \left(e^{-\frac{t}{T_j}} - 1 \right) \tag{6.35}$$

Setting $t = 0$ in the above implies $g_1(0) = 0$. Differentiating leads to $\dot{g}_1(t) = -g_E(t)$ (cf. (6.21)). As $g_E(t)$ is increasing on $[0, \infty)$ this means that $g_1(t)$ is decreasing on $[0, \infty)$. Since $L_+ < 0$, it follows that $\hat{g}_+(t)$ is increasing on $[0, t_L]$.

6.1.4 The form of $\hat{g}_+(t)$ in the range $t \geq t_L$

Equation (6.34) implies that for $t \geq t_L$:

$$\hat{g}_+(t) = (\Delta g)\, g_E(t) + \int_0^{t_L} u_g(t-s)\, \hat{\varepsilon}_+(s)\, ds + \int_{t_L}^{t} u_g(t-s)\, \hat{\varepsilon}_+(s)\, ds \tag{6.36}$$

Consider the first integral in this sum. Using (6.20) and (6.32) gives:

$$\int_0^{t_L} u_g(t-s)\, \hat{\varepsilon}_+(s)\, ds = L_+ \sum_{j=1}^{3} K_j e^{-\frac{t}{T_j}} \int_0^{t_L} s e^{\frac{s}{T_j}}\, ds + (\Delta g) \sum_{j=1}^{3} K_j e^{-\frac{t}{T_j}} \int_0^{t_L} e^{\frac{s}{T_j}}\, ds$$

Evaluating the integrals and rearranging leads to

$$\int_0^{t_L} u_g(t-s)\, \hat{\varepsilon}_+(s)\, ds = -(\Delta g)\, g_E(t) + \varepsilon_+(t_L)\, g_E(t-t_L) + (\Delta g - \varepsilon_+(t_L))\, g_2(t; t_L) \tag{6.37}$$

where $g_2(t; t_L)$ is defined on $[t_L, \infty)$ by:

$$g_2(t; t_L) = \frac{1}{t_L} \left(g_1(t-t_L) - g_1(t) \right) \tag{6.38}$$

Now consider the second integral in expression (6.36). Using (6.20) and (6.32) gives

$$\int_{t_L}^{t} u_g(t-s)\, \hat{\varepsilon}_+(s)\, ds = \varepsilon_* \sum_{j=1}^{3} K_j e^{-\frac{t}{T_j}} \int_{t_L}^{t} e^{\frac{s}{T_j}}\, ds + g_P^+(t) \tag{6.39}$$

where $g_P^+(t)$ is defined $\forall t \geq t_L$ by:

$$g_P^+(t) = \sum_{j=1}^{3} K_j e^{-\frac{t}{T_j}} \int_{t_L}^{t} e^{\frac{s}{T_j}} w_L^+(s - t_L)\, ds \tag{6.40}$$

Evaluating the integral in (6.39) leads to:

$$\int_{t_L}^{t} u_g(t-s)\,\hat{\varepsilon}_+(s)\, ds = -\varepsilon_* g_E(t - t_L) + g_P^+(t) \tag{6.41}$$

Substituting (6.37) and (6.41) into (6.36) then implies that for $t \geq t_L$

$$\hat{g}_+(t) = g_I^+(t; t_L) + g_P^+(t) \tag{6.42}$$

where the function $g_I^+(t; t_L)$ is defined on $[t_L, \infty)$ by:

$$g_I^+(t; t_L) = (\Delta g - \varepsilon_+(t_L))\, g_2(t; t_L) + (\varepsilon_+(t_L) - \varepsilon_*)\, g_E(t - t_L) \tag{6.43}$$

The properties of the function $g_I^+(t; t_L)$ on $[t_L, \infty)$ will now be examined. Following this, expressions will be obtained for $g_P^+(t)$ in each of the $\boldsymbol{\alpha}$ ranges of interest. This will enable the morphology of $\hat{g}_+(t)$ on $[t_L, \infty)$ to be examined in these ranges. Since $\hat{g}_+(t)$ has been shown to be an increasing function on $[0, t_L]$, this will allow the morphology of $\hat{g}_+(t)$, and hence $g_+(t)$, on $[0, \infty)$ to be inferred.

The form of $g_I^+(t; t_L)$

First consider the function $g_2(t; t_L)$ defined on $[t_L, \infty)$ in (6.38):

$$g_2(t; t_L) = \frac{1}{t_L}(g_1(t - t_L) - g_1(t))$$

Setting $t = t_L$ in the above gives $g_2(t_L; t_L) = -\frac{1}{t_L} g_1(t_L)$. As $g_1(t) < 0\ \forall t > 0$, $g_2(t_L; t_L) > 0$. Additionally, numerics indicate that $g_2(t_L; t_L)$ is an increasing function of t_L on $[0.01, 0.1]$. Figure (6-2) shows plots of $g_2(t; t_L)$ on $[t_L, 0.3]$ for several values of t_L in $[0.01, 0.1]$. Also shown is a plot of $g_E(t)$ on the interval $[0, 0.3]$. As suggested by the figure, numerical evidence seems to indicate that for each $t_L \in [0.01, 0.1]$, $g_2(t; t_L)$ can be approximated on $[t_L, \infty)$ as a rightward displacement of $g_E(t)$ along the t-axis. i.e. there is a $t_D(t_L) > 0$ for which $g_2(t; t_L) \approx g_E(t - t_D(t_L))$. Figure (6-3) shows values of $t_D(t_L)$ obtained for choices of t_L in $[0.01, 0.1]$ by estimating the value of t, $t_2^M(t_L)$,

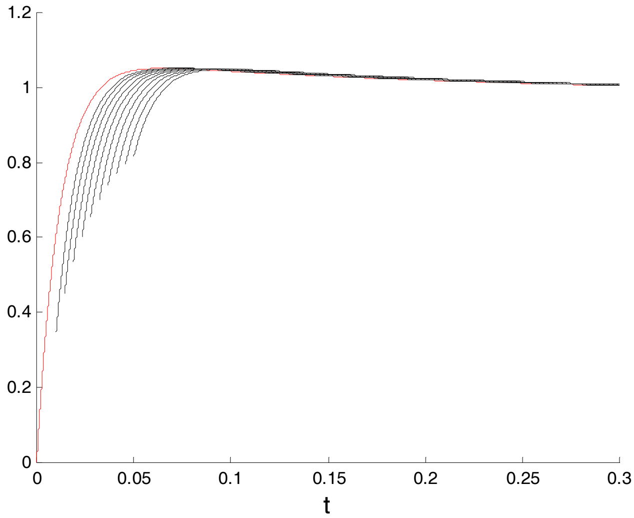

Figure 6-2: Plots of the function $g_2(t;t_L)$ on $[t_L, 0.3]$ for 10 equally spaced values of t_L in the range $[0.01, 0.1]$ (black lines). Also shown is a plot of the function $g_E(t)$ on $[0, 0.3]$ (red line).

at which $g_2(t;t_L)$ has a maximum on $[t_L,\infty)$, and then setting $t_D(t_L) = t_2^M(t_L) - t_E^M$. It can be seen that $t_D(t_L)$ is an increasing, approximately linear function of t_L with $\frac{1}{2}t_L < t_D(t_L) < t_L$. Plots of the function pairs $\{g_2(t;t_L), g_E(t - t_D(t_L))\}$ on $[t_L, 0.3]$ for $t_L = 0.01$, 0.02, 0.05 and 0.1 are given in figure (6-4) to illustrate the accuracy of the estimate $g_E(t;t_L) \approx g_1(t - t_D(t_L))$. The estimate suggests that on $[t_L,\infty)$, $g_2(t;t_L)$ will increase to a maximum at $t_2^M(t_L)$ before decreasing to 0 with $g_2(t;t_L) \approx L_3 e^{-\frac{t}{T_3}}$ for $t > t_2^M(t_L)$. Moreover, $g_2\left(t_2^M(t_L);t_L\right) \approx g_E^M$. (6.43) therefore suggests that as t is increased from t_L, $g_I(t;t_L)$ will increase to a maximum at some value $t_I^M(t_L) \approx t_2^M(t_L)$, before decreasing to 0 with $g_I^+(t;t_L) \approx L_3(\Delta g - \varepsilon_*) e^{-\frac{t}{T_3}}$ for $t > t_I^M(t_L)$. Moreover, $g_I^+\left(t_I^M(t_L);t_L\right) \approx (\Delta g - \varepsilon_*) g_E^M$. Numerics seem to support these claims. Figure (6-5) is a proposed schematic of $g_I^+(t;t_L)$ on $[t_L,\infty)$ based on these arguments.

It will be useful in what follows to have a lower bound on $g_I^+(t;t_L)$ in the range $\left(t_L, t_I^M(t_L)\right)$. Since $\varepsilon_+(t_L) > \varepsilon_*$ and $g_E(t - t_L)$ is nonnegative on $[t_L,\infty)$, $\forall t \geq t_L$:

$$g_I^+(t;t_L) \geq (\Delta g - \varepsilon_+(t_L))\, g_2(t;t_L)$$

(cf. equation (6.43)). As was stated earlier, $g_2(t;t_L)$ is increasing on $\left(t_L, t_2^M(t_L)\right)$, and so $g_2(t;t_L) \geq g_2(t_L;t_L)$ on $\left(t_L, t_2^M(t_L)\right)$. Since $g_2(t_L;t_L)$ is an increasing function of t_L for $t_L \in [0.01, 0.1]$, it follows that $g_2(t;t_L) \geq g_2(0.01;0.01)$ on $\left(t_L, t_2^M(t_L)\right)$. Numerics give

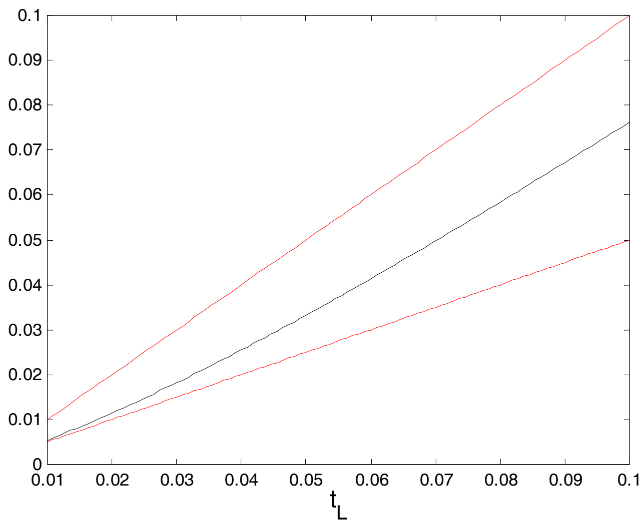

Figure 6-3: Computed values of $t_D\left(t_L\right)$ on the range $[0.01, 0.1]$ (black line: see text for details). Also shown are the functions $\frac{1}{2}t_L$ and t_L (red lines).

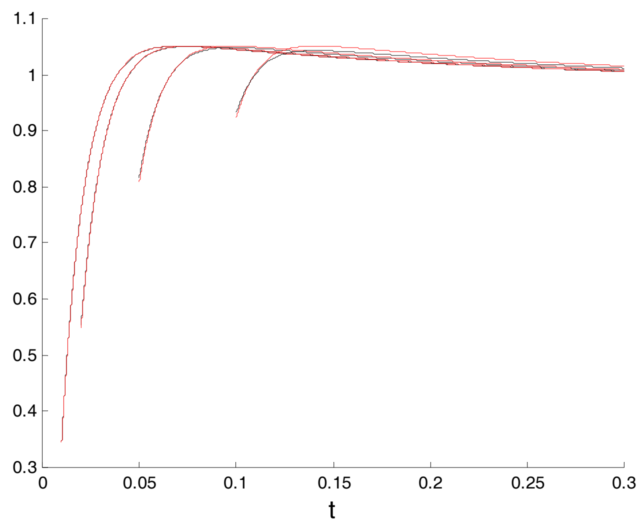

Figure 6-4: Plots of $g_2\left(t; t_L\right)$ (black lines) and $g_E\left(t - t_D\left(t_L\right)\right)$ (red lines) on $[t_L, 0.3]$ for $t_L = 0.01$, 0.02, 0.05 and 0.1.

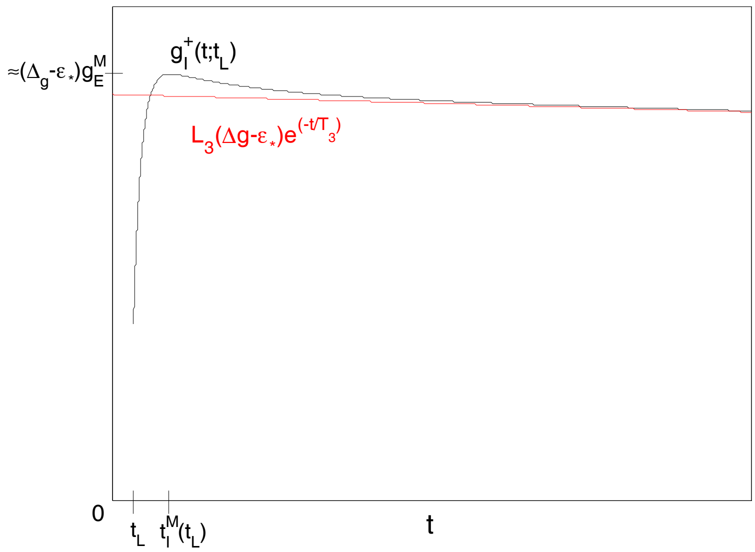

Figure 6-5: Schematic of the function $g_I^+(t;t_L)$ on $[t_L,\infty)$ (see text for details).

$g_2(0.01;0.01) \approx 0.346634$ and so the above inequality implies that for $t_L < t < t_2^M(t_L)$:

$$g_I^+(t;t_L) \geq 0.34\,(\Delta g - \varepsilon_+(t_L))$$

The approximation $t_2^M(t_L) \approx t_I^M(t_L)$ then implies that for $t_L < t < t_I^M(t_L)$:

$$g_I^+(t;t_L) \gtrapprox 0.34\,(\Delta g - \varepsilon_+(t_L))$$

The form of $g_P^+(t)$ in region A

Recall the expression (6.40) for $g_P^+(t)$:

$$g_P^+(t) = \sum_{j=1}^{3} K_j e^{-\frac{t}{T_j}} \int_{t_L}^{t} e^{\frac{s}{T_j}} w_L^+(s-t_L)\,ds \tag{6.44}$$

It was shown earlier that there are two possible expressions for $w_L^+(t)$ on $[0,\infty)$, depending on whether $\epsilon < \epsilon_F^0(\alpha,\beta)$ or $\epsilon > \epsilon_F^0(\alpha,\beta)$. The corresponding expressions for $g_P^+(t)$ are now found for each case in turn.

1. $\epsilon < \epsilon_F^0(\alpha,\beta)$.

(6.24)-(6.25) imply that in this range, $\forall t \geq t_L$

$$w_L^+(t-t_L) = Ae^{\frac{\lambda_2(t-t_L)}{\epsilon}} + Be^{\frac{\lambda_3(t-t_L)}{\epsilon}}$$

with

$$\begin{aligned}
d &= \sqrt{1-4\epsilon\left(\Lambda_+ - \frac{\alpha}{\beta}\right)} \\
\lambda_2 &= \tfrac{1}{2}(-1+d) \\
\lambda_3 &= \tfrac{1}{2}(-1-d) \\
A &= -\tfrac{1}{d}\left(\lambda_3\varepsilon_+(t_L) + \epsilon b_+(t_L)\right) \\
B &= \tfrac{1}{d}\left(\lambda_2\varepsilon_+(t_L) + \epsilon b_+(t_L)\right)
\end{aligned}$$

and $b_+(t_L) = r_+(t_L) - l_+(t_L)$. Substituting the above into (6.44) leads to the following expression for $g_P^+(t)$ on $[t_L, \infty)$

$$g_P^+(t) = \sum_{j=1}^{3} K_j \left(\left(A_j e^{\frac{\lambda_2(t-t_L)}{\epsilon}} + B_j e^{\frac{\lambda_3(t-t_L)}{\epsilon}}\right) - (A_j + B_j)\, e^{-\frac{(t-t_L)}{T_j}}\right) \tag{6.45}$$

where for $1 \leq j \leq 3$:

$$\begin{aligned}
A_j &= -\frac{\epsilon T_j\left(\lambda_3\varepsilon_+(t_L) + \epsilon b_+(t_L)\right)}{d\left(T_j\lambda_2 + \epsilon\right)} \\
B_j &= \frac{\epsilon T_j\left(\lambda_2\varepsilon_+(t_L) + \epsilon b_+(t_L)\right)}{d\left(T_j\lambda_3 + \epsilon\right)}
\end{aligned}$$

Taylor expanding d, λ_2 and λ_3 as functions of ϵ about 0 leads to the approximations $A_j \approx \hat{A}_j$ and $B_j \approx \hat{B}$ for sufficiently small ϵ, where for $1 \leq j \leq 3$

$$\hat{A}_j = \frac{T_j\varepsilon_+(t_L)}{\left(\frac{\alpha}{\beta} - \Lambda_+\right)T_j + 1} \tag{6.46}$$

and:

$$\hat{B} = \left(\left(\Lambda_+ - \frac{\alpha}{\beta}\right)\varepsilon_+(t_L) - b_+(t_L)\right)\epsilon^2$$

Taking moduli of (6.45) and using $A_j \approx \hat{A}_j, B_j \approx \hat{B}$ implies that given ϵ sufficiently small, $\forall t \geq t_L$:

$$\left|g_P^+(t)\right| \lessapprox 2\left(\sum_{j=1}^{3}\left|K_j\hat{A}_j\right| + \left|\hat{B}\right|\sum_{j=1}^{3}|K_j|\right) \tag{6.47}$$

(6.46) implies that for $1 \leq j \leq 3$:

$$\left|K_j\hat{A}_j\right| \leq \frac{|L_j|\,\varepsilon_+(t_L)}{\left|\left(\frac{\alpha}{\beta} - \Lambda_+\right)T_j + 1\right|}$$

As was stated earlier, $L_1 = 0.080395$, $L_2 = -1.086914$, $L_3 = 1.006519$. Hence, for $1 \leq j \leq 3$:

$$\left|K_j\hat{A}_j\right| \leq \frac{|L_2|\,\varepsilon_+(t_L)}{\left|\left(\frac{\alpha}{\beta} - \Lambda_+\right)T_j + 1\right|} \tag{6.48}$$

It was also argued during the discussion of $g_I^+(t;t_L)$ that for $t_L < t < t_I^M(t_L)$:

$$g_I^+(t;t_L) \gtrapprox 0.34\left(\Delta g - \varepsilon_+(t_L)\right)$$

The form of $\hat{B}$ implies $\hat{B} \to 0$ as $\epsilon \to 0$. It therefore follows from (6.47), (6.48) and the above expression that provided Δg is large compared to $\varepsilon_+(t_L)$, and $\left|\left(\frac{\alpha}{\beta} - \Lambda_+\right)T_j + 1\right|$ is not small compared to $|L_2|$ for $1 \leq j \leq 3$, then $\left|g_P^+(t)\right|$ will be small compared to $g_I^+(t;t_L)$ on $\left(t_L, t_I^M(t_L)\right)$, for ϵ sufficiently small. Noting that $\varepsilon_* = 0$ in the parameter range considered here, the analysis of $g_I^+(t;t_L)$ implies $g_I^+(t;t_L) \approx L_3(\Delta g)\,e^{-\frac{t}{T_3}}$ for $t > t_I^M(t_L)$ (cf. figure (6-5)). (6.47) and (6.48) therefore also suggest that, under the assumptions made above regarding the relative sizes of $\{\Delta g, \varepsilon_+(t_L)\}$ and $\left\{\left|\left(\frac{\alpha}{\beta} - \Lambda_+\right)T_j + 1\right|, |L_2|\right\}$, for sufficiently small ϵ, $\left|g_P^+(t)\right|$ will be small compared to $g_I^+(t;t_L)$ for $t > t_I^M(t_L)$ with t small compared to T_3. So fix $t_M > t_I^M(t_L)$ such that t_M is small compared to T_3. Since

$$\hat{g}_+(t) = g_I^+(t;t_L) + g_P^+(t)$$

on $[t_L, \infty)$, the arguments above imply that, provided the assumptions made hold, $\hat{g}_+(t)$ will be a small perturbation of $g_I^+(t;t_L)$ on $[t_L, t_M]$ for ϵ sufficiently small. The discussion of the form of $g_I^+(t;t_L)$ on $[t_L, \infty)$ together with the fact that $\hat{g}_+(t)$ is increasing on $[0, t_L]$ therefore suggests that as t is increased from 0 to t_M, $\hat{g}_+(t)$ will increase to a maximum at $t_+^M(t_L)$ with $t_+^M(t_L) \approx t_I^M(t_L)$, before decreasing with $\hat{g}_+(t) \approx L_3(\Delta g)\,e^{-\frac{t}{T_3}}$ for $t > t_+^M(t_L)$. Moreover, $\hat{g}_+\left(t_+^M(t_L)\right) \approx (\Delta g)\,g_E^M$. Since $g_E^M \approx 1$, this suggests that

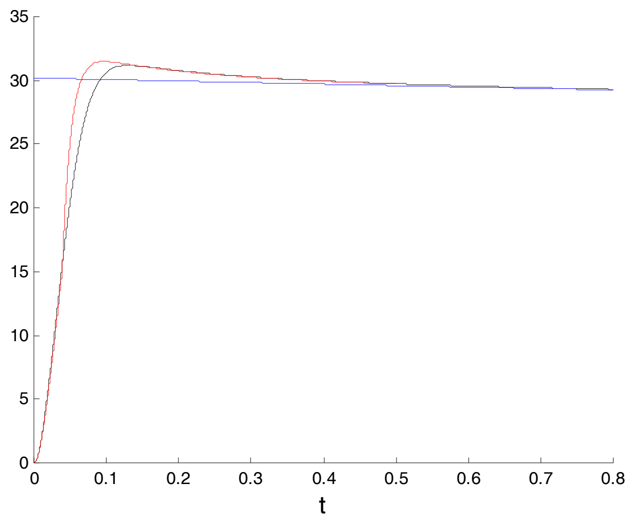

Figure 6-6: Plot of $g_+(t)$ on $[0, 0.8]$ for $\alpha = 80$, $\beta = 3$, $\epsilon = 0.0005$ and $\Delta g = 30$ (black line). The function $L_3(\Delta g)\, e^{-\frac{t}{T_3}}$ is plotted in blue while $\hat{g}_+(t)$ on $[0, t_L]$ and $g_I^+(t; t_L)$ on $[t_L, 0.8]$ are plotted in red. $t_L = 0.0391$.

$\hat{g}_+(t)$, and hence $g_+(t)$, has the form of a normometric saccade to Δg degrees on $[0, t_M]$, which drifts back towards 0 like $L_3(\Delta g)\, e^{-\frac{t}{T_3}}$ as $t \to t_M$ (cf. section 1.1.2). Note that since $g_-(t) = -g_+(t)$, this implies $g_-(t)$ will model a normometric saccade to $-(\Delta g)$ degrees which drifts back towards 0 like $-L_3(\Delta g)\, e^{-\frac{t}{T_3}}$ as $t \to t_M$.

Figures (6-6)-(6-8) are plots of $g_+(t)$ on $[0, 0.8]$ obtained for choices of Δg and $\boldsymbol{\alpha}$ such that $\boldsymbol{\alpha}$ lies in A with $\epsilon < \epsilon_F^0(\alpha, \beta)$. Also shown are the function $L_3(\Delta g)\, e^{-\frac{t}{T_3}}$ on $[0, 0.8]$ together with $\hat{g}_+(t)$ on $[0, t_L]$ and $g_I^+(t; t_L)$ on $[t_L, 0.8]$. In each case $g_+(t)$ can be seen to model an accurate saccade to Δg degrees which drifts towards back towards 0 like $L_3(\Delta g)\, e^{-\frac{t}{T_3}}$ as $t \to 0.8$.

2. $\epsilon > \epsilon_F^0(\alpha, \beta)$.

(6.26)-(6.27) imply that in this range, $\forall t \geq t_L$

$$w_L^+(t - t_L) = Ae^{-\frac{(t-t_L)}{2\epsilon}} \cos\left(\frac{d}{\epsilon}(t - t_L) + B\right)$$

where

$$d \;=\; \tfrac{1}{2}\sqrt{4\epsilon\left(\Lambda_+ - \tfrac{\alpha}{\beta}\right) - 1}$$

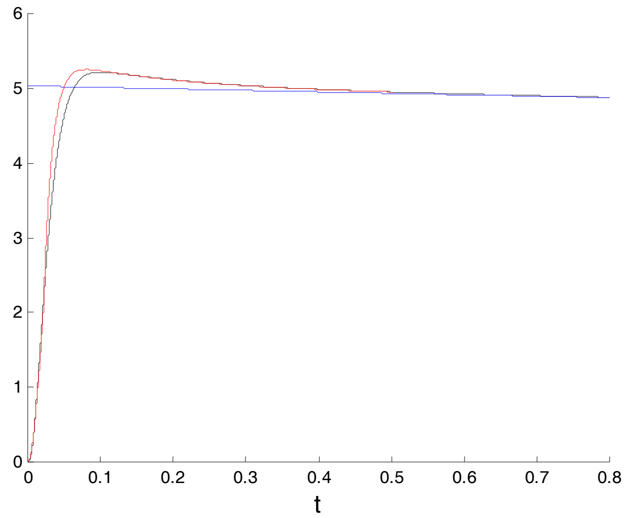

Figure 6-7: Plot of $g_+(t)$ on $[0, 0.8]$ for $\alpha = 120$, $\beta = 4.5$, $\epsilon = 0.002$ and $\Delta g = 5$ (black line). The function $L_3(\Delta g)\, e^{-\frac{t}{T_3}}$ is plotted in blue while $\hat{g}_+(t)$ on $[0, t_L]$ and $g_I^+(t; t_L)$ on $[t_L, 0.8]$ are plotted in red. $t_L = 0.0213$.

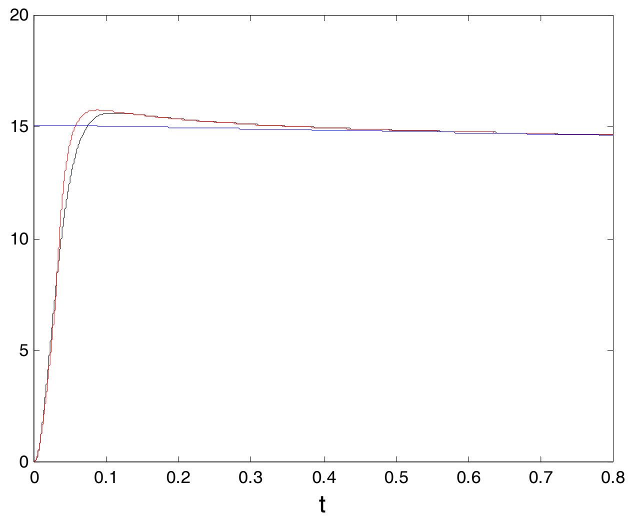

Figure 6-8: Plot of $g_+(t)$ on $[0, 0.8]$ for $\alpha = 160$, $\beta = 6$, $\epsilon = 0.0015$ and $\Delta g = 15$ (black line). The function $L_3(\Delta g)\, e^{-\frac{t}{T_3}}$ is plotted in blue while $\hat{g}_+(t)$ on $[0, t_L]$ and $g_I^+(t; t_L)$ on $[t_L, 0.8]$ are plotted in red. $t_L = 0.0309$.

$$
\begin{array}{rcl}
A & = & \frac{1}{d}\sqrt{\left(\frac{1}{4}+d^2\right)\varepsilon_+\left(t_L\right)^2-\epsilon\varepsilon_+\left(t_L\right)b_+\left(t_L\right)+\epsilon^2 b_+\left(t_L\right)^2} \\
B & = & -\arctan\left(\frac{\varepsilon_+(t_L)-2\epsilon b_+(t_L)}{2d\varepsilon_+(t_L)}\right)
\end{array}
$$

and $b_+\left(t_L\right)=r_+\left(t_L\right)-l_+\left(t_L\right)$. Substituting the above into (6.44) leads to the following expression for $g_P^+\left(t\right)$ on $[t_L,\infty)$

$$
g_P^+\left(t\right)=e^{-\frac{(t-t_L)}{2\epsilon}}\sum_{j=1}^{3}K_jA_j\cos\left(\frac{d}{\epsilon}\left(t-t_L\right)+B_j\right)+\sum_{j=1}^{3}K_jC_je^{-\frac{(t-t_L)}{T_j}} \tag{6.49}
$$

where for $1\leq j\leq 3$:

$$
\begin{array}{rcl}
A_j & = & \sqrt{\frac{\epsilon\left(\left(\Lambda_+-\frac{\alpha}{\beta}\right)\varepsilon_+\left(t_L\right)^2-b_+\left(t_L\right)\varepsilon_+\left(t_L\right)+\epsilon b_+\left(t_L\right)^2\right)}{\left(\Lambda_+-\frac{\alpha}{\beta}-\frac{1}{T_j}\left(1-\frac{\epsilon}{T_j}\right)\right)\left(\Lambda_+-\frac{\alpha}{\beta}-\frac{1}{4\epsilon}\right)}} \\
B_j & = & -\arctan\left(\dfrac{2T_jd}{2\epsilon-T_j}\right)-\arctan\left(\dfrac{\varepsilon_+\left(t_L\right)-2\epsilon b_+\left(t_L\right)}{2d\varepsilon_+\left(t_L\right)}\right) \\
C_j & = & \dfrac{\left(1-\frac{\epsilon}{T_j}\right)\varepsilon_+\left(t_L\right)-\epsilon b_+\left(t_L\right)}{\left(\Lambda_+-\frac{\alpha}{\beta}-\frac{1}{T_j}\left(1-\frac{\epsilon}{T_j}\right)\right)}
\end{array}
$$

Since $\hat{g}_+\left(t\right)=g_I^+\left(t;t_L\right)+g_P^+\left(t\right)\ \forall t\geq t_L$, (6.49) implies that $\forall t\geq t_L$:

$$
\hat{g}_+\left(t\right)=g_I^+\left(t;t_L\right)+e^{-\frac{(t-t_L)}{2\epsilon}}\sum_{j=1}^{3}K_jA_j\cos\left(\frac{d}{\epsilon}\left(t-t_L\right)+B_j\right)+\sum_{j=1}^{3}K_jC_je^{-\frac{(t-t_L)}{T_j}} \tag{6.50}
$$

Since $T_3\gg T_1>T_2$, for t large compared to T_1:

$$
\sum_{j=1}^{3}K_jC_je^{-\frac{(t-t_L)}{T_j}}\approx K_3C_3e^{-\frac{(t-t_L)}{T_3}}
$$

From the expression for C_j:

$$
C_3=\frac{\left(1-\frac{\epsilon}{T_3}\right)\varepsilon_+\left(t_L\right)-\epsilon b_+\left(t_L\right)}{\left(\Lambda_+-\frac{\alpha}{\beta}-\frac{1}{T_3}\left(1-\frac{\epsilon}{T_3}\right)\right)}
$$

By assumption, $T_3\gg 1>\epsilon$. This yields the approximations $1-\frac{\epsilon}{T_3}\approx 1$ and $\frac{1}{T_3}\left(1-\frac{\epsilon}{T_3}\right)\approx 0$. It follows that for t large compared to T_1

$$
\sum_{j=1}^{3}K_jC_je^{-\frac{(t-t_L)}{T_j}}\approx\hat{K}_3e^{-\frac{(t-t_L)}{T_3}} \tag{6.51}
$$

where:

$$\hat{K}_3 = \frac{K_3\left(\varepsilon_+\left(t_L\right) - \epsilon b_+\left(t_L\right)\right)}{\Lambda_+ - \frac{\alpha}{\beta}} \tag{6.52}$$

As was shown earlier, $g_I^+\left(t;t_L\right) \approx L_3\left(\Delta g\right)e^{-\frac{t}{T_3}}$ for $t > t_I^M\left(t_L\right)$. Assume that $\alpha < \left(\Lambda_+ - 1\right)\beta$. (Since $\Lambda_+ \gg 1$, this will typically be true). (6.52) then implies:

$$\left|\hat{K}_3\right| \leq K_3\varepsilon_+\left(t_L\right) + K_3\epsilon\left|b_+\left(t_L\right)\right|$$

Since $K_3 = 0.040261$, $L_3 = 1.006519$ and $\Delta g > \varepsilon_+\left(t_L\right)$, $K_3\varepsilon_+\left(t_L\right) \ll L_3\left(\Delta g\right)$. The above inequality therefore shows that provided $K_3\epsilon\left|b_+\left(t_L\right)\right|$ is small compared to Δg, $\left|\hat{K}_3\right|$ is small compared to $L_3\left(\Delta g\right)$. As $\left|b_+\left(t_L\right)\right|$ is a bounded function of t_L, and $\epsilon, K_3 \ll 1$, this should be true for sufficiently large Δg. (6.52) and the fact that $g_I^+\left(t;t_L\right) \approx L_3\left(\Delta g\right)e^{-\frac{t}{T_3}}$ for $t > t_I^M\left(t_L\right)$ therefore imply that given sufficiently large Δg, for t large compared to $\max\left\{T_1, t_I^M\left(t_L\right)\right\}$, $\sum_{j=1}^{3} K_j C_j e^{-\frac{\left(t-t_L\right)}{T_j}}$ will be small compared to $g_I^+\left(t;t_L\right)$. It then follows from (6.50) that for t large compared to $\max\left\{T_1, t_I^M\left(t_L\right)\right\}$

$$\hat{g}_+\left(t\right) \approx g_I^+\left(t;t_L\right) + e^{-\frac{\left(t-t_L\right)}{2\epsilon}}\sum_{j=1}^{3} K_j A_j \cos\left(\frac{d}{\epsilon}\left(t-t_L\right) + B_j\right)$$

which suggests $\hat{g}_+\left(t\right)$ will be a damped oscillation about $g_I^+\left(t;t_L\right)$ in this range.

Since $\hat{g}_+\left(t\right)$ is increasing on $\left[0, t_L\right]$, it can be concluded that provided Δg is sufficiently large, as t is increased from 0, $\hat{g}_+\left(t\right)$ will increase to a maximum at $t_+^M\left(t_L\right) > t_L$ before decreasing to 0 by executing damped oscillations about $g_I^+\left(t;t_L\right)$. Moreover, as $g_I^+\left(t;t_L\right) \approx L_3\left(\Delta g\right)e^{-\frac{t}{T_3}}$ for $t > t_I^M\left(t_L\right)$ and $L_3 \approx 1$, these oscillations may cause $\hat{g}_+\left(t_+^M\left(t_L\right)\right)$ to exceed Δg. In such cases $\hat{g}_+\left(t\right)$, and hence $g_+\left(t\right)$, will therefore model a saccade towards Δg degrees with a dynamic overshoot (cf. section 1.1.2). Note that since $g_-\left(t\right) = -g_+\left(t\right)$, this implies $g_-\left(t\right)$ will model a saccade towards $-\left(\Delta g\right)$ degrees with a dynamic overshoot.

Figures (6-9)-(6-11) are plots of $g_+\left(t\right)$ on $\left[0, 0.8\right]$ obtained for choices of Δg and $\boldsymbol{\alpha}$ such that $\boldsymbol{\alpha}$ lies in A with $\epsilon > \epsilon_F^0\left(\alpha,\beta\right)$. Also shown on the plots are $\hat{g}_+\left(t\right)$ on $\left[0, t_L\right]$ and $g_I^+\left(t;t_L\right)$ on $\left[t_L, 0.8\right]$. For these choices of Δg and $\boldsymbol{\alpha}$, $g_+\left(t\right)$ can indeed be seen to simulate a dynamic overshoot.

In contrast to the more mathematical treatment above, there is a geometric interpretation

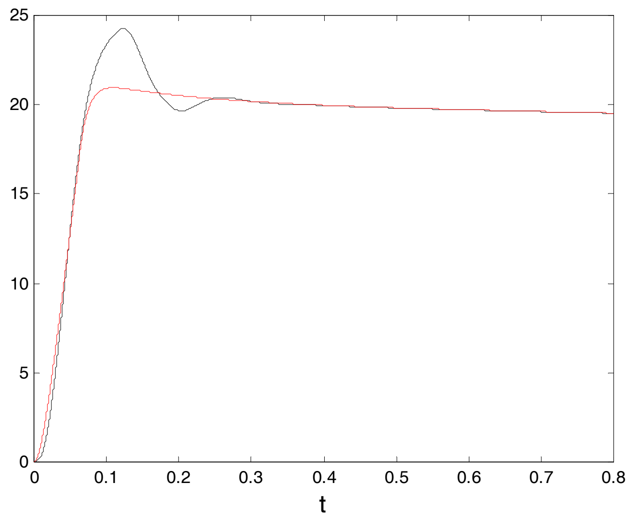

Figure 6-9: Plot of $g_+(t)$ on $[0, 0.8]$ for $\alpha = 100$, $\beta = 4.5$, $\epsilon = 0.015$, $\Delta g = 20$ (black line). The functions $\hat{g}_+(t)$ on $[0, t_L]$ and $g_I^+(t; t_L)$ on $[t_L, 0.8]$ are plotted in red. $t_L = 0.063$.

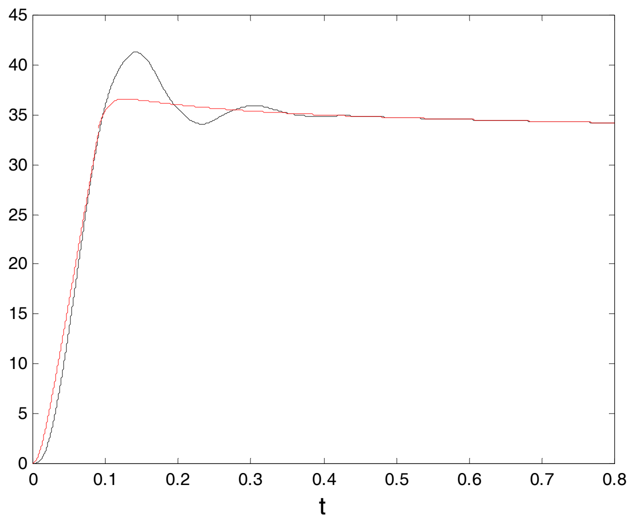

Figure 6-10: Plot of $g_+(t)$ on $[0, 0.8]$ for $\alpha = 40$, $\beta = 1.5$, $\epsilon = 0.02$, $\Delta g = 35$ (black line). The functions $\hat{g}_+(t)$ on $[0, t_L]$ and $g_I^+(t; t_L)$ on $[t_L, 0.8]$ are plotted in red. $t_L = 0.08$.

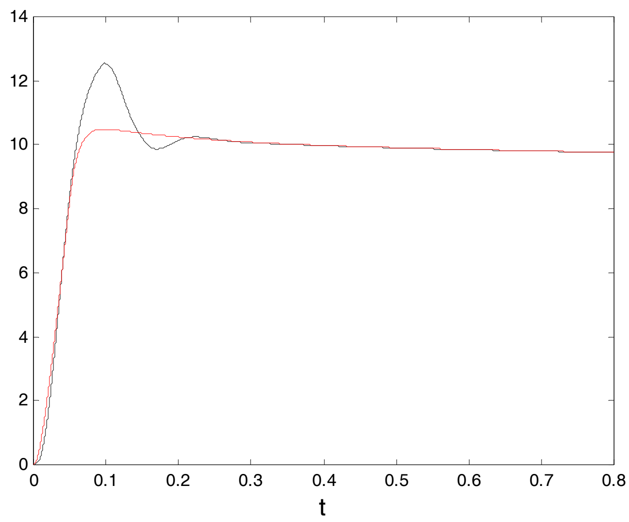

Figure 6-11: Plot of $g_+(t)$ on $[0, 0.8]$ for $\alpha = 100$, $\beta = 6$, $\epsilon = 0.015$, $\Delta g = 10$ (black line). The functions $\hat{g}_+(t)$ on $[0, t_L]$ and $g_I^+(t; t_L)$ on $[t_L, 0.8]$ are plotted in red. $t_L = 0.05$.

of the observation that $g_\pm(t)$ models a normometric saccade for small values of ϵ with $\epsilon < \epsilon_F(\alpha, \beta)$, while $g_\pm(t)$ models a dynamic overshoot for $\epsilon > \epsilon_F(\alpha, \beta)$. Recall from section 3.6.3 that as ϵ is increased from $\mathbf{0}$ through $\epsilon_F(\alpha, \beta)$ for a fixed α and β with $\alpha < \Lambda_+\beta$, trajectories of $\dot{\mathbf{y}} = \mathbf{Y}(\mathbf{y})$ with initial condition in $\mathcal{B}(\mathbf{0})$ begin to follow the slow manifold S_M less and less closely, until they eventually begin to spiral around the invariant line L_0 as they approach the origin. This suggests that the evolution from normometric saccades to dynamic overshoots as ϵ is increased from 0 can be viewed as a consequence of the corresponding burster system trajectories following S_M less closely as they converge to the origin. Figures (6-12)-(6-13) show the effects on both $g_-(t)$ and the corresponding trajectories of $\dot{\mathbf{y}} = \mathbf{Y}(\mathbf{y})$ of increasing ϵ from 0 through $\epsilon_F^0(\alpha, \beta)$ for $\{\alpha = 100, \beta = 3.75, \Delta g = 20\}$. The behaviour shown in these figure seem consistent with this interpretation.

The form of $g_P^+(t)$ in region B

As stated above, it is being assumed that ϵ is sufficiently small for $\mathbf{0}$ to be a stable node of $\dot{\mathbf{y}} = \mathbf{Y}(\mathbf{y})$, and for $\mathbf{y}_+(0) \in \mathcal{B}(\mathbf{y}_1^+)$. Recall the expression (6.44) for $g_P^+(t)$:

$$g_P^+(t) = \sum_{j=1}^{3} K_j e^{-\frac{t}{T_j}} \int_{t_L}^{t} e^{\frac{s}{T_j}} w_L^+(s - t_L)\, ds \tag{6.53}$$

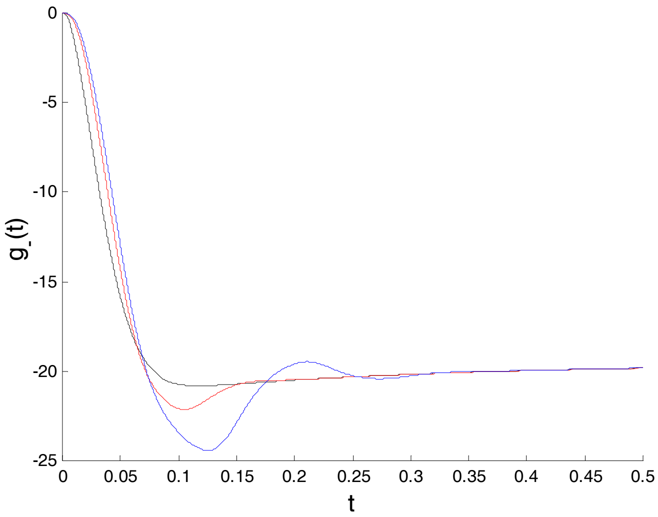

Figure 6-12: Plots of $g_{-}(t)$ on [0 0.5] for $\alpha = 100$, $\beta = 3.75$, $\Delta g = 20$ and the ϵ values 0.001 (black line), 0.01 (red line) and 0.015 (blue line). For this choice of (α, β), $\epsilon_F^0(\alpha, \beta) = 0.065$.

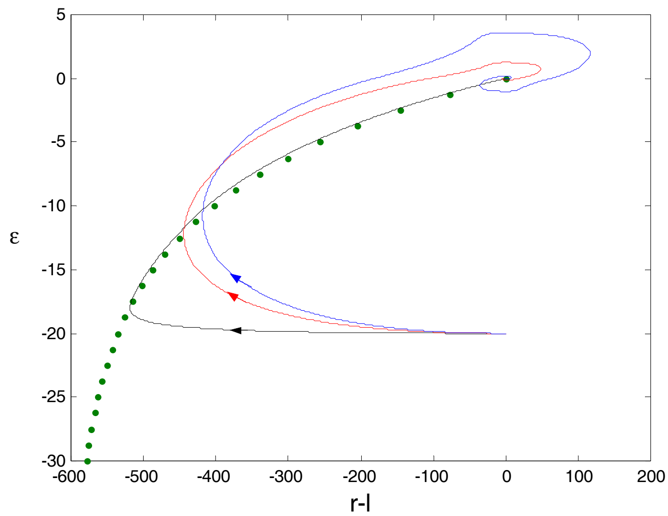

Figure 6-13: Projection onto the $(r - l, \varepsilon)$ plane of the trajectories of $\dot{\mathbf{y}} = \mathbf{Y}(\mathbf{y})$ corresponding to the simulated saccades of figure (6-12). The dotted line represents the slow manifold S_M.

Equations (6.29)-(6.30) imply that in this range, $\forall t \geq t_L$

$$w_L^+ (t - t_L) = Ae^{\frac{\mu_{12}}{\epsilon}(t-t_L)} + Be^{\frac{\mu_{13}}{\epsilon}(t-t_L)}$$

with

$$\begin{aligned}
d &= \sqrt{\Delta_1(\alpha,\beta)^2 - 4\epsilon\left(\Gamma_1^+(\alpha,\beta) + \Gamma_1^-(\alpha,\beta)\right)} \\
\mu_{12} &= \tfrac{1}{2}\left(\Delta_1(\alpha,\beta) + d\right) \\
\mu_{13} &= \tfrac{1}{2}\left(\Delta_1(\alpha,\beta) - d\right) \\
A &= -\tfrac{1}{d}\left(\mu_{13}\left(\varepsilon_+(t_L) - \varepsilon_1\right) + \epsilon b_+(t_L)\right) \\
B &= \tfrac{1}{d}\left(\mu_{12}\left(\varepsilon_+(t_L) - \varepsilon_1\right) + \epsilon b_+(t_L)\right)
\end{aligned}$$

and $b_+(t_L) = r_+(t_L) - l_+(t_L)$. Substituting the above into (6.53) leads to the following expression for $g_P^+(t)$ on $[t_L, \infty)$

$$g_P^+(t) = \sum_{j=1}^{3} K_j \left(\left(A_j e^{\frac{\mu_{12}(t-t_L)}{\epsilon}} + B_j e^{\frac{\mu_{13}(t-t_L)}{\epsilon}}\right) - (A_j + B_j)\, e^{-\frac{(t-t_L)}{T_j}}\right) \tag{6.54}$$

where for $1 \leq j \leq 3$:

$$\begin{aligned}
A_j &= -\frac{\epsilon T_j\left(\mu_{13}\left(\varepsilon_+(t_L) - \varepsilon_1\right) + \epsilon b_+(t_L)\right)}{d\left(T_j\mu_{12} + \epsilon\right)} \\
B_j &= \frac{\epsilon T_j\left(\mu_{12}\left(\varepsilon_+(t_L) - \varepsilon_1\right) + \epsilon b_+(t_L)\right)}{d\left(T_j\mu_{13} + \epsilon\right)}
\end{aligned}$$

A very similar analysis to that of case 1 in the analysis of region A implies that given ϵ sufficiently small, $\forall t \geq t_L$:

$$\left|g_P^+(t)\right| \lessapprox 2\left(\sum_{j=1}^{3}\left|K_j\hat{A}_j\right| + \left|\hat{B}\right|\sum_{j=1}^{3}|K_j|\right) \tag{6.55}$$

where for $1 \leq j \leq 3$

$$\left|K_j\hat{A}_j\right| \leq \frac{|L_2|\,|\Delta_1(\alpha,\beta)|\left(\varepsilon_+(t_L) - \varepsilon_1\right)}{\left|\left(\Gamma_1^+(\alpha,\beta) + \Gamma_1^-(\alpha,\beta)\right)T_j + \Delta_1(\alpha,\beta)\right|} \tag{6.56}$$

and:

$$\hat{B} = -\frac{1}{\Delta_1(\alpha,\beta)^2}\left(b_+(t_L) + \left(\frac{\Gamma_1^+(\alpha,\beta) + \Gamma_1^-(\alpha,\beta)}{\Delta_1(\alpha,\beta)}\right)\left(\varepsilon_+(t_L) - \varepsilon_1\right)\right)\epsilon^2$$

As stated earlier, for $t_L < t < t_I^M(t_L)$:

$$g_I^+(t;t_L) \gtrapprox 0.34\left(\Delta g - \varepsilon_+(t_L)\right)$$

The form of $\hat{B}$ implies $\hat{B} \to 0$ as $\epsilon \to 0$. It therefore follows from (6.55), (6.56) and the above expression that provided Δg is large compared to $\varepsilon_+(t_L)$, and $\left|\left(\Gamma_1^+(\alpha,\beta) + \Gamma_1^-(\alpha,\beta)\right)T_j + \Delta_1(\alpha,\beta)\right|$ is not small compared to $|L_2|\,|\Delta_1(\alpha,\beta)|$ for $1 \le j \le 3$, then $\left|g_P^+(t)\right|$ will be small compared to $g_I^+(t;t_L)$ on $\left(t_L, t_I^M(t_L)\right)$, for ϵ sufficiently small. Noting that $\varepsilon_* = \varepsilon_1$ in the parameter range considered here, the analysis of $g_I^+(t;t_L)$ given earlier implies $g_I^+(t;t_L) \approx L_3(\Delta g - \varepsilon_1)\,e^{-\frac{t}{T_3}}$ for $t > t_I^M(t_L)$ (cf. figure (6-5)). Under the assumptions on the relative sizes of $\{\Delta g, \varepsilon_+(t_L)\}$ and $\left\{\left|\left(\Gamma_1^+ + \Gamma_1^-\right)T_j + \Delta_1\right|, |L_2|\,|\Delta_1|\right\}$, (6.55) and (6.56) therefore also suggest that for sufficiently small ϵ, $\left|g_P^+(t)\right|$ will be small compared to $g_I^+(t;t_L)$ for $t > t_I^M(t_L)$ with t small compared to T_3. Fix $t_M > t_I^M(t_L)$ such that t_M is small compared to T_3. Since

$$\hat{g}_+(t) = g_I^+(t;t_L) + g_P^+(t)$$

on $[t_L,\infty)$, the arguments above imply that, provided the assumptions made hold, $\hat{g}_+(t)$ will be a small perturbation of $g_I^+(t;t_L)$ on $[t_L, t_M]$ for ϵ sufficiently small. The form of $g_I^+(t;t_L)$ on $[t_L,\infty)$ therefore suggests that as t is increased from 0 to t_M, $\hat{g}_+(t)$ will increase to a maximum at $t_+^M(t_L)$ with $t_+^M(t_L) \approx t_I^M(t_L)$, before decreasing with $\hat{g}_+(t) \approx L_3(\Delta g - \varepsilon_1)\,e^{-\frac{t}{T_3}}$ for $t > t_+^M(t_L)$. Moreover, $\hat{g}_+\left(t_+^M(t_L)\right) \approx (\Delta g - \varepsilon_1)\,g_E^M$. Since $g_E^M \approx 1$, this suggests two possibilities for the form of $\hat{g}_+(t)$, and hence of $g_+(t)$ on $[0, t_M]$, depending on the size of Δg relative to ε_1. If Δg is large compared to ε_1, $g_+(t)$ will model a normometric saccade to Δg degrees on $[0, t_M]$, which drifts back towards 0 like $L_3(\Delta g - \varepsilon_1)\,e^{-\frac{t}{T_3}}$ as $t \to t_M$. As $g_-(t) = -g_+(t)$, $g_-(t)$ will therefore model a normometric saccade to $-(\Delta g)$ degrees on $[0, t_M]$, which drifts back towards 0 like $-L_3(\Delta g - \varepsilon_1)\,e^{-\frac{t}{T_3}}$ as $t \to t_M$. If $\Delta g > \varepsilon_1$, but is of the same order as ε_1, $g_+(t)$ will model a hypometric saccade towards Δg degrees on $[0, t_M]$, which drifts back towards 0 like $L_3(\Delta g - \varepsilon_1)\,e^{-\frac{t}{T_3}}$ as $t \to t_M$ (cf. section 1.1.2). Conversely, $g_-(t)$ will model a hypometric saccade towards $-(\Delta g)$ degrees on $[0, t_M]$ which drifts back towards 0 like $-L_3(\Delta g - \varepsilon_1)\,e^{-\frac{t}{T_3}}$ as $t \to t_M$. Figures (6-14)-(6-16) are plots of $g_+(t)$ on $[0, 0.8]$ obtained for choices of Δg and $\boldsymbol{\alpha}$ such that $\boldsymbol{\alpha}$ lies in B, with ϵ sufficiently small for $\mathbf{0}$ to be a stable node of $\dot{\mathbf{y}} = \mathbf{Y}(\mathbf{y})$ and for $\mathbf{y}_+(0) \in \mathcal{B}\left(\mathbf{y}_1^+\right)$. Also shown are the function $L_3(\Delta g - \varepsilon_1)\,e^{-\frac{t}{T_3}}$ on $[0, 0.8]$ together with $\hat{g}_+(t)$ on $[0, t_L]$ and $g_I^+(t;t_L)$ on $[t_L, 0.8]$. For the parameters used

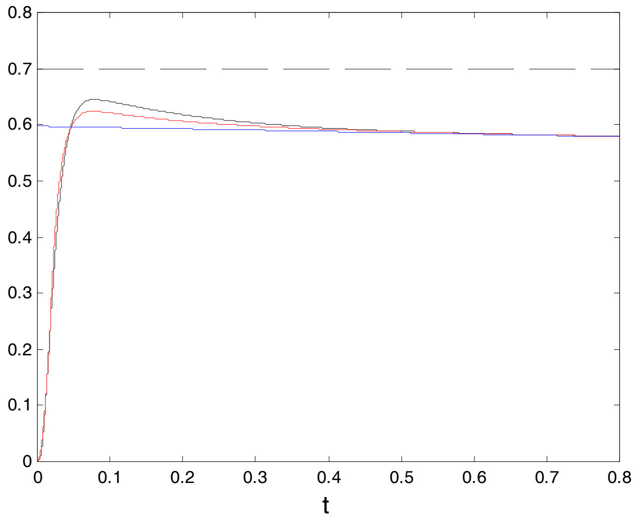

Figure 6-14: Plot of $g_+(t)$ on $[0, 0.8]$ for $\alpha = 206$, $\beta = 3$, $\epsilon = 0.002$, $\Delta g = 0.7$ (black line). $\varepsilon_1 = 0.106391$ in this case. The function $L_3 (\Delta g - \varepsilon_1) e^{-\frac{t}{T_N}}$ is plotted in blue while $\hat{g}_+(t)$ on $[0, t_L]$ and $g_I^+(t; t_L)$ on $[t_L, 0.8]$ are plotted in red. $t_L = 0.0174$.

to obtain figures (6-14) and (6-15), Δg is of a similar size to ε_1, while for the choice of parameters used to obtain figure (6-16), Δg is large compared to ε_1.In all 3 cases, the shape of $g_+(t)$ is as predicted. Note that since ε_1 is bounded above by ε_H, for sufficiently large values of Δg, $g_\pm(t)$ will model a normometric saccade.

6.2 The form of the gaze time series for limit cycle attractors

Assume that $\boldsymbol{\alpha}$ lies in one of C and D, where the attractors are the limit cycles $\hat{\mathcal{C}}_+$ and $\hat{\mathcal{C}}_-$, or in one of E and F, where the attractor is the limit cycle $\hat{\mathcal{C}}_2$ (cf. figure (5-25)). As in section 6.1, fix $\Delta g > 0$, set $\mathbf{z}_0^\pm = (\mathbf{0}, 0, 0, \pm(\Delta g))^T$ and define $\mathbf{z}_\pm(t)$ $\forall t \geq 0$ by:

$$\mathbf{z}_\pm(t) = (\mathbf{x}_\pm(t), \mathbf{y}_\pm(t))^T = (g_\pm(t), v_\pm(t), n_\pm(t), r_\pm(t), l_\pm(t), \varepsilon_\pm(t))^T = \psi_t\left(\mathbf{z}_0^\pm\right)$$

Again, $g_+(t)$ simulates a saccade to Δg degrees and $g_-(t)$ simulates a saccade to $-(\Delta g)$ degrees. Also, $\forall t \geq 0$, $\mathbf{z}_-(t) = \Sigma \mathbf{z}_+(t)$, which implies $g_-(t) = -g_+(t)$. Write $\hat{\mathcal{C}}$ for the limit cycle associated with $\mathbf{z}_+(t)$. Then $\exists \mathbf{z}'_+ \in \hat{\mathcal{C}}$ such that $\mathbf{z}_+(t) \to \psi_t\left(\mathbf{z}'_+\right)$ as $t \to \infty$. The symmetry therefore implies $\mathbf{z}_-(t) \to \psi_t\left(\mathbf{z}'_-\right)$ as $t \to \infty$, where $\mathbf{z}'_- = \Sigma \mathbf{z}'_+$. Define the

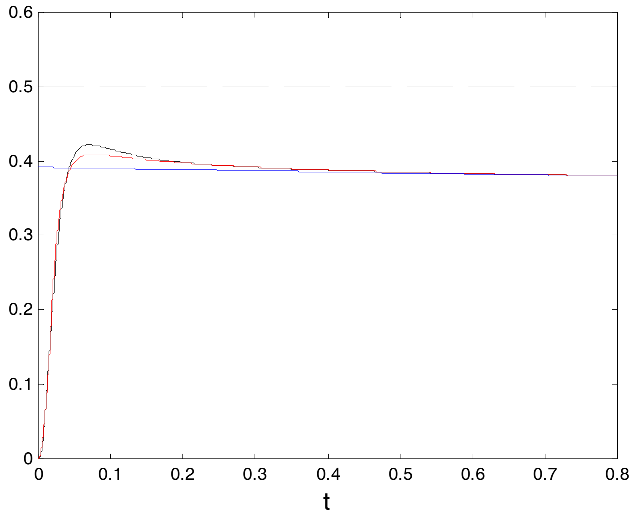

Figure 6-15: Plot of $g_+(t)$ on $[0, 0.8]$ for $\alpha = 107$, $\beta = 1.5$, $\epsilon = 0.0015$, $\Delta g = 0.5$ (black line). $\varepsilon_1 = 0.110704$ in this case. The function $L_3 (\Delta g - \varepsilon_1) e^{-\frac{t}{T_N}}$ is plotted in blue while $\hat{g}_+(t)$ on $[0, t_L]$ and $g_I^+(t; t_L)$ on $[t_L, 0.8]$ are plotted in red. $t_L = 0.016$.

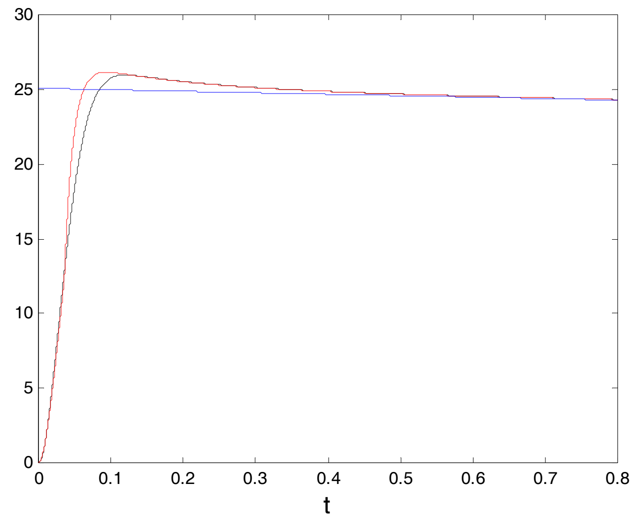

Figure 6-16: Plot of $g_+(t)$ on $[0, 0.8]$ for $\alpha = 404$, $\beta = 6$, $\epsilon = 0.001$, $\Delta g = 25$ (black line). $\varepsilon_1 = 0.089516$ in this case. The function $L_3 (\Delta g - \varepsilon_1) e^{-\frac{t}{T_N}}$ is plotted in blue while $\hat{g}_+(t)$ on $[0, t_L]$ and $g_I^+(t; t_L)$ on $[t_L, 0.8]$ are plotted in red. $t_L = 0.0358$.

functions $\mathbf{z}_S^{\pm}(t)$ and $\mathbf{z}_T^{\pm}(t)$ for $t \geq 0$ by:

$$\begin{aligned}\mathbf{z}_S^{\pm}(t) &= \left(g_S^{\pm}(t), v_S^{\pm}(t), n_S^{\pm}(t), r_S^{\pm}(t), l_S^{\pm}(t), \varepsilon_S^{\pm}(t)\right)^T = \psi_t\left(\mathbf{z}'_{\pm}\right) \\ \mathbf{z}_T^{\pm}(t) &= \left(g_T^{\pm}(t), v_T^{\pm}(t), n_T^{\pm}(t), r_T^{\pm}(t), l_T^{\pm}(t), \varepsilon_T^{\pm}(t)\right)^T = \mathbf{z}_{\pm}(t) - \psi_t\left(\mathbf{z}'_{\pm}\right)\end{aligned}$$

Then $\forall t \geq 0$

$$\mathbf{z}_{\pm}(t) = \mathbf{z}_S^{\pm}(t) + \mathbf{z}_T^{\pm}(t)$$

where $\mathbf{z}_T^{\pm}(t) \to 0$ as $t \to \infty$. In particular, $\forall t \geq 0$:

$$g_{\pm}(t) = g_S^{\pm}(t) + g_T^{\pm}(t) \tag{6.57}$$

where $g_T^{\pm}(t) \to 0$ as $t \to \infty$. The uniqueness of solutions of the saccadic equations implies that $\forall t \geq 0$, $\mathbf{z}_S^{-}(t) = \Sigma \mathbf{z}_S^{+}(t)$. This in turn implies that $\mathbf{z}_T^{-}(t) = \Sigma \mathbf{z}_T^{+}(t)$ $\forall t \geq 0$. It therefore follows from the form of Σ that $\forall t \geq 0$, $g_S^{-}(t) = -g_S^{+}(t)$ and $g_T^{-}(t) = -g_T^{+}(t)$.

It has thus been shown that as $t \to \infty$, the gaze time series $g_{\pm}(t)$ converges to a periodic time series associated with the corresponding limit cycle attractor. The analysis of the morphology of these periodic time series given in section 5.8.4 forms the basis of the discussion of the morphology of $g_{\pm}(t)$ in the ranges C to F given below.

6.2.1 Region C

The analysis of section 5.8.4 suggested that in this region, $g_S^{\pm}(t)$ is a small amplitude oscillation. Figures (6-17) and (6-18) are plots of $g_{+}(t)$ and $g_{-}(t)$ respectively for two choices of Δg and $\boldsymbol{\alpha}$ such that $\boldsymbol{\alpha}$ lies in C. Each time series is shown on the interval $[0, 5]$. It can be seen in each case that $g_{\pm}(t)$ models a normometric saccade to $\pm(\Delta g)$ degrees with a post-saccadic small-amplitude oscillation. This was the typical behaviour observed in this parameter range.

6.2.2 Region D

The analysis of section 5.8.4 suggested that in this region, $g_S^{\pm}(t)$ has the form of a jerk nystagmus waveform which has extended foveation periods for ϵ close to $\epsilon_G(\alpha, \beta)$. Figures

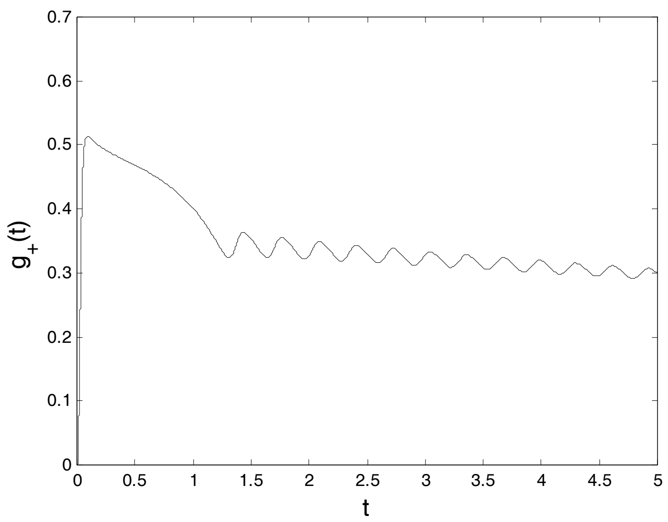

Figure 6-17: The gaze time series $g_+(t)$ on $[0, 5]$ for $\alpha = 207.656$, $\beta = 3$, $\epsilon = 0.006$, $\Delta g = 0.5$.

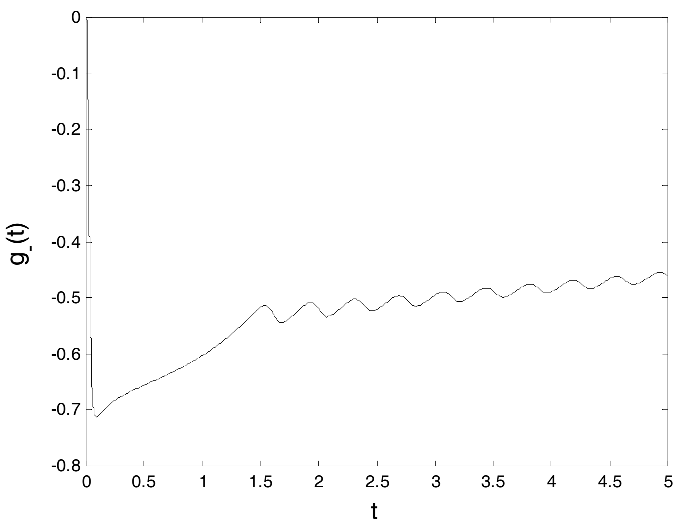

Figure 6-18: The gaze time series $g_-(t)$ on $[0, 5]$ for $\alpha = 306.84$, $\beta = 4.5$, $\epsilon = 0.005$, $\Delta g = 0.7$.

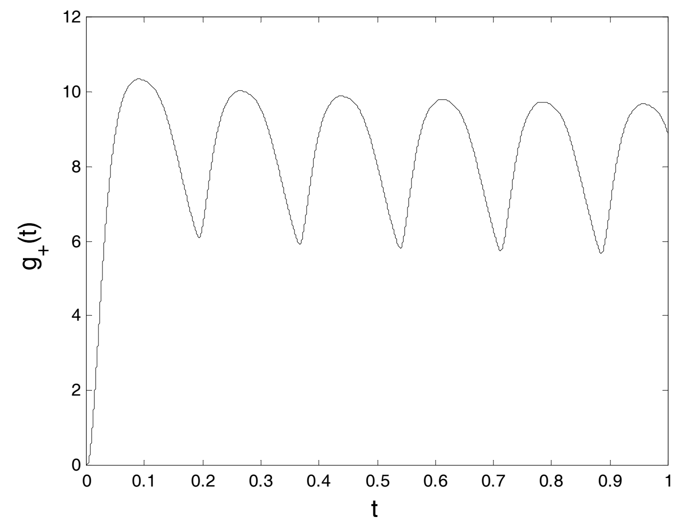

Figure 6-19: The gaze time series $g_+(t)$ on $[0,1]$ for $\alpha = 180$, $\beta = 2.25$, $\epsilon = 0.002$, $\Delta g = 10$.

(6-19)-(6-20) and (6-21)-(6-22) are plots of $g_+(t)$ and $g_-(t)$ respectively for two choices of Δg and $\boldsymbol{\alpha}$ such that $\boldsymbol{\alpha}$ lies in D, and ϵ is small compared to $\epsilon_G(\alpha, \beta)$. Each time series is shown on the interval $[0,1]$ and an interval of the form $[t_1, t_2]$ with $t_1 \gg 1$. $g_\pm(t)$ is seen to have the form of a normometric saccade to $\pm(\Delta g)$ degrees, with a post-saccadic large-amplitude oscillation that decays slowly to a periodic jerk nystagmus waveform. This was the typical behaviour observed for ϵ small compared to $\epsilon_G(\alpha, \beta)$.

Figures (6-23)-(6-24) and (6-25)-(6-26) are plots of $g_+(t)$ and $g_-(t)$ respectively for two choices of Δg and $\boldsymbol{\alpha}$ such that $\boldsymbol{\alpha}$ lies in D, and ϵ is close to $\epsilon_G(\alpha, \beta)$. Each time series is shown on the interval $[0, 3.5]$ and an interval of the form $[t_1, t_2]$ with $t_1 \gg 3.5$. $g_\pm(t)$ is seen to have the form of a normometric saccade to $\pm(\Delta g)$ degrees, with a post-saccadic large-amplitude oscillation that converges slowly to a periodic jerk nystagmus waveform with an extended foveation period. This was the typical behaviour observed for ϵ close to $\epsilon_G(\alpha, \beta)$.

Note that since $g_S^-(t) = -g_S^+(t)$, the direction of the beat of the simulated nystagmus is dependent on the initial direction of the saccade. (This can be seen clearly in figures (6-19)-(6-26)). In more detail, assume that $\mathbf{y}_+(0) \in \mathcal{B}(\mathcal{C}_+)$ so that $\varepsilon_S^+(t)$ is associated with the limit cycle $\mathcal{C}_+$. In this case, the fast motion of $\varepsilon_S^+(t)$ is towards $-\infty$ (cf. section 4.6.1). The approximation $g_S^+(t) \approx -\varepsilon_S^+(t - t_g) + \langle \varepsilon_S^+(t) \rangle$ established in section 5.8.3 therefore implies that the fast motion in $g_S^+(t)$ will be towards $+\infty$, and hence $g_S^+(t)$ will have the

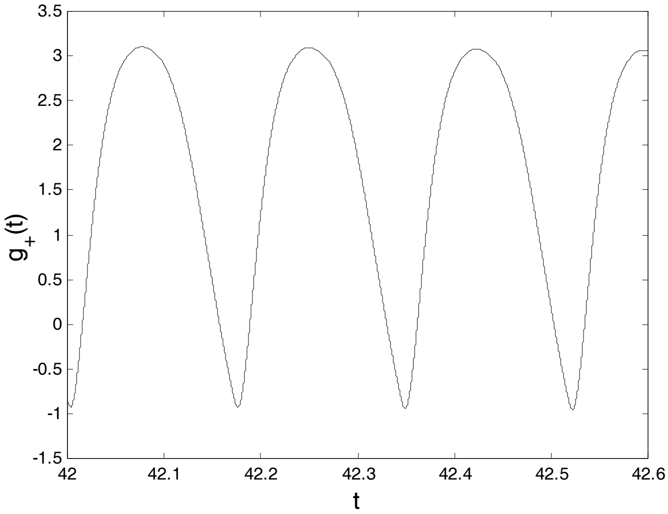

Figure 6-20: The gaze time series $g_+(t)$ on $[42, 42.6]$ for $\alpha = 180$, $\beta = 2.25$, $\epsilon = 0.002$, $\Delta g = 10$.

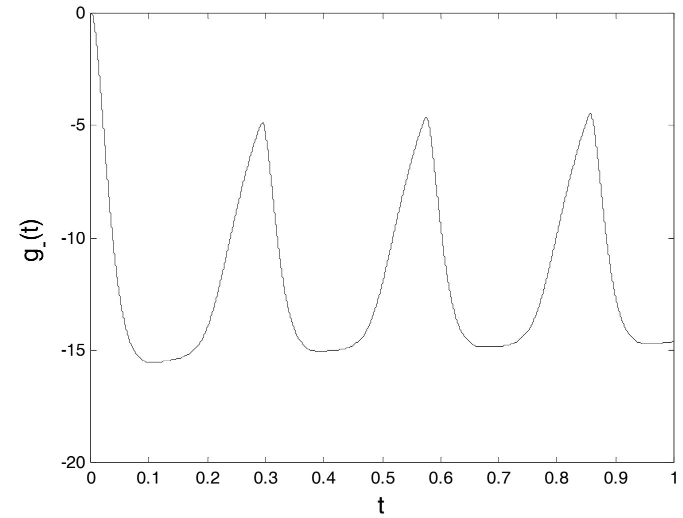

Figure 6-21: The gaze time series $g_-(t)$ on $[0, 1]$ for $\alpha = 310$, $\beta = 4.5$, $\epsilon = 0.001$, $\Delta g = 15$.

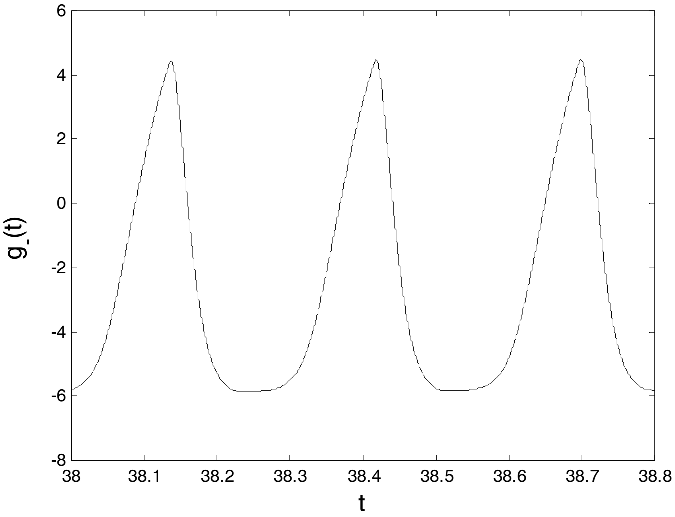

Figure 6-22: The gaze time series $g_-(t)$ on $[38, 38.8]$ for $\alpha = 310$, $\beta = 4.5$, $\epsilon = 0.001$, $\Delta g = 15$.

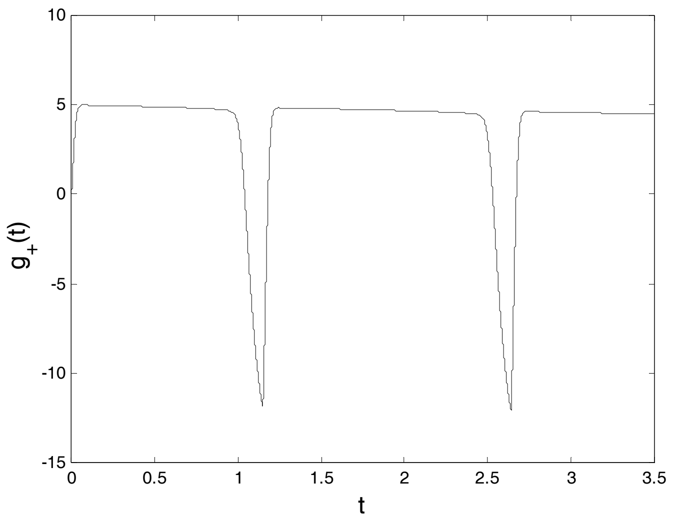

Figure 6-23: The gaze time series $g_+(t)$ on $[0, 3.5]$ for $\alpha = 420$, $\beta = 6$, $\epsilon = 0.0048$, $\Delta g = 5$.

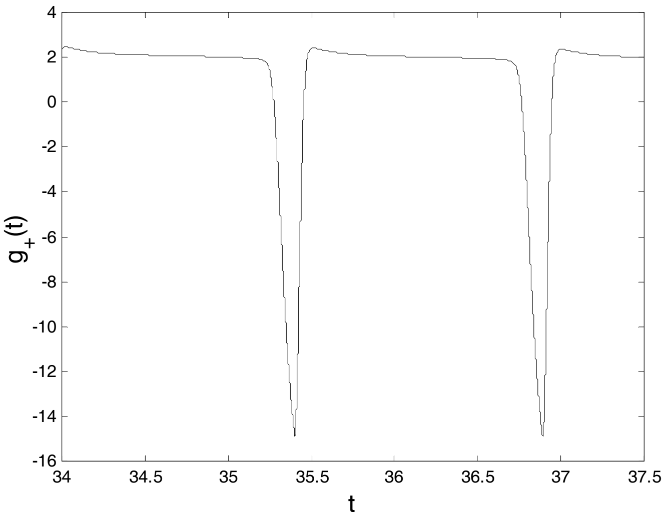

Figure 6-24: The gaze time series $g_+(t)$ on $[34, 37.5]$ for $\alpha = 420$, $\beta = 6$, $\epsilon = 0.0048$, $\Delta g = 5$.

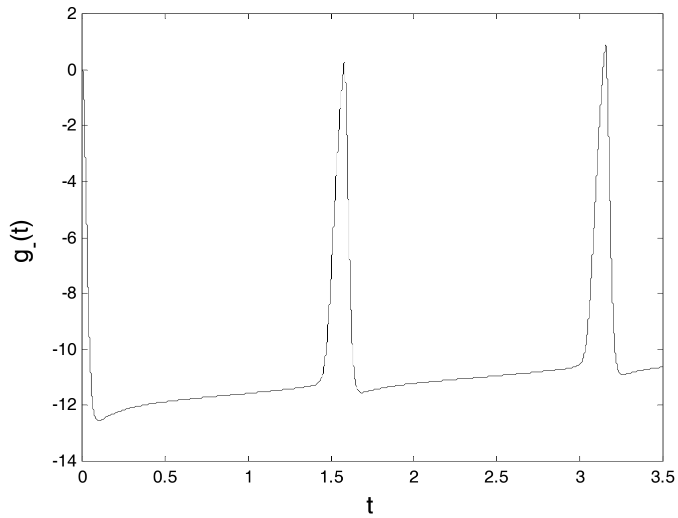

Figure 6-25: The gaze time series $g_-(t)$ on $[0, 3.5]$ for $\alpha = 320$, $\beta = 4.65$, $\epsilon = 0.0047$, $\Delta g = -12$.

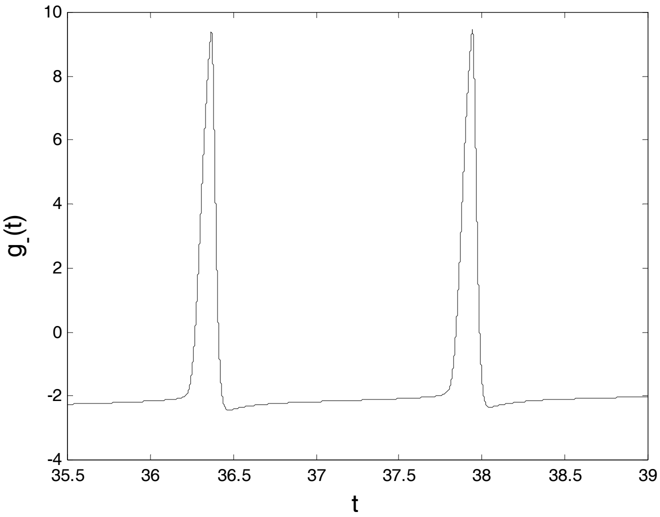

Figure 6-26: The gaze time series $g_{-}(t)$ on $[35.5, 39]$ for $\alpha = 320$, $\beta = 4.65$, $\epsilon = 0.0047$, $\Delta g = -12$.

form of a right-beating jerk nystagmus. As $g_S^-(t) = -g_S^+(t)$, $g_S^-(t)$ will therefore have the form of a left-beating jerk nystagmus. Conversely, if $\mathbf{y}_+(0) \in \mathcal{B}(\mathcal{C}_-)$, $g_S^+(t)$ will be a left-beating nystagmus and $g_S^-(t)$ a right-beating nystagmus. Note that if ϵ is sufficiently small for trajectories of $\dot{\mathbf{y}} = \mathbf{Y}(\mathbf{y})$ not to cross the plane P, then as $\Delta g > 0$, $\mathbf{y}_+(0) \in N_+$, and hence $\mathbf{y}_+(t)$ is confined to N_+ $\forall t \geq 0$. This implies $\mathbf{y}_+(0) \in \mathcal{B}(\mathcal{C}_+)$.

6.2.3 Region E

The analysis of 5.8.4 suggested that in this parameter range, $g_S^{\pm}(t)$ resembles a bilateral jerk nystagmus which has extended foveation periods for ϵ close to $\epsilon_G(\alpha, \beta)$. Figures (6-27)-(6-28) and (6-29)-(6-30) are plots of $g_+(t)$ and $g_-(t)$ respectively for two choices of Δg and $\boldsymbol{\alpha}$ such that $\boldsymbol{\alpha}$ lies in E, and ϵ is large compared to $\epsilon_G(\alpha, \beta)$. Each time series is shown on the interval $[0, 2]$ and an interval of the form $[t_1, t_2]$ with $t_1 \gg 2$. $g_{\pm}(t)$ is seen to have the form of a normometric saccade to $\pm(\Delta g)$ degrees with a post-saccadic large-amplitude oscillation that converges slowly to a periodic bilateral jerk nystagmus. Such behaviour was typical for ϵ large compared to $\epsilon_G(\alpha, \beta)$ in this range.

Figures (6-31)-(6-32) and (6-33)-(6-34) are plots of $g_+(t)$ and $g_-(t)$ respectively for two choices of Δg and $\boldsymbol{\alpha}$ such that $\boldsymbol{\alpha}$ lies in E, and ϵ is close to $\epsilon_G(\alpha, \beta)$. Each time series is plotted on the interval $[0, 4]$ and on an interval of the form $[t_1, t_2]$ with $t_1 \gg 4$. $g_{\pm}(t)$ is

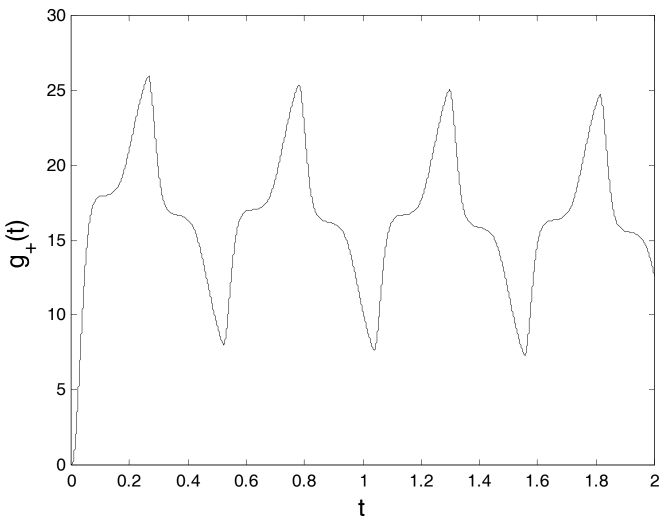

Figure 6-27: The gaze time series $g_+ (t)$ on $[0, 2]$ for $\alpha = 260$, $\beta = 3.75$, $\epsilon = 0.006$, $\Delta g = 17$.

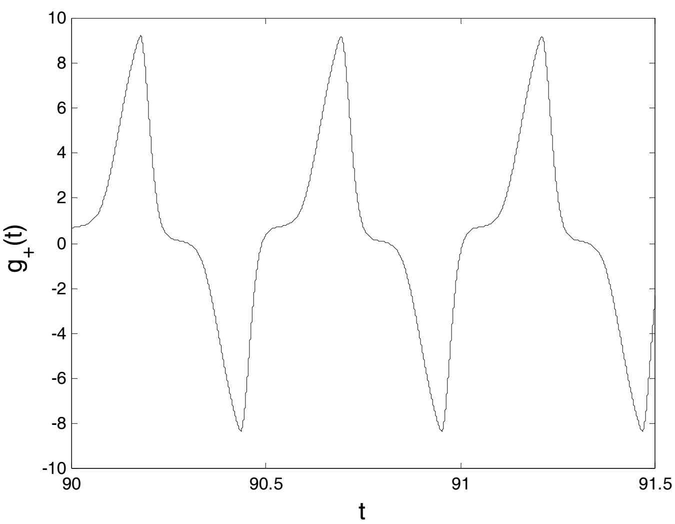

Figure 6-28: The gaze time series $g_+ (t)$ on $[90, 91.5]$ for $\alpha = 260$, $\beta = 3.75$, $\epsilon = 0.006$, $\Delta g = 17$.

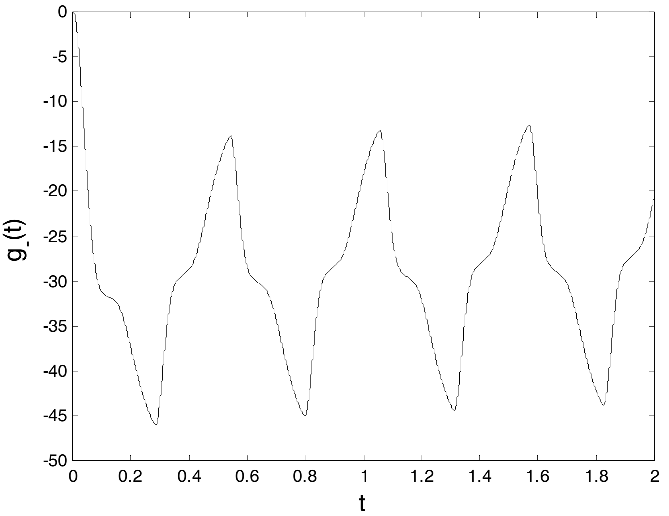

Figure 6-29: The gaze time series $g_-(t)$ on $[0, 2]$ for $\alpha = 400$, $\beta = 5.55$, $\epsilon = 0.0065$, $\Delta g = 30$.

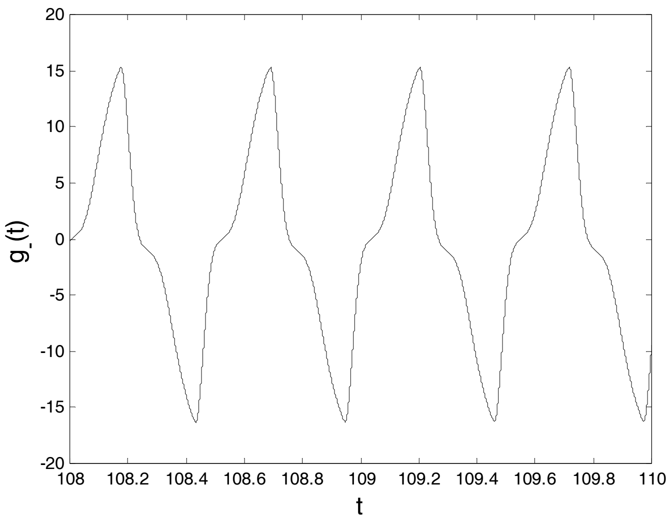

Figure 6-30: The gaze time series $g_-(t)$ on $[108, 110]$ for $\alpha = 400$, $\beta = 5.55$, $\epsilon = 0.0065$, $\Delta g = 30$.

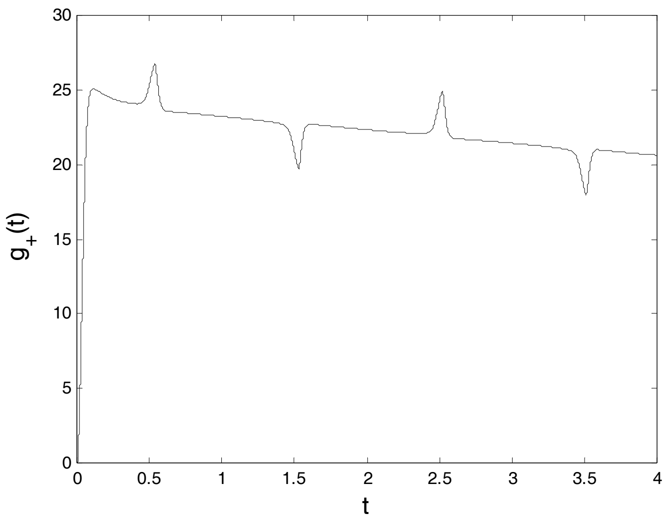

Figure 6-31: The gaze time series $g_+(t)$ on $[0, 4]$ for $\alpha = 134$, $\beta = 1.8$, $\epsilon = 0.005$, $\Delta g = 24$.

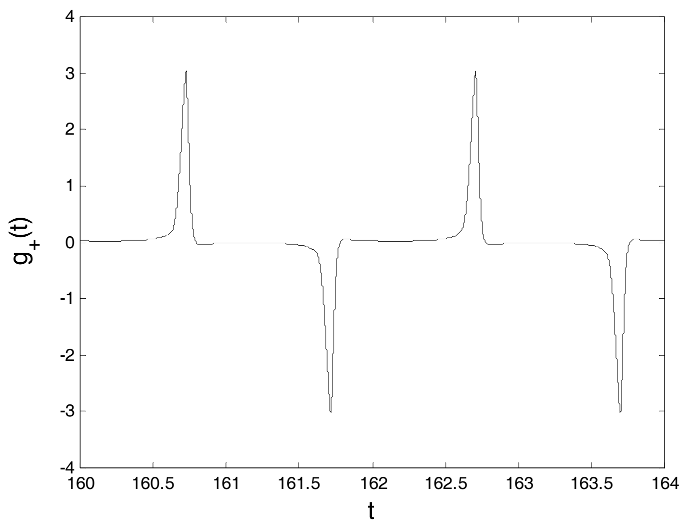

Figure 6-32: The gaze time series $g_+(t)$ on $[160, 164]$ for $\alpha = 134$, $\beta = 1.8$, $\epsilon = 0.005$, $\Delta g = 24$.

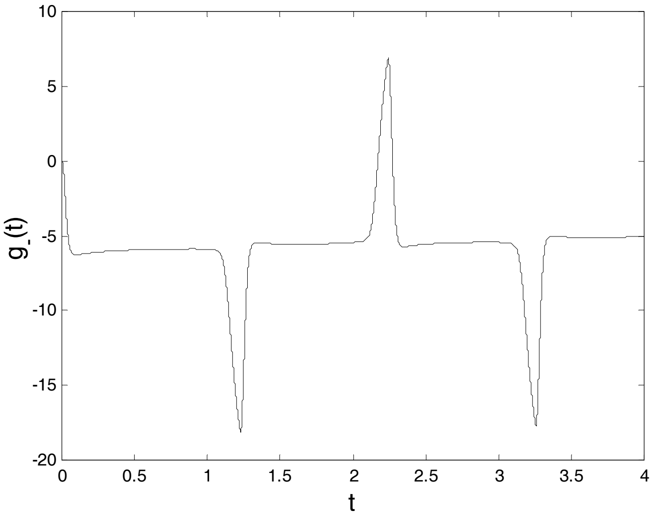

Figure 6-33: The gaze time series $g_{-}(t)$ on $[0, 4]$ for $\alpha = 340$, $\beta = 4.8$, $\epsilon = 0.0049$, $\Delta g = -6$.

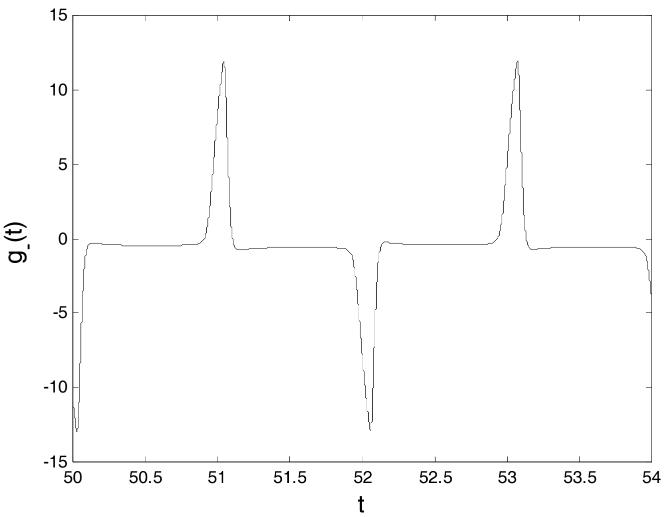

Figure 6-34: The gaze time series $g_{-}(t)$ on $[50, 54]$ for $\alpha = 340$, $\beta = 4.8$, $\epsilon = 0.0049$, $\Delta g = -6$.

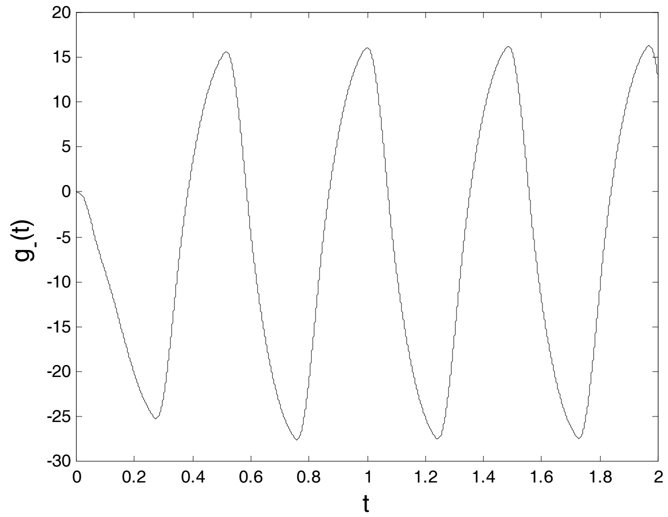

Figure 6-35: The gaze time series $g_-(t)$ on $[0,2]$ for $\alpha = 380$, $\beta = 5.1$, $\epsilon = 0.05$, $\Delta g = -6$.

seen to have the form of a normometric saccade to $\pm(\Delta g)$ degrees, with a post-saccadic large-amplitude oscillation that converges slowly to a periodic bilateral jerk nystagmus with an extended foveation period. This was the typical behaviour observed for ϵ close to $\epsilon_G(\alpha,\beta)$ for parameters in this range.

6.2.4 Region F

It was argued during section 5.8.4 that in this parameter range, $g_S^{\pm}(t)$ has the form of a pendular nystagmus. Plots of $g_-(t)$ and $g_+(t)$ for two choices of Δg and $\boldsymbol{\alpha}$ such that $\boldsymbol{\alpha}$ lies in F are given in figures (6-35)-(6-36) and (6-37)-(6-38) respectively. Each time series is plotted on the interval $[0,2]$ and on an interval of the form $[t_1,t_2]$ with $t_1 \gg 2$. The figures indicate that $g_\pm(t)$ has the form of a hypermetric saccade to $\pm(\Delta g)$ degrees, with a post-saccadic large-amplitude oscillation that decays slowly to a periodic pendular nystagmus. This was the typical behaviour observed in this parameter range.

6.3 Classification of the simulated saccadic behaviours

Collecting the analysis and observations of the last two sections leads to figure (6-39).

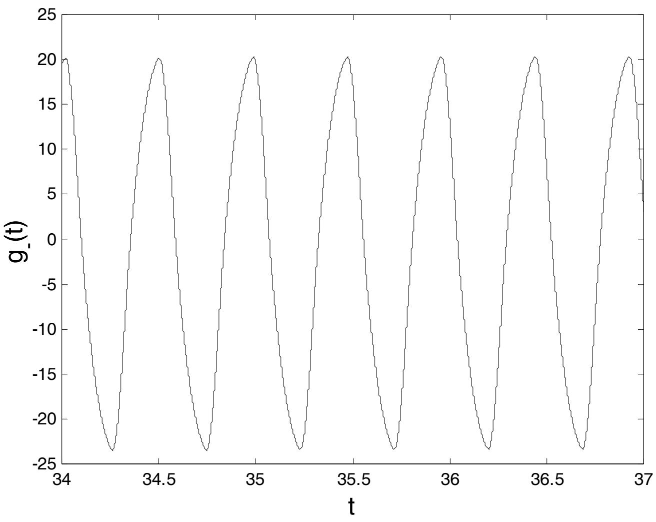

Figure 6-36: The gaze time series $g_-(t)$ on $[34, 37]$ for $\alpha = 380$, $\beta = 5.1$, $\epsilon = 0.05$, $\Delta g = -6$.

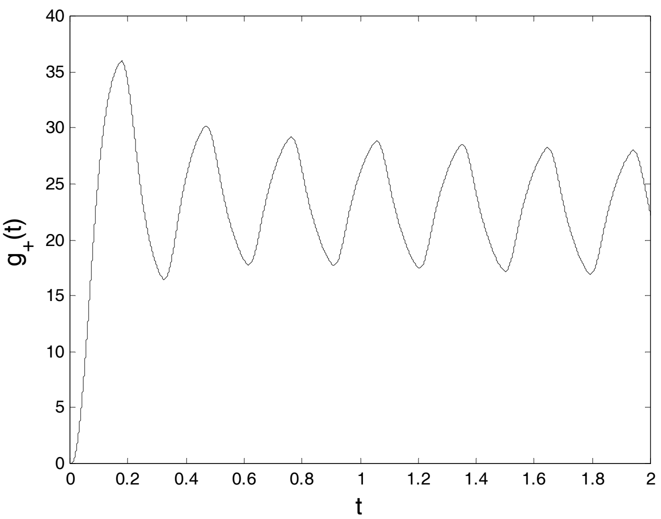

Figure 6-37: The gaze time series $g_+(t)$ on $[0, 2]$ for $\alpha = 140$, $\beta = 1.8$, $\epsilon = 0.05$, $\Delta g = 24$.

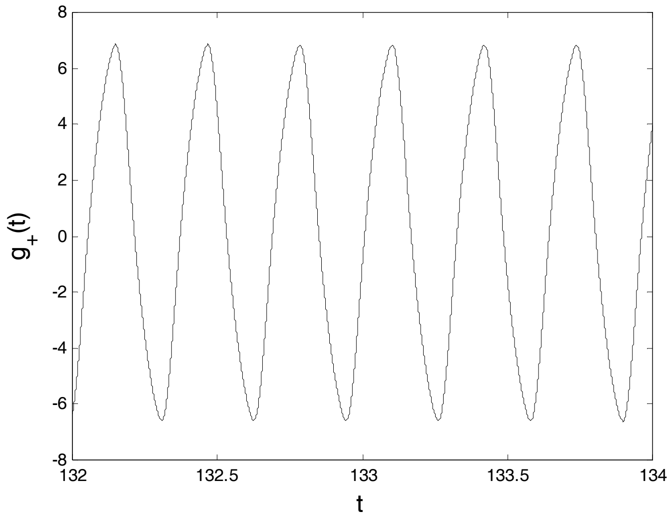

Figure 6-38: The gaze time series $g_+(t)$ on $[132, 134]$ for $\alpha = 140$, $\beta = 1.8$, $\epsilon = 0.05$, $\Delta g = 24$.

6.4 Biological implications

This section presents a number of possible implications for the understanding of saccadic dysmetria and CN that can be inferred from the analysis of the saccadic equations. Where appropriate, experiments are outlined to further investigate these hypotheses.

6.4.1 The existence of a continuum of saccadic behaviours

One of the most significant implications of this work is that a single model of the saccadic system is able to simulate both normal and abnormal behaviour. This suggests that the oculomotor pathologies simulated by the model, such as CN, may simply be a consequence of the components of the saccadic system operating outside of their normal range, while remaining structurally intact. The pathologies are therefore what are sometimes referred to as **dynamical diseases** [40]. This proposed characterisation of CN as a dynamical disease contrasts with the work of Optican et al, who proposed that CN is a consequence of miswiring in the oculomotor system (cf. section 1.1.3).

Another important prediction of the model is that it is possible to move between the different types of behaviour classified in figure (6-39), by altering the parameters of the system. This is consistent with experimental observations that, depending on the environmental

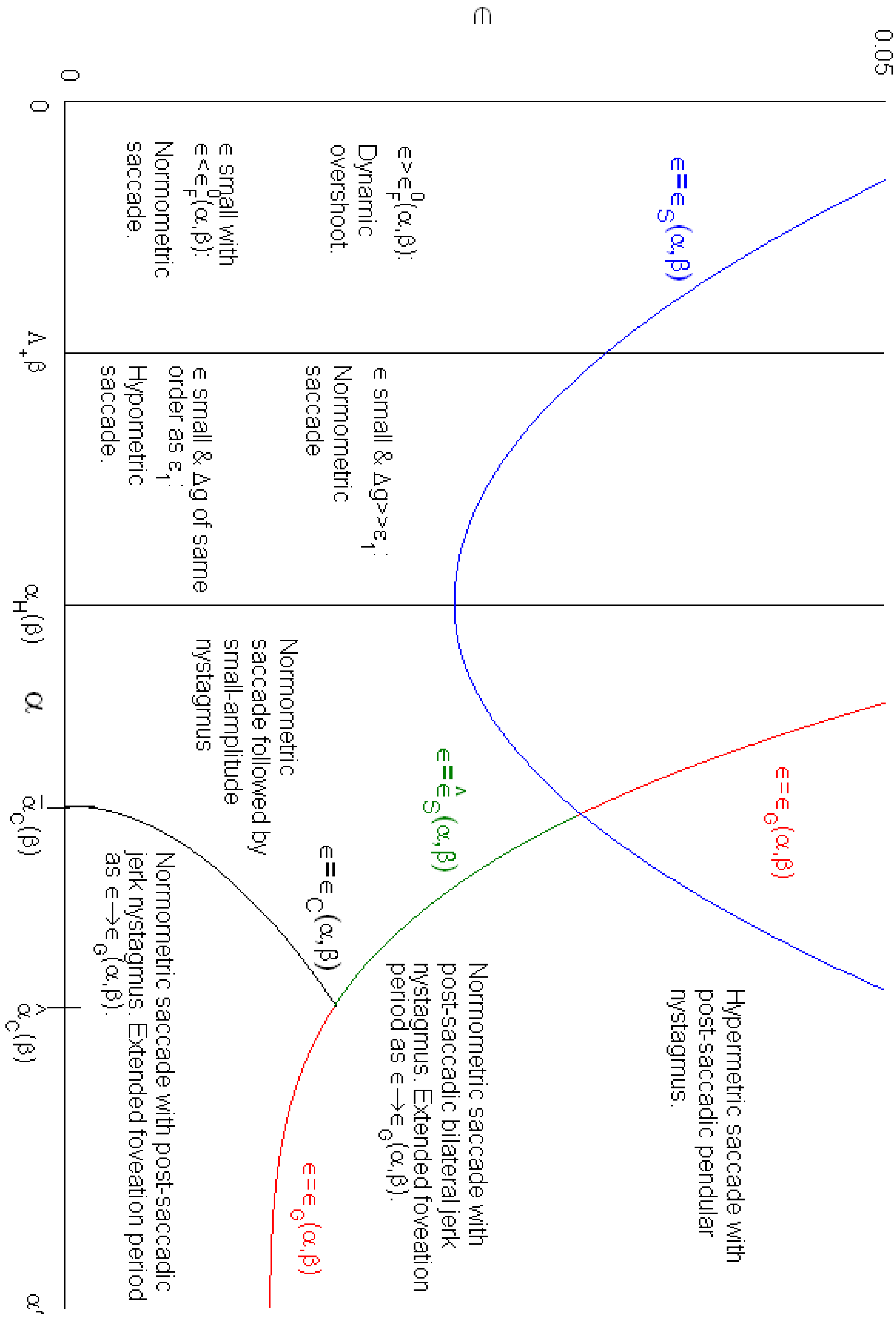

Figure 6-39: Saccadic behaviours modelled by the saccadic equations for initial conditions $(0,0,0,0,0,\pm(\Delta g))^T$ when $\boldsymbol{\alpha}$ lies in the intersection of Π_P with the union of regions A-F of $\hat{\Pi}_P$.

conditions, non-nystagmats can produce both normometric and dysmetric saccades, while nystagmats can exhibit several types of CN waveform (cf. 1.1.3). Additionally, the model predicts which behaviours may be associated with each other in parameter space. Since α and β relate to the basic firing properties of neurons, it seems reasonable to assume that they will be fixed quite early on in the development of the oculomotor system. As stated in section 2.3, the parameter ϵ can be characterised as a measure of how quickly the bursters respond to the driving motor error signal. ϵ might therefore be expected to show greater variability than α and β, as it will be affected by factors such as the chemical environment of the bursters. Under these assumptions on the variability of the parameters, the model suggests, for example, that a normometric saccade is unlikely to develop a post-saccadic oscillation, but may develop into a dynamic overshoot. It also suggests that a jerk oscillation has the capacity to develop into both a bilateral jerk and a pendular nystagmus (cf. figure (6-39)). Such observations can provide the basis of experiments to determine the validity of the model as a predictor of saccadic behaviour (cf. 6.4.2 and 6.4.3 below).

6.4.2 Dynamic overshoots in non-nystagmats result from a large value of ϵ

The discussion of section 6.1 suggested that for $0 < \alpha < \Lambda_+\beta$, normometric saccades evolve into dynamic overshoots with increasing ϵ, as a consequence of the corresponding burster system trajectories following the slow manifold S_M less closely as they converge to the origin. This predicted capacity of normometric saccades to develop into dynamic overshoots is consistent with experimental evidence showing that both behaviours can be observed in the same subject (cf. section 1.1.3). In the case of humans, the hypothesis that dynamic overshoots result from large values of ϵ cannot be tested directly by observing trajectories in the burst neuron firing against motor error phase plane, as this would involve invasive single neuron recording techniques such as those used by Van Gisbergen et al (cf. section 2.3). However, under the assumption that decreased burst neuron reaction times can be associated with reduced attention, simple experiments based on reducing the attention of a subject in a controlled manner could be conducted, to test this hypothesis indirectly.

One such approach to reducing attention would be the measured administration of known tranquillising agents to the subject over a recording period. Another recognised technique is to use visual distractions to break the attentional state [41]. Finally, since visual inattention is known to be correlated with fatigue, it would be interesting to investigate whether dynamic overshoots became more prevalent in a subject during recording periods spread out over the course of a day.

6.4.3 Jerk nystagmus can evolve into both bilateral jerk and pendular nystagmus

One of the most interesting predictions of the model is the possibility of moving between the jerk, bilateral jerk and pendular nystagmus waveforms by varying the ϵ parameter in the range $\alpha > \hat{\alpha}_C(\beta)$ (cf. figure (6-39)). This prediction appears to be consistent with the observation that jerk nystagmus can exhibit transient periods of the bilateral oscillation. Assuming again that the ϵ parameter can be identified with attention, the prediction is also consistent with experimental evidence which shows that some subjects who exhibit jerk nystagmus in high attention conditions can switch to a pendular waveform under conditions of reduced attention (cf. section 1.1.3). The prediction could be explored by using the same techniques to reduce attention in a subject as those suggested above in the discussion of dynamic overshoots. In the event that reasonable control over the waveform could be established, a secondary experiment would be to investigate whether jerk and bilateral jerk waveforms with extended foveation times may be induced by varying the level of attention so as to bring ϵ close to $\epsilon_G(\alpha, \beta)$.

6.4.4 Hypometric saccades and nystagmus are caused by a pathological off response

The analysis of the saccadic equations showed that given a fixed β and ϵ in the ranges of interest, hypometria is observed in saccades of small amplitude for $\Lambda_+\beta < \alpha < \alpha_H(\beta)$, while nystagmus is observed for $\alpha > \alpha_H(\beta)$ (cf. figure (6-39)). This suggests that small amplitude hypometric saccades and the modelled nystagmuses (jerk, pendular etc.) both result from an inappropriately large off response. The interpretation of the off response as a braking saccade (cf. section 2.3) provides a physiological interpretation of these pathologies. Recall that the braking saccade is a small centrifugal tug on the eye towards the end of the movement, which prevents the eye overshooting the target. Hypometric saccades can be attributed to a braking saccade which has increased in magnitude to a level where it is causing the eye to be brought to a halt before the target gaze angle is achieved. Similarly, the modelled oscillations may be thought of as resulting from a braking saccade of sufficient magnitude to produce a large movement of the eye in the opposite direction to that of the saccade. This reverse motion in turn causes the onset of an oscillatory instability through the reciprocal inhibition of the bursters.

6.4.5 For small ϵ, the most likely oscillatory behaviour is jerk nystagmus

The bifurcation structure of the saccadic model implies that in the oscillatory regime $\alpha > \alpha_H(\beta)$, there are two possible types of behaviour that may occur for small ϵ, depending on the sign of $\alpha - \bar{\alpha}_C(\beta)$. If $\alpha < \bar{\alpha}_C(\beta)$, the oscillation is a small-amplitude nystagmus, while if $\alpha > \bar{\alpha}_C(\beta)$, the oscillation is a large-amplitude jerk nystagmus (cf. figure (6-39)). It should be noted that the absence of a steady progression from a small oscillation to a fully developed jerk waveform as α is increased from $\alpha_H(\beta)$ for small ϵ is a consequence of the canard structure of the model discussed in section 4.6.

It was shown in section 3.6.1 that $\alpha_H(\beta)$ is an increasing function of β on (ε_H, β_2). Since $\varepsilon_H < 1.5$ and $\beta_2 > 6$, this implies that $\alpha_H(\beta)$ is increasing on $(1.5, 6)$, the β range of Π_P (cf. (6.1)). It was also stated on the basis of numerical evidence in section 4.6 that $\bar{\alpha}_C(\beta) - \alpha_H(\beta)$ is a decreasing function of β on (β_C, β_2). Since $\beta_C < 1.5$ and $\beta_2 > 6$, $\bar{\alpha}_C(\beta) - \alpha_H(\beta)$ is therefore decreasing on $(1.5, 6)$. Combining these facts implies that the quantity

$$\frac{\bar{\alpha}_C(\beta) - \alpha_H(\beta)}{\alpha_H(\beta)}$$

is a decreasing function of β on $(1.5, 6)$. Hence, $\forall 1.5 < \beta < 6$:

$$\frac{\bar{\alpha}_C(\beta) - \alpha_H(\beta)}{\alpha_H(\beta)} < \frac{\bar{\alpha}_C(1.5) - \alpha_H(1.5)}{\alpha_H(1.5)}$$

Numerics indicate that $\frac{\bar{\alpha}_C(1.5) - \alpha_H(1.5)}{\alpha_H(1.5)} < 0.001$. Hence, $\bar{\alpha}_C(\beta) \approx \alpha_H(\beta)$ on $(1.5, 6)$. This suggests that given ϵ small, the most likely oscillatory instability is jerk nystagmus. Assuming again that ϵ can be identified with attention, the implication of this analysis appears to be that nystagmats are most likely to exhibit the large-amplitude jerk oscillation under high attention conditions, rather than the small-amplitude oscillation.

During the investigation of the canard surface $\epsilon = \epsilon_C(\alpha, \beta)$, determining the value of $\hat{\alpha}_C(\beta)$ for a given $1.5 < \beta < 6$ accurately proved to be computationally very difficult.

Numerics did however suggest that in this range, $\hat{\alpha}_C(\beta) \approx \bar{\alpha}_C(\beta)$. The model therefore also predicts that jerk nystagmus is most likely to evolve into bilateral jerk and pendular nystagmus with increasing ϵ; the transition to a small-amplitude nystagmus is unlikely to be observed.

6.4.6 The fast phases of jerk and bilateral jerk nystagmus may not be corrective

Recall from section 1.1.3 that in the model of congenital nystagmus proposed by Optican et al, the fast phases of CN are believed to be a corrective motion, which counters drift of the eye caused by an instability of the gaze-holding system [7]. The bilateral saccadic model challenges this idea. In this model, the existence of a periodic gaze time series $g_S(t)$ resembling jerk or bilateral jerk nystagmus is attributable to the slow-fast form of the associated error time series $\varepsilon_S(t)$. This slow-fast form is inherited by $g_S(t)$ as a consequence of the properties of the filter relating the error and gaze time series of periodic solutions (cf. section 5.8.3). The slow fast-form of $\varepsilon_S(t)$ itself results from the orientation of the slow manifold S_M in the $(r-l, \varepsilon)$ plane, as discussed in more detail in section 4.6.1. The implication is that in the case of jerk and bilateral jerk nystagmus, the fast phase of the nystagmus may not be a corrective motion, but simply a consequence of the underlying geometry of the dynamics.

6.4.7 The modelled nystagmuses are periodic, with the beat direction of jerk nystagmus dependent on the saccade direction

As stated in section 1.1.3, congenital nystagmus waveforms are nonperiodic, although they do have a strong periodic component. By contrast, all oscillatory behaviour predicted by the model is asymptotically periodic, due to the equations having only fixed points and limit cycles as attractors. The inability of the model to generate nonperiodic behaviour is one area that requires investigation, and is elaborated on further in chapter 7.

Another implication of the model is that in jerk nystagmus, the direction of the beat following a saccade is dependent on the saccade direction (cf. section 6.2.2). This conflicts with experimental evidence showing that jerk nystagmus tends to have a preferred beat direction, which is unaffected by a saccadic movement [22]. The predicted correlation of beat and saccade direction is a consequence of the fact that the saccadic equations are symmetric. Consequently, breaking the symmetry of the system may dissociate the beat and saccade directions. Other possible consequences of breaking the symmetry are discussed in chapter 7.

Chapter 7

Conclusions and further work

7.1 Summary of the model analysis

The primary aim of this study was to obtain a classification of the gaze time series associated with saccade-modelling solutions of the bilateral saccadic model, for choices of $\boldsymbol{\alpha}$ in the physiological range Π_P that produce biologically realistic simulations of eye movements. This classification was to be used to provide insight into the mechanisms underlying the abnormal oculomotor behaviour simulated by the model, such as dynamic overshoot and congenital nystagmus.

The first phase of the study was an analysis of the burster equations $\dot{\mathbf{y}} = \mathbf{Y}(\mathbf{y})$. This work was presented in chapters 3 and 4. The initial stage of the analysis involved establishing that solutions exist and are unique. It was then observed that the burster system has a symmetry, and it was also remarked that the system would be assumed eventually compact. Following this, the equations were observed to be of slow-fast form for small ϵ, and restrictions were placed on the behaviour of solutions for small ϵ on the basis of their interaction with the slow manifold. The fixed points of the equations were then identified, and their stabilities determined. During this part of the analysis, approximations to the error time series $\varepsilon(t)$ of solutions that converge to fixed points of $\dot{\mathbf{y}} = \mathbf{Y}(\mathbf{y})$ were obtained for large t. This was done by using the linearised dynamics of the burster equations about a given fixed point to approximate the nonlinear dynamics in the neighbourhood of the fixed point.

Next, a local analysis of the equations about each of the fixed points was carried out.

It was discovered that for a fixed ϵ, the bifurcations in the (β, α) plane are organised by a pair of codimension two points. The first point (β_2, α_2) was demonstrated to be a Takens-Bogdanov point, at which curves of saddlenode, homoclinic and supercritical Hopf bifurcations intersect. The second point $\left(2\beta', 2\alpha'\right)$ was found to correspond to a nonsmooth pitchfork bifurcation changing from supercritical to subcritical. This bifurcation was observed to result from a transcritical bifurcation in the related smooth system $\dot{\mathbf{y}} = \mathbf{Y}_+(\mathbf{y})$. Additionally, evidence was found for the existence of a curve of Hopf-initiated canards in the (β, α) plane for β greater than a cut-off value β_C, when ϵ is small. It was suggested on the basis of numerical evidence that this curve also intersects the Takens-Bogdanov point. The results of the local analysis, together with the restrictions on solutions imposed by the existence of the slow manifold for small ϵ, were combined to propose a full description of the attractors of the equations in this range. It was concluded that for small ϵ, the attractors are stable fixed points or stable limit cycles. Moreover, limit cycles in $\beta > \beta_2$ and post-canard limit cycles in $\beta < \beta_2$ both have the form of large-amplitude relaxation oscillations, owing to the interaction of the cycles with the slow manifold.

The next stage in the analysis of the burster equations involved examining the qualitative changes in the dynamics caused by increasing ϵ from 0 to 0.05 in the reduced β range $\beta_C < \beta < 2\beta'$. Increasing ϵ meant that solutions were no longer constrained by the slow manifold, which introduced the possibility of bifurcations and attractors other than those observed for small ϵ. It was in fact discovered that in the (α, ϵ) range $\{0 < \alpha < 2.5\alpha', 0 < \epsilon < 0.05\}$, there are two global bifurcations, in addition to the bifurcations associated with the codimension two points and the canard. The first of these bifurcations was characterised as a nonsmooth gluing bifurcation, in which a pair of symmetry-related limit cycles become simultaneously homoclinic at the origin, forming a symmetric limit cycle. The bifurcation was observed to be qualitatively equivalent to a smooth gluing bifurcation of the saddle type, with saddle index greater than 1.

The second global bifurcation that was found also involves the creation of a symmetric limit cycle. This bifurcation, termed the H-bifurcation, occurs in one of two ways; in the type I bifurcation, the creation of the cycle does not appear to involve any other trajectories, while in the type II bifurcation, the creation of the cycle coincides with the catastrophic destruction of a pair of symmetry-related cycles. The type I bifurcation was found to occur for all $\beta_C < \beta < 2\beta'$. The type II bifurcation was observed to occur for $\hat{\beta}_C < \beta < 2\beta'$, where $\hat{\beta}_C > \beta_C$ is a value of β at which the curve of canards begins to intersect the curve of gluing bifurcations in the (α, ϵ) plane. No obvious explanation for the occurrence of the H-bifurcation could be found. The mechanism underlying the H-bifurcation could provide an interesting area for further investigation.

Following the discussion of the H- and gluing bifurcations, the morphology of the error time series associated with limit cycles in the range $\left\{\bar{\beta}_C < \beta < 2\beta', \hat{\alpha}_C(\beta) < \alpha < 2.5\alpha', 0 < \epsilon < 0.05\right\}$ was examined. Here, for each $\hat{\beta}_C < \beta < 2\beta'$, $\hat{\alpha}_C(\beta)$ is the α value corresponding to the intersection of the curve of canards with the curve of gluing bifurcations in the (α, ϵ) plane. Also, $\bar{\beta}_C > \hat{\beta}_C$ represents a value of β such that for all $\bar{\beta}_C < \beta < 2\beta'$, the only bifurcation in the (α, ϵ) plane for $\alpha > \hat{\alpha}_C(\beta)$ is the gluing bifurcation. It was discovered that for ϵ less than $\epsilon_G(\alpha, \beta)$ in $\left\{\bar{\beta}_C < \beta < 2\beta', \hat{\alpha}_C(\beta) < \alpha < 2.5\alpha', 0 < \epsilon < 0.05\right\}$, the error time series associated with the pair of pre-gluing symmetry-related limit cycle attractors have a slow-fast form. This form causes the error time series to resemble jerk nystagmus waveforms, and was attributed to the asymmetric double-loop form of the slow manifold in the $(r - l, \varepsilon)$ plane. As ϵ is increased towards $\epsilon_G(\alpha, \beta)$ and the limit cycles approach homoclinicity, the corresponding error time series take on the form of a jerk nystagmus with an extended foveation period. For ϵ greater than $\epsilon_G(\alpha, \beta)$ with $|\epsilon - \epsilon_G(\alpha, \beta)|$ not too large, the error time series associated with the post-gluing symmetric limit cycle were also observed to have a slow-fast form. The slow-fast form causes the time series to resemble bilateral jerk nystagmus waveforms, and was again attributed to the asymmetric double-loop form of S_M in the $(r - l, \varepsilon)$ plane. As ϵ is decreased towards $\epsilon_G(\alpha, \beta)$ and the limit cycle nears homoclinicity, the error time series take on the form of a bilateral jerk nystagmus with an extended foveation period. Increasing ϵ from $\epsilon_G(\alpha, \beta)$ to 0.05 was seen to result in the symmetric limit cycle becoming progressively less confined to S_M, causing the corresponding error time series to lose the slow-fast form. For sufficiently large $\epsilon < 0.05$, the error time series appear sinusoidal and resemble pendular nystagmus waveforms.

The analysis outlined above was used to obtain a proposed classification of the bifurcations and attractors of the burster equations in the parameter range

$$\hat{\Pi}_P = \left\{\bar{\beta}_C < \beta < 2\beta', 0 < \alpha < 2.5\alpha', 0 < \epsilon < 0.05\right\}$$

containing Π_P. Similarly to the small ϵ case, all attractors in this range were observed to be stable fixed points or stable limit cycles. On the basis of the classification, $\hat{\Pi}_P$ was divided into regions labelled A to J. This classification concluded the investigation of the burster equations.

The second phase of the study was an analysis of the saccadic equations $\dot{\mathbf{z}} = \mathbf{Z}(\mathbf{z})$, modelled on the preceding analysis of the burster equations $\dot{\mathbf{y}} = \mathbf{Y}(\mathbf{y})$. This work was presented in chapter 5. The initial stage of the analysis involved showing that solutions exist and are unique. Next, it was established that the saccadic system has a symmetry and is eventually compact. Following this, the skew-product form of the saccadic equations was used to demonstrate that the projection map π provides a bijection from the set of ω-limit sets of the saccadic equations to the set of ω-limit sets of the burster equations. Moreover, if $\mathcal{A}$ is an attractor of $\dot{\mathbf{z}} = \mathbf{Z}(\mathbf{z})$, then $\pi\mathcal{A}$ is an attractor of $\dot{\mathbf{y}} = \mathbf{Y}(\mathbf{y})$. It was then established that there is a one-to-one relationship between the fixed points of the burster and saccadic equations, and that the stability of a given fixed point of $\dot{\mathbf{z}} = \mathbf{Z}(\mathbf{z})$ is determined by the stability of the corresponding fixed point of $\dot{\mathbf{y}} = \mathbf{Y}(\mathbf{y})$.

The next stage in the investigation involved using Fourier analysis and linear systems theory, to prove that a stable limit cycle $\mathcal{C}$ of $\dot{\mathbf{y}} = \mathbf{Y}(\mathbf{y})$ corresponds to a stable limit cycle $\mathcal{C}$ of $\dot{\mathbf{z}} = \mathbf{Z}(\mathbf{z})$. It was concluded from this that the projection map π provides a bijection from the set of attractors of the saccadic equations to the set of attractors of the burster equations, when the attractors of the burster equations are fixed points or limit cycles. This was noted to be the case for choices of $\boldsymbol{\alpha}$ in $\hat{\Pi}_P$, meaning that the attractors of $\dot{\mathbf{z}} = \mathbf{Z}(\mathbf{z})$ could be inferred from those of $\dot{\mathbf{y}} = \mathbf{Y}(\mathbf{y})$ in this range. By utilising the one-to-one correspondence between stable limit cycles of $\dot{\mathbf{y}} = \mathbf{Y}(\mathbf{y})$ and $\dot{\mathbf{z}} = \mathbf{Z}(\mathbf{z})$, it was then argued that the nonsmooth gluing bifurcation that occurs at the origin $\mathbf{0}$ in $\dot{\mathbf{y}} = \mathbf{Y}(\mathbf{y})$ induces a nonsmooth gluing bifurcation at the origin $(\mathbf{0}, \mathbf{0})^T$ in $\dot{\mathbf{z}} = \mathbf{Z}(\mathbf{z})$. This bifurcation was observed to be qualitatively equivalent to a smooth gluing bifurcation of the saddle type with saddle index greater than 1.

Following the discussion of the gluing bifurcation, the previous Fourier analysis was used to demonstrate that the gaze time series $g_S(t)$ associated with a given limit cycle $\hat{\mathcal{C}}$ of $\dot{\mathbf{z}} = \mathbf{Z}(\mathbf{z})$ is related to the corresponding error time series $\varepsilon_S(t)$ by a linear filter. Investigation of the properties of this filter led to the approximation $g_S(t) \approx -\varepsilon_S(t - t_g) + \langle \varepsilon_S(t) \rangle$, where $t_g > 0$ is a delay, and $\langle \varepsilon_S(t) \rangle$ represents the mean value of $\varepsilon_S(t)$. It was observed that this approximation resulted in $g_S(t)$ inheriting the morphology of $\varepsilon_S(t)$ for limit cycle attractors in the parameter range $\hat{\Pi}_P$. In particular, for limit cycles where $\varepsilon_S(t)$ models a congenital nystagmus waveform, $g_S(t)$ was seen to model the same waveform.

The investigation of the saccadic equations concluded with a proposed classification of the attractors for $\boldsymbol{\alpha} \in \hat{\Pi}_P$, based on the one-to-one correspondence between the attractors of $\dot{\mathbf{y}} = \mathbf{Y}(\mathbf{y})$ and $\dot{\mathbf{z}} = \mathbf{Z}(\mathbf{z})$.

The final phase of the study involved examining the form of the gaze time series $g_{\pm}(t)$ associated with saccade-modelling solutions of $\dot{\mathbf{z}} = \mathbf{Z}(\mathbf{z})$, for $\boldsymbol{\alpha}$ in the intersection of Π_P with the union of regions A to F of $\hat{\Pi}_P$. Here, for a given $\Delta g > 0$, $g_+(t)$ simulates a saccade of Δg degrees from an initial gaze angle of 0, while $g_-(t)$ simulates a saccade of $-(\Delta g)$ degrees from 0. This work was presented in chapter 6.

The examination of the gaze time series was performed in two stages. During the first stage, the form of $g_{\pm}(t)$ was investigated for $\boldsymbol{\alpha}$ lying in regions A and B, in which the attractors are fixed points. As a consequence of the symmetry of the saccadic equations, $g_-(t) = -g_+(t)$. Hence, in order to determine the forms of both $g_+(t)$ and $g_-(t)$ for a given $\boldsymbol{\alpha}$ in A or B, it was necessary to only determine the form of $g_+(t)$. This was achieved by first using Laplace transforms to get an expression for $g_+(t)$ in terms of the corresponding error time series $\varepsilon_+(t)$. Next, a piecewise approximation $\hat{\varepsilon}_+(t)$ to $\varepsilon_+(t)$ was obtained. $\hat{\varepsilon}_+(t)$ was constructed by combining the observation that $\varepsilon_+(t)$ is approximately linear for small t, with an approximation to $\varepsilon_+(t)$ for large t that had been established previously by considering the linearised dynamics of $\dot{\mathbf{y}} = \mathbf{Y}(\mathbf{y})$ about its fixed points. Setting $\hat{\varepsilon}_+(t)$ into the expression for $g_+(t)$ yielded a piecewise approximation $\hat{g}_+(t)$ to $g_+(t)$. Assuming that $\hat{g}_+(t)$ is a good approximation to $g_+(t)$ for $t \geq 0$, the morphology of $g_+(t)$ could then be inferred.

In region A, the attractor of $\dot{\mathbf{z}} = \mathbf{Z}(\mathbf{z})$ is the origin $(\mathbf{0}, \mathbf{0})^T$. The analysis of the burster equations had shown that the origin $\mathbf{0}$ is a stable node of $\dot{\mathbf{y}} = \mathbf{Y}(\mathbf{y})$ for $\epsilon < \epsilon_F^0(\alpha, \beta)$, while for $\epsilon > \epsilon_F^0(\alpha, \beta)$, $\mathbf{0}$ is a stable fixed point such that trajectories spiral around the stable manifold L_0 as they contract to $\mathbf{0}$. By examining the form of $\hat{g}_+(t)$ in both these ranges, it was shown that $g_{\pm}(t)$ models a normometric saccade for small $\epsilon < \epsilon_F^0(\alpha, \beta)$, and a dynamic overshoot for $\epsilon > \epsilon_F^0(\alpha, \beta)$. Moreover, it was observed that the evolution from normometric saccades to dynamic overshoots which occurs as ϵ is increased through $\epsilon_F^0(\alpha, \beta)$ could be viewed as a consequence of the corresponding burster system trajectories following the slow manifold less closely as they converge to $\mathbf{0}$. In region B, the attractors of $\dot{\mathbf{z}} = \mathbf{Z}(\mathbf{z})$ are the symmetry-related pair of fixed points $\left(\mathbf{0}, \mathbf{y_1^{\pm}}\right)^T$, where $\mathbf{y_1^{\pm}} = (x_1, x_1, \pm\varepsilon_1)^T$. The burster system analysis had shown that $\mathbf{y_1^{\pm}}$ is a stable node of $\dot{\mathbf{y}} = \mathbf{Y}(\mathbf{y})$ for small ϵ. By examining the form of $\hat{g}_+(t)$ for small ϵ, it was demonstrated that $g_{\pm}(t)$ models a normometric saccade if Δg is large compared to ε_1, and a hypometric saccade if Δg is of the same order as ε_1.

The second stage in the gaze time series analysis involved determining the form of $g_{\pm}(t)$ for $\boldsymbol{\alpha}$ lying in regions C-F, where the attractors of $\dot{\mathbf{z}} = \mathbf{Z}(\mathbf{z})$ are limit cycles, with corresponding gaze time series that simulate congenital nystagmus waveforms. In each of these parameter ranges, $g_{\pm}(t)$ was seen to have the form of a saccade towards the required gaze angle $\pm(\Delta g)$, followed by a slow convergence to a periodic time series $g_S^{\pm}(t)$ associated with the corresponding limit cycle. For $\boldsymbol{\alpha}$ in C, $g_{\pm}(t)$ was observed to have the form of a normometric saccade with a post-saccadic small-amplitude nystagmus. In the range D, $g_{\pm}(t)$ was seen to model a normometric saccade with a post-saccadic jerk nystagmus that develops an extended foveation period as $\epsilon \to \epsilon_G(\alpha, \beta)$. It was shown that the relation $g_S^-(t) = -g_S^+(t)$, derived from the symmetry of $\dot{\mathbf{z}} = \mathbf{Z}(\mathbf{z})$, means that the direction of the beat of the simulated nystagmus is coupled to that of the saccade. For $\boldsymbol{\alpha}$ in E, $g_{\pm}(t)$ was observed to simulate a normometric saccade, followed by a post-saccadic bilateral jerk nystagmus that develops an extended foveation period as $\epsilon \to \epsilon_G(\alpha, \beta)$. Finally for $\boldsymbol{\alpha}$ in F, $g_{\pm}(t)$ was seen to have the form of a hypermetric saccade with a post-saccadic pendular nystagmus.

On the basis of the classification obtained in the manner described above, several biological implications of the model were then discussed. One important implication was the proposed characterisation of congenital nystagmus as a dynamical disease. This opposes the prevalent control model explanation of CN in terms of structural abnormalities proposed by Optican et al. The bilateral saccadic model was also observed to suggest the possibility of moving between different types of oculomotor behaviour, by varying the parameters α, β and ϵ. It was noted that this is consistent with experimental observations, which show that the type of saccadic or oscillatory behaviour exhibited by a given subject is dependent on environmental conditions. Furthermore, under the assumption that α and β are fixed while ϵ is variable, the model suggests that inducing an increase in ϵ could cause normometric saccades to develop into dynamic overshoots. In addition, the model predicts that increasing ϵ could cause jerk nystagmus to develop into both bilateral jerk and pendular nystagmus. Under the assumption that the ϵ parameter can be equated with attention, a number of experiments to systematically investigate these claims were then suggested.

The model also proposes that both hypometria in small-amplitude saccades and nystagmus are caused by an inappropriately large off response, or, equivalently, by an inappropriately strong braking saccade. Hypometric saccades were attributed to an over-powerful breaking saccade bringing the eye to a premature halt, while nystagmus was viewed as resulting from a stronger braking saccade causing a reverse in the direction of the eye, leading to oscillations. It was also noted that the existence of canards in the saccadic equations implied that the type of oscillation most likely to be observed for small ϵ is jerk nystagmus. Consequently, assuming that ϵ corresponds to attention, this suggests that nystagmats are most likely to exhibit jerk oscillations in high attention conditions. Furthermore, the canard structure implies that jerk is most likely to develop into bilateral jerk and pendular nystagmus with increasing ϵ.

Another important implication of the model concerns the nature of the fast phase in congenital nystagmus. The analysis of the saccadic equations demonstrated that the fast phases of the simulated jerk and bilateral jerk waveforms are a consequence of the form of the slow manifold in the $(r - l, \varepsilon)$ plane. This suggests that the fast phases of jerk and bilateral jerk are not corrective movements, as postulated by Optican et al, but may in fact be a consequence of an underlying slow-fast system.

Finally, two biologically unrealistic implications of the model were noted. These were the asymptotic periodicity of all simulated oscillations, and the coupling of beat direction to saccade direction in jerk nystagmus.

7.2 Suggestions for further development of the model

As was mentioned in section 6.4.7, one important limitation of the model in its current form is that the CN oscillations it simulates are periodic, while actual CN oscillations are nonperiodic. There are a number of approaches to modifying the model on the grounds of biological realism that may result in nonperiodic or even chaotic behaviour. Three such approaches are outlined here. Each of these is based on modification of the burster equations.

7.2.1 Incorporation of signal-dependent noise

The first approach involves incorporating the variable responses of burst neurons observed experimentally. Recall from section 2.3 that the burster function $F(\varepsilon)$ is based on a response curve that was obtained by Van Gisbergen et al by averaging over all the individual burst neuron responses they recorded. This suggests replacing the terms $F(\varepsilon(t))$ and $F(-\varepsilon(t))$ with random variables $F_R(t)$ and $F_L(t)$ respectively, where for all $t \geq 0$, $F_R(t)$ has mean $F(\varepsilon(t))$ and $F_L(t)$ has mean $F(-\varepsilon(t))$. Making these changes yields the system of stochastic differential equations (SDEs) below:

$$\dot{r} = \frac{1}{\epsilon}\left(-r - \gamma r l^2 + F_R(t)\right) \tag{7.1}$$

$$\dot{l} = \frac{1}{\epsilon}\left(-l - \gamma l r^2 + F_L(t)\right) \tag{7.2}$$

$$\dot{\varepsilon} = -(r - l) \tag{7.3}$$

The modified full saccadic equations comprising the plant equations together with (7.1)-(7.3) will also be a system of SDEs. The particular form of the solutions of this modified system will of course depend on the distributions of $F_R(t)$ and $F_L(t)$. Recent work on the role of signal-dependent noise in neural control systems may provide some insight into the most appropriate distributions to choose. In a study investigating the effect of noise on the saccadic control signal, Harris et al found evidence supporting empirical observations that the variance of burst neuron firing increases with the mean level of firing [42]. Assuming a well known control model of the saccadic system based on the position feedback model, Harris et al modelled the pulse $b(t)$ as a deterministic signal augmented with noise, whose variance increases with the mean value of the signal. Explicitly, $b(t)$ was assumed to have the form $b(t) = u(t) + w(t)$, where $u(t)$ is a deterministic signal and $w(t)$ is a zero-mean white noise process with variance proportional to $|u(t)|^2$. Using optimal control techniques, Harris et al discovered that the choices of $u(t)$ which minimised post-movement positional variance produced saccades that had position and velocity profiles very similar to those observed experimentally [42].

Other evidence for the existence of signal-dependent noise in the saccadic system is provided by some recent work on the analysis of congenital nystagmus time series data using nonlinear dynamics techniques [43]. Part of this work involved estimating the local dimension of delay-embedded CN time series at points corresponding to different phases of the CN cycle. For the traces analysed, the local dimension was observed to increase during the slow phase, before peaking at the beginning of the fast phase, and decreasing again as the eye returns to the foveation position. On the basis that motor error increases with the distance from the foveation position, these observations were proposed to be consistent with the hypothesis that the variance of burster firing increases with the mean firing level [43].

The discussion above suggests that, in the first instance, it may be constructive to model $F_R(t)$ and $F_L(t)$ as Poisson random variables. A Poisson random variable X with parameter λ is defined by the probability mass function:

$$P(X = x) = e^{-\lambda}\frac{\lambda^x}{x!}$$

The mean and variance of X are both equal to λ [44]. Modelling $F_R(t)$ and $F_L(t)$ as Poisson random variables, with parameters $F(\varepsilon(t))$ and $F(-\varepsilon(t))$ respectively, would therefore be a simple way of incorporating the signal-dependent noise hypothesis.

It seems reasonable to assume that modifying the bilateral saccadic model through the inclusion of stochastic terms in the manner described here could produce nonperiodic solutions resembling CN waveforms. However, determining whether any observed nonperiodicity is biologically meaningful would require further investigation. In order to confidently assert that any simulated nonperiodicity was biologically realistic, it would need to be demonstrated that the modelled variability was not simply a predictable consequence of adding noise to a periodic system, but was qualitatively similar to the variability observed in real CN waveforms. Simulated nonperiodic waveforms in which the amplitude of oscillations or the interval between slow and fast phases were confined to a narrow range would not, for example, be considered biologically realistic, since actual CN waveforms show an appreciable variation in these quantities [21].

One approach to deciding whether the stochastic model was capable of producing biologically viable nonperiodicity would be to compare the Fourier spectra of modelled and experimentally recorded CN waveforms. Another would be to delay-embed simulated waveforms, and examine whether the changes in local dimension observed in actual CN waveforms was reproduced. If it was found that the stochastic equations are unable to generate biologically realistic nonperiodicity, this could be taken to suggest that either signal-dependent noise is not a significant factor in the observed variability of CN waveforms, or that the noise needs to be incorporated into the model in a different way (e.g. by assuming different distributions for $F_R(t)$ and $F_L(t)$).

7.2.2 Splitting the symmetry of the equations

Another possible modification to the burster equations on the basis of biological realism would be to break the symmetry of the burster equations. This can be done in a number of different ways. One method would be to drop the unrealistic assumption that the equations for the left and right bursters are the same, up to the change of variables $(r, l, \varepsilon)^T \longmapsto (l, r, -\varepsilon)^T$. Instead of using the single function $F(\varepsilon)$ to represent the mean responses of both classes of bursters, separate functions $F_L(\varepsilon)$ and $F_R(\varepsilon)$ could be used to model the left and right responses respectively. If the basic properties of $F(\varepsilon)$ were preserved, the mean left response function $F_L(\varepsilon)$ would have the form

$$F_L(\varepsilon) = \begin{cases} \alpha'_L \left(1 - e^{-\varepsilon/\beta'_L}\right) & \text{if} \quad \varepsilon \geq 0 \\ -\frac{\alpha_L}{\beta_L}\varepsilon e^{\varepsilon/\beta_L} & \text{if} \quad \varepsilon < 0 \end{cases}$$

where $\alpha'_L, \beta'_L, \alpha_L$ and β_L are positive parameters. Here α'_L and β'_L determine the properties of the left on response, while α_L and β_L determine those of the left off response. The form of the right response function $F_R(\varepsilon)$ would be similar with parameters $\alpha'_R, \beta'_R, \alpha_R$ and β_R. In addition to invoking separate burster response functions, two separate parameters γ_L and γ_R could be used in place of the single parameter γ to represent the strength of the mutual inhibition. The quantity γ_L would determine the strength of the inhibition of the left bursters by the right bursters. Conversely, γ_R would determine the strength of the inhibition of the right bursters by the left bursters. Also, the parameter ϵ which measures the speed with which bursters react to the motor error signal could be replaced with separate parameters ϵ_L and ϵ_R, representing the reaction speeds of left and right bursters respectively. The most general equations for r and l that incorporate each of these suggested changes are:

$$\dot{r} = \frac{1}{\epsilon_R}\left(-r - \gamma_R r l^2 + F_R(\varepsilon)\right) \tag{7.4}$$

$$\dot{l} = \frac{1}{\epsilon_L}\left(-l - \gamma_L l r^2 + F_L(-\varepsilon)\right) \tag{7.5}$$

(cf. equations (2.7)-(2.8)). Another modification to the burster equations that would break their symmetry would be to model the resettable integrator as a 'leaky' integrator. Writing T_R for the time constant of the leaky RI would give the following equation for the eye displacement s:

$$\dot{s} = -\frac{1}{T_R}s + b$$

Setting $b = r - l$ and $\varepsilon = \Delta g - s$ in the above and rearranging yields:

$$\dot{\varepsilon} = -\frac{1}{T_R}\varepsilon - (r - l) + \frac{\Delta g}{T_R} \quad (7.6)$$

(cf. equation (2.9)). The original burster equations can be recovered from the asymmetric equations (7.4)-(7.6) by setting $F_R(\varepsilon) = F_L(\varepsilon) = F(\varepsilon)$, $\epsilon_R = \epsilon_L = \epsilon$, $\gamma_R = \gamma_L = \gamma$ and $T_R = \infty$.

The basis for supposing that the symmetry-breaking modifications discussed above could lead to greater variability in the simulated waveforms, is the nonsmooth gluing bifurcation of the saccadic equations. Recall that as ϵ increases through $\epsilon_G(\alpha, \beta)$ in region D of Π_P, the asymmetric limit cycles $\hat{\mathcal{C}}_+$ and $\hat{\mathcal{C}}_-$ merge at the origin to form the symmetric limit cycle $\hat{\mathcal{C}}$ in a nonsmooth gluing bifurcation. Moreover, this bifurcation appears to be qualitatively equivalent to a smooth gluing bifurcation of the saddle type with saddle index $\delta > 1$. Breaking the symmetry of a smooth gluing bifurcation results in dynamics involving stable limit cycles with more complicated structures than those observed in the symmetric case [33], [34], [35]. This suggests that breaking the symmetry of the saccadic equations by breaking the symmetry of the burster equations may lead to simulated CN waveforms with a more complex morphology.

In the absence of symmetry, smooth gluing bifurcations have a codimension of 2, since one parameter is needed to control the homoclinic connection of each limit cycle [33], [34], [35]. A bifurcation diagram for the imperfect gluing bifurcation of the saddle type with $\delta > 1$ is shown in figure (7-1). It comprises a 2-dimensional parameter plot in which it is assumed that the parameters controlling the homoclinic connections are μ_1 and μ_2. At the point $\mu_1 = \mu_2 = 0$, there are a pair of symmetry-related homoclinic orbits. Writing these orbits as Γ_0 and Γ_1, a given limit cycle attractor of the system can be represented by a binary 'code' describing the order in time in which the cycle passes through neighbourhoods of these orbits. The code 011, for example, would correspond to a cycle that winds around Γ_0 once before winding around Γ_1 twice. Increasing μ_1 through 0 along the line $\mu_1 = \mu_2$ corresponds to the symmetric gluing bifurcation: a pair of asymmetric cycles 0 and 1 combine to form the symmetric cycle 01. If an asymmetric path which crosses the shaded

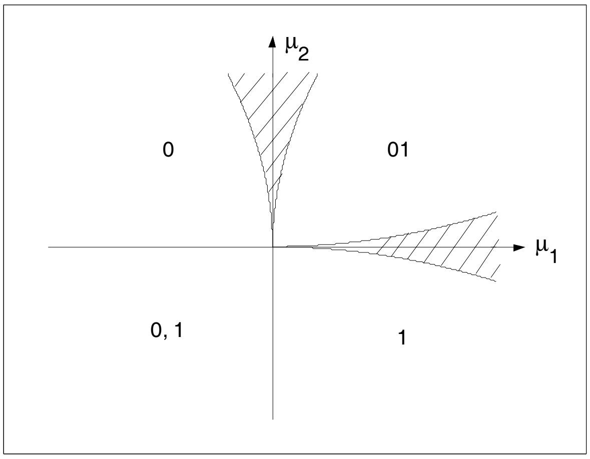

Figure 7-1: Bifurcation set for the imperfect gluing bifurcation of the saddle type with $\delta > 1$.

region is followed, a more complex sequence of bifurcations occurs. Within the shaded region there exists intricate curves of homoclinic bifurcations which create and destroy cycles with complicated codes [33], [34], [35]. The exact nature of the bifurcations depends on both the configuration (figure-of-eight or butterfly) and orientability of the homoclinic orbits Γ_0, Γ_1. It can, however, be shown that for a given choice of (μ_1, μ_2) in the shaded region, there are at most two stable cycles. Moreover, these cycles have what are called rotation-compatible codes. These are codes of the form

$$xy^{k_1}xy^{k_2}xy^{k_3}\dots$$

where $x, y \in \{0, 1\}$, and for all j, $k_j \in \{n, n+1\}$ for some $n > 0$. Examples of such codes are 0111011 and 100101010. Each cycle with a rotation-compatible code has a corresponding rotation number. This is defined as the number of 1s in the code divided by the total length of the code. The two examples given above have rotation numbers $\frac{5}{7}$ and $\frac{4}{9}$ respectively. For the butterfly configuration with orientable orbits, there is at most one cycle for each (μ_1, μ_2) in the shaded region. Moreover, the rotation number varies continuously along a typical parameter path crossing the shaded region, implying the existence of nonperiodic attractors [33], [34], [35].

For the nonsmooth gluing bifurcation of interest, the cycles with codes 0 and 1 can be identified with $\hat{\mathcal{C}}_+$ and $\hat{\mathcal{C}}_-$ respectively, while the cycle 01 can be identified with $\hat{\mathcal{C}}$. If the unfolding of the nonsmooth gluing bifurcation is similar to that of the smooth bifurcation, the discussion above suggests that splitting the symmetry of the model could result in limit cycle attractors, or even nonperiodic attractors, with rotation-compatible codes. Such cycles would have gaze time series with a more complicated beat cycle than in the symmetric case. Since $\hat{\mathcal{C}}_+$ corresponds to a right-beating nystagmus and $\hat{\mathcal{C}}_-$ to a left-beating nystagmus, a cycle with code 011, for example, would correspond to an oscillation that beats once to the right before beating twice in succession to the left. A cycle with an irrational rotation number would correspond to an oscillation with a seemingly random pattern of beats. Although such oscillations would have greater morphological complexity than those produced by the symmetric oscillations, it would need to be investigated whether this complexity was biologically meaningful or not (cf. the discussion of the stochastic saccadic equations above). If no cycles with rotation compatible codes were observed upon splitting the symmetry, this could be taken to imply that either the rotation-compatible codes exist in parameter regions of very small measure, or that the unfolding of the nonsmooth gluing bifurcation is unrelated to that of the smooth bifurcation.

Finally, it may also be instructive to investigate whether splitting the symmetry causes beat and saccade direction to be dissociated in simulated jerk waveforms.

7.2.3 Incorporation of the omnipause neurons

The final approach to modifying the burster equations to generate more biologically realistic behaviour involves incorporating the omnipause neurons. As was stated in section 1.1.2, omnipause neurons discharge continuously in their normal state, inhibiting the burst neurons. Immediately prior to and during a saccade, the omnipause neurons are themselves inhibited causing them to release their inhibition of the bursters, which then generate the saccadic velocity command. The bilateral saccadic model in its current form does not include the time-dependent dynamics of the omnipause neurons; it implicitly assumes that they *instantaneously* release their inhibition of the burst neurons just before the onset of a saccade. It may be that including this time-dependence could lead to nonperiodic or chaotic dynamics. However, constructing a biologically viable model of omnipause neuron dynamics may be problematic. This is because, in contrast to burst neurons, relatively little is currently known about their firing characteristics [2].

7.3 Concluding remarks

The work presented here provides a comprehensive classification of the normal and abnormal eye movements simulated by a novel nonlinear dynamics model of the saccadic system. This classification was based on relating the morphology of the simulated movements to the underlying bifurcations and attractors of the model equations. Many of the implications of the model analysis are in agreement with experimental evidence, while others challenge existing ideas relating to the aetiology of both congenital nystagmus and saccadic dysmetria. Additionally, the analysis suggests a number of simple experiments to determine the viability of the model as a predictor of oculomotor behaviour. Finally, the work provides the framework for the development of more complex models incorporating physiological properties of the saccadic system that are not represented in the basic model. It is hoped that these modified models will be able to simulate a wider range of eye movements that more accurately reflect those found experimentally.

Appendix A

Appendices to the chapters

A.1 Appendix to Chapter 3

A.1.1 Proof that X is locally Lipschitz on $\mathbb{R}^3$

It is first shown that F is Lipschitz on $\mathbb{R}$. It then follows easily that $\mathbf{X}$ is locally Lipschitz on $\mathbb{R}^3$.

Lemma 1 *F is Lipschitz on $\mathbb{R}$ with Lipschitz constant Λ, where $\Lambda = \max\{\Lambda_+, -\Lambda_-\}$. i.e. $|F(\varepsilon_1) - F(\varepsilon_2)| \leq \Lambda |\varepsilon_1 - \varepsilon_2|$ $\forall \varepsilon_1, \varepsilon_2 \in \mathbb{R}$.*

Proof. To prove the Lemma it is sufficient to show that $|F(\varepsilon_1) - F(\varepsilon_2)| \leq \Lambda |\varepsilon_1 - \varepsilon_2|$ $\forall \varepsilon_1, \varepsilon_2 \in \mathbb{R}$ with $\varepsilon_1 < \varepsilon_2$. The proof uses the fact that $|Df(\varepsilon)| \leq \Lambda$ $\forall \varepsilon \geq 0$ and $|Dh(\varepsilon)| \leq \Lambda$ $\forall \varepsilon \leq 0$. So let $\varepsilon_1 < \varepsilon_2$ be given. There are 3 cases to consider: $\varepsilon_2 < 0$, $\varepsilon_1 > 0$ and $\varepsilon_1 < 0 < \varepsilon_2$.

1. $\varepsilon_2 < 0$. By definition, $F|_{(-\infty,0]} = h|_{(-\infty,0]}$. Thus:

$$F(\varepsilon_1) - F(\varepsilon_2) = h(\varepsilon_1) - h(\varepsilon_2) \tag{A.1}$$

h is differentiable on $[\varepsilon_1, \varepsilon_2]$ so by the Mean Value Theorem (MVT) $\exists \xi \in (\varepsilon_1, \varepsilon_2)$ such that:

$$Dh(\xi) = \frac{h(\varepsilon_2) - h(\varepsilon_1)}{\varepsilon_2 - \varepsilon_1} \tag{A.2}$$

Substituting (A.2) into (A.1) and taking the modulus of both sides leads to:

$$|F(\varepsilon_1) - F(\varepsilon_2)| \leq |Dh(\xi)|\,|\varepsilon_1 - \varepsilon_2| \tag{A.3}$$

Since $\xi < 0$, $|Dh(\xi)| \leq \Lambda$. Substituting into (A.3) gives:

$$|F(\varepsilon_1) - F(\varepsilon_2)| \leq \Lambda\,|\varepsilon_1 - \varepsilon_2|$$

2. $\varepsilon_1 > 0$. Similar to case 1.

3. $\varepsilon_1 < 0 < \varepsilon_2$. By definition, $F|_{(-\infty,0]} = h|_{(-\infty,0]}$ and $F|_{[0,\infty)} = f_{[0,\infty)}$. Thus:

$$F(\varepsilon_1) - F(\varepsilon_2) = h(\varepsilon_1) - f(\varepsilon_2) \tag{A.4}$$

f is differentiable on $[0, \varepsilon_2]$, so by the MVT $\exists \xi_2 \in (0, \varepsilon_2)$ such that

$$\begin{aligned} Df(\xi_2) &= \frac{f(\varepsilon_2) - f(0)}{\varepsilon_2 - 0} = \frac{f(\varepsilon_2)}{\varepsilon_2} \\ &\Rightarrow f(\varepsilon_2) = Df(\xi_2)\,\varepsilon_2 \end{aligned} \tag{A.5}$$

Also, h is differentiable on $[\varepsilon_1, 0]$, so by the MVT $\exists \xi_1 \in (\varepsilon_1, 0)$ such that:

$$\begin{aligned} Dh(\xi_1) &= \frac{h(0) - h(\varepsilon_1)}{0 - \varepsilon_1} = \frac{h(\varepsilon_1)}{\varepsilon_1} \\ &\Rightarrow h(\varepsilon_1) = Dh(\xi_1)\,\varepsilon_1 \end{aligned} \tag{A.6}$$

Substituting (A.5) and (A.6) into (A.4) and taking the modulus of both sides leads to:

$$|F(\varepsilon_1) - F(\varepsilon_2)| \leq |Dh(\xi_1)\,\varepsilon_1| + |Df(\xi_2)\,\varepsilon_2| \tag{A.7}$$

Since $\xi_2 > 0$, $|Df(\xi_2)| \leq \Lambda$. Thus $-\Lambda \leq Df(\xi_2) \leq \Lambda$. Multiplying this inequality by $\varepsilon_2 > 0$ implies $|Df(\xi_2)\,\varepsilon_2| \leq \Lambda\varepsilon_2$. Also, since $\xi_1 < 0$, $|Dh(\xi_1)| \leq \Lambda$. Thus $-\Lambda \leq Dh(\xi_1) \leq \Lambda$. Multiplying by $\varepsilon_1 < 0$ gives $|Dh(\xi_1)\,\varepsilon_1| \leq -\Lambda\varepsilon_1$. Substituting into (A.7) implies:

$$|F(\varepsilon_1) - F(\varepsilon_2)| \leq \Lambda(\varepsilon_2 - \varepsilon_1) = \Lambda\,|\varepsilon_1 - \varepsilon_2|$$

It has been shown that in all three cases, $|F(\varepsilon_1) - F(\varepsilon_2)| \leq \Lambda\,|\varepsilon_1 - \varepsilon_2|$, completing the proof. ■

Proposition 2 $\mathbf{X}$ *is locally Lipschitz on* $\mathbb{R}^3$.

Proof. First note that $\mathbf{X}$ can be written as $\mathbf{X} = \mathbf{X}_1 + \mathbf{X}_2$ where the maps $\mathbf{X}_1, \mathbf{X}_2 : \mathbb{R}^3 \to \mathbb{R}^3$ are defined $\forall \mathbf{y} \in \mathbb{R}^3$ by:

$$\mathbf{X}_1(\mathbf{y}) = \begin{pmatrix} -r\left(1+\gamma l^2\right) \\ -l\left(1+\gamma r^2\right) \\ -\epsilon(r-l) \end{pmatrix}, \mathbf{X}_2(\mathbf{y}) = \begin{pmatrix} F(\varepsilon) \\ F(-\varepsilon) \\ 0 \end{pmatrix}$$

$\mathbf{X}_1$ is C^1, and therefore locally Lipschitz [23]. Hence, it will be sufficient to show that $\mathbf{X}_2$ is Lipschitz to prove the Proposition. Let $\|.\|_1$ denote the vector 1-norm. It is shown that for $\mathbf{y}, \mathbf{y}' \in \mathbb{R}^3$

$$\left\|\mathbf{X}_2(\mathbf{y}) - \mathbf{X}_2\left(\mathbf{y}'\right)\right\|_1 \leq 2\Lambda \left\|\mathbf{y} - \mathbf{y}'\right\|_1$$

where $\Lambda = \max\{\Lambda_+, -\Lambda_-\}$. So let $\mathbf{y} = (r, l, \varepsilon)^T, \mathbf{y}' = (r', l', \varepsilon')^T \in \mathbb{R}^3$ be given. Then:

$$\mathbf{X}_2(\mathbf{y}) - \mathbf{X}_2\left(\mathbf{y}'\right) = \begin{pmatrix} F(\varepsilon) - F(\varepsilon') \\ F(-\varepsilon) - F(-\varepsilon') \\ 0 \end{pmatrix}$$

$$\Rightarrow \left\|\mathbf{X}_2(\mathbf{y}) - \mathbf{X}_2\left(\mathbf{y}'\right)\right\|_1 = \left|F(\varepsilon) - F\left(\varepsilon'\right)\right| + \left|F(-\varepsilon) - F\left(-\varepsilon'\right)\right|$$

Hence by Lemma 1:

$$\left\|\mathbf{X}_2(\mathbf{y}) - \mathbf{X}_2\left(\mathbf{y}'\right)\right\|_1 \leq \Lambda\left|\varepsilon - \varepsilon'\right| + \Lambda\left|-\varepsilon + \varepsilon'\right| = 2\Lambda\left|\varepsilon - \varepsilon'\right| \leq 2\Lambda\left\|\mathbf{y} - \mathbf{y}'\right\|_1$$

■

A.1.2 Proof that solutions of $\dot{\mathbf{y}} = \mathbf{X}(\mathbf{y})$ can be extended infinitely far forward in time

It is shown in this section that given $\mathbf{y} \in \mathbb{R}^3$, the unique solution $\mathbf{y}(\tau)$ to $\dot{\mathbf{y}} = \mathbf{X}(\mathbf{y})$ with $\mathbf{y}(0) = \mathbf{y}$ exists $\forall \tau \geq 0$. In order to prove this, the following results are required.

Theorem 3 ([26]) *Let* W *be an open subset of* $\mathbb{R}^n$ *and* $\mathbf{F} : W \to \mathbb{R}^n$ *be a locally Lipschitz* *map. Then a solution to $\dot{\mathbf{x}} = \mathbf{F}(\mathbf{x})$ with initial condition in a compact subset of W can be continued forward (respectively backward) either infinitely far, or to the boundary of the compact set.*

Corollary 4 *Let $\mathbf{F} : \mathbb{R}^n \to \mathbb{R}^n$ be a locally Lipschitz map, and $\mathbf{x_0} \in \mathbb{R}^n$ with $\mathbf{x}(t)$ the unique solution to $\dot{\mathbf{x}} = \mathbf{F}(\mathbf{x})$ such that $\mathbf{x}(0) = \mathbf{x_0}$. Then the following hold:*

1. If $\exists$ some maximal $b > 0$ such that $\mathbf{x}(t)$ is defined on $[0, b)$, $\|\mathbf{x}(t)\|$ is unbounded on $[0, b)$.

2. If $\exists$ some minimal $a < 0$ such that $\mathbf{x}(t)$ is defined on $(a, 0]$, $\|\mathbf{x}(t)\|$ is unbounded on $(a, 0]$.

Proof.

1. Let $\delta > \|\mathbf{x_0}\|$ be given, and consider the compact subset S_δ of $\mathbb{R}^n$ defined by $S_\delta = \{\mathbf{x} \in \mathbb{R}^n : \|\mathbf{x}\| \leq \delta\}$. $\mathbf{x_0} \in S_\delta$ and $\mathbf{x}(t)$ cannot be continued forward infinitely far since it does not exist for $t \geq b$. Hence, by Theorem 3, $\mathbf{x}(t)$ can be continued forward to the boundary of S_δ. Thus, $\exists s \in [0, b)$ with $\|\mathbf{x}(s)\| = \delta$. Such an s can be found $\forall \delta > \|\mathbf{x_0}\|$, from which it follows that $\|\mathbf{x}(t)\|$ is unbounded on $[0, b)$.

2. Similar. ■

The main result can now be proved.

Proposition 5 *Let $\mathbf{y} \in \mathbb{R}^3$. Then the unique solution $\mathbf{y}(\tau)$ to $\dot{\mathbf{y}} = \mathbf{X}(\mathbf{y})$ with $\mathbf{y}(0) = \mathbf{y}$ exists $\forall \tau \geq 0$.*

Proof. This is by contradiction. Assume that there is some maximal $b > 0$ such that $\mathbf{y}(\tau)$ is defined on $[0, b)$. Then by Corollary 4, $\|\mathbf{y}(\tau)\|_1$ is unbounded on $[0, b)$. So write $\mathbf{y}(\tau) = (r(\tau), l(\tau), \varepsilon(\tau))^T$ for $\tau \geq 0$ and consider the r and l derivatives of the burster equations in the (r, l) plane. The equations for $\dot{r}$ and $\dot{l}$ are:

$$\begin{aligned}
\dot{r} &= -r\left(1 + \gamma l^2\right) + F(\varepsilon) \\
\dot{l} &= -l\left(1 + \gamma r^2\right) + F(-\varepsilon)
\end{aligned}$$

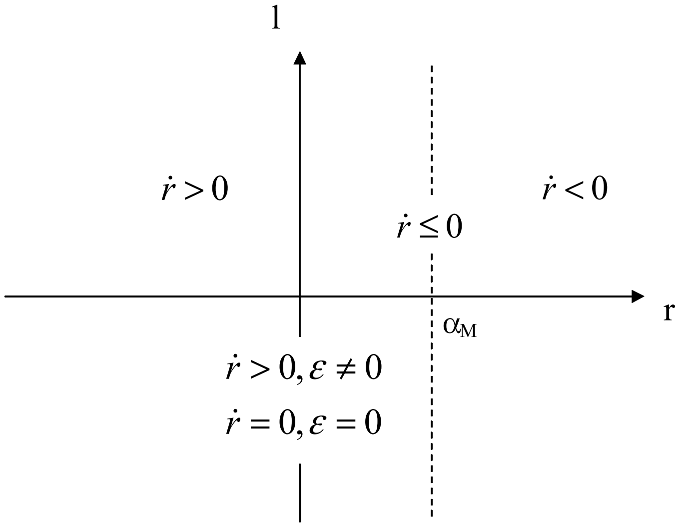

Figure A-1: The sign of $\dot{r}$ in the (r, l) plane.

(cf. (3.2)-(3.3)). Now $\forall \varepsilon \in \mathbb{R}$, $0 \leq F(\varepsilon) \leq \alpha_M$, where $\alpha_M = \max\left\{\frac{\alpha}{e}, \alpha'\right\}$. This implies that $\dot{r} < 0$ for $r > \alpha_M$ and $\dot{r} \leq 0$ for $r = \alpha_M$. Also, $\dot{r} > 0$ for $r < 0$. When $r = 0$, $\dot{r} = F(\varepsilon)$ and so $\dot{r} > 0$ unless $\varepsilon = 0$. By symmetry, it can be concluded that $\dot{l} < 0$ for $l > \alpha_M$, $\dot{l} \leq 0$ for $l = \alpha_M$, $\dot{l} > 0$ for $l < 0$, and when $l = 0$, $\dot{l} > 0$ unless $\varepsilon = 0$. The sign of $\dot{r}$ in the (r, l) plane is shown in figure (A-1). The sign of $\dot{l}$ in the (r, l) plane can be inferred from the figure using the symmetry. Set $M_2 = \max\{\alpha_M, r(0)\}$. Then $r(0) \leq M_2$ and since $M_2 \geq \alpha_M$, $\dot{r}(\tau) < 0$ whenever $r(\tau) > M_2$. This implies that $r(\tau) \leq M_2$ $\forall \tau \in [0, b)$. Now set $M_1 = \min\{0, r(0)\}$. Then $r(0) \geq M_1$ and since $M_1 \leq 0$, $\dot{r}(\tau) > 0$ whenever $r(\tau) < M_1$. This implies that $r(\tau) \geq M_1$ $\forall \tau \in [0, b)$. It follows that $|r(\tau)| \leq M_r$ $\forall \tau \in [0, b)$, where $M_r = \max\{M_1, -M_2\}$. Using a similar argument, it can be shown that $\exists M_l > 0$ with $|l(\tau)| \leq M_l$ $\forall\ \tau \in [0, b)$.

Now consider $\varepsilon(\tau)$ on $[0, b)$. Let $\tau \in [0, b)$ be given. Then $\forall s \in [0, \tau]$:

$$\dot{\varepsilon}(s) = -\epsilon\,(r(s) - l(s))$$

(cf. (3.4)). Taking moduli of the above and using $|r(s)| \leq M_r$ and $|l(s)| \leq M_l$ leads to

$$-L \leq \dot{\varepsilon}(s) \leq L$$

where $L = \epsilon\,(M_r + M_l)$. Integrating the above inequality over $[0, \tau]$ gives:

$$\begin{aligned} -L\tau \leq \varepsilon(\tau) - \varepsilon(0) \leq L\tau \\ \Rightarrow -L\tau + \varepsilon(0) \leq \varepsilon(\tau) \leq L\tau + \varepsilon(0) \\ \Rightarrow -L\tau - |\varepsilon(0)| \leq \varepsilon(\tau) \leq L\tau + |\varepsilon(0)| \\ \Rightarrow |\varepsilon(\tau)| \leq L\tau + |\varepsilon(0)| \leq Lb + |\varepsilon(0)| \end{aligned}$$

Set $M_\varepsilon = Lb + |\varepsilon(0)|$. Then from the above, $|\varepsilon(\tau)| \leq M_\varepsilon$. This holds $\forall \tau \in [0, b)$, showing that $|\varepsilon(\tau)|$ is bounded on $[0, b)$.

It has been shown that $|r(\tau)|, |l(\tau)|$ and $|\varepsilon(\tau)|$ are all bounded on $[0, b)$, implying that $\|\mathbf{y}(\tau)\|_1$ is bounded on $[0, b)$. This gives a contradiction, as required. ■

A.1.3 Result concerning the eigenvalues of linearisation of $\mathbf{y}_1^{\pm}$

Lemma 6 *Given* $\boldsymbol{\alpha}$ *with* (β, α) *lying between* $\alpha = \alpha_-(\beta)$ *and* $\alpha = R_-(\beta, \epsilon)$, $\mu_{11} < \mu_{13}$.

Proof. Recall from section 3.6.1 that $\{\mu_{11}, \mu_{12}, \mu_{13}\}$ are given by

$$\begin{aligned} \mu_{11} &= -(4 + 3\Delta_1) \\ \mu_{12} &= \tfrac{1}{2}\left(\Delta_1 + \sqrt{\Delta_1^2 - 4\epsilon\Gamma_P}\right) \\ \mu_{13} &= \tfrac{1}{2}\left(\Delta_1 - \sqrt{\Delta_1^2 - 4\epsilon\Gamma_P}\right) \end{aligned}$$

where $\Delta_1 = \gamma x_1^2 - 1$ and $\Gamma_P = \Gamma_1^+ + \Gamma_1^- > 0$. In the range of interest, $-1 < \Delta_1 < 0$ and $\Delta_1^2 - 4\epsilon\Gamma_P > 0$. The condition $\mu_{11} < \mu_{13}$ is equivalent to:

$$-(4 + 3\Delta_1) < \frac{1}{2}\left(\Delta_1 - \sqrt{\Delta_1^2 - 4\epsilon\Gamma_P}\right)$$

Rearranging the above gives:

$$8 + 7\Delta_1 > \sqrt{\Delta_1^2 - 4\epsilon\Gamma_P}$$

Squaring both sides of this expression and simplifying leads to:

$$(3\Delta_1 + 4)(\Delta_1 + 1) > \frac{-\epsilon\Gamma_P}{4}$$

As $\Gamma_P > 0$, this condition will be true, and hence μ_{11} will be less than μ_{13}, provided $(3\Delta_1 + 4)(\Delta_1 + 1) > 0$. Since $\Delta_1 > -1$, both $3\Delta_1 + 4$ and $\Delta_1 + 1$ are > 0 implying that $(3\Delta_1 + 4)(\Delta_1 + 1) > 0$. This completes the proof. ■

A.1.4 Solutions of the general linear harmonic oscillator equation $\ddot{X} + a_1\dot{X} + a_2X$

This section lists the solutions of the general linear harmonic oscillator equation

$$\ddot{X} + a\dot{X} + bX = 0$$

for each possible choice of $a, b \in \mathbb{R}$. These solutions are used when discussing the linearised dynamics of the burster system about $\mathbf{0}$ and $\mathbf{y}_1^{\pm}$. The results of this section are based on chapter 3 of [45].

1. $a^2 - 4b > 0$. In this range, $\forall t \in \mathbb{R}$

$$X(t) = Ae^{r_1 t} + Be^{r_2 t}$$

where

$$\begin{aligned} r_1 &= -\frac{1}{2}\left(a - \sqrt{a^2 - 4b}\right) \\ r_2 &= -\frac{1}{2}\left(a + \sqrt{a^2 - 4b}\right) \end{aligned}$$

and:

$$\begin{aligned} A &= \frac{1}{\sqrt{a^2 - 4b}}\left(\dot{X}(0) - r_2 X(0)\right) \\ B &= \frac{1}{\sqrt{a^2 - 4b}}\left(r_1 X(0) - \dot{X}(0)\right) \end{aligned}$$

2. $a^2 - 4b = 0$. In this range, $\forall t \in \mathbb{R}$

$$X(t) = (A + Bt)\, e^{-\frac{a}{2}t}$$

where:

$$\begin{aligned} A &= X(0) \\ B &= \dot{X}(0) + \frac{a}{2} X(0) \end{aligned}$$

3. $a^2 - 4b < 0$. In this range, $\forall t \in \mathbb{R}$

$$X(t) = Ae^{-\frac{a}{2}t} \cos(dt + B)$$

where

$$d = \frac{1}{2}\sqrt{4b - a^2}$$

and:

$$\begin{aligned} A &= \frac{1}{d}\sqrt{\left(\frac{a^2}{4} + d^2\right) X(0)^2 + aX(0)\dot{X}(0) + \dot{X}(0)^2} \\ B &= -\arctan\left(\frac{aX(0) + 2\dot{X}(0)}{2dX(0)}\right) \end{aligned}$$

A.1.5 Equations for the error variable in the system $\dot{\mathbf{z}} = D\mathbf{X}(\mathbf{y}_1^{\pm})\mathbf{z}$

Write $\mathbf{z} = (u, v, w)^T$. It is shown here that in the system $\dot{\mathbf{z}} = D\mathbf{X}(\mathbf{y}_1^{\pm})\mathbf{z}$ obtained by linearising the burster system about the nontrivial fixed point $\mathbf{y}_1^{\pm}$, w satisfies the equation for a general linear harmonic oscillator, and the equation $\dot{w} = -\epsilon(u - v)$. So first consider the equations for $\dot{\mathbf{z}} = D\mathbf{X}(\mathbf{y}_1^{+})\mathbf{z}$. (3.58) implies that these are:

$$\begin{aligned} \dot{u} &= -\left(1 + \gamma x_1^2\right) u - 2\gamma x_1^2 v + \Gamma_1^{+} w && \text{(A.8)} \\ \dot{v} &= -2\gamma x_1^2 u - \left(1 + \gamma x_1^2\right) v - \Gamma_1^{-} w && \text{(A.9)} \\ \dot{w} &= -\epsilon(u - v) && \text{(A.10)} \end{aligned}$$

Differentiating (A.10) gives:

$$\ddot{w} = -\epsilon(\dot{u} - \dot{v})$$

Substituting (A.8) and (A.9) into the above yields:

$$\ddot{w} = -\epsilon\left(\Delta_1\left(u-v\right)+\Gamma_P w\right)$$

where $\Delta_1 = \gamma x_1^2 - 1$ and $\Gamma_P = \Gamma_1^+ + \Gamma_1^-$. Substituting (A.10) back into the above and rearranging implies:

$$\ddot{w} - \Delta_1 \dot{w} + \epsilon \Gamma_P w = 0 \tag{A.11}$$

Using the relation $D\mathbf{X}(\mathbf{y}_1^-) = \sigma D\mathbf{X}\left(\mathbf{y}_1^+\right)\sigma$ shows that the equations for $\dot{\mathbf{z}} = D\mathbf{X}(\mathbf{y}_1^+)\mathbf{z}$ are:

$$\begin{aligned}
\dot{u} &= -\left(1+\gamma x_1^2\right)u - 2\gamma x_1^2 v + \Gamma_1^- w \\
\dot{v} &= -2\gamma x_1^2 u - \left(1+\gamma x_1^2\right)v - \Gamma_1^+ w \\
\dot{w} &= -\epsilon\left(u-v\right)
\end{aligned}$$

Performing similar calculations on this set of equations gives (A.11) again. Thus in both cases, $w\left(\tau\right)$ satisfies both $\dot{w} = -\epsilon\left(u-v\right)$ and the general linear harmonic oscillator equation $\ddot{X} + a\dot{X} + bX = 0$ with $a = -\Delta_1$ and $b = \epsilon\Gamma_P$ (cf. section A.1.4).

A.1.6 Proof that solutions of $\dot{\mathbf{z}} = \mathbf{L}_{\mathbf{X}}\left(\mathbf{z}\right)$ exist and can be extended infinitely far forward in time

The analysis is simplified by introducing the change of coordinates $x = u+v, y = u-v, z = w$. Write $\mathbf{x} = \left(x,y,z\right)^T$, $\Lambda_M = \Lambda_+ - \Lambda_-$ and $\Lambda_P = \Lambda_+ + \Lambda_-$. Then in the new coordinates, the linearised burster system $\dot{\mathbf{z}} = \mathbf{L}_{\mathbf{X}}\left(\mathbf{z}\right)$ is $\dot{\mathbf{x}} = \mathbf{A}\left(\mathbf{x}\right)$, where the transformed vector field $\mathbf{A} : \mathbb{R}^3 \to \mathbb{R}^3$ is given by:

$$\mathbf{A}\left(\mathbf{x}\right) = \begin{cases} \begin{pmatrix} -1 & 0 & \Lambda_M \\ 0 & -1 & \Lambda_P \\ 0 & -\epsilon & 0 \end{pmatrix}\mathbf{x} & \text{if} \quad \mathbf{x} \in N_+ \\ \begin{pmatrix} -1 & 0 & -\Lambda_M \\ 0 & -1 & \Lambda_P \\ 0 & -\epsilon & 0 \end{pmatrix}\mathbf{x} & \text{if} \quad \mathbf{x} \in N_- \end{cases} \tag{A.12}$$

Note that $\Lambda_M > 0$. By introducing the matrices

$$A_+ = \begin{pmatrix} -1 & 0 & \Lambda_M \\ 0 & -1 & \Lambda_P \\ 0 & -\epsilon & 0 \end{pmatrix}, A_- = \begin{pmatrix} -1 & 0 & -\Lambda_M \\ 0 & -1 & \Lambda_P \\ 0 & -\epsilon & 0 \end{pmatrix}$$

$\mathbf{A}(\mathbf{x})$ can be written in the concise form:

$$\mathbf{A}(\mathbf{x}) = \begin{cases} A_+\mathbf{x} & \text{if} \quad \mathbf{x} \in N_+ \\ A_-\mathbf{x} & \text{if} \quad \mathbf{x} \in N_- \end{cases} \tag{A.13}$$

It will be useful during this section to be have an alternative form for $\mathbf{A}(\mathbf{x})$. Define the matrix $\bar{A}$ as below:

$$\bar{A} = \begin{pmatrix} -1 & 0 & 0 \\ 0 & -1 & \Lambda_P \\ 0 & -\epsilon & 0 \end{pmatrix}$$

Also define the map $\mathbf{S} : \mathbb{R}^3 \to \mathbb{R}^3$ by:

$$\mathbf{S}(x, y, z) = \begin{pmatrix} \Lambda_M |z| \\ 0 \\ 0 \end{pmatrix} \tag{A.14}$$

Then $\mathbf{A}(\mathbf{x})$ can be written as:

$$\mathbf{A}(\mathbf{x}) = \bar{A}\mathbf{x} + \mathbf{S}(\mathbf{x}) \tag{A.15}$$

It is first shown here that $\mathbf{A}$ is Lipschitz, from which it follows that solutions exist and are unique (cf. section 1.2). It is then shown that all solutions can be extended infinitely far forward in time.

Proposition 7 $\mathbf{A}$ *is Lipschitz.*

Proof. Set $K = \left\|\bar{A}\right\|_1 + \Lambda_M$. It is shown that for $\mathbf{x}, \mathbf{x}' \in \mathbb{R}^3$, $\|\mathbf{A}(\mathbf{x}) - \mathbf{A}(\mathbf{x}')\|_1 \leq K\|\mathbf{x} - \mathbf{x}'\|_1$, from which the result follows. So let $\mathbf{x} = (x, y, z)^T, \mathbf{x}' = (x', y', z')^T \in \mathbb{R}^3$ be given. By (A.15)

$$\begin{aligned}\mathbf{A}(\mathbf{x}) - \mathbf{A}(\mathbf{x}') &= \bar{A}(\mathbf{x}-\mathbf{x}') + \mathbf{S}(\mathbf{x}) - \mathbf{S}(\mathbf{x}') \\ \Rightarrow \left\|\mathbf{A}(\mathbf{x}) - \mathbf{A}(\mathbf{x}')\right\|_1 &\leq \left\|\bar{A}\right\|_1 \left\|\mathbf{x}-\mathbf{x}'\right\|_1 + \left\|\mathbf{S}(\mathbf{x}) - \mathbf{S}(\mathbf{x}')\right\|_1 \end{aligned} \tag{A.16}$$

Now by (A.14):

$$\begin{aligned}\mathbf{S}(\mathbf{x}) - \mathbf{S}(\mathbf{x}') &= \left(\Lambda_M\left(|z| - |z'|\right), 0, 0\right)^T \\ \Rightarrow \left\|\mathbf{S}(\mathbf{x}) - \mathbf{S}(\mathbf{x}')\right\|_1 &= \Lambda_M \left||z| - |z'|\right| \leq \Lambda_M \left|z - z'\right| \leq \Lambda_M \left\|\mathbf{x}-\mathbf{x}'\right\|_1\end{aligned}$$

Setting the above into (A.16) gives $\|\mathbf{A}(\mathbf{x}) - \mathbf{A}(\mathbf{x}')\|_1 \leq K \|\mathbf{x}-\mathbf{x}'\|_1$, as required. ■

It is now shown that solutions of the linearised system can be extended infinitely far forward in time.

Proposition 8 *Let* $\mathbf{x_0} \in \mathbb{R}^3$. *Then the unique solution* $\mathbf{x}(\tau)$ *to* $\dot{\mathbf{x}} = \mathbf{A}(\mathbf{x})$ *with* $\mathbf{x}(0) = \mathbf{x_0}$ *exists* $\forall \tau \geq 0$.

Proof. There are 2 cases:

1. $\mathbf{x_0} = \mathbf{0}$. $\mathbf{0}$ is a fixed point of $\dot{\mathbf{x}} = \mathbf{A}(\mathbf{x})$ and so $\mathbf{x}(\tau)$ exists $\forall \tau \in \mathbb{R}$ with $\mathbf{x}(\tau) = \mathbf{0}$.

2. $\mathbf{x_0} \neq \mathbf{0}$. Proceed by contradiction. Assume that there is some maximal $b > 0$ such that $\mathbf{x}(\tau)$ is defined on $[0, b)$. Then by Corollary 4, $\mathbf{x}(\tau)$ is unbounded on $[0, b)$. Let $J_L(\mathbf{x}_0)$ be the maximal open interval on which $\mathbf{x}(\tau)$ is defined. Then $J_L(\mathbf{x}_0) = (a, b)$ for some $a < 0$ (a may be $= -\infty$). Since $\mathbf{x_0} \neq \mathbf{0}$, $\mathbf{x}(\tau) \neq \mathbf{0}$ $\forall \tau \in J_L(\mathbf{x}_0)$ and so $\|\mathbf{x}(\tau)\|_2$ is differentiable on $J_L(\mathbf{x}_0)$ with derivative $\frac{d}{d\tau}\|\mathbf{x}(\tau)\|_2$ given by

$$\frac{d}{d\tau}\|\mathbf{x}(\tau)\|_2 = \frac{\mathbf{x}(\tau)\cdot\dot{\mathbf{x}}(\tau)}{\|\mathbf{x}(\tau)\|_2}$$

where $\cdot$ denotes scalar product. Now $\mathbf{x}(\tau)\cdot\dot{\mathbf{x}}(\tau) \leq |\mathbf{x}(\tau)\cdot\dot{\mathbf{x}}(\tau)| \leq \|\mathbf{x}(\tau)\|_1 \|\dot{\mathbf{x}}(\tau)\|_1 \leq 3\|\mathbf{x}(\tau)\|_2 \|\dot{\mathbf{x}}(\tau)\|_2$. Thus, from above:

$$\frac{d}{d\tau}\|\mathbf{x}(\tau)\|_2 \leq 3\|\dot{\mathbf{x}}(\tau)\|_2 \tag{A.17}$$

Also, by (A.13):

$$\|\dot{\mathbf{x}}(\tau)\|_2 = \|\mathbf{A}(\mathbf{x}(\tau))\|_2 \leq \begin{cases} \|A_+\|_2 \|\mathbf{x}(\tau)\|_2 & \text{if} \quad \mathbf{x} \in N_+ \\ \|A_-\|_2 \|\mathbf{x}(\tau)\|_2 & \text{if} \quad \mathbf{x} \in N_- \end{cases}$$

Hence, $\|\dot{\mathbf{x}}(\tau)\|_2 \leq K \|\mathbf{x}(\tau)\|_2$ where $K = \max\{\|A_+\|_2, \|A_-\|_2\}$. Substituting into (A.17) gives

$$\frac{d}{d\tau} \|\mathbf{x}(\tau)\|_2 \leq 3K \|\mathbf{x}(\tau)\|_2$$

Let $\tau \in [0, b)$. Integrating the above inequality over $[0, \tau]$ gives $\|\mathbf{x}(\tau)\|_2 \leq \|\mathbf{x}_0\|_2 e^{3K\tau} \Rightarrow \|\mathbf{x}(\tau)\|_2 \leq \|\mathbf{x}_0\| e^{3Kb}$. This is true $\forall \tau \in [0, b)$ implying that $\mathbf{x}(\tau)$ is bounded on $[0, b)$. This gives a contradiction, as required. ■

A.1.7 Proof that the origin is stable in the linearised burster system for $\alpha < \Lambda_+ \beta$

It is shown here that the origin is globally attracting in the linearised burster system $\dot{\mathbf{z}} = \mathbf{L}_{\mathbf{X}}(\mathbf{z})$ when $\alpha < \Lambda_+ \beta$, or equivalently $\Lambda_+ + \Lambda_- > 0$. As in the previous section, write $\Lambda_M = \Lambda_+ - \Lambda_-$ and $\Lambda_P = \Lambda_+ + \Lambda_-$.

Proposition 9 *Assume $\Lambda_+ + \Lambda_- > 0$. Then $\exists -\frac{1}{2} < \mu < 0$ such that given a solution $\mathbf{z}(\tau)$ of $\dot{\mathbf{z}} = \mathbf{L}_{\mathbf{X}}(\mathbf{z})$, $\exists$ a constant $C = C(\mathbf{z}(0), \dot{\mathbf{z}}(0)) \geq 0$ with $\|\mathbf{z}(\tau)\| \leq Ce^{\mu\tau}$ $\forall \tau \geq 0$.*

Proof. It is shown that $\exists -\frac{1}{2} < \mu < 0$ such that given a solution $\mathbf{x}(\tau)$ of the transformed system $\dot{\mathbf{x}} = \mathbf{A}(\mathbf{x})$ introduced in the previous section, $\exists$ a constant $K = K(\mathbf{x}(0), \dot{\mathbf{x}}(0)) \geq 0$ with $\|\mathbf{x}(\tau)\| \leq Ke^{\mu\tau}$ $\forall \tau \geq 0$. The result then follows. Write $\mathbf{x}(\tau) = (x(\tau), y(\tau), z(\tau))^T$. Explicitly, the system $\dot{\mathbf{x}} = \mathbf{A}(\mathbf{x})$ is given by:

$$\dot{x} = -x + \Lambda_M |z| \tag{A.18}$$

$$\dot{y} = -y + \Lambda_P z \tag{A.19}$$

$$\dot{z} = -\epsilon y \tag{A.20}$$

(cf. equation (A.12)). Differentiating equation (A.19) and substituting in equation (A.20) gives the following second order differential equation for $y(\tau)$:

$$\ddot{y} + \dot{y} + \epsilon \Lambda_P y = 0$$

Differentiating equation (A.20) and substituting in equations (A.19) and (A.20) gives the following second order differential equation for $z(\tau)$:

$$\ddot{z} + \dot{z} + \epsilon \Lambda_P z = 0$$

$y(\tau)$ and $z(\tau)$ therefore both satisfy the linear harmonic oscillator equation $\ddot{X} + a\dot{X} + bX = 0$, with $a = 1$ and $b = \epsilon \Lambda_P$. It follows from the discussion of this equation in section A.1.4 that there are 3 possibilities for the solution $X(\tau)$ for this choice of a and b, depending on the sign of $1 - 4\epsilon \Lambda_P$.

1. $1 - 4\epsilon\Lambda_P > 0$. From case 1 of section A.1.4, $\forall \tau \geq 0$

$$X(\tau) = Ae^{\lambda_2 \tau} + Be^{\lambda_3 \tau}$$

where $\lambda_2 = -\frac{1}{2} + \frac{1}{2}\sqrt{1 - 4\epsilon\Lambda_P}$ and $\lambda_3 = -\frac{1}{2} - \frac{1}{2}\sqrt{1 - 4\epsilon\Lambda_P}$ are eigenvalues of $D\mathbf{X}_{\pm}(0)$, and:

$$\begin{aligned} A &= \frac{1}{\sqrt{1 - 4\epsilon\Lambda_P}} \left(\dot{X}(0) - \lambda_3 X(0) \right) \\ B &= \frac{1}{\sqrt{1 - 4\epsilon\Lambda_P}} \left(\lambda_2 X(0) - \dot{X}(0) \right) \end{aligned}$$

2. $1 - 4\epsilon\Lambda_P = 0$. From case 2 of section A.1.4, $\forall \tau \geq 0$

$$X(\tau) = (A + B\tau) e^{-\frac{1}{2}\tau}$$

where:

$$\begin{aligned} A &= X(0) \\ B &= \dot{X}(0) + \frac{1}{2} X(0) \end{aligned}$$

3. $1 - 4\epsilon\Lambda_P < 0$. From case 3 of section A.1.4, $\forall \tau \geq 0$

$$X(\tau) = Ae^{-\frac{1}{2}\tau}\cos(d\tau + B)$$

where $d = \frac{1}{2}\sqrt{4\epsilon\Lambda_P - 1}$ and:

$$\begin{aligned} A &= \frac{1}{d}\sqrt{\left(\frac{1}{4} + d^2\right)X(0)^2 + X(0)\dot{X}(0) + \dot{X}(0)^2} \\ B &= -\arctan\left(\frac{X(0) + 2\dot{X}(0)}{2dX(0)}\right) \end{aligned}$$

Thus, in all 3 cases, $\exists -\frac{1}{2} < \mu < 0$ and a constant $K = K\left(X(0), \dot{X}(0)\right) \geq 0$ such that $\forall \tau \geq 0$:

$$|X(\tau)| \leq Ke^{\mu\tau}$$

Note that μ can be chosen to depend only on $\boldsymbol{\alpha}$. The fact that $y(\tau)$ and $z(\tau)$ both satisfy the equation in X therefore implies that $\exists$ constants $K_1 = K_1(y(0), \dot{y}(0)) \geq 0$ and $K_2 = K_2(z(0), \dot{z}(0)) \geq 0$ such that $\forall \tau \geq 0$:

$$|y(\tau)| \leq K_1 e^{\mu\tau} \tag{A.21}$$

$$|z(\tau)| \leq K_2 e^{\mu\tau} \tag{A.22}$$

Now consider the x equation, (A.18). Let $\tau \geq 0$ be given. Multiplying both sides of (A.18) by e^{τ} and integrating over $[0, \tau]$ gives:

$$e^{\tau}x(\tau) = x(0) + \Lambda_M \int_0^{\tau} e^s |z(s)|\, ds$$

Taking moduli of both sides and using (A.22) implies:

$$\begin{aligned} e^{\tau}|x(\tau)| \leq\ & |x(0)| + \Lambda_M K_2 \textstyle\int_0^{\tau} e^{(\mu+1)s} ds = |x(0)| + \frac{\Lambda_M K_2}{\mu+1}\left(e^{(\mu+1)\tau} - 1\right) \\ \leq\ & |x(0)| + \tfrac{\Lambda_M K_2}{\mu+1} e^{(\mu+1)\tau} \end{aligned}$$

Multiplying both sides of the above by $e^{-\tau}$ gives:

$$\begin{aligned} \Rightarrow |x(\tau)| \leq\ & |x(0)|e^{-\tau} + \tfrac{\Lambda_M K_2}{\mu+1} e^{\mu\tau} \leq |x(0)|e^{\mu\tau} + \tfrac{\Lambda_M K_2}{\mu+1} e^{\mu\tau} \\ =\ & \left(|x(0)| + \tfrac{\Lambda_M K_2}{\mu+1}\right) e^{\mu\tau} \end{aligned}$$

Set $K_3 = |x(0)| + \frac{\Lambda_M K_2}{\mu+1} \geq 0$. Then $\forall \tau \geq 0$:

$$|x(\tau)| \leq K_3 e^{\mu\tau} \tag{A.23}$$

It follows from equations (A.21)-(A.23) that $\forall \tau \geq 0$, $\|\mathbf{x}(\tau)\| \leq K e^{\mu\tau}$ where $K = K_1 + K_2 + K_3$. Note that $K = K(\mathbf{x}(0), \dot{\mathbf{x}}(0)) \geq 0$. ■

Remark: It follows from the proof above that a given solution $\mathbf{z}(\tau)$ of the linearised system $\dot{\mathbf{z}} = \mathbf{L}_\mathbf{X}(\mathbf{z})$ can only cross the plane P an infinite number of times if $1 - 4\epsilon\Lambda_P < 0$.

A.2 Appendix to Chapter 5

A.2.1 The projection operator π

Proposition 10 *The following hold for the projection operator* $\pi : \mathbb{R}^6 \to \mathbb{R}^3$ *defined through the* 3×6 *matrix:*

$$\pi = \begin{pmatrix} \mathbf{0}_{3\times 3} & \mathbf{1}_3 \end{pmatrix}$$

1. π *is linear.*

2. π *is continuous.*

3. If U *is open in* $\mathbb{R}^6$ *then* $\pi(U)$ *is open in* $\mathbb{R}^3$.

4. $\forall \mathbf{z} \in \mathbb{R}^6$, $\|\pi\mathbf{z}\|_1 \leq \|\mathbf{z}\|_1$

Proof.

1. Follows from the fact that π is defined through a matrix.

2. Follows from the fact that a linear map between Euclidian spaces is continuous [24].

3. Since $\mathbb{R}^6 = \mathbb{R}^3 \times \mathbb{R}^3$, U can be written in the form

$$U = \bigcup_{i\in I} A_i \times B_i \tag{A.24}$$

where I is an index set and $\forall i \in I$, A_i and B_i are open in $\mathbb{R}^3$. For each $i \in I$:

$$A_i \times B_i = \left\{ (\mathbf{x}, \mathbf{y})^T : \mathbf{x} \in A_i, \mathbf{y} \in B_i \right\}$$

Hence:

$$\pi (A_i \times B_i) = \left\{ \pi (\mathbf{x}, \mathbf{y})^T : \mathbf{x} \in A_i, \mathbf{y} \in B_i \right\} = \{ \mathbf{y} : \mathbf{x} \in A_i, \mathbf{y} \in B_i \} = B_i$$

Applying π to both sides of (A.24) therefore gives:

$$\pi (U) = \pi \left(\bigcup_{i \in I} A_i \times B_i \right) = \bigcup_{i \in I} \pi (A_i \times B_i) = \bigcup_{i \in I} B_i$$

Since an arbitrary union of open sets is open, $\pi (U)$ is open in $\mathbb{R}^3$.

4. Let $\mathbf{z} = (\mathbf{x}, \mathbf{y})^{\mathbf{T}} \in \mathbb{R}^6$. Then by the definition of the 1-norm, $\|\mathbf{z}\|_1 = \|\mathbf{x}\|_1 + \|\mathbf{y}\|_1 = \|\mathbf{x}\|_1 + \|\pi\mathbf{z}\|_1$. Thus, $\|\pi\mathbf{z}\|_1 \leq \|\mathbf{z}\|_1$. ■

A.2.2 Proof that $\mathbf{Z}$ is locally Lipschitz on $\mathbb{R}^6$

Proposition 11 $\mathbf{Z}$ *is locally Lipschitz.*

Proof. First recall that for $\mathbf{z} = (\mathbf{x}, \mathbf{y})^T \in \mathbb{R}^6$, $\mathbf{Z} (\mathbf{z})$ is given by

$$\mathbf{Z} (\mathbf{z}) = \begin{pmatrix} A\mathbf{x} + B\mathbf{y} \\ \mathbf{Y} (\mathbf{y}) \end{pmatrix}$$

where $A, B \in \mathbb{R}^{3 \times 3}$ are constant matrices, and $\mathbf{Y} (\mathbf{y}) = \frac{1}{\epsilon} \mathbf{X} (\mathbf{y})$ $\forall \mathbf{y} \in \mathbb{R}^3$ (cf. (5.2) and (5.3). So let $\mathbf{z}_0 \in \mathbb{R}^6$. To prove the result, it is sufficient to show that there is an open set $W_{\mathbf{z}_0} \in \mathbb{R}^6$ containing $\mathbf{z}_0$ and a constant $K_{\mathbf{z}_0} \geq 0$ such that $\forall \mathbf{z}, \mathbf{z'} \in W_{\mathbf{z}_0}$:

$$\left\| \mathbf{Z} (\mathbf{z}) - \mathbf{Z} (\mathbf{z'}) \right\|_1 \leq K_{\mathbf{z}_0} \left\| \mathbf{z} - \mathbf{z'} \right\|_1$$

Write $\mathbf{z}_0 = (\mathbf{x_0}, \mathbf{y_0})^T$ where $\mathbf{x}_0, \mathbf{y}_0 \in \mathbb{R}^3$. It was shown in Proposition 2 that $\mathbf{X}$ is locally Lipschitz on $\mathbb{R}^3$. Thus, there exists an open set $V_{\mathbf{y}_0}$ containing $\mathbf{y}_0$ and a constant $L_{\mathbf{y}_0} \geq 0$ such that $\forall \mathbf{y}, \mathbf{y'} \in V_{\mathbf{z}_0}$:

$$\left\|\mathbf{X}\left(\mathbf{y}\right)-\mathbf{X}\left(\mathbf{y}'\right)\right\|_1 \leq L_{\mathbf{y}_0}\left\|\mathbf{y}-\mathbf{y}'\right\|_1 \tag{A.25}$$

Define the set $W_{\mathbf{z}_0}$ by $W_{\mathbf{z}_0} = \mathbb{R}^3 \times V_{\mathbf{y}_0}$. Then $W_{\mathbf{z}_0}$ is open in $\mathbb{R}^6$ and contains $\mathbf{z}_0$. Let $\mathbf{z} = (\mathbf{x}, \mathbf{y})^T$, $\mathbf{z}'= (\mathbf{x}', \mathbf{y}')^T \in W_{\mathbf{z}_0}$. Then:

$$\begin{aligned}\left\|\mathbf{Z}\left(\mathbf{z}\right)-\mathbf{Z}\left(\mathbf{z}'\right)\right\|_1 &= \left\|A\left(\mathbf{x}-\mathbf{x}'\right)+B\left(\mathbf{y}-\mathbf{y}'\right)\right\|_1+\left\|\mathbf{Y}\left(\mathbf{y}\right)-\mathbf{Y}\left(\mathbf{y}'\right)\right\|_1 \\ &\leq \|A\|_1\left\|\left(\mathbf{x}-\mathbf{x}'\right)\right\|_1+\|B\|_1\left\|\left(\mathbf{y}-\mathbf{y}'\right)\right\|_1+\frac{1}{\epsilon}\left\|\mathbf{X}\left(\mathbf{y}\right)-\mathbf{X}\left(\mathbf{y}'\right)\right\|_1\end{aligned}$$

Substituting (A.25) into the above yields:

$$\left\|\mathbf{Z}\left(\mathbf{z}\right)-\mathbf{Z}\left(\mathbf{z}'\right)\right\|_1 \leq \|A\|_1\left\|\mathbf{x}-\mathbf{x}'\right\|_1+\left(\|B\|_1+\frac{L_{\mathbf{y}_0}}{\epsilon}\right)\left\|\mathbf{y}-\mathbf{y}'\right\|_1$$

Define the constant $K_{\mathbf{z}_0} \geq 0$ by $K_{\mathbf{z}_0} = \max\left\{\|A\|_1, \|B\|_1+\frac{L_{\mathbf{y}_0}}{\epsilon}\right\}$. Then from the above:

$$\left\|\mathbf{Z}\left(\mathbf{z}\right)-\mathbf{Z}\left(\mathbf{z}'\right)\right\|_1 \leq K_{\mathbf{z}_0}\left\|\mathbf{x}-\mathbf{x}'\right\|_1+K_{\mathbf{z}_0}\left\|\mathbf{y}-\mathbf{y}'\right\|_1 = K_{\mathbf{z}_0}\left\|\mathbf{z}-\mathbf{z}'\right\|_1$$

This is true $\forall \mathbf{z}, \mathbf{z}' \in W_{\mathbf{z}_0}$, completing the proof. ■

A.2.3 Solutions of the initial value problem $\{\dot{\mathbf{x}} = A\mathbf{x}+B\mathbf{r}\left(t\right) : \mathbf{x}\left(0\right) = \hat{\mathbf{x}}\}$

Proposition 12 *Assume that $\mathbf{r}\left(t\right)$ is a C^1 function defined on an open interval (t_1, t_2) containing 0 (t_1 may be $-\infty$ and t_2 may be ∞). Then given $\hat{\mathbf{x}} \in \mathbb{R}^3$, the following hold:*

1. The unique solution to the initial value problem $\{\dot{\mathbf{x}} = A\mathbf{x} + B\mathbf{r}\left(t\right) : \mathbf{x}\left(0\right) = \hat{\mathbf{x}},\ t_1 < t < t_2\}$ is $\mathbf{x}_r\left(t\right)$ where $\forall t \in (t_1, t_2)$:

$$\mathbf{x}_r\left(t\right) = e^{At}\hat{\mathbf{x}} + \int_0^t e^{A(t-s)}B\mathbf{r}\left(s\right)ds \tag{A.26}$$

2. $\forall t \in [0, t_2)$

$$\left\|\mathbf{x}_r\left(t\right)\right\|_1 \leq P_C\left(e^{-\frac{t}{T_N}}\left\|\hat{\mathbf{x}}\right\|_1 + \int_0^t e^{-\frac{(t-s)}{T_N}}\left\|B\mathbf{r}\left(s\right)\right\|_1 ds\right)$$

where P_C is a constant with $P_C \geq 1$.

Proof.

1. It can be verified by direct substitution that $\mathbf{x}_r(t)$ satisfies $\dot{\mathbf{x}} = A\mathbf{x} + B\mathbf{r}(t)$ on (t_1, t_2) with $\mathbf{x}_r(0) = \hat{\mathbf{x}}$. Moreover, as $\mathbf{r}(t)$ is C^1 on (t_1, t_2), the right hand side of the system $\dot{\mathbf{x}} = A\mathbf{x} + B\mathbf{r}(t)$ is C^1 on $\mathbb{R}^3 \times (t_1, t_2)$, and so $\mathbf{x}_r(t)$ is the unique such solution [4].

2. Assume $0 \leq t < t_2$. Taking 1-norms of both sides of (A.26) yields:

$$\|\mathbf{x}_r(t)\|_1 \leq \left\|e^{At}\right\|_1 \|\hat{\mathbf{x}}\|_1 + \int_0^t \left\|e^{A(t-s)}\right\|_1 \|B\mathbf{r}(s)\|_1 \, ds \tag{A.27}$$

Recall that the constant matrix A is given by

$$A = \begin{pmatrix} 0 & 1 & 0 \\ -P_2 & -P_1 & P_2 \\ 0 & 0 & -\frac{1}{T_N} \end{pmatrix}$$

where

$$\begin{aligned} P_1 &= \frac{1}{T_1} + \frac{1}{T_2} \\ P_2 &= \frac{1}{T_1 T_2} \end{aligned}$$

with $T_1 = 0.15$, $T_2 = 0.012$ and $T_N = 25$ (cf. (5.4)-(5.7)). The eigenvalues of A are $\left\{-\frac{1}{T_1}, -\frac{1}{T_2}, -\frac{1}{T_N}\right\}$. Let the corresponding eigenvectors be $\{\mathbf{p}_1, \mathbf{p}_2, \mathbf{p}_3\}$, and define the 3×3 constant matrix P by $P = [\mathbf{p}_1 \; \mathbf{p}_2 \; \mathbf{p}_3]$. Then since the eigenvalues of A are distinct

$$A = P \Lambda P^{-1}$$

where $\Lambda = \text{diag}\left\{-\frac{1}{T_1}, -\frac{1}{T_2}, -\frac{1}{T_N}\right\}$. Fix $0 \leq r < t_2$. Multiplying the above by r and taking exponentials of both sides gives:

$$\begin{aligned} e^{Ar} &= P e^{\Lambda r} P^{-1} \\ \Rightarrow \left\|e^{Ar}\right\|_1 &\leq \|P\|_1 \left\|e^{\Lambda r}\right\|_1 \left\|P^{-1}\right\|_1 \\ \Rightarrow \left\|e^{Ar}\right\|_1 &\leq P_C \left\|e^{\Lambda r}\right\|_1 \end{aligned}$$

where $P_C = \|P\|_1 \left\|P^{-1}\right\|_1 \geq 1$. Now $e^{\Lambda r} = \operatorname{diag}\left\{e^{-\frac{r}{T_1}}, e^{-\frac{r}{T_2}}, e^{-\frac{r}{T_N}}\right\}$ and so $\left\|e^{\Lambda r}\right\|_1 = \max\left\{e^{-\frac{r}{T_1}}, e^{-\frac{r}{T_2}}, e^{-\frac{r}{T_N}}\right\}$. Thus, since $r \geq 0$ and $T_N > T_1, T_2$, $\left\|e^{\Lambda r}\right\|_1 = e^{-\frac{r}{T_N}} \Rightarrow \left\|e^{Ar}\right\|_1 \leq P_C e^{-\frac{r}{T_N}}$. This is true $\forall 0 \leq r < t_2$, and so $\left\|e^{At}\right\|_1 \leq P_C e^{-\frac{t}{T_N}}$ and $\left\|e^{A(t-s)}\right\|_1 \leq P_C e^{-\frac{(t-s)}{T_N}}$ $\forall 0 \leq s \leq t$. Substituting into (A.27) implies

$$\|\mathbf{x}_r(t)\|_1 \leq P_C \left(e^{-\frac{t}{T_N}} \|\hat{\mathbf{x}}\|_1 + \int_0^t e^{-\frac{(t-s)}{T_N}} \|B\mathbf{r}(s)\|_1 \, ds\right)$$

as required. ■

Remark: It follows from the above proof that $\left\|e^{At}\right\|_1 \leq P_C e^{-\frac{t}{T_N}}$ $\forall t \geq 0$. Hence, given $\mathbf{x} \in \mathbb{R}^3$, $\left\|e^{At}\mathbf{x}\right\|_1 \leq P_C e^{-\frac{t}{T_N}} \|\mathbf{x}\|_1$ $\forall t \geq 0$, and so $e^{At}\mathbf{x} \to \mathbf{0}$ as $t \to \infty$. Also, $\left\|e^{-At}\right\|_1 \leq P_C e^{\frac{t}{T_N}}$ $\forall t \leq 0$. Thus, given $\mathbf{x} \in \mathbb{R}^3$, $\left\|e^{At}\mathbf{x}\right\|_1 \geq \frac{1}{P_C} e^{-\frac{t}{T_N}} \|\mathbf{x}\|_1$ $\forall t \leq 0$, and so $e^{At}\mathbf{x} \nrightarrow \mathbf{0}$ as $t \to -\infty$.

A.2.4 Proof that $\dot{\mathbf{z}} = \mathbf{Z}(\mathbf{z})$ has a compact absorbing set if $\dot{\mathbf{y}} = \mathbf{Y}(\mathbf{y})$ has a compact absorbing set

Proposition 13 *Assume that $\dot{\mathbf{y}} = \mathbf{Y}(\mathbf{y})$ has an absorbing set C of the form:*

$$C = \left\{(r, l, \varepsilon)^T \in \mathbb{R}^3 : 0 \leq r, l \leq \alpha_M, |\varepsilon| \leq \varepsilon_M\right\}$$

(cf.5.27). Then $\exists M_{\bar{\varepsilon}} > 0$ such that given $\mathbf{z} \in \mathbb{R}^6$, there is $t_C(\mathbf{z}) > 0$ for which $\psi_t(\mathbf{z}) \in \bar{B}_{M_{\bar{\varepsilon}}}(\mathbf{0}) \times C$ $\forall t \geq t_C(\mathbf{z})$, where:

$$\bar{B}_{M_{\bar{\varepsilon}}}(\mathbf{0}) = \left\{\mathbf{x} \in \mathbb{R}^3 : \|\mathbf{x}\|_1 \leq M_{\bar{\varepsilon}}\right\}$$

Proof. Fix $M_{\bar{\varepsilon}} > 0$ with $M_{\bar{\varepsilon}} > 2P_C \|B\|_1 T_N (2\alpha_M + \varepsilon_M)$, where $P_C \geq 1$ is the constant which was defined during the proof of Proposition 12. Let $\mathbf{z} = (\mathbf{x}, \mathbf{y})^T \in \mathbb{R}^6$, and define $\mathbf{z}(t) = (\mathbf{x}(t), \mathbf{y}(t))^T$ by $\mathbf{z}(t) = \psi_t(\mathbf{z})$ $\forall t \in J(\mathbf{z})$. $\mathbf{y}(t)$ solves $\dot{\mathbf{y}} = \mathbf{Y}(\mathbf{y})$, and so all solutions of $\dot{\mathbf{y}} = \mathbf{Y}(\mathbf{y})$ are by assumption eventually confined to C, there is $t_C(\mathbf{y}) > 0$ such that $\mathbf{y}(t) \in C$ $\forall t \geq t_C(\mathbf{y})$. Also, $\mathbf{x}(t)$ satisfies the initial value problem $\{\dot{\mathbf{x}} = A\mathbf{x} + B\mathbf{y}(t) : \mathbf{x}(0) = \mathbf{x},\ t \in J(\mathbf{z})\}$. As $J(\mathbf{z})$ is an open interval of the form (a, ∞) where $a < 0$, Proposition 12 therefore implies that $\forall t \geq 0$:

$$\|\mathbf{x}(t)\|_1 \leq P_C\left(e^{-\frac{t}{T_N}}\mathbf{x} + \int_0^t e^{-\frac{(t-s)}{T_N}}\|B\mathbf{y}(s)\|_1\, ds\right)$$

If follows that for all $t \geq t_C(\mathbf{y})$:

$$\|\mathbf{x}(t)\|_1 \leq P_C e^{-\frac{t}{T_N}}\left(\mathbf{x} + \int_0^{t_C(\mathbf{y})} e^{\frac{s}{T_N}}\|B\mathbf{y}(s)\|_1\, ds + \|B\|_1 \int_{t_C(\mathbf{y})}^t e^{\frac{s}{T_N}}\|\mathbf{y}(s)\|_1\, ds\right) \tag{A.28}$$

Now since $\mathbf{y}(t) \in C\ \forall t \geq t_C(\mathbf{y})$:

$$\begin{aligned}\int_{t_C(\mathbf{y})}^t e^{\frac{s}{T_N}}\|\mathbf{y}(s)\|_1\, ds &\leq (2\alpha_M + \varepsilon_M)\int_{t_C(\mathbf{y})}^t e^{\frac{s}{T_N}}\, ds \\ &\leq T_N(2\alpha_M + \varepsilon_M)\left(e^{\frac{t}{T_N}} - e^{\frac{t_C(\mathbf{y})}{T_N}}\right) \\ &< T_N(2\alpha_M + \varepsilon_M)\, e^{\frac{t}{T_N}}\end{aligned}$$

Substituting the above into (A.28) implies that for $t \geq t_C(\mathbf{y})$:

$$\begin{aligned}\|\mathbf{x}(t)\|_1 &< P_C e^{-\frac{t}{T_N}}\left(\mathbf{x} + \int_0^{t_C(\mathbf{y})} e^{\frac{s}{T_N}}\|B\mathbf{y}(s)\|_1\, ds\right) + P_C\|B\|_1 T_N(2\alpha_M + \varepsilon_M) \\ &< P_C e^{-\frac{t}{T_N}}\left(\mathbf{x} + \int_0^{t_C(\mathbf{y})} e^{\frac{s}{T_N}}\|B\mathbf{y}(s)\|_1\, ds\right) + \frac{M_{\bar{\varepsilon}}}{2}\end{aligned}$$

As $e^{-\frac{t}{T_N}} \to 0$ monotonically as $t \to \infty$, it is possible to choose $t_C(\mathbf{z}) > t_C(\mathbf{y})$ such that $\forall t \geq t_C(\mathbf{z})$, $\|\mathbf{x}(t)\|_1 \leq M_{\bar{\varepsilon}}$, and so $\mathbf{x}(t) \in \bar{B}_{M_{\bar{\varepsilon}}}(\mathbf{0})$. As $\mathbf{y}(t) \in C\ \forall t \geq t_C(\mathbf{y})$, $\mathbf{z}(t) \in \bar{B}_{M_{\bar{\varepsilon}}}(\mathbf{0}) \times C\ \forall t \geq t_C(\mathbf{z})$, giving the result. ■

A.2.5 Results concerning the ω-limit sets of the saccadic system $\dot{\mathbf{z}} = \mathbf{Z}(\mathbf{z})$

The results of this section pertain to the discussion on the ω-limit sets of $\dot{\mathbf{z}} = \mathbf{Z}(\mathbf{z})$ at the end of section 5.2.

Proposition 14 *Given* $\mathbf{y} \in \mathbb{R}^3$, $\omega\left((\mathbf{x}_1, \mathbf{y})^T\right) = \omega\left((\mathbf{x}_2, \mathbf{y})^T\right)\ \forall \mathbf{x}_1, \mathbf{x}_2 \in \mathbb{R}^3$.

Proof. To prove this, it is sufficient to show that given $\mathbf{x}_1, \mathbf{x}_2 \in \mathbb{R}^3$, $\omega\left((\mathbf{x}_1, \mathbf{y})^T\right) \subseteq \omega\left((\mathbf{x}_2, \mathbf{y})^T\right)$. So let $\mathbf{x}_1, \mathbf{x}_2 \in \mathbb{R}^3$. Assume $\mathbf{z}' = (\mathbf{x}', \mathbf{y}')^T \in \omega\left((\mathbf{x}_1, \mathbf{y})^T\right)$. Then by definition, there is a sequence (t_n) with $t_n \to \infty$ as $n \to \infty$ and $\psi_{t_n}(\mathbf{x}_1, \mathbf{y}) \to \mathbf{z}'$ as $n \to \infty$. The form of ψ_{t_n} then implies that $L_{t_n}(\mathbf{x}_1, \mathbf{y}) \to \mathbf{x}'$ as $n \to \infty$ and $\varphi_{t_n}(\mathbf{y}) \to \mathbf{y}'$ as $n \to \infty$. Now $\forall n \geq 1$:

$$L_{t_n}(\mathbf{x}_1, \mathbf{y}) = e^{At_n}\mathbf{x}_1 + \int_0^{t_n} e^{A(t_n - s)} B\varphi_s(\mathbf{y})\, ds$$

It was remarked at the end of Proposition 12 that for all $\mathbf{x} \in \mathbb{R}^3$, $e^{At}\mathbf{x} \to \mathbf{0}$ as $t \to \infty$. Since $t_n \to \infty$ as $n \to \infty$, this means that $e^{At_n}\mathbf{x}_1 \to \mathbf{0}$ as $n \to \infty$, which implies:

$$\int_0^{t_n} e^{A(t_n - s)} B\varphi_s(\mathbf{y})\, ds \to \mathbf{x}' \text{ as } n \to \infty \tag{A.29}$$

By definition, $\forall n \geq 1$:

$$L_{t_n}(\mathbf{x}_2, \mathbf{y}) = e^{At_n}\mathbf{x}_2 + \int_0^{t_n} e^{A(t_n - s)} B\varphi_s(\mathbf{y})\, ds \tag{A.30}$$

As $n \to \infty$, $e^{At_n}\mathbf{x}_2 \to \mathbf{0}$. Thus (A.29) and (A.30) imply $L_{t_n}(\mathbf{x}_2, \mathbf{y}) \to \mathbf{x}'$ as $n \to \infty$. Since $\varphi_{t_n}(\mathbf{y}) \to \mathbf{y}'$ as $n \to \infty$, it follows that $\psi_{t_n}(\mathbf{x}_2, \mathbf{y}) \to \mathbf{z}'$ as $n \to \infty$. Thus, $\mathbf{z}' \in \omega\left((\mathbf{x}_2, \mathbf{y})^T\right)$. This holds $\forall \mathbf{z}' \in \omega\left((\mathbf{x}_1, \mathbf{y})^T\right)$, and so $\omega\left((\mathbf{x}_1, \mathbf{y})^T\right) \subseteq \omega\left((\mathbf{x}_2, \mathbf{y})^T\right)$, as claimed. ■

Proposition 15 *$\pi\omega(\mathbf{z}) = \omega(\pi\mathbf{z})$ for all $\mathbf{z} \in \mathbb{R}^6$.*

Proof. *Let $\mathbf{z} \in \mathbb{R}^6$. It is first shown that $\pi\omega(\mathbf{z}) \subseteq \omega(\pi\mathbf{z})$. So let $\mathbf{y}' \in \pi\omega(\mathbf{z})$. Then $\exists \mathbf{z}' \in \omega(\mathbf{z})$ with $\mathbf{y}' = \pi\mathbf{z}'$. Since $\mathbf{z}' \in \omega(\mathbf{z})$, there is a sequence (t_n) with $t_n \to \infty$ as $n \to \infty$ such that $\psi_{t_n}(\mathbf{z}) \to \mathbf{z}'$ as $n \to \infty$. As π is continuous, $\pi\psi_{t_n}(\mathbf{z}) \to \pi\mathbf{z}' = \mathbf{y}'$ as $n \to \infty$. Also π semi-conjugates ψ_t and φ_t (cf. (5.19)), and so $\varphi_{t_n}(\pi\mathbf{z}) \to \mathbf{y}'$ as $n \to \infty$. Hence, $\mathbf{y}' \in \omega(\pi\mathbf{z})$. This holds $\forall \mathbf{y}' \in \pi\omega(\mathbf{z})$ proving that $\pi\omega(\mathbf{z}) \subseteq \omega(\pi\mathbf{z})$.*

It is now shown that $\omega(\pi\mathbf{z}) \subseteq \pi\omega(\mathbf{z})$. So let $\mathbf{y}' \in \omega(\pi\mathbf{z})$. Then there is an increasing sequence (t_n) with $t_n \to \infty$ as $n \to \infty$ such that $\varphi_{t_n}(\pi\mathbf{z}) \to \mathbf{y}'$ as $n \to \infty$. It was shown in Proposition 13 that the set $\{\psi_t(\mathbf{z}) : t \geq 0\}$ is eventually confined to the compact subset $\hat{C}$ of $\mathbb{R}^6$. $(\psi_{t_n}(\mathbf{z}))$ is therefore a sequence in a compact set, and thus has a convergent subsequence $(\psi_{s_n}(\mathbf{z}))$. Write $\mathbf{z}' = \lim_{n\to\infty} \psi_{s_n}(\mathbf{z})$. Since (s_n) is a subsequence of (t_n), and (t_n) is increasing with $t_n \to \infty$ as $n \to \infty$, $s_n \to \infty$ as $n \to \infty$. Hence, $\mathbf{z}' \in \omega(\mathbf{z})$. Also, as π is continuous, $\pi\psi_{s_n}(\mathbf{z}) \to \pi\mathbf{z}'$ as $n \to \infty$. The fact that π semi-conjugates ψ_t and φ_t then implies $\varphi_{s_n}(\pi\mathbf{z}) \to \pi\mathbf{z}'$ as $n \to \infty$. However $(\varphi_{s_n}(\pi\mathbf{z}))$ is a subsequence of $(\varphi_{t_n}(\pi\mathbf{z}))$ and so $\mathbf{y}' = \pi\mathbf{z}'$. Thus as $\mathbf{z}' \in \omega(\mathbf{z})$, $\mathbf{y}' \in \pi\omega(\mathbf{z})$. This holds $\forall \mathbf{y}' \in \omega(\pi\mathbf{z})$

proving that $\omega(\pi\mathbf{z}) \subseteq \pi\omega(\mathbf{z})$. ■

Proposition 16 *Given* $i_1, i_2 \in I_B$, $\left[(\mathbf{0}, \mathbf{y}_{i_1})^T\right] \cap \left[(\mathbf{0}, \mathbf{y}_{i_2})^T\right] = \phi$ *if* $i_1 \neq i_2$.

Proof. This is by contradiction. So assume that the intersection is nonempty. Then there is some $\mathbf{z} \in \mathbb{R}^6$ with $\omega(\mathbf{z}) = \omega\left((\mathbf{0}, \mathbf{y}_{i_1})^T\right)$ and $\omega(\mathbf{z}) = \omega\left((\mathbf{0}, \mathbf{y}_{i_2})^T\right)$. Hence:

$$\begin{gathered}\omega\left((\mathbf{0}, \mathbf{y}_{i_1})^T\right) = \omega\left((\mathbf{0}, \mathbf{y}_{i_2})^T\right) \\ \Rightarrow \pi\omega\left((\mathbf{0}, \mathbf{y}_{i_1})^T\right) = \pi\omega\left((\mathbf{0}, \mathbf{y}_{i_2})^T\right)\end{gathered}$$

So by Proposition 15:

$$\omega(\mathbf{y}_{i_1}) = \omega(\mathbf{y}_{i_2})$$

But $\{\omega(\mathbf{y}_i) : i \in I_B\}$ is a collection of distinct sets, implying $i_1 = i_2$. This gives a contradiction, and so the intersection must be empty. ■

Proposition 17 *Assume that* I_S *has been chosen so that* $I_B \subseteq I_S$. *Then for all* $i \in I_S$, $\left[(\mathbf{0}, \mathbf{y}_i)^T\right] = \mathbb{R}^3 \times [\mathbf{y}_i]$.

Proof. It is first demonstrated that $\left[(\mathbf{0}, \mathbf{y}_i)^T\right] \subseteq \mathbb{R}^3 \times [\mathbf{y}_i]$ for all $i \in I_S$. So let $i \in I_S$. Then given $\mathbf{z} = (\mathbf{x}, \mathbf{y})^T \in \left[(\mathbf{0}, \mathbf{y}_i)^T\right]$:

$$\begin{gathered}\omega(\mathbf{z}) = \omega\left((\mathbf{0}, \mathbf{y}_i)^T\right) \\ \Rightarrow \pi\omega(\mathbf{z}) = \pi\omega\left((\mathbf{0}, \mathbf{y}_i)^T\right)\end{gathered}$$

Hence, by Proposition 15:

$$\begin{gathered}\omega(\mathbf{y}) = \omega(\mathbf{y}_i) \\ \Rightarrow \mathbf{y} \in [\mathbf{y}_i] \\ \Rightarrow \mathbf{z} \in \mathbb{R}^3 \times [\mathbf{y}_i]\end{gathered}$$

This holds $\forall \mathbf{z} \in \left[(\mathbf{0}, \mathbf{y}_i)^T\right]$, and so $\left[(\mathbf{0}, \mathbf{y}_i)^T\right] \subseteq \mathbb{R}^3 \times [\mathbf{y}_i]$. So now assume that there is some $j \in I_S$ for which $\left[(\mathbf{0}, \mathbf{y}_j)^T\right] \subset \mathbb{R}^3 \times [\mathbf{y}_j]$. It is shown this leads to a contradiction, giving the required result. By assumption:

$$\mathbb{R}^6 = \bigcup_{i \in I_S} \left[(\mathbf{0}, \mathbf{y}_i)^T \right]$$

Hence, since $\left[(\mathbf{0}, \mathbf{y}_j)^T \right] \subset \mathbb{R}^3 \times [\mathbf{y}_j]$:

$$\mathbb{R}^6 \subset \bigcup_{i \in I_S} \mathbb{R}^3 \times [\mathbf{y}_i] = \mathbb{R}^3 \times \bigcup_{i \in I_S} [\mathbf{y}_i] \tag{A.31}$$

Also $I_B \subseteq I_S$, and so:

$$\bigcup_{i \in I_B} [\mathbf{y}_i] \subseteq \bigcup_{i \in I_S} [\mathbf{y}_i]$$

Thus, since $\bigcup_{i \in I_B} [\mathbf{y}_i] = \mathbb{R}^3$, the expression above implies $\bigcup_{i \in I_S} [\mathbf{y}_i] = \mathbb{R}^3$. Substituting into (A.31) yields $\mathbb{R}^6 \subset \mathbb{R}^3 \times \mathbb{R}^3 = \mathbb{R}^6$, which is a contradiction. ■

Proposition 18 *Assume that $\hat{\mathcal{A}}$ is an attractor of $\dot{\mathbf{z}} = \mathbf{Z}(\mathbf{z})$. Then $\pi\hat{\mathcal{A}}$ is an attractor of $\dot{\mathbf{y}} = \mathbf{Y}(\mathbf{y})$.*

Proof. It is first shown that there is an open set $N_{\pi\hat{\mathcal{A}}}$ of $\mathbb{R}^3$ with $\pi\hat{\mathcal{A}} \subseteq N_{\pi\hat{\mathcal{A}}}$ such that $N_{\pi\hat{\mathcal{A}}}$ is positively invariant, and $\varphi_t\left(N_{\pi\hat{\mathcal{A}}}\right) \to \pi\hat{\mathcal{A}}$ as $t \to \infty$. Since $\hat{\mathcal{A}}$ is an attractor of $\dot{\mathbf{z}} = \mathbf{Z}(\mathbf{z})$, there is an open set $N_{\hat{\mathcal{A}}}$ of $\mathbb{R}^6$ with $\hat{\mathcal{A}} \subseteq N_{\hat{\mathcal{A}}}$ such that $N_{\hat{\mathcal{A}}}$ is positively invariant, and $\psi_t\left(N_{\hat{\mathcal{A}}}\right) \to \hat{\mathcal{A}}$ as $t \to \infty$. Define $N_{\pi\hat{\mathcal{A}}} \subseteq \mathbb{R}^3$ by $N_{\pi\hat{\mathcal{A}}} = \pi N_{\hat{\mathcal{A}}}$. Then $N_{\pi\hat{\mathcal{A}}}$ is open (cf. (3) of Proposition 10) and as $\hat{\mathcal{A}} \subseteq N_{\hat{\mathcal{A}}}$, $\pi\hat{\mathcal{A}} \subseteq \pi N_{\hat{\mathcal{A}}} = N_{\pi\hat{\mathcal{A}}}$. So let $\mathbf{y} \in N_{\pi\hat{\mathcal{A}}}$. Then $\mathbf{y} = \pi\mathbf{z}$ for some $\mathbf{z} \in N_{\hat{\mathcal{A}}}$. The positive invariance of $N_{\hat{\mathcal{A}}}$ implies that for all $t \geq 0$:

$$\begin{aligned} &\psi_t(\mathbf{z}) \in N_{\hat{\mathcal{A}}} \\ \Rightarrow\ &\pi\psi_t(\mathbf{z}) \in \pi N_{\hat{\mathcal{A}}} \\ \Rightarrow\ &\varphi_t(\mathbf{y}) \in N_{\pi\hat{\mathcal{A}}} \end{aligned}$$

Also $\psi_t(\mathbf{z}) \to \hat{\mathcal{A}}$ as $t \to \infty$, and so as π is continuous and $\hat{\mathcal{A}}$ is compact, $\pi\psi_t(\mathbf{z}) \to \pi\hat{\mathcal{A}}$ as $t \to \infty$. Since π semi-conjugates ψ_t and φ_t, it follows that $\varphi_t(\mathbf{y}) \to \pi\hat{\mathcal{A}}$ as $t \to \infty$. It has thus been shown that given $\mathbf{y} \in N_{\pi\hat{\mathcal{A}}}$, $\varphi_t(\mathbf{y}) \in N_{\pi\hat{\mathcal{A}}}$ $\forall t \geq 0$, and $\varphi_t(\mathbf{y}) \to \pi\hat{\mathcal{A}}$ as $t \to \infty$. Hence, $N_{\pi\hat{\mathcal{A}}}$ is positively invariant and $\varphi_t\left(N_{\pi\hat{\mathcal{A}}}\right) \to \pi\hat{\mathcal{A}}$ as $t \to \infty$.

It is now proved that $\pi\hat{\mathcal{A}}$ has a dense orbit with respect to the 1-norm. Since $\hat{\mathcal{A}}$ is an attractor of $\dot{\mathbf{z}} = \mathbf{Z}(\mathbf{z})$, it has a dense orbit $\left\{\psi_t(\mathbf{z}_0) : t \in \mathbb{R},\ \mathbf{z}_0 \in \hat{\mathcal{A}}\right\}$. Let $\mathbf{z}_0 = (\mathbf{x}_0, \mathbf{y}_0)^T$. It is shown that $\left\{\varphi_t(\mathbf{y}_0) : t \in \mathbb{R},\ \mathbf{y}_0 \in \pi\hat{\mathcal{A}}\right\}$ is a dense orbit of $\pi\hat{\mathcal{A}}$. So fix $\mathbf{y} \in \pi\hat{\mathcal{A}}$ and let $\epsilon > 0$ be given. $\mathbf{y} = \pi\mathbf{z}$ for some $\mathbf{z} \in \hat{\mathcal{A}}$. Thus, as $\left\{\psi_t(\mathbf{z}_0) : t \in \mathbb{R},\ \mathbf{z}_0 \in \hat{\mathcal{A}}\right\}$ is a dense orbit of $\hat{\mathcal{A}}$, $\exists t' \in \mathbb{R}$ such that $\psi_{t'}(\mathbf{z}_0) \in B_\epsilon(\mathbf{z})$, which implies $\|\pi(\psi_{t'}(\mathbf{z}_0) - \mathbf{z})\|_1 < \epsilon$. It then follows from the linearity of π that:

$$\begin{aligned} &\|\pi\psi_{t'}(\mathbf{z}_0) - \pi\mathbf{z}\|_1 < \epsilon \\ &\Rightarrow \|\varphi_{t'}(\mathbf{y}_0) - \mathbf{y}\|_1 < \epsilon \\ &\Rightarrow \varphi_{t'}(\mathbf{y}_0) \in B_\epsilon(\mathbf{y}) \end{aligned}$$

Such a $t' \in \mathbb{R}$ can be found for all $\epsilon > 0$. This argument holds $\forall \mathbf{y} \in \pi\hat{\mathcal{A}}$ implying that $\left\{\varphi_t(\mathbf{y}_0) : t \in \mathbb{R},\ \mathbf{y}_0 \in \pi\hat{\mathcal{A}}\right\}$ is a dense orbit of $\pi\hat{\mathcal{A}}$. ■

A.2.6 A result concerning convolutions

The following Proposition is used in section 5.6.

Proposition 19 *Let $f(t), g(t)$ be real, continuous functions defined on $[0, \infty)$ for which the following hold:*

1. *$f(t) \to 0$ as $t \to \infty$.*

2. *$\exists N, \mu > 0$ such that $|g(t)| \leq Ne^{-\mu t}$ for all $t \geq 0$.*

Then $(f * g)(t) \to 0$ as $t \to \infty$, where $f * g$ is the convolution of f and g.

Proof. To prove the result, it is necessary to show that given $\epsilon > 0$, there is a $t' > 0$ such that $|(f * g)(t)| < \epsilon$ for all $t \geq t'$. So let $\epsilon > 0$. By definition, $\forall t \geq 0$, $(f * g)(t)$ is given by:

$$(f * g)(t) = \int_0^t f(s)\, g(t - s)\, ds$$

Hence, $\forall t \geq 0$:

$$|(f * g)(t)| = \left| \int_0^t f(s)\, g(t - s)\, ds \right|$$

$$\begin{aligned}|(f*g)(t)| &\leq \int_0^t |f(s)|\,|g(t-s)|\,ds \\ &\leq Ne^{-\mu t}\int_0^t |f(s)|\,e^{\mu s}ds\end{aligned}$$

Now since $f(t) \to 0$ as $t \to \infty$, there is a $\bar{t} > 0$ such that $|f(t)| < \frac{\epsilon\mu}{2N}$ for all $t \geq \bar{t}$. Also $f(t)$ is continuous, and so is bounded on $[0, \bar{t}]$, implying that there is an $M > 0$ with $|f(t)| \leq M\ \forall t \in [0, \bar{t}]$. It thus follows from the above inequality that for all $t \geq \bar{t}$:

$$\begin{aligned}|(f*g)(t)| &\leq Ne^{-\mu t}\left(M\int_0^{\bar{t}} e^{\mu s}ds + \frac{\epsilon\mu}{2N}\int_{\bar{t}}^t e^{\mu s}ds\right) \\ &= Ne^{-\mu t}\left(\frac{M}{\mu}\left(e^{\mu\bar{t}}-1\right) + \frac{\epsilon}{2N}\left(e^{\mu t}-e^{\mu\bar{t}}\right)\right) \\ &< Ne^{-\mu t}\left(\frac{M}{\mu}e^{\mu\bar{t}} + \frac{\epsilon}{2N}e^{\mu t}\right) \\ |(f*g)(t)| &< \frac{MN}{\mu}e^{-\mu(t-\bar{t})} + \frac{\epsilon}{2}\end{aligned}$$

$\frac{MN}{\mu}e^{-\mu(t-\bar{t})}$ converges to 0 monotonically as $t \to \infty$. Consequently, there is a $t' > \bar{t}$ such that $\frac{MN}{\mu}e^{-\mu(t-\bar{t})} < \frac{\epsilon}{2}$ for all $t \geq t'$. The inequality above therefore implies that $|(f*g)(t)| < \epsilon$ for all $t \geq t'$. This completes the proof. ■

Bibliography

[1] P. Brodal, *The Central Nervous System*, Oxford University Press, 1998.

[2] R. J. Leigh and D. S. Zee, *The Neurology of Eye Movements*, Oxford University Press, 1999.

[3] J. A. M. VanGisbergen, D. A. Robinson, and S. Gielen, A Quantitative Analysis of Generation of Saccadic Eye Movements by Burst Neurons, J. Neurophysiology **45**, 417–442 (1981).

[4] P. Glendinning, *Stability, Instability and Chaos*, CUP, 1994.

[5] D. A. Robinson, Is the Oculomotor System a Cartoon of Motor Control?, Progress in Brain Research **64**, 411–417 (1986).

[6] D. A. Robinson, The Windfalls of Technology in the Oculomotor System, Investigative Opthalmology and Vision Science **28**, 1912–1924 (1987).

[7] L. M. Optican and D. S. Zee, A Hypothetical Explanation of Congenital Nystagmus, Biological Cybernetics **50**, 119–134 (1984).

[8] A. J. VanOpstal, J. A. M. VanGisbergen, and J. J. Eggermont, Reconstruction of the Neural Control Signal for Saccades Based on an Inverse Method, Vision Research **25**, 789–801 (1985).

[9] C. A. Scudder, A New Local Feedback Model of the Saccadic Burst Generator, J. Neurophysiology **59**, 1455–1475 (1988).

[10] A. K. Moschovakis, Neural Network Simulations of the Primate Oculomotor System, Biological Cybernetics **70**, 291–302 (1994).

[11] B. Breznen and J. W. Gnadt, Analysis of the Step Response of the Saccadic Feedback: Computational Models, Experimental Brain Research **117**, 181–191 (1997).

[12] R. V. Abadi, D. S. Broomhead, R. A. Clement, J. P. Whittle, and R. Worfolk, Dynamical Systems Analysis: A New Method of Analysing Congenital Nystagmus Waveforms, Experimental Brain Research **117**, 355–361 (1997).

[13] M. Shelhamer, On the Correlation Dimension of Optokinetic Nystagmus Eye Movements: Computational Parameters, Filtering, Nonstationarity and Surrogate Data, Biological Cybernetics **76**, 237–250 (1997).

[14] D. S. Broomhead, R. A. Clement, M. R. Muldoon, J. P. Whittle, C. Scallan, and R. V. Abadi, Modelling of Congenital Nystagmus Waveforms Produced by Saccadic System Abnormalities, Biological Cybernetics **82**, 391–399 (2000).

[15] R. V. Abadi, C. J. Scallan, and R. A. Clement, The Characteristics of Dynamic Overshoots in Square-Wave-Jerks and in Congenital and Manifest Latent Nystagmus, Vision Research **40**, 2813–2829 (2000).

[16] R. A. Clement, J. P. Whittle, M. R. Muldoon, R. V. Abadi, D. S. Broomhead, and O. E. Akman, Characterisation of Congenital Nystagmus Waveforms in Terms of Periodic Orbits, Vision Research **42**, 2123–2130 (2002).

[17] O. E. Akman, D. S. Broomhead, and R. A. Clement, Mathematical Models of Eye Movements, Mathematics Today **39**(2), 54–59 (2003).

[18] R. Worfolk, The Control of Eye Movements, A series of articles published in Optometry Today: 5/10/92 (pp 26-29), 11/01/93 (pp 24-26), 08/03/93 (pp 30-32),.

[19] L. A. Breen, Nystagmus and Related Ocular Oscillations, in *Walsh and Hoyt's Clinical Opthalmology*, chapter 17, pages 544–561, Williams (Baltimore), 1998.

[20] R. V. Abadi and C. M. Dickinson, Waveform Characteristics in Congenital Nystagmus, Documenta Opthalmologica **64**, 153–167 (1986).

[21] R. V. Abadi, C. M. Dickinson, E. Pascal, J. Whittle, and R. Worfolk, Sensory and Motor Aspects of Congenital Nystagmus, in *Oculomotor Control and Cognitive Processes*, edited by R. Schmid and D. Zambarbieri, pages 249–262, Elsevier Science Publishers B. V. (North-Holland), 1991.

[22] R. V. Abadi and R. Worfolk, Harmonic Analysis of Congenital Nystagmus Waveforms, Clinical Vision Science **6**, 385–388 (1991).

[23] M. W. Hirsch and S. Smale, *Differential Equations, Dynamical Systems and Linear Algebra*, Academic Press, 1974.

[24] D. R. J. Chillingworth, *Differential Topology with a View to Applications*, Pitman, London, 1976.

[25] J. Guckenheimer and P. Holmes, *Nonlinear Oscillations, Dynamical Systems and Bifurcations of Vector Fields*, Springer Verlag, 1983.

[26] V. I. Arnold, *Ordinary Differential Equations*, Springer Verlag, 1992.

[27] D. K. Arrowsmith and C. M. Place, *Dynamical Systems*, CRC, London, 1992.

[28] M. Demazure, *Bifurcations and Catastrophes*, Springer Verlag, 2000.

[29] E. C. Zeeman, Differential Equations for the Heartbeat and Nerve Impulse, in *Towards a Theoretical Biology*, edited by C. H. Waddington, pages 8–67, University Press, Edinburgh, 1972.

[30] J. Guckenheimer, K. Hoffman, and W. Weckesser, Numerical Computation of Canards, International Journal Of Bifurcations and Chaos **10**(12), 2669–2687 (2000).

[31] J. Stark, Invariant Graphs for Forced Systems, Physica D **109**, 163–179 (1997).

[32] P. Glendinning and C. Laing, A Homoclinic Hierarchy, Phys Lett A **211**, 155–160 (1996).

[33] P. Glendinning, J. Ashbagen, and T. Mullin, Imperfect Homoclinic Bifurcations, Phys. Rev. E **64**, 036208:1–036208:8 (2001).

[34] T. Peacock and T. Mullin, Homoclinic Bifurcations in a Liquid Crystal Flow, J. Fluid Mech **432**, 369–386 (2001).

[35] P. Holmes and R. Ghrist, Knotting Within the Gluing Bifurcation, Preprint (2002).

[36] E. Kreyszig, *Advanced Engineering Mathematics*, John Wiley, 7th edition, 1993.

[37] S. Barnett, *Matrices: Methods and Applications*, Clarendon (Oxford), 1996.

[38] P. A. Lynn, *An Introduction to the Analysis and Processing of Signals*, Macmillan, 1989.

[39] C. F. Gerald and P. O. Wheatley, *Applied Numerical Analysis*, Addison Wesley, 1994.

[40] L. Glass and M. C. Mackey, Pathological Conditions Resulting from Instabilities in Physiological Control Systems, Ann NY Acad Sci **316**, 214–235 (1979).

[41] N. Moray, *Attention. Selective Processes in Vision and Hearing.*, Hutchinson Educational, 1969.

[42] C. M. Harris and D. M. Wolpert, Signal-Dependent Noise Determines Motor Planning, Nature **394**, 780–784 (1998).

[43] O. E. Akman, Nonlinear Time Series Analysis of Congenital Nystagmus Waveforms, First year report, Dept. of Mathematics, UMIST, 2000.

[44] A. Papoulis, *Probablilty, Random Variables and Stochastic Processes*, McGraw Hill, 1991.

[45] G. R. Fowles, *Analytical Mechanics*, Saunders College, 1986.